JOURNAL OF GEOPHYSICAL RESEARCH: ATMOSPHERES, VOL. 118, 5380–5552, doi:10.1002/jgrd.50171, 2013

Bounding the role of black carbon in the climate system: A scientific assessment

T. C. Bond,[1] S. J. Doherty,[2] D. W. Fahey,[3] P. M. Forster,[4] T. Berntsen,[5] B. J. DeAngelo,[6] M. G. Flanner,[7] S. Ghan,[8] B. Kärcher,[9] D. Koch,[10] S. Kinne,[11] Y. Kondo,[12] P. K. Quinn,[13] M. C. Sarofim,[6] M. G. Schultz,[14] M. Schulz,[15] C. Venkataraman,[16] H. Zhang,[17] S. Zhang,[18] N. Bellouin,[19] S. K. Guttikunda,[20] P. K. Hopke,[21] M. Z. Jacobson,[22] J. W. Kaiser,[23] Z. Klimont,[24] U. Lohmann,[25] J. P. Schwarz,[3] D. Shindell,[26] T. Storelvmo,[27] S. G. Warren,[28] and C. S. Zender[29]

Received 26 March 2012; revised 6 December 2012; accepted 4 January 2013; published 6 June 2013.

[1] Black carbon aerosol plays a unique and important role in Earth's climate system. Black carbon is a type of carbonaceous material with a unique combination of physical properties. This assessment provides an evaluation of black-carbon climate forcing that is comprehensive in its inclusion of all known and relevant processes and that is quantitative in providing best estimates and uncertainties of the main forcing terms: direct solar absorption; influence on liquid, mixed phase, and ice clouds; and deposition on snow and ice. These effects are calculated with climate models, but when possible, they are evaluated with both microphysical measurements and field observations. Predominant sources are combustion related, namely, fossil fuels for transportation, solid fuels for industrial and residential uses, and open burning of biomass. Total global emissions of black carbon using bottom-up inventory methods are 7500 Gg yr^{-1} in the year 2000 with an uncertainty range of 2000 to 29000. However, global atmospheric absorption attributable to black

Additional supporting information may be found in the online version of this article.

[1]University of Illinois at Urbana-Champaign, Urbana, Illinois, USA.
[2]Joint Institute for the Study of the Atmosphere and Ocean, University of Washington, Seattle, Washington, USA.
[3]NOAA Earth System Research Laboratory and Cooperative Institute for Research in Environmental Sciences, University of Colorado, Boulder, Colorado, USA.
[4]University of Leeds, Leeds, UK.
[5]Center for International Climate and Environmental Research-Oslo and Department of Geosciences, University of Oslo, Oslo, Norway.
[6]US Environmental Protection Agency, Washington, District of Columbia, USA.
[7]University of Michigan, Ann Arbor, Michigan, USA.
[8]Pacific Northwest National Laboratory, Richland, Washington, USA.
[9]Deutsches Zentrum für Luft- und Raumfahrt Oberpfaffenhofen, Wessling, Germany.
[10]US Department of Energy, Washington, District of Columbia, USA.
[11]Max Planck Institute, Hamburg, Germany.
[12]University of Tokyo, Tokyo, Japan.
[13]NOAA Pacific Marine Environment Laboratory, Seattle, Washington, USA.
[14]Forschungszentrum Jülich GmbH, Jülich, Germany.
[15]Norwegian Meteorological Institute, Oslo, Norway.
[16]Indian Institute of Technology, Bombay, India.
[17]China Meteorological Administration, Beijing, China.
[18]Peking University, Beijing, China.
[19]Met Office Hadley Centre, Exeter, UK.
[20]Division of Atmospheric Sciences, Desert Research Institute, Reno, Nevada, USA.
[21]Clarkson University, Potsdam, New York, USA.
[22]Stanford University, Stanford, California, USA.
[23]European Centre for Medium-range Weather Forecasts, Reading, UK; King's College London, London UK; Max Planck Institute for Chemistry, Mainz, Germany.
[24]International Institute for Applied System Analysis, Laxenburg, Austria.
[25]Eidgenössische Technische Hochschule Zürich, Zurich, Switzerland.
[26]NASA Goddard Institute for Space Studies, New York, New York, USA.
[27]Yale University, New Haven, Connecticut, USA.
[28]University of Washington, Seattle, Washington, USA.
[29]University of California, Irvine, California, USA.

Corresponding author: T. C. Bond, University of Illinois at Urbana-Champaign, Urbana, IL, USA. (yark@uiuc.edu)

©2013 The Authors. *Journal of Geophysical Research: Atmospheres* published by Wiley on behalf of the American Geophysical Union.
This is an open access article under the terms of the Creative Commons Attribution License, which permits use, distribution and reproduction in any medium, provided the original work is properly cited, the use is non-commercial and no modifications or adaptations are made.
2169-897X/13/10.1002/jgrd.50171

carbon is too low in many models and should be increased by a factor of almost 3. After this scaling, the best estimate for the industrial-era (1750 to 2005) direct radiative forcing of atmospheric black carbon is +0.71 W m^{-2} with 90% uncertainty bounds of (+0.08, +1.27) W m^{-2}. Total direct forcing by all black carbon sources, without subtracting the preindustrial background, is estimated as +0.88 (+0.17, +1.48) W m^{-2}. Direct radiative forcing alone does not capture important rapid adjustment mechanisms. A framework is described and used for quantifying climate forcings, including rapid adjustments. The best estimate of industrial-era climate forcing of black carbon through all forcing mechanisms, including clouds and cryosphere forcing, is +1.1 W m^{-2} with 90% uncertainty bounds of +0.17 to +2.1 W m^{-2}. Thus, there is a very high probability that black carbon emissions, independent of co-emitted species, have a positive forcing and warm the climate. We estimate that black carbon, with a total climate forcing of +1.1 W m^{-2}, is the second most important human emission in terms of its climate forcing in the present-day atmosphere; only carbon dioxide is estimated to have a greater forcing. Sources that emit black carbon also emit other short-lived species that may either cool or warm climate. Climate forcings from co-emitted species are estimated and used in the framework described herein. When the principal effects of short-lived co-emissions, including cooling agents such as sulfur dioxide, are included in net forcing, energy-related sources (fossil fuel and biofuel) have an industrial-era climate forcing of +0.22 (−0.50 to +1.08) W m^{-2} during the first year after emission. For a few of these sources, such as diesel engines and possibly residential biofuels, warming is strong enough that eliminating all short-lived emissions from these sources would reduce net climate forcing (i.e., produce cooling). When open burning emissions, which emit high levels of organic matter, are included in the total, the best estimate of net industrial-era climate forcing by all short-lived species from black-carbon-rich sources becomes slightly negative (−0.06 W m^{-2} with 90% uncertainty bounds of −1.45 to +1.29 W m^{-2}). The uncertainties in net climate forcing from black-carbon-rich sources are substantial, largely due to lack of knowledge about cloud interactions with both black carbon and co-emitted organic carbon. In prioritizing potential black-carbon mitigation actions, non-science factors, such as technical feasibility, costs, policy design, and implementation feasibility play important roles. The major sources of black carbon are presently in different stages with regard to the feasibility for near-term mitigation. This assessment, by evaluating the large number and complexity of the associated physical and radiative processes in black-carbon climate forcing, sets a baseline from which to improve future climate forcing estimates.

Citation: Bond, T. C., et al. (2013), Bounding the role of black carbon in the climate system: A scientific assessment, *J. Geophys. Res. Atmos.*, *118*, 5380–5552, doi:10.1002/jgrd.50171.

TABLE OF CONTENTS

1. Executive Summary
   1.1. Background and Motivation
   1.2. Major Findings
      1.2.1. Black Carbon Properties
      1.2.2. Black Carbon Emissions and Abundance
      1.2.3. Synthesis of Black-Carbon Climate Forcing Terms
      1.2.4. Black-Carbon Direct Radiative Forcing
      1.2.5. Black-Carbon Cloud Effects
      1.2.6. Black-Carbon Snow and Ice Effects
      1.2.7. Impacts of Black-Carbon Climate Forcing
      1.2.8. Net Climate Forcing by Black-Carbon-Rich Source Categories
      1.2.9. Major Factors in Forcing Uncertainty
      1.2.10. Climate Metrics for Black Carbon Emissions
      1.2.11. Perspective on Mitigation Options for Black Carbon Emissions
      1.2.12. Policy Implications
2. Introduction
   2.1. What Is Black Carbon?
   2.2. How Does Black Carbon Affect the Earth's Radiative Budget?
   2.3. Assessment Terms of Reference
      2.3.1. Assessment Structure
      2.3.2. Use of Radiative Forcing Concepts
      2.3.3. Contrast With Previous Assessments
3. Measurements and Microphysical Properties of Black Carbon
   3.1. Section Summary
   3.2. Definitions
      3.2.1. Black Carbon
      3.2.2. Organic Matter and Other Carbon Aerosols
      3.2.3. Other Particulate Light Absorbers
   3.3. Black Carbon Formation and Evolution
   3.4. Measurement of BC Mass
   3.5. Optical Properties of Black Carbon

3.6. Measurement of Absorption Coefficients
3.7. Microphysical Properties Affecting MAC and ω_0
3.7.1. Optical Models and Required Inputs
3.7.2. Density
3.7.3. Refractive Index
3.7.4. Particle Size
3.7.5. Configuration of BC-Containing Particles
3.8. Measured and Modeled MAC and ω_0
3.8.1. MAC_{BC} Derived From Measurements
3.8.2. Microphysical Model Ability to Simulate MAC
3.8.2.1. MAC_{BC} of Unmixed BC
3.8.2.2. MAC of BC Mixed With Other Substances
3.8.3. Measured and Modeled Single-Scattering Albedo
3.8.4. Aerosol Properties in Global Models
3.9. CCN Activity of Black Carbon
3.9.1. Measurements of CCN Activity
3.9.2. Global Model Treatment of CCN Activity
4. Emission Magnitudes and Source Categories
4.1. Section Summary
4.2. Introduction
4.2.1. Geographic Aggregation
4.2.2. Definitions and Aggregation of Emission Sources
4.3. Bottom-Up Inventory Procedures
4.3.1. Energy-Related Emissions
4.3.2. Open Burning Emissions
4.3.3. Waste Burning Emissions
4.4. Total BC Emissions and Major Source Categories
4.4.1. Diesel Engines
4.4.2. Industrial Coal
4.4.3. Residential Solid Fuels
4.4.4. Open Burning
4.4.5. Other Emission Sources
4.5. Regional Emissions
4.6. Comparison Among Energy-Related Emission Estimates
4.6.1. Differences in Power Generation Emissions
4.6.2. Differences in Industrial Coal Emissions
4.6.3. Differences in Diesel Engine Emissions
4.6.4. Differences in Residential Solid Fuel Sector
4.6.5. Asian Emission Inventories
4.7. Major Sources of Uncertainty in Emissions
4.7.1. Energy-Related Combustion
4.7.1.1. Activity Data
4.7.1.2. Emission Factors
4.7.1.3. Summary of Uncertainties in Energy-Related Emissions
4.7.2. Open Biomass Burning
4.7.2.1. Burned Area
4.7.2.2. Fuel Load and Combustion Completeness
4.7.2.3. Emission Factors
4.7.2.4. Summary of Uncertainties in Open Burning Emissions
4.8. Trends in BC Emissions
4.9. Receptor Modeling to Evaluate Source Contributions
4.9.1. Receptor Modeling in Urban Areas
4.9.2. Receptor Modeling in Continental Plumes
4.9.3. Summary of Findings From Receptor Modeling
5. Constraints on Black-Carbon Atmospheric Abundance
5.1. Section Summary
5.2. Introduction
5.3. Atmospheric Absorption and Extinction by Absorbing Species
5.4. Observations of Atmospheric Black Carbon Concentrations
5.4.1. In Situ Monitoring
5.4.1.1. Intensive Field Campaigns
5.4.1.2. Long-Term In Situ Monitoring
5.4.2. Remote Sensing
5.4.2.1. Ground-Based Remote Sensing
5.4.2.2. Remote Sensing From Space
5.5. Comparison Between Modeled and Observed BC Concentrations and AAOD
5.5.1. Estimating Emissions by Integrating Models and Observations
5.6. Vertical Distribution of BC
5.6.1. Comparison Between Modeled and Observed Vertical Distributions
5.7. Causes of Model Biases
5.8. Summary of Limitations in Inferring Black Carbon Atmospheric Abundance
6. Black-Carbon Direct Radiative Forcing
6.1. Section Summary
6.2. Introduction
6.3. Emission, Lifetime, and Burden
6.4. Mass Absorption Cross Section
6.5. Scaling Modeled BC AAOD to Observations
6.5.1. Sensitivities in AAOD Scaling
6.5.2. Reasons for Low Bias in Modeled AAOD
6.6. Forcing Efficiency
6.6.1. Vertical Location of BC
6.6.2. Horizontal Location of BC
6.7. All-Source and Industrial-Era BC DRF
6.7.1. Scaled Estimates of BC DRF
6.7.2. Central Estimate of BC DRF
6.7.3. Uncertainties in BC DRF
6.8. Previous Observationally Scaled Radiative-Forcing Estimates
6.9. Implications of Increased BC AAOD
6.9.1. Apportionment of Bias in BC AAOD
6.9.2. Revised Estimate of BC Emissions
6.9.3. Scaling of Modeled AAOD in the Context of Other Evidence
6.10. Summary of Uncertainties in BC DRF
7. Black Carbon Interactions With Clouds
7.1. Section Summary
7.2. Introduction
7.3. Black-Carbon Semi-Direct Effects on Cloud Cover
7.3.1. Cloud Scale and Regional Studies

7.3.2. Global Model Semi-Direct Estimates
7.3.3. Increased Absorption by Cloud Droplet Inclusions
7.4. BC Indirect Effects on Liquid Clouds
7.5. BC Indirect Effects on Mixed-Phase and Ice Clouds
7.5.1. Laboratory Evidence for BC Effectiveness as IN
7.5.2. BC Effects on Mixed-Phase Clouds
7.5.2.1. Mechanisms
7.5.2.2. Experimental Studies
7.5.2.3. Modeling Results
7.5.3. BC Effects on Ice-Phase Clouds
7.5.3.1. Mechanisms
7.5.3.2. Field Evidence for BC Acting as IN
7.5.3.3. Modeling Evidence for BC Atmospheric Abundance and Mixing State
7.5.3.4. Global Model Studies of BC Effects on Cirrus
7.5.3.5. Aircraft Impacts on High Ice-Cloud Properties
7.6. Comprehensive Modeling of BC Cloud Effects
7.7. Summary of Uncertainties in Estimating Indirect Effects
7.7.1. Model Uncertainties Beyond Aerosol-Cloud Interactions
7.7.2. Aerosol-Cloud Interactions
8. Cryosphere Changes: Black Carbon in Snow and Ice
8.1. Section Summary
8.2. Introduction
8.3. Modeled Forcing
8.3.1. BC Concentrations in Snow and Sea Ice and the Resulting Change in Albedo
8.3.2. Snow-Covered Area
8.3.3. Masking by Clouds and Vegetation
8.3.4. Snow Grain Size
8.3.5. Albedo Dependence on Downwelling Radiation
8.3.6. Concentration of BC With Sublimation and Melting
8.3.7. Representation of All Light Absorbing Particles in Snow
8.4. Measurements of BC in Snow and Comparison With Models
8.4.1. Measurement Methods
8.4.2. Arctic and Sub-Arctic Snow
8.4.3. Mid-Latitude Snow Measurements
8.4.4. BC in Mountain Glaciers
8.4.5. Trends in Arctic Snow BC
8.4.6. Trends in Mountain Snow
8.5. Sources of BC to Arctic and Himalayan Snow
8.6. Estimate of Forcing by BC in the Cryosphere
8.6.1. Adjusted Forcing by BC in Snow
8.6.2. Radiative Forcing by BC in Sea Ice
8.6.3. Forcing by BC in Snow in the Himalaya and Tibetan Plateau
9. Climate Response to Black Carbon Forcings
9.1. Section Summary
9.2. Introduction to Climate Forcing, Feedback, and Response
9.3. Surface Temperature Response to Atmospheric Black Carbon
9.3.1. Global-Mean Temperature Change
9.3.2. Regional Surface Temperature Change
9.4. Precipitation Changes Due to Black-Carbon Direct and Semi-Direct Effects
9.5. Climate Response to the Snow Albedo Effect
9.6. Detection and Attribution of Climate Change Due to Black Carbon
9.7. Conclusions
10. Synthesis of Black-Carbon Climate Effects
10.1. Section Summary
10.2. Introduction
10.3. Global Climate Forcing Definition
10.4. BC Global Climate Forcing Components and Uncertainties
10.4.1. BC Direct Forcing
10.4.2. BC Cloud Indirect Effects
10.4.2.1. Liquid Cloud and Semi-Direct Effects
10.4.2.2. BC Inclusion in Cloud Drops
10.4.2.3. Mixed-Phase Cloud Effect
10.4.2.4. Ice Cloud Effect
10.4.3. BC in Snow and Cryosphere Changes
10.4.4. BC in Sea Ice
10.4.5. Net Effect of BC and Co-Emitted Species
10.5. Uncertainties in BC Global Climate Forcings
10.5.1. Atmospheric Burden, Emissions, and Rate of Deposition
10.5.2. Selection of Preindustrial Emissions
10.5.3. Scaling to Emission Rate or Atmospheric Burden
10.5.4. Dependence on Atmospheric and Surface State
10.6. Total Forcing Estimates and Comparison With Previous Work
11. Net Climate Forcing by Black-Carbon-Rich Source Categories
11.1. Section Summary
11.2. Introduction
11.3. Approach to Estimating Forcing From BC-Rich Source Categories
11.4. Climate Forcing Per Emission for Co-Emitted Aerosols and Precursors
11.4.1. Direct Effect for Co-Emitted Aerosol and Precursors
11.4.2. Liquid Cloud Effect for Co-Emitted Aerosol and Precursors
11.4.3. Other Cloud Effects for Co-Emitted Aerosol and Precursors
11.4.4. Snow Albedo Forcing for Co-Emitted Aerosol
11.4.5. Forcing by Co-Emitted Gaseous Species
11.4.6. Climate Forcing by Secondary Organic Aerosol

11.4.7. Forcing in Clear and Cloudy Skies
11.5. Net Climate Forcing by BC-Rich Source Categories
11.5.1. Diesel Engines
11.5.2. Industrial Coal
11.5.3. Residential Solid Fuel
11.5.4. Open Biomass Burning
11.5.5. Summary of BC-Rich Source Categories
11.5.6. Cumulative Sum of Forcing by BC-Rich Source Categories
11.6. Climate Forcing by Selected Sources
11.7. Comparison With Forcing on Longer Time Scales
11.8. Cautions Regarding Net Forcing Estimates
11.8.1. Constraints on Emissions of BC and Co-Emitted Species Are Limited
11.8.2. Forcing Dependence on Emitting Region Is Not Captured
11.8.3. Regional Impacts Are Not Well Captured by Global Averages
11.8.4. Large Uncertainties Remain in Deriving and Apportioning Cloud Impacts
11.8.5. Climate Forcing by Additional Co-Emitted Species May Affect Total Category Forcing
12. Emission Metrics for Black Carbon
12.1. Section Summary
12.2. Introduction
12.3. The GWP and GTP Metrics
12.4. Calculations of Metric Values for BC
12.5. Uncertainties
12.6. Shortcomings of Global Metrics
12.7. Choice of Time Horizon
12.8. Towards Metrics for the Net Effect of Mitigation Options
13. Mitigation Considerations for BC-Rich Sources
13.1. Section Summary
13.2. Mitigation Framework for Comprehensive Evaluation
13.3. Costs and Benefits of Mitigation
13.3.1. Health Benefits
13.3.2. Valuing Climate Benefits of BC Mitigation
13.4. Technical and Programmatic Feasibility for Individual BC-Rich Source Categories
13.4.1. Diesel Engines
13.4.2. Industry
13.4.3. Residential Solid Fuel: Heating
13.4.4. Residential Solid Fuel: Cooking
13.4.5. Open Burning
13.4.6. Other Sources
13.5. International Perspective on BC Reductions in Aggregate
13.5.1. Projected Future Emissions
13.5.2. Comprehensive International Assessments of BC Mitigation Actions
13.6. Policy Delivery Mechanisms
13.7. Synthesis of Considerations for Identifying Important Mitigation Options

1. Executive Summary

1.1. Background and Motivation

[2] Black carbon is emitted in a variety of combustion processes and is found throughout the Earth system. Black carbon has a unique and important role in the Earth's climate system because it absorbs solar radiation, influences cloud processes, and alters the melting of snow and ice cover. A large fraction of atmospheric black carbon concentrations is due to anthropogenic activities. Concentrations respond quickly to reductions in emissions because black carbon is rapidly removed from the atmosphere by deposition. Thus, black carbon emission reductions represent a potential mitigation strategy that could reduce global climate forcing from anthropogenic activities in the short term and slow the associated rate of climate change.

[3] Previous studies have shown large differences between estimates of the effect of black carbon on climate. To date, reasons behind these differences have not been extensively examined or understood. This assessment provides a comprehensive and quantitative evaluation of black carbon's role in the climate system and explores the effectiveness of a range of options for mitigating black carbon emissions. As such, this assessment includes the principal aspects of climate forcing that arise from black carbon emissions. It also evaluates the net climate forcing of combustion sources that emit large quantities of black carbon by including the effects of co-emitted species such as organic matter and sulfate aerosol precursors. The health effects of exposure to black carbon particles in ambient air are not evaluated in this assessment.

1.2. Major Findings

1.2.1. Black Carbon Properties

[4] 1. *Black carbon is a distinct type of carbonaceous material that is formed primarily in flames, is directly emitted to the atmosphere, and has a unique combination of physical properties*. It strongly absorbs visible light, is refractory with a vaporization temperature near 4000K, exists as an aggregate of small spheres, and is insoluble in water and common organic solvents. In measurement and modeling studies, the use of the term "black carbon" frequently has not been limited to material with these properties, causing a lack of comparability among results.

[5] 2. *Many methods used to measure black carbon can be biased by the presence of other chemical components*. Measured mass concentrations can differ between methods by up to 80% with the largest differences corresponding to aerosol with low black carbon mass fractions.

[6] 3. *The atmospheric lifetime of black carbon, its impact on clouds, and its optical properties depend on interactions with other aerosol components*. Black carbon is co-emitted with a variety of other aerosols and aerosol precursor gases. Soon after emission, black carbon becomes mixed with other aerosol components in the atmosphere. This mixing increases light absorption by black carbon, increases its ability to form liquid-cloud droplets, alters its capacity to form ice nuclei, and, thereby, influences its atmospheric removal rate.

1.2.2. Black Carbon Emissions and Abundance

[7] 1. *Sources whose emissions are rich in black carbon* ("*BC-rich*") *can be grouped into a small number of categories,*

broadly described as diesel engines, industry, residential solid fuel, and open burning. The largest global sources are open burning of forests and savannas. Dominant emitters of black carbon from other types of combustion depend on the location. Residential solid fuels (i.e., coal and biomass) contribute 60 to 80% of Asian and African emissions, while on-road and off-road diesel engines contribute about 70% of emissions in Europe, North America, and Latin America. Residential coal is a significant source in China, the former USSR, and a few Eastern European countries. These categories represent about 90% of black-carbon mass emissions. Other miscellaneous black-carbon-rich sources, including emissions from aviation, shipping, and flaring, account for another 9%, with the remaining 1% attributable to sources with very low black carbon emissions.

[8] 2. *Total global emissions of black carbon using bottom-up inventory methods are* 7500 *Gg* yr^{-1} *in the year* 2000 *with an uncertainty range of* 2000 *to* 29,000. Emissions of 4800 (1200 to 15000) Gg yr^{-1} black carbon are from energy-related combustion, which includes all but open burning, and the remainder is from open burning of forests, grasslands, and agricultural residues.

[9] 3. *An estimate of background black carbon abundances in a preindustrial year is used to evaluate climate effects*. In this assessment, we use the term "industrial era" to denote differences in the atmospheric state between present day and the year 1750. We use a preindustrial value of 1400 Gg of black carbon per year from biofuel and open biomass burning, although some fraction was anthropogenic at that time.

[10] 4. *Current emission estimates agree on the major sources and emitting regions, but significant uncertainties remain*. Information gaps include the amounts of biofuel or biomass combusted, and the type of technology or burning, especially in developing countries. Emission estimates from open biomass burning lack data on fuel consumed, and black-carbon emission factors from this source may be too low.

[11] 5. *Black carbon undergoes regional and intercontinental transport during its short atmospheric lifetime*. Atmospheric removal occurs within a few days to weeks via precipitation and contact with surfaces. As a result, black carbon is found in remote regions of the atmosphere at concentrations much lower than in source regions.

[12] 6. *Comparison with remote sensing observations indicates that global atmospheric absorption attributable to black carbon is too low in many global aerosol models*. Scaling atmospheric black carbon absorption to match observations increases the modeled globally averaged, industrial-era black carbon absorption by a factor of 2.9. Some of the model underestimate can be attributed to the models lacking treatment of enhanced absorption caused by mixing of black carbon with other constituents. The remainder is attributed to underestimates of the amount of black carbon in the atmosphere. Burden underestimates by factors of 1.75 to 4 are found in Africa, South Asia, Southeast Asia, Latin America, and the Pacific region. In contrast, modeled burdens in North America, Europe, and Central Asia are approximately correct. The required increase in modeled BC burdens is compatible with in situ observations in Asia and space-based remote sensing of biomass burning aerosol emissions.

[13] 7. *If all differences in modeled black carbon abundances were attributed to emissions, total emissions would be* 17,000 *Gg* yr^{-1} *compared to the bottom-up inventory estimates of* 7500 *Gg* yr^{-1}. The industrial-era value of about 14,000 *Gg* yr^{-1}, obtained by subtraction of estimated preindustrial emissions, is used as the best estimate of emissions to determine final forcing values in this assessment. However, some of the difference could be attributed to poorly modeled removal instead of emissions. Both energy-related burning and open biomass burning are implicated in underestimates of emission rates, depending on the region.

1.2.3. Synthesis of Black-Carbon Climate Forcing Terms

[14] 1. *Radiative forcing used alone to estimate black-carbon climate effects fails to capture important rapid adjustment mechanisms*. Black-carbon-induced heating and cloud microphysical effects cause rapid adjustments within the climate system, particularly in clouds and snow. These rapid adjustments cause radiative imbalances that can be represented as adjusted or effective forcings, accounting for the near-term global response to black carbon more completely. The effective forcing accounts for the larger response of surface temperature to a radiative forcing by black carbon in snow and ice compared to other forcing mechanisms. These factors are included in the climate forcing values reported in this assessment.

[15] 2. The best estimate of industrial-era climate forcing of black carbon through all forcing mechanisms is +1.1 W m^{-2} with 90% uncertainty bounds of +0.17 to +2.1 W m^{-2}. This estimate includes cloud forcing terms with very low scientific understanding that contribute additional positive forcing and a large uncertainty. This total climate forcing of black carbon is greater than the direct forcing given in the fourth Intergovernmental Panel on Climate Change (IPCC) report. There is a very high probability that black carbon emissions, independent of co-emitted species, have a positive forcing and warm the climate. This black carbon climate forcing is based on the change in atmospheric abundance over the industrial era (1750 to 2005). The black-carbon climate-forcing terms that make up this estimate are listed in Table 1. For comparison, the radiative forcings including indirect effects from emissions of the two most significant long-lived greenhouse gases, carbon dioxide (CO_2) and methane (CH_4), in 2005 were +1.56 and +0.86 W m^{-2}, respectively.

[16] 3. *The fossil fuel direct effect of black carbon of* +0.29 *W* m^{-2} *is higher than the value provided by the IPCC in* 2007. This increase is caused by higher absorption per mass and atmospheric burdens than used in models for IPCC. The black-carbon-in-snow forcing estimate in this assessment is comparable, although more sophisticated. Our total climate forcing estimate of +1.1 W m^{-2} includes biofuel and open-biomass sources of black carbon, as well as cloud effects that the IPCC report did not explicitly isolate for black carbon.

1.2.4. Black-Carbon Direct Radiative Forcing

[17] 1. *Direct radiative forcing of black carbon is caused by absorption and scattering of sunlight*. Absorption heats the atmosphere where black carbon is present and reduces sunlight that reaches the surface and that is reflected back to

Table 1. Black Carbon Climate Forcing Terms, Evaluated for Industrial Era (1750–2005) Unless Otherwise Stated

Climate Forcing Term	Forcing Components	Forcing ($W m^{-2}$) (90% Uncertainty Range)
Black carbon direct effect	Atmosphere absorption and scattering	+0.71 (+0.09 to +1.26)
Direct radiative forcing split	Fossil fuel sources	+0.29
	Bio fuel sources	+0.22
	Open burning sources	+0.20
Black carbon cloud semi-direct and indirect effects	Combined liquid cloud and semi-direct effect	−0.2 (−0.61 to +0.10)
	Black carbon in cloud drops	+0.2 (−0.1 to +0.9)
	Mixed phase cloud	+0.18 (+0.0 to +0.36)
	Ice clouds	0.0 (−0.4 to +0.4)
	Combined cloud and semi-direct effects	+0.23 (−0.47 to +1.0)
Black carbon in snow and sea-ice effects	Snow effective forcing	+0.10 (+0.014 to +0.30)
	Sea-ice effective forcing	+0.03 (+0.012 to +0.06)
	Combined surface forcing terms	+0.13 (+0.04 to 0.33)
Total climate forcings[a]	Black carbon only (all terms)	+1.1 (0.17 to +2.1)
	Net effect of black carbon + co-emitted species:	
	All sources	−0.06 (−1.45 to +1.29)
	Excluding open burning	+0.22 (−0.50 to +1.08)
All source (includes pre-industrial) forcings	Direct radiative forcing	+0.88 (+0.18 to +1.47)
	Snow pack effective forcing	+0.12 (+0.02 to +0.36)
	Sea-ice effective forcing	+0.036 (+0.016 to +0.068)

[a]Note that the total best estimate is the median of the combined probability distribution functions across all terms, which differs from the mean of the best estimates.

space. Direct radiative forcing is the most commonly cited climate forcing associated with black carbon.

[18] 2. *The best estimate for the industrial-era* (1750 *to* 2005) *direct radiative forcing of black carbon in the atmosphere is* +0.71 *W m*$^{-2}$ *with* 90% *uncertainty bounds of* +0.08 *to* +1.27 *W m*$^{-2}$. Previous direct forcing estimates ranged from +0.2 to +0.9 W m^{-2}, and the median value was much lower. The range presented here is altered because we adjust global aerosol models with observational estimates of black carbon absorption optical depth as done in some previous studies.

[19] 3. *Direct radiative forcing from all present-day sources of black carbon (including preindustrial background sources) is estimated to be* +0.88 *W m*$^{-2}$ *with* 90% *uncertainty bounds of* +0.17 *to* +1.48 *W m*$^{-2}$. This value is 24% larger than industrial-era forcing because of appreciable preindustrial emissions from open burning and biofuel use.

[20] 4. *Estimates of direct radiative forcing are obtained from models of black carbon abundance and location*. The ability to estimate radiative forcing accurately depends on the fidelity of these models. Modeling of and observational constraints on the black-carbon vertical distribution are particularly poor.

1.2.5. Black-Carbon Cloud Effects

[21] 1. *Black carbon influences the properties of ice clouds and liquid clouds through diverse and complex processes*. These processes include changing the number of liquid cloud droplets, enhancing precipitation in mixed-phase clouds, and changing ice particle number and cloud extent. The resulting radiative changes in the atmosphere are considered climate *indirect effects* of black carbon. In addition, in the *semi-direct effect*, light absorption by black carbon alters the atmospheric temperature structure within, below, or above clouds and consequently alters cloud distributions. Liquid-cloud and semi-direct effects may have either negative or positive climate forcings. The best estimates of the cloud-albedo effect and the semi-direct effect are negative. Absorption by black carbon within cloud droplets and mixed-phase cloud changes cause positive climate forcing (warming). At present, even the sign of black-carbon ice-cloud forcing is unknown.

[22] 2. *The best estimate of the industrial-era climate forcing from black carbon cloud effects is positive with substantial uncertainty (*+0.23 *W m*$^{-2}$ *with a* −0.47 *to* +1.0 *W m*$^{-2}$ 90% *uncertainty range).* This positive estimate has large contributions from cloud effects with a very low scientific understanding and large uncertainties. The cloud effects, summarized in Table 1, are the largest source of uncertainty in quantifying black carbon's role in the climate system. Very few climate model studies have isolated the influence of black carbon in these indirect effects.

1.2.6. Black-Carbon Snow and Ice Effects

[23] 1. *Black carbon deposition on snow and ice causes positive climate forcing*. Even aerosol sources with negative globally averaged climate forcing, such as biomass combustion, can produce positive climate forcing in the Arctic because of their effects on snow and ice.

[24] 2. *The best estimate of climate forcing from black carbon deposition on snow and sea ice in the industrial era is* +0.13 *W m*$^{-2}$ *with* 90% *uncertainty bounds of* +0.04 *to* +0.33 *W m*$^{-2}$. The all-source present-day climate forcing including preindustrial emissions is somewhat higher at +0.16 W m^{-2}. These climate forcings result from a combination of radiative forcing, rapid adjustments, and the stronger snow-albedo feedback caused by black-carbon-on-snow forcing. This enhanced climate feedback is included in the +0.13 W m^{-2} forcing estimate.

[25] 3. *Species other than black carbon are a large fraction of the absorbing aerosol mass that reduces reflectivity of snow and ice cover*. These species include dust and absorbing organic carbon; the latter is co-emitted with black carbon or may come from local soils.

[26] 4. *The role of black carbon in the melting of glaciers is still highly uncertain*. Few measurements of glacial black-carbon content exist, and studies of the impact on glacial snow melt have not sufficiently accounted for natural impurities such as soil dust and algae or for the difficulty in modeling regions of mountainous terrain.

1.2.7. Impacts of Black-Carbon Climate Forcing

[27] 1. *The black-carbon climate forcings from the direct effect and snowpack changes cause the troposphere and the top of the cryosphere to warm, inducing further climate response in the form of cloud, circulation, surface temperature, and precipitation changes*. In climate model studies, black-carbon direct effects cause equilibrium global warming that is concentrated in the Northern Hemisphere. The warming response to black-carbon-in-snow forcing is greatest during local spring and over mid-to-high northern latitudes. In terms of equilibrium global-mean surface temperature change, the BC total climate forcing estimate over the industrial era would correspond to a warming between 0.1 and 2.0K. Note that not all this warming has been realized in the present day, as the climate takes more than a century to reach equilibrium and many co-emitted species have a cooling effect, countering the global-mean warming of BC.

[28] 2. *Regional circulation and precipitation changes may occur in response to black-carbon climate forcings*. These changes include a northward shift in the Inter-Tropical Convergence Zone and changes in Asian monsoon systems where concentrations of absorbing aerosols are large. Black-carbon cloud indirect effects are also expected to induce a climate response. However, global models do not simulate robust responses to these complex and uncertain climate-forcing mechanisms.

1.2.8. Net Climate Forcing by Black-Carbon-Rich Source Categories

[29] 1. *Other species co-emitted with black carbon influence the sign and magnitude of net climate forcing by black-carbon-rich source categories*. The net climate forcing of a source sector is a useful metric when considering mitigation options. Principal co-emitted species that can change the sign of short-lived forcing are organic matter and sulfur species. The direct radiative forcing is positive for almost all black-carbon-rich source categories, even when negative direct forcings by sulfate and organic matter are considered. Liquid-cloud forcing by co-emitted aerosol species can introduce large negative forcing. Therefore, high confidence in net positive total climate forcing is possible only for black-carbon source categories with low co-emitted species, such as diesel engines.

[30] 2. *The best estimate of the total industrial-era climate forcing by short-lived effects from all black-carbon-rich sources is near zero with large uncertainty bounds*. Short-lived effects are defined as those lasting less than 1 year, including those from aerosols and short-lived gases. This total is +0.22 (−0.50 to +1.08) W m^{-2} for fossil fuel and biofuel-burning emissions and −0.06 W m^{-2} with 90% uncertainty bounds of −1.45 to +1.29 W m^{-2} when open burning emissions are included.

[31] 3. *The climate forcings from specific sources within black-carbon source categories are variable depending upon the composition of emissions*. Some subsets of a category may have net positive climate forcing even if the whole category does not. Selecting such individual source types from each category can yield a group of measures that, if implemented, would reduce climate forcing. However, the positive forcing reduction would be much less than the total climate forcing of +1.1 W m^{-2} attributable to all industrial-era black-carbon emissions in 2005.

[32] 4. *Short-lived forcing effects from black-carbon-rich sources are substantial compared with the effects of long-lived greenhouse gases from the same sources, even when the forcing is integrated over* 100 *years*. Climate forcing from changes in short-lived species in each source category amounts to 5 to 75% of the combined longer-lived forcing by methane, effects on the methane system, and CO_2, when the effects are integrated over 100 years.

1.2.9. Major Factors in Forcing Uncertainty

[33] 1. *Observational constraints on global, annual average black carbon direct radiative forcing are limited by a lack of specificity in attributing atmospheric absorption to black carbon, dust, or organic aerosol*. These constraints are required to correct demonstrated biases in the distributions of atmospheric black carbon in climate models.

[34] 2. *Altitude and removal rates of black carbon are strong controlling factors*. They determine black-carbon absorption forcing efficiency, microphysical effects on clouds, and the sign of semi-direct effects. Models do not accurately represent black-carbon vertical distributions. Removal rates, particularly wet removal, affect most facets of black carbon forcing, including its lifetime, horizontal, and vertical extent, and deposition to the cryosphere.

[35] 3. *Black-carbon emission rates from both energy-related combustion and biomass burning currently appear underestimated*. Underestimates occur largely in Asia and Africa. Uncertainties in biomass burning emissions also affect preindustrial black-carbon emission rates and net forcing.

[36] 4. *Black carbon effects on clouds are a large source of uncertainty*. Models of liquid-cloud and semi-direct effects disagree on signs and magnitudes of forcing. However, potentially large forcing terms and uncertainties come from black carbon effects on mixed-phase clouds, cloud-absorption, and ice clouds, which have been estimated in a very small number of studies.

[37] 5. *Estimates of forcing rely on accurate models of the Earth system*. Black-carbon cloud interactions rely on fidelity in representation of clouds without black carbon present, and likewise, reductions in snow and sea ice albedo by black carbon depend on accurate representation of coverage of snow and sea ice. Uncertainties due to model biases of these distributions have not been assessed.

1.2.10. Climate Metrics for Black Carbon Emissions

[38] 1. *The* 100 *year global-warming-potential (GWP) value for black carbon is* 900 *(*120 *to* 1800 *range) with all forcing mechanisms included*. The large range derives from the uncertainties in the climate forcings for black carbon effects. The GWP and other climate metric values vary by about ±30% between emitting regions. Black-carbon metric values decrease with increasing time horizon due to the short lifetime of black carbon emissions compared to CO_2.

Black carbon and CO_2 emission amounts with equivalent 100 year GWPs have different impacts on climate, temperature, rainfall, and the timing of these impacts. These and other differences raise questions about the appropriateness of using a single metric to compare black carbon and greenhouse gases.

1.2.11. Perspective on Mitigation Options for Black Carbon Emissions

[39] 1. *Prioritization of black-carbon mitigation options is informed by both scientific and non-scientific factors*. Scientific issues include the magnitude of black carbon emissions by sector and region, and net climate forcing including co-emissions and impacts on the cryosphere. Non-science factors, such as technical feasibility, costs, policy design, and implementation feasibility, also play roles. The major sources of black carbon are presently in different stages with regard to technical and programmatic feasibility for near-term mitigation.

[40] 2. *Mitigation of diesel-engine sources appears to offer the most confidence in reducing near-term climate forcing*. Mitigating emissions from residential solid fuels also may yield a reduction in net positive forcing. The net effect of other sources, such as small industrial coal boilers and ships, depends on the sulfur content, and net climate benefits are possible by mitigating some individual source types.

1.2.12. Policy Implications

[41] 1. *Our best estimate of black carbon forcing ranks it as the second most important individual climate-warming agent after carbon dioxide, with a total climate forcing of +1.1 W m^{-2} (+0.17 to +2.1 W m^{-2} range)*. This forcing estimate includes direct effects, cloud effects, and snow and ice effects. The best estimate of forcing is greater than the best estimate of indirect plus direct forcing of methane. The large uncertainty derives principally from the indirect climate-forcing effects associated with the interactions of black carbon with cloud processes. Climate forcing from cloud drop inclusions, mixed phase cloud effects, and ice cloud effects together add considerable positive forcing and uncertainty. The relative importance of black carbon climate forcing will increase following reductions in the emissions of other short-lived species or decrease if atmospheric burdens of long-lived greenhouse gases continue to grow.

[42] 2. *Black carbon forcing concentrates climate warming in the mid-high latitude Northern Hemisphere*. As such, black carbon could induce changes in the precipitation patterns from the Asian Monsoon. It is also likely to be one of the causes of Arctic warming in the early twentieth century.

[43] 3. *The species co-emitted with black carbon also have significant climate forcing*. Black carbon emissions are primarily attributable to a few major source categories. For a subset of these categories, including diesel engines and possibly residential solid fuel, the net impact of emission reductions can be a lessening of positive climate forcing (cooling). However, the impact of *all* emissions from black-carbon-rich sources is slightly negative (−0.06 W m^{-2}) with a large uncertainty range (−1.45 to +1.29 W m^{-2}). Therefore, uniform elimination of all emissions from black-carbon-rich sources could lead to no change in climate warming, and sources and mitigation measures chosen to reduce positive climate forcing should be carefully identified. The uncertainty in the response to mitigation is larger when more aerosol species are co-emitted.

[44] 4. *All aerosol that is emitted or formed in the lower atmosphere adversely affects public health*. Mitigation of many of these sources would increase positive climate forcing (warming). In contrast, reduction of aerosol concentrations by mitigating black-carbon-rich source categories would be accompanied by very small or slightly negative changes in climate forcing. These estimates of climate forcing changes from source mitigation are associated with large uncertainties.

[45] 5. *Forcings by greenhouse-gases alone do not convey the full climate impact of actions that alter emission sources*. Black-carbon-rich source sectors emit short-lived species, primarily black carbon, other aerosols and their precursors, and long-lived greenhouse gases (e.g., CO_2 and CH_4). The total climate forcing from the short-lived components is a substantial fraction of the total (up to 75%) even when both short-lived and long-lived forcings are integrated over 100 years after emission.

2. Introduction

[46] In the year 2000, a pair of papers [*Jacobson*, 2000; *Hansen et al*., 2000] pointed out that black carbon—small, very dark particles resulting from combustion—might presently warm the atmosphere about one third as much as CO_2. Because black carbon absorbs much more light than it reflects, it warms the atmosphere through its interaction with sunlight. This warming effect contrasts with the cooling effect of other particles that are primarily scattering and, thus, reduce the amount of energy kept in the Earth system. Radiative forcing (RF) by atmospheric BC stops within weeks after emissions cease because its atmospheric lifetime is short unlike the long timescale associated with the removal of CO_2 from the atmosphere. Thus, sustained reductions in emissions of BC and other short-lived climate warming agents, especially methane and tropospheric ozone (O_3), could quickly decrease positive climate forcing and hence climate warming. While such targeted reductions will not avoid climate change, their value in a portfolio to manage the trajectory of climate forcing is acknowledged in the scientific community [e.g., *Molina et al*., 2009; *Ramanathan and Xu*, 2010].

[47] Discussions of black carbon's role in climate rest on a long history. Urban pollution had been a concern for hundreds of years [*Brimblecombe*, 1977], and blackness was used as an indicator of pollution since the early 1900s [*Uekoetter*, 2005]. Black carbon was first isolated in urban pollution, as *Rosen et al*. [1978] and *Groblicki et al*. [1981] found that graphitic, refractory particles were responsible for light absorption. Shortly after *McCormick and Ludwig* [1967] suggested that aerosols could influence climate, *Charlson and Pilat* [1969] pointed out that aerosol absorption causes warming rather than cooling. The magnitude of climate effects was first estimated hypothetically to examine post-nuclear war situations [*Turco et al*., 1983] and later using realistic distributions from routine human emissions [*Penner et al*., 1993; *Haywood and Shine*, 1995]. It was known that particles traveled long distances from source regions [*Rodhe et al*., 1972], reaching as far as the Arctic [*Heintzenberg*, 1980]. International experiments

organized to examine aerosol in continental outflow were initiated in the late 1990s [*Raes et al*., 2000]. They confirmed that absorbing aerosol was prevalent in some regions and an important component of the atmospheric radiation balance [*Satheesh and Ramanathan*, 2000]. This coincident confirmation of atmospheric importance and proposal of policies for mitigation triggered further debate.

[48] In the decade since the initial proposals, the speed of Arctic climate change and glacial melt has increased the demand for mitigation options which can slow near-term warming, such as reductions in the emissions of short-lived warming agents. The impact of air quality regulations that reduce sulfate particles is also being recognized. Most particles, including sulfates, cool the climate system, masking some of the warming from longer-lived greenhouse gases (GHGs) and BC. Thus, regulating these particles to protect human health may have the unintended consequence of increasing warming rapidly. BC also plays a direct role in surface melting of snow and ice and, hence, may have an important role in Arctic warming [*Quinn et al*., 2008]; if so, targeted reductions could have disproportionate benefits for these sensitive regions.

[49] Particulate matter was originally regulated to improve human health. Evidence supporting the link between particles and adverse respiratory and cardiovascular health continues to mount [*Pope et al*., 2009]. High human exposures to particulate matter in urban settings are linked to sources that emit black carbon [*Grahame and Schlesinger*, 2007; *Naeher et al*., 2007; *Janssen et al*., 2011] and to intense exposures in indoor air [*Smith et al*., 2010]. Thus, reducing particulate matter is desirable to improve human welfare, regardless of whether those reductions reduce climate warming.

[50] For the past few years, the opportunity to reduce black carbon has received pervasive policy attention at high levels. The G8 declaration, in addition to promising GHG reductions, is committed to "...taking rapid action to address other significant climate forcing agents, such as black carbon." [9 July 2009, L'Aquila, Italy]. The Arctic Council, recognizing that "...reductions of emissions have the potential to slow the rate of Arctic snow, sea ice and sheet ice melting in the near-term...," established a task force in 2009 to offer mitigation recommendations [29 April 2009, Tromsø, Norway] and "encouraged" the eight member states to implement certain black-carbon reduction measures [12 May 2011, Nuuk, Greenland]. The United States has complemented this international interest with passage of a bill [H.R. 2996] requiring a study of the sources, climate and health impacts, and mitigation options for black carbon both domestically and internationally. A proposed revision to the Gothenburg Protocol [*UNECE*, 1999] states that parties "should, in implementing measures to achieve their national targets for particulate matter, give priority, to the extent they consider appropriate, to emission reductions measures which also significantly reduce black carbon." [*UNECE*, 2011]. In February 2012, the Climate and Clean Air Coalition was formed with the aim of reducing climate warming and air pollutants through action on short-lived pollutants—in particular, BC, methane, and hydrofluorocarbons (http://www.unep.org/ccac).

[51] The prospect of achieving quick climate benefits by reducing BC emissions is tantalizing, but the scientific basis for evaluating the results of policy choices has not yet been fully established. This assessment is intended to provide a comprehensive and quantitative scientific framework for such an evaluation. In the remainder of this section, we briefly define black carbon, present our terms of reference for the assessment, and describe its structure.

2.1. What Is Black Carbon?

[52] Black carbon is a distinct type of carbonaceous material, formed only in flames during combustion of carbon-based fuels. It is distinguishable from other forms of carbon and carbon compounds contained in atmospheric aerosol because it has a unique combination of the following physical properties:

[53] 1. It *strongly absorbs visible light* with a mass absorption cross section of at least 5 m^2g^{-1} at a wavelength of 550 nm.

[54] 2. It is *refractory*; that is, it retains its basic form at very high temperatures, with a vaporization temperature near 4000K.

[55] 3. It is *insoluble* in water, in organic solvents including methanol and acetone, and in other components of atmospheric aerosol.

[56] 4. It exists as an *aggregate* of small carbon spherules.

[57] The strong absorption of visible light at all visible wavelengths by black carbon is the distinguishing characteristic that has raised interest in studies of atmospheric radiative transfer. No other substance with such strong light absorption per unit mass is present in the atmosphere in significant quantities. BC has very low chemical reactivity in the atmosphere; its primary removal process is wet or dry deposition to the surface. BC is generally found in atmospheric aerosol particles containing a number of other materials, many of which are co-emitted with BC from a variety of sources.

[58] In this assessment, the term "black carbon" and the abbreviation "BC" are used to denote ambient aerosol material with the above characteristics. Note that this definition of black carbon has not been used rigorously or consistently throughout most previous literature describing absorbing aerosol and its role in the atmosphere. Section 3 gives further discussion of terminology.

2.2. How Does Black Carbon Affect the Earth's Radiative Budget?

[59] Figure 1 illustrates the multi-faceted interaction of BC with the Earth system. A variety of combustion sources, both natural and anthropogenic, emit BC directly to the atmosphere. The largest global sources are open burning of forests and savannas, solid fuels burned for cooking and heating, and on-road and off-road diesel engines. Industrial activities are also significant sources, while aviation and shipping emissions represent minor contributions to emitted mass at the global scale. The difficulty in quantifying emissions from such diverse sources contributes to the uncertainty in evaluating BC's climate role. Once emitted, BC aerosol undergoes regional and intercontinental transport and is removed from the atmosphere through wet (i.e., in precipitation) and dry deposition to the Earth's surface, resulting in an average atmospheric lifetime of about a week.

[60] Radiative forcing over the industrial era (1750–present) has typically been used (e.g., by the IPCC [*Forster et al*., 2007]) to quantify and compare first-order climate effects from

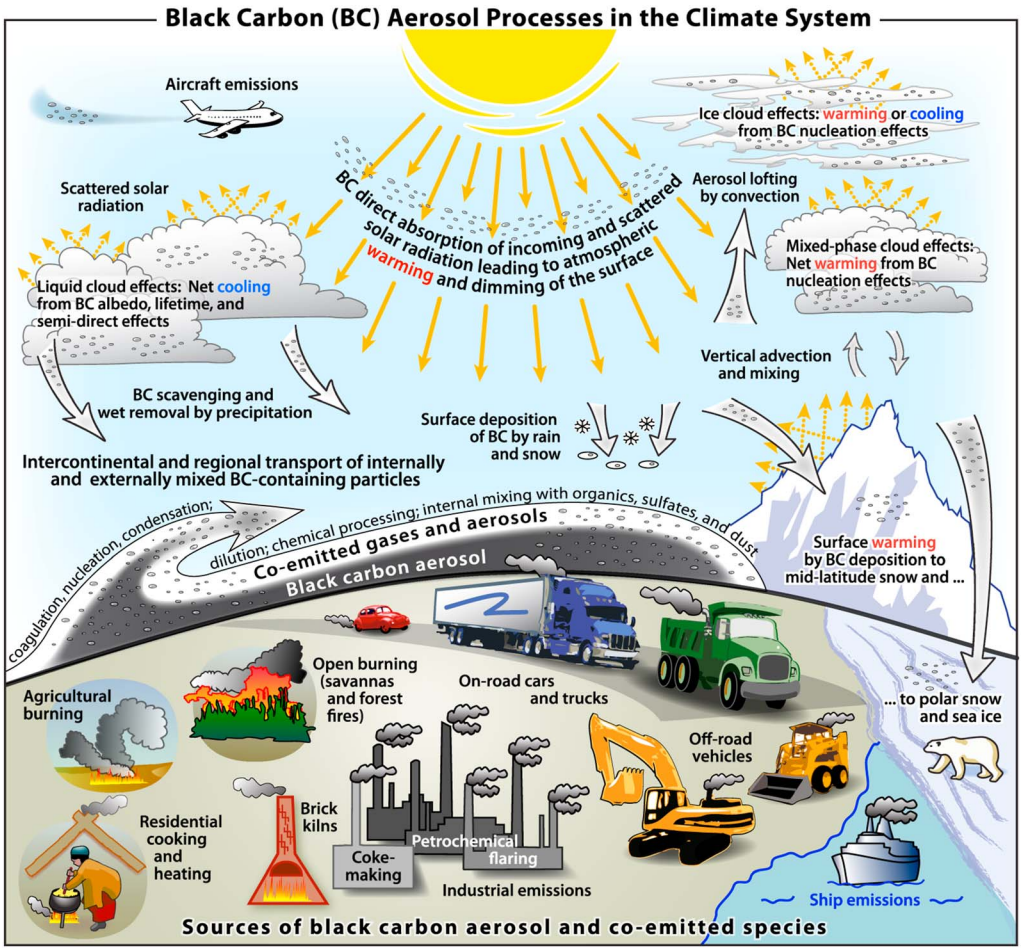

Figure 1. Schematic overview of the primary black-carbon emission sources and the processes that control the distribution of black carbon in the atmosphere and determine its role in the climate system.

different climate change mechanisms. Many of BC's effects on clouds and within the cryosphere are not easily assessed within this framework. These effects result in rapid adjustments involving the troposphere and land surface that lead to a perturbed energy balance that can also be quantified in units of radiative forcing. We employ the term "climate forcing" to encompass both traditional radiative forcing and the rapid adjustment effects on clouds and snow (Table 2); this is discussed further in section 2.3.2.

[61] The best quantified climate impact of BC is its atmospheric *direct radiative forcing*—the consequent changes in the radiative balance of the Earth due to an increase in absorption of sunlight within the atmosphere. When BC is located above a reflective surface, such as clouds or snow, it also absorbs solar radiation reflected from that surface. Heating within the atmosphere and a reduction in sunlight reaching the surface can alter the hydrological cycle through changes in latent heating and also by changing convection and large-scale circulation patterns.

[62] A particularly complex role of BC and other aerosols in climate is associated with changes in the formation and radiative properties of liquid water and ice clouds. BC particles may increase the reflectivity and lifetime of warm (liquid) clouds, causing net cooling, or they may reduce cloudiness, resulting in warming. Aerosol particles can change cloud droplet number and cloud cover in ice clouds, or in mixed-phase clouds made up of both ice and liquid water. Changes in droplet number may also alter cloud emissivity, affecting longwave radiation.

[63] BC also produces warming when it is deposited on ice or snow because BC decreases the reflectivity of these surfaces, causing more solar radiation to be absorbed. The direct absorption of sunlight produces warming which affects snow and ice packs themselves, leading to additional climate changes and ultimately to earlier onset of melt and amplified radiative forcing.

[64] An important consideration in evaluating the climate role of BC emissions is the role of co-emitted aerosols, aerosol precursors, and other gases. Many of these co-emitted species arise in the same combustion sources that produce BC. The greatest emissions by mass include sulfur-containing particles or precursors, organic aerosols that are directly emitted, organic compounds that are precursors to aerosols and ozone, nitrogen oxides that play roles in ozone formation and methane destruction and are precursors to nitrated aerosols, and long-lived GHGs. Sources also emit smaller quantities of ionic species such as potassium and chloride. With the exception of "brown" organic carbon, non-BC particles absorb little or no light, so they often cool rather than warm climate. They also play a role in many, but not all, of the same cloud processes as BC.

[65] In contrast to BC, most other aerosols and precursors are chemically reactive in the atmosphere. Because of

Table 2. Definition of Climate Forcing and Response Terms

Forcing Term	Definition	Model Calculation
Climate forcing	Generic term encompassing all forcing types below, quantifying a perturbation to the Earth's energy balance in $W\,m^{-2}$	
Radiative forcing (RF)	RF is the change in the net vertical irradiance at the tropopause caused by a particular constituent. Usually, RF is computed after allowing for stratospheric temperatures to readjust to radiative equilibrium but with all tropospheric properties held fixed at their unperturbed values. Radiative forcing without stratospheric adjustment is called instantaneous.	Difference between simulations: (1) with radiative effect of the constituent change (2) without radiative effect of constituent change Held constant: All other tropospheric quantities, including cloud
Rapid adjustment	Globally averaged flux change from the adjustment of the troposphere and land surface to a radiative forcing while holding the globally averaged surface temperature constant.[a] Energy balance perturbations arise from temperature, cloud, and constituent changes in the troposphere and from land-surface temperature and moisture changes. These changes occur within 1 year after a forcing is applied, usually within a few days but up to a season in the case of snowpack changes. For BC, the rapid adjustment to the direct effect is also called the "semi-direct effect." The radiative forcing plus the rapid adjustment gives the "adjusted forcing" (see below).	Difference between models: (1) with radiative effect of constituent change and changes in cloud and land-surface temperature (2) with radiative effect of constituent change and no tropospheric response Held constant: global mean surface temperature[a]
Adjusted forcing	Flux perturbation from a given mechanism, allowing for changes in the stratosphere, troposphere, and some surface properties but not allowing a full response of global surface temperatures. This is the sum of a radiative forcing plus its rapid adjustment.	Difference between models: (1) with atmospheric constituent change and full atmospheric response (2) without atmospheric constituent change Held constant: sea-surface temperatures and/or global mean surface temperature response[a]
Effective forcing	A radiative forcing or adjusted forcing multiplied by its efficacy (see below) to give a climate forcing that is comparable to an equivalent climate forcing from a pre-industrial to 2× pre-industrial carbon dioxide change in terms of its globally averaged temperature response. Effective radiative forcing includes rapid adjustments, and it also accounts for differences in globally averaged responses due to latitudinal dependence of forcing.	The efficacy is calculated for the constituent of interest in a climate model (see below). This is then multiplied by the associated radiative forcing or adjusted forcing to give the effective forcing.[b]
Climate response	Large-scale long-term changes in temperature, snow and ice cover, and rainfall caused by a specific forcing mechanism. One of the most important climate responses is that of equilibrium globally averaged surface temperature (ΔT).	Diagnostics from a global atmospheric climate model, coupled to either a mixed layer ocean for equilibrium experiments or a full ocean model for transient experiments
Climate sensitivity (λ)	Equilibrium globally averaged surface warming per $W\,m^{-2}$ of forcing (F), either radiative forcing or adjusted forcing. $\lambda = \Delta T/F$.	Computed from the climate response and radiative forcing diagnostics of a equilibrium climate model integration (see above)
Efficacy (E)	Ratio of the climate sensitivity for a given forcing agent (λ_i) to the climate sensitivity for pre-industrial to 2× pre-industrial CO_2 changes (i.e., $E_i = \lambda_i / \lambda_{CO2}$). Efficacy can then be used to define an effective forcing ($=E_i F_i$), where F_i can either be radiative forcing or the adjusted forcing.	Computed from equilibrium climate model experiments with the constituent of interest, compared these with equivalent climate model diagnostics for a $2\times CO_2$ experiment. Global mean equilibrium temperature and radiative forcing diagnostics are needed.
Climate impact	Regional or local changes in weather and or climate indicators such as heat waves and storms that impact human livelihoods.	Diagnosed from a climate model integration

[a]The adjusted forcing can be computed in different ways. Either regression can be used to determine the forcing at zero global temperature change or a fixed SST model forcing can be modified to account for a change in land temperatures, after *Hansen et al*. [2005], to give an estimate of the zero global surface T response forcing, or the fixed SST flux change can be used directly. The semi-direct effect is computed as the difference between the whole atmosphere adjusted forcing and the radiative forcing when the aerosol direct effect is included. The adjusted forcing for the cryosphere terms employs a different methodology (section 8.2.)

[b]For all changes apart from the snow and sea ice terms, we assume that this effective forcing is the same as the adjusted forcing. This is justified from *Hansen et al*. [2005] and *Shine et al*. [2003] who showed that for most forcings, the rapid adjustment accounted for the non-unity efficacy of the radiative forcing terms. However, for snow and sea ice changes, this is not the case. Their forcings directly influence surface snow and ice, and because they occur at high latitudes, the resulting heating is confined to the near surface. These forcings accelerate snow and ice melt, leading to a strong positive surface albedo feedback. These feedbacks lead to a very high efficacy that their associated rapid adjustments do not account for. Hence, the snow and sea-ice forcings are scaled to account for their enhanced climate response to give an effective forcing.

transport and chemical and microphysical transformation after emission, the atmospheric aerosol becomes a complex array of atmospheric particles, some of which contain BC. Pure BC aerosol rarely exists in the atmosphere, and because it is just one component of this mixed aerosol, it cannot be studied in isolation. Compared with pure BC, mixed-composition particles differ in their lifetimes, interaction with solar radiation, and interactions with clouds. The components of these mixed particles may come from the same or different sources than BC.

[66] The overall contribution of natural and anthropogenic sources of BC to climate forcing requires aggregating the multiple aspects of BC's interaction with the climate system, as well as the climate impacts of constituents that are co-emitted with BC. Each contribution may lead to positive climate forcing (generally leading to a warming) or negative climate forcing (generally cooling). As discussed in the body of this assessment, BC impacts include both warming and cooling terms. While globally averaged climate forcing is a useful concept, BC concentration and deposition are spatially heterogeneous. This means that climate forcing by aerosols and climate response to aerosols is likely distributed differently than the forcings and responses of well-mixed GHGs.

2.3. Assessment Terms of Reference

[67] We use the term "scientific assessment" to denote an effort directed at answering a particular question by evaluating the current body of scientific knowledge. This assessment addresses the question: "What is the contribution of black carbon to climate forcing?" The terms of reference of this assessment include its scope and approach. The primary scope is a comprehensive evaluation of annually averaged, BC global climate forcing including all known forcing terms, BC properties affecting that forcing, and climate responses to BC forcing. Climate forcing of BC is evaluated for the industrial era (i.e.,1750 to 2000). A secondary evaluation addresses the potential interest of BC sources for mitigation. Therefore, we discuss the analyses and tools required for a preliminary evaluation of major BC sources: climate change metrics, net forcing for combined BC and co-emitted species, and factors relating to feasibility.

[68] Our approach relies on synthesizing results of global models from the published literature to provide central estimates and uncertainties for BC forcing. This analysis was guided by the principles of being comprehensive and quantitative, described in more detail as follows:

[69] 1. *Comprehensiveness with regard to physical effect*. As discussed in the foregoing section, BC affects multiple facets of the Earth system, all of which respond to changes in emissions. In evaluating the total climate forcing of BC emissions, we included all known and relevant processes. The main forcing terms are direct solar absorption; influence on liquid, mixed-phase, and ice clouds; and reduction of surface snow and ice albedo.

[70] 2. *Comprehensiveness with regard to existing studies*. Multiple studies have provided estimates of BC climate forcing caused by different mechanisms. These studies often rely on dissimilar input values and assumptions so that the resulting estimates are therefore not comparable. In order to include all possible studies, we sometimes harmonized dissimilar estimates by applying simplified adjustments.

[71] 3. *Comprehensiveness with regard to source contribution*. Atmospheric science has historically focused on individual pollutants rather than the net impacts of sources. However, each pollutant comes from many sources, and each source produces multiple pollutants. Mitigation of BC sources will reduce warming due to BC, but it will also alter emissions of cooling particles or their precursors; short-lived warming gases, such as ozone precursors; and long-lived GHGs. Multi-pollutant analyses of climate impacts have been demonstrated in other work, and we continue that practice here for key sources that account for most of the BC emissions. We include forcing for other pollutants emitted by BC sources by scaling published model results. Although such scaling may yield imprecise estimates of impact, we assert that ignoring species or effects could result in misconceptions about the true impact of mitigation options.

[72] 4. *Quantification and diagnosis*. For each aspect of BC climate forcing, we provide an estimate of the central value and of the uncertainty range representing the 90% confidence limits. When understanding of physical processes is sufficiently mature that the factors governing forcing are known, observations and other comparisons can assist in weighting modeled forcing estimates. Model sensitivity studies based on this physical understanding allow estimates of uncertainty. When the level of scientific understanding is low, an understanding of the dominant factors is not well established. In this situation, the application of observations to evaluate global models is not well developed, and only model diversity was used to estimate the uncertainty. When possible, we identified the causes of variation and key knowledge gaps that lead to persistent uncertainties. In this pursuit, we highlighted critical details of individual studies that may not be apparent to a casual reader. This synthesis and critical evaluation is one of the major value-added contributions of this assessment. The terms of reference require that new calculations be conducted if and only if required to harmonize diverse lines of evidence, including differences between simulations and observations.

[73] The target audience for this assessment includes scientists involved in climate, aerosol, and cloud research and non-specialists and policymakers interested in the role of BC in the climate system. The document structure reflects this audience diversity by including an Executive Summary (section 1), individual section summaries, and introductory material that is required to support understanding of principles.

2.3.1. Assessment Structure

[74] The remaining eleven sections of this document reflect the scope of this assessment. They include seven providing in-depth analysis of the science surrounding BC alone (sections 3 to 9), a climate forcing synthesis (section 10), additional necessary context for discussions of the net climate forcing from BC-rich sources (section 11), a climate metrics analysis (section 12), and mitigation considerations for BC-rich sources (section 13). They are described in more detail as follows:

[75] 3. *Measurements and microphysical properties of black carbon*. The assessment begins with a review of BC-specific properties, including the techniques used to measure BC. The interactions of BC with the climate system depend upon its microphysical properties, optical properties, and mixing with other aerosol components. These govern all impacts shown in Figure 1.

[76] 4. *Emission magnitudes and source categories*. The origins and emission rates of BC are basic components of understanding its total impact. This section identifies major sources of BC and those containing high fractions of BC (i.e., "BC-rich sources"). It also identifies other climate-active aerosols or aerosol precursors emitted from these sources. Finally, data from ambient measurements are reviewed to evaluate emission estimates and the contributions of particular source types.

[77] 5. *Constraints on black-carbon atmospheric abundance*. The burden of BC in the atmosphere and its geographic distribution are basic quantities that directly affect all climate forcing estimates. Observations that constrain the magnitude and location of modeled atmospheric burdens are discussed here.

[78] 6. *Black-carbon direct radiative forcing*. The direct interaction between BC and sunlight unquestionably results in a net positive radiative forcing of climate. This section discusses the basic components that affect direct radiative forcing and the best estimates for each of these components, and it explores the reasons for differences in published radiative forcing values.

[79] 7. *Black carbon interactions with clouds*. BC influences clouds by changing droplet formation and microphysical properties and by altering the thermal structure of the atmosphere. BC is not uniformly distributed with altitude in the lower atmosphere. It directly warms the atmosphere where it is located and alters atmospheric dynamics, the meteorological conditions affecting cloud formation, and the quantity of clouds. In addition, BC, as well as other particles, influences the size and number of water droplets and ice crystals in water and ice clouds through microphysical interactions. All of these changes produce climate forcing by altering cloud properties. This section evaluates the magnitude of changes in water clouds, mixed-phase clouds, and ice clouds. The section emphasizes changes caused by BC alone, instead of the more common examination of cloud changes by all particles.

[80] 8. *Cryosphere changes: Black carbon in snow and ice*. This section evaluates BC that is removed from the atmosphere both in precipitation and through dry deposition and, thereby, is incorporated into surface snow and ice, reducing reflectivity. This initial radiative forcing is amplified by a series of rapid adjustments. This section evaluates modeled cryosphere forcing estimates, including discussion of the microphysical factors that affect radiative transfer in snow and ice packs, and model choices that affect the amplification of that forcing through rapid adjustments. The section also compares the sources and magnitudes of modeled cryospheric BC concentrations with observations and uses this comparison to scale model estimates of forcing for a best estimate.

[81] 9. *Climate response to black carbon forcings*. Forcing is a common measure of radiative impact but of ultimate concern is the climate response to BC, especially if it differs from that of other forcing agents. This section discusses the adjustments in the climate system that affect the efficacy of the forcing by BC in the atmosphere and cryosphere. It also reviews the sparse knowledge about how regional and global climate respond to changes in top-of-atmosphere (ToA) forcing and atmospheric heating.

[82] 10. *Synthesis of black-carbon climate effects*. In this section, best estimates of climate forcing from direct atmospheric light absorption, microphysical cloud changes, the rapid adjustment to direct atmospheric absorption, and the darkening of surface snow and ice by BC are combined with estimates of the forcing efficacy to estimate the total climate forcing of BC in the industrial era (1750 to 2000). Total present-day (i.e., "all-source") forcing is also given for direct radiative forcing and snow and ice forcings.

[83] 11. *Net climate forcing by BC-rich source categories*. While the preceding sections examine the total climate forcing for BC emissions alone, many other species are co-emitted from BC sources, even when they are BC rich. This section examines the total climate forcing of BC-rich sources by quantifying the forcing per emission of all species from a given source.

[84] 12. *Emission metrics for black carbon*. One method of evaluating mitigation of BC versus mitigation of other climate-active species like greenhouse gases is to compare forcing per emitted mass of different compounds in a common framework. This comparison involves scientific issues as well as value judgments. This section summarizes metrics commonly used in climate policy discussions and provides metrics for BC based on the forcing values summarized in section 10 for direct use in the policy community.

[85] 13. *Mitigation considerations for BC-rich sources*. The preceding sections estimate the contributions to climate forcing of BC emissions alone and of the net effect from BC and co-emitted species from BC-rich sources. Future decisions regarding mitigation of climate forcing will include other considerations, including cost and availability of alternatives, additional benefits, and feasibility of implementation. This section discusses these elements for the major BC-rich sources, including regional differences among emission types and potential reduction policies. In addition, this section describes an evaluation framework that extends beyond purely scientific considerations, consistent with our goal of a comprehensive discussion. However, a thorough evaluation of the factors required for a complete mitigation analysis is beyond the scope of this assessment.

2.3.2. Use of Radiative Forcing Concepts

[86] In synthesizing results for BC climate forcing from the published literature, inconsistencies are regularly encountered in the use of radiative forcing concepts, conventions, and terminology. Our definitions for these terms as used in this assessment are listed in Table 2 along with descriptions of their derivation from climate models. Most discussions about climate change refer to measures that are variously called "radiative forcing" or "climate forcing." Our use of the term "radiative forcing" follows the IPCC definition given by Forster *et al*. [2007] that keeps tropospheric and surface temperatures fixed. Many aerosol effects (e.g., rapid adjustments in aerosol, cloud, or snow distributions in response to the initial radiative forcing) can also be measured as changes in fluxes at the tropopause, making them amenable to comparison with radiative forcings. The sum of the radiative forcing and forcing due to these rapid adjustments yields the adjusted forcing. For the atmosphere and most of the land surface, such rapid adjustments occur within a few days of applying the forcing. For the cryosphere, there is more of a continuum of adjustment processes and timescales, and rapid adjustments are usually considered to occur on seasonal timescales or less. For comparability to other forcing agents such as long-lived GHGs, these forcings can be scaled by their efficacy to yield the "effective forcing."

We give the sum of radiative forcing and all other forcing-like terms the name "climate forcing," and this usage is similar to that in the IPCC assessments [*IPCC*, 2007].

[87] Radiative forcing employed in IPCC reports assumes that anthropogenic impact is well represented by the difference between present day and the year 1750, the beginning of the industrial era. This may not be true for BC, where there is evidence of considerable anthropogenic biofuel and open burning before 1750. For the purposes of this assessment, the global climate forcings of BC and co-emitted species are evaluated from the beginning of the industrial era (1750). This definition gives forcing that can be compared with the temperature change since that time, without requiring attribution to a particular cause. Rather than assuming that this value represents the present-day contribution of humans to climate forcing, we refer to the difference between year-2000 forcing and year-1750 forcing as "industrial-era forcing." For direct and cryosphere forcing, we also estimate forcing from all sources, even those that might have been ongoing before 1750. This is referred to as the "all-source" forcing.

2.3.3. Contrast With Previous Assessments

[88] Motivation to undertake this assessment derived, in part, from the scope of previous and concurrent assessments, namely, the IPCC Fourth Assessment Report (AR4) [*IPCC*, 2007] and the UNEP/WMO Integrated Assessment of Black Carbon and Tropospheric Ozone [*UNEP/WMO*, 2011a, 2011b], respectively. A comprehensive and quantitative evaluation of BC sources and associated climate forcing terms was beyond the scope of IPCC AR4 (see section 10.6 for more details). The primary focus in AR4 was the direct radiative forcing of fossil fuel sources of BC, and that forcing was estimated by weighting all studies equally without examining variation. Other terms beyond direct forcing were not evaluated; without these, even the sign of the total forcing cannot be estimated. The focus of the UNEP/WMO assessment was identification of mitigation strategies for short-lived climate forcing agents that would significantly reduce short-term anthropogenic climate forcing through examination with two climate models. Evaluation of model results in the context of observations, the microphysical properties of BC, and findings from other models were beyond the scope of the UNEP/WMO effort.

3. Measurements and Microphysical Properties of Black Carbon

3.1. Section Summary

[89] 1. The term "black carbon" has not been used rigorously or consistently in measurement studies or in modeling studies that use measurements. For future work, we recommend that the term "refractory black carbon," or rBC, be adopted for the distinctive material defined herein as black carbon.

[90] 2. Either during or soon after emission, BC becomes internally mixed with other aerosol components such that it and other chemical species exist together within the same particle. This mixing can alter the optical properties of BC and influence its atmospheric lifetime and ability to form cloud droplets and ice crystals. Hence, the climate impacts of BC must be evaluated in the context of changes in its physico-chemical properties due to interactions with other aerosol components.

[91] 3. Freshly emitted BC particles are small in diameter and hydrophobic and, therefore, make very poor cloud condensation nuclei. Aging of BC after emission and associated accumulation of soluble mass increases the size and hygroscopicity of the internally mixed BC and enhances its cloud condensation nuclei (CCN) activity.

[92] 4. The mass absorption cross section of BC (MAC_{BC}) is a fundamental input to models of radiative transfer. Measured values for freshly generated BC fall within a relatively narrow range of 7.5 ± 1.2 m^2g^{-1} at 550 nm. MAC_{BC} increases by approximately 50% as BC becomes internally mixed with other aerosol chemical components.

[93] 5. Filter-based measurements of both absorption coefficient and BC mass concentrations can be biased by the presence of other chemical components in internally or externally mixed aerosol. Measured mass concentrations can differ between methods by up to 80% with the largest differences corresponding to aerosol with lower BC to organic carbon (OC) ratios. These measurement uncertainties may confound our understanding of trends, spatial and temporal variability, and impacts on climate.

3.2. Definitions

3.2.1. Black Carbon

[94] Black carbon (BC) is distinct from other forms of carbon and carbon compounds contained in atmospheric aerosol. As stated in section 2.1, it has a unique combination of properties. These properties are strong visible light absorption of at least 5 m^2g^{-1} at 550 nm [*Bond and Bergstrom*, 2006], refractory with vaporization temperature near 4000K [*Schwarz et al.*, 2006], aggregate morphology [*Medalia and Heckman*, 1969], and insolubility in water and common organic solvents [*Fung*, 1990]. Its absorption is consistent with a wavelength-independent refractive index across the visible spectrum [*Marley et al.*, 2001]. The combination of these properties distinguishes BC from other light absorbing material, such as some organic carbon compounds. The individual spherules are formed in flames, and the aggregate nature is caused by rapid coagulation [*Haynes and Wagner*, 1981], differentiating black carbon from planar graphite.

[95] In this assessment, the term "black carbon" and the notation "BC" are used to denote ambient aerosol material that has the above characteristics. The term "black carbon" given here has not been used rigorously or consistently throughout all previous modeling and measurement literature, and as we discuss later in this section, most measurement techniques do not respond only to this substance. Measurements and nomenclature that uniquely identify this substance would assist in more rigorous evaluation.

3.2.2. Organic Matter and Other Carbon Aerosols

[96] "Organic aerosol" (OA) is a broad term indicating carbon-containing compounds that contain hydrogen and, usually, oxygen. All sources that emit BC also emit primary organic aerosol (POA), as well as gases that may become secondary organic aerosol (SOA) in the atmosphere. In atmospheric chemistry, the combination of BC and OA is often called "carbonaceous aerosol." As used in this assessment, this term excludes primary organic particles directly

emitted from plants [*Heald and Spracklen*, 2009] and organisms such as fungi and bacteria, which tend to be much larger in size than BC. It also excludes biogenic SOA, which may have small sizes but are emitted from natural, non-combustion sources [*Guenther et al.*, 2006]. This usage is consistent with previous IPCC reports [*Forster et al.*, 2007]. *Gelencsér* [2005] further describes the chemical nature of OA. Mineral dust also contains carbon as carbonate, which is also not included in the carbon aerosol considered in this assessment.

[97] The term "organic carbon" (OC) refers to the carbon mass within OA, excluding the associated oxygen and hydrogen content. Although OA is the quantity most relevant to climate, measurements and emission inventories have usually reported values of OC because it was more commonly measured. The ratio between OA and OC mass (OA : OC ratio) depends on the amount of oxygen incorporated in the organic molecules. It varies from about 1.1 to 2.2 [*Russell*, 2003], depending on the combustion source, with lower values of OA : OC from coal or diesel and higher values from biomass combustion. A default value for POA : OC of 1.3 or 1.4 is often assumed in global modeling [*Penner et al.*, 1998; *Dentener et al.*, 2006].

3.2.3. Other Particulate Light Absorbers

[98] Two other types of atmospheric particles absorb visible light: dust and "brown carbon." Most of the dust in the atmosphere originates from deserts [e.g., *Chin et al.*, 2009], and smaller amounts come from construction, on-road and off-road traffic, and agriculture. Dust particles are more weakly absorbing per mass than BC: about 0.009 m^2g^{-1} at 550nm for Asian dust [*Clarke et al.*, 2004]. They can be distinguished from BC particles because they are typically large (i.e., greater than 2 μm in diameter), crystalline, and composed of crustal elements. They also have relatively more absorption at shorter wavelengths compared with long visible wavelengths. Although dust is more weakly absorbing than BC, globally averaged total absorption by dust is significant due to its relatively high mass abundance [*Sokolik and Toon*, 1996].

[99] Brown carbon, a subset of OA, is a complex mixture of organic compounds lacking a formal analytical definition. Its light absorption is weak, with MAC less than 1 m^2g^{-1} at 550 nm, and has a strong wavelength dependence [*Kirchstetter et al.*, 2004; *Chakrabarty et al.*, 2010]. This strong wavelength dependence can be used to distinguish its absorption from that of BC [*Wonaschütz et al.*, 2009]. Unlike BC, brown carbon is soluble in some organic compounds and responds to analytical techniques that use solubility to isolate humic-like substances [*Andreae and Gelencsér*, 2006; *Graber and Rudich*, 2006]. Brown carbon particles and BC are similar in size.

3.3. Black Carbon Formation and Evolution

[100] BC is produced during the combustion of carbon-based fuels when oxygen is insufficient for complete combustion. Even if adequate oxygen is supplied overall, fuel-rich, oxygen-poor zones can occur when the reactants are not well mixed. A complex series of reactions involving polycyclic aromatic hydrocarbon molecules forms precursors of BC. These precursors coagulate to sizes large enough to serve as particle nuclei and grow through reactions on the surface. Electron microscopy images show that these spherules are unique among atmospheric particles, with wrinkled graphite layers forming a shell around a hollow or disordered interior [*Heidenreich et al.*, 1968]. They have diameters on the order of tens of nanometers [e.g., *Martins et al.*, 1998a; *Pósfai et al.*, 1999; *Li et al.*, 2003] and high carbon-to-hydrogen ratios. Soon after formation, the graphitic spherules coagulate to form aggregates or fractal chain-like structures consisting of hundreds or thousands of spherules [e.g., *Medalia and Heckman*, 1969; *Li et al.*, 2003] (Figure 2). If the combustion exhaust is kept hot, and if sufficient oxygen is well mixed with the flame products, these carbon particles may be eliminated by oxidation reactions before they leave the combustion chamber [e.g., *Lee et al.*, 1962]. Otherwise, they are emitted.

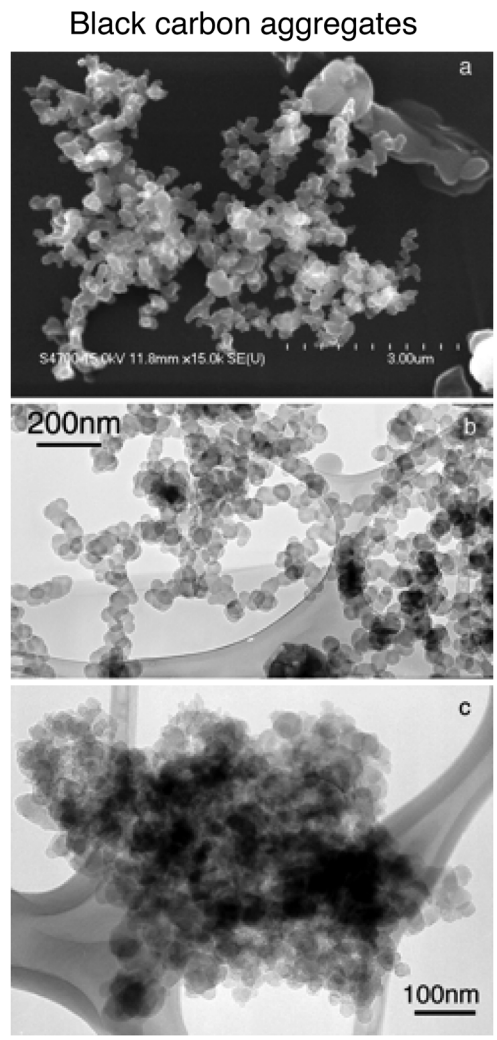

Figure 2. (a) Scanning electron microscope image of BC aggregates in young smoke from the Madikwe Game Reserve fire, South Africa, on 20 August 2000; (b) transmission electron microscope (TEM) image of chain-like BC aggregates in flaming smoke from the dambo fire near Kaoma, Zambia, on 5 September 2000; (c) TEM image of a compact BC aggregate in regional haze near Skukuza, South Africa, on 22 August 2000 [*Li et al.*, 2003]. (Reproduced with permission of the American Geophysical Union).

[101] The morphology of emitted chain-like aggregates changes rapidly after emission. Water vapor and other gas-phase species condense upon the aggregates, which collapse into more densely packed clusters [*Huang et al*., 1994; *Ramachandran and Reist*, 1995; *Weingartner et al*., 1997; *Martins et al*., 1998b]. Other particulate and gas phase species present in the surrounding atmosphere also coagulate with the combustion aerosol. Electron microscopy images and measurements of optical properties indicate that freshly emitted particles often exist as an external mixture in which organic and inorganic light-scattering components and strongly light-absorbing components (BC) reside in different particles [*Pósfai et al*., 2003; *Li et al*., 2003; *Mallet et al*., 2004]. After emission, condensation and coagulation cause individual chemical components to become internally mixed (i.e., different aerosol components existing together within a single particle). Such particles are no longer pure BC but contain sulfate and organic material [*Lee et al*., 2002; *Shiraiwa et al*., 2007]. We refer to these internally mixed particles as "BC-containing" particles. Mixing has been observed to occur within a few hours after emission at some locations [*Moteki et al*., 2007; *Moffet and Prather*, 2009], but there are insufficient measurements to estimate the extent of internal mixing throughout the atmosphere. Global aerosol models that simulate microphysical processes predict that most BC is mixed with other substances within 1 to 5 days [*Jacobson*, 2001a] and this prevalent internal mixing is found at all altitudes [*Aquila et al*., 2011].

[102] The top portion of Figure 3 summarizes particle properties that are used as input into global and radiative transfer models and that can be constrained by measurements. Each characteristic may affect the representation of atmospheric processes and resulting modeled concentrations, as shown in the lower portion of Figure 3. Pure BC and BC-containing particles are separated in Figure 3 because their microphysical, optical, hygroscopic, and cloud-nucleating properties differ [*Abel et al*., 2003; *Slowik et al*., 2004]. For example, as BC ages, it becomes coated or internally mixed with non-BC components and the resulting BC-containing particles become more hydrophilic, which can lead to a reduced lifetime and atmospheric loading [*Stier et al*., 2006b]. Internal mixing with other compounds can enhance absorption of solar radiation according to microphysical models [*Fuller et al*., 1999; *Jacobson*, 2001a; *Lack and Cappa*, 2010] and measurements, primarily laboratory based [*Schnaiter et al*., 2005; *Slowik et al*., 2007]. As a result, the

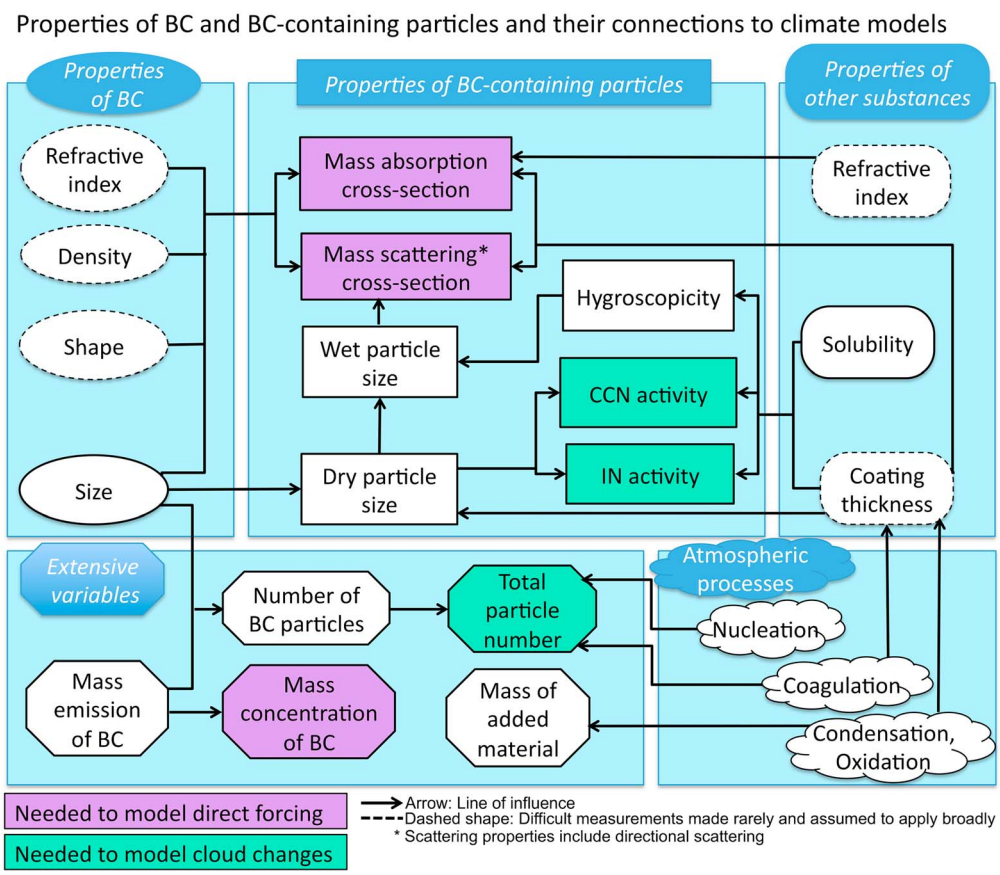

Figure 3. Schematic of the connections between properties of BC and BC-containing particles. A combination of these properties determines the contribution of BC and BC-containing particles to climate forcing. The properties depend on those of other substances produced in the atmosphere or co-emitted with BC and on atmospheric processes such as nucleation and condensation. Mass and number of BC and BC-containing particles (extensive variables) depend, in part, on particle properties that affect the lifecycle of BC (not represented here).

additional material in BC-containing particles must be taken into account when modeling both radiative transfer and atmospheric lifetime [*Stier et al*., 2006a].

[103] In the remainder of this section, we discuss the physical properties that affect estimates of climate forcing, measurements of these properties, and representation of these properties in global models. We begin with a discussion of BC mass concentration in section 3.4. Important optical properties of BC, including absorption, are discussed in section 3.5, followed by a review of absorption measurements in section 3.6. Section 3.7 reviews microphysical properties affecting the mass absorption cross section and single-scattering albedo, while section 3.8 discusses measurements and modeling of these two parameters. Finally, section 3.9 discusses properties of BC and BC-containing particles that are relevant to nucleating liquid cloud droplets. The discussion of microphysical properties, which also affect the interaction of BC-containing particles with ice clouds, appears in section 7.5.

3.4. Measurement of BC Mass

[104] Ambient air samples of particles that contain BC always contain other constituents as well. The mass fraction of BC in atmospheric aerosol is typically less than 10%. Thus, BC mass concentration (in g m^{-3}) cannot be measured directly by collecting aerosol in an air sample and weighing it. Instead, BC mass must be determined indirectly, usually through optical methods, thermal heating combined with optical methods, or laser-induced incandescence (Table 3). BC is associated with high sp^2-bonded carbon content [*Hopkins et al*., 2007] and with Raman spectroscopic responses similar to graphite [*Rosen et al*., 1979; *Dippel et al*., 1999], but these analyses do not respond uniquely to all materials identified as BC.

[105] The measurement of BC mass concentrations by some methods can be biased when BC is sampled with other aerosol components. This mixing can take place either within ambient aerosol particles before sampling or in the sample itself if BC and other particles are collected and measured simultaneously. Biases occur either because the mixing increases absorption or extinction (section 3.6), because BC is incorrectly classified as another material, or because another material is incorrectly classified as BC (i.e., lack of specificity). Most techniques measure similar BC mass concentrations when they are applied to pure BC or when other aerosol components are removed by applying heat [*Knox et al*., 2009; *Kondo et al*., 2009] or by solvent rinsing [*Subramanian et al*., 2006]. For that reason, measurements of untreated samples are usually in closer agreement for diesel exhaust, which contains little non-BC material, than they are for aged (i.e., internally mixed) aerosol [*Schmid et al*., 2001; *Chow et al*., 2004; *Hitzenberger et al*., 2006] or biomass burning aerosol (BB), which has a high content of organic matter and other inorganic substances that could cause interferences [*Novakov and Corrigan*, 1995; *Reid et al*., 1998]. The major uncertainty in some measurements of BC mass is associated with isolating BC from the other constituents with which it is internally or externally mixed. A summary of measurement techniques for BC mass is listed in Table 3 along with common terminology and any directions and causes of bias. In addition, more explicit names for the measured quantities are suggested; some of these follow *Andreae and Gelencsér* [2006]. Details of the measurement of BC mass concentrations are given below.

[106] The most common separation between BC and OC is accomplished by volatilizing and combusting material collected on a filter and by detecting the CO_2 produced as a function of temperature. The discrimination between these two classes of aerosol is based on the idea that BC is nonvolatile or refractory, whereas OC is volatile. This thermal method does not detect BC directly, and the amount of refractory material detected depends on the details of the method. The analytical result is therefore an operational definition and is traditionally called elemental carbon (EC).

[107] In thermal methods based on volatility, the sample filter is first heated in inert gas to volatilize OC and then heated again with oxygen to combust the EC; cooling sometimes occurs before the second heating [e.g., *Chow et al*., 1993; *Birch and Cary*, 1996; *Watson et al*., 2005]. This technique measures all OC, not just combustion-derived primary aerosol. Inaccuracies in this method result from interpreting OC as EC, or vice versa, when properties of the sample cause EC to be released too early or OC to be held too long. One complication is "charring" of OC (i.e., conversion of OC to EC) at high temperatures, which reduces its volatility. Variations of thermal methods include different temperature ramping programs and correcting for the charring of OC during pyrolysis by monitoring the optical reflectance of the sample filter [*Huntzicker et al*., 1982] or light transmission [*Turpin et al*., 1990]. Comparisons among protocols with differing temperature and optical corrections show that derived EC concentrations can differ by over an order of magnitude [*Schmid et al*., 2001] and that large differences can be caused by the lack of correction for charring, which leads to considerable overestimates of EC. There are also significant differences between methods that correct for charring using optical reflectance or light transmission [*Chow et al*., 2001; *Chow et al*., 2004]. The two corrections yield comparable EC concentrations if the filter contains a shallow surface deposit of EC. If EC and OC are distributed throughout the filter, the two corrections yield different EC values, and the variability also depends on the temperature protocol used. Hence, the difference between the two methods depends, in part, on the OC/EC ratio in the sample. As a result, the correction schemes yield similar results for diesel exhaust, which is dominated by EC, but can differ widely for complex atmospheric mixtures. Optimization of temperature programs seeks to minimize charring and release EC and OC during the expected period of the analysis [*Conny et al*., 2003; *Cavalli et al*., 2010]. The accuracy of thermal measurements can also be increased by extracting OC with organic solvents before analysis, since BC is insoluble [*Fung*, 1990; *Subramanian et al*., 2006].

[108] Detection of refractory BC (rBC) mass by laser-induced incandescence (i.e., visible thermal radiation) has become increasingly widespread [*Schwarz et al*., 2006, 2008a; *Moteki and Kondo*, 2010]. The Single Particle Soot Photometer (SP2) is able to provide continuous, real-time, size and coating information for individual particles containing rBC over a wide dynamic range of mass concentration. In the SP2, the rBC component of individual particles is heated to vaporization temperatures (i.e., about

Table 3. Techniques for Measuring BC Mass, Method-Defined Terminology for BC, and Sources of Systematic Biases

Technique	Common Name	Suggested Name	Common Instruments	Sources of Bias	Direction of Bias[a]
Optical absorption with in situ detection	BC	Equivalent BC (BC + other absorbing material)	Photoacoustic	Change in MAC with aerosol aging[b]	+, –
				Presence of other absorbers (dust, organic carbon)[c]	+
Optical absorption by collection on filters	BC	Equivalent BC	Aethalometer; Particle Soot Absorption Photometer (PSAP);	Same as optical absorption above, plus:	
				Optical interactions between particles and filter matrix[d]	+
			Multi-angle Absorption Photometer (MAAP)	Modification of particle morphology by organic carbon	+
Optical absorption with heated inlet	BC	Equivalent BC	Continuous Soot Monitoring System (COSMOS)	Charring of low volatility organic species	+
Thermal heating and optical absorption	Elemental carbon (EC)	Apparent elemental carbon (EC_a)	Thermal Optical Reflectance (TOR); Thermal Optical Transmittance (TOT)	Failure to accurately correct for charred organic carbon;	+
				Catalytic oxidation of BC in presence of metals or metal oxides;	–
				Absorption by charred material affects split between OC and EC[e]	–
				Detection of less volatile organic carbon	+
Laser-induced incandescence	BC or Refractory BC (rBC)	Refractory BC (rBC)	Single Particle Soot Photometer (SP2)	Lack of detection of small particles[f]	–

[a](+) = BC measured too high; (–) = BC measured too low.
[b]If calibrated with fresh, unmixed BC, measurement overestimates BC mass after mixing with non-absorbing species and increase in absorption.
[c]Depends on wavelength; measurements around 630 nm often are unaffected unless dust concentrations are high.
[d]Positive bias if uncorrected filter-based measurements are used; otherwise, it can be either positive or negative.
[e]More extreme for transmission-based monitoring of charring.
[f]Particles with mass below about 0.5 fg, corresponding to a spherical particle of about 80 nm diameter.

4000K) with an infrared intra-cavity laser, and incandescence proportional to rBC mass is detected. Essentially all rBC particles between 80 and 700 nm mass-equivalent diameter are measured, assuming void-free rBC has a density of 2 g cm^{-3}. The response of the SP2 to rBC mass and the lack of interference in measuring rBC mass when non-rBC aerosol components are present have been evaluated in the laboratory [*Schwarz et al.*, 2006; *Slowik et al.*, 2007; *Moteki and Kondo*, 2007]. The dominant uncertainty in the measured mass lies in calibrating its sensitivity to ambient rBC material. The range of this sensitivity is around 15% [*Moteki and Kondo*, 2010; *Laborde et al.*, 2012]. However, the limitations of the size range detected by the SP2 may introduce additional uncertainty, depending on the air mass. Typically, in remote regions, the size range captured by the SP2 contains most of the rBC mass and about 50% of the rBC number [*Schwarz et al.*, 2008b; *Shiraiwa et al.*, 2008]. In urban environments, a correction to total measured mass concentration of about 25% may be required. Pulsed laser-induced incandescence has also been used for environmental rBC measurements [*Chan et al.*, 2011].

3.5. Optical Properties of Black Carbon

[109] Models of radiative transfer require the amount of particulate absorption and scattering in the atmosphere, known as the absorption and scattering coefficients (m^2 m^{-3} or simply m^{-1}). Atmospheric models convert modeled mass concentrations to these optical coefficients using intensive properties (i.e., optical cross section per mass in m^2g^{-1}) known as the mass absorption cross section (MAC) and mass scattering cross section (MSC). Estimates of these values are needed at all wavelengths, and the directional distribution of scattering (dimensionless) is also needed for radiative transfer models.

[110] From atmospheric measurements, MAC can be calculated in reverse: the light-absorption coefficient divided by mass concentration. Throughout this assessment, we often refer to MAC that is determined for BC alone (MAC_{BC}). MAC_{BC} is calculated by dividing the absorption coefficient attributable to BC by the BC mass concentration. The simple term MAC indicates the value determined by dividing by the total mass concentration of BC-containing particles, which is smaller than MAC_{BC}. All other properties are usually measured for BC-containing particles, not for pure BC. Optical properties depend on refractive index, density, size distribution, mixing state, and particle shape. The propensity for water uptake affects the MSC and MAC of BC-containing particles, as well as their ability to form cloud droplets and their atmospheric lifetime due to removal by precipitation. For sub-saturated conditions (i.e., relative humidity below 100%), this water uptake is characterized in terms of hygroscopicity or growth factor. When air is supersaturated, the climate-relevant quantity is the fraction of particles that act as CCN [*Hallett et al.*, 1989].

[111] The MAC was mentioned earlier as a distinguishing feature of BC. Values of MAC and MSC are fundamental inputs to radiative transfer models, required for all aerosols or aerosol components. These quantities are necessary to translate mass concentrations simulated by chemical transport models to their effects on radiative transfer. The wavelength dependence of MAC must also be represented in models for the full solar spectrum. As its name implies, BC strongly absorbs light at all visible wavelengths. In contrast, other atmospheric aerosols that absorb light (OA, soil, and dust) are more yellow, brown, or red, meaning they absorb more blue light than red light. The quantity generally used to characterize the spectral dependence of light absorption is the absorption Ångstrom exponent:

$$\text{Å}_{abs} = -\log(\mathrm{MAC}(\lambda_1)/\mathrm{MAC}(\lambda_2))/\log(\lambda_1/\lambda_2) \qquad (3.1)$$

where $MAC(\lambda_1)$ and $MAC(\lambda_2)$ are the mass absorption cross sections at wavelengths λ_1 and λ_2, respectively. Two wavelengths spanning the visible range are commonly used, such as 450 and 650 nm. Alternatively, Å_{abs} can be calculated from absorption coefficients at the two wavelengths. The value of Å_{abs} for particles is usually greater than that of the bulk material. If the refractive index of the bulk material has no wavelength dependence, as does graphite [*Borghesi and Guizzetti*, 1991], then Å_{abs}=1 for particles much smaller than the wavelength of light [*Rosen et al.*, 1979; *Moosmüller et al.*, 2011].

[112] Measurement studies have confirmed the value of Å_{abs} = 1 in regions where externally mixed BC dominates absorption [*Rosen et al.*, 1978; *Bergstrom et al.*, 2002, 2007; *Kirchstetter et al.*, 2004; *Clarke et al.*, 2007]. When BC becomes coated, Å_{abs} can theoretically be as low as 0.8 or as high as 1.9 [*Lack and Cappa*, 2010]. In contrast, Å_{abs} for OA has been observed to be between 3.5 to 7 [e.g., *Kirchstetter et al.*, 2004; *Sun et al.*, 2007; *Lewis et al.*, 2008; *Yang et al.*, 2009]. Å_{abs} for dust is typically about 2 to 3 but can be higher for very red (iron-rich) dust [e.g., *Fialho et al.*, 2006; *Alfaro et al.*, 2004; *Bergstrom et al.*, 2007]. This difference in the wavelength dependence of absorption of BC versus other absorbing aerosol has been used to approximate relative fractions of BC versus other light-absorbing constituents.

[113] The single-scattering albedo, ω_0, is scattering divided by extinction (i.e., the sum of scattering and absorption) or

$$\omega_0 = \mathrm{MSC}/(\mathrm{MSC} + \mathrm{MAC}) \qquad (3.2)$$

[114] Values of ω_0 near 1 indicate that the aerosol is mainly scattering. Values below about 0.8 indicate that the particles could have a net warming effect [*Haywood and Shine*, 1995]. The value that divides warming from cooling also depends on the albedo of the underlying surface or clouds and the fraction of light that is scattered upward by the particles [*Chylek and Wong*, 1995]. When the addition of aerosol causes a local increase in the planetary albedo, more shortwave radiative energy is reflected back to space, and aerosol exerts a negative forcing. In contrast, when aerosols locally decrease the planetary albedo, the forcing is positive. MAC and ω_0 are the aerosol properties most relevant to the balance between negative and positive forcing, so we emphasize these two parameters in this section instead of MSC. Forcing is not very sensitive to ω_0 for strongly absorbing aerosol with values below 0.4.

3.6. Measurement of Absorption Coefficients

[115] Comprehensive reviews of absorption measurements have been provided by *Horvath* [1993] and by *Moosmüller*

et al. [2009]. Here we summarize only the major challenges in these measurements. The most widely used technique to measure the absorption coefficient involves collecting aerosol on a filter and inferring atmospheric absorption from the resulting change in transmission of light through the filter [*Gundel et al*., 1984], often at one mid-visible wavelength but sometimes at multiple wavelengths. Common instruments using this approach are the Particle Soot Absorption Photometer (PSAP) [*Bond et al*., 1999; *Virkkula et al*., 2005], which has been used to obtain a worldwide data base through the Global Atmospheric Watch program; the Hybrid Integrating Plate System (HIPS), which has been used to collect data by the Interagency Monitoring of Protected Visual Environments (IMPROVE) in U.S. National Parks [*Malm et al*., 1994]; and the Aethalometer [*Hansen et al*., 1982]. Other filter-based absorption instruments include the Integrating Plate [*Lin et al*., 1973] and the Multi-Angle Absorption Photometer (MAAP) [*Petzold et al*., 2005b]. These filter-based methods overestimate absorption if light transmission is also affected by particulate light scattering [*Horvath*, 1997; *Bond et al*., 1999]. With the application of empirical corrections to overcome this artifact, accuracies of the PSAP, IP, HIPS, and Aethalometer range between 20 and 30% [*Bond et al*., 1999; *Weingartner et al*., 2003, *Virkkula et al*., 2005], and accuracy of the MAAP is about 12% [*Petzold et al*., 2005b]. However, these correction schemes are based on laboratory-generated aerosols that may limit their application and accuracy for the measurement of atmospheric aerosols. In addition, coating of BC with volatile compounds can greatly contribute to variation in filter-based measurements of light absorption [*Lack et al*., 2008; *Cappa et al*., 2008; *Kondo et al*., 2009]. For example, PSAP absorption coefficients can be biased high (50 to 80%) when the ratio of organic aerosol to BC is high (15 to 20). *Lack et al*. [2008] postulated that this high bias was due to the redistribution of liquid-like OC that affected either light scattering or absorption. This difficulty can be overcome by removing most of the mass of volatile aerosol components before the BC particles are collected on filters. This removal can be accomplished without significant charring of organic compounds with a heated sampling inlet. This technique is used for the Continuous Soot Monitoring System (COSMOS) instrument [*Kondo et al*., 2011b]. Under those conditions, comparisons of ambient BC mass concentrations measured by light absorption (COSMOS), thermal-optical measurements, and laser-induced incandescence (i.e., SP2) measurements have been found to agree within 10% [*Kondo et al*., 2011b].

[116] Filter-based optical measurements of absorption are sometimes used to derive "effective" BC mass concentrations by using an assumed MAC_{BC} to convert measured absorption to BC mass [e.g., *Sharma et al*., 2002]. Given the artifacts and uncertainties associated with filter-based measurements and the choice of MAC_{BC}, the resulting BC mass concentrations also can be highly uncertain.

[117] Techniques that do not use filters are also available for the measurement of absorption by BC. In the photoacoustic spectrometer (PAS) [*Petzold and Niessner*, 1996; *Arnott et al*., 1997; *Lack et al*., 2006], particles are drawn into an acoustic cavity and irradiated by power-modulated laser light. The heat that is produced when the particles absorb laser light is transferred to the surrounding gas creating an increase in pressure. Sensitive microphones are used to detect the standing acoustic wave that results from the pressure change, and this signal is interpreted to infer the absorption coefficient. Gas phase absorbers can interfere with BC detection in PAS systems. The overall uncertainty of the PAS with respect to aerosol absorption has been reported at about 5% [*Lack et al*., 2006].

[118] Absorption techniques, whether filter based or non-filter based, are not specific for BC. Any light-absorbing aerosol other than BC that absorbs at the measurement wavelength is detected. The degree to which other light absorbing species interfere with the measurement of BC absorption depends on the relative abundance of light absorbing species and the size range and wavelength of the measurement. Measurement of the chemical composition of the aerosol and measurement of absorption at several wavelengths can help determine the interference from all atmospheric species. BC-containing aerosol generally fall into the submicron size range, so measurements of the submicron aerosol only can also reduce the interference of dust absorption.

3.7. Microphysical Properties Affecting MAC and ω_0

3.7.1. Optical Models and Required Inputs

[119] Values of MAC and ω_0 can be predicted with several theories that describe how the particles interact with light. Particle density and refractive index of the bulk material are required to calculate MAC for all models. The assumed particle shape and size affect the model chosen. Common optical-modeling treatments that account for the fractal nature of fresh BC particles include the Rayleigh-Debye-Gans approximation [*Nelson*, 1989; *Dobbins and Megaridis*, 1991], superposition T-matrix theory [*Mishchenko et al*., 2004], and discrete-dipole approximation [*Draine and Flatau*, 1994]. *Sorenson et al*. [2001] reviews many of the key optical relationships for aggregates. These models are useful for exploring how particle properties affect particle optics [e.g., *Liu and Mishchenko*, 2005].

[120] Global-model calculations of radiative transfer usually do not account for complex particle shapes. Instead, they use Mie theory, which can describe homogeneous or core-shell spherical particles. Although BC particles, especially freshly emitted ones, are not spherical, modeling radiative transfer accurately requires only that MAC, ω_0, and angular scattering are correct.

[121] BC non-sphericity creates difficulties in inferring other properties used in optical modeling from measurements. Air drag is different between spherical and non-spherical particles and affects inferences of particle size based on mobility [*Lall and Friedlander*, 2006]. The SP2 measurement detects BC mass and provides equivalent spherical diameters. Inferences of refractive index are often taken from optical measurements with the assumption of spherical particles or from particles that are collected and compacted into a pellet. In either case, the material is not pure BC but contains an unknown fraction of voids. Ideally, the refractive index, density, and size used for modeling would be obtained for the pure material, but observed properties may be obtained for material with unknown and inconsistent void fractions. Despite these

uncertainties, measurements of material properties and sizes are described below.

3.7.2. Density

[122] *Fuller et al*. [1999] compiled reported densities for several types of graphitic material and found values ranging from 0.625 to 2.25 g cm^{-3}. Based on the type of BC emitted from diesel combustion, they adopted the highest density, which was measured for paracrystalline graphite, as representative of strongly absorbing atmospheric BC. BC is not perfectly crystalline, so its microstructure, density, and refractive index differ from those of graphite. The density of pure graphite is 1.9 to 2.1 g cm^{-3} [*Hess and Herd*, 1993]. Densities for pressed pellets of BC with corrections for air volume fractions in the surface layer are slightly lower at 1.8 to 1.9 g cm^{-3} [*Medalia and Richards*, 1972; *Janzen*, 1980]. *Park et al.* [2004] reported a density of 1.8 g cm^{-3}, and *Kondo et al*. [2011b] found 1.718 ± 0.004 g cm^{-3} for fullerene soot. Some global models still use the density of 1 g cm^{-3} recommended by OPAC (Optical Properties of Aerosols and Clouds), which would result in an overestimate of absorption if all other factors are correct.

3.7.3. Refractive Index

[123] The refractive index of a material is critical in determining the scattering and absorption of light, with the imaginary part of the refractive index having the greatest effect on absorption. Refractive index values are derived by assuming a theory for the interaction of BC with light (i.e., reflectance or absorption) and adjusting optical parameters (including refractive index) until predictions match measurements. Three possible methods include (1) fitting Fresnel's formula to reflectance and transmittance data measured for a compressed pellet, (2) fitting Mie theory to light-scattering data for individual spherical particles, and (3) fitting either Mie theory or an approximation formula to scattering and extinction data for particle ensembles. Method 1 has been used widely to estimate refractive indices of solid aerosols like combustion-generated BC [*Mullins and Williams*, 1987]. However, direct evidence of the optical flatness of pellet surfaces, which is necessary for application of Fresnel's formula, has never been shown for wavelengths shorter than the infrared region [*Janzen*, 1979]. Method 2, which is limited to spherical particles, uses measurements of resonance structures in Mie scattering to determine the refractive index [*Chylek et al*., 1983a], but its application to strongly absorbing particles is limited. In method 3, the refractive index and a size distribution function are inferred simultaneously from extinction or scattering data for an ensemble of particles. Solving this inversion problem requires a theory to connect microphysical and light-scattering properties; Mie theory has been used for spherical particles [*Lack et al*., 2009] and the Rayleigh-Gans approximation for non-spherical particles [*Charalampopoulos et al*., 1989; *Van-Hulle et al*., 2002]. For polydisperse or non-spherical particles, the inversion results may have large errors if the assumed size distributions or shapes differ from those of the actual particles. *Moteki et al*. [2010] developed a method to estimate refractive indices that accounted for non-spherical particles by measuring the relationship between the scattering cross section and the particle volume.

[124] A variety of values for the refractive index of BC has been used in global climate models including the OPAC value of $1.74 - 0.44i$ [*Hess et al*., 1998]. As reviewed by *Bond and Bergstrom* [2006], reported values of the refractive index of light absorbing carbon vary widely; the real part, n, appears to vary from that of water to that of diamond, and the imaginary part, k, varies from that of negligibly absorbing material to that of graphite. *Bond and Bergstrom* [2006] hypothesize that strongly absorbing carbon with a single refractive index exists and that some of the variation in reported values results from void fractions in the material. Based on agreement between measured real and imaginary parts of the refractive index of light absorbing carbon, *Bond and Bergstrom* [2006] recommended a value of $1.95 - 0.79i$ at 550 nm. They caution, however, that this value may not represent void-free carbon. *Stier et al*. [2007] found that this value led to better agreement with observed atmospheric absorption, compared with the OPAC value. *Moteki et al*. [2010] found that the refractive index of ambient BC in the Tokyo urban area was about $2.26 - 1.26i$ at 1064 nm. The OPAC assumption for imaginary refractive index is not taken from combustion-generated particles, is lower than either of the latter two recommendations, and would lead to a MAC prediction about 30% lower if all other factors were equal.

[125] Radiative inversion methods can also infer values of refractive indices from remote-sensing measurements [*Dubovik and King*, 2000], but only for the entire mixed aerosol, which includes water and many other constituents other than BC. Currently, such data are available from about 500 globally distributed Aerosol Robotic Network (AERONET) surface sites [*Holben et al*., 1998].

3.7.4. Particle Size

[126] Size distributions of the BC component in ambient aerosol are affected by the size of BC at emission and by subsequent coagulation. Condensation of non-BC material changes the overall aerosol size distribution, but the underlying size distribution of BC does not change except through coagulation. BC size can be diagnosed separately. The first measurements of ambient BC size distributions relied on impactors, which identify the size at which greatest mass appears [*Mallet et al*., 2003; *Riddle et al*., 2008]. SP2 measurements have provided BC number distributions in fresh urban plumes dominated by fossil fuel (FF) combustion [e.g., *Kondo et al*., 2011c; *Schwarz et al*., 2008b], in aged plumes in Asian outflow [*Shiraiwa et al*., 2008], and in the remote upper troposphere and lower stratosphere [*Schwarz et al*., 2006; 2008b]. In the urban areas of Tokyo and Nagoya (Japan) and Seoul (Korea), the mass median diameter (MMD) and count median diameter (CMD) of fresh BC ranged from 120 to 160 nm and 50 to 80 nm, respectively. In plumes associated with wildfires, the MMD was measured to be about 200 nm and the CMD to be 120 nm [*Kondo et al*., 2011a]. The distinct difference in the size between BC particles from fossil fuel combustion and biomass burning seems to be a general feature (Figure 4). The CMD and MMD of BC observed in the Asian outflow were significantly higher than those in fresh urban plumes [*Shiraiwa et al*., 2008], suggesting the growth of BC size by coagulation during transport after emissions. BC particles are largely found in the Aitken mode (i.e., less than 100 nm diameter) and the accumulation mode because of their formation mechanism. Large concentrations of BC in the Aitken mode can result from high combustion temperatures and efficient fuel burn. For example, BC particles produced

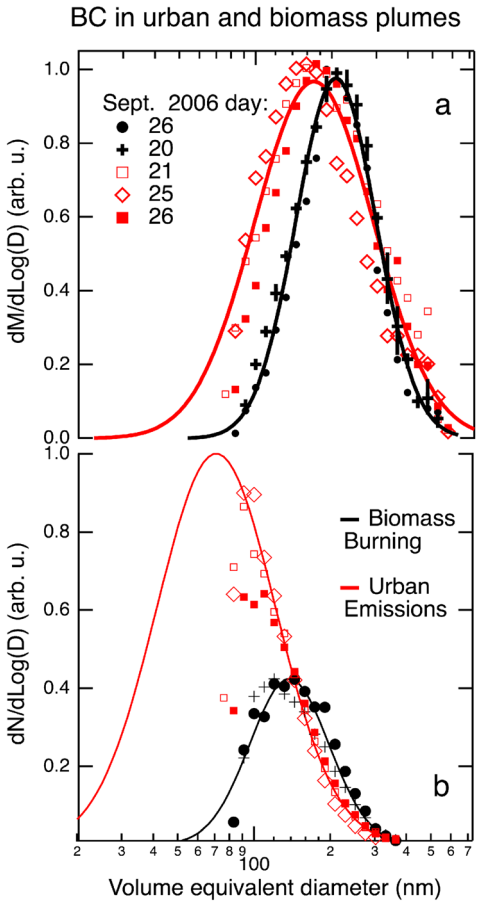

Figure 4. Mass and number size distributions of BC particles observed in three fresh urban (red) and two fresh biomass burning (black) plumes as identified in the legend. The measurements are made on board an aircraft using an in situ, single-particle detection instrument (SP2). The variable coatings on the BC particles is not shown. The observed (a) mass and (b) number amounts are plotted as symbols versus volume equivalent diameter based on assuming a spherical particle shape. The mass distributions are normalized to the same peak value. The observations are fit by a lognormal function between 90 and 600 nm (solid lines). The number distribution fits are those consistent with the fit to the respective mass distribution and are scaled to represent the same BC mass. From *Schwarz et al.* [2008b].

by aircraft jet engines have mean number diameters of about 30 nm [*Petzold et al.*, 2005a].

3.7.5. Configuration of BC-Containing Particles

[127] Internal mixing between BC and other compounds increases absorption of visible light, in part because the non-absorbing material can refract light toward the absorbing particle [*Ackerman and Toon*, 1981]. Because BC is insoluble, it is always distinctly separated from the other material in an internally mixed particle. It is often assumed that non-BC material surrounds the BC completely and approximately symmetrically, known as a "core-shell" configuration. However, BC may also exist near the surface of the particle [*Sedlacek et al.*, 2012]. The presence, relative quantities, and location of non-absorbing material in BC-containing particles require a complex characterization commonly summarized in the single term "mixing state."

3.8. Measured and Modeled MAC and ω_0

[128] As discussed above, optical models can either represent aggregates or rely upon Mie theory with the assumption of spherical particles. Here we review measured values of MAC_{BC} and ω_0, and discuss whether models can simulate these values.

3.8.1. MAC_{BC} Derived From Measurements

[129] Empirical values of MAC_{BC} have been obtained from measurements of light absorption by filter or photoacoustic methods, divided by measurements of EC mass from thermal evolution methods [e.g., *Martins et al.*, 1998a; *Moosmüller et al.*, 2001]. Measured values for freshly generated BC, where care has been taken to eliminate non-BC material, fall within a relatively narrow range of 7.5 ± 1.2 m^2g^{-1} [*Clarke et al.*, 2004; *Bond and Bergstrom*, 2006]. The MAC_{BC} may be reduced as the particles collapse into more compact forms with higher fractal dimensions [*Schnaiter et al.*, 2003; *Lewis et al.*, 2009]. Instrumental artifacts, as shown in Table 3, can hamper accurate inferences of MAC_{BC}.

[130] Laboratory measurements show that absorption increase is low for very thin coatings [*Slowik et al.*, 2007] and reaches a factor of 1.8 to 2 for thicker coatings [*Schnaiter et al.*, 2005; *Khalizov et al.* 2009; *Shiraiwa et al.*, 2010; *Cross et al.*, 2010; *Bueno et al.*, 2011]. Filter-based and photoacoustic measurements report different degrees of enhancement in the measured absorption [*Slowik et al.*, 2007; *Knox et al.*, 2009].

[131] Values of MAC_{BC} enhancement are harder to confirm for atmospheric aerosol and require measuring MAC_{BC} before and after removal of coatings. *Knox et al.* [2009] found enhancement by a factor of 1.2 to 1.6 near source regions. *Lack et al.* [2012] observed a factor of 1.4 enhancement for BC in biomass burning plumes. In contrast, similar measurements of absorption enhancement using a PAS in large urban centers revealed an average absorption enhancement of only 6%, although the MAC_{BC} of aged aerosol was 20 to 40% higher than that of freshly generated BC [*Cappa et al.*, 2012]. *Cappa et al.* hypothesize that the low values of enhancement are caused by BC inclusions at the edge of the sampled particles. Measurements made downwind (up to hundreds of kilometers) of BC source regions also give a wide range of enhancements. *Chan et al.* [2011] found MAC_{BC} values ranging from 10 to 50 m^2g^{-1}, showing a rough relationship with the ratio between non-BC and BC components. This study, which derived time-resolved MAC_{BC} from a photoacoustic spectrometer and laser-induced incandescence instrument system, appeared to contradict earlier work by the same group [*Chan et al.*, 2010] that found no apparent increase in MAC_{BC} using a PSAP to measure absorption and thermal-optical technique to measure EC. MAC_{BC} values inferred from filter-based techniques are more plentiful but may suffer from artifacts; *Cheng et al.* [2011] summarized MAC_{BC} from several studies ranging from 2 to 17 m^2g^{-1} but used empirical correction factors to adjust some of the methods prior to calculating MAC_{BC}. A series of intensive experiments with identical sampling and analysis protocols gave MAC_{BC} values ranging from 6 to 20 m^2g^{-1} [*Quinn and Bates*, 2005].

[132] Most of the above measurements of MAC_{BC} after mixing with non-BC material were made under dry conditions or at relatively low humidity. However, water is also a component of mixed aerosols, both in clear air at high relative humidity and in clouds. Particles that have taken up water become even larger than mixed, dry atmospheric particles, but measurements at such elevated humidities are difficult. *Mikhailov et al.* [2006] measured a threefold increase in absorption of BC at 100% relative humidity. *Brem et al.* [2012] also found an amplification factor of up to 2.7 for an absorbing organic material at 95% relative humidity.

3.8.2. Microphysical Model Ability to Simulate MAC

3.8.2.1. MAC_{BC} of Unmixed BC

[133] Particle size distribution has almost no influence on calculated MAC when particle diameter is below about 80 nm [*Bergstrom*, 1973]. The simplest theory that accounts for aggregate particles indicates that MAC depends only on the size of the component spherules. Therefore, modeled MAC_{BC} should not be very sensitive to particle size if either small, spherical particles are assumed or if modeled aggregates are composed of spherules below 80 nm. However, measured MAC_{BC} values, at 7.5 ± 1.2 m^2g^{-1}, are about 30% higher than values calculated with either method, using best estimates of refractive indices and density. This comparison remains unchanged even with the higher refractive index values found by *Moteki et al.* [2010]. *Bond and Bergstrom* [2006] suggest that the 30% higher absorption of actual particles could be caused by interactions between neighboring BC spherules [*Iskander et al.*, 1991; *Fuller*, 1995]. *Liu and Mishchenko* [2005] calculated a 15 to 25% increase for many changes in aggregate parameters, compared with no interaction but up to 20% decrease for spherule sizes larger than 30 nm. *Kahnert* [2010] showed that spherule interaction alone could not account for the discrepancy of 30%, and MAC modeled by *Adachi et al.* [2010] was similar for aggregates and spheres. The inability of microphysical models to reproduce measured MAC from best estimates of refractive index and density remains unresolved.

[134] Although MAC_{BC} is sensitive to the large differences in both refractive index and density used by different models, *Bond and Bergstrom* [2006] note some compensating errors. For models using OPAC refractive index and density, the low refractive imaginary index would underestimate MAC_{BC}, while the low assumed density (1 g cm^{-3}) would overestimate it. Therefore, the MAC_{BC} simulated with the OPAC refractive index and density is comparable to MAC using the values of refractive index and density recommended by *Bond and Bergstrom* [2006], although the model inputs are quite different. However, it may not be possible to simulate MAC and ω_0 of mixed particles using these erroneous values.

3.8.2.2. MAC of BC Mixed With Other Substances

[135] Internal mixtures of BC and non-absorbing material, including water, are usually modeled either as a core-shell configuration or as a homogeneous particle for which the effective refractive index is obtained using "mixing rules." Some frequently used mixing rules are volume mixing, in which refractive indices are proportional to substance volume; Bruggeman or Maxwell-Garnet effective medium approximations [*Heller*, 1965]; or the dynamic effective medium approximation [*Chylek et al.*, 1996].

[136] Different representations of mixing often produce comparable estimates of absorption. For example, using the *Bond and Bergstrom* [2006] refractive index and density, *Adachi et al.* [2010] calculated MAC_{BC} for uncoated spheres as 6.4 m^2g^{-1}, with increases for volume mixing (13.6 m^2g^{-1}), core shell (13.3 m^2g^{-1}), Maxwell-Garnet effective medium approximation (12.0 m^2g^{-1}), and realistic coated BC particles (9.9 m^2g^{-1}) at 550 nm wavelength. The assumption of a perfectly concentric core within a shell gives the highest absorption among core-shell particles [*Fuller*, 1995]. However, *Jacobson* [2006] showed that the dynamic effective medium approximation suggested for cloud droplets produced a much higher MAC_{BC} than a core-shell treatment. The absorption efficiency of BC may also be higher when it is coated by water, such as in cloud droplets (section 7.3.3).

[137] The optics of mixed particles vary widely in space and time because they depend on the relative concentrations of BC and non-BC components, which may include water, liquid, and solid components. A single value of MAC for an internally mixed aerosol is not appropriate due to the widely varying amounts of non-absorbing material surrounding BC cores. *Moffet and Prather* [2009] estimate that the increase above unmixed aerosol could be 80 to 200% for individual particles. This increase depends upon the relative sizes of the shell and the core, and the location of the core within the particle [*Fuller*, 1995]. *Bond et al.* [2006] suggest a smaller enhancement, concluding that MAC_{BC} is 80% higher for mixed than for unmixed spheres. However, because the absorption of aggregate BC appears to be 30% higher than that of spheres, the increase between uncoated, aggregate BC to coated, mixed spherical particles might be only 50%. The MAC_{BC} of 7.5 m^2g^{-1} for freshly emitted BC, plus an enhancement of 50%, agrees approximately with observed MAC_{BC} at dry conditions. A more precise evaluation of the agreement between models and observations is hampered by artifacts in the measurements.

3.8.3. Measured and Modeled Single-Scattering Albedo

[138] Single-scattering albedo of freshly generated BC has been measured as 0.10 to 0.28, as summarized by *Bond and Bergstrom* [2006]. *Khalizov et al.* [2009] and *Cross et al.* [2010] report similar values of ω_0 for fresh BC. Models of aggregate, pure-BC particles predict ω_0 of 0.1 to 0.3 [*Liu and Mishchenko*, 2005]. This value depends strongly on component spherule size but not on overall particle size [*Sorensen*, 2001]. Scattering and ω_0 for spherical BC depend greatly on the size distribution chosen. For example, ω_0 for particles of 50 and 250 nm diameter is 0.02 and 0.44, respectively, for a refractive index of $1.95 - 0.79i$. Forcing by BC scattering is small compared to that by BC absorption, so small variations in ω_0 produce only small changes in total forcing.

[139] As BC becomes mixed with other components, a large increase in scattering and, hence, in ω_0 occurs [*Khalizov et al.*, 2009; *Cross et al.*, 2010]. For mixed particles, values of ω_0 range from that of fresh particles to 0.9, depending upon the amount of added material. For these particles, forcing can be quite sensitive to ω_0. However, much of the added scattering and the tendency toward negative forcing are attributable to other chemical components, not to BC. Therefore, the forcing by BC alone should be estimated with the difference of two radiative-transfer scenarios, not just the change in ω_0.

3.8.4. Aerosol Properties in Global Models

[140] In global simulations of radiative transfer, BC particles are assumed to be either externally or internally mixed with other aerosol components. For external mixing, the material properties of pure BC are used. If internal mixing is assumed, the non-BC material is either treated as a spherical shell around a BC core, or the refractive index and density of BC and non-BC material are averaged and a homogeneous particle is modeled. *Koch et al*. [2009b] summarize predicted MAC_{BC} and treatments of aging, removal, and optical properties for many global models.

[141] All global models consider how aging affects removal rates of BC. Early models of atmospheric BC expressed the aging of BC by prescribing a timescale for converting hydrophobic BC to hydrophilic BC, typically about 1 day [*Koch et al*., 2009b]. Many models have evolved to express aging explicitly in terms of coagulation with sulfate particles and condensation of sulfuric acid and secondary organic vapor on BC. Some models represent BC-containing aerosol with discrete size-resolved bins [*Jacobson*, 2001a]. Others, known as "multi-modal" models, represent different aerosol classes, such as unmixed BC and BC coagulated with other material [*Whitby and McMurry*, 1997]. Representations of removal rates vary from constant empirical values, to parameterization based on composition and particle number [*Abdul-Razzak and Ghan*, 2000], to explicit dependence on aerosol and cloud droplet size and composition [*Jacobson*, 2002].

[142] Although global models of BC consider mixing when determining removal rates, some do not incorporate enhanced MAC_{BC} due to mixing. Values of MAC_{BC} used in global models range from 2.3 to 18 m^2g^{-1} [*Koch et al*., 2009b; *Jacobson*, 2012]. The diversity in MAC_{BC} arises either from whether the mixing state is assumed or calculated, from whether it is determined at ambient RH or constant RH, or from other choices of aerosol properties. Many of the values are similar to or lower than the value for unmixed BC and are, therefore, lower than the average value of BC in the atmosphere.

3.9. CCN Activity of Black Carbon

3.9.1. Measurements of CCN Activity

[143] Particle size, hygroscopicity, and mixing state also affect the interaction of particles and clouds [*Pruppacher and Klett*, 1997; *McFiggans et al*., 2006]. While BC-induced cloud changes are mainly discussed in section 7, we review the processes of CCN activation here because they are closely related to the microphysical properties of BC-containing aerosol.

[144] Aerosol particles serve as nucleation sites for forming cloud droplets through a process known as *activation*. The ability of an aerosol particle to act as a cloud condensation nucleus depends on its size, composition, and mixing state, and the supersaturation with respect to water vapor within the cloud. The *critical supersaturation* for a given particle is the lowest supersaturation at which that particle activates and produces a cloud droplet. Any particle can activate in extremely supersaturated air. Particles that activate more easily (i.e., that have a lower critical supersaturation) have a greater chance of affecting cloud droplet number concentration and cloud reflectivity, and they may also be more easily removed by wet deposition. Early studies found that soluble species were incorporated in cloud droplets more often than BC [e.g., *Hallberg et al*., 1994] but could not confirm whether this was caused by differences in activation or in scavenging.

[145] If all other factors are equal, small particles require greater supersaturation to activate than do large particles. Less hygroscopic particles have larger critical supersaturations than more hygroscopic particles. Because freshly emitted BC particles are small in diameter and hydrophobic, they have very large critical supersaturations and make very poor CCN [*Dusek et al*., 2006a]. Aging of BC after emission lowers the critical supersaturation of the BC-containing particle, as the addition of soluble mass increases both particle volume and hygroscopicity. Figure 5 shows the dependence of the critical supersaturation on particle diameter and BC mass fraction as simulated by a particle-resolved model [*Riemer et al*., 2009]. For a given particle size, a higher BC mass fraction increases the critical supersaturation, although particle size has a stronger effect on CCN than does chemical composition [*Dusek et al*., 2006b].

[146] "Closure" studies compare measured CCN concentrations with values predicted from particle size and composition, assuming that only soluble components serve as CCN. Predicted CCN concentrations are usually greater than measured values, with large variability in the degree of agreement [*Medina et al*., 2007]. This overprediction is

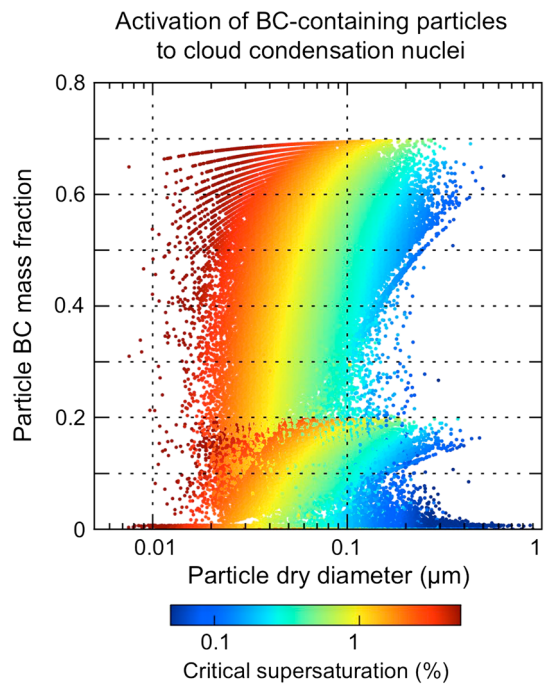

Figure 5. Critical supersaturation required to activate particles of varying size and BC content into cloud condensation nuclei. Higher supersaturation values mean that particles are less likely to become cloud droplets. Results are from a particle-resolved model that simulates coagulation and condensation in ambient air onto individual particles. The two branches show aged particles from diesel exhaust (70% BC) and gasoline exhaust (20% BC), assuming that Köhler theory describes activation. Particle diameter has the greatest effect on activation, with BC content inhibiting activation to a lesser extent. Figure is based on simulations [*Deville et al*., 2011] of particle-resolved model [*Riemer et al*., 2009].

worse with a mixture of hydrophobic and hygroscopic particles [*Wex et al*., 2010]. Near source regions, externally mixed BC plays little role in CCN [*Rose et al*., 2011] and closure is improved when externally mixed BC is assumed not to be CCN active [*Lance et al*., 2009]. However, closure studies to date have insufficient precision to confirm the contribution of coated BC to CCN. A comparison of heated and unheated particle size distributions can indicate the quantity of non-refractory material in atmospheric particles [*Sakurai et al*., 2003; *Philippin et al*., 2004; *Kuwata et al*., 2007]. Figure 6 shows the relationship between the condensed mass per particle and the CCN activity of 100 nm BC particles observed in Tokyo [*Kuwata et al*., 2009]. The number fraction of CCN-active BC particles increases with increasing condensed mass, indicating that 0.18×10^{-15} g of condensed coating material is required to activate these BC-containing particles at 0.9% supersaturation. In this case, the condensed compounds were primarily organic.

3.9.2. Global Model Treatment of CCN Activity

[147] Treatment of BC in global climate models (GCMs) does not always reflect the theoretical dependence on size and soluble fraction. In some GCMs, the activation of BC to form cloud droplets is not considered at all. The simplest formulation, a *mass-based* parameterization, assumes that the number of cloud droplets activated is empirically related to the submicron aerosol mass. In turn, that mass is determined from the hydrophilic aerosol species sulfate, submicron sea salt, and hydrophilic carbonaceous aerosol, where carbonaceous aerosol is the sum of OA and BC [*Rotstayn et al*., 2009]. This simple parameterization ignores differences in activation for particles of different sizes and composition. Many models have advanced to represent this behavior. Cloud droplet number concentration is sometimes empirically related to aerosol number concentration of certain sizes and to updraft velocities [*Lohmann et al*., 2007]. Parameterizations of cloud droplet formation derived from Köhler theory have been developed by *Abdul-Razzak and Ghan* [2000] and *Nenes and Seinfeld* [2003]. In these schemes, dependence on size and hygroscopicity can be taken into account, including the competition between different types of particles. For example, large hygroscopic particles take up water, reduce supersaturation, and therefore result in less activation of smaller or less hygroscopic particles such as those containing BC [*Ghan et al*., 1998]. Models of greater complexity represent size-resolved incorporation of aerosols in cloud droplets and their removal [*Jacobson*, 2006]. Section 7 describes studies of BC effects on clouds using some of these advanced representations.

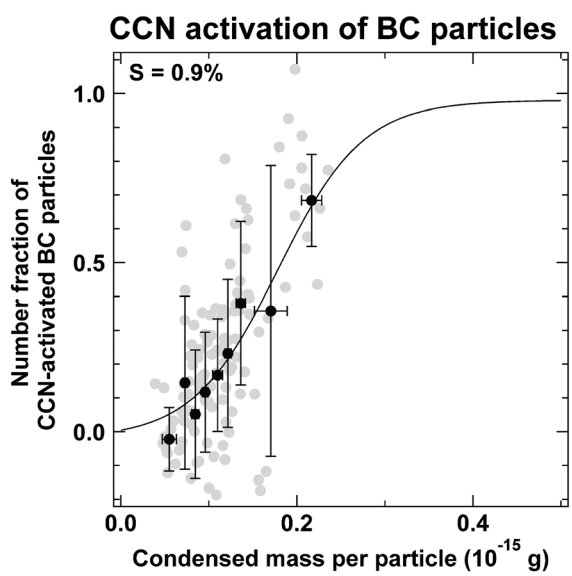

Figure 6. The number fraction of CCN-active BC particles versus mass of coating material for supersaturation of 0.9%. The data represent the response of 100 nm BC particles sampled in Tokyo in April 2007. The black points with 1 σ error bars are averages of the individual runs shown as gray data points. The solid curve is a sigmoidal fit to the averaged data points. A sigmoidal function is used because the ordinate should fall in the region between 0 and 1 by definition, although some deviations are apparent likely due to the measurement errors as well as some deviations from the assumptions employed for the calculation. Adapted from *Kuwata et al*. [2009, Figure 11].

4. Emission Magnitudes and Source Categories

4.1. Section Summary

[148] 1. Global emission estimates use the "bottom-up" method of multiplying emission factors by activity data. With this method, a bottom-up estimate of total global emissions in the year 2000 is about 7500 Gg BC yr^{-1}, with an uncertainty range of 2000 to 29,000 Gg yr^{-1}. About 4800 Gg BC yr^{-1} is from energy-related burning, with the remainder of about 2800 Gg BC yr^{-1} from open biomass burning. Total primary organic aerosol (POA) emissions excluding biogenic matter are 47,000 Gg POA yr^{-1} for the global total, with an uncertainty range of 18,000 to 180,000 Gg POA yr^{-1}. Energy-related burning and open burning produce 16,000 and 31,000 Gg POA yr^{-1}, respectively; the largest uncertainties are in open burning.

[149] 2. Industrial-era emissions are the difference between present-day and the preindustrial background year, 1750. These values are 6100 Gg BC yr^{-1} (4400 Gg BC yr^{-1} from energy-related burning and the remainder of about 1700 Gg BC yr^{-1} from open burning) and 33,000 Gg POA yr^{-1} (14,000 Gg POA yr^{-1} from energy-related sources and the rest from open burning).

[150] 3. Black-carbon emission sources are changing rapidly due to greater energy consumption, which increases emissions, and cleaner technology and fuels, which decreases them. Bottom-up inventories indicate that Asian emissions may have increased by 30% between 2000 and 2005.

[151] 4. Sources whose emissions are rich in BC can be grouped into a small number of categories, broadly described as diesel engines, industry, residential solid fuel, and open burning. Dominant emitters of BC from energy-related combustion depend on the location. Asia and Africa are dominated by residential coal and biomass fuels (60–80%), while on-road and non-road diesel engines are leading emitters (about 70%) in Europe, North America, and Latin America. Residential coal contributes significantly in China, the former USSR, and a few Eastern European countries.

[152] 5. Estimates of energy-related emissions agree broadly on the major contributing sectors and approximate magnitudes of BC emission. However, current inventories in many world regions lack information regarding the factors governing

emissions. These include the type of technologies or burning, and the amounts of biofuel (BF) combusted. Major differences in estimates of energy-related emissions result from a few knowledge gaps. For energy-related emissions, these include sparse emission measurements of sources with the highest emissions. In industrialized countries, these may be a small fraction of the emitting sources. Only energy-use inventories in North America, Europe, and urban East Asia provide a high level of detail. Measurements in developing countries are scarce for all source types.

[153] 6. Current emission factors from biomass burning, and thus emission estimates, might be biased low by a factor of at least two. Emission estimates from open burning are generally uncertain due to insufficient data on burned area and fuel consumed. Quantification of BC emissions from this source is also difficult because they strongly depend on the burning behavior and because of inherent problems with sampling and analyzing BC in smoke plumes from vegetation fires.

[154] 7. The majority (80%) of open fire emissions occurs in tropical latitudes, and inter-annual variability of BC emissions from forest or savanna fires can exceed one order of magnitude in some regions.

[155] 8. Because the net aerosol effect on climate depends on the ratio of absorbing to reflective particles such as OA and sulfate, we group emission sources into categories based on their combustion type and co-emissions. Major sources of BC, ranked in order of increasing POA : BC ratio, are diesel vehicles, residential burning of coal, small industrial kilns and boilers, burning of wood and other biomass for cooking and heating, and all open burning of biomass. A few of these sources also emit significant quantities of SO_2.

[156] 9. Receptor modeling studies of BC in urban areas that use chemical composition to identify dominant emission sources find source categories that are qualitatively similar to those in bottom-up inventories based on activity data.

4.2. Introduction

[157] Emission inventories, or global and regional tabulations of emission quantities, have a dual role. They are required inputs for atmospheric models that assess the environmental consequences of these emissions, and they also provide necessary information for the development of air quality and climate policies by indicating the largest or most easily manageable sources of emission. For BC and POA, inventories used in global models are typically "bottom-up" tabulations constructed from estimates of activity (e.g., mass of fuel burned or number of kilometers driven) combined with emission factors (e.g., grams BC emitted per mass of fuel burned or per kilometer driven). To address major fractions of particulate air pollution, or climate forcing related to BC, identification of the sources that contribute to total emissions is needed. The identification of emitting sectors is important not only for mitigation policies but also for historical reconstructions and future projections, as each sector has a different temporal evolution. The major BC emitters in each country or region depend on technological development and on practices common in each society.

[158] In this section, we first provide definitions of the terms, groupings of emission sources, and groupings of countries used throughout this assessment. Section 4.3 outlines general procedures for producing bottom-up inventories. We then present global totals and major source sectors, and regional contributions in section 4.4, and several regional estimates are tabulated in section 4.5. Major causes of differences among inventories are reviewed in section 4.6. Section 4.7 discusses major sources of uncertainty in emission estimates, focusing on the sectors identified as most important. Section 4.8 briefly discusses trends in BC emissions and causes of change. In section 4.9, we discuss studies that have inferred the major sources of particulate matter based on the chemical composition of ambient aerosol, known as receptor modeling. These studies have been conducted primarily in urban areas.

[159] The forcing by species co-emitted with BC is important in determining the net radiative forcing by BC sources (section 11). In this section, we also discuss emissions of POA, the aerosol species most commonly emitted with BC. For BC sources, we also summarize co-emissions of SO_2, which is a precursor to sulfate. Dust and sea salt are other major aerosol components, but they are generally not co-emitted with BC and they usually have larger particle sizes than BC or its co-emissions. Aged aerosol, however, may contain all of these components. The discussion of uncertainties in this section emphasizes BC emissions.

4.2.1. Geographic Aggregation

[160] In this assessment, we summarize emissions and concentrations based on 10 groups of countries (called "regions"), depicted in Figure 7. These groups were chosen based on proximity, development status, and basic meteorological similarity, although there is heterogeneity within each region. Countries in each region are listed in the auxiliary material (Table S1).

4.2.2. Definitions and Aggregation of Emission Sources

[161] 1. *Activity*. The term "activity," as it is commonly used in the emission community, indicates a quantitative measure of an event that leads to emission, such as the quantity of fuel burned, product manufactured, or kilometers driven.

[162] 2. *Emission factor*. The term "emission factor" gives mass of BC emission per activity, as opposed to total

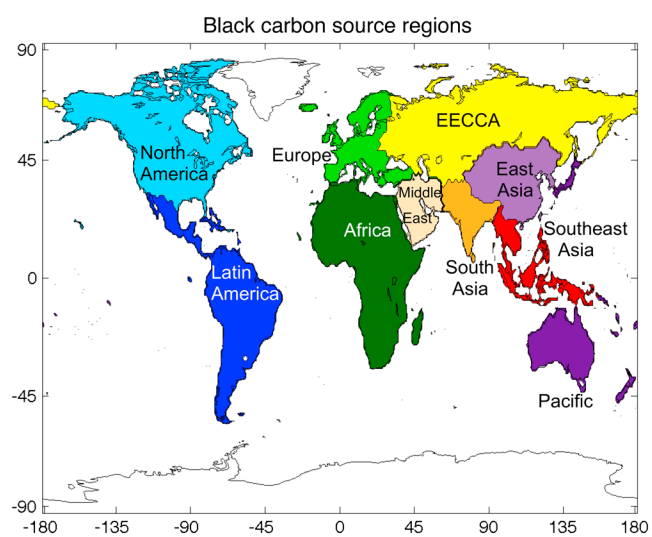

Figure 7. Regions (country groups) used for summarizing emissions and concentrations in this assessment. EECCA = Eastern Europe, Caucasus and Central Asia. The regional country groups are listed in Table S1.

emissions. Emission factors for BC vary by region and end-use, even for the same fuel.

[163] 3. *Source categories*. Because this assessment focuses on BC sources and their impacts, we isolate sources that contain large fractions of BC relative to other aerosol components or precursors. We group sources with some similarities into aggregates called "source categories," although there are some heterogeneities within these categories. For example, we lump both modern diesel engines with emission reduction technology and high-emitting, poorly maintained diesel engines into the category "on-road diesel engines." These categories are discussed further in section 4.4.

[164] 4. *BC-rich sources*. This assessment examines sources that have non-negligible BC emissions and that, therefore, have a positive component of forcing. We differentiate between sources that are rich in BC with respect to co-emitted species and those whose aerosol forcing is dominated by inorganic species. For our purposes in this assessment, a "BC-rich" source is defined as having an estimated SO_2 : BC emission ratio below 200 : 1.

[165] 5. *Sectors*. The term "sectors," as used throughout emission literature, refers to broad activity categories used for reporting by the International Energy Agency and the United Nations. These sectors are energy or transformation (which includes electricity generation), industrial activity, transportation, agriculture, and residential. The sector frequently termed "residential combustion" may also contain commercial, agriculture, and miscellaneous activities. Energy-related combustion is conducted deliberately in pursuit of economic activity or to meet personal or industrial energy demands. Open biomass burning also produces large quantities of atmospheric pollutants, and this activity has also become known as a sector in atmospheric literature. Because sectors consist of many types of activity, they include both BC-rich sources and sources that emit little BC. For that reason, we present emissions from source categories rather than from sectors.

[166] 6. *Aggregated emissions*. We use some additional terms to describe aggregated emission categories. "Energy-related" emissions include power plants, industrial activity, transportation, and residential fuel use. "Open burning" includes combustion of forests and grasslands or savannah, regardless of the cause of the fire. We also include open burning of waste for disposal, including crop residue or urban waste, in the latter category. The term "fossil fuel" indicates emissions from combustion of all fossil fuels, including diesel fuel and coal used in residential and industrial sectors. The term "biofuel" denotes biomass burned intentionally to meet energy needs and includes solid, unprocessed biofuel such as wood and agricultural waste.

[167] 7. *Industrial-era versus anthropogenic emissions*. A distinction of importance to the IPCC, among others, is the identification of "anthropogenic" emission sources. As discussed in section 2.3.2, we follow IPCC practice and use a time-based definition of climate forcing that is more accurately described as "industrial-era" forcing: the difference between the near-current year 2000 and the background year 1750. Industrial-era emissions are required to evaluate climate changes since 1750. "All-source" emissions include the component that occurred both in 1750 and in the present day. Industrial-era emissions are more uncertain than all-source emissions because of the large uncertainties in activity during the background year, especially for open biomass burning. Anthropogenic emissions may not be the same as industrial-era emissions, as some emissions in 1750 may have been human caused. Nominally, energy-related sources are all anthropogenic, as are sources associated with waste disposal. Vegetation fires are the only BC emission source that sometimes occurs without human activity.

4.3. Bottom-Up Inventory Procedures

[168] Emissions from energy-related combustion and from open vegetative burning are derived from different types of input data and often created by separate communities. In this section, we summarize information needed to create inventory estimates to clarify the sources of uncertainties.

4.3.1. Energy-Related Emissions

[169] Emission estimates for activities related to energy use were first developed to evaluate air quality in urban areas, where both high concentrations and high population led to severe exposure to health risks. Urban regulations have historically targeted total particulate matter mass concentrations, not individual chemical species. For that reason, early source characterization focused on mass emissions, and many source measurements did not provide emission rates of individual components such as BC.

[170] Bottom-up inventory estimates from energy use are based on the following simple equation:

$$Emission = \sum_i A_i \; EF_i(1 - eff_i) \tag{4.1}$$

[171] In the equation above, A_i represents activity of a particular type (e.g., fuel consumption or commodity production, conducted in a specific way), EF_i is an emission factor in grams per activity, and eff_i is the pollutant removal efficiency by a particular type of abatement. The subscript i represents different types of activity that result in emissions of the same pollutant. Both emission factors and removal efficiency depend on the type of activity and the pollutant. For global or regional emission inventories, activity is almost always given as mass of fuel burned.

[172] BC emission inventories from energy-related emissions are available for all countries. However, the level of detail used in each inventory varies greatly. Quantification of emissions and the identification of major contributing sources could be substantially refined by disaggregating the activity definitions used in equation (4.1). For example, activity for a country might be given as total coal consumption in the residential sector, with a single emission factor used for all coal burning installations. This lumping ignores the fact that large boilers might have very different emission factors or better control devices than small coal stoves.

[173] Bottom-up inventories can be graded based on the level of refinement used in emission estimation. Table 4 proposes such criteria for grading energy-related emissions. Major uncertainties in current bottom-up inventories include insufficient knowledge of activity rates and emission characteristics. Emission factors are not as well understood for sources largely found in rural areas, such as off-road diesel engines. Furthermore, measurement resources have been concentrated in developed countries, so there are still relatively few measurements of key emission sources in

Table 4. Recommended Grade Levels for Inventories of Energy-Related Emissions

Level	Activity Data	Emission Factors
Low	National fuel use for each fuel and sector or commodity	Sectoral averages *Low*−: Global average *Low*+: Regionally specific average
Medium	National fuel use for each fuel and sector or commodity, apportioned by technology	Specific to each technology and fuel *Medium*−: Some extrapolation from other countries *Medium*+: Full participation of country in specifying activity
High	Country tabulations of technology divided by substantially different emission characteristics; identification of major individual point sources	Measured at each installation or closely matched to emitting technology, including control

developing countries. Section 4.7 gives further details on uncertainties, which vary by emission sector and by region.

4.3.2. Open Burning Emissions

[174] In contrast to energy use, open burning emissions are usually not included in national activity reports. There are thousands of open fires burning globally each day, and most of these are caused by humans, either purposefully or involuntarily. Open fires are ignited for many purposes, and their emissions differ by region and ecosystem type. In contrast to residential and industrial emission sources, which are predominantly located in the northern hemisphere mid-latitudes, open fires occur largely in tropical regions, with 80% of emissions occurring there. National regulations about fire use and their enforcement vary among countries. Another important distinction between emissions from open fires and emissions from energy use is the very large interannual variability of the former. This is caused by variations in the accumulation of wooded or grass fuels, in fuel characteristics such as dryness, and in other factors influencing fire spread and fire severity. An extreme case in point is fires in Indonesia that are strongly influenced by the El Niño-Southern Oscillation in combination with the draining of peatlands. According to *Schultz et al*. [2008], BC emissions from Indonesian fires ranged between 40 and 1400 Gg yr^{-1} during the 1990s. *Mack et al*. [2011] report a single tundra fire whose fuel consumption was similar in magnitude to the annual net carbon sink for the entire Arctic tundra biome.

[175] The method for estimating emissions from large open fires is similar to equation (4.1) but using different input data.

$$M_{\text{emitted}} = \sum_i BA_i\, FL_i\, CC_i\, EF_i \tag{4.2}$$

[176] Here BA_i is the burned area (km^2), FL_i the available fuel load (kg dry matter per km^2), CC_i the combustion completeness (fraction), and EF_i the emission factor (g compound per kg dry matter). The first three parameters combine to produce activity, or total mass burned. The index i usually stands for one ecosystem type in each inventory grid cell. As fire activity has a pronounced seasonal cycle, *BA, FL*, and *CC* must also consider temporal variability of fires, although this is not yet state of the art in global inventories for *FL* and *CC*. Similar to estimates of energy-related combustion, emissions for open burning can be accomplished at different levels of refinement, as summarized in Table 5.

[177] Burned area is either derived from aerial surveillance or retrieved from satellite instruments that measure surface temperature and reflectance [*Stocks et al*., 2002; *Kasischke and French*, 1995]. Space-borne retrievals of burned area are generally based on the changes in surface reflectance as a result of the dark burn scar after a fire, but they occasionally make use of active fire detection as well [*Giglio et al*., 2009]. These retrievals can be confounded by apparent changes caused by the viewing geometry, cloud shadows, snow melt or temporary flooding, and other factors [*Roy et al*., 2002; *Simon et al*., 2004]. Some studies have also related fire radiative power from active burns to the amount of biomass combusted [e.g., *Wooster et al*., 2005; *Kaiser et al*. 2009; *Kaiser et al*., 2012] or to the amount of aerosol emitted [e.g., *Ichoku and Kaufman*, 2005; *Sofiev et al*., 2009].

[178] Fuel loads and combustion completeness are normally extrapolated from smaller-scale field studies. Grassland fires often consume nearly 100% of the aboveground biomass [e.g., *Shea et al*., 1996; *Keene et al*., 2006]. In contrast, the combustion completeness in forests varies strongly depending on the fuel and burning conditions. If the fuel is sufficiently dry, the dead plant material and plant litter are often consumed almost completely. Larger branches and stems rarely burn entirely, and living tree biomass is generally affected only in severe fires. The actual consumption of biomass in a given fire depends strongly on the ecosystem type and the fire size, severity, and persistence. Fires can consume substantial amounts of soil material, which can dominate fire emissions, for example, in peat areas of Indonesia or Siberia [e.g., *Goldammer and Seibert*, 1990; *Soja et al*., 2004].

[179] Emission factors are obtained from laboratory experiments or field measurements in the smoke plumes of actual open burns. Different measurement methods for BC in each field study, systematic sampling biases, and the use of ecosystem mean emission factors to represent both flaming and smoldering combustion introduce uncertainties in the estimated emissions (section 4.7.2.3).

4.3.3. Waste Burning Emissions

[180] Combustion may be used to dispose of agricultural, household, or industrial waste. Well-controlled combustion systems, such as incinerators, emit little particle mass, and the discussion here focuses on uncontrolled burning. Activity data are among the most difficult to estimate, as they are not of economic interest and, therefore, not quantified by any organization. Large agricultural fires are detected with remote sensing, but the smaller fires are not and may be excluded from open burning emission estimates.

[181] Agricultural wastes, such as cereal straws, woody stalks, and sugarcane leaves and tops, are generated during harvest periods. Some of this biomass finds use as animal

Table 5. Recommended Grade Levels for Inventories of Open-Burning Emissions

Level	Forest, Grassland, or Woodland Burned Area	Fuel Load (FL) and Combustion Completeness (CC)	Emission Factors	Agricultural Waste
Low	Global satellite product	Aggregated ecosystem-dependent estimates at grid cell level	Default (three ecosystem average values)	Global data compilations of burned mass
Medium−	Satellite product, plus fire hot spot data and retrieval uncertainty assessment	Ecosystem-dependent estimates at fire pixel level, FL and CC highly aggregated (<12 ecosystem classes)	Three ecosystem average values with adjustments for peat soils	Bottom-up inventory using regional-scale information
Medium+	Satellite product, plus fire hot spot data and retrieval uncertainty assessment	Finer aggregation of FL and CC	Three ecosystem average values with adjustments for peat soils	
High	High-resolution (spatial and temporal) satellite product or complete aerial surveillance, fire hot spot, and fire radiative power;	Information on available fuel load and combustion parameters at tree stand level	Ecosystem-based emission factors with adjustments dependent on fire behavior (at least 12 global ecosystem classes)	Cross-validation of satellite-derived and bottom-up estimates for agricultural waste burning emissions

fodder, thatching for rural homes, and fuel for residential cooking and agricultural and rural industry. A fraction of agricultural waste is burned in fields, often to clear them for a new sowing season, or sometimes as part of the harvesting process. The practice of agricultural waste burning has strong regional and crop-specific differences and has large seasonal variations. Emissions from agricultural waste burning are typically calculated by multiplying crop production of a particular type, a fraction of residue per product, a fraction burned in the field, a fraction of dry matter, and the combustion completeness. Reported residue-to-product ratios [*Koopmans and Koppejan*, 1997] are larger for straw and stalks of crops like cereals (rice, wheat, millets) and legumes but smaller for husks and hulls from rice and groundnut. Reported ranges of dry matter fraction are 0.71 to 0.85, and combustion efficiencies range from 0.68 to 0.89 [*Streets et al.*, 2003a]. However, the assumed fraction burned in field is subject to large uncertainties and is sometimes computed based on local practice and knowledge of competing uses of the agricultural waste [*Venkataraman et al.*, 2006].

[182] Emissions from garbage burning are estimated using per-capita waste generation rates, along with fraction burned and emission factors. Both waste generation rates and fraction burned are location specific [e.g., *Christian et al.*, 2010]. Waste generation is higher in industrialized countries and urban areas, but the fraction burned is higher in developing countries. Burning of industrial waste is quantified in industrialized countries, but it is highly controlled so that emissions are small. In contrast, informal disposal of industrial waste has not been quantified in developing countries, and these emissions are not included in these estimates.

4.4. Total BC Emissions and Major Source Categories

[183] Table 6 summarizes the best estimates and their ranges for BC and POA emissions in the year 2000 as derived in this assessment from a variety of information sources described in this section. Figure 8 summarizes sources of global BC emissions from two global inventories, along with estimates of their uncertainty; it also shows emission ratios for co-emitted, cooling aerosol species or precursors. Figure 9 shows the same estimates tabulated by region. Estimates from SPEW (Speciated Pollutant Emissions Wizard) [*Bond et al.*, 2004, 2007; *Lamarque et al.*, 2010] and GAINS (Greenhouse Gas and Air Pollution Interactions and Synergies) [*Kupiainen and Klimont*, 2007; *Cofala et al.*, 2007; *Amann et al.*, 2011; *UNEP*, 2011] are used as a reference for energy-related emissions throughout this assessment because they have the technological detail required to explore mitigation. SPEW estimates contain bottom-up

Table 6. Best-Estimate Bottom-Up Values for BC and POA Emissions in Year 2000[a] ($Gg\,yr^{-1}$)

	BC	BC Range	POA	POA Range
All sources				
Energy related[b]	4770	1220 to 15,000	15,900	8800 to 23,800
Open burning[c]	2760	800 to 13,800	31,100	9000 to 156,000
Total all-source	7530	2020 to 28,800	47,000	17,800 to 179,000
1750 background				
Energy related	390		1560	
Open burning	1020		12,800	
Total background	1410		14,360	
Industrial era				
Energy related	4380		14,300	
Open burning	1740		18,300	
Total industrial era	6120		32,600	

[a]Energy-related emissions are from year 2000; open-burning emissions are a climatological average of years around year 2000.
[b]Refer to section 4.4 for a derivation of the totals and ranges.
[c]Refer to section 4.4 for a derivation of the totals and section 4.7.2.4 for a derivation of the ranges.

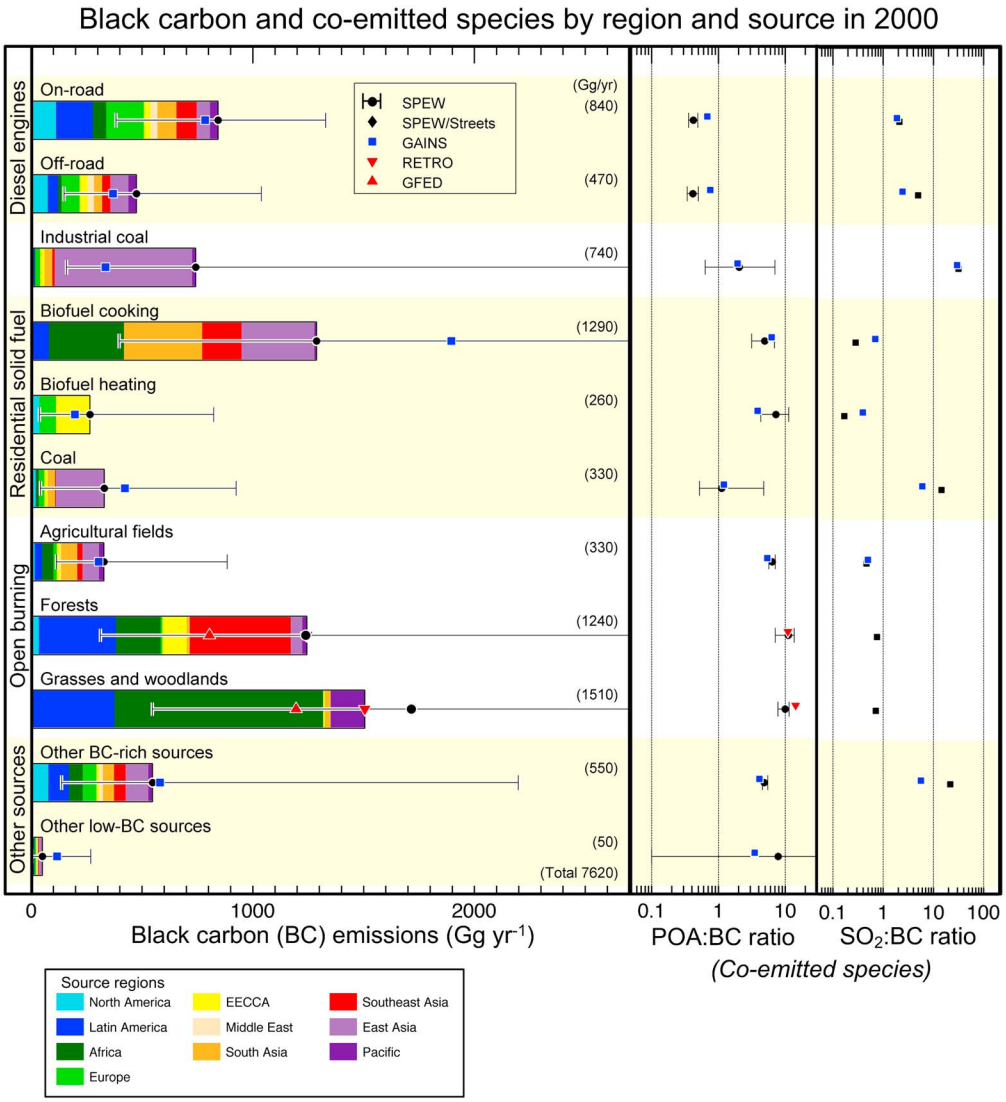

Figure 8. Emission rates of BC in the year 2000 by source category and ratios of co-emitted aerosols (e.g., primary organic aerosol, POA) and aerosol precursors (e.g., SO_2) to BC. For reference, it is often assumed that the ratio of OA to primary organic carbon (OC) varies from 1.1 to 1.4, depending on the source (section 3.2.2). SPEW emissions are shown as colored bars and are described by *Lamarque et al.* [2010]. GAINS estimates are from *UNEP/WMO* [2011a, 2011b], and RETRO emissions for open burning are described by *Schultz et al.* [2008]. Sulfur emissions from *Streets et al.* [2009] were used for ratios to SPEW. Regions are shown in Figure 7.

uncertainties and are therefore used as the basis for Figure 8. GAINS estimates have the advantage of providing all co-emitted species, including gaseous emissions, and are used in the discussion of source category impacts in section 11. Section 4.6 discusses differences between these inventories and compares other global and regional emission estimates.

[184] Figure 8 and Table 7 also give bottom-up estimates from open burning. Both RETRO (REanalysis of the TROposphere over the last 40 years) [*Schultz et al.*, 2008] and GFED (Global Fire Emissions Database) [*van der Werf et al.*, 2006] incorporate remote sensing information on fires to provide seasonal and inter-annual emission variation and are frequently used by atmospheric models. Figure 10 shows the seasonal and inter-annual variability of open burning in five regions. However, because remote sensing poorly detects small agricultural fires, we rely on estimated activity data (SPEW and GAINS) for agricultural waste burning emissions. The figure and table also compare SPEW open-burning emissions, which are based on country information about total quantities burned.

[185] The left panel of Figure 8 presents total BC emissions for each source category, also indicating the regions of emission. This panel shows ranges calculated from uncertainties in both activity data and emission factors in SPEW, and a comparison with the same sectors in the GAINS database. Although totals for each category vary, there is general agreement that the three largest contributors are open burning, diesel engines, and residential solid fuels. A small number of industrial sources in developing countries also make a significant contribution.

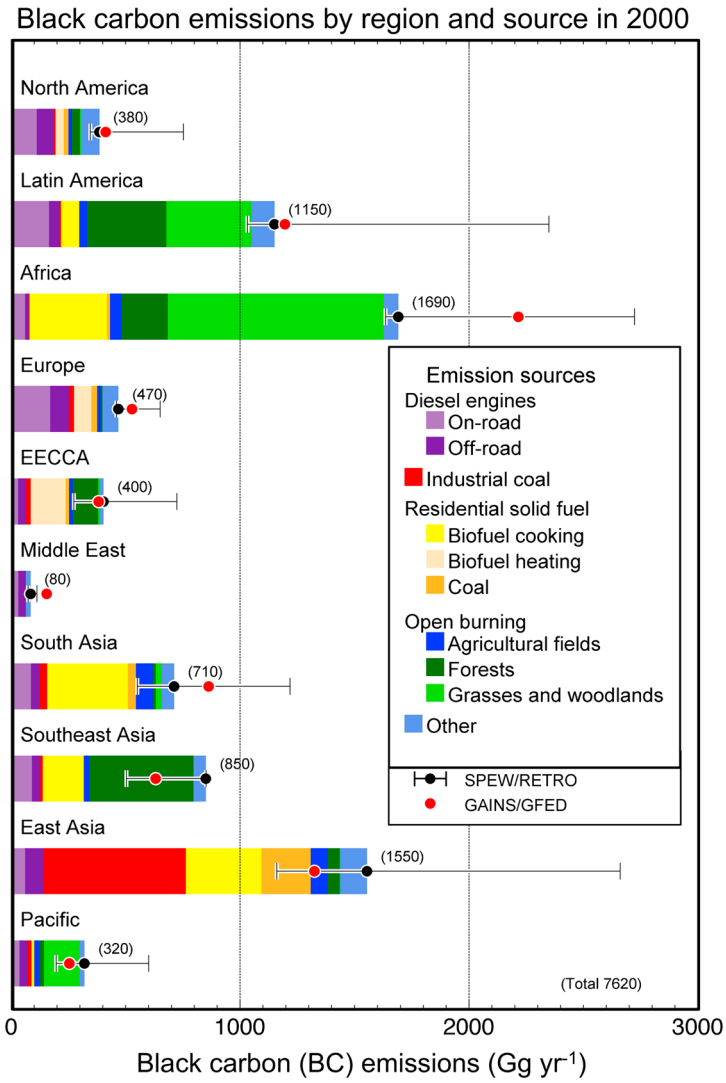

Figure 9. Emission rates of BC in the year 2000 by region, indicating major source categories in each region. SPEW, GAINS, and RETRO emission data are the same as in Figure 8. Regions are shown in Figure 7.

[186] The two right panels of Figure 8 show emission ratios between POA and BC, and sulfur dioxide and BC. Higher ratios indicate that more aerosol species are co-emitted that could offset direct warming by BC. For BC in snow and sea ice, co-emission of non-absorbing aerosol (e.g., sulfate) does not affect BC forcing, and co-emission of absorbing aerosol (e.g., some POA) adds to the forcing. Not represented in the figure are gaseous species such as carbon monoxide and O_3 precursors, many of which contribute to warming (section 11).

[187] Table 8 provides numeric values for energy-related emission estimates in Figure 8, including additional disaggregation. For an estimate of energy-related BC emissions in the year 2000, we average the GAINS and SPEW totals without flaring, aircraft at cruise altitudes, and international shipping yielding 4430 Gg yr^{-1}. We then add those three sources for a total of 4770 Gg yr^{-1}. Relative uncertainties in BC emissions are taken from the SPEW bottom-up calculations, giving 90% uncertainty bounds of 1220 to 15,000 Gg yr^{-1}. A similar estimate for POA gives a central estimate of 15,900 Gg yr^{-1} with uncertainty bounds of (8800 to 23,800) Gg yr^{-1}.

[188] Table 7 provides numeric values for biomass-burning emission estimates in Figure 8, including additional disaggregation. For an estimate of all-source, bottom-up emissions in 2000 from open burning, we average the RETRO and GFED climatological values for forests, grasslands, and woodlands, yielding approximately 2450 Gg BC yr^{-1}. We add estimated activity-based data (average of SPEW and GAINS) for estimates of agricultural waste burning emissions (310 Gg BC yr^{-1}). The total is 2760 Gg BC yr^{-1}. A parallel estimate for POA gives 29,200 Gg POA yr^{-1} from forests, grasses, and woodlands, and 1910 Gg POA yr^{-1} from agricultural waste burning. Bottom-up uncertainty estimates are discussed in section 4.7.

[189] For energy-related emissions in the background year of 1750, we assume the values of 390 Gg BC yr^{-1} and 1560 Gg POA yr^{-1} given by *Dentener et al.* [2006]. These emissions are entirely from biofuel use. Industrial-era emissions are the difference, 4380 Gg BC yr^{-1} and 14300 Gg POA yr^{-1}. We also assume the *Dentener et al.* [2006] values for background open-burning emissions: 1230 Gg BC yr^{-1} and

Table 7. Central Estimates of All-Source Global Black-Carbon Emissions From Open Biomass Burning (Gg yr^{-1})

	Inventory					
	GFED[a]		RETRO[b]	RETRO[c]	GAINS	SPEW
	2000	clim.	2000	clim.	2000	clim.[d]
Grassland and woodland fires[e]						
Grassland and open savanna	820	850	310	290		
Woodland	330	350	1220	1220		
Total grassland and woodland	1150	1200	1530	1510		1710
Forest fires						
Deforestation and degradation	230	440	n.s.	n.s.		
Forest (excluding deforestation and degradation)	300	370	n.s.	n.s.		
Peat	2	130	n.s.	n.s.		
Total forest fires	530	940	830	1240		1240
Agricultural waste burning[f]	50	60	n.e.	n.e.	290	330
Grand total	1730	2200	2370	2750		3280

[a]Version 3.1 from http://www.falw.vu/~gwerf/GFED/GFED3/tables/emis_BC_absolute.txt; clim.: mean climatological values from 1997 to 2006.
[b]n.s. = not specified; n.e. = not estimated.
[c]clim.: mean climatological values for 1996 to 2000.
[d]SPEW totals provide a climatological average rather than representing any particular year.
[e]GFED and RETRO have different classifications of grasslands and woodlands.
[f]GFED agricultural waste burning is inferred from remote-sensing data and includes only large fires, while GAINS and SPEW are based on activity estimates.

12800 Gg POA yr^{-1}. Industrial-era emissions are the difference, 1740 Gg BC yr^{-1} and 18300 Gg POA yr^{-1}. With no constraints in the year 1750, the background values are crude assumptions, scaled by population and land cover. Other work has estimated BC emissions in the middle to late 1800s [*Novakov et al.*, 2003; *Ito and Penner*, 2005; *Bond et al.*, 2007; *Junker and Liousse*, 2008], but none has provided estimates for earlier years.

[190] In the following sections, we briefly review contributions from individual source categories. Section 4.6 discusses some reasons for differences between the estimates presented in the figures, as well as other emission estimates.

4.4.1. Diesel Engines

[191] On-road diesel engines include diesel cars and trucks, while off-road engines include engines used in agriculture, construction, and other heavy equipment. The diesel-engine category in this assessment specifically excludes shipping emissions, which are summarized separately. Diesel engines contributed about 20% of global BC emissions in 2000. These sources have the lowest co-emissions of aerosols or aerosol precursors of all the major BC sources. In order to enable use of the most advanced exhaust controls, sulfur must be removed from the diesel fuel during refining. Therefore, in regions with fewer controls, primary particulate matter emission factors are higher, but SO_2 emissions are also higher.

4.4.2. Industrial Coal

[192] Industrial coal combustion is estimated to provide about 9% of global emissions, mainly in small boilers, process heat for brick and lime kilns, and coke production for the steel industry. Although coal combustors can be designed to produce little BC, coal can also be highly polluting when burned in simple combustors, which are still present in small industries, particularly in developing countries. Co-emitted SO_2 is estimated from coal sulfur content and exhaust control. The SO_2/BC ratio for industrial coal is much higher than that for the other emission categories, where the fuel has little sulfur or more efficient flue-gas controls are in place. Emissions from coal-fired power plants, which emit much less BC because of their better combustion efficiency, are not included here.

4.4.3. Residential Solid Fuels

[193] Wood, agricultural waste, dung, and coal are used for cooking or heating in homes, providing another 25% of BC emissions. Most of the emissions occur in single-family devices, which are often of simple design. When infrastructure and income do not allow access to low-emission residential energy sources such as electricity and natural gas, solid fuels are used extensively for cooking. Otherwise, they are used more often for heating. Coal and, less frequently, wood are also used for heating in multi-family building boilers. The designation "cooking" in Figure 8 refers to regions where wood is primarily used for cooking, even if some heating occurs. Similarly, "heating" includes all uses in regions where heating is dominant. This sector also includes emissions from both production and consumption of charcoal. The poor combustion and mixing in these simple devices result in relatively high POA : BC ratios, but SO_2 emissions are low except for coal.

4.4.4. Open Burning

[194] Open burning of biomass in the location where it is grown is a very large contributor to global BC emissions, with bottom-up estimates predicting that it contributes about 40% of the total. Table 7 compares estimates of open-burning BC emissions for the periods 1997 to 2006 (GFED 3.1) and 1996–2000 (RETRO) with the climatological values from SPEW. Current global emissions estimated from open burning range between 2000 and 11,000 Gg yr^{-1} for BC and between 18,000 and 77,000 Gg yr^{-1} for OC in average years, as summarized by *Schultz et al.* [2008] and confirmed by subsequent work [*Lamarque et al.*, 2010; *van der Werf et al.*, 2010]. Most studies fall into the range of 2000 to 6000 Gg yr^{-1} for BC and

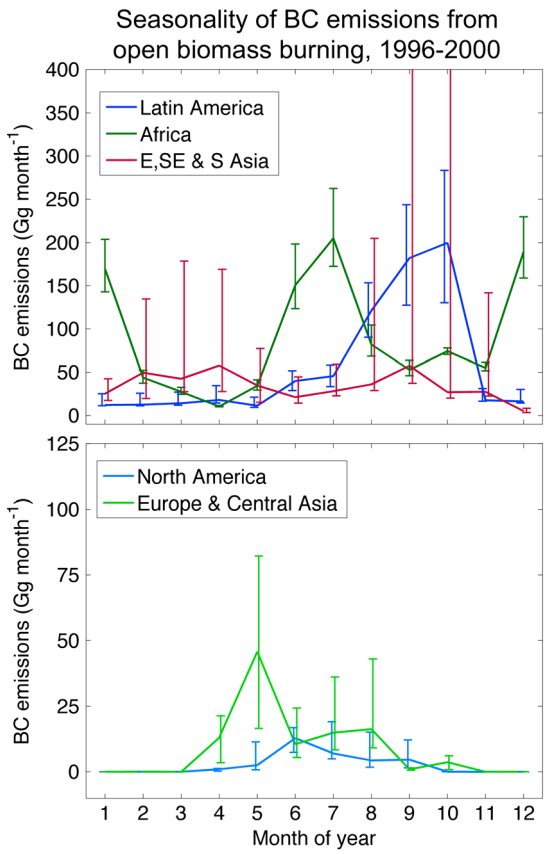

Figure 10. Seasonality of BC emissions from forest, grassland, and woodland burning. Average monthly emissions estimated by RETRO for the period 1996–2000 are shown [*Schultz et al.*, 2008]. Error bars indicate minima and maxima during each period. Regions correspond to those in Figure 7. Africa, which includes the small Middle East emissions, has two burning seasons because the equator bisects it. The group of East, Southeast, and South Asia (E, SE, and S Asia) includes emissions from Oceania. The very large error bars in that region results from the very high fire season in 1997. Note the different vertical scales in the two panels.

20,000 to 27,000 Gg yr^{-1} for OC. The highest BC and OC emission estimates by *Chin et al.* [2002] resulted from the use of larger emission factors. A smaller contribution originates from open burning in agricultural fields, which is often done to clear residues after harvest. This source contributes about 300 Gg yr^{-1} BC and 1500 Gg yr^{-1} OC. In regions like south Asia, this source can contribute about 20% of carbonaceous aerosol emissions [*Venkataraman et al.*, 2006].

[195] The average of 2760 Gg BC yr^{-1} in Table 7 (including emissions from agricultural waste burning) agrees well with the mean value of global BC estimates from the review of *Schultz et al.* [2008] after they adjusted the literature estimates to standard emission factors. However, modeling studies that constrain emissions using satellite observations indicate substantially larger biomass burning emissions of particulate matter. Section 5.5.1 discusses these studies further.

[196] Because fuel-air mixing is completely unmanaged in open burning, large quantities of organic matter can escape and average POA : BC ratios are highest of all sectors. This ratio can vary greatly depending on the burning conditions; *Andreae and Merlet* [2001] give an inter-quartile range of 4 to 14. If the burning is natural or accidental, vegetation may burn while it is still rooted and standing, thus allowing for some greater ventilation and oxygen supply. Deliberate burning may involve land clearing before collecting, piling, and burning the material, which tends to favor oxygen-poor conditions.

Table 8. Bottom-Up Central Estimates of All-Source Global Black Carbon Emissions From Energy-Related Combustion in the Year 2000 (Gg yr^{-1})[a]

Source	Inventory	
	SPEW	GAINS
Diesel engines		
On-road diesel engines	840	780
Off-road diesel engines	480	370
Total diesel	1320	1150
Industrial coal		
All coal in industry	740	340
Total industrial coal	740	340
Residential solid fuel		
Wood, cooking regions	1000	1580
Other biofuel, cooking regions[b]	290	310
All biofuel, heating regions[b]	260	200
Coal, cooking, and heating	330	420
Total residential solid fuel	1880	2510
Other sources		
Non-coal industry, including biofuel	170	30
On-road gasoline engines	110	80
Residential, including diesel generation	100	170
Aviation	20	1[c]
Shipping	100	40[d]
Flaring	-[e]	260
All other BC-rich sources	70	20
Power plants [f]	20	20
Other low-BC sources	-[e]	60
Total other sources	590	690
Grand total	4510	4690

[a]Data are based on year-2000 energy data and technology. Totals do not match exactly due to rounding.
[b]"Cooking regions" are those where solid fuel is primarily used for cooking, even if some heating occurs; the opposite is true for the definition of "heating regions."
[c]This inventory only includes landing and takeoff (i.e., no cruise) emissions.
[d]This inventory only does not include international shipping.
[e]Not estimated.
[f]Considered to be low-BC sources.

4.4.5. Other Emission Sources

[197] BC emissions from the four major source types above are about 90% of the global total. Significant contributors of the remainder of BC emissions are listed in Table 8. Two of the largest groups are industrial and residential emissions that are not included in one of the preceding categories. In industry, biofuels are responsible for the higher BC emissions estimated by SPEW. Like coal-burning sources, these small sources are challenging to characterize. About half of the miscellaneous residential emissions come from middle distillate oil, and stationary diesel engines used for distributed power generation are estimated to produce about 85% of that. Charcoal, kerosene, and liquefied petroleum gas make up the remainder of residential emissions.

[198] Although aviation emits BC at altitudes that otherwise have low aerosol concentrations, its contribution to BC mass is quite small. Likewise, shipping emits aerosol

into regions that otherwise have low concentrations, but it ranks with minor sources of BC. These statements are supported by more refined emission estimates than those in Table 8. *Lee et al*. [2010] estimated "soot" from aviation as 6 Gg yr^{-1} for 2004. *Eyring et al*. [2010] summarized shipping emission studies, giving a best estimate of 130 Gg yr^{-1} and a range of 5 to 280 Gg yr^{-1}.

[199] Other BC-rich sources include gasoline engines and flaring in the oil and gas industry. Gasoline engines have much lower particulate matter emission rates than diesel engines, so total emissions from gasoline are less than 10% of diesel BC emissions, although gasoline vehicles are more numerous. Flaring in the oil and gas industry is a poorly understood source both in terms of activity and emissions. Considering data from *Elvidge et al*. [2009], *Johnson et al*. [2011a], and *Johnson and Coderre* [2011], GAINS estimated BC emissions at nearly 4% of the anthropogenic global total with the majority originating in Russia, Nigeria, and the Middle East.

[200] All BC-rich sources together constitute 99% of the global inventory. Low-BC sources include coal power plants for generating electricity. These are not considered a large source of BC because the high temperatures and well-managed combustion promote burnout of any BC that is formed. However, BC emission rates from power generation in developing countries are not well known (section 4.6.1).

4.5. Regional Emissions

[201] The level of refinement in current inventories, limited by the availability of data, varies greatly among world regions (Table 9). Figure 9 presents emission estimates tabulated by region, rather than by source category. Substantial BC emissions occur in all regions, with the largest contributions in regions where open burning is high (Africa and Latin America). Dominant sources of BC emissions from energy-related combustion change with development from residential coal and biomass fuels (60–80%) in Asia and Africa, to on-road and non-road diesel transport (about 70%) in Europe, North America, and Latin America. Industrial uses of coal are also important in East Asia.

[202] The largest open burning emissions occur in Africa, Latin America, and Southeast Asia. Tropical savanna and forest burning contribute about 45% and 40% of global open fire emissions, respectively. Globally, burned area and fire emissions are mostly decoupled because most of the burned area occurs within savanna ecosystems with relatively low fuel loads and emissions per unit area, while forest lands have less burned area but higher and more variable fuel loads. As a consequence, inter-annual variability is higher in equatorial Asia than in Africa. Open burning at northern middle to high latitudes does not constitute a large fraction of global, annual BC emissions, but the timing and location of Eurasian open burning emissions in particular (i.e., high-latitude spring in Figure 10) mean they have especially large contributions to BC cryosphere climate forcing, which has very high efficacy (section 8). Figure 11 shows the distribution of the major source types by latitude. The Northern Hemisphere contains about 70% of the emissions (i.e., 85% of energy-related emissions and 45% of open-burning emissions).

Table 9. Black Carbon Emission Inventory Grades[a]

	Energy Use		
Region	Urban	Rural	Open Burning
North America	High	High	Medium+
Latin America	Medium+	Low	Low
Europe	High	High	Medium+
EECCA	Low	Low	Medium−
Middle East	Low	Low	Low
Pacific	Low	Low	Low
Africa	Low	Low	Medium−
East Asia	High	Medium+	Medium−
South Asia	Medium+	Low	Low
Southeast Asia	Low	Low	Low

[a]Highest possible inventory grades based on current available disaggregation of activity and emission data for different world regions. Regions are shown in Figure 7. Grades defined in Tables 4 and 5.

4.6. Comparison Among Energy-Related Emission Estimates

[203] Thus far, emission estimates from GAINS and SPEW have provided a perspective on the major sources of global BC emissions. Other estimates of global and regional emissions are summarized in Table 10. These differ substantially, by up to factors of 3 for specific regions. We begin by reviewing global emission estimates. Differences in the totals can usually be ascribed to choices of emission factors or other characteristics within the major source categories, which we discuss individually. We then use this background to discuss differences among Asian emission estimates.

[204] *Penner et al*. [1993] developed one of the first global BC emission estimates based on applying constant global emission factors to broad sectors. *Cooke and Wilson* [1996] were the first to apply emission factors that depend on development level. An updated version of that inventory [*Cooke et al*. [1999], abbreviated as *Cooke99* for the following discussion] is commonly used in atmospheric modeling. *Liousse et al*. [1996] developed an early estimate of biofuel-burning emissions based on consumption estimates from the Food and Agriculture Organization. Bond *et al*. [2004] discussed the main sources of differences between SPEW and *Cooke99*. As discussed below, the largest differences are for power generation and diesel engines. A composite of national inventories reflecting growth between 2000 and 2006 was developed for the field campaign Arctic Research of the Composition of the Troposphere from Aircraft and Satellites (ARCTAS). The global estimate totaled 5200 Gg yr^{-1} [www.cgrer.uiowa.edu/arctas/emission.html].

4.6.1. Differences in Power Generation Emissions

[205] GAINS and SPEW agree on the magnitude of BC from power generation. However, *Cooke99* has much higher emissions from coal-fired power plants (an increase of 1600 Gg yr^{-1} BC and 2400 Gg yr^{-1} OC above both GAINS and SPEW). This difference resulted from assumptions of very high BC fractions in *Cooke99*, while the other estimates relied on existing measurements. New measurements [*Zhang et al*., 2008b] and subsequent harmonization of emission factors [*Lamarque et al*., 2010] support the use of lower emission factors and values nearer the SPEW and GAINS emissions for this sector. However, there remains a persistent but informal perception (e.g., G. Beig, personal communication, 2009) that BC fractions of particulate matter in developing countries, especially in power plants and industrial installations, could be higher than that represented by existing measurements. Even

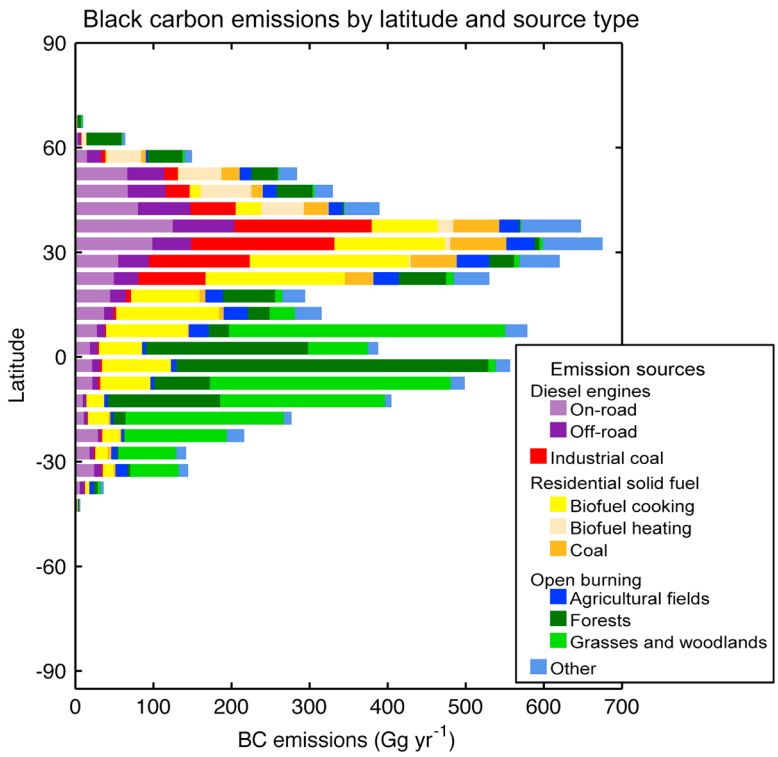

Figure 11. Latitude plot of the data shown in Figures 8 and 9 using 5° latitude bins.

if older, poorly operating power plants have high BC emission factors, there is no evidence that newly installed, modern power plants do. Thus, rapid growth in electricity generation is unlikely to cause sharp increases in BC emissions.

4.6.2. Differences in Industrial Coal Emissions

[206] SPEW estimates of industrial coal emissions are about double those of GAINS. This difference is almost entirely due to assumptions in emission factors and BC fractions for the two major emitting categories, brick kilns, and coke ovens. A few particulate matter (PM) measurements were available for brick kilns, but no measurements of total PM from uncaptured coking were available at the time of inventory development. Composition measurements for both sources were estimated based on expert judgment, as no composition measurements were available for either source.

4.6.3. Differences in Diesel Engine Emissions

[207] GAINS and SPEW have similar emissions for year 2000 from on-road and off-road diesel engines, with SPEW being somewhat higher due to different assumptions about emission factors and the fraction of high-emitting vehicles. In previous versions of SPEW [e.g., *Bond et al.*, 2007], diesel emissions were higher than those given here due to different assumptions about the implementation of standards. The *Cooke99* inventory had much higher emissions from diesel engines, resulting from very large assumed emission factors in developing countries that were not based on measurements. Measurements have confirmed higher emission factors in locations with delayed emission standards [*Subramanian et al.*, 2009; *Assamoi and Liousse*, 2010], although no measurements are as high as the assumptions in the *Cooke99* inventory. However, an evaluation of trends in California [*Kirchstetter et al.*, 2008] indicates that emissions prior to regulation could have been higher by a factor of 10, greater than either the emission factors used in SPEW and GAINS, or in any reported measurements.

4.6.4. Differences in Residential Solid Fuel Sector

[208] Small-scale residential combustors constitute the largest difference between SPEW and GAINS. Estimates from SPEW are lower by 30% for biofuel used in cooking and all uses of coal, and higher by 35% for biofuel used in heating. The discrepancies in heating biofuel and coal emissions are largely due to activity data. For cooking stoves, activity in SPEW is lower by about 15%, and emission factor choices cause the remainder of the difference. GAINS uses the highest emission factor from fireplace measurements for cooking stoves (about 1.1 g BC [kg fuel]$^{-1}$), while SPEW uses an average of cooking stove measurements (about 0.8 g BC [kg fuel]$^{-1}$). Both are consistent with observed emission factors.

4.6.5. Asian Emission Inventories

[209] Detailed emission inventories have been developed for the Asian region and for individual countries within Asia. Here we compare these inventories and identify some reasons for differences. Similar studies are not available in other world regions.

[210] Three emission inventories have been developed for Asia alone. Streets *et al.* [2003b] provided inventories to support modeling during the TRACE-P field campaign [*Jacob et al.*, 2003]. Emission factors in that inventory were an earlier version of those in SPEW [*Bond et al.*, 2004]. Two primary differences were the addition of small industries (brick kilns and coking) in SPEW and adjustment of emission factors for residential fuel, where BC emission factors were reduced slightly and those for organic matter were greatly reduced. In addition, the

Table 10. Bottom-Up Estimates of All-Source Global and Regional BC and OC Emission Rates From Energy-Related Sources (Fossil Fuel and Biofuel Combustion)[a]

Source	Emission Rate ($Gg\,yr^{-1}$) BC	OC[b]	Inventory Level[c]	Year of Estimate
Global				
GAINS [*Cofala et al.*, 2007][d]	4700	12,300	Med−/+	2000
SPEW [*Bond et al.*, 2007][d]	4530	8700	Med−	2000
Junker and Liousse [2008]	4800	7300	Low+	1997
Ito and Penner [2005][e]	4800	10,100	Med−	2000
Cooke et al. [1999] and *Liousse et al.* [1996]	6100[f]	16,000[f]	Low+	1984
Penner et al. [1993]	12,600	-	Low−	1980
India				
Reddy and Venkataraman [2002a, 2002b]	400	1150	High/Med	1997
Sahu et al. [2008]	1300	-	Low+	2001
Parashar et al. [2005]	900[g]	2300[g]	Low+	1995
Ohara et al. [2007]	800	3300	Low+/Med−	2000
Streets et al. [2003b]	600	2800	Med−	2000
Klimont et al. [2009]	750	1600	Med+	2000
Lu et al. [2011]	680	1700	Med+	2000
	920	2200		2010
GAINS	580	1900	Med+	2000
SPEW	500	1600	Med−	2000
China				
Cao et al. [2006]	1500	4200		2000
Streets et al. [2003b]	1000	3400	Med−	2000
Zhang et al. [2009b]	1600	2800	Med+	2001
	1800	3200	Med+	2006
Klimont et al. [2009]	1200	2800	Med+	2000
Lu et al. [2011]	1200	2400	Med+	2000
	1700	3400		2010
GAINS	1100	3500	Med+	2000
SPEW	1200	2800	Med−	2000
United States				
Reff et al. [2009]	440	960	High	2000
Battye et al. [2002]	430	-	High	1999
SPEW	350	500	Med−	2000
GAINS	260	370	Med−	2000

[a]Subsets of global inventories are given under each country for comparison. All emission rate values are rounded.
[b]Because most inventories report OC emission rates rather than POA, OC values are given here.
[c]See Table 9 for definitions of inventory levels.
[d]GAINS and SPEW emission factors and technology divisions have been updated since the original publications describing the methodology. Updates to SPEW are described in *Lamarque et al.* [2011].
[e]Digitized from figures to obtain fossil fuel plus biofuel only.
[f]Combined estimate is fossil fuel emissions from *Cooke et al.* [1999] (5100 $Gg\,yr^{-1}$ BC, 7000 $Gg\,yr^{-1}$ OC) and biofuel emissions from *Liousse et al.* [1996]; the two inventories are often used together. Bulk BC emissions in *Cooke et al.* [1999] (rather than only submicron emissions) are estimated to be 6400 $Gg\,yr^{-1}$.
[g]Average of range: 400–1400 for BC, 1200–3300 for OC.

TRACE-P inventory relies on some projected energy use because it was developed before year 2000 data became available. *Ohara et al.* [2007] developed an Asian emission inventory and also provided time trends for 1980–2003. They used a single emission factor for each sector drawn from *Streets et al.* [2003b], except for transportation where they developed a representation based on differing vehicle types. *Klimont et al.* [2009] drew on additional national data collected during the GAINS-Asia project to estimate emissions of BC and OC for the period 1990–2005 and projections to 2030. They developed technology specific factors, although they did not distinguish among some uses (e.g., cooking versus heating), with the result that estimates were about 25% higher estimates than those of *Streets et al.* [2003b], *Ohara et al.* [2007], SPEW, and the current GAINS global model.

[211] For India, central values of BC emissions differ by a factor of about 3. The lowest central value [*Reddy and Venkataraman*, 2002a, 2002b; *Venkataraman et al.*, 2005] is from a difference (compared to SPEW) in the residential sector, where the India-only mean emission factor is about 16% lower than the global mean used by *Bond et al.* [2004]. Estimates by *Sahu et al.* [2008] are a factor of 3 larger, resulting from the use of the high power-plant and diesel emission factors from *Cooke et al.* [1999]. *Parashar et al.* [2005] estimated emissions a factor of 2 larger than those of *Reddy and Venkataraman*, largely caused by their new measurements of very high emission factors for biofuel (especially dung). Estimates from *Ohara et al.* [2007] and *Streets et al.* [2003b] are based on the same emission factors, so the large difference between them is surprising. Most of the 200 Gg yr^{-1} difference is attributable to biofuels in the residential sector (616 versus 420 Gg yr^{-1}, respectively). Activity data are frequently given in terms of total fuel calorific content rather than mass, and in these units, the Ohara and Streets inventories are only 16% different. The

difference, therefore, must be caused by differing assumptions in the conversion between fuel calorific content and mass. *Klimont et al*. [2009] used higher emission factors for cooking and national energy use statistics and estimated nearly 30% higher BC than current global GAINS implementation or SPEW, while OC was well within the range of GAINS and SPEW. *Lu et al*. [2011] obtained similar estimates to *Klimont et al*. [2009] and also estimated that BC emissions rose 35% between 2000 and 2010. The *Lu et al*. [2011] trends in Asian aerosol emissions compare favorably with remote-sensing data.

[212] For China, regional inventories are in broad agreement with global inventories on magnitudes and sources of BC emissions. *Cao et al*. [2006] developed an emission inventory based on Chinese data and some new emission factors. SPEW and the inventory of *Cao et al*. [2006] are quite similar. The *Streets et al*. [2003b] inventory lacks treatment of small industry. *Zhang et al*. [2009b] included small industry, particularly brick and cement kilns, following the approach of *Streets et al*. [2006] and estimated significantly higher total BC emissions from China. *Lu et al*. [2011] estimated generally higher growth in BC emissions between 2000 and 2010 (+46%) than previous studies. Organic matter emissions in *Cao et al*. [2006] are higher than those of the other studies due to the use of different emission factors. *Klimont et al*. [2009] estimates for BC are higher by about 15% than *Streets et al*. [2003b] and global inventories but lower than *Zhang et al*. [2009b]. While comparing total emissions for China yields in general fairly good agreement across the studies, there are significant sectoral shifts resulting primarily from uncertainties in coal versus briquette use in the residential sector and assumptions for the brick-making sector. For example, *Zhang et al*. [2009b] and GAINS use comparable assumptions for coal, while *Klimont et al*. [2009] assumes more briquettes, leading to lower emissions from this sector in *Klimont et al*. On the other hand, for brick making both *Zhang et al*. and *Klimont et al*. rely on *Bond et al*. [2004] emission factors and estimate higher emissions than GAINS, which considers anecdotal evidence about the transition in this industry that leads to significantly lower emission factors.

4.7. Major Sources of Uncertainty in Emissions

4.7.1. Energy-Related Combustion

[213] As discussed in section 4.6, large differences between emission estimates are attributable to a few choices regarding emission factors made by inventory developers. Some of the diversity is not supported by measurements at emission sources, while other disagreements reflect true uncertainty in knowledge. A bottom-up estimate of uncertainty is about a factor of two using either a simple uncertainty combination for global emissions [*Bond et al*., 2004] or a Monte Carlo approach for individual countries [*Lu et al*., 2011].

4.7.1.1. Activity Data

[214] For fossil fuel combustion, activity estimates for many inventories in Table 10 have the same source (International Energy Agency (IEA), or United Nations fuel-consumption data), although many inventory developers adjust these data when inconsistencies are found or when finer allocation of activities is required (e.g., road and off-road vehicles or vehicle type). For several larger countries, regional statistics are also available and using them allows for better spatial resolution; however, national and international statistics are not always consistent. Finally, some models chose to use data sets specifically developed for particular projects. For example, GAINS often uses national fuel-consumption estimates for most of the European countries, China, India, and Pakistan. These may differ from IEA statistics, especially with regard to sectoral allocation. Total fuel consumption can be affected by the use of regional information on the calorific value of fuels.

[215] Consumption of residential solid fuels, especially biofuel, is not well constrained. Biofuel consumption data are frequently drawn from disparate sources. For example, GAINS relies on IEA and national data, while SPEW uses the tabulation of *Fernandes et al*. [2007]. Fuel production and sales are not centralized in this sector, and many fuels are collected by the consumers or by small sellers. Activity data are therefore much more uncertain than for liquid or gaseous fuels or consumption in large installations. Estimates of fuel consumption are often based on per-capita consumption estimates multiplied by the number of people using solid fuels. Comparison of the residential biofuel consumption for the past years in India and China [*Streets and Aunan*, 2005; *Venkataraman et al*., 2005; *Ohara et al*., 2007; GAINS] shows significant differences, typically ranging within about ±25%.

4.7.1.2. Emission Factors

[216] Emission rates of both BC and organic carbon depend on the combustion process, including fuel composition, flame temperature, mixing between fuel and air during combustion, and post-combustion treatment of the exhaust. Carbonaceous aerosols can be destroyed if the exhaust is kept hot and well mixed with air. Large, properly operating combustors, such as power plants and some modern installations using biofuel, tend to achieve this burnout, resulting in little emitted BC. Mixing between fuel and air before combustion also limits BC formation, so that gasoline engines emit much less BC than do diesel engines. Finally, BC may be removed through end-of-pipe controls that capture fine particles, as it is in particulate filters after diesel engines.

[217] The strong dependence of BC emissions on combustion processes means that the disaggregation of activity to represent combustion quality explicitly is an important component of inventories. The dependence also demands the development of emission factors under realistic operating conditions. Because most sources have several operating modes, it is important to obtain emission factors by measuring during a realistic sequence. This sequence of conditions may be called "driving cycles" for vehicles, or "burn cycles" for stoves, small boilers, or open combustion. Although design of existing cycles seeks to represent real-world operation, unrealistic choices of operating conditions may yield emission factors that are poorly representative. For example, very cold conditions or startup phases, which promote poor efficiency and high emissions, may be omitted from vehicle and stove emission testing or tests may not include the poorest quality fuels.

[218] Uncertainties are particularly acute outside the United States and Europe. A few measurements are becoming

available, but the limited number of studies has not dispelled concern that the highest emitters have been missed or significantly underrepresented.

[219] 1. *Diesel engines*. There is a good understanding of on-road emissions from normal vehicles in developed countries, although questions exist about how in-use vehicle emissions compare with those from tests in laboratories because of differences in driving conditions. Both averages and ranges of vehicle emissions in developing countries are not well quantified. Compared with on-road engines, there are many fewer measurements of off-road equipment, including engines used for agriculture and construction. A large uncertainty in determining total emissions is the contribution of poorly functioning vehicles with very high emissions, or "super-emitters." The fraction of such vehicles and their emission factors are not well known, and these assumptions result in major discrepancies between inventories, because a single super-emitter can produce many times more BC than a properly operating engine with an emission control system. Super-emitters are likely to be more widespread in developing countries, but data on the fraction of vehicles with such high emissions are extremely limited.

[220] 2. *Industrial solid fuels*. Emission estimates from the industrial sector are dominated by small, simple kilns in traditional production processes and old boilers. Activity data and emission factors for these sources are particularly difficult to obtain. Magnitudes and composition of emissions are the most uncertain of any of the major source categories due to lack of measurements.

[221] 3. *Residential solid fuels*. Although the residential sector is highly heterogeneous with regard to the types of fuels and devices used, a relatively small number of emission measurements have been made and many of these are from laboratory rather than in-use measurements. Limited data on emission magnitudes and composition are available to characterize this sector.

4.7.1.3. Summary of Uncertainties in Energy-Related Emissions

[222] Major contributors to uncertainty in BC and OC emissions from energy use are (1) measured particle emission factors obtained under laboratory conditions (i.e., rather than in-use or in-field) for residential combustion, traditional industry, and vehicles with high emissions due to malfunction; (2) speciation of PM from high-emitting technologies into BC and OC; (3) quantification of individual emitters in sectors that contain even a small fraction of highly polluting devices; and (4) amounts offuel burned in sectors where fuel and output are not formally monitored and tabulated. While most of the estimates tabulated here are given for the year 2000, rapid economic growth in countries with large BC emissions may have caused energy-related BC emissions to increase dramatically over the last decade. The year used for the inventory estimate is important when comparing atmospheric models with observations.

[223] In addition to the factors that affect total emission quantities, the location of emission may be poorly known for sources such as small industry and passenger or freight vehicles. These inaccuracies affect comparisons between measured and modeled concentrations.

4.7.2. Open Biomass Burning

4.7.2.1. Burned Area

[224] Considerable uncertainties remain in the quantification of burned area. Current satellite retrievals cannot detect burn scars much smaller than 1 km^2, and the size of the burned area is sometimes wrongly determined. Active fires can be detected when they are larger than about 0.1 ha, but many fires cannot be observed during their flaming stage because of incomplete coverage of satellite orbits or clouds obscuring the scene. Given the current resolution of satellite instruments that are used for burned area retrievals (typically 0.25 to 1 km^2 at the sub-satellite point and 5 to 10 times larger at swath edges), only burn scars with a size of at least 12 to 40 ha can be detected from space. Field data and satellite retrievals of fire radiative power [*Wooster et al*., 2005] show that the majority of fires are smaller, particularly in tropical regions [*cf. Schultz and Wooster*, 2008]. Uncertainties arising from the limited spatial resolution of current instruments could be as large as −30% to +40%, but in reality, they are smaller due to compensating errors. Validation of individual fire scenes from the MODIS burned-area data set with high-resolution Landsat data indicates that burned areas are probably underestimated by about 10% on average (M. Wooster, personal communication, 2009).

4.7.2.2. Fuel Load and Combustion Completeness

[225] Field studies, such as those in the savanna regions of South Africa [*Shea et al*., 1996] or in boreal North America (summarized by *McKenzie et al*. [2007]), reveal that fuel loads can easily vary by a factor of 3–20 within a region of limited ecosystem diversity. This uncertainty is consistent with estimates of fuel load derived from analysis of satellite data [*Ito and Penner*, 2004]. Combustion completeness strongly depends on the weather conditions because bulk fuel, which constitutes a large fraction of fuel mass in wooded ecosystems, burns only when the fuel is sufficiently dry and when it is windy. Uncertainties in vegetation modeling for calculation of available fuel load and combustion completeness are highest in deforestation regions and in regions where peat fires occur [*van der Werf et al*., 2006] (e.g., Southeast Asia) where problems in modeling the combustion of organic soil layers containing peat leads to an uncertainty of about a factor of 5. In some regions, like southern hemisphere Africa, models incorrectly predict seasonality, with peak emissions in bottom-up estimates occurring about 1–2 months earlier than the peak in satellite-detected AOD [*van der Werf et al*., 2006]. This is attributed to an increase in emissions as the fire season progresses, caused by a shift from grassland fires early in the dry season to woodland fires later in the dry season, associated with different fuel moistures and burning behaviors. Ecosystem modeling frameworks are moving toward capturing such temporal variations. Assuming that errors in fuel load estimates are uncorrelated across different regions, the global uncertainty in fuel load densities would be substantially lower than the variance encountered in individual field studies but greater than the 50% model diversity reported by *Knorr et al*. [2012]. Our conservative estimate of the global uncertainty caused by fuel load densities and combustion completeness is a factor of 2.

4.7.2.3. Emission Factors

[226] As shown in section 5.5, current models of the atmosphere underestimate absorption aerosol optical depth (AAOD) in Africa and Latin America, which are major biomass burning regions [*Koch et al*., 2009b]. Some of the extra absorption in Africa could be caused by dust, but an explanation is needed for the underestimate in Latin America. The underestimate could be caused by low biases in burned area or fuel loads (see above), but inverse models [*Arellano et al*., 2004; *Arellano et al*., 2006; *Stavrakou and Müller*, 2006] indicate little bias in carbon monoxide (CO) emissions from biomass burning in these regions. The remaining suspects are fire emission factors, the relationship between emitted mass of BC and optical absorption in fire plumes, or incorrectly modeled aerosol lifetimes.

[227] Although biomass burning is a large component of global BC emissions, particulate and BC emission factors for this source are poorly constrained. As discussed in section 3, measurements of BC depend on the analysis method. These method-dependent biases are more critical for biomass-burning emissions than for other sources, because these emissions pyrolyze and also contain materials that catalyze BC emission. The comprehensive literature review of *Andreae and Merlet* [2001] has become widely used, in particular for the compilation of global inventories [e.g., *van der Werf et al*., 2006; *Schultz et al*., 2008]. However, this review included only values based on thermal oxidation techniques and excluded optical absorption measurements. Even the highest BC emission factor in *Andreae and Merlet* [2001] is lower than values inferred from absorption measurements, which have been used in other studies [*Patterson and McMahon*, 1984; *Liousse et al*, 1996; *Chin et al*., 2002; *Liley et al*., 2003]. In part due to higher emission factors, *Liousse et al*. [2010] estimated African biomass burning emissions that were about 2.5 higher than GFED. *Martins et al*. [1998a] showed that thermal oxidation measurements underestimated BC mass, leading to unrealistically high MAC_{BC} values. Therefore, it is possible that the use of imperfect thermal methods yields BC emission factors that are too low.

[228] Comparisons between chemical and optical measurements would increase confidence in biomass-burning emission factors for BC. A review by *Watson et al*. [2005] showed differences of up to a factor of 7 between different BC field measurements and discussed the various uncertainties related to both thermal and optical measurements. In contrast to *Martins et al*. [1998a], thermal measurements did not always yield lower BC mass estimates than absorption measurements.

[229] Representativeness of measured emission factors is another concern. Open fires have a high inherent variability. Some emission factors and characteristics are inferred from small, better-controlled fires in laboratory settings. The combustion intensity and the burning and airflow characteristics of these small fires may differ from those of fires in the real world [*Reid et al*., 2005]. Oxygen-rich flaming combustion is generally associated with more BC and more heat release, while lower-temperature smoldering fires have higher overall particulate matter emission factors and CO emissions than flaming fires [*Lobert et al*., 1991; *Ward et al*., 1992; *Yokelson et al*., 1997]. If a sample is dominated by emissions from one of these phases, then ratios of BC to total PM, or BC to CO, do not represent the overall emission profile.

[230] The relationship between emitted mass of BC and absorption of the fire plume can be biased because of aging processes. As smoke ages, organic material condenses, but no further BC is created. BC/PM ratios in aged plumes are lower than those in fresh plumes, and single-scattering albedos are higher (more scattering relative to absorption). Emission ratios are generally determined in fresh smoke plumes, while models are evaluated with data from long-term regional averages, which are mostly of aged aerosol. If the relatively low BC ratios are then applied to fresh plumes, either BC emissions or absorption by BC could be underestimated.

[231] Data are presently insufficient to support firm conclusions about what updates should be made to BC emission rates from open burning of vegetation. However, thermal measurements may underpredict absorption, and using regional-average optical properties as constraints could also underpredict absorption at the time of emission. This body of evidence suggests that current emission factors from biomass burning might be biased low. Based on the data from *Andreae and Merlet* [2001], we estimate the lower uncertainty of BC emission factors to be a factor of 0.6 multiplied by the central value. Our estimate for the upper bound is a factor of 4.

4.7.2.4. Summary of Uncertainties in Open Burning Emissions

[232] The dominant uncertainty term for open burning emissions is the emission factor (error range: factor of 0.6 to 4). Fuel load and combustion completeness are uncertain by about a factor of 2, while burned area is probably known within 10% on the global scale, although regional differences can be larger (cf. auxiliary material of *Schultz et al*. [2008]). Neglecting the independent error estimates from agricultural waste burning and assuming that errors are independent, error propagation yields an uncertainty range of a factor of 0.29 to 5. Based on the emission estimates in section 4.4, bottom-up uncertainty ranges are 740 to 12,800 Gg yr^{-1} for BC, and 8400 to 144,000 Gg yr^{-1} for POA. These ranges are quite asymmetric.

4.8. Trends in BC Emissions

[233] *Novakov et al*. [2003], *Ito and Penner* [2005], *Bond et al*. [2007], and *Junker and Liousse* [2008] all estimate large changes in BC emissions during the industrial era. All of these studies demonstrate that BC emissions are related but not directly proportional to fuel consumption. Typically, emission rates become greater as population and economic activity increase and then decrease as cleaner technology is deployed. The resulting trend is an emission increase followed by a decrease and is broadly consistent with measurement records downwind of industrializing countries [*McConnell et al*., 2007].

[234] This discussion has focused primarily on the situation in the year 2000, but historical trends suggest how emissions may have changed since the year 2000 and how they will continue to change (see also section 13.5). In regions where emission factors decrease faster than fuel consumption is growing, BC emissions and concentrations decline. *Murphy et al*. [2011] observed a 25% decrease across the United States between 1990 and 2004, and *Bahadur et al*. [2011] found a 50% decrease over a similar period in California, a state with more stringent standards. Ice-core measurements in Europe [*Legrand et al*., 2007] also indicate a decrease in BC deposition since the 1970s. In contrast, when growth is rapid and

clean technology has not yet been implemented, BC emissions and concentrations rise. *Lei et al*. [2011] suggests a 30% increase in Chinese BC emissions between 2000 and 2005. *Lu et al*. [2011] conclude that Asian BC emissions increased strongly since 2000, with emissions from the largest contributors, China and India, growing by about 40%. Increasing BC deposition is recorded in Himalayan ice cores [*Ming et al*., 2008], although more measurements would help constrain the high spatial variability in deposition in this region.

[235] Besides increases in fuel use and decreases in emission factors, other trends in fuel use affect net emissions. Cleaner fuels are chosen because of environmental regulations. Households switch to more convenient fuels as income rises, and those fuels tend to be cleaner. Fuels may be adopted for different uses (e.g., energy production from agricultural waste).

[236] Historical records of charcoal deposits and anecdotal evidence suggest a decline of global emissions from open burning between the end of the nineteenth century and present day, with strong regional differences [*Moulliot and Field*, 2005; *Power et al*., 2008; *Marlon et al*., 2008]. These changes have been attributed to the expansion of intensive grazing, agriculture, and fire management [*Marlon et al*., 2008]. Fire records from North America suggest that fire severity, and hence carbon loss, increased during the last three decades [*Turetsky et al*., 2010]. This is consistent with climate model simulations indicating that fire activity will increase in the future because of increased temperatures and reduced rainfall [*Pechony and Shindell*, 2010; *Liu et al*., 2010]. However, there have not yet been estimates of BC emissions from future increases in open burning.

4.9. Receptor Modeling to Evaluate Source Contributions

[237] Most BC is emitted from sources that are either small and numerous or large but episodic, so monitoring data for individual sources are not available to validate emission inventories. The quality of emission inventories and the contributions of dominant sources can be determined only by inferences drawn from atmospheric measurements. The use of measured atmospheric chemical composition to deduce the influence of emission source types is generally known as *receptor modeling*. Another type of study that uses the magnitude and spatial distribution of atmospheric constituents to infer emission source strengths is called *inverse modeling*. The latter type of study requires atmospheric measurement networks, which are discussed in section 5.4. A discussion of inverse modeling results is given in section 5.5. In this section, we summarize information from receptor studies that have used chemical composition to identify particular source categories.

[238] Receptor methods based on the chemical composition of particles include examining the ratios of target chemical compounds, such as isotope ratios measured in time-averaged aerosol samples [*Gustafsson et al*., 2009] or in single particles [*Guazzotti et al*., 2003]. Other approaches use an expanded suite of chemical species to elucidate additional sources, including elemental and ionic composition and organic and elemental carbon [*Watson et al*., 1994] and additional organic molecular markers [*Schauer et al*., 1996; *Zheng et al*., 2002]. A limitation common to all receptor models is the inability to distinguish sources whose emissions have a very similar chemical composition.

[239] Among receptor models, the chemical mass balance model [*Friedlander*, 1973; *Watson et al*., 1984; *Chow and Watson*, 2002, *Watson et al*., 2002] and positive matrix factorization [*Paatero*, 1997; *Hopke*, 2010] have seen wide application in air quality assessment. Receptor modeling may also exploit ensembles of atmospheric trajectories [*Ashbaugh et al*., 1985]. The outcome is the identification of the pollution source types and estimates of the contribution of each source type to the observed concentrations. Elemental carbon (as measured by thermal techniques) is often used as a tracer of certain emission sources. As discussed in section 3, this measurement may not be equivalent to light-absorbing carbon. However, it is referred to as BC in this section for congruency with other sections.

4.9.1. Receptor Modeling in Urban Areas

[240] Table 11 summarizes source apportionment studies conducted to determine the sources of particulate matter pollution, usually in urban areas. The most detailed information exists in the United States, based on measurements from the U.S. Environmental Protection Agency's network of speciation samplers. Source contributions shown are specific to BC, in decreasing order of influence. For United States urban areas, it is possible to separate approximately 6–10 major sources of BC, including diesel, gasoline, biomass, residual oil, and local traffic. Several other sources also contribute to BC concentrations, depending on the location: steel mills, railroad emissions, and metal processing facilities.

[241] For Europe and other world regions, no separate apportionment of BC has been done. Instead, reviews [e.g., *Viana et al*., 2008; *Johnson et al*., 2011b] were used to identify the largest contributors to the mass of particles smaller than 2.5 μm diameter ($PM_{2.5}$). Major sources of BC are also major sources of $PM_{2.5}$, but the converse is not always true; major sources of $PM_{2.5}$ may produce little BC if their emissions are primarily inorganic. Sources that are BC and OC emitters are shown in the table. Resuspended dust, secondary pollutants like sulfate and nitrate, or sea salt, could also be contributors to $PM_{2.5}$ at some locations but are not included in Table 11.

[242] Globally, BC from gasoline combustion is only about 10% that from diesel (Table 8), but in the urban atmosphere, this source may constitute a significant fraction of particulate emissions. There are considerable problems in separating emissions from diesel and gasoline vehicles. For example, *Shah et al*. [2004] showed that slow-moving and stop-and-go diesel vehicles emit organic and elemental carbon in patterns that are very similar to those of gasoline powered vehicles. Thus, their mass contributions of diesel engines might be mis-allocated to gasoline engines. In a growing number of urban centers, especially in the developing countries like India and Bangladesh, *Guttikunda and Jawahar* [2012] showed that a significant fraction of BC emissions also originate from the brick kilns surrounding the city administrative boundaries, which consume a mix of coal, agricultural waste, and bunker fuel (in coastal cities).

[243] For European urban areas, the main sources of BC are vehicles, oil or solid-fuel combustion, and industrial and shipping emissions. Emissions from burning of biomass or biofuel were originally reported to be significant only in Denmark and Spain. Later, this source was shown to contribute relatively large fractions in rural and even urban areas [*Szidat et al*., 2006; *Alfarra et al*., 2007; *Puxbaum et al*.,

Table 11. Major Sources Contributing to Urban BC (USA) and PM2.5 (Other World Regions)[a,b]

Region	Sources	Cities	Sample References
North America	TR, IN, SA, RE	Anchorage, Atlanta, Baltimore, Buffalo, Burlington, Camden, Chester, Chicago, Cleveland, Detroit, Dover, Elizabeth, Indianapolis, Los Angeles, New Brunswick, New York City, Portland, Rochester, San Jose, San Diego, Seattle, St Louis, Wilmington	*Chen et al.* [2010b]; *Sheesley et al.* [2010]; *Zhou et al.* [2009]; *Watson et al.* [2008]; *Gildemeister et al.* [2007]; *Kim and Hopke* [2007]
Latin America	TR, IN, RE	Mexico City, Santiago, Sao Paolo	*Johnson et al.* [2006]; *Johnson et al.* [2011b]
Europe	TR, IN, SA	Areao, A Coruña, Ballinasloe, Birkenes, Skrealaden, Coimbra, Lisbon, L'Hospitalet, Milan, Gent, Waasmunster, Amsterdam, Dublin, Cork, Birmingham, Duisburg, Erfurt, Helsinki, Dresden, Huelva	*Viana et al.* [2008]; *van Dingenen et al.* [2004]; *Hazenkamp-von Arx et al.* [2004]; *Manoli et al.* [2002]; *Gotschi et al.* [2005]; *Houthuijs et al.* [2001]
Africa	OB, RE, IN, TR	Cairo, Oalabotjha, Addis Ababa (qualitative)	*Abu-Allaban et al.* [2002]; *Engelbrecht et al.* [2002]; *Etyemezian et al.* [2005]
East Asia	IN, RE, TR	Shanghai (TC), Beijing, Xi'an	*Song et al.* [2006]; *Zheng et al.* [2005]; *Cao et al.* [2005]
South Asia	TR, IN, OB, RE	Delhi, Mumbai, Kolkata, Chandigarh, Hyderabad, Dhaka, Rajshahi	*Chowdhury et al.* [2007]; *Johnson et al.* [2011b]
Southeast Asia	TR, IN, RE	Bangkok, Hanoi, Bandung, Manila	*Hien et al.* [2004]

[a]Estimated from receptor modeling, in order of decreasing importance. TR = transport (vehicle exhaust including gasoline and diesel); IN = industry including coal and oil and biomass burning; coal burning power plants; RE = residential energy; OB = open burning of biomass and refuse; SA = secondary aerosols; O = Others.

[b]In receptor modeling, quantity assessed is usually elemental carbon from thermal-optical analysis rather than BC. Here, the major sources of both substances are assumed to be the same.

2007] suggesting that this source was not discriminated in the earlier studies.

[244] Information on urban areas in other world regions is largely qualitative, because many studies in these regions did not measure the complete suite of pollutants used for receptor modeling. Furthermore, they often use source profiles that were not locally measured and therefore may be unrepresentative [*Johnson et al.*, 2011b]. Table 11 shows that in Latin America, traffic, oil combustion, and small industry, including copper smelters, are important sources of fine particle mass. *Mugica et al.* [2009] attributed 42% of fine particulate matter in Mexico City to vehicles, but they were unable to separate wood burning due to their similarity with diesel sources. In Africa, open burning of biomass and refuse, residential coal combustion, and traditional industries (brick making, lead smelters, and foundries) are significant contributors. In East Asia, coal burning industries are dominant sources followed by traffic and biomass burning. Residential coal burning is a large wintertime contributor. In Southeast Asia, traffic is the dominant source in more urbanized locations, while local burning (for cooking and brick making) is important in less urban locations. In South Asia, traffic and burning of refuse and biomass are important sources, followed by industrial sources. Brick kilns are important in some locations, while lumped small industrial sources contribute 10 to 30% of fine particle mass. Overall, where traffic is an important source, an aging motor vehicle fleet containing high emitters is of concern. Coal and biomass combustion for residential cooking and heating and small-scale industrial applications is widespread, likely under poor combustion conditions.

4.9.2. Receptor Modeling in Continental Plumes

[245] Urban studies constrain sources that affect cities, but many emissions, such as residential solid-fuel burning or agricultural use of diesel engines, occur preferentially outside urban areas. Source apportionment studies have been applied to carbonaceous aerosol in the continental plume from South Asia. *Novakov et al.* [2000] suggested that fossil fuel was responsible for 80% of the BC in the continental outflow, while studies in Dhaka [*Salam et al.*, 2003] indicated a negligible contribution of biomass burning in South Asian cities. However, these findings relied on ratios between total carbon and BC that are representative of open biomass burning but not biofuel burning. Studies that do consider differences between emissions from biomass and biofuel burning estimate an approximately equal contribution of biofuel and fossil fuel [*Stone et al.*, 2007]. In continental outflow, a strong biofuel influence on total carbonaceous particles is indicated by single-particle measurements (74%) [*Guazzotti et al.*, 2003] and radiocarbon measurements (66%) [*Gustafsson et al.*, 2009]. In Indian cities, fossil fuel burning dominates fine particulate matter concentrations, but biofuel burning is not negligible, according to organic marker studies [*Chowdhury et al.*, 2007]. Fossil fuel and biofuel burning contribute 20 to 60% and 7 to 20%, respectively.

4.9.3. Summary of Findings From Receptor Modeling

[246] Results from receptor modeling agree qualitatively that major BC sources identified by global or regional emission inventories are similar to the major sources of fine particulate matter. Traffic is the largest source in North and Latin America and Europe, and contributions from residential solid-fuel burning and open burning are found in Asia and

Africa. This broad agreement lends confidence to the identification of the largest BC sources. However, receptor modeling of regional aerosols with specific source markers capable of resolving similar sources is needed before the approach can be extended beyond this qualitative assessment. Further examination of both urban and rural sources is required to constrain the dominant sources in continental plumes.

5. Constraints on Black-Carbon Atmospheric Abundance

5.1. Section Summary

[247] 1. Black carbon concentrations, like those of all short-lived species, are variable in space and time and are largest around source regions. Constraints on black carbon abundance are provided by in situ measurements of BC concentration and by ground- and satellite-based remote sensing of AAOD. Aerosol absorption inferred from satellite-based remote sensors is nearly global in coverage, but these data are less quantitative than ground-based data.

[248] 2. Ground-based remote sensing provides information on the atmospheric aerosol column burden and optical properties, which is directly relevant to radiative forcing. However, BC AAOD is inferred indirectly from these measurements. Aerosol can be sensed only when the sky is cloud free, absorption sensing has large uncertainties when aerosol loading is low, and the interpretation of BC amount is confounded by the presence of other light-absorbing aerosol in the column.

[249] 3. National and global networks of measurements are used to evaluate chemical transport models that provide estimates of BC surface concentrations (in situ monitoring) and column AAOD (ground-based remote sensing). Measurements are most sparse in some of the regions with the highest BC loadings: Africa and most of Asia. Measurements from field campaigns, which typically sample only one region over periods shorter than a year, can also be used to test processes within models more comprehensively but within a limited domain and time.

[250] 4. Comparisons with in situ observations indicate that many models simulate near-surface BC concentrations approximately correctly for North America and East Asia, have a slight high bias in Europe, and have a strong low bias in parts of Asia.

[251] 5. On the other hand, many model estimates of column BC AAOD over continents have a low bias in all regions. In many regions, this underestimate can be explained at least in part by the fact that these models do not account for aerosol internal mixing, and thus, their modeled mass absorption cross section (MAC_{BC}) is too low. However, even if this factor is taken into account, models would still underestimate AAOD in some regions.

[252] 6. Comparisons with satellite observations indicate that bottom-up estimates of aerosol emitted from biomass burning are too low by factors of 2–4, and emission estimates should be revised upward.

[253] 7. Airborne campaigns measuring vertical profiles of BC now allow for comparisons of vertically resolved concentrations away from continents. These measurements suggest that models overpredict BC in remote Pacific regions—on average by a factor of five—and that the overestimate is generally greatest in the upper troposphere. An exception is in the Arctic, where models appear to underpredict upper tropospheric BC. While concentrations in these regions are generally low, the large spatial area and bright underlying surfaces means the contribution of Arctic BC to globally averaged radiative forcing may be significant.

[254] 8. These combined results suggest that modeled removal of BC is an important source of model error. Further, inter-model comparisons indicated that differences between modeled BC concentrations and AAOD can only be attributed in part to differences in assumed emissions; differences in vertical transport and aerosol removal also play a large role, and MAC_{BC} differs between models.

5.2. Introduction

[255] The impact of BC on climate depends on its atmospheric abundance. Aerosol concentrations vary in space and time, and coverage by observations is insufficient to capture all such variations. Therefore, atmospheric models must be used to determine global concentration fields, and these models can be partially evaluated by comparisons with

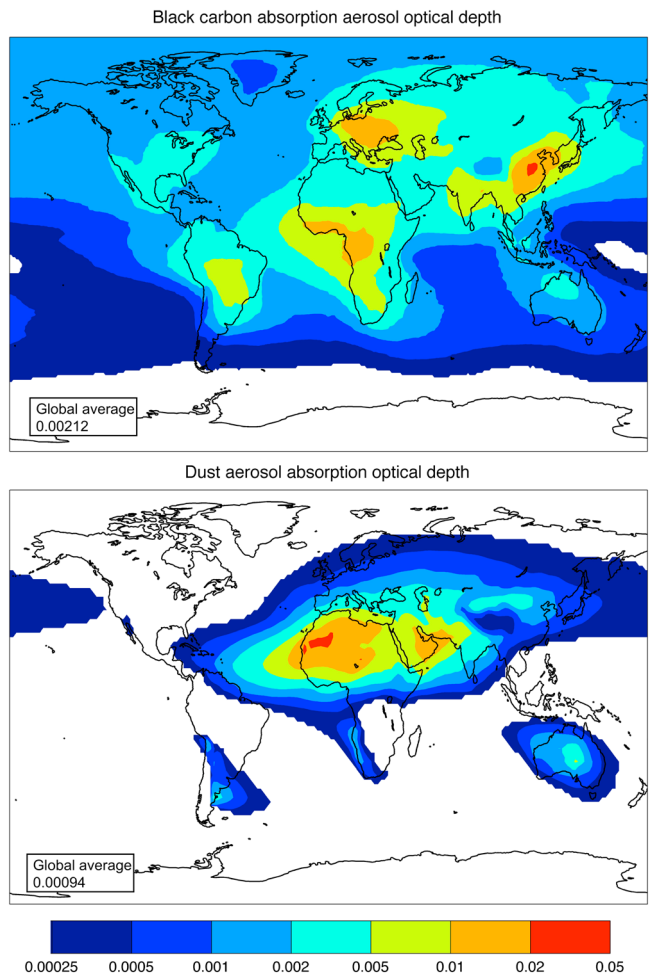

Figure 12. Aerosol absorption optical depth (AAOD) at 550 nm attributable to BC and dust. BC-AAOD fields are from the AeroCom median model fields [*Schulz et al.*, 2006] of all-source BC, including AAOD that would have been present before the pre-industrial era. Dust distribution is from *Luo et al.* [2003], with AAOD calculated from particle size in *Mahowald et al.* [2006] and optical properties in *Yoshioka et al.* [2007].

available observational data. Figure 12 shows modeled atmospheric absorption by two absorbing aerosols: BC and dust. The figure shows that BC, like all short-lived species, is most concentrated around source regions. For energy-related combustion, sources and concentrations are largest where population density is highest, as can be seen by comparing the east and west coasts of the United States, or Eastern Asia with Central Asia. Large BC concentrations also occur in and around biomass burning regions, especially South America and central Africa. Continental outflow also contains high concentrations, especially to the east of Asia and the west of Africa. Although BC is not well mixed throughout the atmosphere, some of it is carried to remote regions. Most energy-related BC emissions occur in the Northern Hemisphere, and BC is found in remote regions there, including in the deep Arctic. In contrast, there is very little BC throughout large remote regions in the Southern Hemisphere.

[256] Section 5.3 discusses atmospheric absorption and extinction by absorbing species. This section highlights the fact that if all absorption is attributed to BC, then concentrations of BC using measured absorption would be overestimated, especially in dusty regions. In section 5.4, we review measurements that report the spatial and temporal variation of BC concentrations. Section 5.5 examines how well global models simulate BC concentration over broad regions, and section 5.6 compares modeled vertical BC distributions with observations. These evaluations are used in section 6 to derive a best estimate of BC direct radiative forcing. Throughout this assessment, modeled BC concentrations are often drawn from an intercomparison project known as AeroCom (Aerosol Comparisons between Observations and Models) [*Kinne et al.*, 2006; *Schulz et al.*, 2006]. The AeroCom results described here reflect the first round of model experiments, known as Phase I.

5.3. Atmospheric Absorption and Extinction by Absorbing Species

[257] Section 3.4 discussed measurements of BC mass concentration (with units of g m^{-3}). Another measure of particle abundance, albeit indirect, is AOD, which is the vertically integrated extinction of aerosols in an atmospheric column. Aerosol light extinction and AOD values are given for a specific wavelength; small (submicron) aerosols have higher AOD at shorter solar wavelengths. For illustration, if we neglect losses of sunlight to molecular scattering by gases, an aerosol AOD of 1.0 at a given wavelength indicates that only 37% [e^{-1}] of the direct solar beam at that wavelength reaches the surface without being scattered or absorbed, if the sun is directly overhead.

[258] Of particular relevance for inferring absorbing aerosol amount is the column single-scattering albedo (ω_0), which relates the amount of light scattered to the amount attenuated (similar to equation (3.2)). The value of ω_0 is influenced by microphysical properties (section 3.7) and by compositional properties, which are quantified by refractive indices. These optical coefficients are usually determined through laboratory or in situ measurements. The fraction of AOD attributable to absorption, or AAOD, is

$$\mathrm{AAOD} = \mathrm{AOD} \times (1 - \omega_0) \tag{5.1}$$

where ω_0 denotes a column-averaged single-scattering albedo. For any species, the product of mass concentration (with units of g m^{-3}) and mass absorption cross section (MAC) ($m^2 g^{-1}$) is the absorption coefficient (m^{-1}). AAOD (dimensionless) is the result of integrating absorption coefficient over the entire atmospheric column and is the quantity shown in Figure 12. AAOD is more closely related to BC column abundance than AOD because BC is responsible for a much larger fraction of total absorption than of total extinction.

[259] As discussed in section 3, atmospheric concentrations of BC are often inferred from observations of absorption. Absorption measured in the atmosphere is attributable to all light-absorbing aerosols: BC, mineral dust, soil, and light-absorbing organic carbon (i.e., brown carbon) from combustion. If all AAOD is attributed to BC, then inferences of BC may be overestimated, especially in dusty regions. Measured absorption may also include contributions from nitrogen dioxide and ozone. The relative contributions of each component to AAOD are required to infer BC column abundance.

[260] Figure 12 shows that although the regions most affected by BC and dust are somewhat different, both species make significant contributions to globally averaged absorption, and in some regions, the contributions are equal. Dust has a much greater total AOD than does BC, but a smaller fraction of that AOD is absorption (i.e., ω_0 is larger), so globally averaged AAOD of BC and dust are of similar magnitudes at visible wavelengths.

5.4. Observations of Atmospheric Black Carbon Concentrations

[261] Monitoring studies provide information about BC concentrations in the atmosphere. These studies incorporate either in situ observations, in which sampled air is drawn into an instrument for measurement, or remote observations, which measure the intensity of light coming from the atmosphere, and from this infer information on the atmospheric distributions and properties of aerosols. In this section, we illustrate the contributions of different types of studies to the understanding of BC and other aerosol concentrations and properties (Table 12).

[262] Data gathered from intensive field campaigns or observational networks are subject to the limitations of the measurement techniques used, as discussed in section 3. Furthermore, when measurements are made at a single point, the measured values may not represent an average of the surrounding area, so comparisons between these point measurements and the average of a large model grid box should be done cautiously [e.g., *Tegen et al.*, 1997; *Vignati et al.*, 2010]. Thus, model simulations of the BC burden are evaluated by comparison with observations, which themselves may be biased. If the bias were known for each observation, or if it were the same for all observations, it might not affect our understanding of BC's life cycle, but this is not the case. Some biases may depend on aerosol age, source type, or location, and these relationships are poorly known.

5.4.1. In Situ Monitoring

[263] The in situ BC measurement techniques described in section 3, especially thermal-optical measurements on filter

Table 12. Observations That Contribute to the Understanding of Black-Carbon Distributions

Type of Monitoring	Spatial Coverage	Major Contributions
Intensive field campaigns	Single point, surface, or aircraft	In-depth examination of aerosol properties and transformation processes
In situ monitoring (includes networks)	Single point, surface	Long-term average aerosol concentrations, properties, and fluctuations in remote or urban locations
Ground-based remote sensing (includes networks)	Single point, column	Long-term averages and fluctuations of aerosol optical depth and inferences about other optical properties, often with unattended operation
Space-based remote sensing	Global coverage, column	Global coverage of aerosol optical depth, with limited information on properties

samples and optical measurements, have been employed in several intensive field campaigns (section 5.4.1.1) and in routine monitoring networks (section 5.4.1.2) at national or continental scales. The uses and limitations of these measurements are described in the following subsections, and inferences drawn from these measurements are discussed in sections 5.5 and 5.6.

5.4.1.1. Intensive Field Campaigns

[264] Multi-investigator field campaigns have examined the nature of atmospheric aerosol in many world regions. Such campaigns typically take place over the course of a few weeks and provide "snapshots" of regional aerosol. They often combine measurements from several platforms, beginning with heavily instrumented surface stations but also adding aircraft and shipboard platforms to measure vertical and horizontal distributions in continental plumes. Intensive campaigns provide information about aerosol composition, microphysical properties including scattering and absorption, and reaction rates. Because they incorporate large arrays of measurements, they provide a wealth of information on aerosol and gaseous precursors, and can often be used to evaluate some aspects of emission inventories. This type of observational approach generally has limited temporal and spatial coverage and, alone, does not provide the information required to determine the average influence of BC or other aerosols on climate. The value of this type of effort in the context of evaluating BC concentrations and climate impacts lies in the richness of simultaneous measurements that they provide. These studies provide detailed physical understanding for evaluation and the improvement of the modeling of aerosol processes.

[265] Examples of early field campaigns that studied carbonaceous particles included a mission to the Arctic [*Rosen et al*., 1984] and the search for the light-absorbing component in the Denver Brown Cloud [*Groblicki et al*., 1981]. Coordinated campaigns to study aerosol-climate interactions in particular regions began with the Aerosol Characterization Experiments (ACE) series of experiments [*Quinn and Coffman*, 1998; *Raes et al*., 2000], and these have frequently examined the outflow regions from major source areas [*Russell et al*., 1999; *Ramanathan et al*., 2001b; *Mayol-Bracero et al*., 2002; *Jacob et al*., 2003; *Huebert et al*., 2003]. Large field campaigns in more recent years have focused on aerosol evolution and properties in large regions with high aerosol loadings [*Bates et al*., 2005, *Querol et al*., 2008, *Zhang et al*., 2008a]. Equally intensive efforts have examined aerosol in urban areas or heavily source-influenced regions [*Watson et al*., 2000; *Neususs et al*., 2002; *Solomon et al*., 2003; *Cabada et al*., 2004; *Parrish et al*., 2009; *Wang et al*., 2010].

[266] Intensive field campaigns have provided information on emissions in addition to aerosol properties. Experiments to evaluate emissions from open biomass burning [*Lindesay et al*., 1996; *Kaufman et al*., 1998; *Eck et al*., 2003] have determined aerosol characteristics and emission ratios. Chemical and transport models have also been used in conjunction with measurements to evaluate regional emission inventories [*Rasch et al*., 2001; *Dickerson et al*., 2002; *Carmichael et al*., 2003; *Minvielle et al*., 2004]. The interaction between atmospheric models and campaign measurements can be iterative, as models have also been used to guide aircraft flights to intercept urban and biomass burning plumes.

[267] The long history of intensive measurements now allows analyses across many campaigns and pollutants. For example, *Clarke and Kapustin* [2010] combined aerosol and trace gas measurements from 11 campaigns to relate anthropogenic aerosol concentrations to concentrations of CCN, AOD, and CO. This type of relationship can be used to test modeled emissions and transport.

[268] One recent campaign relied on a single well-instrumented aircraft performing near-continuous vertical profiling over global scales in remote areas over a period of a few weeks [*Wofsy et al*, 2011]. The sampling approach of reaching both high northern and southern latitudes was repeated 5 times in different seasons, so the spatial and temporal coverage is greater than intensive field campaigns. This type of measurement, along with vertical profile measurements in a single location over several years [*Andrews et al*., 2011], can provide constraints on background aerosol loadings and removal processes. Here they are used to estimate biases in modeled vertical distributions of BC (section 5.6.1) and to correct biases in modeled BC forcing efficiency (section 6.6.1).

[269] Intensive field campaigns usually include both in situ and remote-sensing measurements from multiple surface (either land- or ship-based) platforms and from one or more aircraft, as well as integrating satellite remote sensing measurements. Research aircraft often fly over surface stations and ships, so measurements can be compared between platforms and used to determine vertical profiles of the full aerosol column. This rich set of data allows comparisons of different techniques for measuring BC and other aerosol properties and applications of the same technique in different environments [e.g., *Livingston et al*., 2000; *Schmid et al*., 2003;

Doherty et al., 2005]. Understanding of the applicability and limitations of each type of measurement is fostered by comparisons between properties measured at the surface, columnar properties measured by satellite-based remote sensing, and vertically resolved information from aircraft measurements [e.g., *Redemann et al.*, 2000; *Magi et al.*, 2003].

5.4.1.2. Long-Term In Situ Monitoring

[270] Long-term monitoring networks usually combine relatively simple measurement techniques with tens or even hundreds of stations to create a widely spaced network of observations that operate under uniform techniques. Surface sites may be influenced by orography and local sources, although such effects are usually considered when selecting sites. Because network sites are spatially sparse and have relatively simple data products, they do not provide the same level of insight into the fine details of aerosol processes as intensive field campaigns. However, they do provide valuable information on aerosol trends and broad spatial concentration patterns, and these long records contribute strongly to evaluation of the modeling of emissions, transport, and removal.

[271] Table 13 lists the major networks contributing information on aerosol absorption and BC concentrations. Continuous in situ measurements to monitor pollution levels were initiated as early as 1962 [*Novakov and Hansen*, 2004]. The IMPROVE network in the United States [*Malm et al.*, 1994] and the European Monitoring and Evaluation Programme network in Europe [*Kahnert et al.*, 2004] are among the most extensive and have historically focused on chemical speciation rather than on aerosol properties. Stations participating in the WMO Global Atmosphere Watch monitor aerosol properties relevant to climate, including light absorption, in a sparse, but worldwide, network of rural and remote sites that are predominantly operated in the EUSAAR- and NOAA-coordinated sub-networks. While they have achieved broad coverage within their regions, similar coverage is not available in many other world regions, such as South America and Africa. Monitoring stations are being developed throughout Asia [*Oanh et al.*, 2006; *Cao et al.*, 2007; *Ramana and Ramanathan*, 2006; *Marcq et al.*, 2010], although coverage is still poor.

[272] As multiple measurement locations are required to evaluate emissions, transport, and removal processes in global and regional models, measurements from all of these networks have been used for model evaluation [*Cooke et al.*, 2002; *Park et al.*, 2003; *Solmon et al.*, 2006; *Koch et al.*, 2009b]. Most national networks have rigorous quality control procedures that ensure comparability of their measurements among similar network stations. However, as discussed in section 3, important differences in sampling or measurement practices may affect comparisons between networks.

5.4.2. Remote Sensing

[273] Remote sensing methods measure changes in the amount of sunlight reaching the Earth's surface, or the amount of radiation leaving the Earth's atmosphere, rather than the actual atmospheric BC or aerosol content. Through a process known as *inversion*, the nature and quantity of aerosol is inferred from its observed physical effect on the light. The procedure is also called a *retrieval*, because aerosol properties are retrieved from observed changes in radiance. Radiance properties that may be measured include wavelength dependence, angular distribution, and polarization. These can be used to infer the columnar amount of aerosol, the average aerosol size, the presence of non-spherical particles (such as dust), and even estimates of columnar light absorption.

[274] Advantages of remote sensing are the multi-year nature of the measurements and the ability to obtain measurements without continuous maintenance. Remote measurements sense column properties of aerosol, rather than concentrations at the surface as are typically quantified by in situ measurements. Column properties are more directly relevant for quantifying climate impacts. The relationship between surface in situ observations and column data depends on many factors, including the stability of the boundary layer, the presence of atmospheric layers, and measurement conditions that affect in situ and remote measurements differently. When in situ measurements are made from an aircraft that profiles the depth of the atmosphere, however, robust comparisons with column-integrated remote sensing measurements are possible. Disadvantages of passive remote sensing include a lack of specificity to individual chemical species and an inability to retrieve the properties of aerosols in distinct layers independently, such as a dust layer overlying a pollution layer.

Table 13. Largest Global or Regional Ground-Based Observations Providing Long-Term Measurement Information Related to Aerosol Absorption or Black-Carbon Abundances in the Atmosphere

Network	Location and # of Sites	Dates	Products	Comments (Reference or URL)
AERONET	World 400+	1996–present	AAOD (column)	AOD*(1-SSA), less accuracy at lower AOD (http://aeronet.gsfc.nasa.gov/)
IMPROVE	US 100+	1985–present	Absorption coefficient, EC measurement (ground)	http://vista.cira.colostate.edu/improve/
EMEP	Europe 70	1989–present	PM and EC/OC (ground)	http://www.emep.int/
WMO/GAW	World 39 (EUSAAR 19 Europe, NOAA: 15 World)	1994–present	Absorption coefficient (ground)	http://www.gaw-wdca.org/ http://www.eusaar.net http://www.esrl.noaa.gov/gmd/aero
ABC	10	2004–present	Absorption coefficient, EC (ground)	*Ramanathan et al.* [2007] *Bonasoni et al.* [2010]
AIRPET	Asia 6	2001–2004+	EC/OC, BC by reflectance, $PM_{2.5}$ (ground)	*Oanh et al.* [2006]
CARIBIC	1 commercial aircraft	2005–Present	Impactor with single-particle carbon content	*Nguyen et al.* [2008]

[275] Information from retrievals may be used to infer the column burdens of chemical species that have distinctive physical or optical characteristics. However, many assumptions are required for these inferences, resulting in large uncertainties, especially at low optical depths (low concentrations). Furthermore, most remote sensing techniques can obtain valid data only in cloud-free conditions.

5.4.2.1. Ground-Based Remote Sensing

[276] The utility of ground-based remote sensing for constraining BC atmospheric abundance is similar to that of long-term in situ sampling. Networks of measurements can be combined to evaluate model performance, but they do not provide fine-scale or global coverage. However, unlike ground-based in situ measurements, they do measure the whole atmospheric column which is more directly relevant to radiative forcing.

[277] Passive, ground-based remote sensing with upward-looking sun or sky photometers can be used to estimate AAOD. AERONET is the largest global network of these photometers [*Holben et al*. 1998; *Dubovik et al*., 2002]. These instruments use information measured at multiple wavelengths and multiple angles by sun- and sky-photometers [*Dubovik and King*, 2000]. Properties derived from the sky radiance measurements include the aerosol size distribution, AOD, and refractive indices at four solar wavelengths; from this, single-scattering albedo can be determined. However, the retrieved refractive indices are obtained for the total aerosol. No distinction is made between the fine and coarse mode aerosol components, which are compositionally different and have different refractive indices. Thus, when both dust and BC are present in an aerosol column, the retrieved imaginary refractive index (which dictates aerosol absorption) does not accurately reflect that of BC alone.

[278] We have calculated values of BC AOD from retrievals of AAOD at AERONET sites and use these values in section 6 to produce a scaled estimate of BC direct radiative forcing. The process of extracting BC AAOD from total AAOD requires certain assumptions. Limitations in the derivation of AAOD and specifically BC AAOD are discussed next.

[279] First, AAOD values are overestimated by the averaged AERONET Version 2.0 data product. Values of AAOD are based on aerosol extinction optical depth and single-scatter albedo, and single-scatter albedo can only be retrieved reliably for rather polluted conditions. For this reason, the AERONET Version 2.0 values of AAOD are published only when AOD is greater than 0.33 at 550 nm. The exclusion of low-AAOD conditions introduces a significant sampling bias that *Reddy et al*. [2005b] estimate to be a factor of two. This issue, and its implication for inferred BC quantities, is explored further in section 6.5.1 and Appendix B.

[280] Second, not all solar absorption by aerosol is caused by BC; some is due to dust and some to organic matter. Dust is less absorbing per mass than BC, but its AOD is often much larger. The net effect is that global average dust AAOD is comparable to that of BC AAOD but differently distributed in space and time. Thus, the BC contribution to AAOD needs to be isolated to use AERONET absorption for model evaluation. Dust particles tend to be larger than BC particles, so retrieved size distribution data might be used to attribute absorption by super-micron particles to dust, and absorption by submicron particles to BC and light-absorbing organic matter. However, AERONET retrievals provide a single ω_0 and refractive index for the entire size distribution. Although this refractive index can be used to estimate AAOD of the total aerosol, the composition and, hence, the refractive indices and ω_0 of the separate fine and coarse modes may differ greatly [*Quinn and Bates*, 2005]. As a consequence, a method is needed to apportion AAOD among the two modes. Separating the sub-micron AAOD into contributions of organic matter and BC would require a further inference not based on size distribution. The spectral absorption properties of the total aerosol have been combined with assumptions about the wavelength dependence of absorption for dust, BC, and organic matter to estimate their contributions to AAOD [*Arola et al*., 2011; *Chung et al*., 2012].

[281] Third, sample biases may occur because AERONET AAOD retrievals are made only during daylight hours and in cloud-free conditions. Two potential sources of bias oppose each other. Clear conditions can be expected to favor larger concentrations and column burdens of BC because fires are more likely and because scavenging by clouds (i.e., the primary removal mechanism for BC) cannot occur under clear skies. To estimate biases in retrievals of BC AAOD, we averaged modeled BC AAOD at AERONET locations only during days when AERONET retrievals were possible. Bias was determined by comparing with the average BC AAOD. For four AeroCom models, biases were regionally dependent, but the average was only 1%. This is consistent with a small global clear-sky bias in AOD found by *Zhang and Reid* [2009]. Another factor is that solar absorption by BC is enhanced when BC is coated by water, which may be much more likely in the vicinity of clouds. The model of *Jacobson* [2010] estimated solar absorption enhancement to be a factor of 2 to 4, depending on the size of the BC particle. Clear-sky measurements, which exclude partially cloudy scenes, likely miss this near-cloud absorption enhancement. To explore this sensitivity, we used the GATOR model [*Jacobson*, 2010], the only aerosol model that treats the full effect of optical focusing on absorption, to compare the AAOD for clear-sky versus all conditions. Although the global mean MAC_{BC} for cloudy conditions (14.4 m^2g^{-1}) was higher than that for clear-sky (13.9 m^2g^{-1}) conditions, the global mean burden was greater by 35% and BC AAOD was 20% higher for clear sky conditions than for cloudy conditions, so it is unlikely that AERONET observations are missing large enhanced absorption under cloudy conditions. However, this finding is not specific to AERONET sites or days of retrieval.

[282] A method to infer BC column mass loading is to determine the volume concentrations of components of aerosol mixtures required to fit the AERONET retrieved total column refractive index. These can then be used, along with assumptions about densities, to determine the column mass of each component, including BC [*Schuster et al*., 2005]. The BC column mass uncertainty is estimated at −15% to +40%, although the imaginary refractive indices used affect the retrieval and the AAOD. For analyses in this assessment, we use AAOD rather than inferred BC column loadings, as the former requires fewer assumptions.

5.4.2.2. Remote Sensing From Space

[283] Knowledge of BC concentrations is needed in regions with few or no ground sites, such as over oceans. Remote

sensing from space-borne sensors on satellites has near-global coverage and can, therefore, fill observational gaps in ground-based networks. AOD can be inferred from retrievals from satellite data, but the procedure also requires general assumptions regarding environmental properties (e.g., surface reflectance), and aerosol properties [*Torres et al*., 1998; *Levy et al*., 2007; *Kahn et al*., 2010], so that uncertainties are greater than those in ground-based sensing. Satellite-based instruments that provide data on column aerosol absorption and, therefore, information specific to constraining light-absorbing aerosol, are discussed below.

[284] The longest satellite data record on aerosol absorption, dating to 1978, is provided by the TOMS sensor (Total Ozone Mapping Spectrometer, http://jwocky.gsfc.nasa.gov/aerosols/aerosols_v8.html). The TOMS Aerosol Index is a retrieved quantity that indicates whether the column aerosol is largely absorbing or scattering. Over the last decade, TOMS-type retrievals have been continued with measurements from OMI (Ozone Measurement Instrument, http://disc.sci.gsfc.nasa.gov/Aura/data-holdings/OMI). This instrument senses reflection and its spectral variability in the ultraviolet region (UV) of the solar spectrum [*Torres et al*., 2002]. Aerosol retrieval at UV wavelengths has two advantages: first, surface contributions to the signal are small, especially over land, and second, small aerosols have stronger signals in the UV than at visible wavelengths. On the other hand, in addition to BC, both dust and organic carbon contribute to UV absorption. Another complication is a reduced sensitivity towards the surface, so that BC near the surface (approximately the lowest kilometer) may not be detected. Therefore, a separate estimate of the vertical distribution of aerosol is an essential element of the retrieval. In the past, the vertical profile of aerosol concentration was prescribed using estimates from global modeling; more recently, aerosol profiles inferred from the CALIPSO space-borne lidar have been applied [*Winker et al*., 2010]. Even with this constraint, this type of retrieval is mostly useful for identifying atmospheric aerosol from large events such as biomass burning [*Zhang et al*., 2005].

[285] Satellite-based aerosol sensors that provide spectrally resolved information allow general estimates of aerosol size and separate contributions from fine and coarse particles. Moderate Resolution Imaging Spectroradiometer (MODIS) sensors have the greatest temporal resolution [*Remer et al*., 2005]. Additional information on aerosol shape and difficult retrievals over bright surface come from polarization sensing (e.g., POLDER) [*Deuzé et al*., 2001] and multiple views of the same scene (e.g., Multi-angle Imaging Spectro-Radiometer (MISR)) [*Kahn et al*., 2009b]. Active remote sensing with a space-borne lidar (CALIPSO) [*Winker et al*., 2010] offers information on aerosol vertical distribution. This information may provide estimates of total aerosol amount, or even total fine-mode aerosol, but they do not constrain the amount of absorbing aerosol.

[286] The satellite-based MISR instrument [*Kahn et al*., 2009b] provides another constraint on aerosol absorption. The MISR instrument detects radiance at multiple angles and multiple wavelengths. This additional information is used to estimate surface radiance, and it allows inversion for additional aerosol properties, including estimates of aerosol absorption. The MISR standard retrieval algorithm identifies two to four classes of absorbing aerosol, rather than providing exact values of absorption. The atmosphere must be relatively uniform and cloud free, and the mid-visible AOD must be at least 0.15 or 0.2 [*Chen et al*., 2008; *Kahn et al*., 2009c].

[287] While all these satellite-based instruments provide some constraint on atmospheric absorption, several factors limit their utility in determining global, annual average BC AAOD. Signals reaching satellite-based sensors are influenced by both atmospheric constituents and by the reflectance properties of the Earth's surface. This increases the uncertainty in AOD and, especially, AAOD, particularly over spatially heterogeneous or highly reflective surfaces. Thus, quantitative atmospheric aerosol absorption cannot be retrieved from existing satellite-based sensors. Conversion of AOD to AAOD requires use of an assumed column aerosol single-scatter albedo, such as from a model [e.g., as employed by *Chung et al*., 2012]. Although satellite retrievals may infer the separation between fine and coarse particles, they cannot distinguish AOD from BC versus that from other fine mode aerosols like OA or sulfate. The division must be estimated either from the relative magnitude of modeled concentration fields or from ground-based observations. The relatively coarse resolution at which most satellite sensors can provide retrieved aerosol fields also makes them susceptible to cloud contamination. Finally, while polar-orbiting satellites have nearly global coverage, data coverage at any given location is limited and does not always allow for sufficient sampling for good statistics.

5.5. Comparison Between Modeled and Observed BC Concentrations and AAOD

[288] Estimates of forcing by individual aerosol species, including BC, are all based on aerosol distributions generated by global chemistry transport models (CTMs). Even estimates that incorporate observations require model results to expand concentration fields beyond observed locations or to separate observed aerosol influences among chemical species. Evaluation of BC concentrations in these models is therefore critical in assessing our understanding of climate forcing. A first-order evaluation of these models is accomplished by comparing either simulated aerosol concentrations or simulated optical depths with independent observations. This comparison requires long-term, spatially distributed aerosol measurements, so that observations from nationwide or global networks, such as the ones discussed above, are particularly useful.

[289] Comparisons between models and observations shed light on our understanding of the quantity of BC in the atmosphere, but they often cannot distinguish between various possible causes of model error. For example, a model could underestimate atmospheric concentrations if its emissions are too low or if its overall removal rate is too high.

[290] *Koch et al*. [2009b] evaluated the AeroCom suite of global models by comparing modeled BC concentrations with observations from several intensive campaigns and long-term in situ measurements. Figure 13 summarizes this comparison, showing the ratio between observed and modeled surface concentrations of BC. The figure shows that the median model predicts surface BC concentrations in the North America fairly closely, slightly overestimates BC in Europe, and clearly underestimates it in Asia. The

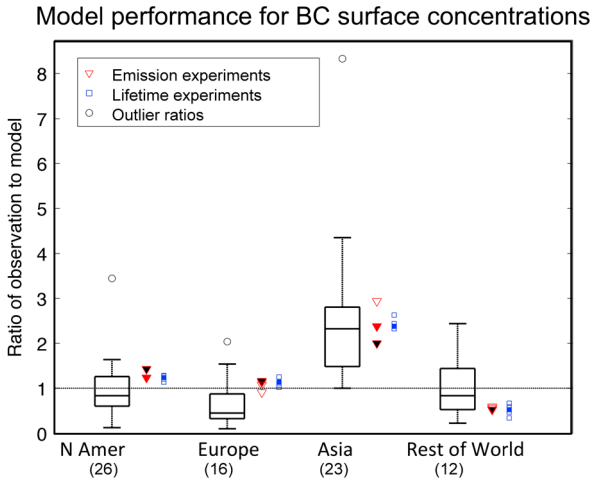

Figure 13. Evaluation of model performance and model sensitivities for simulating BC concentrations in surface air for specific regions and the rest of the world. Box plots show ratios between observations and models (i.e., the factor by which modeled values are multiplied to obtain observed values). The middle bar in each box shows the median model value. Box boundaries show 25th and 75th percentiles. Data points outside 1.5 times the interquartile distance from the box are marked as outliers; otherwise, they are included in the whiskers. Symbols show sensitivity experiments using different emission databases (red triangles) and removal rates (blue squares) in a single model (GISS) with the base case shown as filled symbols. For emission experiments, SPEW is shown with red fill and GAINS with black fill; unfilled symbols show results using two other emission databases. The number of surface observations is shown below each region name. Data from *Koch et al.* [2009b].

global annual average difference among models in this suite was about 30% of the median concentration; variations in individual seasons can be greater.

[291] *Koch et al.* [2009b] also compared modeled fields with values of AAOD inferred from AERONET. Modeled AAOD was lower than observed values in all regions. Column BC AAOD is the sum over altitude of the product of BC concentration and MAC_{BC}. Because most of the models used in the comparison do not represent internal mixing, the modeled MAC_{BC} (section 3.7) was underestimated. This bias could explain the disagreement in North America and Europe but not in other areas of the world. However, AAOD data were not separated into contributions from BC and dust. A refined analysis, which considers this separation and incorporates more AERONET stations, appears in section 6 and is more fully described in Appendix B.

[292] The sources of differences between model predictions are not completely understood. For any given location, the inter-quartile range of the concentrations predicted by the 15 models participating in AeroCom was a factor of about 3, and the range excluding outliers was a factor of about 5 [*Kinne et al.*, 2006; *Schulz et al.*, 2006]. *Koch et al.* [2009b] provided sensitivity experiments to explore the sources of this variability by using one model from the suite (GISS, shown as symbols in Figure 13). Simulations with different emission inventories are given in red, and concentrations with removal rates increased or decreased by a factor of 2 are shown as blue squares. Filled symbols indicate base-case results. Varying removal rates and emissions do cause significant variations in a single model, but these uncertainties do not explain most of the inter-model differences. *Textor et al.* [2007] also found that inter-model differences were only partially explained by differences in emission inventories. Large differences in modeled horizontal and vertical transport are largely responsible for the diversity. Once BC is lifted into the free troposphere, removal processes are slower, and its atmospheric lifetime may be extended.

[293] Figure 14 compares modeled and observed values of BC AAOD. The left panel shows BC AAOD inferred from AERONET observations (Appendix B). Although these values include absorption by organic matter, we use them as our observational estimate for BC AAOD. Section 11.4 discusses implications of this combination. Modeled BC AAOD from the 15 AeroCom models are shown in the middle panels of the figure. We use this particular collection because it contains a large number of consistent modeled fields, but this presentation excludes subsequent improvements in many of these models. The AAOD fields shown in Figures 12 and 14 are from the AeroCom "median model," for which a median of the local ($1° \times 1°$ grid resolution) values from all AeroCom models was calculated every month. These median fields, unlike averages, lose their additivity, but the use of median values excludes the influence of individual outlier models. Figure 14 also presents differences in BC AAOD between co-located AERONET and model median values, showing that these models tend to underestimate BC AAOD. The regional dependence of model biases are discussed further in section 6.

[294] The quantity and representativeness of observation sites is fundamentally important in interpreting comparisons between models and measurements. North America and Europe have the best coverage of all long-term measurement sites, followed by Asia. The number of sites is not in proportion to the strength of emissions, and concentrations in regions with large emissions and, therefore, highest aerosol forcing, are relatively poorly constrained.

[295] Remote regions with low concentrations also have few measurement sites and hence are also poorly constrained. Although aerosol forcing in these regions is small, their large spatial coverage means that contribution to the global-average forcing may be important. Compared with BC concentrations measured during a field campaign over the remote Pacific Ocean (Figure 15) [*Schwarz et al.*, 2010], the median model overpredicted remote BC concentrations by a factor of 5. Some models, such as the lower quartile of the AeroCom model suite or GATOR [*Jacobson*, 2012], show better comparisons with these remote measurements.

[296] *Koch et al.* [2009b] note that model diversity in atmospheric BC concentrations is particularly high for the Arctic. Models almost universally underestimated concentrations in the free troposphere during spring, and they did not match the observed decrease in concentrations from spring to summer. This finding is based on a very limited data set from intensive field campaigns, but it is consistent with multi-year observations from surface sites in the Arctic, which show that most models underestimate BC concentrations in the winter and spring and generally do not capture strong seasonal

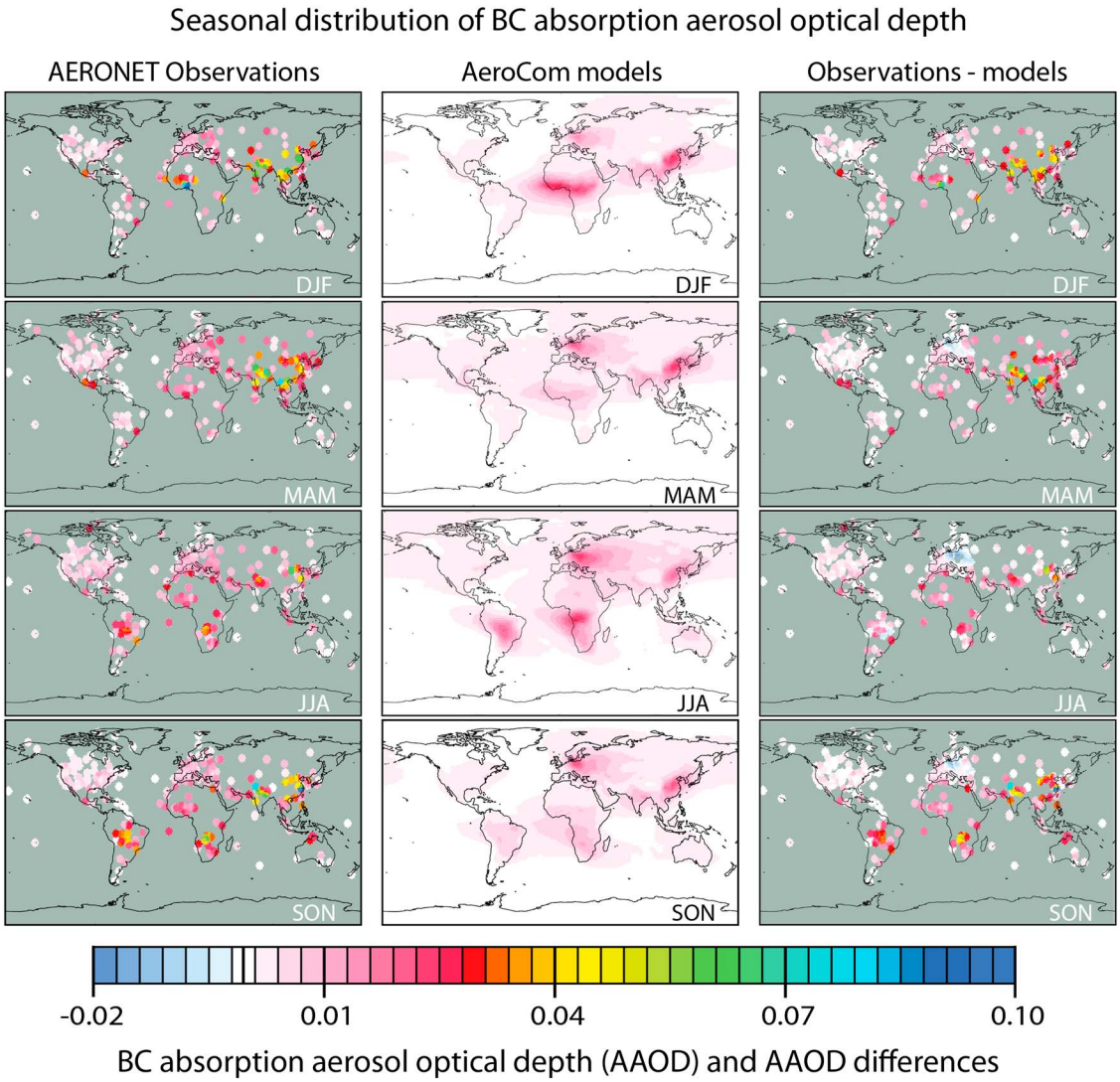

Figure 14. Seasonal absorption aerosol optical depth (AAOD) at 550 nm due to BC as inferred from observations and from models. The left panels show seasonal averages for BC AAOD at AERONET sites, as they were derived from sky-inversion data that were sampled during the last decade (2000–2010). Each symbol represents an AERONET site. The middle panels show seasonal BC-AAOD median maps of AeroCom models (listed in Table 14) for year 2000 conditions (see text for methods). The right panel shows differences between the BC-AAOD values inferred from AERONET observations (left column) and AeroCom modeling efforts (middle column) at each location, illustrating deficiencies in global modeling of BC.

variations in boundary-layer BC concentrations [*Shindell et al*., 2008; *Huang et al*., 2010; *Liu et al*., 2011].

5.5.1. Estimating Emissions by Integrating Models and Observations

[297] The comparisons between modeled and observed BC concentrations and column absorption described above are a first step in evaluating model performance. More detailed evaluations have been conducted, usually focusing on inferring the most likely sources of error. The simplest of these compare the temporal or spatial dependence of atmospheric concentrations with that given by models. More complex approaches use a mathematically strict evaluation of sources and sinks using a formulation of Bayes' theorem, which has been demonstrated for CO_2, CO, and aerosols [e.g., *Chevallier et al*., 2005; *Dubovik et al*., 2008; *Chevallier et al*., 2009; *Huneeus et al*., 2012]. Evaluation methods that use measurements of atmospheric abundance in combination with modeled fields are broadly called *inverse methods*. Inverse modeling of gaseous concentrations on continental scales, particularly CO and oxides of nitrogen (NO_x), can also provide information about emission sources. Although this technique has usually been applied to infer emissions, it should not be forgotten that model processes such as transport and removal can also contribute to errors and that the initial estimate of emissions has a strong influence on the inferred emissions. Here we summarize the results of inverse modeling studies that have focused on particular regions.

[298] 1. *North America*. An inverse model by *Hu et al*. [2009] found that USA BC emission estimates using data mainly from a rural network (IMPROVE) was about 30 to

35% lower than an estimate that also included urban sites. This implies that in order to constrain concentrations on continental scales, measurements in high-concentration areas should be included if models have sufficient resolution, and that this inclusion may affect the total continental burden of aerosol. There are also differences in the thermal evolution methods for measuring BC (section 3.3) between urban and rural sites in the United States. The former tends to use a transmittance-corrected thermal-optical method, while the latter corrects using reflectance and heats the sample to a lower temperature. Before performing an inverse estimate, these authors had to multiply the transmittance-corrected values by factors ranging from 1.7 to 2.6, depending on the season. The resulting emission estimates were similar to the bottom-up emission estimate in Figure 9. On the other hand, an inverse model by *Park et al.* [2003] estimated a BC emission rate of about 750 Gg yr^{-1}, which is about 70% higher than the bottom-up estimate.

[299] *Bhave et al.* [2007] used organic markers to show that USA emission estimates of total aerosol carbon (OC plus BC) from vehicle exhaust and biomass combustion were not biased. They did find a large unexplained source of total aerosol carbon unassociated with combustion, but this would not affect BC totals.

[300] Inverse modeling of carbon monoxide has indicated that inventories overestimate fossil fuel sources in North America by a factor of 3 in summer and two in spring [*Miller et al.*, 2008]. *Kopacz et al.* [2010] found a large underestimation especially in winter, ascribing this difference to heating and poor vehicle efficiency at cold temperatures. Although BC model results in the United States do not appear highly biased, these findings indicate that some small sources that could affect BC emissions are not well understood.

[301] 2. *Europe. Tsyro et al.* [2007] found that a model based on the IIASA inventory underestimated BC concentrations by about 20%. Significant overestimate and underestimate of BC were correlated with concentrations of levoglucosan, a tracer of wood smoke, indicating that biofuel or open biomass burning could be responsible for the difference. Modeled concentrations were generally too high in Northern Europe and too low in Southern Europe. Mobile source emissions were thought to be underestimated in Austria and some Eastern European countries.

[302] 3. *East Asia. Hakami et al.* [2005] used BC concentrations observed in field campaigns to constrain emission over eastern Asia. They found that the magnitude of the total emission inventory given by *Streets et al.* [2003b] did not change significantly as a result of the assimilation. However, anthropogenic emissions over southeastern China were reduced, while those in northeast China and Japan were increased. The increase in the industrialized regions is consistent with the low bias in estimates of CO emissions [*Kasibhatla et al.*, 2002; *Heald et al.*, 2004], which is more strongly associated with the more northern industrialized regions [*Yumimoto and Uno*, 2006]. The observed CO bias has been largely resolved by improving the fraction of small combustors [*Streets et al.*, 2006], as discussed in section 4.6.5. *Tan et al.* [2004] suggested that modeled particulate carbon emissions in East Asia should increase in order to be consistent with observations, but they did not separate BC and OC nor account for the formation of secondary organic aerosol, which could increase atmospheric concentrations. Studies that compare ground and aircraft measurements with modeled BC values over the East China Sea estimate an annually averaged BC emission flux of 1920 Gg yr^{-1} [*Kondo et al.*, 2011a], close to bottom-up emission estimates for the late 2000s. Inverse modeling of NO_x emissions in East Asia indicates rapid growth in high-temperature sources [*Kurokawa et al.*, 2009], although high-NO_x sources are presently a small part of the East Asian BC inventory.

[303] 4. *South Asia. Rasch et al.* [2001] estimated that increases of about 10 to 20% in fine-mode aerosols were needed in the model to match satellite observations over South Asia, but this study did not specifically identify biases in BC. *Dickerson et al.* [2002] suggested a BC emission rate of 2000–3000 Gg yr^{-1}, much higher than bottom-up estimates, based on atmospheric ratios of BC and CO that are much higher than is given by bottom-up estimates. *Menon et al.* [2010] also find that modeled concentrations in South Asia are much too low compared with in situ measurements.

[304] The inverse modeling studies discussed above rely on in situ data from a small number of sites to represent continental-scale concentrations of aerosols. Satellite measurements have much broader spatial coverage and could produce global emission estimates. This approach has been applied in biomass burning regions, where optical depths are large and seasonal. *Freitas et al.* [2005] found that emission estimates derived from observed AOD were larger than bottom-up estimates. *Zhang et al.* [2005] used aerosol index from the TOMS instrument to estimate BC from biomass burning as 5700 to 6900 Gg yr^{-1}, depending on the assumptions used, and total smoke (BC plus OM) emissions as 60,000 to 73,000 Gg yr^{-1}. *Reid et al.* [2009] estimated that bottom-up emission estimates of particulate matter from biomass burning need to be enhanced by factors of 1.5 to 3. The global emission flux derived for 2006 to 2008 was about 140,000 Gg yr^{-1}, as compared with the value of 30,000 to 44,000 Gg yr^{-1} BC plus POA given in section 4.4.4, if OA is assumed to be 1.4 times OC. Similarly, *Kaiser et al.* [2012] derived a global average enhancement factor of 3.4 for the OA and BC resulting from biomass burning, summarizing several other top-down studies that recommended emissions 2–4 times larger than the bottom-up estimates. These studies indicate that BC emissions from biomass burning should be much larger than represented in models, although they may not scale linearly with total aerosol emissions. However, the fraction of the discrepancy attributable to BC is uncertain. Formation of SOA may contribute to the observed OA and particulate matter loading.

[305] In summary, inverse modeling studies have produced inconsistent results for North America, indicating that either BC emissions are estimated well or are too low by 70%. European BC concentrations appear slightly underestimated. East Asian concentrations appear reasonable, especially after the addition of small combustors. Although observations are limited, measurements in South Asia suggest that concentrations are greatly underestimated there. All of the studies described have used single models and await further confirmation. On the other hand, there is a consensus that aerosol concentrations, including BC, may be too low in biomass burning regions. Considering also the likely bias in emission factors (section 4.7.2.3), emission

values that are greater than bottom-up estimates appear warranted.

5.6. Vertical Distribution of BC

[306] As discussed in sections 6 and 7, the vertical distribution of absorbing aerosol affects its forcing. Vertically resolved measurements below 8 km of the refractory aerosol concentration, which correlates strongly with BC concentration, have been carried out since the 1990s [*Clarke and Kapustin*, 2010]. Remotely piloted airborne sensors have measured optical properties and total aerosol absorption below 3 km [*Corrigan et al.*, 2008].

[307] BC vertical profiles extending through the troposphere have been made with a variety of measurement methods, but the development of the SP2 instrument (section 3.5) has allowed measurements of vertical profiles of BC in very clean air where they were previously unobtainable [*Schwarz et al.*, 2006, *Schwarz et al.*, 2010]. These profiles extend vertically from near the surface to the lower stratosphere, as shown in Figure 15. Although BC vertical profiles are quite variable, in polluted regions they generally show a declining BC mass mixing ratio from the surface to about 4 km altitude, and relatively constant values up to well above the tropopause. However, in remote regions influenced by the transport of pollution from source regions, BC loadings tend to peak in the free troposphere or above. BC that has been lifted above the low altitude ranges where aerosol removal is fast due to precipitation is more likely to have a longer lifetime in the atmosphere.

[308] Important BC properties, such as mixing state (section 3), also change with altitude. One set of vertical profile observations in the tropics indicates that the coatings of BC-containing particles become thicker and more prevalent with increasing altitude between the surface and the lower stratosphere [*Schwarz et al.*, 2008a]. The fraction of coated BC particles and the acquired coating mass depend on both the BC source and the history of the particle and the air it is contained in. Thus, MAC_{BC} (section 3.8) can be expected to depend on altitude.

5.6.1. Comparison Between Modeled and Observed Vertical Distributions

[309] Correctly modeling the vertical distribution of AAOD is important for calculations of direct radiative forcing, as discussed in section 6.6.1. *Schwarz et al.* [2010] compared the AeroCom set of models with a global-scale "snapshot" of SP2 BC measurements from remote locations (Figure 15). The AeroCom model ensemble captured the vertical trends of BC concentration in the southern mid to high latitudes, but in northern middle and equatorial latitudes, the models underestimated the decrease in concentration with altitude. This comparison in regions far from sources suggests that modeled removal of BC is an important source of error. However, the aircraft data in this comparison were obtained over a limited time range; in particular, the profile for the northernmost band (60–80°N) was from a single flight. *Koch et al.* [2009b] also compared BC vertical distributions between AeroCom models and SP2 measurements from several intensive field campaigns, mainly over North America and the

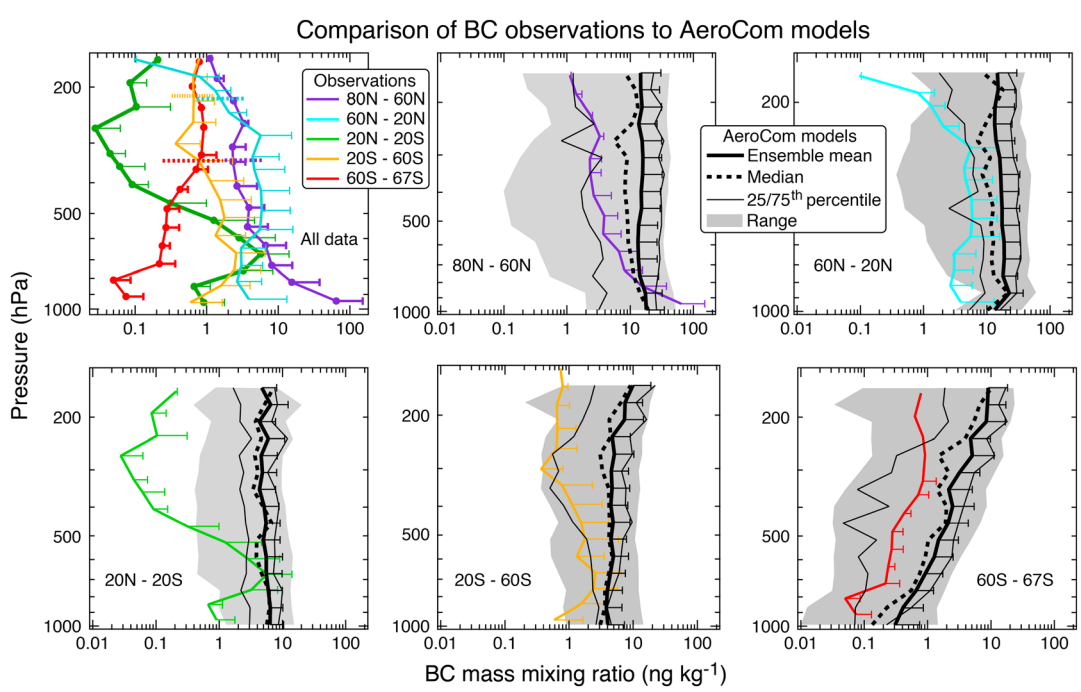

Figure 15. Airborne, in situ measurements of BC made in the remote Pacific Ocean between 80°N and 67°S in January 2009 using an SP2 instrument. Upper left panel: average measured BC mass concentrations observed in five latitude bands with whiskers representing atmospheric variability. In the additional panels, colored lines repeat the observed average profiles and include the range of BC mass mixing ratios from the AeroCom model suite. The legend explains lines and shading used to represent model results. The whiskers are numerically symmetric about the average values but are omitted on the left side to simplify the presentation on a log scale. Adapted from *Schwarz et al.* [2010].

Arctic. That comparison indicated that models overestimate middle and upper troposphere BC at mid-latitudes, consistent with *Schwarz et al*. [2010], but underestimate BC in the Arctic. In urban areas, model predictions of column loadings were consistent with observations [*Schwarz et al*., 2006], but the vertical distribution was not well predicted.

[310] Observations of the vertical distribution of AOD have become available in recent years with active remote sensing by the space-borne CALIOP lidar [*Winker et al*., 2010], for which multi-year averages are shown in Figure 16. AOD includes scattering and absorption by BC, dust, and other aerosol types (e.g., sulfates, organics, and sea salt) with sizes greater than 0.1 μm diameter [*Omar et al*., 2009]. Although chemical speciation is not possible, limited inferences about aerosol type can be obtained through depolarization data that identify non-spherical particles and permit estimates of dust contributions. Geographical distributions of full-column CALIOP AOD (Figure 16) are very similar to BC and dust AAOD from AeroCom models (Figures 12 and 14), with high loadings in South and East Asia, the Middle East, Africa, and Latin America. Maximum total AAOD values are a few percent of maximum AOD values. The panels in Figure 16 show that AOD is confined largely to altitudes below about 4 km. Although interpretation of CALIOP data is still undergoing refinement, these data also indicate that models tend to place aerosol at higher altitudes than is observed [*Koffi et al*., 2012].

5.7. Causes of Model Biases

[311] The comparisons between models and observations and the inverse model studies discussed above provide some consistent messages regarding modeled atmospheric distributions of BC. In the following sections, these observations are used to adjust modeled BC AAOD and direct radiative forcing (section 6) and cloud forcing (section 7). The source of these model biases is less clear. Large underestimates in modeled BC concentrations strongly argue that there are low biases in emission estimates. However, it is difficult to attribute these biases wholly to errors in model emissions, because transport patterns and removal rates can also affect spatial distributions. Transport and removal rates are not independent factors, because aerosol transported to higher altitudes is less likely to be removed and, therefore, has a longer lifetime and greater horizontal transport.

[312] At least one model sensitivity study [*Koch et al*., 2009b] (section 5.5; Figure 13) indicates that varying removal rates by a factor of 2 cannot fully explain the

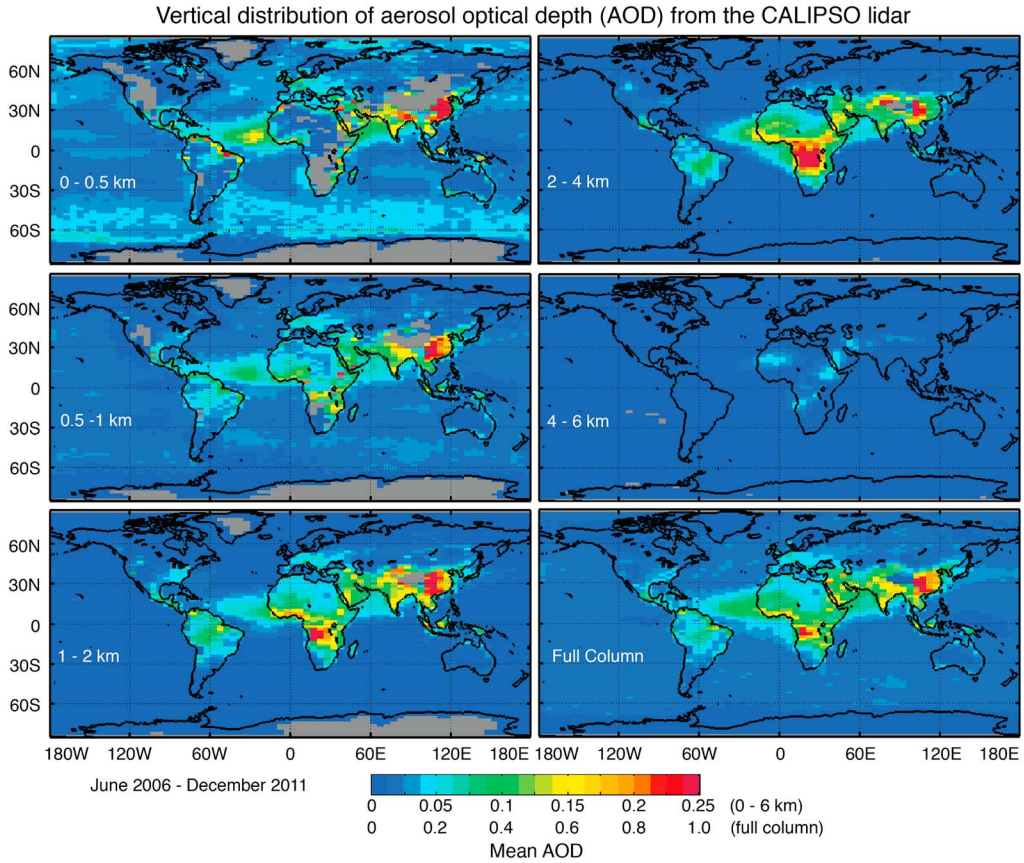

Figure 16. Multi-year averages of the global vertical distribution of mid-visible (532 nm) AOD from the Cloud-Aerosol Lidar with Orthogonal Polarization (CALIOP) spaceborne lidar on the NASA CALIPSO satellite. The panel colors show average AOD derived from CALIOP observations from June 2006 to December 2011 (version 3) for specific altitude intervals referenced to sea level (see legends). The color bar has separate scales for the 0 to 6 km and full-column data panels as indicated. The full-column AOD is shown in the bottom right panel. The gray shading indicates "no observations" usually because of elevated land surfaces. CALIOP statistics were provided by D. Winker of NASA Langley Research Center (Hampton, VA, USA).

inter-model range in concentrations or the bias between models and observations. Significant overestimates in BC concentrations over the remote Pacific are consistent with vertical transport that is too strong or scavenging rates that are too low, but significant underestimates in concentrations in the Arctic free troposphere indicate opposite biases in these processes. Across-the-board adjustments such as altering wet scavenging rates may improve biases in one region but make them worse in another. It is likely that different regions have different sensitivities to each of these processes, requiring focused studies in regions where biases have been observed. For example, Garrett *et al*. [2010] argue that scavenging plays a dominant role in controlling Arctic BC distributions, but this may not be true in other regions such as the remote Pacific. Concentrations near sources are most sensitive to emissions, while concentrations in remote regions depend on transport and removal as well as emissions. Although concentration biases could be reduced by first constraining emissions with near-source concentration measurements and then focusing on transport and removal using measurements downstream from sources, such an activity is beyond the scope of this study, which instead resorted to an after-simulation adjustment that can be applied to all previous simulations that save the requisite information.

5.8. Summary of Limitations in Inferring Black Carbon Atmospheric Abundance

[313] Like all aerosols, BC concentrations are spatially and temporally variable. No measurement strategy provides global coverage of BC concentrations or of AAOD. Space-based sensors have varying limitations: they detect aerosol abundance but not composition (MODIS), provide qualitative measurements of absorption (MISR), or preferentially detect BC at greater altitudes (OMI). Estimating global distributions of BC or absorbing aerosol must therefore rely on modeled aerosol fields, which in turn are constrained by ground-based observations. Ground-based AERONET stations are widespread and produce reasonably accurate AAOD, but coverage is not complete and techniques to separate BC, OM, and dust absorption from these observations are not yet mature. In situ surface measurements have less coverage than AERONET but greater specificity in identifying individual species. These measurements have been used to broadly evaluate modeled global fields and to assess modeled emissions in selected regions. However, observations are sparse in some of the regions with the greatest emissions. A systematic evaluation of model biases caused by emissions, removal rates, and vertical transport, leveraging near-source and remote measurements, has not yet been accomplished.

6. Black-Carbon Direct Radiative Forcing

6.1. Section Summary

[314] 1. Black carbon in the atmosphere reduces the planetary albedo by increasing the absorption of sunlight. The perturbation in the radiative balance resulting from this change is called black-carbon direct radiative forcing (BC DRF).

[315] 2. The best estimate for the BC DRF in the industrial-era is +0.71 W m^{-2} with an uncertainty range of +0.08 to +1.27 W m^{-2}. The best estimate of the global annual mean all-source BC DRF is +0.88 W m^{-2} with an uncertainty of +0.17 to +1.48 W m^{-2}. Locally, BC-DRF forcing can be larger, on the order of +10 W m^{-2}, for example, over regions of East and South Asia. These values are estimated by scaling modeled forcing to the observationally constrained estimate of BC absorption aerosol optical depth (BC AAOD) and reducing the estimated forcing by 15% to account for the incorrect vertical distribution of BC. Our estimate of BC AAOD includes absorption by organic aerosol (OA).

[316] 3. Most BC-DRF estimates originate with simulations of BC lifecycle and radiative transfer using global aerosol models. To improve confidence in these estimates, model-derived fields, such as aerosol optical depth, BC AAOD, or BC distributions, are often adjusted to match observations of AOD, BC AAOD, or concentration, either by direct scaling or by tuning removal rates.

[317] 4. BC DRF can be considered the product of four factors: emissions, lifetime, mass absorption cross section (MAC_{BC}), and radiative forcing per unit absorption optical depth (termed forcing efficiency). Diversity in previous global annual estimates of industrial-era BC DRF (+0.2 to 0.9 W m^{-2}) is caused by variations in modeling assumptions, as evident in the modeled diversity of these four factors: 6000 to 18,000 Gg yr^{-1} for industrial-era BC emissions, 3.8 to 11.4 days for BC lifetime, 4.4 to 13.4 m^2g^{-1} for MAC_{BC}, and 90 to 270 W m^{-2} per AAOD for forcing efficiency.

[318] 5. BC emissions, lifetime, and mass absorption cross section—three of the governing factors—combine to produce BC AAOD, which can be constrained by measurements. Comparison with remote-sensing fields indicates that BC AAOD from most models appears too low. Applying regionally dependent scale factors to match observations increases globally averaged, industrial-era BC AAOD by a factor of 2.9, from 0.0017 to 0.0049. Some of the underestimate can be attributed to the lack of modeled enhanced absorption due to internal mixing, which would increase BC AAOD by about 50%.

[319] 6. If the remaining model bias is caused by burdens that are too low, then model burdens should be increased by factors of 1.75 to 4 in five regions (Africa, South Asia, Southeast Asia, Latin America, Middle East, and the Pacific region). Simulated burdens in North America, Europe, and Central Asia are approximately correct considering uncertainty in BC AAOD and MAC.

[320] 7. The altitude of BC in the atmosphere and its location relative to clouds affects its interaction with solar radiation and hence the forcing efficiency. Solar absorption by BC above low clouds is particularly important and is poorly constrained in models. Limited observations suggest that most models overestimate high-altitude BC at tropical and mid-latitudes and, thus, BC DRF. Our central estimate of forcing includes a 15% reduction to account for this bias.

[321] 8. If all of the differences in modeled burden were attributed to emissions, global emissions would be 17,000 Gg BC yr^{-1}, or an 87% increase above modeled emissions and a 100% increase above the bottom-up emissions in section 4. Industrial-era emissions would be 13,900 Gg BC yr^{-1}. These values are associated with concentrations in approximately the year 2005. We use the latter value as a best estimate of emissions throughout the remainder of this

assessment, although poorly modeled aerosol lifetimes could also explain the discrepancies.

[322] 9. The interpretation of remote-sensing data involves assumptions that affect the amount of absorption and, hence, radiative forcing, that is attributed to BC versus dust. Uncertainties in this division are responsible for nearly half the uncertainty in BC forcing.

[323] 10. If OA does contribute significantly to absorption at 550 nm, then our estimate of observationally constrained BC DRF is biased high, but total forcing by OA would correspondingly become less negative or more positive. About 10% of our BC AAOD may be due to absorption by OA.

[324] 11. The uncertainty range (+0.08 to +1.27 W m^{-2}) for the best estimate of industrial-era BC DRF includes relative uncertainties of about 40% associated with the extrapolation of global BC AAOD, about 50% in the radiative forcing efficiency per unit BC AAOD, and asymmetric uncertainty due to the difficulty in separating BC AAOD from dust AAOD.

6.2. Introduction

[325] Direct radiative forcing by BC refers to the change in the energy balance at the top of the atmosphere due to absorption and scattering of sunlight by BC in the atmosphere. All estimates of BC DRF are based on the difference between radiative transfer calculations for the atmosphere with present-day BC and with a background level of BC. The BC spatial distribution is generally taken from global models of the BC atmospheric lifecycle, which includes emissions, transport, aging, and removal. As described in section 2.3.2, the background level of BC for industrial-era radiative forcing is set by models using year-1750 emissions. For all-source radiative forcing, the background level of BC is zero. Thus, "industrial-era" in this section, when used for any quantity including BC burden, means the difference between modeled quantities with present-day emissions and the same quantities modeled with 1750 emissions.

[326] As with aerosol concentrations, radiative forcing is highly variable in space and time. Global modeling of BC concentrations [*Liousse et al.*, 1996; *Cooke and Wilson*, 1996] and radiative forcing [*Penner et al.*, 1998] began in the middle to late 1990s. Since then, many groups have estimated both concentration and radiative forcing fields. An example of modeled direct forcing is illustrated in Figure 17, which shows radiative forcing simulated by the Community Atmosphere Model CAM5 [*Ghan et al.*, 2012]. As discussed in section 2.3.2, any estimated industrial-era forcing depends on the selection of the "preindustrial background." Industrial-era BC DRF is estimated to be negative in regions such as the eastern United States and the United Kingdom, due to declines in biomass burning since 1750. However, the emission inventories used for the background are associated with considerable uncertainties, especially for open burning. The largest forcing is over the Congo Basin in Africa and southeast China, and Bangladesh, with significant forcing also in the Amazon Basin, over northern India and Indonesia, and off the eastern coasts of South America and Africa where BC is transported over low clouds from distant fires.

[327] To understand the factors that affect radiative forcing in models, it is useful to express the global-mean direct

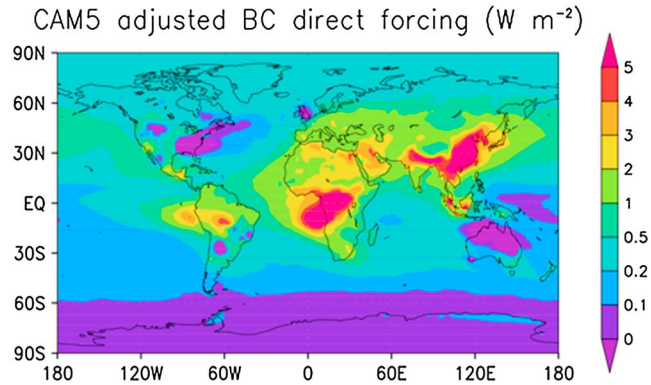

Figure 17. Annual mean direct radiative forcing by BC from 1850 to present day, as estimated by the CAM5 AeroCom model and adjusted according to the global annual-mean BC-AAOD scale factor of 3.0 derived in the comparison with AERONET observations (Table 15 and section 6.7.1). Forcing is negative in regions where biomass or fossil fuel (e.g., coal) emissions were large in 1850. Year 1750 emissions from these regions would be lower, so the total radiative forcing would be more positive. Based on *Liu et al.* [2012] and *Ghan et al.* [2012].

radiative forcing by BC, BC DRF, as the product of four factors [*Schulz et al.*, 2006]:

$$\text{BC DRF} = E \times L \times \text{MAC}_{\text{BC}} \times \text{AFE} \tag{6.1}$$

where E is the global mean BC emission rate, L is the global mean lifetime of BC governed by removal, MAC_{BC} is the global-mean mass absorption cross section discussed in section 3.7.3.3, and AFE is the global mean absorption forcing efficiency (forcing per aerosol absorption optical depth). This relationship is summarized in Figure 18. Three-dimensional models simulate many complex processes that are captured only to first order by the factors in equation (6.1).

[328] Additional diagnostics shown in Figure 18 can be used to compare model results and identify the reasons for differences in simulated radiative forcing. Modeled L can be determined from the ratio of global mean column burden of BC to E, and global average MAC_{BC} is the ratio of the global mean absorption optical depth of BC to the global mean burden. Modeled AFE can be determined from the ratio of the global mean BC radiative forcing to BC AAOD, which is the global mean product of E, L, and MAC_{BC}. BC AAOD is a particularly powerful diagnostic that can be compared with atmospheric measurements and is therefore emphasized in this section. Although AOD can also be used to evaluate modeled aerosol quantities, atmospheric AOD is dominated by scattering and thus has large contributions from other non-absorbing aerosol components.

[329] Table 14 summarizes modeled global mean estimates of each term in equation (6.1) as well as other model diagnostics. Many of these models were used as the basis for IPCC radiative forcing estimates [*Forster et al.*, 2007]. Estimates of industrial-era BC DRF range from +0.2 to +0.9 W m^{-2}. The large diversity is due to different model choices that affect one or more of the factors in equation (6.1). Global emissions of BC range from 5700 to

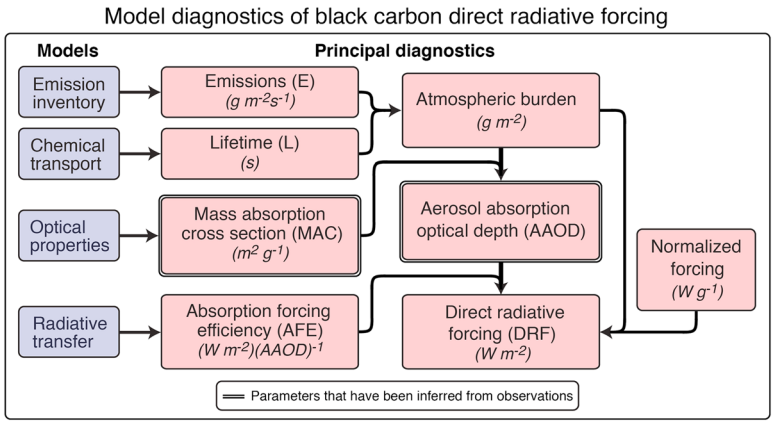

Figure 18. Schematic showing the relationships between principal diagnostics of models used to simulate BC direct radiative forcing (DRF) and the role of models in deriving these diagnostics. The arrows show which diagnostics can be multiplied to yield another diagnostic. The schematic expands upon equation (6.1) which expresses DRF as a product of factors DRF = E L MAC_{BC} AFE. The diagnostics shown within double lines can be directly inferred from observations.

Table 14. Global Industrial-Era or All-Source Black-Carbon Mass-Related Properties as Simulated by Several Models[a]

Model	Reference	EMI[b]	Lifetime[c]	Load Above 5 km[d]	Ind-Era Fraction BC AOD[e]	Load[f]	Mixing[g]	MAC[h]	BC AAOD[i]
		$Tg\,yr^{-1}$	d	%	%	$mg\,m^{-2}$		$m^2\,g^{-1}$	*1000
AeroCom									
GISS	*Schulz et al.* [2006]	6.3	7.2	21.2	80	0.24	Ext	8.4	1.83
LOA	*Schulz et al.* [2006]	6.3	7.3	19.1	80	0.25	Ext	8.0	1.98
LSCE	*Schulz et al.* [2006]	6.3	7.5	40.6	73	0.25	Ext	4.4	1.11
MPI-HAM	*Schulz et al.* [2006]	6.3	4.9	6.1		0.16	Int	7.7	1.23
SPRINTARS	*Schulz et al.* [2006]	6.3	10.6	19.1	78	0.37	Ext	9.8	3.50
UIO-CTM	*Schulz et al.* [2006]	6.3	5.5	14.5	88	0.19	Ext	7.2	1.34
UIO-GCM	*Schulz et al.* [2006]	6.3	5.5	32.7	89	0.19	Int	10.5	1.95
UMI	*Schulz et al.* [2006]	6.3	5.8	17.5	79	0.19	Ext	6.8	1.29
Other models									
BCC_AGCM[k]	*Zhang et al.* [2012]	7.7	3.31	16		0.14	Ext	4.3	0.60
CAM3 ECA	*Kim et al.* [2008]	14.4	3.75			0.29	Ext	10.6	3.06
CAM5 3-mode	*Ghan et al.* [2012]	5.7	3.6		68	0.11	Int	15.0	1.65
GATOR[k]	*Jacobson* [2010]	4.7	9.9			0.25	Ext + Int	14	3.11
GISS-GCM II	*Chung and Seinfeld* [2002]	11.5	6.4		91	0.39	Ext	7.8	3.01[j]
		11.5	6.4		91	0.39	Int		
GISS-MATRIX	*Bauer and Menon* [2012]	2.3	6.3			0.08	Int	8.2	0.66
GOCART[k]	*Textor et al.* [2006]	13.9	7.16	32		0.53	Ext	8.1	4.1
MACR-Assim[k]	*Ramanathan and Carmichael* [2008]	13.9[l]					n/a		5.8[m]
MACR[k]	*Chung et al.* [2012]	6.3	5.5		91	0.19	Ext	n/a	7.7
UIO-CTM	*Myhre et al.* [2009]	6.3	5.5		91	0.19	Int	7.3	1.39[j]

[a]AeroCom models UMI-SPRINTARS represent difference between present day and preindustrial simulations: AeroCom experiments B and PRE.
[b]EMI = Emissions. For comparison to emission totals in the rest of the document, 1 Tg = 1000 Gg.
[c]Lifetime computed from load and emissions.
[d]Load above 5 km refers to the fraction of BC mass above 5 km altitude [from *Textor et al.*, 2006].
[e]Ind-era fraction BC AOD: Industrial-era fraction of BC aerosol optical depth.
[f]Load is global area weighted column mass of BC.
[g]Int = Treatment or explicit assumption of internal mixing; Ext = External mixing, or no explicit treatment of internal mixing, even if a relatively high value of MAC was uniformly applied to all aerosol. Some models used external mixing for the AeroCom study [*Schulz et al.*, 2006] but are capable of internally mixed treatments too.
[h]MAC: Mass absorption coefficient due to BC.
[i]Absorption aerosol optical depth due to industrial-era BC, except for MACR-Assim, GOCART, GATOR, and BCC_AGCM, which use all-source BC.
[j]Inferred from column burden of BC and MAC_{BC} given for pure BC. This calculation cannot be done for internal mixtures, as MAC_{BC} depends on the aerosol composition.
[k]All-source BC is reported for these models rather than the industrial-era component.
[l]Emissions in underlying GOCART model but modified through assimilation.
[m]C.E. Chung, personal communication [2010] and *Chung et al.* [2005].
n/a = not applicable.

Table 15. Global Averages of Aerosol Absorption Optical Depth (AAOD) Industrial-Era (ind.-era) or All-Source BC Direct Radiative-Forcing (DRF) Measures as Simulated in Several Models[a]

	Model Values				Normalized Values		Scaled BC-DRF	
Model	BC Quantity	BC AAOD[b]	BC-DRF ToA[c]	BC-Atm RF[d]	AFE[e]	Normalized DRF[f]	Ind.-era ToA[g]	All-Source ToA[h]
Units		*1000	$W\,m^{-2}$	$W\,m^{-2}$	$W\,m^{-2}$/AAOD	$W\,g^{-1}$	$W\,m^{-2}$	$W\,m^{-2}$
AeroCom models								
GISS	Ind. era	1.83	0.22		120	920	0.59	0.73
LOA	Ind. era	1.98	0.32		159	1280	0.78	0.96
LSCE	Ind. era	1.11	0.30	0.85	270	1200	1.32	1.63
MPI-HAM	Ind. era	1.23	0.20		165	1250	0.81	1.00
SPRINTARS	Ind. era	3.50	0.32	1.00	91	870	0.44	0.55
UIO-CTM	Ind. era	1.34	0.22		164	1160	0.80	0.99
UIO-GCM	Ind. era	1.95	0.36		184	1900	0.90	1.11
UMI	Ind. era	1.29	0.25	0.89	194	1320	0.95	1.17
Other models								
BCC-AGCM	All	0.60	0.10		166	710	0.82	1.01
CAM3 ECA	Ind. era	3.06	0.57	1.57	186	1970	0.91	1.13
CAM5 3-mode	Ind. era	1.65	0.30		182	2730	0.89	1.10
GATOR	All	3.11	0.55		177	1830	0.86	1.07
GISS-GCM II ext	Ind. era	3.01	0.51		170	1310	0.83	1.03
GISS-GCM II int	Ind. era		0.79			2030		
GISS-MATRIX	Ind. era	0.66	0.15		227		1.11	1.38
GOCART	All	4.1						
MACR-Assim	All	5.80	0.90	2.6	155		0.76	0.94
MACR	All	7.70	0.75	2.75	97		0.48	0.59
UIO-CTM ext	Ind. era	1.30	0.26		187	1370	0.98	1.21
UIO-CTM int	"		0.33			1740		
Average $\pm 1\sigma$					171		0.84 ± 0.21[i]	1.03 ± 0.26[i]

[a]All model values are those reported by the listed model for either industrial-era (Ind. era) or all-source (All) BC emissions. See Table 14 for references associated with each model.
[b]BC AAOD: Absorption optical depth due to modeled BC, either industrial era or all-source emissions.
[c]BC-DRF ToA: Top of atmosphere all-source (MACR-Assim and GOCART) or industrial-era (all other models) shortwave radiative forcing from unscaled AeroCom models.
[d]BC-Atm-RF: This is the warming by BC of the atmospheric column, which is much greater than the ToA radiative forcing.
[e]AFE: Normalized radiative forcing per unit absorption aerosol optical depth.
[f]Normalized DRF: Direct radiative forcing normalized to BC column load.
[g]Industrial-era BC-DRF ToA scaled: Top-of-atmosphere industrial-era shortwave radiative forcing after scaling to 0.0049 industrial-era absorption optical depth.
[h]All-source BC-DRF ToA adjusted: Top-of-atmosphere all-source shortwave radiative forcing by BC after scaling to 0.0060 all-source absorption optical depth.
[i]Final central estimate of direct forcing is 15% lower than these values to account for BC vertical distribution (section 6.7.2).

18,000 Gg yr^{-1}. Lifetime ranges from 3.3 to 10.6 days. Global mean MAC_{BC} ranges from 4.3 to 15 m^2g^{-1}. AFE ranges from 91 to 270 W $m^{-2}AAOD^{-1}$ (Table 15). Because the correlation among these four factors can be negative [*Schulz et al*., 2006], and because no model has maximum or minimum values of all four factors, the diversity in the radiative forcing in Table 15 (+0.2 to +0.9 W m^{-2}) is much smaller than the diversity estimated by multiplying the minima and maxima of the four factors (+0.05 to +3.7 W m^{-2}). The lower net diversity in simulated BC DRF is to some extent due to tuning simulations to match observational constraints on BC concentration and AOD. The best estimates of each component are summarized in sections 6.3 through 6.6 before providing a best estimate of BC DRF in section 6.7.

6.3. Emission, Lifetime, and Burden

[330] As discussed in section 4, BC emission rates used in estimates of radiative forcing vary regionally and globally [*Haywood and Boucher*, 2000; *Bond et al*., 2004]. Commonly used values of global industrial-era emissions are 6300 Gg yr^{-1} for AeroCom [*Schulz et al*., 2006], but emissions as high as 18000 Gg yr^{-1} have been used [*Chin et al*., 2002]. For the Climate Model Intercomparison Program simulations for the IPCC Fifth Assessment Report, the value was 5700 Gg yr^{-1} for present-day emissions [*Lamarque et al*., 2010].

[331] Column burden is proportional to BC emissions and to modeled lifetime. Lifetime is determined by removal, which is represented differently in each model and varies by location and season. Global average lifetime for BC varies by a factor of more than 3 for the models reported in Table 14. Removal in precipitation plays a large role in aerosol lifetime [*Ogren and Charlson*, 1983], which is difficult to represent accurately at the coarse resolution of global modeling [*Rasch et al*., 2000; *Textor et al*., 2007; *Croft et al*., 2010]. Differences in dry deposition contribute to uncertainty as well [*Easter et al*., 2004; *Bauer et al*., 2008; *Vignati et al*., 2010]. Because removal processes depend on altitude, aerosol lofting also affects lifetime. For example, *Koch et al*. [2007] showed that lofting of biomass-burning aerosols from South America led to longer lifetimes compared with African emissions. Most developers of aerosol models have applied surface observations of BC concentrations and surface and satellite retrievals of AOD to constrain emissions or the treatment of scavenging, so one would expect the product of emissions and lifetime (burden) to agree broadly with observations [*Vignati et al*., 2010].

[332] Early models used a limited number of parameters to account for sub-grid variability in precipitation and the

efficiency with which particles are scavenged. These scavenging treatments used crude parameters that were applied globally. More advanced models treat the coating of BC with hygroscopic material to form particles that are more readily activated to form cloud droplets and scavenged more efficiently. The representation of scavenging affects the magnitude and seasonality of BC concentrations, especially at remote locations [*Croft et al*., 2005]. Model representation of the BC seasonal cycle in the Arctic improves with more accurate microphysical treatments [*Vignati et al*., 2010; *Lund and Berntsen*, 2012; *Park et al*., 2011].

[333] The global mean column burden of BC ranges from 0.11 to 0.53 mg m^{-2} in Table 14. The studies with the largest radiative forcing estimate (MACR-Assim) [*Ramanathan and Carmichael*, 2008; *Chung et al*., 2012] did not calculate a burden, but the BC simulation [*Chin et al*., 2002] that the studies relied on for absorption far from AERONET sites [*Chung et al*., 2005] had a global mean BC column burden of 0.6 mg m^{-2}. Some of the models did not constrain the combination of emissions and lifetime with BC concentration measurements [*Vignati et al*., 2010], including the model that estimated the largest BC burden (i.e., SPRINTARS; Table 15) [*Takemura et al*., 2005]. Some of the diversity in the column burden of BC in Table 14 can be attributed to differences in emissions. Yet many of the estimates used the same BC emission inventory and still yielded BC burdens differing by more than a factor of 2 (0.16 to 0.38 mg m^{-2}) due to differences in lifetime [*Schulz et al*., 2006]. As discussed in section 5.5, most models simulate surface BC concentrations within a factor of 2 of measurements in most regions, with weak over-predictions in Europe, underpredictions in biomass burning regions, and large underpredictions for eastern and southern Asia [*Koch et al*., 2009b].

[334] Vertical lofting of BC affects its prospects for wet scavenging and hence its lifetime. Vertical profiles of BC show that simulated concentrations have large biases in the free troposphere [*Koch et al*., 2009b]. High biases of a factor of 3 to 15 (average 8) are found in tropospheric BC concentrations above the boundary layer at tropical and subtropical latitudes, while most models underestimate the BC concentrations in the Arctic troposphere, on average by a factor of 2.5 [*Koch et al*., 2009b, Table 8]. Adjustments to simple scavenging treatments cannot reproduce these observed distributions; increased removal in tropical regions would reduce the over-prediction at high altitudes there (section 5.5) but would enhance the low bias in the Arctic troposphere where abundances may be controlled by scavenging processes [*Garrett et al*., 2010]. However, improved treatments of scavenging may result in greater fidelity.

6.4. Mass Absorption Cross Section

[335] Section 3.5 discussed measured and modeled MAC of BC and particles that contain BC. Section 3.5 also summarized how mixing of BC with other aerosol components would increase MAC_{BC}, and field measurements have found that BC particles are largely mixed with other components. Since MAC depends on refractive index, water content, particle size, and mixing with other aerosol components, measured MAC_{BC} data provide a useful diagnostic check for models when information about each variable is also known.

[336] The global mean MAC_{BC} listed in Table 14 ranges from 4.3 to 15 m^2g^{-1}, with the AeroCom median around about 6.5 m^2g^{-1}. Many models have MAC_{BC} values similar to the *Bond and Bergstrom* [2006] estimate of 7.5 $\pm$ 1.2 m^2g^{-1} for freshly emitted, externally mixed BC, and a few others are close to the estimates of about 12.5 m^2g^{-1} for internally mixed aerosol. Two models (LSCE and BCC-AGCM) are much lower than this range. If models that assumed external mixing were excluded or adjusted for the increase in MAC_{BC}, the model average MAC_{BC} and the average estimated DRF would increase [*Jacobson*, 2000; *Myhre et al*., 2009]. The internally mixed value of MAC_{BC} may be an upper limit on the global mean value because the actual global mean depends on how much of the BC is mixed with other components throughout the atmosphere.

[337] All global models that represent internal mixing report a large increase in absorption and positive forcing for internally mixed particles. *Haywood and Shine* [1995] reported doubled forcing due to internal versus external mixing in a simple model. *Jacobson* [2001a] was the first to confirm that finding with realistic BC spatial distributions and accounting for the evolution of mixing state. *Chung and Seinfeld* [2002] found a forcing increase of 36% for BC with homogeneous internal mixing compared with external mixing. *Bauer et al*. [2010] included a core-shell representation in a multi-modal model. *Flanner et al*. [2007] and *Myhre et al*. [2009] associated internally mixed values of MAC_{BC} with aged BC, and *Adachi et al*. [2010] explored several mixing assumptions in a global model. Model treatment of aging and mixing affects both absorption and lifetime, often with compensating effects. *Ghan et al*. [2012] found that two treatments of BC produced similar forcing estimates, as internally mixed BC had higher MAC_{BC} but was removed faster. *Stier et al*. [2006b] found regional differences in which effect of BC mixing state dominates.

6.5. Scaling Modeled BC AAOD to Observations

[338] BC AAOD is the product of three of the factors that determine BC DRF (i.e., E, L, and MAC_{BC} in equation (6.1)), and constraining this product can reduce uncertainty in radiative forcing. In this section, we present an estimate of observationally constrained BC AAOD that is used to produce scaled forcing estimates in section 6.7.

[339] Measurements of AAOD are sparsely distributed, and many models underestimate BC AAOD, as shown in Figure 14. In section 5.4.2.1, we cautioned that both sampling bias and dust absorption could produce a high bias in BC AAOD inferred from AERONET AAOD. Comparisons between model and observationally derived total AAOD in *Koch et al*. [2009b] include contributions from both BC and dust. As a result, either or both BC and dust could be responsible for model discrepancies. However, AAOD comparisons for regions and seasons not affected by dust still show that many models simulate too little absorption in the atmosphere and, therefore, underestimate BC DRF.

[340] To obtain an estimate of BC AAOD constrained more closely by observations, a method was developed to scale modeled BC AAOD fields using BC AAOD inferred from the AERONET ground-based network. Appendix B gives the details and background of this method. Briefly,

sampling biases in the AERONET retrievals of total AAOD were removed, and BC AAOD was estimated from total aerosol AAOD by subtracting the contribution to AAOD by dust. This process allocates all non-dust absorption to BC. To the extent that organic aerosol contributes to AAOD, our estimate of BC AAOD is biased high. Biases in the AeroCom median model BC AAOD were quantified by calculating the ratio of the observationally constrained and modeled values at the same month and location. The scale factors so determined were then extended to other grid boxes within the region, including outflow from that region over the ocean. This expansion of scale factors relies on the spatial distribution of BC in the AeroCom median model.

[341] BC AAOD estimated this way is found to be much greater than modeled BC AAOD, so the procedure increases the globally averaged estimate of total BC AAOD from 0.0021 before scaling to 0.0060 after scaling. As discussed in section 6.9, causes of the resulting BC AAOD changes would likely have affected preindustrial BC AAOD as well, so we applied the same scaling factors to preindustrial BC AAOD. Hence, the global mean industrial-era BC AAOD increases by the same factor, from 0.0017 before scaling to 0.0049 after scaling. These increases in BC AAOD are large, but previous estimates that employ observations have also found BC AAOD much greater than model values (section 6.8).

6.5.1. Sensitivities in AAOD Scaling

[342] A summary of modeled BC AAOD values before scaling is presented in Table 15 and summarized in Figure 19. Industrial-era, global-mean BC AAOD from models without any scaling ranges from 0.0006 to 0.0035, with two models that included internal mixing giving values above 0.0030 and the remainder lying within 30% of the median value. Figure 19 also shows BC AAOD estimates scaled to observations for industrial-era sources and for all sources. For both scaled and unscaled fields, all-source BC AAOD is higher than the industrial-era average by about 23%.

[343] Error bars in the scaled estimates in Figure 19 reflect uncertainty in the spatial distribution of BC in the model used to extend scaling to regions without observations. This uncertainty is estimated by applying the full scaling procedure to three additional modeled fields (SPRINTARS, GOCART, and UMI) that were chosen to represent high and low average BC AAOD. The scaled value of global BC AAOD ranges from 0.0046 for SPRINTARS to 0.0064 for UMI, so the highest initial model field results in the lowest scaled value.

[344] The BC AAOD values derived in Appendix B are very sensitive to assumptions imposed in the use of the AERONET data fields, as discussed in Appendix B. To demonstrate this, Figure 19 shows estimates of all-source BC AAOD with three different changes in basic assumptions used in deriving BC AAOD from AERONET observations. The revised AERONET fields are then used to rescale the AeroCom model fields, and a new global estimate is calculated. First, BC AAOD is separated from total AAOD by combining the AERONET size distribution for submicron particles and the retrieved AERONET refractive index. This method of separation reduces the mean BC AAOD from the baseline estimate of 0.0060 to 0.0034 but does not account for the differing properties of submicron and super-micron aerosol. This method ascribes a relatively small AAOD to BC and a large AAOD to dust. Second, the selection of AERONET stations introduces an uncertainty of 30%. When

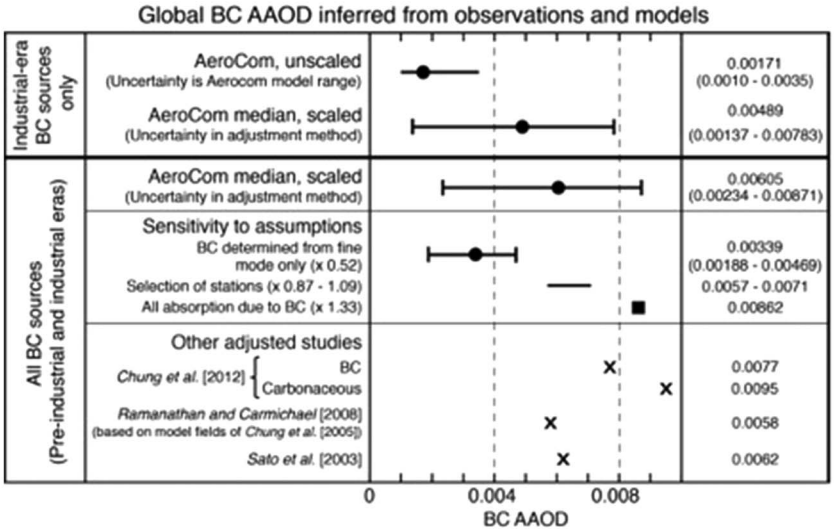

Figure 19. Summary of the sensitivity of global BC-AAOD derived from AeroCom models. The scaling of AeroCom BC-AAOD values is based on AERONET observations following the method in Appendix B and discussed in section 6.5. Separate unscaled and scaled AeroCom model values are shown in Table 15. Data points (circles) are AeroCom median values. Ranges are shown with lines and uncertainty with whiskers. Not shown on the figure due to limited scale is an estimate of scaling to average BC AAOD inferred from AERONET version 2.0 averages (0.0143). The sensitivity of scaled all-source BC-AAOD to key assumptions in using the AERONET observations is shown for three cases (see text). Three other model study results are shown at the bottom for comparison. Central estimates, value ranges, and uncertainty ranges are shown in the right-hand column.

four different subsets of stations were used for the scaling of all-source BC AAOD, global averages ranged from 0.0057 to 0.0071. The analysis presented here includes this uncertainty. Third, if all absorption were attributed to BC, the modeled BC-AAOD field would increase by a factor of 1.33 to 0.0086. Fourth, the AERONET Version 2.0 data exclude low-AOD conditions, so that average AAOD values in that dataset are biased high. If the AERONET Version 2.0 data were used, estimated BC AAOD would increase by a factor of 2.2, to 0.0143 (not shown in Figure 19 due to limited scale). The interpretation applied here does not suffer from this bias because of the method used to interpret the AERONET data. BC-DRF estimates relying on averages of published AERONET AAOD data cannot account for this bias and are expected to be much greater than those derived in this assessment. These sensitivity calculations highlight the importance of clearly stating assumptions and their consequences when using AERONET observations to scale modeled fields of absorbing aerosol. Other uncertainties in this analysis, used to set bounds on BC DRF, are discussed in section 6.7.3.

6.5.2. Reasons for Low Bias in Modeled AAOD

[345] Because BC AAOD is the product of MAC_{BC} and BC burden (section 6.2), the mismatch between modeled and observed BC AAOD may derive from errors in modeling both factors. Apportionment is considered separately for AAOD resulting from open biomass burning and energy-related combustion in the ten regions shown in Figures 7–9.

[346] We first assume that the MAC_{BC} scale factor for all months and regions is 1.5 (i.e., the approximate ratio between the MAC of internally and externally mixed BC). Most models in the Phase I AeroCom group described here did not account for internal mixing, and the AeroCom median BC AAOD at each grid box likely represents aerosol with this lower MAC_{BC}. We also assume that AAOD attributable to open burning and energy-related sources are proportional to their emissions; that is, aerosol lifetimes from the two sources are similar in each month. The scaled BC AAOD values for each source are then averaged over the year to produce an annual BC AAOD and then divided by the original BC AAOD to give an annually averaged scaling factor.

[347] Figure 20 displays the annual scale factors for each region and source group. Although our assumption of similar lifetimes between the source groups may be questionable, the method should produce dissimilar scale factors if more correction is needed during months with high or low biomass burning. The bars for each scale factor show the portions attributable to BC burden (closed) and MAC_{BC} (open). The middle panel of Figure 20 also shows the annual

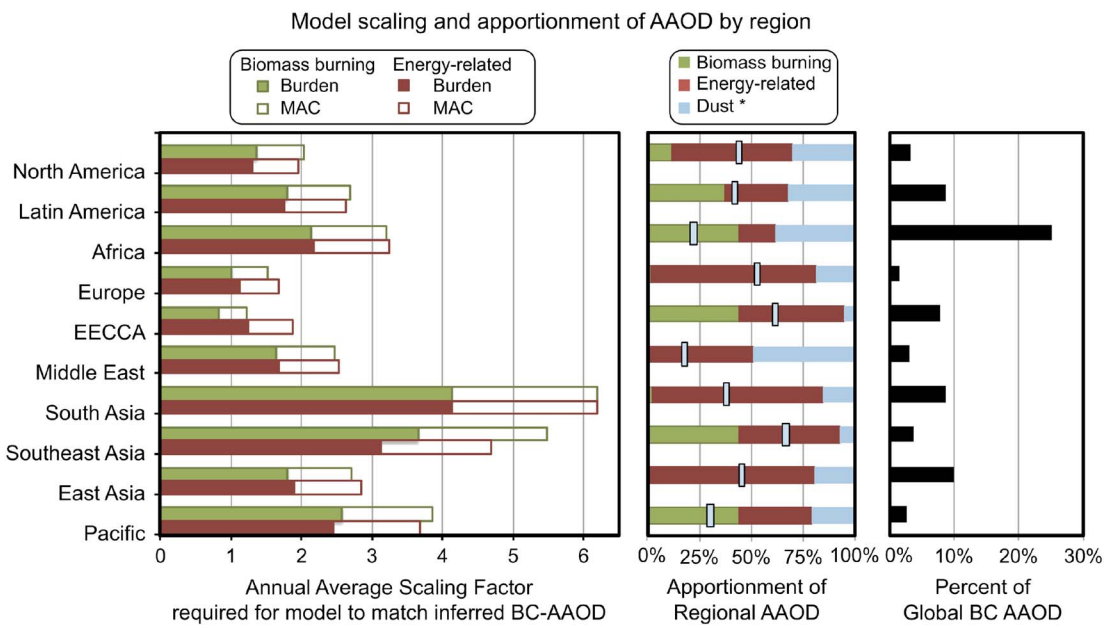

Figure 20. Summary of regional BC aerosol absorption optical depth (BC AAOD) scaling and contributions. Left: Summary of regional scaling factors required for AeroCom median model values to match BC AAOD constrained by AERONET observations. The regions are shown in Figure 7. Scaling factors are effective annual averages apportioned between open biomass burning and energy-related burning. Each factor is an annual average of monthly scaling factors in each region and includes a prescribed MAC_{BC} scaling of 1.5 for all months and regions (open bar), the approximate ratio between the MAC_{BC} of internally and externally mixed BC. The remainder of the scaling is attributed to burden. Center: Estimate of BC AAOD fraction in each region due to energy-related combustion, biomass burning, and dust; the dust contribution is not a true estimate of dust AAOD but of dust AAOD in AERONET. The small blue rectangles indicate where the left boundary of the dust AAOD would lie if BC AAOD were determined by applying AERONET refractive indices to the fine mode of the retrieved size distribution. Right: Contribution of modeled, scaled BC AAOD over land to global total BC AAOD. These percentages do not sum to 100% because BC AAOD over oceans is excluded.

fraction of BC AAOD attributed to energy-related emissions versus biomass burning emissions and also shows estimates of the amount attributed to dust in each region. This fraction is not a true estimate of regional dust AAOD, as it does not account for the difference in the dust spatial distribution. Instead, it shows the amount of AAOD that would be added if BC-AAOD fields were scaled to total AAOD instead of BC AAOD. Regions with a high apparent dust fraction have greater uncertainty in BC AAOD because of the difficulties in separating the two. The narrow blue box shows the dust fraction that would be inferred using an alternate technique: applying the AERONET-retrieved refractive index to the fine fraction of the retrieved size distribution. Finally, the rightmost panel of Figure 20 shows the contribution of each land region to scaled global BC AAOD. These percentages do not sum to 100% because 35% of the BC AAOD occurs over oceans. Over half of this BC AAOD, or 20% of the global total, occurs in outflow regions for which scaling was affected by adjacent continents.

[348] Burden scale factors greater than unity (solid bars) in Figure 20 indicate that the AeroCom median model usually underestimates the burden. Differences between energy-related and biomass burning scaling factors are small, indicating that corrections are not wholly attributable to either one. The greatest burden underestimates, by factors of 3–4, are found in South and Southeast Asia. Most other regions require significant increases of 60 to 160%. Modeled burdens are more realistic, within 40%, in North America, EECCA, and Europe; this analysis is consistent with surface observations in Europe (Figure 13 and section 5.5). Some regions requiring large scaling factors are dominated by energy-related emissions, and the underestimate must occur in those emissions. In other regions, particularly Africa and Southeast Asia, open burning is a large fraction of BC AAOD. Uncertainties in attribution between BC and dust are greatest when apparent dust fractions are large, which could affect the global burden greatly in Africa. Section 6.9 discusses the implications for emission rates, and compares the findings presented here with previous model-measurement comparisons.

6.6. Forcing Efficiency

[349] Radiative effects of BC are estimated by comparing radiative transfer calculations with and without BC emissions, accounting for scattering and absorption by the surface and by gases, clouds, and other aerosol components throughout the atmosphere. Aerosol optical properties are important inputs to determine the magnitude and location of aerosol absorption and scattering. However, once the optical depths and single-scattering albedo are known, variations in global-average radiative forcing per absorption optical depth are largely driven by environmental variables, especially the reflectivity of the underlying surface. BC aerosol alters the ToA net energy balance much more over a bright reflective surface or cloud layer than above a dark one [*Haywood and Shine*, 1995; *Chylek and Coakley*, 1974]. This sensitivity produces the threefold diversity in the global mean absorption forcing efficiencies (AFE) listed in Table 15, with values ranging from 91 to 270 W $m^{-2}AAOD^{-1}$. Figure 21 shows the spatial distribution of annually averaged AFE from the AeroCom median model. It tends to be higher for aerosol located over land and stratus clouds, and the highest values occur over snow.

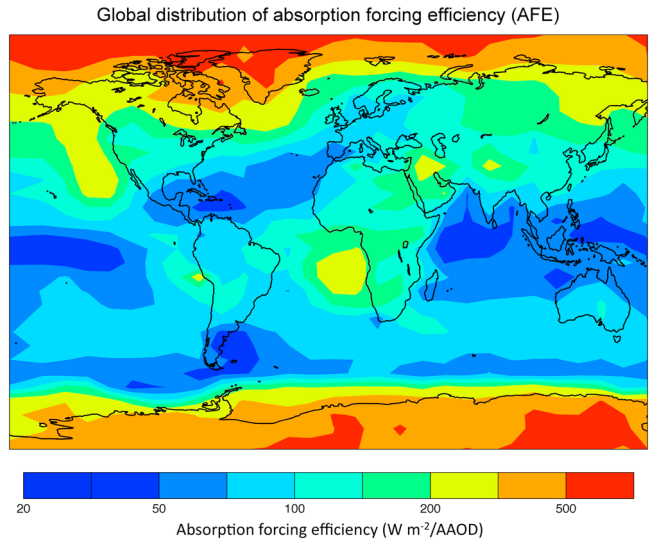

Figure 21. Global distribution of absorption forcing efficiency (AFE) defined as direct radiative forcing divided by aerosol absorption optical depth (AAOD). Both forcing and AAOD used are AeroCom median values as described in section 5.3.

6.6.1. Vertical Location of BC

[350] Top-of-atmosphere AFE is enhanced considerably when BC is located over clouds compared with over the dark ocean surface. Thus, some of the diversity in AFE is caused by differences in the BC vertical distribution because elevated BC is more likely to overlie low clouds [*Haywood and Ramaswamy*, 1998]. BC over low clouds increases forcing disproportionately compared with BC in clear skies, while BC under clouds has a decreased contribution [*Haywood and Ramaswamy*, 1998; *Zarzycki and Bond*, 2010]. Greater solar flux at high altitudes can also increase forcing by high-altitude BC [*Samset and Myhre*, 2011]. Comparing forcing from models that all use the same emissions, the model with the lowest AFE of 91 W $m^{-2}AAOD^{-1}$ places 14% of the total BC mass above 5 km, and the model that simulates the highest forcing efficiency of 270 W $m^{-2}AAOD^{-1}$ has 37% of its BC above 5 km. *Textor et al.* [2006] find that the fraction of the simulated BC mass above 5 km ranges from 7 to 37% for 16 AeroCom models. Direct forcing by BC can be greatly intensified when aerosol-cloud collocation on sub-grid scales is considered [*Chand et al.*, 2009], and this is not treated in global models or in this estimate.

[351] How realistic are simulated vertical distributions of BC? As discussed in section 5.5, recent measurements have shown that aerosol models generally simulate too much BC in the upper troposphere, especially at tropical and mid-latitudes [*Schwarz et al.*, 2010]. Models also underestimate the decrease in aerosol extinction with altitude [*Yu et al.*, 2010]. Adjustments to reduce these biases are likely to put more of the BC below rather than above clouds and, hence, reduce estimates of the ToA radiative forcing by BC. Thus, the highest values of AFE shown in Table 15 are probably unrealistic. *Zarzycki and Bond* [2010] estimate that radiative forcing would decrease by approximately 15% if a model with an intermediate BC vertical profile was scaled to match measured profiles. *Koffi et al.* [2012] compared AeroCom models and CALIPSO measurements and found that aerosol

was too high by about 400 m (range of 50 to 1080 m) in source regions. This finding also suggests a forcing decrease of approximately 15% when combined with the sensitivities given by *Samset and Myhre* [2011].

6.6.2. Horizontal Location of BC

[352] Some of the diversity in AFE could also be due to differences in the BC horizontal distribution, particularly with respect to the albedo of the underlying surface or the amount of sunlight at different latitudes. *Kinne et al.* [2006] find the greatest diversity in the simulated BC burden is in polar regions, *Textor et al.* [2006] find that the fraction of BC mass between 80° and 90°N varies greatly in the AeroCom models, and *Shindell et al.* [2008] find that all BC models in their study simulate far too little BC at Barrow and Alert (both in the Arctic), particularly during winter and early spring.

6.7. All-Source and Industrial-Era BC DRF

[353] Figure 22 summarizes the two major determinants of direct radiative forcing—BC AAOD and AFE—for the model results reported in Tables 14 and 15. Figure 22(top) shows that modeled radiative forcing has a strong relationship with modeled AAOD. AFE is the ratio between forcing and AAOD and varies among models. Figure 22(bottom) shows larger AFE for models with more BC above 5 km altitude, which suggests that AFE can be strongly affected by the amount of BC above 5 km altitude.

6.7.1. Scaled Estimates of BC DRF

[354] Many of the models with results reported in Tables 14 and 15 simulate too little BC AAOD compared to atmospheric observations and, therefore, too little BC DRF. If modeled values of AFE were trustworthy, then a best estimate of all-source radiative forcing could result from multiplying those values by a best estimate of BC AAOD for every grid cell and season and averaging over the globe. A map of the increase in radiative forcing obtained by applying this method with the AeroCom median model is shown in Figure 23. Because we do not have all the modeled forcing fields to perform this scaling, we capture the diversity in AFE by scaling each of the model-based estimates of industrial-era radiative forcing using the observation-based estimate of industrial-era BC AAOD, which has a global annual mean of 0.0049. These estimates are only approximate because the scaling ignores regional and seasonal variations. However, this scaling method does improve absorption fields that are too low when models do not include internal mixing or sufficient emissions.

[355] Table 15 shows the industrial-era BC-DRF values from each model, scaled by the ratio of the observationally based BC AAOD to the modeled BC AAOD. These scaled values range from +0.48 to +1.32 W m^{-2}, with a mean and standard deviation of +0.84 ± 0.21 W m^{-2}. Radiative forcing is increased for all models because all models simulate a lower BC AAOD. Similarly, this scaling can be used to estimate DRF by all BC sources. Model BC-DRF values scaled to the total BC AAOD of 0.0060 are also listed in Table 15. Estimates range from +0.59 to +1.63 W m^{-2}, with a mean and standard deviation of +1.03 ± 0.26 W m^{-2}.

6.7.2. Central Estimate of BC DRF

[356] For a central estimate of BC DRF, we use an average of the scaled radiative forcing estimates in Table 15. However, section 5.6 showed that most models overpredict BC at high altitudes, leading to an overestimate of BC DRF. Therefore, we estimate a central value of 15% less than the mean of all estimates to compensate for the tendency of models to place BC at too high altitudes and, hence, produce an unrealistically high radiative forcing efficiency, as discussed in section 6.6.1.

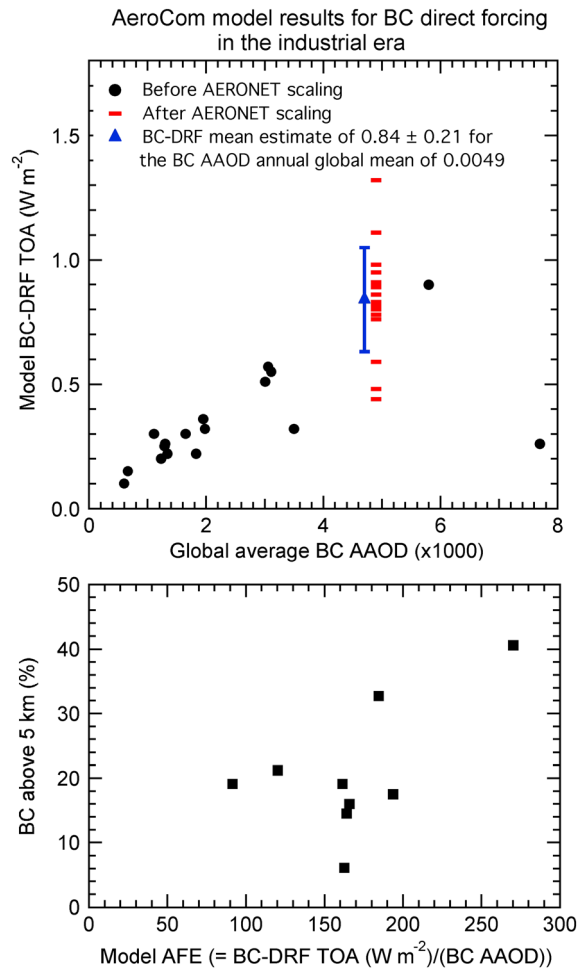

Figure 22. AeroCom model results for BC DRF in the industrial era. Top: Unscaled Aerocom BC DRF versus global average BC AAOD in each model (circles) and scaled BC-DRF values (short lines) plotted at the scaled industrial-era AAOD value (0.0049). BC AAOD is proportional the amount of BC in the atmosphere. Unscaled models with higher BC AAOD generally have higher BC DRF. When BC DRF from each model is scaled to the BC AAOD global mean value of 0.0049, the resulting BC DRF has a mean and standard deviation of 0.84 ± 0.21 W m^{-2} (blue triangle slightly offset for clarity). Bottom: The percentage of BC above 5 km versus absorption forcing efficiency (AFE) in several Aerocom models. Data presented here are also provided in Tables 14 and 15. The scaling of BC DRF in AeroCom models is discussed in section 6.7.1. The forcing average shown here is reduced for the best estimate of forcing, as discussed in section 6.7.2.

[357] With this scaling, the central estimate of global annual DRF by industrial-era BC is +0.71 W m^{-2}. The central estimate of DRF by all-source BC is +0.88 W m^{-2}. These values may be considered an observationally constrained model average. This estimate includes forcing due to

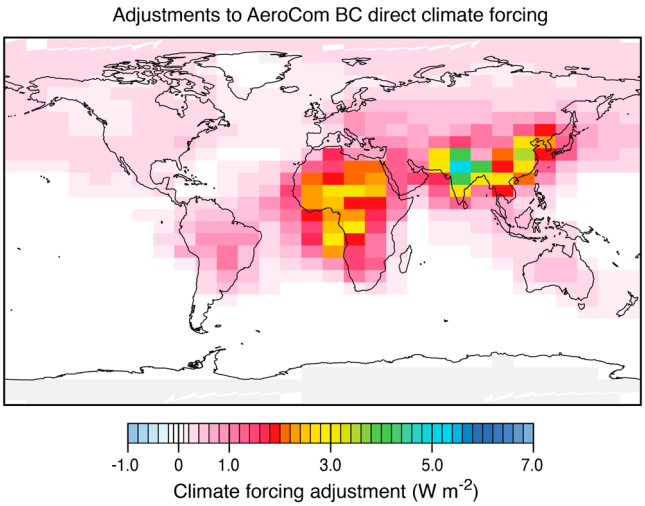

Figure 23. Adjustments to the annual mean, direct radiative forcing (W m^{-2}) by BC in the median AeroCom model required for consistency with the AERONET retrieved aerosol absorption optical depth (AAOD).

atmospheric absorption by organic carbon since our estimate of BC AAOD includes absorption by both BC and OA. In section 11, total aerosol DRF from sources that emit BC is estimated, and there we do not account for atmospheric absorption by OA, so while BC DRF may be biased high, the total forcings by emissions from sources that include both BC and OA do not include this bias.

[358] The modeled forcing discussed above was calculated only at visible wavelengths, except for the work of *Jacobson* [2010]. Aerosols can also interact with infrared radiation, especially in source regions [*Lubin and Simpson*, 1994]. *Reddy et al.* [2005a] estimated infrared forcing by BC as +0.006 W m^{-2}. *Jacobson* [2001b] presented a graphical summary in which ToA direct infrared forcing by BC was small relative to forcing at visible wavelengths. Therefore, we assume that the central estimate given above encompasses infrared forcing, even if most models have neglected it.

6.7.3. Uncertainties in BC DRF

[359] A 90% confidence range for BC DRF is based on independent uncertainties in the industrial-era BC AAOD and the radiative forcing efficiency, AFE. The final estimate of uncertainty is higher than that reflected in the diversity of scaled BC DRF estimates listed in Table 15, which do not account for uncertainty in BC AAOD.

[360] Appendix B provides an estimate of the uncertainty in BC AAOD. Uncertainties are caused by the spatial patterns of BC AAOD used in filling gaps between AERONET sites, ambiguity in how the scale factor is defined, the limited number of AERONET sites, clear-sky biases in the BC AAOD, the influence of BC transport from sources to oceanic regions, and the impacts of fine-mode dust and OA on the estimate of BC AAOD. The industrial-era BC-AAOD estimate has an additional 18% uncertainty due to a 50% uncertainty in the estimate of the preindustrial background. We assume that the overall uncertainty of the total AAOD retrieval contributes to the above-mentioned sources of uncertainty, although the degree of this contribution is unknown, and we thus do not account separately for it. One factor that could decrease the BC DRF is the attribution of more AAOD to dust. As discussed in Appendix B, we allow this factor to introduce an asymmetric uncertainty. The 90% uncertainty range is from 0.0023 to 0.0087 for all-source BC AAOD and from 0.0014 to 0.0078 for industrial-era BC AAOD.

[361] The uncertainty in AFE is estimated from the standard deviation of the model AFE values listed in Table 15. This uncertainty is attributable to the vertical and horizontal location and the temporal covariance of the clouds and BC. Other uncertainties included are the vertical location of BC relative to clouds (25%) [*Zarzycki and Bond*, 2010], the effect of surface albedo (20%), and the choice of radiative transfer code (20%) [*Boucher et al.*, 1998]. *Schulz et al.* [2006] attributed a variation in total aerosol cloudy-sky radiative forcing of $\pm$0.26 W m^{-2} among nine AeroCom models mainly to diversity in forcing above clouds. However, this diversity in AFE has not been apportioned to individual sources of uncertainty.

[362] Our final estimate of 90% uncertainty bounds comes from combining the uncertainties in AAOD and the 50% uncertainty in AFE. The global annual DRF by industrial-era BC is estimated to have an uncertainty range of +0.08 to +1.27 W m^{-2} about the central estimate of +0.71 W m^{-2}. This range spans all scaled estimates listed in Table 15. The uncertainty range for all-source BC is +0.17 to +1.48 W m^{-2} about the central estimate of +0.88 W m^{-2}.

[363] A final uncertainty not estimated here is caused by interpretation of AERONET remote-sensing data. Such data sets are subject to periodic revision, and changes in the interpretation would shift the estimate of AAOD and forcing presented here.

6.8. Previous Observationally Scaled Radiative-Forcing Estimates

[364] Three previous studies have reported similar estimates of all-source BC DRF by scaling to AERONET data. *Sato et al.* [2003] scaled modeled fields to the AERONET Version 2.0 product to obtain modeled forcing of +1.0 W m^{-2}. As discussed previously (section 6.5.1), this product eliminates low-AOD observations, with the result that the average AAOD has a high bias, and any scaling of BC AAOD using that product is also biased high. The *Sato et al.* BC AAOD relied on data from earlier years, so their value of 0.006 is not as high as our value extracted from AERONET Version 2.0 averages (0.0143).

[365] *Ramanathan and Carmichael* [2008] estimated forcing of +0.9 W m^{-2} by combining modeled fields with AERONET data, MODIS data, and estimated ω_0. Modeled fields were based on *Chung et al.* [2005], which reports BC AAOD of about 0.0068. Both BC AAOD and AFE are similar to those derived here, and the DRF estimate for all-source BC (+0.9 W m^{-2}) is similar to the value given here. *Chung et al.* [2005] also point out that correcting MODIS AOD with those of AERONET decreases the estimated global AOD by 25%.

[366] The most recent observationally based estimate, by *Chung et al.* [2012], used a combination of AERONET retrievals, partitioning to distinguish BC AAOD from contributions by dust and organic carbon, satellite retrievals of AOD, and model estimates of single-scattering albedo. Their estimate of BC AAOD (0.0077) is 28% larger than our best

estimate. However, this study also estimates a relatively low AFE value (97 W m^{-2} $AAOD^{-1}$); applying this value to our best estimate of BC AAOD produces a BC DRF that is much smaller than that of most estimates in Table 15. *Chung et al.* [2012] estimate an uncertainty range for all-source BC AAOD of 0.006 to 0.009. The lower bound is much higher than ours, because we have more strongly weighted the possibility that more AAOD is attributable to dust.

6.9. Implications of Increased BC AAOD

6.9.1. Apportionment of Bias in BC AAOD

[367] It is of interest to attribute the model bias in BC AAOD to causes beyond the division between MAC_{BC} and burden presented in Figure 20. The required burden scaling could be caused by emissions, by atmospheric lifetime, or a combination of the two. Inverse modeling that explored adjustment of both removal processes and emissions might help to apportion the bias with more confidence, but these studies are beyond the scope of this assessment. However, because the scaling factors were mainly determined using land-based AERONET observations, they are less strongly affected by modeled removal than they would be if the observation sites were very distant from sources. Sensitivity studies reported by *Koch et al.* [2009b], as shown in Figure 13, show that the ratios between observed and modeled concentrations could change by 10% if aging rates were altered by a factor of 2 in either direction. An exception to this finding is North America, for which altered lifetimes would alter the comparison more greatly, but modeled burdens in that region are modeled reasonably well. It is likely that underestimates of emissions are a major cause of the observed discrepancies.

6.9.2. Revised Estimate of BC Emissions

[368] Emission rates that would be required to match observations were estimated by applying the monthly regional scale factors described above to modeled emissions in each region. Then annual emissions were determined by summing the monthly emissions. Table 16 shows the annual scaled totals for energy-related and open-burning emissions and compares them with the bottom-up emission estimates in section 4. This division between energy-related and open-burning scale factors depends on the modeled seasonality of these major source groups, as well as the assumption that monthly scale factors for each group are equal. The scaling of emission totals is more robust than the apportionment of scaling between the two categories.

[369] Table 16 summarizes these scaled annual emissions. Three emission estimates are given in the table: modeled emissions, which are an estimate of the median used by AeroCom models; scaled emissions, which are inferred using the burden scale factors applied to monthly emissions; and current emissions, which are the bottom-up estimates summarized in section 4. Current emission estimates are different than those used by the AeroCom models that produced the fields for analysis. Although energy-related emissions are similar, modeled open-burning emissions in AeroCom models were about 35% higher than the most current values.

[370] Scaled estimates for all-source annual emissions are 17,000 Gg BC yr^{-1}, a factor of 2.2 increase over current emission estimates and modeled values. Because AERONET observations from years 2000 to 2009 were used for scaling, this emission estimate is approximately associated with the year 2005. In this simple scaling exercise, energy-related and open-biomass emissions are scaled each month resulting in similar scaling for annual totals which are 10,100 Gg BC yr^{-1} and 6800 Gg BC yr^{-1}, respectively. Table 16 also gives estimates of industrial-era emissions, inferred by subtracting the scaled preindustrial emission values. The industrial-era total is 9750 Gg BC yr^{-1} for energy-related emissions and 4200 Gg BC yr^{-1} for open biomass emissions.

[371] The industrial-era emission estimate of about 13,900 GgC yr^{-1} is the value obtained with a simple scaling of AAOD. However, several caveats apply to the method described here. First, this scaling method neglects the fact

Table 16. Modeled, Scaled, and Current Bottom-Up Annual BC Emissions by Region in Gg yr^{-1}

	Energy-Related Emissions			Open Biomass Emissions			Total Emissions	
Region	Modeled[a]	Scaled[b]	Current[c]	Modeled[d]	Scaled[b]	Current[c]	Scaled[b]	Current[c]
North America	340	400	330	80	100	40	500	370
Latin America	400	800	360	590	1200	720	2000	1080
Middle East	80	140	140	0	0	0	140	140
Africa	500	1200	680	1520	3200	1140	4400	1820
Europe	450	500	470	10	10	10	510	480
EECCA	270	500	310	280	100	120	600	430
South Asia	610	2500	670	20	80	40	2580	710
East Asia	1440	2800	1310	10	20	50	2820	1360
Southeast Asia	380	800	400	400	1400	460	2200	860
Pacific	130	500	120	190	700	170	1200	290
All-source	4600	10,140	4790	3100	6810	2750	16,950	7540
Pre-industrial	*390*	*390*	*390*	*1030*	*2640*	*1030*	*3030*	*1420*
Industrial-Era	4210	9750	4400	2070	4170	1720	13,920	6120

[a]Based on SPEW emissions, which were used in many AeroCom models.
[b]Modeled regional emissions adjusted by burden scale factors as described in section 6.5.1.
[c]As reported in Tables 7 and 8, and Figures 8 and 9, for comparison with the initial and scaled modeled values given here. Current energy-related emissions are a composite of SPEW and GAINS as described in section 4. Current biomass burning emissions given here are from RETRO only and do not match the central estimate for that reason. Biomass burning estimates have decreased substantially since the initial AeroCom exercise.
[d]Based on GFED 2.0 emission fields, reported as the source of open-burning emissions for AeroCom models [*Dentener et al.*, 2006]. Regions scaled identically to total emission rate reported for AeroCom exercise.
[e]Pre-industrial emissions estimated by *Dentener et al.* [2006] and assumed to be constant to estimate industrial-era forcing.

that burden in some regions may be caused by emissions in other regions. According to tagged-tracer modeling given in *Bond et al*. [2011], Middle Eastern concentrations are affected by South Asian emissions, Southeast Asian concentrations have significant contributions from both South Asia and East Asia, and the Pacific region is affected by all Asian emissions. However, the model used tends to over-transport aerosol, as evidenced by atmospheric burdens at high altitudes. A true inverse modeling approach would give a better estimate of emissions in each region, but modeled transport and removal should be more thoroughly evaluated before embarking on such a study. We caution that inferred emissions in Southeast Asia and the Pacific are particularly uncertain.

[372] Second, as discussed above, uncertainties in modeled lifetimes could also contribute to errors in burdens. Changes in modeled lifetime were shown to alter modeled BC by about 10% at the observation sites (Figure 13), which would alter inferred emissions by the same amount. Third, the MAC_{BC} scale factor used here is also simplified because it assumes that BC is always internally mixed and, therefore, amplifies absorption at the observation sites. If BC were externally mixed at observation sites, the MAC_{BC} scale factor would decrease and the burden scale factor would increase. If the appropriate MAC_{BC} scaling were a 20% increase instead of 50%, all-source emissions would be estimated as 21,000 Gg BC yr^{-1}. For an assumed increase of 80%, the estimate would be 14,000 Gg BC yr^{-1}. Finally, observations are sparse in many of the regions with the largest emissions and the largest estimated increases. In the absence of more definitive studies that explain biases in aerosol absorption, the central value is used as a best estimate of industrial-era BC emissions throughout this assessment.

6.9.3. Scaling of Modeled AAOD in the Context of Other Evidence

[373] Inverse modeling studies and other comparisons between models and measurements were discussed in section 5.5.1. As these studies have attributed errors to emission biases rather than modeling of any other factor, we compare them with the emission increases in Table 16.

[374] Scaled emissions for total biomass burning BC of 6800 Gg yr^{-1} are in good agreement with the upper limit derived by *Zhang et al*. [2005]. The increase by a factor of 2.5 falls within the large uncertainty ranges for biomass smoke given by *Reid et al*. [2009] and *Kaiser et al*. [2012]. Carbon monoxide measurements do not indicate such a large discrepancy, so either modeled emission factors or modeled aerosol lifetimes are suspect. Section 4.7.2.3 discussed some reasons why modeled biomass burning emission factors could be too low. These proposed adjustments should also apply to the preindustrial background used here, and hence, the scaling described here is also represented in our estimate of preindustrial AAOD.

[375] The finding that small to moderate emission increases are required in North America and Europe is in reasonable agreement with inverse modeling studies. Scaled emissions in Figure 20 suggest that emissions for East Asia should increase as suggested by *Kondo et al*. [2011a], but by 90% instead of 30%. Since inverse modeling by *Hakami et al*. [2005] suggested that BC emissions in East Asia were approximately correct at an earlier date, the increased emissions may be related to growth, estimated as 30 to 50% [*Lu et al*., 2011]. The higher emission estimates for South Asia are 30% greater than those estimated by *Dickerson et al*. [2002] for a much earlier year, and they agree with observations that modeled burdens in that region are too low by about a factor of 4 to 5.

[376] Total emissions are in reasonable agreement with predictions of a Kalman filter inverse estimate [*Jason Blake Cohen*, personal communication, 2012]. Scaled global energy-related emissions are estimated at 10,100 Gg yr^{-1}, with 80% of the increase appearing in Africa, South, East, and Southeast Asia. Although the apportionment between energy-related emissions and biomass burning is not certain, it would be difficult for the small amount of biomass burning in South and East Asia to cause such a large discrepancy. Applying the higher BC emission factors recommended by *Cooke et al*. [1999] for power generation would cause much greater discrepancies in North America and Europe than currently exist. The evidence points to underestimation of emissions in regions with low regulation, so that sources such as poorly operating vehicles, industrial installations, or high solid-fuel combustion may be responsible.

[377] Land regions of Latin America, Africa, Southeast Asia, and the Pacific region (Figure 7) are, together, responsible for 40% of the global BC AAOD and suggested scaling factors in these regions are 2 to 3.5. Especially uncertain are findings for Africa, where 25% of global AAOD is found, and partitioning between BC and dust affects inferences about the magnitude of BC AAOD. Inverse modeling studies or continent-wide comparisons with long-term measurements have not been reported for these regions.

[378] In summary, we find that global AAOD from AeroCom models is low compared to that suggested by observations, that this underestimate occurs in particular regions, and that it cannot be fully explained by the absorption enhancement produced by internal mixing or by uncertainties in retrievals. Modeled absorption is reasonable in regions with the best measurement coverage, relevant emission measurements, and low biomass-burning emissions: North America and Europe. The dominance of different source categories and larger uncertainties in the other regions (Figure 9 and section 4.7.1) that require increased scaling to match observations suggests that poorly modeled emissions are a potential cause. Studies using space-based remote sensing indicate that modeled aerosol concentrations and absorption from biomass burning are too low (section 5.5.1), and an independent line of argument indicates that biomass-burning emission factors could lead to underestimates of absorption (section 4.7.2.3). Surface measurements in South and East Asia indicate that models using the emissions summarized in section 4 would underestimate observed BC concentrations (section 5.5.1). In Asia, where emissions have increased since the global emission fields were developed (section 4.8), some of the underestimation is to be expected. Although we cannot fully exclude modeled lifetimes, instrumental uncertainties, and the division of remotely-sensed AAOD into BC and dust components in some regions (particularly Africa) as explanatory factors, multiple lines of evidence support the position that AeroCom models using year-2000 BC emissions substantially underestimate absorption and direct radiative forcing. Despite the inherent limitations of these models, they are required to produce estimates of global forcing,

because global space-based observations cannot separate radiative impact by chemical component. Model fields scaled to observations are therefore used to develop our best estimate of direct radiative forcing.

6.10. Summary of Uncertainties in BC DRF

[379] The discussion in this section shows that several factors affecting BC radiative forcing are not well constrained. First, the most quantitative and widespread data set for determining atmospheric absorption is remote sensing provided by AERONET, but use of these observations requires an estimate of the division between AAOD attributable to BC and dust. Different plausible assumptions can greatly alter the inferred BC AAOD, up to a factor of 2. Parameters retrieved from AERONET observations, such as size distributions or wavelength dependence of absorption, have been used in interpreting AAOD data, but these have not been thoroughly evaluated with in situ measurements. Second, the dust refractive index may have large variability within regions [*Moosmüller et al.*, 2012; *Wagner et al.*, 2012] and could greatly affect the estimate of dust AAOD and the inference of BC AAOD. Third, despite the uncertainties, observations indicate more BC AAOD than is modeled by about a factor of 2.5. A simple scaling procedure indicates that a large increase in emission estimates is warranted for biomass burning and for energy-related sources in developing regions. Emission factors may explain low biases in modeled biomass burning emissions, but the cause of errors in energy-related emissions is unknown. Fourth, despite the fact that emission rates are implicated in underestimates of BC AAOD, a full attribution of differences in BC distributions to errors in model emissions, transport, or removal rates is not yet possible. No simple adjustment to modeled transport can explain the range of model biases (section 5.7). Fifth, the contribution of absorbing organic aerosol to AAOD has not been elucidated. Attribution of some of the absorption to OA rather than BC would reduce the direct forcing estimate for BC and make that of OA less negative or more positive. Finally, model evaluations are limited in regions that contribute large fractions of the global AAOD, because few long-term observations are available.

[380] Although present-day observations can be used to adjust modeled forcing terms, a lack of understanding of the causes of bias limits the accuracy of modeled forcing for the past and future. Further, vertical transport and therefore location of BC is poorly modeled, so that modeled absorption forcing efficiency also contains errors. While biases in BC distributions in the Arctic produce only small errors in global, annual average BC AAOD (and thus forcing), they produce large biases in forcing within the Arctic, where BC may contribute to greater-than-expected warming and declines in sea ice [*Quinn et al.*, 2008, 2011]. In subsequent sections, horizontal and vertical distributions are shown to affect the interaction with clouds (section 7) and forcing in snow and sea ice (section 8). Thus, a lack of understanding of process fundamentals and the resulting modeled biases are large sources of uncertainty in all BC forcing terms.

[381] The amount of aerosol in the preindustrial atmosphere is also poorly known. Biomass burning produced much of this aerosol, and preindustrial estimates used here were based on the emissions given by *Dentener et al.* [2006]. Although biomass burning has increased overall during the industrial era, charcoal records suggest that activity in some regions was similar between 1750 and today [*Marlon et al.*, 2008]. Although this preindustrial background does not affect the estimate of total radiative forcing, it does affect industrial-era forcing and temperature change since preindustrial times. We retain conventional nomenclature and refer to this background value as that of 1750, but we caution that it represents a reference atmosphere rather than a true preindustrial value.

7. Black Carbon Interactions With Clouds

7.1. Section Summary

[382] 1. Black carbon may change cloud cover, emissivity, or brightness in four ways: (1) by changing the vertical temperature structure of the atmosphere, which could shift cloud distributions (semi-direct effect); (2) by changing the number concentration of liquid cloud droplets and the lifetime of liquid clouds; (3) by changing phase partitioning and precipitation in mixed-phase clouds; and (4) by changing ice particle number concentration. These effects may cause either positive or negative radiative forcing. Very few model studies isolate the influence of BC on each effect. All aerosol effects on clouds are highly uncertain, and the isolated effects of BC have even greater relative uncertainty.

[383] 2. Many of the cloud effects described here may be considered rapid adjustments, either to direct radiative forcing or to the presence of BC. However, all effects can be quantified in units of climate forcing, a practice we continue here for consistency with previous studies and for convenience.

[384] 3. In the semi-direct effect, cloud cover can increase or decrease, depending on region and conditions. Some studies examining regional cloud reduction have suggested a positive forcing, but global model studies indicate that the BC semi-direct effect averages -0.1 ± 0.2 W m^{-2} for industrial-era forcing if all BC is emitted at the surface. An additional -0.28 W m^{-2} is added to the lower uncertainty range to account for the potential reduction of high-level clouds from biomass-burning BC, making the 90% uncertainty range –0.44 to +0.1 W m^{-2} over the industrial era. Major uncertainties include poorly modeled BC vertical distributions and the fidelity of modeled cloud responses.

[385] 4. BC has two competing indirect effects on liquid clouds. First, adding BC increases the aerosol number concentration. If the number of cloud droplets also increased, negative forcing by clouds would increase, but BC-rich particles are inferior cloud-forming particles. Second, BC particles may also serve as sites to collect soluble material, reducing overall cloud droplet number concentration and producing a positive forcing. BC alone is estimated to have an indirect climate forcing of about -0.1 W m^{-2}. Many studies do not separate this effect from the semi-direct effect discussed above, so an isolated estimate is difficult to obtain. Therefore, we estimate the combined industrial-era climate forcing from liquid-cloud and semi-direct effects as -0.2 (with a 90% uncertainty range of -0.61 to +0.1 W m^{-2}).

[386] 5. Greater absorption by BC within cloud droplets decreases cloud albedo, heats clouds, and dissipates them. This is a special case of the semi-direct effect that we estimate separately as a climate forcing of +0.2 W m^{-2}, with a 90% uncertainty range of −0.1 to +0.9 W m^{-2} over the industrial era. Model results for this effect are very sensitive to the representation of optical properties for the mixed BC and cloud droplet.

[387] 6. The liquid-cloud indirect effect is sensitive to BC particle size and to mixing with other particles. Many model studies indicate that particles emitted from biofuel combustion appear to have more negative forcing per emission than do particles from fossil fuel combustion, possibly because of size or co-emitted POA.

[388] 7. The BC mixed-phase indirect effect acts on clouds that are part liquid and part ice. BC may act as ice nuclei (IN) that enhance ice formation and increase ice fall-out. An estimate for this effect is +0.18 ± 0.18 W m^{-2} for industrial-era climate forcing and 90% uncertainty range, but the magnitude would be reduced for BC mixed with sulfate.

[389] 8. In the ice-cloud indirect effect, greater IN concentrations either increase or decrease the concentrations of ice particles and the lifetime of cirrus clouds, depending on conditions. Cirrus clouds affect both shortwave and longwave radiative fluxes. The cloud cover change and forcing may, therefore, be positive or negative. Two model studies estimate effects of opposite signs: −0.4 and +0.4 W m^{-2}. Laboratory and field observations suggest that both BC concentration and BC's ability to act as IN are probably less than assumed in these model estimates. We estimate an industrial-era climate forcing of 0 ± 0.4 W m^{-2} (90% uncertainty range) for this highly uncertain effect, which excludes the effects of aviation. These effects are sensitive to assumptions about BC's role as IN and to the number concentration and mixing state of BC particles in the free and upper troposphere. Ice-cloud effects also depend on the assumed background conditions, including concentrations of other IN and updraft velocities.

[390] 9. Few modeling and measurement studies are able to constrain cloud-absorption, mixed-phase and ice-cloud indirect effects. Consequently the uncertainties are large. Model diversity, rather than true uncertainty propagation, provides uncertainties in cloud radiative forcing.

7.2. Introduction

[391] Clouds and their responses to aerosol addition introduce a large uncertainty in the understanding of total climate forcing and climate response [*Heintzenberg and Charlson*, 2009]. The general term "indirect effects" refers to the suite of climate forcings that aerosols impose through the modification of cloud properties [*Forster et al.*, 2007; *Denman et al.*, 2007]. Aerosol indirect effects on clouds have been extensively studied, but the influence of BC alone has received less attention. Although BC makes a small contribution to aerosol mass load in the atmosphere, it may play an important role in determining the CCN or IN particle number concentration that in turn alters indirect effects. Aerosol indirect effects and BC's role in the indirect effect differ depending on the cloud phase: liquid, ice, or "mixed" containing both liquid and ice, and these are discussed individually. Furthermore, absorption by BC embedded within cloud droplets is greater than that of BC alone or with coatings.

[392] Figure 24 summarizes the mechanisms by which BC can influence clouds. A brief overview is given here before the detailed discussions in the remainder of this section. The first general class of effects involves perturbations to the atmospheric temperature structure, which affect cloud distributions. These mechanisms are commonly termed "semi-direct effects," a term that is sometimes used to describe evaporation of cloud droplets when absorbing aerosols heat a cloud layer [*Hansen et al.*, 1997; *Ramanathan et al.*, 2001a]. Additional BC radiative effects have also been documented whereby cloud cover may be either enhanced or reduced, depending on factors such as its altitude relative to cloud cover [e.g., *Hansen et al.*, 2005; *Johnson et al.*, 2004], and meteorological conditions. BC's semi-direct effects are a rapid adjustment to BC direct radiative forcing, through local warming of the atmosphere. Some model calculations treat this adjustment as a distinct forcing term. Following these studies, and consistent with other treatments in this assessment, we review semi-direct estimates in forcing units.

[393] Another general category, commonly termed "indirect effects," involves changes in concentrations of cloud droplets or ice crystals that alter cloud brightness, emissivity, and lifetime, which produce a radiative forcing. This category includes the groups titled "liquid-cloud effects," "mixed-phase cloud effects," and "ice-cloud effects" in Figure 24. These cloud effects are driven by changes in the number of CCN or IN, aerosols on which cloud droplets or ice particles may form. The process of forming a stable liquid droplet or ice particle is known as activation. In principle, any particle can activate in either liquid or ice clouds if high enough supersaturation is reached. However, when many aerosol types are present, the particles that activate the most easily do so first and have the greatest potential influence on the resulting number concentration of cloud particles. Microphysical characteristics of a particular type of aerosol are thus very important in determining its cloud effects.

[394] Warm cloud indirect effects include two components. The cloud albedo effect (i.e., the first indirect or Twomey effect) [*Twomey*, 1959] refers to the change in radiation caused by a change in cloud albedo or brightness resulting from a change in the cloud droplet size distribution. Increased CCN lead to more and smaller cloud liquid droplets for a given cloud water content (case LC1 in Figure 24). This effect can be observed in ship-track studies [e.g., *Ferek et al.*, 1998]. However, if BC attracts condensing gases that would otherwise form particles, the net result is a decrease in CCN and cloud droplets and is, therefore, a positive radiative forcing (case LC2) [*Bauer et al.*, 2010].

[395] The cloud lifetime effect (LC3, second indirect effect) refers to the fact that in the presence of increased aerosol concentrations, more and smaller cloud droplets form, and these collide less efficiently. Factors such as drop evaporation rates and depletion of water vapor can also alter cloud lifetimes. While cloud resolving models suggest that this effect could lead to either an increase or decrease in liquid water [*Ackerman et al.*, 2004; *Sandu et al.*, 2008], the GCMs are parameterized such that this effect can only lead to longer cloud lifetimes with greater overall cloud reflectivity [*Lohmann and Feichter*, 2005]. Thus, although this forcing could be either positive or negative, GCM global estimates of LC3 are always negative. Altered lifetime also plays a role in mixed-phase clouds, where temperatures

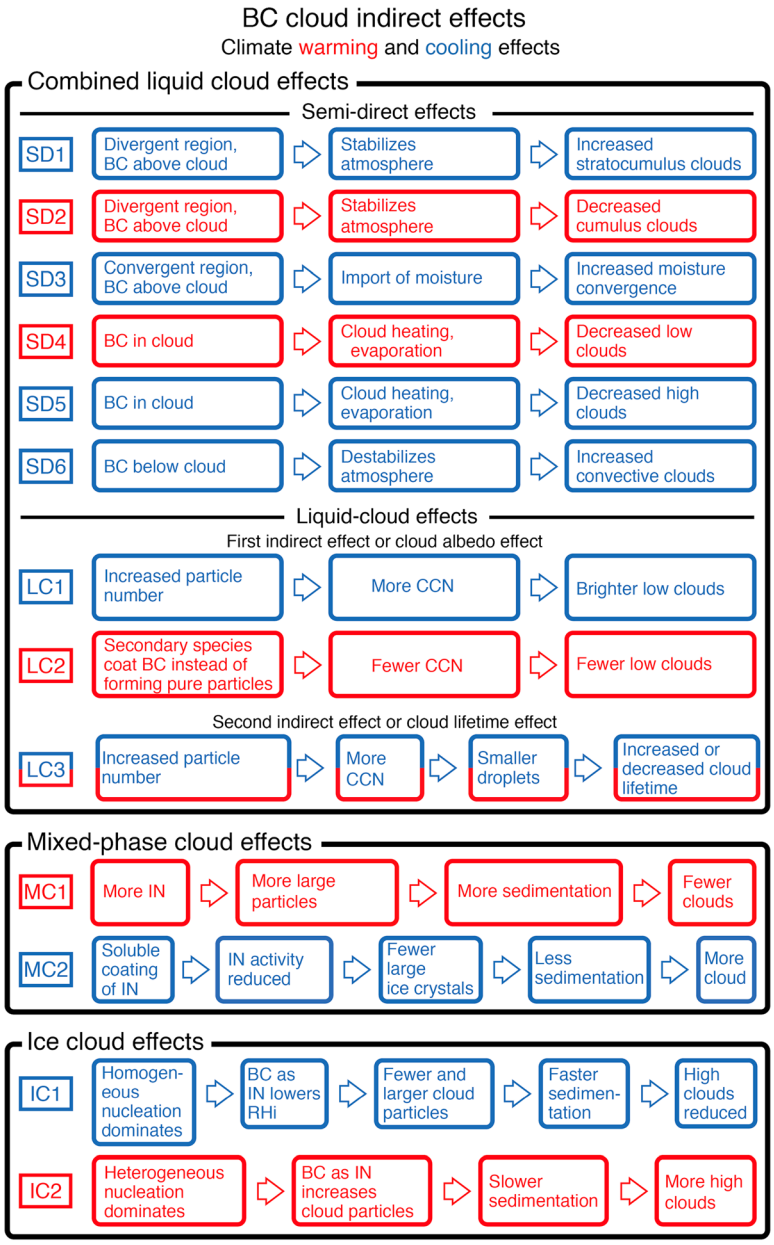

Figure 24. Schematic of the causes and effects that lead to cloud effects from BC emissions. Each row begins with an identifying label followed by a cause, namely, an atmospheric or microphysical parameter representing a potential perturbation to cloud properties. To the right of each cause are the response(s) to the perturbation. On the far right is the associated effect, namely, the cloud parameter that changes in response to the perturbation. The single color of the components in a row indicates a climate system response of warming (red) or cooling (blue). The split coloring in LC3 indicates that the response can be either warming or cooling (section 7.2). Although MC2 is not attributable directly to BC, it is included here because it alters the effects of BC.

typically fall between 0 and −35°C. Two competing effects have been suggested: first, glaciation, which refers to an increase in ice nuclei causing more frequent glaciation of supercooled clouds, and second, de-activation. In the glaciation effect, ice crystals grow at the expense of water droplets because of the difference in vapor pressure between water and ice, referred to as the Bergeron-Findeisen effect. An increase in IN would enhance this process, causing clouds to precipitate more readily (case MC1 in Figure 24) and thereby reducing cloud amount [*Lohmann*, 2002]. However, deactivation occurs when sulfur or secondary organic aerosol coat IN and make them less efficient [*Girard et al.*, 2005] in mixed-phase clouds by changing the mode of freezing from contact to immersion freezing. In global climate models, this leads to less sedimentation and more cloud cover [*Storelvmo et al.*, 2008; *Hoose et al.*, 2008] (case MC2 in Figure 24).

[396] BC may also affect cirrus clouds that occur at high altitude in the upper troposphere [*Kärcher and Spichtinger*, 2009]. Aerosol particles at these high altitudes have long

atmospheric lifetimes [e.g., 4–30 days; *Williams et al*., 2002] and, therefore, extended opportunities for mixing with other aerosol components. Thin, high cirrus clouds are believed to have net positive cloud forcing [*Chen et al*., 2000]. Absorption of infrared radiation and re-emission at colder temperatures dominates scattering of solar radiation, which results in a net positive forcing. Efficient IN may either increase or reduce cirrus cloud forcing. Cirrus cloud particles are mostly formed through homogeneous ice nucleation. Even a small number of particles can initiate heterogeneous freezing well below the homogeneous freezing threshold, depleting some of the supersaturated water vapor, partially preventing homogeneous formation of solution droplets and reducing the number of particles [e.g., *Kärcher et al*., 2006]. Early onset of nucleation from a few efficient BC particles affects forcing less than enhanced sedimentation, yielding case IC1 in Figure 24. If high concentrations of IN already exist, heterogeneous freezing dominates the cloud and additional IN increase the number concentration of cloud particles (case IC2 in Figure 24).

[397] Some challenges are common in obtaining forcing from models of aerosol-cloud interactions. First, models use different emission levels and input assumptions, and variation in values of direct forcing may result from these differences alone. Second, each model study may have a different set of impacts, such as treating aerosol interactions with only liquid or ice clouds, or allowing certain climate responses. The net effect on radiation is usually inferred from two sets of simulations—one with and one without perturbed pollution conditions [*Lohmann et al*., 2010]—so that the individual effects contributing to the changes are difficult to distinguish without well-designed diagnostics. The combination of varying inputs and inconsistent selection of effects makes global cloud-forcing estimates difficult to compare. Third, some aerosol-induced changes are best simulated at scales smaller than a global model grid box. Physical confirmation of the factors governing cloud dynamics and cloud microphysical interactions must also occur on relatively small scales. Cloud-resolving models (CRMs) and large-eddy simulations (LES) may be most appropriate for modeling these scales, but these simulations do not have the spatial extent to calculate globally averaged forcing, and do not always agree with the results of global models that use coarser resolutions. The reasons for these disagreements is not always understood, making it difficult to infer a global, annual average forcing from either set of model studies. Fourth, some effects that cause cloud redistribution on large scales are best simulated with global models, but their broad spatial or temporal extent makes their existence and magnitude difficult to confirm. Fifth, the fidelity of aerosol-cloud simulations depends on accurate representation of the cloud amount and location, yet these factors are not often verified in the model studies. Finally, inter-annual and spatial variability of modeled cloud forcing is large compared with the magnitude of the aerosol-induced changes. Therefore, extracting statistically significant changes is challenging.

[398] While aerosol effects on clouds are complex, accounting for them is critical because they may induce changes similar to or greater than aerosol direct forcing. For a perspective on all aerosol effects, *Denman et al*. [2007] summarized studies ranging from a mean of -1.2 W m^{-2} with a range of -0.2 to -2.3 W m^{-2} for the total effect of all anthropogenic aerosols on climate, including direct forcing, cloud albedo, cloud lifetime, and semi-direct effects. Using a combination of 10 models and input from relationships observed by satellite, *Quaas et al*. [2009] estimated the total aerosol effect on stratiform clouds as -1.5 ± 0.5 W m^{-2}. The global annual mean climate forcing for just the first indirect effect of all aerosols has been estimated from GCMs with some guidance from satellite observations as -0.7 W m^{-2} with a range between -0.3 and -1.8 W m^{-2} [*Forster et al*., 2007]. Notably, *Lohmann et al*. [2010] showed that estimates of total anthropogenic aerosol effects have become smaller with time. GCMs have added processes, such as aerosol effects on mixed-phase clouds, or treating rain as a prognostic variable, which place more emphasis on accretion instead of autoconversion. These more advanced GCMs arrive at smaller total anthropogenic cloud forcing compared with earlier versions. GCMs that are constrained by satellite data also predict a smaller total anthropogenic aerosol effect.

[399] This assessment mainly presents global, annually averaged climate forcing by semi-direct and indirect effects. However, forcing within a given region may differ significantly from this average. For example, in the Arctic the combined semi-direct and indirect effect of aerosols may produce a much smaller negative forcing than on the global average, or possibly even a positive forcing [*Koch et al*., 2009a; *Jacobson*, 2010; *Alterskjær et al*., 2010], because of the Arctic's high surface albedo and because changes in cloud emissivity due to aerosol microphysical effects may produce significant positive forcing in late winter and spring [*Garrett and Zhao*, 2006].

[400] In summary, BC may affect clouds by perturbing the atmospheric thermal structure, or by changing liquid cloud droplet number concentration, ice crystal number concentration, or some combination of the two in mixed-phase clouds. Each of these processes affects the distributions or reflectivity of clouds, which, in turn, alters the radiative balance of the Earth. As such, these are rapid adjustments to the climate system that can be quantified as adjusted forcings (section 2.3 and Table 2). The role of BC in each of these cloud effects is presented below, including increased absorption by BC inclusions in cloud droplets (section 7.3.3), semi-direct effects (section 7.3.2), indirect effects on liquid clouds (section 7.4), and mixed and ice phase clouds (section 7.5). Although modeled cloud forcing depends on assumed emission rates or simulated atmospheric burden, this dependence may not be linear, so scaling modeled forcing to the new emission rates or forcing determined in section 6 is also discussed for each effect. Best estimates of adjusted forcings are calculated for the combined semi-direct and liquid-cloud effects for mixed-phase clouds and ice clouds. These estimates are followed by a discussion of uncertainties (section 7.7). All cloud forcings discussed here are industrial-era forcings; all-source forcings are not estimated. Clouds in a clean atmosphere are much more susceptible to change than clouds in an atmosphere with even a small aerosol background [*Boucher and Pham*, 2002], so cloud forcing is always calculated against a preindustrial background.

7.3. Black-Carbon Semi-Direct Effects on Cloud Cover

[401] Atmospheric BC absorbs solar radiation, perturbs the temperature structure of the atmosphere and, therefore, influences the cloud distribution. The first of these effects to be documented, the original semi-direct effect, is the evaporation and dissolution of clouds by BC suspended near or within clouds [*Hansen et al*., 1997]. Since then, numerous studies have demonstrated this effect, as well as additional mechanisms by which BC either increases or reduces cloud cover. Some of these studies use cloud-scale models, some are observational—typically with focus on a particular region—and some use global models. *Koch and Del Genio* [2010] reviewed many studies on this topic, which are summarized here. The top segment of Figure 24 summarizes a framework proposed by *Koch and Del Genio* [2010] to classify previous studies.

[402] Each of the effects shown in the top portion of Figure 24 is the result of a rapid adjustment to the initial direct radiative forcing by BC. Following the terminology defined in section 2, the sum of the direct effect and the semi-direct effect can be interpreted as a single "adjusted forcing." However, model studies to date have either calculated the semi-direct effect as an independent forcing, derived a combined forcing for the semi-direct and liquid cloud effects, or report a reduced efficacy for BC direct radiative forcing, attributing this decrease to semi-direct effects. Because semi-direct effects are diverse, all changes other than cloud microphysical changes might be grouped under this label [e.g., *Ghan et al*., 2012]. For consistency with the existing literature, we also discuss the semi-direct effect here as a climate forcing term and include the efficacy studies in our estimate of that forcing.

7.3.1. Cloud Scale and Regional Studies

[403] The altitude of BC relative to a cloud or potential cloud layer plays an important role in determining the cloud response. For aerosols embedded near cloud, cloud evaporation is enhanced due to their heating and reduction of relative humidity (Figure 24, case SD4). This effect was demonstrated in the LES experiments of *Ackerman et al*. [2000] for trade cumulus and *Hill and Dobbie* [2008] and *Johnson et al*. [2004] for marine stratocumulus clouds.

[404] Absorbing aerosol aloft increases atmospheric stability. Increased stability over stratocumulus clouds reduces cloud-top entrainment of overlying dry air and tends to strengthen the underlying clouds (Figure 24, case SD1). LES experiments by *Johnson et al*. [2004] showed that absorbing aerosols above cloud increased cloud cover, because they increased the difference in potential temperature across the inversion, decreased entrainment rate, and caused a shallower, moister boundary layer with higher liquid-water path. The same model had demonstrated cloud reduction when absorbing aerosols were within the cloud layer (Figure 24, case SD4). *Brioude et al*. [2009] analyzed satellite cloud observations and modeled biomass-burning tracers for a field study near the coast of California. They found that biomass-burning aerosols enhanced cloud cover, especially for high-humidity conditions and for low lower tropospheric stability conditions, when the aerosols increased lower tropospheric stability. Similarly, *Wilcox* [2012] analyzed satellite data of subtropical, South Atlantic biomass-burning smoke overlying marine stratocumulus clouds and found that the smoke enhanced the cloud liquid-water path, countering more than 60% of the smoke direct radiative effect.

[405] While the stabilizing effect of absorbing aerosols aloft can enhance stratocumulus cloud cover, they may suppress cumulus cloud development (Figure 24, case SD2). *Fan et al*. [2008] performed experiments in a cloud-resolving model for the Houston area and demonstrated that absorbing aerosols aloft decreased the temperature lapse rate, leading to a more stable atmosphere and decreased convection. MODIS observational studies for the Amazon biomass burning season by *Koren et al*. [2004, 2008] also demonstrated cumulus cloud cover reduction due to increased smoke. They argued that smoke plumes stabilized the boundary layer, reducing convective activity and boundary layer cloud formation. The smoke also reduced radiation penetration to the surface, therefore reducing evaporation and atmospheric moisture. *Ten Hoeve et al*. [2011] used satellite observations of biomass-burning regions to show that cloud optical depth increased with AOD for low values, consistent with cloud brightening (case LC1). At higher AOD values, cloud optical depth decreased with AOD, possibly due to cloud evaporation (case SD4).

[406] On the other hand, in some land regions, lofted absorbing aerosols may enhance upper level convection, promoting low-level moisture convergence of oceanic air masses, which could increase continental clouds (Figure 24, case SD3). Monsoon enhancement due to lofted absorbing aerosols (known as the "Elevated Heat Pump" hypothesis) was shown in the global model studies of *Lau et al*. [2006], *Randles and Ramaswamy* [2008], and *Chung et al*. [2002]. However, global climate models are limited by relatively coarse spatial resolution, which may preclude accurate representation of aerosol transport over the Tibetan Plateau. In a study using observed vertically resolved aerosol distributions over the Tibetan Plateau and surrounding regions, *Kuhlmann and Quaas* [2010] use observed surface albedo and a radiative transfer model to show that aerosols do not produce the large elevated heating needed to drive the Elevated Heat Pump. In the non-monsoon season, wintertime pollution as observed in the Indian Ocean Experiment reduced the meridional temperature gradient in the global model study of *Ramanathan et al*. [2005], which included a coupled ocean response. These SST shifts were found to enhance precipitation over sub-Saharan Africa [*Chung and Ramanathan*, 2006]. Many studies predicting enhanced convergence over land indicate a shift in clouds and precipitation rather than an overall enhancement.

[407] BC below cloud generally promotes convective activity and can enhance cloud cover (Figure 24, case SD6). Cloud resolving model studies of *McFarquhar and Wang* [2006] for trade wind cumuli demonstrated that absorbing aerosols placed below cloud promoted vertical motion and increased liquid water path. Similarly, LES experiments of *Feingold et al*. [2005] found that Amazon smoke emitted at the surface could destabilize the surface layer and increase convection and cloud cover. However, smoke at cloud level decreased cloud cover and promoted dissipation in both of these studies.

7.3.2. Global Model Semi-Direct Estimates

[408] Consistent with the variety of responses found in regional studies, global model studies also find that regional variations and global-average forcing include positive and negative forcing effects over all regions. Although semi-direct effects cause positive forcing in some regions, most

Table 17. Studies Used to Estimate Values of the Semi-Direct Effect

Study	Reported Semi-direct Effect ($W\,m^{-2}$) and Efficacy	Adjustment Type (Value Used in Study)[a]	Adjusted Effect ($W\,m^{-2}$)
Semi-direct effect calculated directly			
Penner et al. [2003]	−0.01, surface emissions	EM (12.2 $Tg\,yr^{-1}$)	−0.01
	−0.39, lofted BB emissions	EM (BB) (5.6 $Tg\,yr^{-1}$)	−0.28
Wang [2004]	−0.16	EM (14 $Tg\,yr^{-1}$)	−0.16
Ghan et al. [2012]	−0.10 to +0.08	EM (7.6 $Tg\,yr^{-1}$)	−0.18 to +0.15
Semi-direct effect inferred from efficacy[b]			
Hansen et al. [2005]	−0.08 (0.58)	DRF (+0.19 $W\,m^{-2}$)	−0.30
Hansen et al. [2005]	−0.11 (0.78)	DRF (+0.49 $W\,m^{-2}$)	−0.16
Chung and Seinfeld [2005]	−0.1 (0.70)	DRF (+0.33 $W\,m^{-2}$)	−0.21
Yoshimori and Broccoli [2007]	−0.40 (0.59)	DRF (+0.99 $W\,m^{-2}$)	−0.29
Jones et al. [2007]	−0.11 (0.71)	DRF (+0.39 $W\,m^{-2}$)	−0.21

[a]Adjustments: EM = scaled from BC emissions used in study to our estimate of BC emissions (13.9 $Tg\,yr^{-1}$ or 4.0 $Tg\,yr^{-1}$ for biomass); DRF = scaled from BC direct forcing found in study to industrial-era direct forcing of +0.71 $W\,m^{-2}$; BB = biomass burning. For comparison to emission values in the remainder of the document, 1 Tg = 1000 Gg.

[b]Reported effect = −DRF × (1 − efficacy). The two values from *Hansen et al.* [2005] are together weighted equally to the other studies.

models indicate that the global average is negative. Table 17 tabulates the studies discussed here.

[409] *Wang* [2004] performed experiments in the NCAR model, with and without BC. One type of experiment included an ocean temperature response; a second experiment had fixed observed sea-surface temperatures. He found that BC in the experiments with ocean response had enhanced convective activity and cloud cover in the northern branch of the intertropical convergence zone, with a smaller magnitude reduction in clouds and convective activity in the south. The cloud forcing change (i.e., the difference between all-sky and clear-sky radiative flux change due to BC) was −0.16 W m^{-2} at the ToA. However, the simulation using observed sea-surface temperatures gave a cloud forcing of −0.06 W m^{-2}. BC did not warm the climate in these experiments, due to compensating cooling from increased cloud cover.

[410] In sensitivity studies of a coupled transient climate model study, *Koch et al.* [2011b, section 6] showed that removal of BC from 1970 to 2000 would not have caused significant climate cooling. BC removal cooled the atmospheric column, but it also reduced low-level stability and caused a decrease in low-level clouds. Therefore, the surface air temperatures were not significantly decreased, probably due to the loss of low-level clouds. *Koch et al.* [2011a] did not isolate the forcing by the semi-direct effect from that of the direct effect, so it is not included in Table 17.

[411] *Roeckner et al.* [2006] performed future transient climate simulations in the ECHAM5 model, with one simulation including projected increases for carbonaceous aerosols (37% BC and 25% particulate organic matter relative to year 2000). This model included indirect as well as direct and semi-direct effects and did not separately diagnose the individual forcings, so it is not included in Table 17. Increased BC in a region caused cooling there, mostly near African biomass burning regions. In these regions, liquid water path and precipitation increased, possibly due to enhanced instability (Figure 24, case SD6); the additional cloud cover reduced surface solar radiation and cooled the surface. For this study, the increased organic carbon together with the indirect effects might also contribute to the increased cloud cover.

[412] Some global model studies show reduced high-level clouds from BC, also a cooling effect (Figure 24, case SD5) [*Penner et al.*, 2003; *Menon and Del Genio*, 2007; *Jacobson*, 2010]. Small-scale models have also simulated this effect [*Fan et al.*, 2008]. *Penner et al.* [2003] found a negligible semi-direct effect for fossil fuel and biomass burning in the GRANTOUR GCM when all aerosols were injected at the surface. However, when biomass-burning aerosols were injected aloft, they found a net negative semi-direct cloud climate forcing response to carbonaceous aerosols (both BC and organic carbon), mostly due to loss of high-level clouds. In most other studies, BC aerosols were injected at the surface and the response was smaller. *Menon and Del Genio* [2007] also reported a negative semi-direct effect of −0.08 W m^{-2} in their GISS simulations due to decreased long-wave cloud forcing and loss of high-level clouds, mostly in biomass burning regions. This study did not specify how the semi-direct effect was calculated nor what was used for emissions in the baseline and forcing scenarios, so it is not included in Table 17. *Lohmann and Feichter* [2001] obtained a negative direct plus semi-direct effect of −0.1 W m^{-2} in their ECHAM simulations. However, this value was smaller than the inter-annual standard deviation. The semi-direct forcing was not isolated, so this study is also not included in Table 17. *Ghan et al.* [2012] isolated liquid-cloud effects by setting aerosol refractive indices to zero, allowing an estimate of the semi-direct effect by difference. Changes in shortwave and longwave radiation were of similar magnitudes and totaled −0.10 to +0.08 W m^{-2} depending on the aerosol representation.

[413] Some studies report BC direct radiative forcing "efficacy" of less than one instead of calculating a negative semi-direct forcing as a rapid adjustment to the direct forcing. The definition of efficacy is temperature change per forcing relative to that for CO_2, so that efficacy of less than one indicates that a mechanism acts to reduce the positive direct radiative forcing (Table 2). In some cases, these studies indicate that either increased low-to-middle level or decreased upper level cloud changes are responsible for radiative forcing efficacies less than one [e.g., *Roberts and Jones*, 2004; *Hansen et al.*, 2005; *Yoshimori and Broccoli*, 2008]. It is noteworthy that BC radiative forcing efficacy estimates are consistently about 0.6 to 0.8. If we assume that the reduced BC radiative forcing efficacy is entirely due to cloud cover changes, we can infer BC semi-direct forcing

estimates for these models. This is justified by the fact that adjusted forcing efficacies for absorbing aerosol are much closer to 1.0, implying that rapid adjustment accounts for most of the small radiative forcing efficacy [*Shine et al.*, 2003; *Hansen et al.*, 2005; *Crook et al.*, 2011].

[414] *Roberts and Jones* [2004] found that the radiative forcing efficacy of BC was 0.62, due mostly to reduction of high-altitude clouds. *Hansen et al.* [2005] found BC radiative forcing efficacy of 0.78 for fossil fuel BC and 0.58 for biomass-burning BC and direct forcing values of +0.49 W m^{-2} and +0.19 W m^{-2}, respectively. If their smaller than 1.0 radiative forcing efficacies are all due to rapid adjustment of clouds, the semi-direct effect forcings are −0.11 and −0.08 W m^{-2}, respectively. *Yoshimori and Broccoli* [2008] had efficacy of 0.59 for direct BC radiative forcing of +0.99 W m^{-2}, giving a maximum semi-direct effect forcing of −0.4 W m^{-2}. *Jones et al.* [2007] report a BC radiative forcing efficacy of 0.71 for BC forcing of +0.39 W m^{-2}, for an inferred semi-direct effect of −0.11 W m^{-2}. *Chung and Seinfeld* [2005] calculated a 0.70 radiative forcing efficacy for 0.33 W m^{-2} direct forcing, giving a −0.1 W m^{-2} semi-direct effect. These efficacy studies give a range of −0.4 to −0.08 W m^{-2} of inferred semi-direct effect of BC. The finding of a narrow range of efficacies implies that this effect is approximately linear with direct forcing. The range is altered to −0.30 to −0.15 W m^{-2} when each study is scaled to either direct forcing of +0.71 W m^{-2} (for those studies that reported forcing) or to industrial-era emissions of 13,900 Gg yr^{-1}. These scaled estimates are given in Table 17.

[415] Our estimate of the climate forcing from the BC semi-direct effect for emissions that do not have significant lofting, scaled to 13,900 Gg yr^{-1} emissions, is -0.1 ± 0.2 W m^{-2}. The central value is the average of the *Wang* [2004] climate forcing estimate, scaled as described above, the near-zero sum of fossil fuel and biomass values from *Penner et al.* [2003], the *Ghan et al.* [2012] value, and the five efficacy estimates scaled to a BC climate forcing of +0.71 W m^{-2}. Most of these estimates come from studies that isolate pure BC, but the *Penner et al.* [2003] estimate is for BC and OC. All estimates used in this average came from models where emissions were injected at the surface. The magnitude of our uncertainty estimate is larger than the standard deviation of the studies but reflects inter-annual variability and sensitivity analyses reported by individual studies.

[416] The semi-direct estimate is influenced by the five studies that cast the response in terms of radiative forcing efficacy. These studies may have included other climate responses in addition to changes in cloud amount, so we caution against comparing this value with pure estimates of the semi-direct effect.

[417] As noted above, *Penner et al.* [2003] also estimated a large negative semi-direct effect when all aerosols from open biomass burning were injected aloft (−0.39 W m^{-2}). This estimate was given for a larger emission rate; scaled to our anthropogenic biomass-burning estimate of 4000 Gg BC yr^{-1}, the additional semi-direct forcing would be −0.28 W m^{-2}, with a 100% uncertainty given by the inter-annual variability. We do not have estimates of the quantity of biomass burning aerosol that is lofted, but it is less than 100%. We have added this value as an asymmetric uncertainty to the lower bound of the semi-direct forcing. When we estimate forcing by individual source categories (section 11), this uncertainty for lofted aerosol is attributed entirely to biomass-burning emissions. All other BC emissions are emitted near the surface.

[418] Semi-direct effects are strongly dependent on the amount of absorption [e.g., *Johnson et al.*, 2004; *Fan et al.*, 2008; *Randles and Ramaswamy*, 2008; *Perlwitz and Miller*, 2010; *Wang*, 2004]. For example, *Perlwitz and Miller* [2010] showed that in GISS model climate simulations, dust with sufficiently large and absorbing AOD caused global mean cloud cover to increase. For weakly absorbing dust, mean cloud cover decreased. *Johnson et al.* [2004] showed that absorbing aerosols above stratocumulus cloud level strongly increase cloud cover, an effect that did not appear with scattering aerosols. Two global model studies found net decreased cloud cover in response to total pollution aerosols, and positive semi-direct effect [*Allen and Sherwood*, 2010; *Lohmann and Feichter*, 2005], but BC effects were not separated in these studies.

[419] Although global models simulate a negative semi-direct effect, the models have substantial uncertainties. Because cloud enhancement is caused mostly by BC above cloud level, model BC altitude distributions must be accurate. As discussed in section 6.6.1, models are especially diverse in their simulated altitude distribution of BC, and measurements to verify vertical distributions are sparse (section 5.6). Many of the models that simulate negative semi-direct effects overestimate BC at high altitude, when compared with a few available BC measurements over North America [*Koch et al.*, 2009b]. Further, global model cloud schemes may not be able to reproduce some small-scale features that would influence the semi-direct effect, such as cloud layer thickness, cloud-top entrainment, cloud fraction, and the tendency to drizzle, which are affected by the scale of interactions among radiation, turbulence, and moist physics on small horizontal and vertical scales. However, the models should capture many larger-scale features, such as stabilizing or destabilizing of the boundary layer, cloud burn-off, and impacts on larger circulation.

[420] Model cloud responses to absorbing aerosols have not been compared carefully with cloud-scale model and field studies for specific conditions. The framework presented here, and in greater detail in *Koch and Del Genio* [2010], requires ongoing revision as future studies provide information.

7.3.3. Increased Absorption by Cloud Droplet Inclusions

[421] Absorption by BC increases when it is covered with non-absorbing material [*Graßl*, 1975; section 2.7.3.2], including water. This increase affects both the amount of atmospheric absorption attributable to BC and the estimated absorption that is collocated with clouds, with both effects possibly leading to positive forcing. The lack of simulated absorption by mixed or cloud-borne BC in most models probably affects the general prediction of the global average semi-direct effect.

[422] Forcing due to altered cloud albedo was first estimated by *Chylek et al.* [1984, 1996] as 1 to 3 W m^{-2} in a simple analysis that assumed fixed volume fractions of BC within cloud droplets. *Chuang et al.* [2002] used a

chemical transport model to estimate the positive forcing as +0.07 W m^{-2}, although it was not clear how they determined the fraction of BC within droplets. Models that simulate the dynamics of aerosols and clouds find that although more than 90% of BC in the atmosphere passes through and is removed by clouds, the short residence time of BC in clouds results in only a few percent of the global BC burden being present in cloud droplets at a given time [*Jacobson*, 2012; *Ghan et al*., 2012]. *Stier et al*. [2007] and *Ghan et al*. [2012] estimated direct forcing by BC in droplets as +0.02 W m^{-2} and less than +0.01 W m^{-2}, respectively, using the Bruggeman mixing rule to represent BC-droplet absorption. The dynamic effective medium approximation predicts the greatest absorption increase for wetted particles [*Jacobson*, 2006]. It is consistent with the small number of laboratory studies measuring absorption at high relative humidity (section 3.7.1) and results in a direct forcing change of +0.05 to 0.07 W m^{-2}. Another mechanism involves droplet heating by BC and subsequent deactivation of CCN, but this has been shown to be insignificant at appreciable supersaturation levels [*Conant et al*., 2002].

[423] A potentially greater forcing results from cloud burn-off when cloud-borne BC increases absorption within clouds. The forcing results summarized in the preceding paragraph do not account for this effect. The choice of model to represent absorption by BC residing within cloud droplets greatly affects the modeled absorption and, thus, the thermodynamic effect on clouds. In the model with lower absorption described above, cloud absorption caused a small negative semi-direct effect [−0.07 W m^{-2}, *Ghan et al*., 2012]. However, predicted heating rates within clouds are 2 to 2.3 times greater when the dynamic effective medium approximation is used, compared with a core-shell treatment [*Jacobson*, 2012]. *Jacobson* [2010] found an increase in temperature of +0.18K for fossil fuel soot and +0.31K for fossil fuel plus biofuel soot and gases, when cloud absorption by BC and its resulting feedbacks were included versus excluded (see their Figure 1a). With the equilibrium climate-sensitivity of this model (0.6K (W $m^{-2})^{-1}$), these temperature changes correspond to a forcing increase of +0.30 W m^{-2} for the effect of cloud absorption by fossil fuel soot effect alone. Cloud absorption by fossil fuel plus biofuel soot and gases has a greater forcing of +0.52 W m^{-2}, but these simulations may include effects other than those of BC. All of these forcing estimates include the small forcing change caused by cloud albedo. When the soot-only values are scaled to our industrial-era emission rate of 13,900 Gg yr^{-1}, this climate forcing would be +0.76 W m^{-2}. However, some plausible optical treatments produce much lower in-cloud heating rates in *Jacobson* [2012] and lower forcing in *Jacobson* [2006].

[424] The cloud absorption effect is highly uncertain because there are few measurements of aerosol optical properties at cloud conditions or of the relationship between in-cloud aerosol absorption and cloud dissipation. Although it is difficult to assign a central estimate under these circumstances, we average the negative estimate of *Ghan et al*. [2012] and an average of the highest and a mid-range estimate from the Jacobson studies (+0.54 W m^{-2}) to obtain a very uncertain central estimate of +0.2 W m^{-2} for this effect, with uncertainty bounds of (−0.1, +0.9) W m^{-2}. The upper bound comes from using the highest forcing-per-emission obtained from *Jacobson* [2010] for the case of fossil fuel and biofuel soot.

7.4. BC Indirect Effects on Liquid Clouds

[425] Although aerosol liquid-cloud indirect effects have been extensively studied, only a few studies isolate the influence of BC alone. Many models do not have adequate sophistication to simulate aerosol microphysics, including mixing between BC and other aerosol species and the evolution of aerosol size distribution. Earlier model studies had minimal treatment of the aerosol microphysics that are important for capturing the gaseous and aerosol interactions that dominate CCN concentrations and, hence, the BC indirect effect. Below we review earlier literature, discuss the importance of aerosol microphysics, and summarize results from studies that include the microphysics of aerosol-cloud interactions.

[426] Two simple global model studies estimated the effect of BC on liquid-cloud indirect effects and found a negative BC indirect effect. *Hansen et al*. [2005] estimated that BC contributed 5% of the aerosol indirect effect in a model study with the net indirect effect magnitude prescribed and parameterized so that cloud cover and cloud albedo are augmented proportionately to the logarithm of the aerosol number concentration. Aerosol number concentration was derived from aerosol mass and assumed size, and aerosols were externally mixed. *Chuang et al*. [2002] estimated the liquid-cloud effects of carbonaceous aerosols, using a parameterization of cloud droplet number concentration (CDNC or the number of cloud droplets per volume of cloud). CDNC was parameterized based on Köhler theory but without explicit aerosol microphysics. They estimated that carbonaceous aerosols from biomass-burning and fossil fuels contributed 63% and 28% of the indirect effect, respectively; these aerosols contained both BC and organic carbon. Sulfate had a smaller effect because of its lower burden. The total indirect effect was approximately proportional to the atmospheric burden, but the effects of different species were slightly less than additive.

[427] BC could have a substantial influence on the indirect effect due to its potentially large contribution to aerosol number concentration rather than aerosol mass. However, number concentration of aerosol and BC mass are not linearly related. BC also provides a surface upon which volatile inorganic or organic compounds may condense. In the absence of BC, sulfate might preferentially nucleate fresh particles and additional sulfate would condense upon pure sulfate particles. In general, larger particles make better CCN or IN, although CCN activity increases when BC is internally mixed with soluble species such as sulfate or OA, while there is evidence that IN activity is optimal for unmixed or pure BC. CCN activation for BC is discussed in section 3.8, where methodology for applying Köhler theory to a BC-solute mixture is described. Activation depends upon particle size, moles of solute in the particle, and water supersaturation in the environment (Figures 5 and 6). The indirect effect dependence on particle number concentration is also nonlinear. Additional particles generally have a greater effect on clouds in clean conditions and relatively less in more polluted environments [e.g., *Twomey*, 1991; *Lohmann and Feichter*, 2005; *Hoose et al*., 2008]. Given these nonlinearities, it is difficult to model

Table 18. Studies That Provide Indirect Effect Estimates

Study	Reported Indirect Effect ($W\,m^{-2}$)	Emissions Changed in Study; (BC/OC ($Tg\,yr^{-1}$))[a]	Adjusted IE for BC ($W\,m^{-2}$); Adjustment Method[b]	Effects[c]; Diagnostic Method[d]
Liquid clouds (microphysics and lifetime)				
Kristjansson [2002]	−0.1	100% BC; 12.4/0	ALL: −0.11 EM	WIE(1/2), SD (DE); M1
Chen et al. [2010a]	−0.13 ± 0.33	50% FF BC + OC; 1.5/2.2	FF: −0.13 EM, SZ	WIE(1/2); M1
	−0.31 ± 0.33	50% ALL BC + OC; 3.9/30	ALL: −0.13 EM	
Bauer et al. [2010]	+0.05	100% FF BC[f]; 3.0/0	FF: +0.18; EM, SD	WIE(1/2), SD (DE); M1
	−0.12	50% FF + BF BC; 2.3/0	BF: −0.10; EM, SD	
	−0.2	100% BF BC + OC; 1.6/6.4	FF + BF: −0.32; EM, SD	
Koch et al. [2011b][e]	−0.08 to +0.31	100% FF BC[f]; 3.0/0	FF: +0.05 (−0.15 to +0.26); EM, SD, DE	WIE(1/2), SD, DE; M3
	−0.2 to +0.08	100% BF BC + OC; 1.6/6.4	BF: −0.05 (−0.12 to +0.02); EM, SD, DE	
Spracklen et al. [2011]	−0.23	100% FF + BF BC + OC 16.9 total	FF + BF: −0.13 EM	WIE(1)
	−0.34	100% ALL BC + OC 54.6 total	ALL: −0.09 EM	
Storelvmo [2012]	0.01	100% FF	ALL: 0.01	WIE
Mixed-phase clouds				
Lohmann and Hoose [2009]	+0.12 [g]	100% BC; 6.3/0	ALL: +0.12; None[h]	MIE (WIE, SD); M2
	+0.2 [g]		ALL: +0.2; None[h]	
Storelvmo et al. [2011]	+0.16 ± 0.08	100% BC; 6.3/0	ALL: +0.16; None[h]	MIE (WIE, SD); M2
Yun and Penner [2012][i]	+0.15	BC (PCT)	ALL: +0.15[h]	MIE; M4
	+0.71 to 0.93	BC + OM (YCT)		
Ice clouds				
Penner et al. [2009]	−0.3, −0.4	100% BC + OC; 13.5/97	ALL: −0.27; None	IIE; M1
Gettelman et al. [2012]	−0.06	100% BC	ALL: −0.06; None	IIE; M2
Liu et al. [2009a]	+0.22, +0.39	100% BC + OC; 13.5/97	ALL: +0.24; None	IIE, SD (WIE, DE); M3
All effects, including direct and cryosphere				
Jacobson [2010][j,k]	+0.47	100% FF BC + OC; 3.2/2.4	FF: +0.47	WIE, SD, DE, MIE, IIE, CRY, CLIM
	+0.68	100% FF + BF BC + OC, BF gases	FF + BF: +0.68	

[a]FF = fossil fuel, BF = biofuel, BB = biomass burning; ALL = FF + BF + BB. When a percentage reduction is given, it refers to all-source emissions. For comparison to emission values in the remainder of the document, 1 Tg = 1000 Gg.

[b]Adjustments: EM = scaled from mass of emissions used in study to our estimate of BC emissions (FF 5.6, BF 4.3, OB 4.0, ALL 13.9 $Tg\,yr^{-1}$); SD = estimate of semi-direct effect deducted assuming −30% of direct forcing; DE = estimate of direct effect in cloudy skies removed by assuming 65% of direct forcing; SZ = adjusted from particle size used in study to 100 nm diameter using dependence reported by *Bauer et al.* [2010].

[c]WIE = warm cloud indirect effect, with 1 = first indirect effect (cloud-albedo) and 2 = second indirect effect (lifetime); MIE = mixed-phase cloud indirect effect, IIE = ice cloud indirect effect, DE = direct effect, SD = semi-direct effect, CRY = cryosphere, CLIM = climate response. Effects in parentheses are included in the simulations but did not affect the indirect effect diagnostic and, therefore, are not included in the values in the "Reported indirect effect" column.

[d]M1 = Change in ToA cloud forcing with and without BC; M2 = Difference between model runs with and without mixed-phase indirect effects; M3 = Change in cloud forcing with and without BC + OC; M4 = Change in cloud forcing with and without BC + OC in mixed-phase clouds only.

[e]Values exclude those from the GISS model, which are reported separately in *Bauer et al.* [2010].

[f]Simulations were also done with reductions of 50% BC + OC emitted from diesel. The results were very similar to those for fossil-fuel BC emissions.

[g]The two estimates use different parameterizations of the Bergeron-Findeisen process.

[h]All estimates were first averaged without adjustment to obtain +0.15 $W\,m^{-2}$ and then scaled for emissions as described in the text.

[i]Contact nucleation parameterizations: PCT = *Phillips et al.* [2008]; YCT = *Young et al.* [1974]. The main effect in PCT is constrained by findings of BC within ice nuclei; YCT includes all OM as contact nucleus, but because the response is quite nonlinear, OM cannot be extracted from the latter treatment and is not used as an estimate of BC effect.

[j]This study included a simulation with biofuel and biomass emissions removed. Emissions of short-lived and long-lived GHGs emitted from BF and BB were also removed, so the results are not comparable with the aerosol-only effects summarized here.

[k]Effective forcing values from this study were not separated by mechanism, so the total forcing is discussed in section 10.

BC-cloud effects without models that include detailed aerosol microphysical schemes.

[428] Several model studies used aerosol microphysical schemes in simulations of the warm-cloud indirect effect of BC (Table 18). These model studies were done by comparing a simulation with all aerosols with another simulation in which BC, or BC and OA, have been removed. For consistency, we report all results as the response to the addition of BC. Below, we discuss the forcing changes actually reported by each study. However, each investigation used different changes in emissions, and Table 18 shows values scaled to the relevant BC emission rate.

[429] *Kristjansson* [2002] calculated a BC indirect forcing of −0.1 W m^{-2} (5–10 % of the total aerosol indirect effect), with regional values reaching about −0.25 W m^{-2} in more polluted regions where BC was an important component of the accumulation mode aerosols. In some remote oceanic regions, the sign was positive because BC reduced aerosol hygroscopicity.

[430] *Chen et al.* [2010a] modeled liquid-cloud indirect effects due to BC and OA emissions. Their results show that 50% of present-day BC and OA emissions from fossil fuel cause a −0.13 W m^{-2} indirect forcing, and 50% of all BC and OA emissions (including biomass-burning emissions) cause a −0.31 W m^{-2} indirect forcing. Fossil fuel BC

particles were assumed to have quite small sizes of 25 nm diameter at emission (compare to section 3.6.2). The indirect effects more than offset the calculated direct effects for fossil fuel and all carbonaceous emissions of +0.07 and +0.12 W m^{-2}, respectively. In the *Chen et al*. model experiments, indirect effects were isolated from semi-direct effects by running the simulation without aerosol-radiation coupling. The authors also estimated the standard deviation of the forcing over multiple years, which was as large as or greater than the forcings for 15 year simulations. While the absolute change in BC + OA emissions was larger for biomass emissions, so one would expect a larger effect, *Chen et al*. also attribute the larger forcing mostly to the larger size of the biomass and biofuel combustion particles as well as to the greater hygroscopicity of the non–fossil fuel emissions.

[431] *Bauer et al*. [2010] performed three BC reduction experiments. Adding either fossil fuel BC or fossil fuel plus biofuel BC decreased CDNC, probably because BC reduces the number of pure sulfate aerosols. The semi-direct effect in these cases was negative (more low-level clouds). The combined warm cloud indirect plus semi-direct effects resulted in positive forcing when fossil fuel BC only was added but negative forcing when a mix of biofuel and fossil fuel BC was added. Adding biofuel combustion emissions apparently produces a larger semi-direct effect, especially at high latitudes of both hemispheres, perhaps due to lofted BC in these regions (section 6.2). A third experiment tested the combined effect of BC and OA from biofuels only. In this case, aerosols caused increased CDNC and cloud cover with a larger negative forcing. The indirect effect was found to depend greatly on assumed particle sizes, with a factor of 2 decrease or increase in diameter producing a 45% increase and 30% decrease in magnitude, respectively.

[432] *Koch et al*. [2011a] presented a multi-model study of the effects of BC and OA from fossil fuel and biofuel burning. Six models examined alterations in cloudy-sky fluxes due to the same emission changes. The response to fossil fuel BC was −0.08 to +0.31 W m^{-2} with an average of +0.08 W m^{-2}, while the response to 50% of biofuel BC and OA ranged from −0.20 to +0.08 W m^{-2} with an average of −0.10 W m^{-2}. Cloud response in this study was diagnosed using the difference in cloudy-sky fluxes between simulations with and without BC, except for one model (GISS, reported separately by *Bauer et al*. [2010] and discussed above). Therefore, these values include not only cloud semi-direct effects and warm-cloud indirect effects but also direct radiative forcing in cloudy skies, which can be more than half of the direct radiative forcing [*Zarzycki and Bond*, 2010]. Removing the above-cloud direct forcing effect would result in more negative liquid-cloud effect.

[433] Many model studies do not separate microphysical effects from semi-direct effects, although such a division could be useful for comparing across studies that do estimate these effects separately. To isolate liquid-cloud microphysical effects in the *Koch et al*. [2011a] study, we estimated semi-direct and direct radiative forcing in cloudy skies for each model. Adjusted values, scaled to our emission estimates, are summarized in Table 18.

[434] *Spracklen et al*. [2011] modeled liquid-cloud effects, comparing CCN against observations. They found that the contribution of carbonaceous aerosols was required to explain observed CCN concentrations. Their estimate of forcing for BC plus OA emissions from fossil fuel and biofuel combustion was −0.23 W m^{-2} and reached −0.34 W m^{-2} with the addition of BC and OA emissions from biomass burning. *Storelvmo* [2012] found that BC had only a +0.01 W m^{-2} indirect effect in a study using four modes to represent BC and OA, while −0.25 W m^{-2} was attributed to OA.

[435] *Jacobson* [2010] studied the effects of fossil fuel and biofuel combustion on climate. Fossil fuel emissions, including BC, OA (some of which absorbs light), and primary sulfate, caused a net decrease in liquid cloud cover. Biofuel combustion emissions, including these species as well as co-emitted gaseous species, caused a net increase in liquid cloud cover. In this case, the cloud effects include the semi-direct effect, which is reported to be a cloud loss in this model. *Jacobson* [2010] argued that fossil fuel emissions contain fewer hygroscopic particles and, therefore, have lesser indirect effect, while the more hygroscopic biofuel combustion particles affect liquid clouds more significantly. This study includes all effects (direct, liquid, mixed, semi-direct, and ice clouds, as well as cryosphere forcing), and they were not separated.

[436] For the studies discussed above, the mean value of the isolated liquid-cloud indirect effect, when scaled to the magnitude of industrial-era BC, from the three studies that modeled all carbonaceous aerosol, is about −0.1 W m^{-2}. These three models give similar forcings when scaled to emissions of 13,900 GgC yr^{-1}. We use the model variation from the *Koch et al*. [2011a] study, about 0.2 W m^{-2}, as the total uncertainty in this effect. However, models are frequently unable to distinguish separate mechanisms, so the separation between liquid-cloud indirect effect and semi-direct effect is somewhat arbitrary. We therefore estimate the combined indirect and semi-direct effect, excluding forcing by cloud droplet inclusions, as -0.2 ± 0.3 W m^{-2}, where the central value is the sum of the separate estimates and the uncertainties have been added in quadrature. This value is more robust than the separate estimates. When the asymmetric uncertainty due to lofted biomass emissions is also added, the uncertainty bounds become −0.82 to 0.08 W m^{-2}.

[437] A common result among the models summarized in *Koch et al*. [2011a] is that aerosol emissions from biofuel combustion cause larger indirect effects per mass than do emissions from fossil fuel. Table 18 shows how the studies discussed above were scaled for emission rate and, in one case, particle size. Studies that isolate fossil fuel or diesel emissions suggest a small positive liquid-cloud forcing, scaled to emissions, averaging +0.08 W m^{-2}, while those that isolate biofuel combustion emissions have a small negative forcing averaging −0.08 W m^{-2}. However, studies that examine the two in combination estimate a larger negative forcing that is greater than the near-zero sum. This finding suggests that the liquid-cloud system contains significant nonlinearities so that the total effect is not equal to the sum of the parts. In contrast, *Spracklen et al*. [2011] attribute greater negative forcing to fossil fuel and biofuel particles compared with particles emitted from open burning.

[438] Biofuel and fossil fuel combustion emissions are different in four ways that may affect cloud responses. The first is chemical; the ratio of organic to black carbon is larger for biofuel and organic carbon is generally more hygroscopic than BC. However, some models do not explicitly treat the difference in hygroscopicity, so that modeled BC and OA

particles are identical. Second, co-emitted aerosol species or precursors also affect the number of particles. For example, altering biofuel sources to remove 1 Gg of BC also removes about 4 Gg of primary OC, so it could reduce primary particle number concentrations much more effectively than altering fossil fuel sources to achieve the same reduction. Third, models assume different emitted particle sizes. Both *Chen et al*. [2010a] and *Bauer et al*. [2010] assumed larger particle size in biofuel combustion emissions than in fossil fuel emissions. Since particles must grow large enough to act as CCN, biofuel combustion particles are closer to activation than fossil fuel particles. Conversely, an assumption of smaller diameter yields many more particles for the same mass emission. The modeled indirect effect depends on assumptions about source-specific particle size, number concentration, and composition, but such observations are limited. Fourth, cloud response has a regional dependence. Fossil fuel consumption is more prevalent at temperate latitudes, where cloud types and atmospheric dynamics differ greatly from tropical regions. Few models have conducted experiments that isolate sensitivities to these factors.

7.5. BC Indirect Effects on Mixed-Phase and Ice Clouds

[439] The influence of aerosols on both mixed-phase and ice clouds depends upon whether they can effectively nucleate ice. Typical IN are mineral dust, biological particles, and possibly BC. Although coating of BC with sulfate or organic material increases its ability to act as a CCN, coatings might reduce BC's IN activity, although there is less evidence for this change. In order to have an influence on ice particle formation, it is not enough that BC have the capability to serve as IN; it must also be equally or more efficient than other types of aerosols.

7.5.1. Laboratory Evidence for BC Effectiveness as IN

[440] The mechanisms by which BC can affect ice clouds require that it activates heterogeneously. In general, IN need to be larger than 0.1 μm in order to have ice-active sites [*Marcolli et al*., 2007]. Such sites can be thought of as imperfections that aid ice nucleation and may result from surface roughness or crevasses. IN activity is thought to be favored for hydrophilic particles, particles with crystallographic structure or with chemical bonds similar to those of water [*Pruppacher and Klett*, 1997]. These requirements mean that dust and crystalline sulfate are good IN and organic carbon or sulfuric acid is a poor IN. The IN behavior of BC is open to question. Two parameters are commonly reported to convey the effectiveness of IN. First, the ice nucleation threshold is the supersaturation with respect to ice at which the IN activates (e.g., a threshold of 1.5 means that the particle initiates nucleation of ice crystals at a relative humidity with respect to ice, RH_i, of 150%). Second, the ice-active fraction is the fraction of particles that serve as IN under any conditions.

[441] Figure 25 summarizes laboratory studies that have examined IN activity of BC-containing samples as a function of temperature. It includes particles from various sources and with different degrees of aging or processing [*Kärcher et al*., 2007]. The figure shows the nucleation threshold of each material, and the dashed (solid) curves indicate the point where supercooled solution droplets (pure water droplets) activate by homogeneous nucleation. In order for BC to compete with solution droplets such as sulfate, it should activate at a lower threshold (i.e., those aerosols that fall below the dashed line in Figure 25). Graphite spark-generated aerosol samples (two red areas in Figure 25) made efficient heterogeneous IN [*Möhler et al*., 2005b], but they are probably least chemically similar to atmospheric BC-containing particles. The remainder of the samples

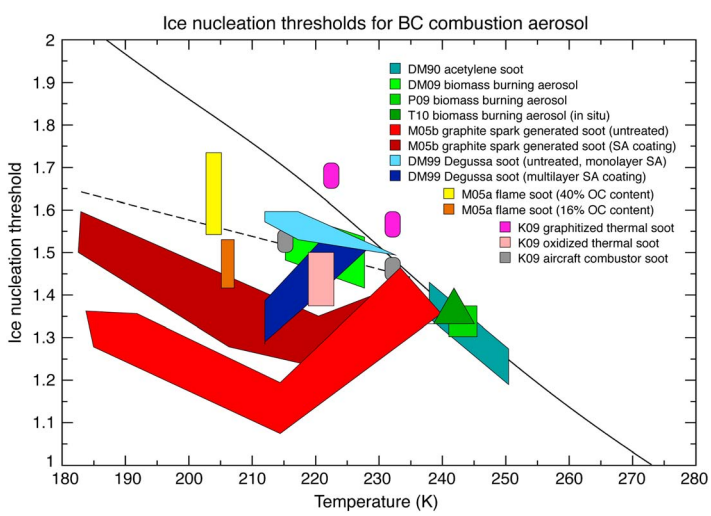

Figure 25. Compilation of heterogeneous ice nucleation threshold ranges of combustion aerosol samples from BC sources as a function of temperature. The ice nucleation threshold is the supersaturation with respect to ice at which the aerosol activates. Color-shaded regions show data from *DeMott* [1990] (DM90), *DeMott et al*. [1999] (DM99), *Möhler et al*. [2005a, 2005b] (M05a/b), *Petters et al*. [2009] (P09), *DeMott et al*. [2009a] (DM09), *Köhler et al*. [2009] (K09), and *Twohy et al*. [2010] (T10). The dashed curve represents the equilibrium ice saturation ratio required to freeze an aqueous solution droplet of diameter 500 nm in 1 s [*Koop et al*., 2000]. The solid curve is the water saturation curve, or the vapor pressure ratio of supercooled liquid water to hexagonal ice [*Murphy and Koop*, 2005]. Figure updated from *Kärcher et al*. [2007].

lie near the homogeneous nucleation line. Thus, despite differences in nucleation threshold definitions and other aspects between studies, the vast majority of studies suggest that combustion particles from a large number of sources are inefficient ice nuclei, regardless of the mode of nucleation [*Kärcher et al*., 2007].

[442] While some studies suggest that coatings reduce the ice nucleation efficiency of BC [*Möhler et al*., 2005b; *Crawford et al*., 2011], others find that they do not significantly alter the IN behavior of BC [*Friedman et al*., 2011] or even enhance it [*DeMott et al*., 1999] or that the influence of sulfuric acid coatings depends on the organic matter within the soot [*Crawford et al*., 2011]. This contrasts with BC CCN activity in liquid clouds, which is always enhanced by coating.

[443] Extensive comparisons of the IN and CCN activity of BC-containing aerosol were reported by *Köhler et al*. [2009], using samples of different hygroscopicity and surface porosity. Larger particles were more ice active than smaller ones, although the size range investigated was limited. The processes that promote water adsorption facilitated both CCN activation and ice nucleation. At 233K, no combustion aerosol particles nucleated ice better than did aqueous solutions of similarly sized particles. At 216–221K, 1 in 100 particles of oxidized combustion aerosol and 1 in 1000 particles of non-oxidized combustion aerosol and aviation kerosene promoted heterogeneous nucleation of ice. BC particles coated with soluble material behaved like fully soluble particles with the same liquid volume and water activity. This suggests, overall, a limited role for BC in promoting ice nucleation.

[444] Biomass burning emissions, composed of BC and OA, also have limited IN activity, due to inhibition by organic carbon. *DeMott et al*. [2009a] found that biomass-burning aerosol from controlled laboratory burns had the same or lower nucleation activity when compared with liquid solution particles. Aerosol with high OC : BC ratios impeded heterogeneous ice nucleation most strongly. A similar impact has been reported for organic coatings on emissions from propane flames [*Möhler et al*., 2005a]. At warmer temperatures, significant IN activity of polydisperse samples of small biomass burning particles (number mode diameters 60–140 nm) has been observed only when they have low organic carbon fraction and high water-soluble ion content, associated with flaming fires [*Petters et al*., 2009]. At warmer temperatures (i.e., greater than 240K), dynamic cloud chamber studies of acetylene combustion emissions suggest no significant IN activity [*DeMott*, 1990], in agreement with the biomass burning aerosol studies.

[445] In contrast, many laboratory studies suggest that mineral dust particles are good to moderate IN as long as they remain uncoated with soluble material [*Kärcher et al*., 2007, section 4.2 and references therein]. The IN activity of dust particles decreases once coated with soluble material, so that the few processed mineral dust particles reaching the upper troposphere and lower stratosphere (UTLS) are likely those with moderate IN activity [*Wiacek and Peter*, 2009]. Therefore, dust is a major competitor for BC with regard to ice formation. Other competitors include some crystalline inorganic and organic phases within partially soluble aerosols such as ammonium sulfate [*Abbatt et al*., 2006], oxalic acid [*Zobrist et al*., 2006], biological particles [*Pratt et al*., 2009], or mineral dusts with lead [*Cziczo et al*., 2009].

[446] The laboratory studies summarized in Figure 25 employed a wide array of combustion sources and surrogates of BC-containing particles for measurements of IN activity. These studies do not provide fully conclusive information about the behavior of BC in the atmosphere for two reasons. First, not all studies provide sufficient information to judge their relevance for cloud formation (i.e., ice active fractions and presence of solutes). Second, most studies have not investigated potentially important atmospheric processes that could affect the particles' IN activity, such as surface oxidation or cloud processing. Moreover, a fundamental understanding of the physico-chemical nature of ice nucleation is lacking, although there is some progress in linking source-dependent surface properties of BC-containing aerosol and their ability to adsorb water [*Popovicheva et al*., 2008].

7.5.2. BC Effects on Mixed-Phase Clouds

[447] Mixed-phase clouds occur at temperatures between 0°C and approximately −35°C because water droplets and ice crystals can co-exist at these temperatures. The water vapor pressure in a mixed-phase cloud lies between water and ice saturation, so the cloud is supersaturated with respect to ice. In these clouds, an increase in IN promotes ice nucleation, and subsequently large ice particles grow in the supersaturated environment. Eventually, this cloud completely becomes an ice cloud (glaciate). This process is called the Bergeron-Findeisen process. As the ice crystals grow in a supersaturated environment, they grow rapidly and start to sediment. The overall effect may be a reduction in cloud cover, causing a positive forcing (Figure 24, case MC1). Reduction in IN may cause the opposite effect (case MC2).

7.5.2.1. Mechanisms

[448] Ice formation in mixed-phase clouds occurs by heterogeneous freezing, with the aid of insoluble IN [*Pruppacher and Klett*, 1997]. Heterogeneous freezing can be initiated either by collision of a supercooled cloud droplet and an IN (contact mode) or from within a cloud droplet on an IN that is immersed in it (immersion mode). Condensation freezing refers to the condensation of water vapor onto a nucleus followed by freezing. Immersion and condensation freezing are conceptually similar and are not easily distinguishable in measurements. At relative humidities below 100% with respect to water but above 100% with respect to ice, nucleation of ice directly on bare IN could take place (deposition mode). Based on lidar observations of Saharan dust particles, *Ansmann et al*. [2008] argue that the time available for deposition nucleation may be too short and, hence, is negligible for mixed-phase clouds. Contact nucleation is initiated at higher temperatures than immersion nucleation [e.g., *Shaw et al*., 2005; *Fornea et al*., 2009], but it is limited by collision rates, especially for accumulation mode particles that are large enough to serve as IN. Therefore, the immersion mode may be the most important ice-forming mechanism in mixed-phase clouds.

7.5.2.2. Experimental Studies

[449] Laboratory and field measurements give conflicting views on the viability of BC as an effective IN. As summarized above, laboratory results indicate that BC appears to be one of the least efficient IN in the atmosphere, because

it nucleates ice at colder temperatures than IN with natural sources such as mineral dust and biological particles. Laboratory studies also suggest that deposition nucleation of ice on most types of BC particles is not important above 243K and below water saturation [*Dymarska et al.*, 2006]. In contrast, in situ observations of lower tropospheric mixed phase clouds find an enrichment of BC in ice particle residuals [*Cozic et al.*, 2008; *Targino et al.*, 2009], so there must be some mechanism for BC to enter ice clouds. BC may act as a contact IN at temperatures between 245 and 251K [*Diehl and Mitra*, 1998; *Fornea et al.*, 2009].

7.5.2.3. Modeling Results

[450] Parameterizations have been developed to represent ice formation affected by mineral dust and BC particles in both contact and immersion modes [*Diehl et al.*, 2006; *Phillips et al.*, 2008]. A GCM study using the parameterization of *Diehl et al.* [2006] found that BC did induce a glaciation effect. However, the importance of BC acting as a contact IN, and hence the glaciation effect, decreases in the presence of natural aerosols such as dust that are more efficient IN than BC [*Lohmann and Diehl*, 2006]. The glaciation effect also decreases with increased sulfate coating thickness. The results also depend on the model's parameterization of the Bergeron-Findeisen process. Taking into account all these uncertainties, the glaciation effect of all BC emissions on mixed-phase clouds was estimated as +0.12 and +0.20 W m^{-2} for two different parameterizations [*Lohmann and Hoose*, 2009] (Table 18).

[451] *Storelvmo et al.* [2011] also studied BC impacts on mixed-phase clouds, including the opposing effects of albedo and lifetime. The magnitude and sign of the forcing depended on the ice-active fraction of BC and the parameterization chosen. Forcing became negative when another parameterization [*DeMott et al.*, 2010] was used, but this treatment led to ice crystal sizes that did not agree with observations. When using an intermediate case for ice-active fraction, this study found a forcing of $+0.16 \pm 0.08$ W m^{-2}, which is used in this assessment in calculating our central estimate of the BC effect on mixed-phase clouds. *Yun and Penner* [2012] also studied the anthropogenic effects of BC and OM on mixed-phase clouds. The effect depends greatly on the contact freezing parameterization; it is +0.15 W m^{-2} when a parameterization from *Phillips et al.* [2008] is used but +0.83 W m^{-2} when the older and simpler *Young* [1974] version is used. However, in the latter treatment, this study also allowed OM to participate in contact nucleation of ice.

[452] While other model studies have not produced forcing estimates, they generally agree that BC addition reduces mixed-phase clouds through enhanced glaciation. *Ekman et al.* [2007] studied the influence of BC particles on continental convective clouds using a cloud-resolving model. They found that BC increased heterogeneous ice nucleation, thereby increasing the latent heat release and updraft velocities in the convective plume. As a result, total precipitation increased and clouds were reduced. One regional climate model study found that externally mixed BC aerosols increase riming and enhance orographic precipitation and cloud loss [*Muhlbauer and Lohmann*, 2009]. In contrast, internally mixed BC aerosols decreased riming rates and orographic precipitation.

[453] Our estimate for mixed-phase cloud indirect effects due to modeled emissions is $+0.15 \pm 0.16$ W m^{-2} based upon estimates of *Lohmann and Hoose* [2009], *Storelvmo et al.* [2011], and *Yun and Penner* [2012] using the *Phillips et al.* [2008] freezing parameterization. Sensitivity experiments in *Storelvmo et al.* [2011] (experiments BC, BC10, and BC01) show that forcing is approximately proportional to the log of ice-active nuclei. To account for the increased industrial-era emissions reported in section 6, we scale the forcing according to the relationship between these studies, and retain the same relative uncertainties, for a forcing of $+0.18 \pm 0.18$ W m^{-2}.

7.5.3. BC Effects on Ice-Phase Clouds

[454] Pure ice-phase clouds (cirrus clouds), which form at temperatures below −35°C, often reside at high altitude and usually exert positive forcing. As discussed in section 7.5.1, BC IN activity may either increase or decrease this forcing.

7.5.3.1. Mechanisms

[455] In cirrus clouds, there are no water droplets and, therefore, no contact nucleation, so heterogeneous ice nucleation in these clouds can only occur in the deposition, immersion, or condensation modes. In these clouds, the total concentration of nucleated ice crystals may either increase or decrease depending on temperature, cooling rate, and number of BC particles [*Kärcher et al.*, 2006]. If heterogeneous nucleation dominates unperturbed clouds (especially in slowly cooling air masses), BC could contribute to this nucleation by increasing the number concentration of IN and thereby decrease the mean size of ice crystals. This leads to longer lifetimes of high clouds that exert a net warming effect, resulting in a positive forcing (case IC2, Figure 24) [*Kärcher et al.*, 2006]. At higher cooling rates, adding IN tends to retard or even prevents homogeneous freezing, which decreases the number of ice crystals, resulting in a negative cloud forcing (case IC1, Figure 24) [*Kärcher et al.*, 2006]. In the UTLS, airborne measurements of relative humidity and cirrus indicate that the latter scenario occurs preferentially under typical atmospheric conditions [*Haag et al.*, 2003].

[456] Figure 26 shows the results of an IN parameterization demonstrating how the number concentration of combustion aerosol affects the total concentration of nucleated ice crystals in the presence of dust IN and liquid background aerosols. Updraft velocities govern the rate at which a developing cloud is cooled and, therefore, the formation rate of new ice crystals, so they play an important role in the initial cloud properties. The two panels show different cloud updraft speeds, where the updraft rate increases the cooling rate. If all IN are combustion aerosols and their concentration decreases (black curves), ice-crystal number concentration is determined by homogeneous nucleation and unaffected by the addition of BC. As more IN are added, more of them nucleate heterogeneously and take up water. As a result, fewer ice crystals form homogeneously and the total ice-crystal number concentration decreases. (This reduction in ice crystals with IN, corresponding to case IC1 in Figure 24, contrasts with liquid clouds where addition of CCN causes increased CDNC.) The resulting larger particles have a shorter atmospheric lifetime, leading to a decrease in cirrus clouds and negative longwave forcing. IN can consist of either combustion particles or dust (Figure 26, colored curves). When IN are numerous enough, heterogeneous nucleation

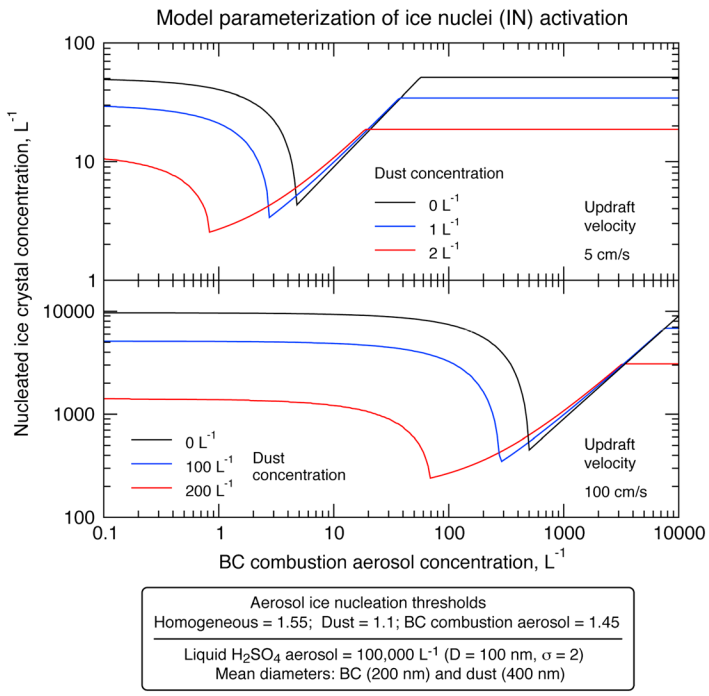

Figure 26. Calculated total number concentration of nucleated ice crystals as a function of BC combustion particle number concentration. Ice particle number results from the competition of three particle types (liquid H_2SO_4/H_2O droplets acting as homogeneous freezing nuclei, and dust and BC particles acting as heterogeneous IN) during ice formation in adiabatically rising air parcels (sharp ice nucleation thresholds for the IN given in the legend). Results are shown for an updraft velocity of 5 cm/s (top panel: synoptic-scale vertical winds), and 100 cm/s (bottom panel: strong orographic waves or convective cells). In the simulations, air parcels start rising at 250 hPa and 220 K at ice saturation and contain mineral dust particles with concentrations noted in the legends, a wide range of BC (10^3 L^{-1} = 1 cm^{-3}) concentrations, and a fixed concentration of lognormally distributed aqueous H_2SO_4 particles. Dust and soot particles are assumed to be monodisperse. Adapted from *Kärcher et al.* [2007].

dominates the formation of ice crystals, and the suppression of homogeneous nucleation has little effect on the final number concentration. Therefore, the addition of IN causes an increase in the number concentration of ice crystals (case IC2 in Figure 24). Under some conditions, ice formation on combustion aerosol could entirely suppress homogeneous freezing.

[457] At small updraft rates (top panel), few ice crystals form and the influence of adding IN occurs at lower combustion aerosol number concentration. Large updraft velocities (bottom panel) cause the formation of a large number of ice crystals, since homogeneous freezing dominates ice formation (the number of aerosol droplets is not a limiting factor). In this case, BC is not capable of causing a notable indirect effect. At intermediate updraft velocities, BC depletes the air mass of moisture, causing much fewer (but still more than BC) background particles to freeze homogenously. This discussion, focused largely on microphysics, addresses only processes that affect the initial ice crystal concentration in single air parcels. This sensitivity study gives a first-order estimate of IN in young clouds but does not quantify the changes in the cloud as it evolves and, therefore, does not reflect global averages.

7.5.3.2. Field Evidence for BC Acting as IN

[458] Laboratory studies indicate that IN activity of BC is, at best, moderate. Field studies, summarized below, confirm these findings. They indicate that homogeneous freezing is the prevalent ice formation mode [*DeMott et al.*, 2003; *Cziczo et al.*, 2004a]. This is consistent with the ubiquity of high ice supersaturations in cloud free areas of the upper troposphere [*Jensen et al.*, 2001; *Haag et al.*, 2003; *Kahn et al.*, 2009a] and with the fact that total cirrus ice-crystal number densities often far exceed estimated IN concentrations [*Gayet et al.*, 2002; *Hoyle et al.*, 2005].

[459] Field measurements using single-particle mass spectrometry, electron microscopy, and X-ray emission or particle elastic scattering analysis demonstrate that BC and organic carbon are present in the troposphere and lower stratosphere [*Murphy et al.*, 2007; *Nguyen et al.*, 2008]. Often, the predominant particles are composed of organic carbon that originates mainly from surface sources. Even particles that reach the stratosphere may have acquired small amounts of carbon during transport through the upper troposphere. Some measurements suggest that BC's effectiveness as an IN is greatest if it is uncoated, but this finding is not yet definitive. Presumably, uncoated BC rarely exists in the UTLS region, and because it is difficult to detect thin coatings on BC, the number of such particles in this region is poorly known.

[460] A constraint that could ascertain whether BC affects ice cloud formation would be direct airborne sampling of particles at high altitudes, along with simultaneous characterization of their chemical composition and measurements

of their ice-forming properties. Ice nuclei counters have been employed in several ground-based and airborne measurements [*Rogers et al.*, 1998; *DeMott et al.*, 2003; *Cziczo et al.*, 2004b; *Richardson et al.*, 2007; *Stith et al.*, 2009; *Prenni et al.*, 2009; *Froyd et al.*, 2009]. In qualitative agreement with most laboratory studies, some of these field measurements support the notion that mineral particles can act as IN in cirrus clouds, while BC-containing aerosol is less ice-active, although it often present in ice-nucleating aerosol. However, without adequate characterization of particle composition and properties, field measurements can infer correlations between IN components and heterogeneous ice nucleation but cannot distinguish the processes by which certain particles partition in cirrus ice; therefore, they cannot provide causal links.

[461] This conclusion is particularly true for measurements of cirrus ice crystal residues that show enhancements in insoluble components relative to ambient particles, throughout the troposphere and in aircraft corridors [*Heintzenberg et al.*, 1996; *Ström and Ohlsson*, 1998; *Twohy and Gandrud*, 1998; *Petzold et al.*, 1998; *Twohy and Poellot*, 2005]. Inertial scavenging of BC particles by ice crystals in clouds was found to be more important than ice nucleation in explaining observed BC-to-ice mass ratios at temperatures of 228–248K [*Baumgardner et al.*, 2008; *Stith et al.*, 2011].

[462] Field data sets that measure IN concentrations have not distinguished BC-containing particles from other particles. Such measurements may be viewed as the maximum concentrations of ice-active BC for comparison with models. Measurements over continental areas and in aircraft corridors reveal highly variable IN number concentrations of 0.1–500 L^{-1}, with 60% of data lying in the range 2–20 L^{-1} [*Rogers et al.*, 1998]. Other data sets point to typical background northern hemispheric IN concentrations of 10 to 30 L^{-1} [*DeMott et al.*, 2003; *Haag et al.*, 2003]. Data in the Arctic report lower values (i.e., less than 1 L^{-1}) with local maxima of 50 L^{-1} [*Prenni et al.*, 2009]. IN concentrations of 100 to 500 L^{-1} are rare and have only been detected locally in dust storms [*DeMott et al.*, 2009b; *Stith et al.*, 2009].

[463] The minimum BC ice active fraction present in lower and middle tropospheric biomass burning plumes required to exert regional impact was estimated to be 10^{-4} or higher [*Petters et al.*, 2009]. A comparison of upper tropospheric refractory particle concentrations of about 10,000 L^{-1} [*Minikin et al.*, 2003] with inferred IN concentrations of about 10 L^{-1} [*Haag et al.*, 2003] yields a BC ice active fraction of 10^{-3}, when assuming that BC contributed 100% by number to the refractory particles. The latter assumption is likely an overestimate, so the BC ice active fraction in nature was probably smaller.

7.5.3.3. Modeling Evidence for BC Atmospheric Abundance and Mixing State

[464] As discussed in section 3, BC particles are commonly mixed with sulfate or organic carbon within a day. If most BC particles in the UTLS are coated, then BC acting as deposition IN, in which ice forms directly on bare BC, would be rare in the upper troposphere.

[465] Most global models are not well validated in terms of UTLS aerosol speciation and particle number concentrations, in particular for BC [*Koch et al.*, 2009b; *Lohmann and Hoose*, 2009]. Problems in simulating tropospheric BC vertical distribution, mixing state, and other properties are mainly tied to poorly parameterized physical and chemical processes that affect BC lifetime and, to a smaller degree, to uncertainties in emission inventories [*Textor et al.*, 2007]. One particularly uncertain process is scavenging in ice clouds.

[466] One climate model has specifically compared UTLS aerosol number and mass concentrations with observations [*Aquila et al.*, 2011]. This model tracks the properties and distribution of potential ice nuclei (defined as the sum of dust and BC particles) separately from soluble particles, so that internally and externally mixed BCs are explicitly represented. The zonal mean ratio of externally mixed potential IN to the total potential IN number is 0.5–2% throughout most of the free troposphere. These values are much smaller than suggested by observations [*Schwarz et al.*, 2008a], but internally mixed particles are not distinguished as easily by the measurements as they are in the model. Simulated transformation times from external to internal mixtures are predicted to be larger for dust than for BC, implying a larger (but still small) fraction of bare dust particles relative to BC in tropospheric accumulation mode IN. These model results suggest the need for careful examination of observed IN mixing state.

[467] For BC particles (or IN in general) to exert a significant effect on ice formation, their ice nucleation thresholds should lie well below the homogeneous freezing limit for fully soluble aerosol particles, and the number concentration of the ice active population should be 10 L^{-1} or larger for typical updraft velocities and temperatures in the upper troposphere [*Kärcher et al.*, 2006]. However, as summarized above, BC particles from a wide range of sources do not appear to be potent IN (Figure 25). Therefore, it is realistic to assume an ice nucleation threshold that is close to but below the homogeneous freezing threshold, as was chosen for the simulations in Figure 26. While Figure 26 explores the effect of BC on IN, the possible range of influence of BC on cirrus properties depend on the details of the ice active fraction and other factors that are not included in those simulations.

[468] Resolving moderate impacts of IN, where ice is formed at supersaturations slightly below the homogeneous freezing threshold, and validating IN impacts on cirrus will be very challenging in UTLS in situ measurements, given the present difficulties in measuring relative humidity and cooling rates on the scale of individual clouds. *Kärcher and Ström* [2003] emphasized the crucial role of dynamical forcing in cirrus formation; small uncertainties in estimating cooling rates in cirrus generating cells can easily mask any indirect effect exerted by IN. Furthermore, it is questionable whether the effects of IN on optically thin ice clouds can be unraveled by means of satellite observations [*Chylek et al.*, 2006; *Seifert et al.*, 2007; *Massie et al.*, 2007].

7.5.3.4. Global Model Studies of BC Effects on Cirrus

[469] Three model studies have estimated the carbonaceous aerosol effect on ice clouds (Table 18). This effect is the difference between present-day conditions and preindustrial (background) conditions, and estimates of forcing are, therefore, strongly affected by the nucleation regime in the background atmosphere. If homogeneous nucleation is most common in the preindustrial atmosphere (left side of Figure 26 or an environment with few IN), BC decreases ice particle number concentration and forcing is negative. If heterogeneous nucleation

was dominant in the preindustrial case (toward the upward slope of Figure 26 or an environment with more dust), BC increases ice particle number concentration and forcing becomes positive. A predominance of droplets or sulfate particles corresponds to natural conditions with homogeneous nucleation, while predominance of refractory particles like dust would result in heterogeneous domination. The influence of adding IN on ice formation is largely controlled by cloud-scale dynamics, and changes in the dynamic regime since the preindustrial era are not fully included in this forcing estimate.

[470] *Penner et al.* [2009] used off-line estimates from a CTM aerosol scheme coupled to the NCAR CAM3. They used two parameterizations that allowed for competition between homogeneous and heterogeneous nucleation in an aerosol mass-only and a three-mode, two-moment versions of the model. Sulfate droplets were assumed to act as homogeneous freezing agents, BC was assumed to be coated with soluble material and, therefore, to act as immersion IN, and dust was assumed to act as IN in the deposition or condensation mode. For the more sophisticated (three-mode) parameterization, two different ice nucleation schemes gave a forcing from fossil fuel and biomass burning emissions of -0.3 to -0.4 W m^{-2}. The dominant effect was that heterogeneous IN activity of BC decreased relative humidity with respect to ice, inhibited homogeneous nucleation, decreased the number concentration of ice particles, and reduced positive forcing by high-level clouds.

[471] The mass-only version of the aerosol model was applied by *Liu et al.* [2009a] in the NCAR CAM3 global model with a double moment ice microphysical scheme. Adding BC resulted in increased high-level clouds, especially over polar regions but also somewhat over tropical regions. The resulting change in forcing due to BC emitted at the surface was +0.22 W m^{-2} or +0.39 W m^{-2} when critical supersaturations of 1.2 to 1.3 or 1.4, respectively, were assigned to BC. The larger forcing for higher ice nucleation threshold is due to a larger decrease in negative shortwave contribution. The change in sign between this study and the *Penner et al.* [2009] results reflects the large uncertainty in this forcing, stemming from the fact that cirrus clouds affect both shortwave and longwave radiative fluxes, and the change in each is determined by specific cloud properties. The forcing is, therefore, a small value calculated by adding two large values of opposing sign, making it very sensitive to changes in the magnitude of either one. Similar uncertainties are seen in the estimation of the climate effects of aviation BC emissions, which are not included here. There are three major differences between this study and *Penner et al.* [2009]. In the preindustrial atmosphere, homogeneous nucleation dominated in *Penner et al.* [2009] while heterogeneous nucleation dominated background conditions in *Liu et al.* [2009a]. *Liu et al.* used a prognostic treatment of the ice-crystal number concentration including source and sink terms while *Penner et al.* diagnosed ice-crystal number concentration from nucleation. *Liu et al.* [2009a] included climate feedbacks, so that aerosols in the UTLS region tended to enhance relative humidities there; however, they were unable to reproduce the observed supersaturations in the atmosphere, so that the modeled supersaturations were never high enough to allow homogeneous nucleation [*Liu et al.*, 2007, Figure 3].

[472] *Gettelman et al.* [2012] analyzed the BC effect on ice clouds as part of a more comprehensive study of ice nucleation in the CAM5 model, exploring the effect of parameterisation changes on background cloud properties and the aerosol indirect effect. They compared study pairs with 1850 and 2000 aerosol emissions. One member of the pair had fixed ice nuclei as a function of temperature and the other used a more complete parameterization, allowing competition between heterogeneous nucleation on dust with homogeneous nucleation on sulphate. The standard model used only coarse-mode dust as potential ice nuclei. BC was incorporated into this scheme by assuming it had the same ice nucleation properties as dust. The ice active fraction for BC was set to 0.1%, 2%, and 100% in different simulations. Only the simulation assuming a 0.1% ice active fraction gave realistic ice water mass and cloud radiative properties, and this simulation was used to estimate the indirect effect. Forcings were estimated from the full ToA radiative-flux change, a cloud forcing change, and a cloud forcing change with a clear-sky flux change correction applied; the quoted result is the average of these three. This study estimates $+0.27 \pm 0.10$ W m^{-2} (1σ uncertainty) for the total ice cloud aerosol indirect effect. The BC component was -0.06 W m^{-2} and was not statistically significant.

[473] *Jacobson* [2010] included ice-cloud effects in a model of the effect of BC on climate. Ice crystal sizes increased slightly due to BC. The study used a temperature-dependent ice-nucleation threshold for uncoated BC (section 7.5.1) that ranged between 1.15 and 1.35. These values are within the range for uncoated spark-generated soot at moderate and low temperatures but below the range of coated soot in Figure 25. Cloud drop and ice-crystal number concentration were calculated by simultaneously solving the mass balance equations for water vapor, liquid, and ice, considering all aerosol and cloud particle sizes. BC in this model study is a more efficient IN than is observed in the laboratory. In the study, relative humidity increased at high altitudes and in the Arctic, and ice clouds increased due to BC, which are results similar to those in *Liu et al.* [2009a]. Forcing due to this IN mechanism was not isolated, but the direction of ice-cloud changes suggests a positive forcing.

[474] In a global model study by *Hendricks et al.* [2011], a multiple-mode ice microphysical scheme was applied in the ECHAM GCM to simulate IN effects on global cirrus properties. The ice nucleation parameterization by *Kärcher et al.* [2006] was applied to simulate the competition between homogeneous and heterogeneous ice formation. *Hendricks et al.* [2011] assumed that only small fractions of the modeled BC and mineral dust particles (0.25% and 1%, respectively) could act as IN, resulting in IN concentrations in the order of 10 L^{-1} at cirrus levels. BC and dust-related IN had similar contributions. Heterogeneous nucleation on both types of particles produced significant reductions in the mean cirrus ice particle number concentrations. The effect was most pronounced in the tropics, where the zonal mean annual average ice particle number concentration decreased by up to 20%. Reductions in the mean ice water content, likely resulting from efficient sedimentation and precipitation of large ice particles generated by heterogeneous nucleation, also occurred. This effect led to reductions in the zonal mean, annually averaged, water-vapor mixing ratio of up to 5% at cirrus

Table 19. Model Studies Used to Derive the Adjusted Forcing of Black Carbon in Snow and Ice[a]

	Hansen and Nazarenko [2004]	*Jacobson* [2004a]	*Hansen et al.* [2005, 2007];[b] *Shindell and Faluvegi* [2009]
Emissions *year* and global, annual BC emissions used to derive forcing ($GgC\,yr^{-1}$)	n/a	FF + BF: 3920 BB: 3140 Total: 7060	Year *1880*, *2000*: FF: 500, 5700 BF: 500, 1000 BB: 2300, 4600 Total *1880, 2000*: 3300, 11300
Emission inventories used	n/a	Early version of *Bond et al.* [2004][e] for year 1996	FF: *Penner et al.* [2001] (via D. Koch, personal communication) BB and BF: *Liousse et al.* [1996]
Gridbox size (latitude × longitude)	4° × 5°	4° × 5°	4° × 5°
BC forcing medium [g]	n/a	SN_L, SN_I, SI	SN_L, SN_I
Present-day adjusted forcing for FF+BF only ($W\,m^{-2}$)	n/a	0.06[h]	{0.05}
Pre-industrial-to-present (*years*) adjusted forcing for FF+BF+BB	n/a	n/a	(*1880–2000*) *Hansen et al.* [2005, 2007] **0.08; 0.05**
Present-day adjusted forcing, for FF+BF+BB ($W\,m^{-2}$)	0.16	{0.08}	{0.07}
Climate forcing per emission ($\mu W\,m^{-2}$) $(GgC\,yr^{-1})^{-1}$ for all-source forcing	n/a	{11}	{6}

[a]"Adjusted forcing" here refers to radiative forcing plus the rapid adjustments to that forcing (Table 20), producing the adjusted forcing as defined in Table 2. However, as shown in Table 20, studies included different rapid adjustments; for the *Rypdal et al.* [2009b], *Skeie et al.* [2011], and *Wang et al.* [2011] studies, no rapid adjustments were included so the climate forcing equals the radiative forcing. Shown are the model BC emission sources and strengths (global, annual average; FF = fossil fuel; BF = biofuel; BB = biomass burning), model gridbox size, and the global, annual average, adjusted forcing for FF + BF only and for FF + BF + BB. The global, annual average forcing per emissions for FF + BF + BB is also given. Values that are either directly reported in the studies or which can be calculated from reported values are given in bold face. Values shown in {brackets} are estimates based on scaling the reported values, as described in section 8.6.1.

[b]*Hansen et al.* [2007] revised down the total BC-in-snow forcing given by *Hansen et al.* [2005] after correcting a programming error. Both sets of data are given here.

[c]*Flanner et al.* [2007] provided calculations for high (1998) and low (2001) biomass burning years.

[d]*Flanner et al.* [2009] selected 2002 biomass burning emissions because this is a "typical" boreal fire year (versus the "high" and "low" cases selected for *Flanner et al.* [2007]).

[e]*Jacobson* [2004a] used an "early version" of the *Bond et al.* [2004] inventory for submicron BC emissions, where FF + BF ~20% lower (global, annual average) than was ultimately given in *Bond et al.* [2004]. However, *Jacobson* [2004a] also included super-micron BC emissions, set at 25% of the mass of sub-micron emissions, so the total BC emissions were, in terms of mass, close to those of *Bond et al.* [2004], though the differing size distributions affect deposition rates and therefore spatial distribution of deposited BC. *Bond et al.* [2004] annual biomass burning emissions were used to determine monthly emissions by scaling using the monthly inventory of *Cooke and Wilson* [1996].

[f]Pre-industrial (1890) BF emissions comes from taking *van Aardenne et al.* [2001] SO_2 biofuel emissions and calculating BC + OC BF emissions using the ratios of SO_2 : BC and SO_2 : OC in 1990 from *van Aardenne* (SO_2) and *Bond et al.* [2004] (BC and OC).

[g]Forcing by BC in snow on land (SN_L), BC in snow on sea ice (SN_I), and BC in bare (non-snow-covered) sea ice (SI).

[h]Estimated value provided via personal communication (M. Z. Jacobson). Radiative forcing was not reported in *Jacobson* [2004a].

[i]*Rypdal et al.* [2009b] BF includes only energy-related biofuel burning.

[j]*Rypdal et al.* [2009b] did not include biomass burning emissions, so here we have used the *Flanner et al.* [2009] 2.7 $TgC\,yr^{-1}$ for BB emissions and have scaled the *Rypdal et al.* (FF + contained BF) forcing linearly to get a forcing for FF + BF + BB.

[k]*Skeie et al.* [2011] include BB aerosols in their model, but forcing is calculated for FF + BF emissions only and all reported forcings are relative to base year 1750.

[l]*Wang et al.* [2011] is surface forcing; ToA forcing was not reported but would be lower than the surface forcing because of the effect of atmospheric transmission.

n/a = not applicable.

levels. The BC contribution to these effects was comparable to that related to mineral dust IN only when the assumed ice nucleation threshold is significantly lower than that assumed for dust particles (threshold of 1.2 for BC and 1.3 for mineral dust). When a larger critical value (ice nucleation threshold of 1.40) was assumed for BC, heterogeneous freezing was dominated by mineral dust particles.

[475] Compared to the global model studies by *Liu et al.* [2009a] and *Penner et al.* [2009], *Hendricks et al.* [2011] and *Gettelman et al.* [2012] simulated a much smaller effect of BC on cirrus ice crystal number concentrations. These differences could result from either a smaller availability of active ice nuclei in the *Hendricks et al.* [2011] and *Gettelman et al.* [2012] studies or from differences in the representation of relative humidity and cooling rates. *Gettelman et al.* [2012] found that an ice active fraction of 0.1% gave realistic ice water content and radiative properties, and ice active fractions of 2% and 100% did not.

[476] Compared with the measurements discussed in section 7.5.3.2, the *Liu et al.* [2009a] and *Penner et al.* [2009] studies may overestimate UTLS BC and IN and may, therefore, overestimate the magnitude of the ice-cloud indirect

Table 19. (Continued)

Flanner et al. [2007]	*Flanner et al.* [2009]	*Koch et al.* [2009a]	*Rypdal et al.* [2009b]	*Skeie et al.* [2011] [k]	*Wang et al.* [2011]
Year *1996* FF + BF: 4700 Year *1998* [c] BB: 4100 Year *2001* BB: 2000 Total *1998*, *2001*: 8800, 6700	Year *1996* FF + BF: 4700 Year *2002* BB [d]: 2700 Total: 7400	Year *1890*, *1995*: FF + BF: 1800, 4500 BB: 2200, 3700 Total *1890*, *1995*: 4000, 8200	FF + contained BF burning: 5300	Year *1750, 2000*: FF+BF: 0400, 4500 BB: 1000, 2600 Total *1750, 2000*: 1400, 7100	n/a
Bond et al. [2004] + GFEDv2 [*van der Werf et al.*, 2006] for open burn	*Bond et al.* [2004] + GFEDv2 [*van der Werf et al.*, 2006] for open burn	BB: GFEDv1; Pre-indust. FF: *Lefohn et al.* [1999] BF: *van Aardenne et al.* [2001][f]; Present day FF + BF: *Bond et al.* [2004]	*Cofala et al.* [2007]	FF+BF: *Bond* *et al.* [2007] BB: *Lamarque* *et al.* [2010]	n/a
2.8° × 2.8° SN_L, SN_I **0.043** n/a	2.8° × 2.8° SN_L, SN_I **0.037** n/a	4° × 5° SN_L, SN_I {0.02} (*1890–1995*) **0.01**	1° × 1° SN_L, SN_I, SI **0.03**[i] n/a	1° × 1° SN_L, SN_I, SI {0.018} (*1750-2000*) {0.021}	2.8° × 2.8° n/a n/a n/a
0.054 (*1998*) **0.049** (*2001*) 6 (*1998* BB), 7 (*2001* BB)	**0.047** 6	**0.03** 4	{0.04} {5} [j]	{0.024} {3}	**0.042** [l] n/a

effect. *Liu et al.* [2009a] reported BC concentrations of about 300 to 3000 L^{-1}, which when compared to a few measurements were roughly a factor of 2 too high. *Penner et al.* [2009] reported reasonable agreement with measurements of IN from one field campaign, but the concentrations exceed those summarized in section 7.5.3.2 for a more geographically diverse set of regions. IN concentrations in the UTLS region are smaller in *Liu et al*. [2009a] than in *Penner et al*. [2009].

[477] Our estimate of the BC influence on ice-cloud indirect effects is 0.0 ± 0.4 W m^{-2} based on the *Gettelman et al*. [2012] study and the average and range of *Liu et al*. [2009a] and *Penner et al*. [2009]. Both *Penner et al*. [2009] and *Liu et al*. [2009a] lack fidelity in some aspects, so that there is no clear choice between the two opposing results. However, we use them to bound the uncertainty range. Unlike all other cloud forcings, this estimate has not been scaled to our best estimate of industrial-era BC emission rate. For ice-cloud effects, many factors other than emission rate affect ice-active BC concentrations in the upper troposphere. Most models, including those used in the *Penner et al*. [2009] and *Liu et al*. [2009a] studies, overestimate these concentrations. Therefore, the model results may represent an upper bound on the magnitude of ice-cloud impact. In the *Gettelman et al*. [2012] study, the BC ice cloud impact was not significant.

7.5.3.5. Aircraft Impacts on High Ice-Cloud Properties

[478] BC emissions from aviation are a very small fraction of direct forcing because they are a very small fraction of global emissions. However, aviation emissions of BC provide an especially potent source of potential ice nuclei [*Kärcher et al*., 1996; *Schröder et al*., 1998]. The *Liu et al.* [2009a] and *Penner et al*. [2009] modeling studies estimate the effect of aviation BC alone on ice cloud to be between −0.16 W m^{-2} to +0.26 W m^{-2}. Aviation emissions potentially have a larger effect on ice clouds than comparable emissions at the surface [*Lee et al*., 2010]. The total BC climate forcing in Figure 35 explicitly excludes aviation emissions. We mention these studies here because they may provide additional clues about how BC particles affect cirrus clouds, although BC emitted from aviation may undergo less mixing with tropospheric particles and gases.

[479] Although contrails would form even in the absence of BC emissions, the optical properties of the contrails and cirrus impacts depend on BC emission levels [*Kärcher and Yu*, 2009; *Lee et al*., 2010]. Water supersaturated conditions during contrail ice formation below approximately 225K activate even rather hydrophobic BC particles into rapidly freezing water droplets [*Kärcher et al*., 1996; *Köhler et al*., 2009]. A decrease in ice cloud particle size for cirrus clouds altered by aircraft may imply that aircraft BC increases the concentration of available IN for these aged contrails or cirrus clouds [*Lee et al*., 2010]. *Jacobson et al*. [2011] found that an assumption of efficient ice nuclei (i.e., ice nucleation threshold of 1.35 at 185K) was required for a good match with observed contrail cloud fractions. The model study of *Hendricks et al*. [2005] suggests that aircraft BC increases IN by 10 to 40% in aircraft cruise altitudes in northern mid-latitudes. However, the ice nucleating properties of aircraft exhaust for the exact composition and coating of exhaust particles, at the temperature and water vapor conditions in cirrus, remain poorly known. The impact of aircraft BC emissions on cirrus cloud formation in the absence of contrail formation remains very uncertain.

7.6. Comprehensive Modeling of BC Cloud Effects

[480] Although the discussion above has separated effects on individual cloud types, one series of model results [*Jacobson*, 2001b; *Jacobson*, 2002; *Jacobson*,

2004a; *Jacobson*, 2010] has implemented a progressively more complex treatment of BC that does not separate forcing by mechanism or by cloud type. Because individual forcing values cannot be extracted from these studies, it is not possible to discuss them in the framework described in the remainder of the section. However, if these models results are greatly different than the forcing values assembled in the remainder of this assessment, then the causes of these differences should be sought. Therefore, we evaluate these model results for consistency with our estimated forcing. The studies give shortwave and longwave irradiance changes, but those values are not effective forcings because they also include climate responses. Instead, our comparison is largely based on the reported temperature responses divided by the GHG climate sensitivity of the model [0.6K (W m^{-2})$^{-1}$, *Jacobson*, 2002]. This quotient gives an approximate effective forcing.

[481] *Jacobson* [2004a] included direct forcing, snow forcing, and responses of liquid, mixed, and ice clouds to estimate a temperature increase of +0.27K for fossil fuel and biofuel combustion emissions. When the effective snow forcing of +0.18 W m^{-2} (Table 19 and section 10) is subtracted from the total effective forcing, an effective forcing of +0.31 W m^{-2} is obtained. This value is similar to the purely direct-forcing total of +0.36 W m^{-2} expected for the emission rates used in that study and the direct forcing of the model reported earlier [*Jacobson*, 2001b]. From this, we infer that the balance of positive and negative forcings exerted by liquid, mixed, and ice clouds is near zero, comparable to the values assessed above when ignoring the cloud absorption effect. On the other hand, aerosol from open biomass burning caused a negative temperature change of −0.17K [*Jacobson*, 2004b].

[482] *Jacobson* [2010] used slightly different emission rates for fossil fuel and biofuel combustion and reported a temperature change of +0.38K (i.e., equivalent to about 0.45 W m^{-2} after removing cryosphere forcing) when cloud absorption was ignored, again similar to the emission-based projection of direct aerosol forcing of +0.39 W m^{-2} and indicating a negligible net cloud influence. However, when cloud absorption by BC in droplets was included in the simulation, the temperature change was +0.69 K, an increase of +0.31K (+0.52 W m^{-2}). This potentially large effect was considered in section 7.3.3.

7.7. Summary of Uncertainties in Estimating Indirect Effects

[483] For all aerosols, model estimates of indirect effects have a much larger relative spread for indirect effects compared with direct effects. For example, the uncertainty estimate for the cloud albedo effect is double that of the aerosol direct effect [*Forster et al.*, 2007].

7.7.1. Model Uncertainties Beyond Aerosol-Cloud Interactions

[484] Aspects of the environment beyond aerosol-cloud interactions have not been addressed nor accounted for in this section. In addition to aerosol effects on clouds, atmospheric dynamics plays a decisive role in cloud formation, properties, and lifetimes [*Heintzenberg and Charlson*, 2009]. If these dynamical relationships are incorrectly represented in models, the resulting errors could overwhelm the magnitude of aerosol influence. Some studies argue that offsetting mechanisms, or "buffering," may reduce the magnitude of perturbations caused by aerosols [*Stevens and Feingold*, 2009].

[485] In some models, the representation of clouds themselves is inaccurate, either in total coverage, location, or optical thickness [*Soden and Held*, 2006; *Bony and Dufresne*, 2005; *Cesana and Chepfer*, 2012]. Global models also suffer from inconsistency between ice microphysics and cloud coverage [*Kärcher and Burkhardt*, 2008], and there are uncertainties in specifying sub-grid-scale vertical velocities, which control the relative roles of IN and liquid particles during cirrus formation [*Kärcher and Ström*, 2003]. These factors may introduce larger uncertainties in determining the indirect effect than do assumptions about variations in the properties of the aerosols, but they have not been evaluated in previous literature and are not included in the uncertainty estimated here.

7.7.2. Aerosol-Cloud Interactions

[486] Uncertainties in BC's influence on clouds are of four general types. First, there are process uncertainties regarding the effects of aerosols on clouds generally and of the role of BC more particularly, and modeled aerosol microphysics and cloud responses have not yet been strongly constrained by observations. A current challenge is obtaining sufficient observational information on aerosol number concentration, size, mixing state, and chemical composition in various regions and altitudes. Cloud-scale measurements determining collocated relative humidity, vertical air motion, and CCN or IN activity and number concentration provide important constraints on these processes. Cloud-resolving models also allow a more detailed evaluation of the importance of individual processes, yet forcing values obtained from models of individual clouds have yet to be reconciled with global average forcing predicted by GCMs. Many models have only recently represented aerosol microphysics and the coupling to both the vapor phase and cloud microphysics. Including these factors changes the magnitude, and sometimes even the sign, of the reported effects.

[487] Only a few model studies have focused on particular types of aerosol-cloud effects and the influence of BC in those changes. Studies frequently lack consistent diagnostics and experimental designs for isolating effects of particular species or emission sectors, in particular regions, or of individual cloud impact mechanisms. Discerning which effects are reported is sometimes difficult; reported liquid-cloud forcing sometimes includes semi-direct responses and even a portion of direct forcing. This inconsistency causes a lack of comparability among model results that is frequently ignored when such reports are tabulated.

[488] Modeling of changes in mixed-phase clouds, ice clouds, and increased absorption in cloud droplets is a relatively new research area. A much smaller number of studies provide these estimates, compared with studies on liquid clouds. Aerosol microphysical effects on convective clouds are poorly known and generally not included in models. For cold ice clouds, GCM cloud schemes do not yet reconcile the physical treatments of fractional coverage, supersaturation, and microphysics.

[489] With few exceptions, modeling of aerosol influence on clouds has been illustrative and has not addressed

sensitivities nor constrained sensitive parameters with observations. Models agree that forcing usually increases as emissions increase, yet some studies do not even report the emission rates used, again making comparability difficult. Forcing may not be linear with regard to emissions or other inputs such as particle size, but sensitivity studies are not available to provide more constrained scaling for cases when modeled aerosol concentrations differ from observed values. Uncertainties estimated for cloud effects are obtained from model diversity rather than from true uncertainty propagation, as the latter has not been achieved with current models and scientific understanding.

[490] Multiple indirect effects exist and the combination of forcings may be nonlinear. Forcing inferred from satellite observations may include the combined response, but in situ observations may be more likely to isolate individual effects. A constraining approach that combines the strengths of all approaches has not yet appeared.

[491] Because of sub-linearity in cloud response to increasing aerosol concentrations, the dependence of industrial-era forcing on assumed preindustrial values is even greater for indirect effects than for direct effects. To determine the impacts of future aerosol changes and for comparison with temperature changes in recent years, examining changes from present-day conditions could provide a more reliable measure than comparison with a nominal preindustrial condition [*Menon et al.*, 2002a].

8. Cryosphere Changes: Black Carbon in Snow and Ice

8.1. Section Summary

[492] 1. Light-absorbing particles in snow can significantly reduce snow albedo. Because of the high albedo of snow, even aerosol with relatively high single-scatter albedo (e.g., aerosol with a high OA : BC ratio) causes positive radiative forcing.

[493] 2. Small initial snow albedo reductions may have a large adjusted forcing because the resulting warming affects the snow morphology (grain size), snow sublimation rates, and snow melt rates, all of which enhance BC-induced snowpack albedo reductions, leading to an amplification of the radiative forcing. Albedo feedback triggered by this forcing drives a large surface temperature response (section 9).

[494] 3. The best estimates for all-source and industrial-era adjusted forcing by BC in snow are +0.04 W m^{-2} and +0.035 W m^{-2}, respectively. The all-source estimate is derived by scaling the results of a suite of model studies to achieve consistent estimates of forcing from all present-day sources (fossil fuel, biofuel, and biomass burning). Measurements of the BC content of Arctic snow were also used to adjust two of the model studies' derived forcing for biases in snow BC concentrations. Industrial-era forcing is calculated by scaling by the ratio of industrial-era to all-source BC emissions, accounting for changes 1750 to present day in the fraction of global emissions from fossil fuel-plus-biofuel and from open biomass burning which are deposited to snow. Changes in snow and ice cover 1750 to present day are not accounted for. These central estimates also do not account for forcing by BC in sea ice but do account for forcing by BC in snow on sea ice.

[495] 4. The bounds for all-source snow BC adjusted forcing are estimated at +0.01 W m^{-2} to +0.09 W m^{-2} and for industrial-era forcing at +0.008 W m^{-2} and +0.078 W m^{-2}. These bounds include rapid adjustments in snow grain size and surface snow BC concentrations due to changes in sublimation and melt rates resulting from the initial snow albedo reduction due to BC. They are based on results of model sensitivity studies applying low and high values of snow cover fraction, rate of snow aging and resulting grain size evolution, scavenging of BC out of the snowpack during melt, and BC emissions, as well as a model estimate of the reduction in forcing by BC caused by the concurrent presence of light-absorbing soil dust. These bounds do not account for uncertainty in how forcing is affected by patchy snow cover, by uncertainties in modeled cloud cover and vegetation cover, or for possible biases in modeled mid-latitude snow BC concentrations.

[496] 5. The best estimate for all-source and industrial-era radiative forcings by BC in melting snow-free sea ice are +0.012 W m^{-2} and +0.011 W m^{-2}, respectively. These forcings do not account for rapid adjustments that may amplify the initial radiative forcing. They are derived using Arctic-wide averages for sea-ice BC concentration, sea-ice area, melt pond fraction, snow cover fraction, and solar irradiance. The bounds on sea-ice BC radiative forcing are +0.008 and +0.017 W m^{-2} for all-source forcing and +0.007 and +0.016 W m^{-2} for industrial-era forcing, based on independently calculating negative and positive deviations from the mean given by realistic possible minima and maxima in these factors.

[497] 6. Chemical analysis of springtime surface snow samples indicate that most BC and other light-absorbing particles in the North American and Russian Arctic snow and in Greenland are associated with biomass burning. Fossil fuel plays a prominent role in the high-latitude Arctic Ocean and in Greenland in the summertime, but in Greenland, concentrations are low. Indirect evidence indicates that pollution may also play a significant role in the Arctic north of Europe, where concentrations are higher.

[498] 7. A large fraction of particulate light absorption in Arctic snow (about 30 to 50%) is due to non-BC constituents. Most of the absorption appears to be due to light-absorbing organic carbon from biofuel and agricultural or boreal forest burning. The forcing estimates given above account for only BC. The total forcing by a source which emits both BC and light-absorbing organic carbon is larger than is given by BC forcing alone.

[499] 8. In some regions, especially areas with thin and patchy snow cover or mountainous regions, soil dust significantly lowers snow albedo, lessening the influence of BC. Models do not capture these potentially large sources of local dust to the snowpack and, therefore, may be overestimating BC forcing, and this is not accounted for here.

[500] 9. There is evidence that snow BC concentrations in the Arctic, Europe, and North America were higher in the early and middle twentieth century than presently. Also, snow cover is declining with time. Thus, snow BC forcing is likely decreasing in many regions.

[501] 10. BC in glacial snow is a concern primarily because of its possible role in altering melt cycles of

glaciers in regions that rely on glacial melt to balance the water supply through the seasons. Forcing due to BC in snow in the Himalaya and Tibetan Plateau is significant in the limited model studies available to date, but there are indications these estimates are biased high due to overestimates in modeled snow BC concentrations and snow cover or by not accounting for the role of dust and soil in snow reducing snow albedo. The available measurements of glacial snow BC in this region show high spatial variability and a springtime maximum that coincides with a maximum in dust deposition to snow, emphasizing the need for accurate model representation of both BC and dust in snow.

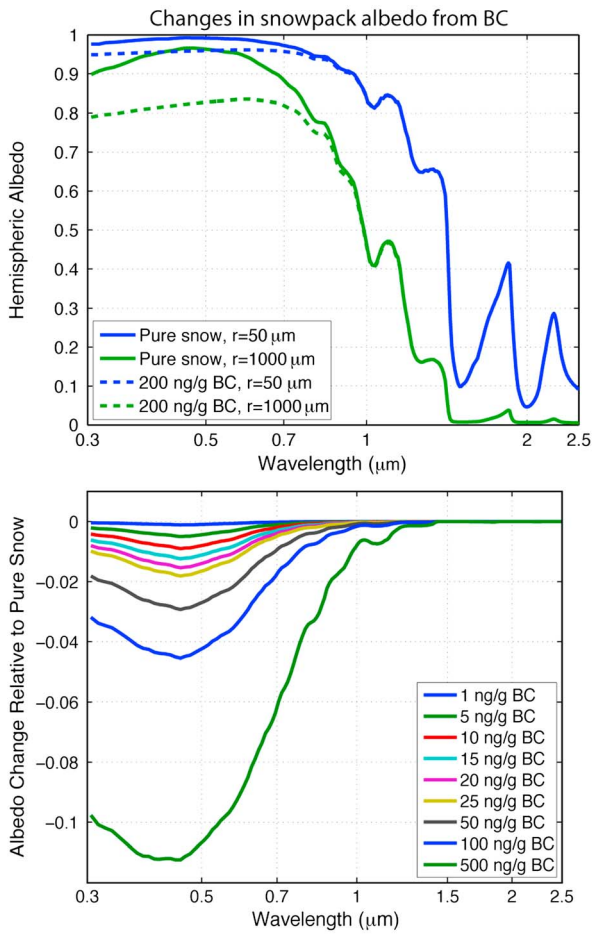

Figure 27. Top: Spectrally resolved, hemispheric albedo for snowpack effective grain sizes of radii (r) of 50 and 1000 μm, with and without BC mixing ratios of 200 ng/g, for a semi-infinite snowpack and with diffuse incident solar radiation. Changes in grain size most strongly affect albedo at near infrared wavelengths, whereas BC lowers albedo most strongly at visible and ultraviolet wavelengths. Bottom: the reduction in hemispheric albedo caused by various mixing ratios of BC as a function of wavelength, for a snowpack with effective grain size of 200 μm. BC optical properties are those used by *Flanner et al*. [2007, 2009] for hydrophobic (uncoated) particles, tuned to match recommendations from *Bond and Bergstrom* [2006]. Albedo calculations were made following *Flanner et al*. [2007, 2009].

8.2. Introduction

[502] Light-absorbing particles in snow can significantly reduce snow albedo and increase the amount of absorbed solar radiation because the albedo of pristine snow at visible wavelengths is high and because snow scatters visible

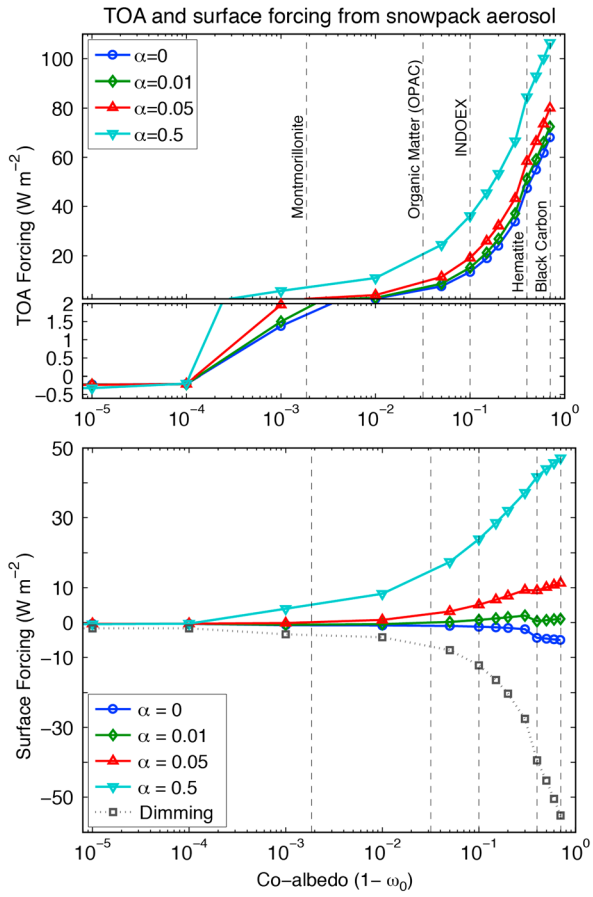

Figure 28. Daily-mean (top) top-of-atmosphere and (bottom) surface changes in net solar power (radiative forcing) as a function of single-scattering co-albedo ($1 - \omega_o$) for all aerosol at 500 nm. Extinction optical depth of the atmospheric aerosol is fixed at 0.2, and the environment represents a clear-sky atmosphere overlying a snowpack with effective grain radius of 200 μm on 1 April at 45°N. Curves are shown for different values of α, which is the ratio of particle mixing ratio in snow to atmospheric column burden ($(\mathrm{kg\,kg^{-1}})\,(\mathrm{kg\,m^{-2}})^{-1}$). Radiative forcings represent the combined influence of particles in the atmosphere and snow. For reference, the change in downwelling surface insolation ("dimming") is also depicted. Vertical lines depict common co-albedo values of BC and organic matter, and that measured during the Indian Ocean Experiment (INDOEX) [*Ramanathan et al*., 2001b]. Also shown are co-albedo values of strongly and weakly absorbing components of dust aerosols. The plot illustrates that (1) any mixture of atmospheric BC and organic matter exerts a positive ToA radiative forcing over snowpack and (2) a small amount of aerosol mixed within the underlying snowpack exerts a darkening effect that exceeds the loss of absorbed energy from surface dimming caused by the atmospheric constituents. Figure from *Flanner et al*. [2009].

radiation very efficiently, producing a large photon path length that amplifies the influence of impurities (Figure 27) [*Warren and Wiscombe*, 1980; *Warren*, 1982; *Chylek et al.*, 1983b]. In contrast to atmospheric aerosol radiative forcing, which may be positive or negative depending on the underlying surface albedo and what species are co-emitted with BC, aerosols with a visible-band single-scatter albedo less than that of ice grains (about 0.9999+), which includes nearly all species except sulfate and sea salt, exert a positive radiative forcing when incorporated into surface layers of optically thick pure snowpacks (Figure 28). Thus, even sources with a high OA : BC ratio produce a warming when deposited on snow exposed to sunlight.

[503] Critically, the large climate effects from BC in snow do not come from the initial change in snow albedo but from the rapid adjustments that follow (Figure 29). Increased solar heating with lower snow albedo affects the snow aging process, in general causing more rapid growth of the snow effective grain size through warmer snowpack temperatures. Coarse-grained snow has a lower albedo than fine-grained snow (*GRA* in Figure 29), and the reduction in albedo due to BC increases with grain size (*GRB* in Figure 29) [*Warren and Wiscombe*, 1980, Figure 7] (Figure 27) so the accelerated aging caused by the warmer snowpack further reduces the snowpack albedo, again increasing the amount of absorbed sunlight. The *GRA* and *GRB* feedback processes lead to earlier melt onset. (A competing effect of BC in snow may be to reduce the snowpack temperature gradient, which could slow the rate of snow aging [*Flanner and Zender*, 2006], but this effect has not been studied in-depth). BC accumulates at the surface with snow sublimation, and sublimation may increase or decrease as surface air temperatures increase, depending on ambient humidity changes. This either enhances or decreases surface snow BC concentrations, albedo reduction, and warming (*SBC* in Figure 29). When melt commences, some of the hydrophobic BC is left at the snow surface [*Conway et al.*, 1996; *Doherty et al.*, 2010, Figure 10], increasing surface snow BC concentrations, further lowering the snow albedo and accelerating melting [*Flanner et al.*, 2007] (*MBC* in Figure 29). Climate changes driven by reduced snow and ice albedo may affect atmospheric transport pathways and wet and dry deposition rates, in turn affecting snow BC concentrations, albedo, and climate forcing (see *DAC* in Figure 29). The magnitude and direction of the feedback is currently unknown. On the other hand, accelerated melting caused by BC in snow leads to earlier exposure of the underlying surface (vegetation, soil, sea ice, etc.), which has a dramatically lower albedo (about 0.2 for tundra or soil [*Bøggild et al.*, 2010]; 0.3–0.6 for sea ice [*Perovich et al.*, 2002]) than snow (about 0.8 for new snow; about 0.7 for melting snow) [*Warren and Wiscombe*, 1985, Figure 1] and thereby warms the surface and adjacent atmosphere, a process commonly known as the snow albedo feedback (*SAF* in Figure 29). The *SAF* feedback only occurs when melt of seasonal snow uncovers a land or ocean surface; the melting of snow on ice sheets (e.g., on Greenland) or on mountain glaciers reveals an almost equally high albedo sub-layer so the strong albedo feedback is missing. The *SAF* feedback facilitates large temperature changes (section 9) in response to the BC snow and ice forcings discussed here. BC-induced changes in snow cover occur on a weeks to months timescale, but the climate system also has a longer-term (months to years) memory for snow cover [e.g., *Déry and Brown*, 2007]. Northern hemisphere albedo feedback is strongest in springtime when the combined effect of snow cover and insolation is maximum, and the snowpack is at or near its melt point [e.g., *Hall and Qu*, 2006; *Flanner et al.*, 2011]. Melt onset and local albedo feedback vary with latitude and altitude, however, for example, occurring later in the year on parts of the Greenland plateau that experience melt and in high-elevation mountain areas.

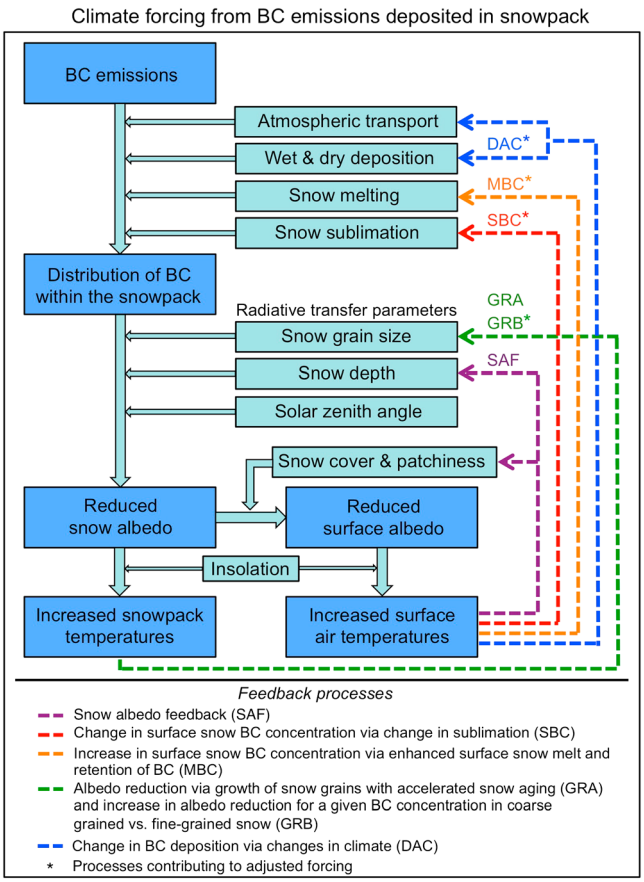

Figure 29. Schematic of the parameters and feedbacks that influence climate forcing by BC in surface snow. BC in the snowpack leads to reduced albedo of the snow surface, with the albedo change depending on BC amounts, snow grain size, and snow depth. Reduced snowpack albedo reduces regional surface albedo and leads to increased snowpack and surface air temperatures. The temperature changes feed back to snow albedo through changes in snow parameters via several processes, as noted in the legend and discussed in the text. This figure emphasizes feedbacks specific to forcing by BC in snow. Changes in climate of any origin may also affect BC emissions, atmospheric transport, rates of BC deposition to the snowpack, and snow accumulation rate.

[504] The rapid adjustments *GRB*, *MBC*, *SBC*, and *DAC* affect the concentrations of BC in the snow (*MBC* and *SBC*) or the change in albedo for a given BC concentration (*GRB*) and constitute "rapid adjustments" to the initial radiative forcing, as defined in section 2.3.2 and Table 2. Modeled radiative forcing is the net effect of the initial

radiative forcing and these rapid adjustments, which together constitute what we have defined here as the adjusted forcing (Table 2). The rapid adjustments *GRA* and *SAF* affect the climate state itself (i.e., the snow cover, *SAF*, and snow grain size, *GRA*), increasing the efficacy of the adjusted forcing. Together the adjusted forcing and high efficacy of that forcing produce an enhanced climate forcing—the effective forcing (section 10).

8.3. Modeled Forcing

[505] *Warren and Wiscombe* [1985] and *Vogelmann et al.* [1988] originally highlighted the climatic importance of snow albedo reduction by pollutants by examining the potential impacts of a "nuclear winter" scenario. At around the same time, measurements demonstrated that sufficient BC was already present in snow around the Arctic margin to affect climate [*Clarke and Noone*, 1985; *Warren and Wiscombe*, 1985, Figure 2]. In contrast, concentrations in Antarctica are too small to be climatically important [*Chylek et al.*, 1987; *Warren and Clarke*, 1990; *Bisiaux et al.*, 2012]. The subject received little attention again until 2004, when *Hansen and Nazarenko* [2004] and *Jacobson* [2004a] published model studies on climate forcing by changes to snow and ice albedos. *Hansen and Nazarenko* used the small number of BC-in-snow measurements available at the time to estimate the change in visible-wavelength (λ less than 770nm) snow albedo due to BC for the Arctic (2.5%), Greenland (1%), and other snow-covered areas in the northern hemisphere (5%). The authors imposed these snow albedo changes and then calculated the radiative forcing and climate response. Subsequent studies have either followed the model of *Hansen and Nazarenko* [2004] in applying regionally uniform snow albedo changes [*Wang et al.*, 2011], have scaled albedo changes based on model-derived BC deposition rates [*Hansen et al.*, 2005; *Hansen et al.*, 2007; *Shindell and Faluvegi*, 2009, which used as input the radiative forcing from *Hansen et al.* 2005], or have prognostically determined the concentrations of BC in snow [*Jacobson*, 2004a; *Flanner et al.*, 2007; *Flanner et al.*, 2009; *Koch et al.*, 2009a; *Rypdal et al.*, 2009b; *Skeie et al.*, 2011], and then calculated the change in snow albedo and finally the forcing and climate response. All of these studies (Table 19) indicate that BC in snow produces warming both in the Arctic and across the northern hemisphere and that the climate efficacy of BC in snow is about 2 to 4 times that of CO_2, so that BC in snow has larger climatic effects than its small direct radiative forcing would suggest.

[506] These studies have raised interest because they indicate that BC may be playing a significant role in two critical areas: the unexpectedly rapid warming of the Arctic and the retreat of mountain glaciers, particularly in areas such as the Himalaya which has high levels of pollution and where local populations rely heavily on a seasonally balanced hydrologic cycle with glacial melt as a water supply in summer [*Menon et al.*, 2010]. BCs in snow may also have contributed to the marked decline in Eurasian springtime snow cover since 1979, which has not been reproduced by models that only account for warming due to GHGs [*Flanner et al.*, 2009]. Accurately modeling these climatic effects requires, first, accurate representation of BC deposition fluxes (i.e., the endpoint of emissions, transport, and deposition along the transport pathway), snow accumulation rates, meltwater scavenging of BC in the snowpack, and snow and sea-ice distributions and cloud cover. All of these vary from model to model. Second, climate forcing calculations must account for the feedback processes shown in Figure 29, not all of which are included in current studies (Table 20). Finally, the climate response to the radiative forcing and rapid adjustments must be accurately represented (section 9, Climate Response).

[507] Interpretation across different model studies is complicated by the fact that they differ in terms of which feedbacks are included in each model (Figure 29 and Table 20) and in that different sources and types of light-absorbing aerosol are used in different models for the baseline and forcing scenarios. Adjusted forcing by BC in the cryosphere was calculated by *Jacobson* [2004a] and *Flanner et al.* [2009] using as a baseline a snowpack that included

Table 20. Indirect Effects and Feedback Processes Induced by Black Carbon in Snow in Model Studies Which Produce Rapid Adjustments to the Radiative Forcing (*GRB*, *MBC*, and *SBC*) or Which Increase the Efficacy of BC-in-Snow Forcing (*GRA* and *SAF*)[a]

Process in Model Studies	*Hansen and Nazarenko* [2004]; *Hansen et al.* [2005]; *Wang et al.* [2011]	*Jacobson* [2004a]	*Flanner et al.* [2007, 2009]	*Koch et al.* [2009a]	*Rypdal et al.* [2009b]; *Skeie et al.* [2011]
Indirect effects and feedbacks driving the climate impact of BC in snow	SAF	SBC, DAC, SAF	GRA, GRB, MBC, SBC, DAC, SAF	GRA, GRB, SBC, DAC, SAF	MBC
Not included	GRA, GRB, MBC, SBC, DAC	GRA, GRB, MBC		MBC	GRA, GRB, SBC, DAC, SAF

[a]Process in model studies that influence the calculation of forcing in various studies, where the processes are as shown in Figure 29 and described in the text. For the MBC process, where hydrophobic soot is left at the snow surface during melt, *Flanner et al.* [2007; 2009] allow for a fraction of the BC to consolidate at the snow surface; *Rypdal et al.* [2009b] leave all BC at the surface when melt commences; and all other models allow the BC to be washed away with the melt water. *Jacobson* [2004a] and *Rypdal et al.* [2009b] used a fixed snow grain radius (150 μm and 500 μm, respectively), so snow grain size does not change with climate. *Jacobson* [2004a] also allows dry-deposited BC to "fall" through the snowpack at a rate of 9 mm/day, and both *Jacobson* [2004a] and *Flanner et al.* [2007, 2009] include frost deposition to the snow surface, which results in a decrease in snow BC concentration. Both of these effects are small and are not included here or in Figure 29.

The abbreviations are snow albedo feedback (*SAF*); albedo reduction via growth of snow grains with accelerated snow aging (*GRA*); increase in albedo reduction for a given BC concentration in coarse grained versus fine-grained snow (*GRB*; see Figure 27); increase in surface snow BC concentration via enhanced sublimation (*SBC*); increase in surface snow BC concentration via enhanced surface snow melt (*MBC*), and changes in deposition resulting from climate changes due to BC in snow and sea ice climate forcings (*DAC*).

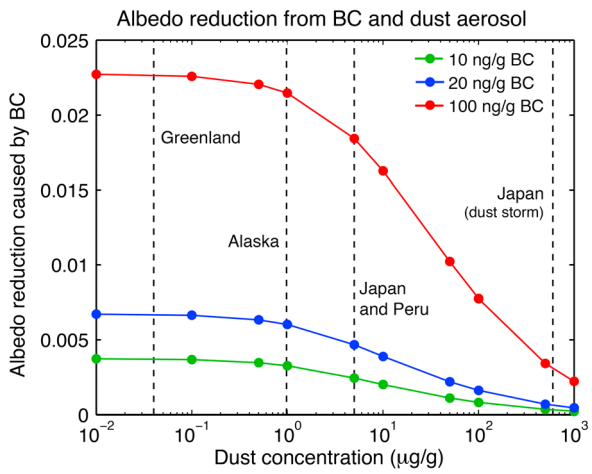

Figure 30. Reduction in hemispheric broadband snow albedo (0.3 to 5.0 μm) caused by BC in the presence of varying amounts of dust. The perturbation caused by BC becomes smaller with increasing dust burden. Conditions represent a clear-sky atmosphere with solar zenith angle of 60° and snowpack effective grain radius of 250 μm. Dust optical properties are similar to those listed in *Flanner et al.* [2009] for a particle effective radius of 1300 nm, and albedo calculations follow *Flanner et al.* [2009]. Vertical dashed lines depict, from left to right, dust-in-snow concentrations measured in Greenland (0.03–0.06 $\mu g\,g^{-1}$) [*De Angelis et al.*, 1997; *Banta et al.*, 2008]; Barrow, Alaska (0.98 $\mu g\,g^{-1}$) [*Darby et al.*, 1974]; Hokkaido, Japan, during pre-melt and Andes, Peru (5 $\mu g\,g^{-1}$) [*Thompson et al.*, 1979; *Higuchi and Nagoshi*, 1977]; and Hokkaido, Japan, after a dust storm (600 $\mu g\,g^{-1}$) [*Aoki et al.*, 2006].

light-absorbing soil dust, which lowers the initial albedo of the snowpack and, therefore, reduces the impact of adding other light-absorbing aerosol (Figure 30). None of the other studies in Table 20 included the impact of soil dust on snow BC radiative forcing. Some model studies calculated forcing due to fossil fuel and biofuel (FF + BF) combustion emissions only [*Jacobson*, 2004a; *Rypdal et al.*, 2009b; *Skeie et al.*, 2011], but others calculated the effect of all sources: fossil fuel, biofuel, and biomass burning (FF + BF + BB) [*Hansen and Nazarenko*, 2004; *Hansen et al.*, 2005, *Hansen et al.*, 2007; *Flanner et al.*, 2007, 2009; *Koch et al.*, 2009a]. Finally, while most studies have calculated the total forcing for a given (near present-day) year, *Hansen et al.* [2005, 2007], *Koch et al.* [2009a], and *Skeie et al.* [2011] focused on the change in forcing from preindustrial to present, defined in these studies as 1880 to 2000, 1890 to 1995, and 1750 to 2000, respectively.

[508] Here the aim is to produce best estimates of the all-source and industrial-era adjusted forcing by BC in the cryosphere and to put uncertainty bounds on that estimate. Some of the sources of uncertainty in this estimate can be quantified using existing measurements and model studies, but for other critical factors, the necessary studies do not yet exist to bound the uncertainty. Sections 8.3.1 to 8.3.6 discuss factors that affect snow BC radiative forcing and rapid adjustments that amplify that forcing. Existing measurements of snow BC concentrations are then used to calculate a best-guess estimate of all-source adjusted forcing for snow BC. Model sensitivity studies are used to estimate the possible range of this forcing, based on the uncertainties that can be bounded. Industrial-era forcing is calculated by scaling the all-source forcing by the ratio of industrial-era to all-source BC emissions.

8.3.1. BC Concentrations in Snow and Sea Ice and the Resulting Change in Albedo

[509] Studies have used a range of values for present-day and preindustrial emissions of BC (Table 19). Here we use observed snow and ice BC concentrations in the present day to account for biases in the net effects of modeled emissions, transport, wet and dry depositional processes, and post-depositional processes such as snow sublimation and melting. However, no such constraint can be placed on preindustrial snow and ice concentrations so derived industrial-era forcing relies on quite uncertain estimates of preindustrial emissions (section 4) and on modeled BC atmospheric transport, BC deposition rates, snow and ice cover, and climate in 1750.

[510] The change in albedo for a given concentration of BC is a function of snow grain size and of the presence of other impurities, as well as of the effective mass absorption cross section of BC in snow. As with atmospheric BC, this cross section depends on BC mixing state and the nature of other constituents in the BC-containing particles. In snow, it also depends on whether the BC is incorporated into the snow or on the surface of snow grains. *Warren* [1982] mentioned the possibility of a factor-of-two enhancement of absorption by situating BC particles inside snow grains, citing *Ackerman and Toon's* [1981] computation for BC inside sulfate aerosols. *Chylek et al.* [1983b] then modeled this effect for snow, obtaining a factor-of-two enhancement. *Flanner et al.* [2007; 2009] obtain about a 50% enhancement for their assumptions of the mixing state.

[511] All model studies considered here other than *Hansen and Nazarenko* [2004], *Hansen et al.* [2005, 2007], and *Wang et al.* [2011] determine deposition of BC to surface snow prognostically, accounting for time-dependent emissions, transport, in-atmosphere chemical processing and aging, and wet and dry deposition rates that depend on aerosol hygroscopicity or age. However, the treatment of atmospheric aerosol processes varies considerably from model to model. For example, *Jacobson* [2004a] determines BC aging by solving coagulation, condensation, and dissolution among multiple, independent, aerosol size bins and resolves cloud-borne and interstitial BC within these bins, whereas other studies track BC in a single mode and assume fixed BC aging rates, internal mixing times, and in-cloud BC fractions [e.g., *Flanner et al*, 2007, 2009; *Koch et al.*, 2009a]. The *DAC* feedback in Figure 29 depends on modeled climate changes due to cryosphere BC forcing, as well as how modeled transport and deposition rates depend, for example, on mixing with other constituents, cloud properties, and precipitation patterns. This feedback does not exist at all in models where albedo changes are prescribed. These factors result in differences in modeled deposition rates of BC to surface snow. Comparisons between modeled and measured surface snow concentrations are discussed in section 8.4.

[512] Calculated albedo change for a given snow BC concentration is also handled differently across models. The *Jacobson* [2004a] study explicitly calculates the changes in

solar albedo of snow and snow thermal-IR emissivity as a function of zenith angle by solving radiative transfer through the atmosphere, snow and ice grains together, by adding a snow or ice layer to the bottom of the atmospheric layers and solving for the upward divided by downward irradiance at the top of the snow layer. The calculation is done for both interstitial BC particles and BC inclusions within snow grains, treated with a core-shell approximation. *Jacobson* [2004a] found that the modeled effect of BC on emissivity is small, as also shown in *Warren* [1982, Table 2]. Effects of BC on IR emissivity are disregarded in all other model studies. The *Flanner et al*. [2007; 2009] studies explicitly calculate the change in solar snow albedo by solving radiative transfer through multiple layers of snow, based on theory from *Warren and Wiscombe* [1980] and the two-stream, multiple scattering radiative approximation of *Toon et al*. [1989]. The snow albedo is then added interactively at each time step as a bottom boundary condition to an atmospheric model that accounts for the effects of atmospheric optics (e.g., aerosol, clouds, etc.) on downwelling solar radiation. They treat sulfate-coated and interstitial BC species with coated BC absorbing about 50% more solar radiation per mass of BC. *Koch et al*. [2009a] parameterizes the change in albedo based on the study of *Warren and Wiscombe* [1985], which treated the BC as being externally mixed with the snow and accounts for absorption enhancement through multiple scattering in the snow. This parameterization provides a spectrally averaged change in albedo, with dependence on snow grain size and BC concentration, but it ignores the zenith angle and atmospheric optical dependence of the albedo. *Rypdal et al*. [2009b] and *Skeie et al*. [2011] use look-up tables of albedo based on snow grain size and BC concentration; these tables are based on Mie theory and radiative transfer calculations. Radiative transfer calculations are done with a multi-stream model using the discrete ordinate method [*Stamnes et al*., 1988], where two snow layers have been added below their atmospheric layers. *Hansen and Nazarenko* [2004], *Hansen et al*. [2005, 2007], and *Wang et al*. [2011] impose albedo changes so there is no dependence on BC concentration or other factors.

[513] As with snow, BC concentrations in bare (non snow-covered) sea ice similarly depend on the amount of BC wet and dry deposition to the surface. However, because sea ice is usually snow-covered in the winter to spring season, the BC concentrations in multi-year summer ice are likely a strong function of how much BC resides in the winter and spring snowpack and on how much is retained in the sea ice during melting. A few measurements of sea-ice BC concentrations are available to test models; they indicate that BC in sea ice is comparable to that in snow from the same region [*Doherty et al*., 2010].

[514] A given concentration of BC produces a larger change in albedo in sea ice than in snow, because the surface of sea ice behaves as large-grained snow. However, sea ice also can contain significant amounts of other light-absorbing impurities, such as sediment, which as discussed below may significantly decrease the forcing by BC. Only three studies in Table 19 include radiative forcing by BC in sea ice: *Jacobson* [2004a], *Rypdal et al*. [2009b], and *Skeie et al*. [2011]. This may explain, in part, the relatively large forcing per emission of *Jacobson* [2004a]. However, forcing by BC in snow on sea ice and by BC in sea ice were not separately diagnosed so it is not possible to know how large a role these forcings played in either study. Below independent estimates are made for forcing by BC in sea ice and its possible upper and lower bounds.

8.3.2. Snow-Covered Area

[515] Climate forcing by BC in snow is a direct function of the amount of land or ice area covered by snow, so seasonal and sub-grid-scale variations in snow cover must be accurately represented. Models allow for fractional snow cover within model grid boxes by employing snow depth dependent parameterizations. The adjusted forcings calculated by *Flanner et al*. [2007] for low and high cases of snow cover are used here to help bound uncertainty in forcing due to errors in fraction of snow covered area.

[516] The allowance for fractional snow coverage within a grid box might not, however, account for very small-scale snow patchiness, which occurs particularly in areas with low snowfall amounts or broken up sea ice. Melt rates are higher in patchy snow than in uniform snowpacks, and melt rates increase with degree of snow patchiness and exposed area [*Liston*, 1995, 1999, 2004; *Essery*, 1997]. Accounting for this patchiness is expected to have two competing effects: Patchy snow warms and starts to melt more quickly due to local heat advection, and when the snowpack is close to its melt point, the feedbacks enhance the effect of the initial direct forcing most powerfully. On the other hand, patchy snow on land is more likely to be loaded with local soil dust, thereby lowering the "baseline" snowpack albedo and decreasing the impact of BC (Figure 30). It is not known if accurately accounting for these two effects would produce a larger or a smaller radiative effect by BC in snow, so this is an unbounded uncertainty.

8.3.3. Masking by Clouds and Vegetation

[517] The planetary albedo of cloud-covered areas is relatively insensitive to surface albedo, so cloud cover must be accurately represented. Similarly, BC in snow masked by vegetation contributes little to ToA forcing, so vegetative cover must be accurately represented. Both cloud cover and vegetation are sub-grid-scale features, complicating their representation in models. Model representation of and forcing sensitivity to realistic ranges of cloud cover and vegetation have not been tested, and this is currently an unbounded uncertainty in cryosphere BC adjusted forcing.

8.3.4. Snow Grain Size

[518] As noted above, snow albedo is highly sensitive to snow grain size. Further, the change in albedo for a given snow BC concentration is greater in larger grained snow than in smaller grained snow (Figure 27). Thus, the snowpack BC concentration and snow-grain size must be well constrained down to the penetration depth of sunlight (about 30 cm for a typical snow density of 0.3 g cm^{-3}) [*Warren and Wiscombe*, 1980, Figure 13c]. "Grain size" must also be defined consistently: in field measurements, reported values are optical grain sizes, which are proportional to the volume-to-area ratio [e.g., *Grenfell et al*., 2005] and inversely proportional to the "specific surface area" [e.g., *Matzl and Schneebeli*, 2006]. *Jacobson* [2004a], *Rypdal et al*. [2009b], and *Skeie et al*. [2011] use globally fixed snow-grain radii in their models of 150, 500, and 500 μm, respectively. Grain radii for new snow are less than 150 μm, and for old, melting snow, they are larger than

500 μm, so the feedbacks that involve grain size (*GRA, GRB* in Figure 29) are not captured. The net effect of applying a fixed snow grain size is not known. However, *Flanner et al*. [2007] used a model to determine how a reasonable range in snow aging rate (i.e., the rate of grain size growth) affects the derived annual mean adjusted forcing. These results are used to help bound the possible range of forcings by BC in snow.

8.3.5. Albedo Dependence on Downwelling Radiation

[519] In addition to being a function of snowpack properties, both pure and contaminated snow albedo depend on solar zenith angle and the fraction of direct versus diffuse solar radiation. Models that prescribe solar-zenith-angle-independent albedos may have a bias in clear-sky albedo of several percent for pristine snow [*Wiscombe and Warren*, 1980, Figure 6], which is of the same magnitude as the albedo perturbation by BC. Direct and diffuse solar radiation must also be accurately represented, in turn requiring accurate representation of cloud cover.

8.3.6. Concentration of BC With Sublimation and Melting

[520] Precipitation rates and relative humidity in much of the Arctic are low, so in some areas appreciable (up to 30–50%) [*Liston and Sturm*, 2004] surface snow is lost to sublimation. This process removes snow water but leaves BC and other non-volatile particulate constituents at the snow surface, increasing their concentration. Similarly, variable fractions of BC are left behind at the snow surface with melt, depending on the hygroscopicity of accompanying constituents [*Conway et al*., 1996]. *Flanner et al*. [2009] apply a "scavenging efficiency" for BC with melt of 0.2 for hydrophilic BC and 0.03 for hydrophobic BC, based on the *Conway et al*. [1996] study. *Rypdal et al*. [2009b] and *Skeie et al*. [2011] leave all BC at the snow surface as the snow melts, and all other models cited here allow all BC to be washed away with snow meltwater. While there are some observational evidence of BC remaining at the surface during melt [*Conway et al*., 1996; *Xu et al*., 2006; *Doherty et al*., 2010], an appropriate BC scavenging ratio remains to be determined. A model sensitivity study which applies a range of melt scavenging efficiencies is used to help bound this source of uncertainty.

8.3.7. Representation of All Light Absorbing Particles in Snow

[521] Particulate matter in snow is never pure BC. BC from biomass, biofuel, and fossil fuel burning is accompanied by varying amounts of brown organic carbon. Other sources also produce light-absorbing carbon [*Andreae and Gelencsér*, 2006] and light-absorbing crustal material (e.g., hematite in soil dust). Calculation of BC effects on snow and ice albedo and melt rates must consider *all* light-absorbing constituents in the snow. Glacial snow especially often has high concentrations of locally sourced soil dust and sand that significantly reduce its albedo. While the *Jacobson* [2004a] and *Flanner et al*. [2009] studies included soil dust in snow in their baseline calculations, these models do not account for very local sources of coarse-grained (i.e., much greater than 10 μm diameter) dust and sand, which have a very short atmospheric lifetime (i.e, less than a few days). Particularly in areas with patchy snow cover, local soil and sand may be present in the snow at high concentrations. This observation was made along the Arctic coast of Siberia (S. Warren and T. Grenfell, personal communication, 2011), in Inner Mongolia [*Huang et al*., 2011], and on summertime Arctic sea ice (B. Light and T. Grenfell, personal communication, 2011) during snow and ice sampling surveys. The bias this introduces to modeled forcing cannot currently be bounded. However, the *Flanner et al*. [2009] model can be used to help constrain the impact of including dust deposition to snow. In this model, when dust is included the snow BC radiative forcing is decreased by about 25% for the global mean dust burden of 4.3 ppm calculated in the model. This result is consistent with Figure 30, which shows a snow albedo reduction of about 0.006 for a pristine snowpack with 20 ng g^{-1} of BC and an albedo reduction of about 0.005 for a snowpack with 4000 ng g^{-1} of dust and 20 ng g^{-1} of BC. These results indicate that the albedo reduction due to BC is 20% less in the presence of dust.

[522] Importantly, most studies that have measured [*Xu et al*., 2006; *Ming et al*., 2009] or estimated [*Yasunari et al*., 2010; *Castelvecchi*, 2009] BC concentrations for Himalayan glaciers have estimated a significant radiative forcing, but this was by comparing clean (dust- and algae-free) snow to clean snow with BC added. In the spring season when the glacier snow starts to melt and when BC may have its maximum impact, it is also late in the dry season, with minimal precipitation and large dust events over the Tibetan Plateau and across the Himalaya [*Ming et al*., 2009; *Marinoni et al*., 2010]. In addition to being exposed to dust from Central Asia and the Middle East, the south side of the Himalaya can experience significant dust loading from sources in northern India [*Marinoni et al*., 2010]. Similarly, dust storms from the Sahara can account for a significant fraction of the impurities in Alpine snow [*Thevenon et al*., 2009; *Haeberli*, 1977], and dust from the Colorado Plateau drives a very large radiative forcing of snowpack in the San Juan Mountains [*Painter et al*., 2007]. The lower parts of many Himalayan glaciers are entirely hidden by thick debris cover [*Nakawo et al*., 2000], actually inhibiting melt. Future studies must account for the effects of crustal and other light-absorbing material (e.g., algae) [*Jones et al*., 2001] in mountain glaciers when determining the effects of BC on snow melt.

[523] Measurements from across the Arctic indicate that typically 30 to 50% of sunlight absorbed in the snowpack by impurities is due to constituents other than BC [*Doherty et al*., 2010]. Either organic matter or soil dust could be responsible, and the spectral absorption measurements cannot distinguish them, but chemical analysis of a geographically diverse subset of these Arctic samples indicates that the non-BC light absorbing particulate matter is overwhelmingly light-absorbing OC, not mineral dust [*Hegg et al*., 2010]. These samples were collected specifically trying to avoid snow that obviously contained significant amounts of soil, dust, or sand, so they may somewhat underrepresent the role of these particles in snow. Regardless, these measurements make it clear that particles other than BC play a significant role in changing snow albedo. While *Flanner et al*. [2007; 2009] did not include snow OC light absorption in their published forcing calculations, they did test for the effect of OC on snow albedo and found it to be sufficiently small that omitting it would not significantly change their results. If organic matter is in fact a significant source of light absorption in snow,

the forcing by sources high in OC (i.e., BF and BB) would be larger because of the addition of light-absorbing OC. However, if biomass burning and soil dust emissions are considered a "natural" source of aerosol, this would mean the natural snowpack has a lower albedo, thus lessening the effect of mitigating anthropogenic sources. On the other hand, mitigating biofuel-burning emissions or any burning which produces light-absorbing OC or decreasing soil dust emissions would have a larger impact than would be implied by only considering the effect of BC.

[524] These results highlight the importance of determining not only the concentration of snow BC but also light-absorbing OC and soil dust in snow. In addition, while the wavelength dependence of absorption of BC has been studied and is relatively well constrained to follow λ^{-1}, the wavelength dependence of absorption (or, equivalently, the size distribution and spectrally resolved indices of refraction) for light-absorbing organics and soil dust appear to be quite variable [e.g., *Bond*, 2001; *Kirchstetter et al.*, 2004; *Bergstrom et al.*, 2007; *Sun et al.*, 2007; *Russell et al.*, 2010], making estimates of the impact of OC and dust on light absorption in snow highly uncertain.

8.4. Measurements of BC in Snow and Comparison With Models

[525] As shown in Table 19, model studies to date have used a range of assumptions about the sources and quantity of BC emissions. Similarly, atmospheric transport processes differ from model to model, as do deposition rates. For example for the suite in Table 19, the fraction of BC deposited to surface snow by wet (versus dry) deposition ranges from 71% [*Koch et al.*, 2009a] to 98% [*Jacobson*, 2004a]. Measurements of snow BC concentrations can be used to test models for the combined influence of all of these factors. Data are available from the Arctic and sub-Arctic, a few mid-latitude locations in the northern hemisphere and the Antarctic. Here we limit model/measurement comparisons to northern hemisphere sites, because concentrations in Antarctic are too small (i.e., generally less than 1 ng g^{-1}) [*Chylek et al.*, 1987; *Warren and Clarke*, 1990; *Bisiaux et al.*, 2012] to be important for forcing evaluations.

8.4.1. Measurement Methods

[526] BC concentrations in snow have been measured using variations of the thermo-optical method [*Chylek et al.*, 1987; *Cachier and Pertuisot*, 1994; *Lavanchy et al.*, 1999; *Xu et al.*, 2006; *Jenk et al.*, 2006; *Hagler et al.*, 2007a, 2007b; *Legrand et al.*, 2007; *Ming et al.*, 2008; *Forsström et al.*, 2009; *Ming et al.*, 2009; *Thevenon et al.*, 2009; *Xu et al.*, 2009a, 2009b; *Hadley et al.*, 2010] and with an SP2 instrument [*McConnell et al.*, 2007; *McConnell and Edwards*, 2008], both of which are described in section 3.5. They have also been measured using a third, filter-based method that optically analyzes BC concentrations, used first by *Clarke and Noone* [1985] in the form of the IP Spectrophotometer and later with an improved instrument, the ISSW Spectrophotometer [*Grenfell et al.*, 2011; *Doherty et al.*, 2010]. Using the wavelength-dependence of the measured light absorption on the filter, it is possible, assuming known BC MAC, to calculate the maximum possible BC concentration, an estimated BC concentration, and the fraction of absorbed solar radiation (integrated 300–750nm) that is due to species other than BC, such as light-absorbing organic carbon and crustal material [*Grenfell et al.*, 2011; *Doherty et al.*, 2010]. Here modeled values are compared with BC concentrations from the IP and ISSW spectrophotometers, thermo-optical measurements and from the SP2.

8.4.2. Arctic and Sub-Arctic Snow

[527] Table 21 gives measured concentrations of BC in surface snow for various regions of the Arctic. Because the snow albedo feedback is greatest in spring, most of these measurements were of surface snow in March, April, or early May; all are from snow that has not yet experienced melting (and therefore the feedback *MBC* in Figure 29) but which may have experienced sublimation (feedback *SBC* in Figure 29). These are compared to average surface snow (top 2 cm) concentrations from the *Flanner et al.* [2009] study and to the concentration of BC deposited in snow (via both wet and dry deposition) in the *Koch et al.* [2009a] study. Model average values were calculated using the modeled concentrations from the same month and location (grid box) as the measurements. In addition, *Skeie et al.* [2011] include a comparison of their modeled snow BC concentrations with measured values reported by *Forsström et al.* [2009] and *Doherty et al.* [2010] for Arctic and sub-Arctic regions. These comparisons are imperfect but allow a first-order check of how well the models are representing BC deposition to the snowpack. The concentrations shown in Table 21 produce a change in snow albedo of less than 5%, which would not be visible to the human eye. In common images of snow visibly darkened by light-absorbing impurities, the impurities are often sand and soil, not BC.

[528] The comparison herein has been limited to two of the six studies which calculated snow BC concentrations [*Flanner et al.*, 2009; *Koch et al.*, 2009a] (Table 20) for which modeled snow BC is readily available, and to discussion of the *Skeie et al.* [2011] model and observation comparison. For reference, total, present-day BC emissions from *Flanner et al.* [2009] (7400 Gg yr^{-1}) and *Koch et al.* [2009a] (8200 Gg yr^{-1}) are between the central bottom-up all-source estimate of 7300 Gg yr^{-1} (section 4) and the all-source emissions (10,100 Gg yr^{-1}) based on a comparison of modeled and measured AAOD (section 6). The *Hansen et al.* [2005] total present-day BC emissions (11,000 Gg yr^{-1}) are larger than either of these estimates. *Jacobson* [2004a] total BC emissions are within 5% of the total emissions of *Flanner et al.* [2009], though there is a higher fraction of BB emissions in *Jacobson et al.* than in *Flanner et al.* (44% versus 35%), and BB emissions are less likely to be deposited to snow [*Flanner et al.*, 2009; *Skeie et al.*, 2011]. The *Rypdal et al.* [2009b] FF + BF emissions are 13% and 18% higher, respectively, than those in *Flanner et al.* [2009] and *Koch et al.* [2009a] studies; *Rypdal et al.* [2009b] did not include BB emissions in their analysis. The *Flanner et al.* [2009] study was specifically run for a representative biomass-burning year and so is a better comparison to measurements than the *Flanner et al.* [2007] study, which explored two extreme (high and low) BB years. Differences in transport and deposition rates also affect the concentration of BC in snow, but this comparison still provides a first-order test of the models. Broad patterns in

Table 21. Arctic Surface Snow Measurements of BC Compared With Model Results[a]

Region	# Sites	Sampling Period	Measured EC, BC (ng g^{-1})	*Flanner et al.* [2009] BC (ng g^{-1})	*Koch et al.* [2009a] BC (ng g^{-1})	Ratio Flanner: Measured	Ratio Koch: Measured	References for Measurements
Greenland (~63°–81°N)	12	April Jul + Aug	Apr: 3 ± 1 Jul + Aug: Cold snow:2 ± 1 Melting snow:16 ± 5	April: 5 ± 1 May: 7 ± 4 June: 13 ± 7 July: 29 ± 18 Aug: 27 ± 30	April: 6 ± 6 May: 4±2 June: 5 ± 2 July: 5 ± 3 Aug: 4 ± 2	April: 1.3 Jul/Aug: 14 (cold snow) 1.8 (melting snow)	April: 1.6 Jul/Aug: 2.3 (cold snow)	*Chylek et al.*, 1987; *Cachier and Pertuisot* [1994]; *Chylek et al.* [1995]; *Hagler et al.* [2007a, 2007b]; *McConnell et al.* [2007]; *Doherty et al.* [2010]
Arctic Ocean (~84°–90°N)	5	April	5 ± 3	7 ± 1	11.8 ± 1.2			*Doherty et al.* [2010]
Arctic Canada,May: 9.2 (~66°–77°N)	25	April–May	8 ± 3	13 ± 8	8.4 ± 2.3	1.5	1.0	*Doherty et al.* [2010]
Sub-Arctic Canada, (~63.5°–67.5°N)	27	March–April	14 ± 9	11 ± 3	7.6 ± 3.3	0.8	0.6	*Doherty et al.* [2010]
Barrow, Alaska (~71.3°N)	1	March–April	9	5	5.8	0.6	0.6	*Doherty et al.* [2010]
Svalbard, Norway (~79°N)	10	Mar–May	Mar:10 ± 20 Apr: 9 ± 8 May: 10	Mar: 17 Apr: 14 May: 16	Mar: 7.6 Apr: 4.9 May: 9.2	1.6	0.7	*Forsström et al.* [2009][b]; *Doherty et al.* [2010]
Tromso, Norway (~69.7°N)	1	March–May	21 ± 12	78	7.6	3.4	0.3	*Doherty et al.* [2010]
Abisko, Sweden (~68.3°N)	1	March–April	31	76	7.8	2.4	0.3	*Clarke and Noone* [1985]
Northern Russia (~62°–74.5°N)	9	March–May	18 ± 28	17 ± 14	17.2 ± 13.2	0.9	1.0	*Doherty et al.* [2010]

[a]Arctic surface snow EC (thermo-optical (T.O.) or SP-2 method) or estimated BC (IP or ISSW Spectrophotometer) from measurements versus in models. Where more than 10 measurements are available, a median and standard deviation are given. The model values are calculated from monthly averages of the model gridboxes that contain the sample sites. Monthly averages for Greenland are shown explicitly because of the large change in concentration in the *Flanner et al.* [2009] study moving from spring to summer.

[b]Excludes *Forsström et al.* [2009] data from Linnébreen because of contamination by local sources.

the observed spatial variability of snow BC concentrations are qualitatively consistent with the model results. Both have higher concentrations of BC in snow over northwestern Russia, Europe, and Scandinavia than across the western Arctic and Greenland. However, there are important quantitative differences.

[529] The *Koch et al*. [2009a] modeled values are in agreement with the measured values for Arctic Canada and northern Russia, are biased high in the Arctic Ocean, and are biased low compared to the measurements in all other regions other than Greenland, where they are about a factor of 2 too high. In contrast, the *Flanner et al*. [2009] model values are somewhat lower than the measured values for northern Russia, Barrow, and sub-Arctic Canada but are higher than the measured values at all other sites. The differences are particularly profound for the Scandinavian sites, where they are 1.6 to 3.4 times the measured concentrations. Notably, these sites also have the highest concentrations and so carry more weight than the other sites at similar latitudes in terms of global radiative forcing. For Greenland, values are shown for both spring (April) and summer (July to August). Only about 25% of the Greenland Ice Sheet is in the "dry snow zone;" everywhere else some melting occurs during summer. There is a striking increase in Greenland values in the *Flanner et al*. model when moving from spring to summer that is also present in the measurements but not as pronounced (Table 21). Based on the timing and spatial pattern of the increase, it appears to be caused by the concentration of BC at the surface with melt, indicating that the *MBC* feedback (Figure 29) may be too strong in *Flanner et al*. [2009] study. The timing and extent of melt is clearly critical in this process and needs to be validated against observations; the limited data presented here are insufficient. Furthermore, improved model treatment may be needed for particle accumulation in perennial snow and ice sheets, where (in the absence of glacier dynamics) snow either accumulates year after year or is "capped."

[530] *Skeie et al*. [2011] prognostically determined snow BC concentrations from all sources (FF + BF + BB) and compared these to measured concentrations. Their forcing was calculated for the FF + BF sources only, but biomass burning only accounted for 4 to 12% of BC in snow north of 65°N. Their comparison with the *Forsström et al*. [2009] measurements indicates that the modeled snow BC concentrations for 2001 to 2008 vary over about the same range as the measured concentrations in 2007 in Ny Ålesund, Svalbard. However, *Doherty et al*. [2010] find concentrations in this region that are about a factor of 2 higher than that measured by *Forsström et al*. The *Skeie et al*. modeled concentrations are much lower than is observed by *Forsström et al*. at the Scandinavian sites Pallas, Tromso, and Abisko, sometimes by more than a factor of 4 and typically by a factor of 2. The exception is in the later spring when the snow starts to melt, and in the model, all BC consolidates at the snow surface. At this time, modeled surface snow BC concentrations increase by approximately 10-fold. The comparison with the geographically broader snow BC data set of *Doherty et al*. [2010] only includes snow samples that had not yet experienced springtime melt. This comparison shows reasonable agreement for the Canadian and Alaskan Arctic and for Greenland; it indicates a low bias in the model over the Arctic Ocean, and it shows large model underestimates for the Canadian sub-Arctic, across Russia, and in Svalbard. Model underestimates vary from about a factor of 2 (Svalbard) up to a factor of 5 (Eastern Russia). Notably, this is the region where BC concentrations (and, thus, forcing) are expected to be largest.

8.4.3. Mid-Latitude Snow Measurements

[531] Few measurements of mid-latitude snow exist, despite the fact that the climate impacts of BC in snow at these latitudes may be larger than for Arctic snow because of the combination of higher BC concentrations and higher insolation. *Flanner et al*. [2007] include a comparison of their modeled values for 1998 and 2001 to those measured in the 1980s and 1990s at select mid-latitude sites in North America and Europe (see their Table 2). Modeled concentrations at some sites are about one third to one half the measured values (in rural and urban Michigan, USA, and in Lithuania). At other sites, they are about equal to the measured values (Cascade mountains in Washington State in the USA and the French Alps in Europe) or are higher by factors of about 1.5 to 7.7 (West Texas and New Mexico in the USA and Halifax, Nova Scotia, in Canada). *Hadley et al*. [2010] measured snow BC concentrations at three remote sites in Northern California and found they were a factor of 2–4 lower than predicted by *Flanner et al*. [2007] and *Qian et al*. [2009]. The sparseness of these data and the mismatch between the years modeled versus the time of the measurements make it difficult to draw conclusions.

[532] A snow survey described by *Huang et al*. [2011] provides the possibility of a more robust comparison of mid-latitude snow concentrations. Huang and colleagues sampled snow across north China, reporting concentrations, for example, in northeast China of 600 $\pm$ 300 ng g^{-1} at latitudes of 41 to 46°N that decreased to about 40 ng g^{-1} at more northerly latitudes (51°N). These values are based on visual estimates of filter samples; estimates for samples from central and western China were not provided.

[533] No other geographically broad data set exists of mid-latitude snow BC concentrations, so it is not possible at this time to bound how well models represent mid-latitude snow BC albedo reductions.

8.4.4. BC in Mountain Glaciers

[534] BC in mountain snow and glaciers is of concern primarily because of the potential for affecting melt rates and, therefore, the seasonality of trends in water supplies. The effect of BC in glacial snow differs from BC's effect on seasonal snow because in the former melting does not lead to exposure of the underlying Earth surface, except perhaps at the very margins of the glacier which are anyhow often loaded with light-absorbing soil dust. Thus, the powerful albedo feedback present for seasonal snow (SAF in Figure 29) is absent. On longer timescales, if BC leads to glacial retreat, a positive albedo feedback would likely accelerate warming and melt near the glacial terminus.

[535] Few measurements exist of BC in mountain glaciers, and in most cases, they do not permit separation of the role of local versus remote sources nor are they accompanied by coincident measurements of other light-absorbing impurities. Using a global model to determine snowfall and aerosol deposition to glaciers is particularly difficult because of their small size relative to a model grid box (Table 19), allowing for only one BC concentration per grid box, regardless of,

for example, the dramatic altitude variations in mountainous regions. As discussed above, forcing by BC in snow also depends on accurate representation of snow and glacier cover. The coarse resolution of most models makes this representation quite difficult in mountainous areas and in areas with sparse snow cover, such as the Tibetan Plateau [e.g., *Qian et al*., 2011, Figure 2].

[536] Ice cores from the European Alps provide historical time series but do not reach present day and are reflective of glacial ice concentrations, not snow concentrations. Nonetheless, they provide information on the trends in BC deposition to the European Alps and some indication of near-present-day levels. *Jenk et al*. [2006] found a 1900–1940 average BC concentration of 31 ng g^{-1} (range: 9 to 22 ng g^{-1}), *Thevenon et al*. [2009] found a 1950–1980 average of about 20 ng g^{-1}, and *Legrand et al*. [2007] reported concentrations for 1960–1990 of about 10 to 17 ng g^{-1}, with the peak concentrations around 1960 and a decline thereafter. These studies also indicate a shift in the dominant source of BC from biomass burning in the nineteenth century to coal and later to non-coal fossil fuel. Modeled snow concentrations for present day from *Flanner et al*. [2009] grid boxes corresponding to the measurement sites in these studies range from approximately 115 to 160 ng g^{-1} in January through March and then decline to about 10 to 50 ng g^{-1} in April. Summertime (May–August) concentrations are zero, because all surface snow is assumed to have melted and BC in the glacier itself is not accounted for. In contrast, BC in the deposited snow in the *Koch et al*. [2009a] model increases from about 20 to 25 ng g^{-1} in January to about 50 ng g^{-1} by early summer, much more in line with the measured concentrations in mid-twentieth century glacial ice.

[537] Analysis by *Xu et al*. [2006], *Xu et al*. [2009a, 2009b], and *Ming et al*. [2009] of surface snow samples taken June–October in the Himalaya and in the Tibetan Plateau region yield typical concentrations of BC in surface snow of about 10 to 40 ng g^{-1}. Excluding samples collected from a site where the surrounding rock is rich in coal, the highest average surface snow concentration was 107 ng g^{-1}, and the lowest less than 1 ng g^{-1}. However, samples from deeper in the glacial snow [*Xu et al*., 2006; *Ming et al*., 2009] and glacier cores [*Xu et al*., 2009a, 2009b] show that BC concentrations are a factor of about 3 to 6 higher outside the summer monsoon (October–May) than during the monsoon (June–September). BC concentrations are highest when snow cover is also highest (October–May), but the concentration maximum also corresponds to a maximum in dust deposition in this region [*Ming et al*., 2009], so the impact of the BC on snow albedo is moderated. The only measurements from the south side of the Himalaya were from the East Rongbuk glacier on Mt. Everest, with concentrations of about 10 to 20 ng g^{-1} [*Xu et al*., 2009b; *Ming et al*., 2009].

[538] Snow samples in these studies were from summer and early fall, but in the model study of *Flanner et al*. [2009], almost all grid boxes corresponding to the sample sites are snow free from May to September. However, a qualitative comparison is possible of monthly averaged model snow BC concentrations from October–April for the grid boxes corresponding to the sample sites. Concentrations in the *Flanner et al*. [2009] model study decrease with latitude across the plateau, with the lowest concentrations corresponding to the measurements sites in northwest China. In contrast, this was where some of the higher concentrations were found in the measurements. Concentrations also are a strong function of season, increasing from about 20 to 30 ng g^{-1} in September (where there is snow) to a high of 70 to 500 ng g^{-1} (median 250 ng g^{-1}) in February. Concentrations remain high in March but drop by about a third in April and by May are back to about 10 to 40 ng g^{-1}. Thus, both the measurements and the models show maximum concentrations in the spring, but the concentrations in the model are notably higher than in the measurements. The *Koch et al*. [2009a] modeled median concentrations are lower (January–May monthly median across sample sites of 30 to 45 ng g^{-1}), they do not exhibit a systematic latitudinal dependence, and they show only a moderate seasonal dependence, peaking in March–April. Thus, they are in better general agreement with the median measured concentrations but perhaps miss strong peaks in springtime BC concentrations seen in some of the measurements. *Kopacz et al*. [2011] compare their modeled snow BC concentrations with this same measurement data set and find both overestimates and underestimates at individual sites but no overall systematic bias in the modeled values.

8.4.5. Trends in Arctic Snow BC

[539] While most model studies (e.g., as given in Table 19) have focused primarily on the role of BC in recent warming trends, anthropogenic emissions of BC in some regions were much higher in the past and are declining, while in others, they are rapidly increasing above historical levels. A small number of ice core records of BC are available to test models' historical representation of BC trends, and atmospheric BC trends for the Arctic can be used as an indicator of likely trends of BC deposition to snow in this region, though atmospheric and snow concentrations are not directly related.

[540] Near-surface atmospheric measurements since 1989 at Alert, Ellesmere Island (82°30′N 62°19′W) [*Sharma et al*., 2006; *Gong et al*., 2010] and since 1998 at Ny Ålesund, Svalbard, Norway (78°55′N 11°56′E) [*Hicks and Isaksson*, 2006; *Eleftheriadis et al*., 2009; *Forsström et al*., 2009] show that Arctic atmospheric BC concentrations have been declining in recent decades. Measurements starting in 1989 at Barrow, Alaska (71°19′N 156°37′W) [*Sharma et al*., 2006] show moderate declines in atmospheric BC up to 2003 and then a possible slight increase from 2003 to 2006. *Hirdman et al*. [2010a] argue that only a fraction of these trends is driven by changes in transport and that most of the observed trends are attributable to emissions changes in source regions, especially northern Eurasia.

[541] Ice cores from the Greenland plateau provide insight to longer-term Arctic trends. The Greenland cores reflect free-troposphere concentrations of BC and are most strongly influenced by fires and anthropogenic activity in North America [*McConnell et al*., 2007]. These records indicate that Greenland snow, preceding any human activity, had BC concentrations of about 1.1 to 2.5 ng g^{-1} (i.e., 4–6000 ybp) [*Chylek et al*., 1987] or about half the concentrations for the past few decades (1 to 4 ng g^{-1}) [*Cachier and Pertuisot*, 1994; *Chylek et al*., 1995] (Table 21). Ice core analyses by *McConnell et al*. [2007] and *McConnell and*

Edwards [2008] that span the industrial era show that from 1788 to about 1850, Greenland had relatively low concentrations (about 2 ng g^{-1}) of BC associated with biomass or biofuel burning and then a rise occurred to an average of about 10 ng g^{-1} (D4 core) or about 20 ng g^{-1} (ACT2 core), peaking around 1910. After this, BC concentrations declined steadily through the 1940s, finally dropping sharply in 1952 to nearly pre-1850 values. This post-1850 peak in BC was associated with coal burning, with the decline in BC in the mid-1900s associated with air pollution controls, improved combustion, and a fuel shift from coal to oil and gas. An ice core on Mt. Logan in the St. Elias range, Yukon, Canada [*Holdsworth et al*., 1996], shows a similar BC increase starting in the mid-1800s, though these data only extend to about 1950 so it is not possible to determine if there was a subsequent decline. An ice core from the St. Elias range is being analyzed and may help elucidate century-timescale trends on that side of the Arctic (J. McConnell, personal communication).

[542] Notably, the early twentieth century peak in BC in the Greenland ice core (about 1890–1950) leads by about 20 years a period of strong positive regional surface-air temperature anomalies from 1920 to 1965 [e.g., *Polyakov et al*., 2002, Figure 2; *Shindell and Faluvegi*, 2009, Figure 3]. It is expected that the full climate response to a forcing lags the imposed forcing, because of the ocean's heat capacity, for example, so this does not necessarily negate the possibility that the high BC concentrations led to the observed warming. This warming has generally been attributed to solar and natural variability. However, *Shindell and Faluvegi* [2009] point out that in their model, only about half of the early twentieth century Arctic (60° to 90°N) temperature rise can be attributed to the combined effects of GHGs, natural forcings, and tropospheric O_3. Natural variability is unable to account for the remainder in most models, implying that a portion of the warming should be interpreted as due to aerosol climate forcing. In a model study of historic aerosol impacts on climate, *Koch et al*. [2011b] calculate a maximum in BC deposition to Arctic snow around 1950 and a peak BC radiative forcing between 1940 and 1970, with declines since then. The peak in radiative forcing correlates well with the Greenland trends of *McConnell et al*. [2007]. *Skeie et al*. [2011] modeled trends in snow BC radiative forcing by fossil fuel and biofuel sources, reporting forcing relative to year 1750 in the year 1850 and then once per decade from 1900 to 2000. Forcing relative to 1750 is about 0.005 Wm^{-2} in 1850, more than doubles between 1850 and 1900 to about 0.013 Wm^{-2} and increases steadily from 1900 to 1960 to about 0.019 W m^{-2}. After this, forcing varies by about 0.03 W m^{-2} with no apparent trend from 1960 to 2000 [*Skeie et al*., 2011, Figure 16b]. Thus, this study does not show a forcing peak in the mid-1900s, but it does indicate that snow BC forcing has not appreciably increased since 1960.

[543] In summary, both observations and model studies indicate that BC may in fact have played a significant role in the observed early twentieth century Arctic warming. Further, radiative forcing by BC in Arctic snow likely has not increased since the mid-1900s and may instead be declining.

8.4.6. Trends in Mountain Snow

[544] Several ice core studies from the European Alps provide insight into trends and sources of BC in snow through the industrial era. These data show two features: first, a sharp increase in BC starting in the late nineteenth century and, second, a transition to fossil fuel as a significant source of BC. At the three locations studied, concentrations increased from the turn of the century to 1940–1950, with peak concentrations of about 15 to 25 ng g^{-1} [*Jenk et al*., 2006; *Legrand et al*., 2007; *Thevenon et al*., 2009]. Only two of the three records extend past 1940 with one showing a slight increasing trend and the other showing a declining trend. These differences may be due to differences in exposure to local pollution sources.

[545] Trends in BC deposition to the Himalaya or Tibetan regions have been measured using ice cores from Mt. Everest [*Ming et al*., 2008; *Xu et al*., 2009b] and at four other sites on the Tibetan Plateau [*Xu et al*., 2009b] using the thermal-optical method, with records extending about 1952–2004. These records show a great deal of spatial and temporal variability in concentrations, reflecting the variations in source regions and meteorology. Values typically average about 10–40 ng g^{-1}. However, some commonalities are apparent: all but the easternmost site show elevated concentrations from about 1950 (the earliest part of the record) to the early to mid-1970s, which *Xu et al*. attribute to eastern European sources. Concentrations then remain somewhat lower up until about 1990–1995, after which concentrations at most sites indicate increasing but variable concentrations. Thus, unlike the Arctic, it appears that BC radiative forcing may be increasing in the Himalaya.

8.5. Sources of BC to Arctic and Himalayan Snow

[546] Currently, there are few sources of pollution within the Arctic itself so almost all BC is transported there from the mid-latitudes. In the winter and spring seasons, when BC deposition to snow is most climatically important, a "dome" of cold air over the Arctic makes it difficult for air from lower latitudes to enter the Arctic troposphere. Typically, the front formed by this dome reaches to lower latitudes on the Eurasian side of the Arctic than on the North American side, making it easier for Eurasian sources to influence the Arctic troposphere [*Stohl*, 2006]. In order for air masses to cross the Arctic front, they must originate in cold, dry locations, and typically follow surfaces of constant potential temperature into the Arctic [*Iversen*, 1984; *Law and Stohl*, 2007]. Thus, air masses originating along the relatively warmer, moister North American, and Asian east coasts cannot readily enter the Arctic troposphere. While they can be lifted (e.g., in warm conveyor belts) to high altitudes where they can be transported over the Arctic, this pollution is unlikely to be deposited to the snow surface via wet or dry deposition, except on the high Greenland plateau.

[547] A model study by *Koch and Hansen* [2005] evaluating regional contributions to the Arctic haze found that Asian sources dominated total atmospheric column aerosol load, but near-surface concentrations were dominated by sources in Europe and Russia. *Stohl* [2006] also found lower tropospheric aerosol sources to be dominated by European and Russian emissions. This was reinforced by a multi-model study of pollutant transport to the Arctic from the source regions of North America, Europe, South Asia, and East Asia, which found that the greatest impact on surface-deposited BC in the Arctic comes from European emissions [*Shindell et al*., 2008], but this study did not include

northern Eurasia as a source region. *Hirdman et al*. [2010b] used a Langrangian particle dispersion model and reanalysis data and found northern Eurasia to be the dominant source region associated specifically with high atmospheric concentrations of BC at Barrow, Alert, and Svalbard. This finding is consistent with the *Koch and Hansen* [2005] and *Stohl* [2006] model studies and with other studies of the source of atmospheric BC at Barrow [*Polissar et al*., 2001] and Svalbard [*Eleftheriadis et al*., 2009].

[548] In the springtime, when deposition of BC to snow is climatically important, there is extensive agricultural burning in western Russia and widespread forest fires, particularly in the east. The former is clearly an anthropogenic source, and it may be that a significant fraction of the latter may be as well [*Mollicone et al*., 2006]. Given this result, the high latitude of this region (50 to 70°N), the tendency of the Arctic front to drop to lower latitudes in the Russian sector, and the model findings cited above, the impact of northern Eurasian biomass burning emissions to Arctic-wide BC (and OC) in snow, may be significant.

[549] Indeed, biomass burning appears to be the source of high-concentration plumes observed in the Arctic in recent years, with Russian biomass burning playing a particularly prominent role during the measurements of the International Polar Year (2007–2008) [*Stohl et al*., 2007; *Warneke et al*., 2009; *Paris et al*., 2009; *Jacob et al*., 2010]. Chemical analysis of snow samples from 36 sites across the Arctic (Alaska, Canada, Greenland, Russia, and the Arctic Ocean near the north pole) also indicates that the majority (in most cases, greater than 75%) of the BC in surface snow is associated with biomass or biofuel burning [*Hegg et al*., 2009; *Hegg et al*., 2010]. Those analyses are from a geographically broad but limited number of samples, all from 2007 to 2009, and they do not yet include samples from the Scandinavian sector of the Arctic, where both models and measurements [*Forsström et al*., 2009; *Doherty et al*., 2010] indicate that concentrations are relatively higher and more influenced by fossil fuel burning than in the rest of the Arctic. These factors may be biasing the conclusions of *Hegg et al*. [2009, 2010] toward the role of biomass or biofuel burning emissions in Arctic BC. The model experiments of *Flanner et al*. [2007] attribute 4.5 ng g^{-1} BC in Arctic snow to FF sources, 1.7 ng g^{-1} to BF sources, and 1.9 to 4.7 ng g^{-1} to BB sources, depending on the strength of the boreal fire year, also suggesting a potentially dominant contribution from biomass or biofuel sources. However, *Skeie et al*. [2011] attribute only about 10% of snow BC to biomass burning sources, and *Flanner et al*. [2009] attribute only 25% of present-day snow BC forcing to biomass burning in a "typical" biomass-burning year. Despite the uncertainty, it is important in the context of mitigation decisions to recognize that biomass and biofuel burning emissions may be a significant source of BC to Arctic snow.

[550] Consistent with Greenland's physical location, the *Shindell et al*. [2008] multi-model study determined that surface-deposited BC in Greenland comes predominantly from North America and Europe in the fall and winter. In the spring, synoptic systems in Asia loft pollutants to higher altitudes, where they can be transported long distances. Accordingly, they calculated that for the Greenland Ice Sheet—most of which is at high altitudes—BC deposition is most strongly influenced in the spring by East Asian emissions. *Hirdman et al*. [2010b] similarly found that the surface air at Summit, Greenland, was strongly influenced by East Asian emissions in the summer, whereas other Arctic sites were not. They emphasize that the high altitude of the Greenland plateau makes it unique in the Arctic in being exposed to free troposphere air. Consistent with these findings, chemical analysis of surface snow samples from the Greenland plateau indicate that the BC is largely from biomass or biofuel burning sources in the spring and that fossil fuel sources dominate in the summer [*Hegg et al*., 2009, 2010]. In any case, as noted above, the Greenland Ice Sheet has very low concentrations of BC in its surface snow (i.e., typically less than 3 ng g^{-1}) and so the radiative forcing by BC in Greenland snow is likely small, except during the melting season when BC becomes concentrated at the surface [*Doherty et al*., 2010, Figure 10a].

[551] At lower latitudes, sources of BC in snow can be either local or the end-point of long-range transport and can be highly variable not only with season but even within a day, due to the influence of, for example, thermal winds in lifting pollution from populated areas up onto the high mountain glaciers [*Marinoni et al*., 2010]. Local sources of BC, terrain, and meteorology are sufficiently varied that it is difficult to make generalized statements about the sources of BC to Himalayan snow using a global model. Acknowledging this, *Kopacz et al*. [2011] used a chemical transport model to determine the seasonally resolved source of BC in year 2001 to the atmospheric column above one site on Mt. Everest and four sites across the Tibetan Plateau. They found that BC in the atmosphere above the Everest site was predominantly from India, China, and Nepal; at the eastern Tibetan Plateau sites, it was primarily from western China, secondarily from India, and also influenced by emissions in Nepal, the Middle East, and Pakistan; and at the western Tibetan Plateau site, it was primarily from western China and secondarily from Pakistan and the Middle East. At all sites, source regions varied with season, with atmospheric BC concentrations at a minima in the summer, consistent with measurements [*Xu et al*., 2006; *Xu et al*., 2009a,2009b; *Ming et al*., 2009]. *Lu et al*. [2012] used a combination of emissions data and modeling to study the source regions and types for BC transported to the boundary layer over the Himalaya and Tibetan Plateau region as a whole for the period 1996 to 2010. They found that India, other South Asian countries, and China were the dominant source regions, but there were also significant contributions from biomass burning in Russia and from the Middle East. The majority of the BC came from residential fuel combustion, with industry and land transport playing secondary roles, agricultural burning a small but significant role, and, in some years, open forest burning made a notable contribution. Over the period studied, total contributions of BC to the region increased by over 40%, which they link to emissions increases in China and India.

[552] These studies focus on the source of BC to the atmosphere, either the entire column [*Kopacz et al*., 2011] or the boundary layer [*Lu et al*., 2012]. Forcing due to reduced snow albedo is driven by BC deposited to snow, which is determined not only by atmospheric BC distributions but by their incorporation into precipitation and inclusion in the surface snowpack. It remains to be seen if the sources

of BC in snow on the Himalaya and Tibetan Plateau are the same as for the atmosphere above it. Further, because of the extreme terrain variations in this region, accurate representation of BC distributions, sources, and deposition to snow will likely require the use of a high-resolution regional model.

8.6. Estimate of Forcing by BC in the Cryosphere

8.6.1. Adjusted Forcing by BC in Snow

[553] Forcing by BC in snow results from the radiative forcing due to the initial albedo reduction when BC is deposited in snow and the rapid adjustment to that forcing through the positive feedbacks *MBC*, *SBC* and *GRB* (Figure 29), resulting in the adjusted forcing. Comparable values of global, annual average forcing by BC in snow are calculated by scaling forcing as derived in model studies to the common base of present-day forcing due to all sources (FF + BF + BB). The *Flanner et al*. [2009] and *Koch et al*. [2009a] modeled adjusted forcings are then scaled based on the biases found in the measurement-model comparison of snow BC concentrations. From these, a representative central estimate is determined. In addition, all studies are normalized to forcing per emission (μW m^{-2} per GgC yr^{-1}) to isolate differences in total emissions from differences in all other model processes that lead to cryosphere BC climate forcing (Table 20). For studies that do not report present-day forcing by BC emissions from FF + BF only, the adjusted forcing is calculated by scaling total to FF + BF emissions, in order to provide comparable forcings for what roughly might be considered the minimum "anthropogenic" BC. Industrial-era (1750 to 2010) forcing is estimated by scaling total present-day forcing based on the ratio of present-day to preindustrial BC emissions. In scaling by emissions, we use two model studies to account for differences in the amount of biomass burning versus fossil and biofuel burning emissions that are deposited to snow. Finally, the model sensitivity studies of *Flanner et al*. [2007] and runs from *Flanner et al*. [2009] are used to establish low and high uncertainty forcing bounds based on uncertainties in emissions, rate of snow aging (grain size), the efficiency with which BC is scavenged from surface snow during snow melt, snow cover fraction, the light absorption efficiency of BC, and the reduction in snow BC radiative forcing due to the presence of dust in the snow.

[554] This analysis does not encompass all sources of uncertainty in snow BC adjusted forcing, only those where information is available to set bounds. There are two weaknesses in this approach. First, forcing does not scale linearly with snow BC concentration. This affects both our uncertainty analysis and the scaling of all-source to industrial-era forcing, which is based on scaling by emissions. As with other agents, the forcing increase per unit mass of additional BC decreases with increasing BC amount, as indicated in *Flanner et al*. [2007, Figure 3a]. Second, snow BC concentrations do not scale linearly with global, annual average changes in BC emissions, since the amount of BC deposited in snow from any given source depends on its location and season—i.e., a large increase in sub-Saharan Africa biomass burning has very little effect on BC concentrations in Arctic snow. We attempt to account for this using information from models on the relative role of biomass burning in snow forcing versus its fraction of global, annual emissions. However, there are likely significant but unquantified uncertainties associated with this adjustment, especially for preindustrial snow BC forcing.

[555] The relative roles of biomass burning, fossil fuel, and biofuel burning in BC cryosphere forcing is a function of their relative emissions, of seasonal timing of emissions, and of the fraction of each that are deposited to surface snow and ice. The present-day fraction of emissions due to BB reported in the studies in Table 20 range from a low of 30% in a low BB year (2001) [*Flanner et al*. [2007]) to a high of 47% in a high BB year (1998) [*Flanner et al*., 2007], with the rest falling in the range 35 to 45% (all other studies in Table 19). *Flanner et al*. [2009] attributed 25% of present-day BC-in-snow forcing to biomass burning emissions. However, *Skeie et al*. [2011] attribute only 10% of the present-day BC in snow north of 65°N to BB. In both studies, biomass burning is about 35% of global, annual average present-day BC emissions, so this discrepancy must be due to differences in modeled source locations, aerosol transport, BC mixing ratios in falling snow, and dry deposition rates from BB versus BF + FF sources, and to feedbacks included in the two models (Table 20). Seasonality and nonlinearities in forcing per change in snow BC concentration may also be contributing, since *Flanner et al*. [2009] report the fraction of forcing whereas *Skeie et al*. [2011] report the fraction of BC in snow due to BB. The source attribution analyses of *Hegg et al*. [2009, 2010] indicate that both of these studies may be underestimating the fraction of cryosphere forcing by BC from biomass burning. Further, the 35% of total emissions attributed to BB by *Flanner et al*. [2009] and *Skeie et al*. [2011] is at the low end of the range (35–45%) by all studies in Table 19. Therefore, the higher value of 25% is selected as the best estimate of the fraction of present-day BC cryosphere forcing due to biomass burning. *Skeie et al*. [2011] also reported that in the year 1750, 20% of snow BC north of 65°N was from biomass burning sources. For consistency with the assumption that present-day cryosphere forcing due to BB is higher than reported by *Skeie et al*., we estimate that approximately 30% of preindustrial (i.e., before 1750) forcing by BC in snow was due to BB.

[556] As noted earlier, *Hansen and Nazarenko* [2004] conducted a sensitivity study based on uniformly imposed albedo changes. *Wang et al*. [2011] followed this approach, applying similar fixed, snow albedo changes within a few broadly defined regions. Thus, there is no basis for applying adjustments for emission sources or amounts to these two studies' reported forcings. The focus of these studies was understanding the climate response to the imposed albedo change, rather than on accurately modeling the forcing. Therefore, these two studies are not included here in determining the estimate or bounds on BC cryosphere forcing.

[557] *Jacobson* [2004a] did not report a forcing value in his study, only the climate response. The adjusted forcing value of 0.06 W m^{-2} for FF + BF emissions shown in Table 19 is an estimate based on this study provided by M. Z. Jacobson. Biomass burning was included in the baseline, with fossil fuel and biofuel burning emissions as the forcing agents. All-source adjusted forcing is estimated as 0.08 W m^{-2} using the assumption that 25% of present-day BC cryosphere forcing is due to BB emissions. This all-source forcing is used to calculate forcing per emission, based on the emissions reported by *Jacobson* [2004a].

[558] *Hansen et al*. [2005] (whose radiative forcing distribution was used directly by *Shindell and Faluvegi* [2009]) followed the approach of *Hansen and Nazarenko* [2004] of imposing a snow albedo change, rather than prognostically calculating snow BC concentrations. However, in this updated study they scaled the imposed albedo based on the deposition rates from the study of *Koch* [2001]. *Hansen et al*. [2005] note they use the emissions of *Koch* [2001] in this context, but emission amounts were also not reported by *Koch* [2001]. The FF emissions provided by D. Koch (private communication) for this study were based on global, annual averages from *Penner et al*. [2001] for year 2000, with 1880 emissions approximated as 10% of the year 2000 emissions, and both biomass and biofuel burning emissions were taken from *Liousse et al*. [1996] (D. Koch, personal communication), resulting in the BC emissions shown in Table 19. To get atmospheric abundances, *Hansen et al*. [2005] scaled these BC emissions by a factor of 1.9, so that their global, annual average direct (atmospheric) radiative forcing by BC matched the 1 W m^{-2} given by *Sato et al*. [2003] based on AERONET observations. The model-measurement discrepancy could result from a bias in emissions, deposition rates or BC mass absorption efficiency, so it is not clear how the model might be biased in terms of light absorption by deposited aerosol. It is specified that the "...resulting albedo effect in the region of Arctic sea ice in our present model is only several tenths of 1%, as opposed to the 1.5% spectrally integrated (2.5% visible wavelengths) albedo change assumed by [*Hansen and Nazarenko*, 2004]." [*Hansen et al*., 2005; also, see their Figure 16]. The *Hansen and Nazarenko* [2004] and *Hansen et al*. [2005] studies did not include the feedbacks *MBC*, *SBC*, or *GRA* (Table 20), so their forcing is a direct radiative forcing due to the initial albedo change alone. This albedo change results in a preindustrial-to-present (1880 to 2000) radiative forcing by BC in snow of 0.08 W m^{-2}, which was later revised down to 0.05 W m^{-2} after correcting for a programming error that caused the modeled albedo change in *Hansen et al*. [2005] to be too high in partially snow-covered land grid boxes and too low for snow on sea ice [*Hansen et al*., 2007]. In Table 19, the present-day adjusted forcings for FF + BF + BB and for FF + BF only are calculated based on the corrected 0.05 W m^{-2} forcing value. Scaling is done by accounting for the change in emissions 1850 to 2000 and by assuming that the fraction of snow BC forcing due to BB is 30% in 1880 and 25% in 2000. Forcing per emission is calculated from this all-source forcing.

[559] The studies of *Flanner et al*. [2007, 2009] calculated present-day adjusted forcing for all emission sources (FF + BF + BB) as well as calculating forcing for (FF + BF) emissions only, as given in Table 19. *Koch et al*. [2009a] report both preindustrial-to-present (1890 to 1995) and present-day (1995) adjusted forcings for all sources (FF + BF + BB). Present-day forcing from FF + BF only is calculated by assuming that 75% of present-day forcing is due to these sources.

[560] *Rypdal et al*. [2009b] do not include biomass burning emissions in either their baseline or forcing scenarios, including BC emissions only from fossil fuel and closed-container biofuel burning. The amount of open- versus closed-container biofuel BC emissions is not sufficiently constrained to apply an adjustment to account for this missing source of BC. Total present-day forcing including biomass burning is calculated by scaling the reported FF + BF forcing, assuming the latter accounts for 75% of total present-day forcing. Forcing per emission is calculated using the sum of the *Rypdal et al*. [2009b] reported FF + BF emissions and the *Flanner et al*. [2009] "typical year" BB emissions of 2700 GgC yr^{-1}.

[561] *Skeie et al*. [2011], using the same model as *Rypdal et al*. [2009b], reported an industrial-era (1750 to 2000) forcing by FF and BF of only 0.016 W m^{-2}. This gives a forcing per emission for FF + BF of 3.9 μW m^{-2} (GgC $yr^{-1})^{-1}$, which in turn yields FF + BF forcing of 0.018 W m^{-2} for present-day (year 2000) emissions. Assuming 25% of present-day BC cryosphere forcing is due to biomass burning emissions, present-day all-source forcing is 0.024 W m^{-2}. This implies an industrial-era forcing by FF + BF + BB of 0.021 W m^{-2}.

[562] With all studies adjusted to the common metrics of all-source forcing and forcing per emissions, a greater degree of convergence is reached. Total present-day adjusted forcings from the five most recent studies that prognostically calculated forcing span a range of a factor of 2 (0.024 to 0.050 W m^{-2}). The *Hansen et al*. [2005] and *Jacobson* [2004a] forcings are notably higher at 0.07 and 0.08 W m^{-2}, respectively. However, when normalized to forcing per emission, all but the *Jacobson* [2004a] study fall in the range of 3 to 7 (μW m^{-2})(GgC $yr^{-1})^{-1}$. If the high biomass-burning year (1998) of *Flanner et al*. [2009] is excluded, this range narrows to 3 to 6 (μW m^{-2})(GgC $yr^{-1})^{-1}$.

[563] The *Jacobson* [2004a] study stands out in two regards: it includes forcing by BC in bare (non–snow-covered) sea ice as well as by BC in snow, and it includes UV and blue absorption of certain types of OC in the derived forcing. *Rypdal et al*. [2009b] and *Skeie et al*. [2011] also include forcing by BC in sea ice, but otherwise, all other studies discussed only include light absorption by BC and only in snow (not sea ice). Other studies include BC in snow on sea ice, but not in the sea ice itself. *Flanner et al*. [2007] excluded light absorption by OC in snow because a sensitivity study indicated that snow forcing from OC was a factor of 200 smaller than BC but acknowledged that modern optical measurements of light-absorbing OC could alter this conclusion. The inclusion of BC in sea ice and OC absorption might explain why the forcing per emission of the *Jacobson* [2004a] study is higher than in the other studies. However, the forcing provided is estimated, not calculated, so it is not possible to know the fraction of forcing due to BC in sea ice versus snow or due to OC versus BC, and it is difficult to know quantitatively how much these factors account for the comparatively high adjusted forcing and forcing per emission of the *Jacobson* [2004a] study. The *Rypdal et al*. [2009b] forcing per emission is more in line with that from the other studies, though again it is not known what fraction of this forcing is due to BC in snow versus bare sea ice. On the other hand, forcing per emission in the *Skeie et al*. [2011] study, which also included BC in sea ice, are lower than in the other studies.

[564] The comparison of measured versus modeled snow BC concentrations (section 8.4) allow us to make a first-order adjustment for biases in the *Flanner et al*. [2009], *Koch et al*. [2009a], and *Skeie et al*. [2011] studies for all-source adjusted forcing. The results of this

comparison (Table 21) indicate that the *Flanner et al*. [2009] model tends to overestimate snow BC concentrations, particularly in locations with relatively higher concentrations (e.g., Scandinavia). There are also indications that this model may exaggerate the enhancement of surface snow BC concentrations with melt and therefore feedback process *MBC* (Figure 29). The *Koch et al*. [2009a] model, on the other hand, tends to underestimate snow BC concentrations (Table 21), and it does not include the *MBC* feedback at all. Some data indicate that this feedback is significant (Dye-3 Greenland samples of *Clarke and Noone* [1985] and work in Norway, Greenland, and Alaska [*Doherty et al*., 2010; *Doherty et al*., 2013]), if perhaps not as large as is given by *Flanner et al*. [2009]. The *Skeie et al*. [2011] comparison indicates that the model tends to underestimate surface snow BC concentrations in many locations by a factor of approximately 2–5 for cold snow. Once the snow starts to melt, the modeled *MBC* feedback leads to large increases in surface snow BC amounts because none of the BC is washed away with the meltwater. Based on these data, the all-source adjusted radiative forcing for FF + BF + BB from *Flanner et al*. [2009] is scaled down from 0.047 W m^{-2} to 0.04 W m^{-2}, and the forcing from *Koch et al*. [2009a] is scaled up from 0.03 W m^{-2} to 0.04 W m^{-2}. The *Flanner et al*. [2009] study accounted for dust impurities in the snowpack (which lessens the impact of adding BC) and so should be a more accurate representation of snow BC forcing than is given by *Flanner et al*. [2007]. Applying a correction factor to the all-source forcing derived from the reported *Skeie et al*. [2011] industrial-era FF + BF forcing based on the comparison to observations is somewhat more difficult. The low bias in modeled concentrations, especially in areas where forcing is expected to be greatest, is both large and variable. While forcing is likely biased low by at least a factor of 2 for cold snow (i.e., winter to early spring), once the surface snow starts to melt, it is assumed that all meltwater BC remains at the snow surface, maximizing the *MBC* feedback (Figure 29). Thus, adjusted forcing is likely underestimated initially but overestimated once the model snowpack warms to the point of melting. It is unclear what the net effect on adjusted forcing would be of increased cold snow BC concentrations coupled with a more realistic, reduced *MBC* feedback. However, an approximate doubling of the all-source radiative forcing from the *Skeie et al*. [2011] study from 0.024 W m^{-2} is reasonable given the reported large underestimates in snow BC concentrations across much of the Arctic. A comparison of snow BC concentrations is not made for the *Rypdal et al*. [2009b] study, but notably the emissions and forcing are intermediate to the *Flanner et al*. [2009] and *Koch et al*. [2009a] values. With this suite of information, the best estimate of all-source adjusted forcing by BC in snow is estimated to be 0.04 W m^{-2}. This yields a forcing per emission of 5 (μW m^{-2})(GgC yr^{-1})$^{-1}$ for the spatial and temporal emission patterns applied in the models.

[565] Industrial-era adjusted forcing is estimated from the total present-day forcing through scaling by the ratio of industrial era to all-source BC emissions, accounting for changes in the relative fractions of FF + BF versus BB from the industrial era to present day and accounting for differences in the fractions of FF + BF versus BB emissions that are deposited to snow. Caveats in this scaling are that significant uncertainties are associated with the preindustrial BC emissions, especially from biomass burning; that forcing does not necessarily scale linearly with emissions; and that for forcing by BC in the cryosphere the forcing-per-emission is very sensitive to the season and location of the emissions. Biomass-burning emissions in 1750 were approximately 39% of present-day biomass-burning emissions, and industrial-era FF + BF emissions were approximately 4% of present-day emissions (see "scaled" values in Table 16). In present day, about 25% of the BC-in-snow forcing is due to biomass-burning emissions and 75% to fossil fuel and biofuel-burning emissions, and in 1750, the split was about 30%/70% (section 8.6.1, para. [555]). Thus, biomass forcing in 1750 was about 0.005 W m^{-2} (0.04 W $m^{-2} \times 0.25 \times 0.39 \times (30/25)$) and FF + BF forcing was 0.001 W m^{-2} (0.04 W $m^{-2} \times 0.75 \times 0.04 \times (70/75)$), for a total forcing in 1750 of 0.006 W m^{-2}. This yields an industrial-era forcing from all sources of 0.034 W m^{-2}. This forcing is the difference between present-day forcing and forcing in 1750. As noted earlier, snow (and likely sea ice) forcing in the later 1800s and early 1900s may have been greater than in 1750 or present day.

[566] As noted earlier, it is not possible at this time to account for all known sources of uncertainty in model calculations of the radiative forcing and feedbacks that amplify that forcing as rapid adjustments. However, it is certain that snow BC radiative forcing is greater than zero (section 8.1 and Figure 28). Further, it is amplified by the rapid adjustments *GRA*, *SBC* and *MBC* (section 8.1 and Figure 29). Thus, the bounds on snow BC forcing are asymmetric about the best estimate.

[567] *Flanner et al*. [2007] calculated ranges of global-mean adjusted forcings resulting from plausible uncertainty bounds of different factors. Ranges of BC emissions produced a forcing range of −46% to +100% of their central estimate; ranges of snow aging (effective grain size): −42% to +58%; ranges of the fraction of BC scavenged from the snowpack with melt: −31% to +8%; ranges of snow cover fraction: −17% to +8%; and ranges of BC mass absorption efficiency −12% to +12%. From these results, uncertainty in three of the factors that directly affect snow BC radiative forcing (emissions or, equivalently, snow BC concentrations; BC absorption efficiency; and snow cover) can be determined, as well as for two of the feedback processes that amplify snow BC radiative forcing (*MBC* and *GRA*; Figure 29). Some bounds can also be placed on the uncertainty in BC radiative forcing due to the presence of soil dust using the *Flanner et al*. [2009] study model, where including dust deposition decreased BC adjusted forcing by 20% relative to adding combustion aerosol to a pristine snowpack. Based on this result, the role of dust in reducing BC forcing is allowed to be as low as 10% or as high as 40%.

[568] The lower (upper) bounds on snow BC adjusted forcing are calculated by adding in quadrature the forcing from low (high) bounds in emissions, rate of snow aging, BC mass absorption efficiency, and snow cover fraction, and using the high (low) bounds in the efficiency of BC scavenging with melt and in the role of dust in reducing snowpack albedo. The resulting lower and upper bounds on the forcing are calculated by subtracting 79% and adding 117% of the central estimate, giving an all-source adjusted forcing uncertainty range of 0.01 to 0.09 W m^{-2} with a

central estimate of 0.04 W m^{-2} and an industrial-era forcing of 0.034 W m^{-2} with a range of 0.007 to 0.074 W m^{-2}. These bounds do not account for uncertainty in how forcing is affected by patchy snow cover or by uncertainties in modeled cloud cover and vegetation cover. They also do not account for possible biases in modeled mid-latitude snow BC concentrations.

8.6.2. Radiative Forcing by BC in Sea Ice

[569] As noted above, both the *Jacobson* [2004a] and *Rypdal et al*. [2009b] studies include forcing by BC in bare sea ice in their calculated climate impact of BC in the cryosphere. However, since these studies do not separate forcing by BC in snow versus in sea ice they cannot be used to estimate forcing by BC in sea ice, and the other studies considered do not include forcing by BC in bare sea ice. Therefore, an independent first-order estimate of this forcing is provided here. This estimate only accounts for the direct radiative forcing by BC in sea ice and does not include feedbacks that may alter sea ice BC concentrations as the ice warms.

[570] After the snow melts in June on Arctic sea ice, the surface then consists of a mixture of puddles ("melt ponds") and drained hummocks. The hummocks have a surface granular layer that resembles coarse-grained snow, with effective grain radii about 2 mm. The BC content of the surface granular layer has been measured in several summer expeditions; it is similar to that of the springtime snow that recently covered it. The median is about 8 ng g^{-1} with estimated bounds of 3 and 15 ng g^{-1} from tables in *Doherty et al*. [2010]. The corresponding broadband albedo reductions under overcast sky (the normal situation in summer) are 0.010 and 0.028, respectively.

[571] The radiative forcing of BC in sea ice is bounded as follows. Only the months June, July, August, and September are considered because the ice is assumed to be completely snow covered in all other months. (New ice forming in winter is not immediately snow covered, but it is exposed to very little sunlight in the dark winter.)

[572] 1. The upper bound on sea ice area is taken as the average for 1978 to 1987 [*Gloersen et al*., 1992, Figure 3.1.45]; the lower bound as that of the extreme summer of 2007 [*Comiso et al*., 2008, Table 1]. These estimates of "ice area" are of ice only; they are smaller than the tabulated "ice extent" because the extent includes areas of open water within the ice pack.

[573] 2. Melt-pond fractions are given in *Fetterer and Untersteiner* [1998, Figure 3]; 100% uncertainty is assumed to get upper and lower bounds for each month.

[574] 3. The average snow depth for each month is given in *Warren et al*. [1999, Figure 13]; using these data, the snow-cover fractions are estimated and an approximately 50% uncertainty assumed to get upper and lower bounds.

[575] 4. The year-to-year variability in downward solar irradiance is mainly determined by varying extent and thickness of the widespread stratus clouds covering the Arctic Ocean in summer. The mean monthly values of surface solar irradiance are adopted, as given in *Fletcher* [1968, Figure 5] and tabulated in *Maykut and Untersteiner* [1971, Table 1]; 15% is added or subtracted to get upper and lower bounds.

[576] These values are shown in Table 22 and used to estimate the lower and upper bounds on all-source radiative forcing by BC in bare sea ice. The uncertainties are combined in quadrature. For example, for June, the relative standard deviations for ice area, non-ponded fraction, non–snow-covered fraction, downward solar flux, and albedo reduction are 0.095, 0.02, 0.33, 0.15, and 0.5, respectively, giving a combined relative standard deviation of 0.625. The bounding values for global annual radiative forcing at the surface are 0.008 and 0.017 W m^{-2}. The central estimate is 0.012 W m^{-2}. As for BC in snow, the industrial-era sea-ice forcing is estimated to be 85% of the all-source forcing (i.e., 0.010 W m^{-2} with bounds of 0.006 and 0.015 W m^{-2}).

8.6.3. Forcing by BC in Snow in the Himalaya and Tibetan Plateau

[577] The Himalaya and Tibetan Plateau comprise a large area of seasonal snow cover and a high concentration of glaciers. This region is also in close proximity to East and South Asia, where BC emissions are large (Figure 9) and increasing (section 4.8), consistent with observed increasing concentrations of BC in glacial snow at some sites [*Ming et al*., 2009, *Xu et al*., 2009a, *Lu et al*., 2012]. These aspects have led to the hypothesis that greater than average warming rates [*Xu et al*., 2009a] and observed acceleration of glacial melt rates [*Lau et al*., 2010] in this region may be in part caused by BC in snow.

[578] Indeed, *Flanner et al*. [2009], in their model study, found that the largest annual average forcing due to BC in snow is over the Tibetan Plateau, namely, 1.3 W m^{-2} averaged over the whole region. The forcing averaged only over snow-covered surfaces reached a maximum of about 10 to 20 W m^{-2} in spring. These forcings are adjusted forcings in that they include the feedbacks *MBC*, *SBC*, and *GRB* (Figure 29). This model study also included reduction in snow albedo due to dust, which moderates the forcing by BC. However, this model may be overestimating snow BC concentrations in this region, especially in spring (section

Table 22. Factors Affecting Albedo Reduction by BC in Bare Sea Ice[a]

Factors	June	July	August	September
Arctic ice area (10^{12} m^2)	9.6, 11.4	6.7, 10.0	4.4, 8.0	3.8, 7.5
Area not covered by melt ponds (fraction)	0.95, 1.00	0.7, 0.9	0.85, 0.95	1.0
Area not snow covered (fraction)	0.4, 0.8	0.8, 0.95	0.8, 1.0	0.1, 0.7
Downward solar flux at surface (W m^{-2})	260, 360	190, 250	120, 170	50, 70
Energy absorbed by BC in sea ice (10^{18} J $month^{-1}$)	94 ± 59	63 ± 36	32 ± 20	7 ± 6
Energy absorbed by BC in sea ice during one Arctic summer (10^{18} J)		196 ± 72		
Global annual radiative forcing (W m^{-2})		0.008 – 0.017		

[a]Lower and upper bounds are shown for each quantity.

8.4.4), as well as overestimating snow cover on the Tibetan Plateau [*Qian et al*., 2011], both of which would lead to a high bias in modeled radiative forcing. Modeled snow dust concentrations have not been evaluated.

[579] Using snow BC concentrations that show general agreement with measured values, *Kopacz et al*. [2011] calculate snow-cover averaged radiative forcing at the sites measured by *Xu et al*. [2006], *Xu et al*. [2009a, 2009b] and *Ming et al*. [2009] of 4 to 16 W m^{-2}, with minima in the winter (4 to 8 W m^{-2} across the different sites) and maxima in summer (8 to 16 W m^{-2}). Total surface forcing (i.e., accounting for snow covered area) is not calculated, and the reported forcings are instantaneous, not adjusted forcings. The forcing is also calculated as the difference between radiative fluxes for clean snow and for snow with BC only; reduction in albedo due to dust or soil in the snow is not accounted for.

[580] A robust estimate of forcing by BC in snow in the Tibetan Plateau region is thus hindered by limited measurements of snow BC concentrations, which show large spatial and seasonal variations, limited knowledge of snow dust concentrations in a region subject to dust storms that occur in the same season as maximum deposition of BC to snow, and the inherent difficulty of using a global model to accurately represent snow cover and atmospheric transport and deposition of BC and dust in a region that is mountainous and in close proximity to a range of intense BC and dust emission sources.

9. Climate Response to Black Carbon Forcings

9.1. Section Summary

[581] 1. The BC direct, in-snow and in-sea-ice radiative forcings cause the troposphere and the top of the cryosphere to warm, which induces further rapid adjustments and climate response in the form of cloud, circulation, surface temperature, snow cover, and precipitation changes. BC microphysical effects on clouds also induce adjustments and climate response, but models have not yet separated the full climate responses to these complicated and uncertain climate forcing mechanisms and their adjustments (section 7).

[582] 2. BC direct radiative forcing causes a surface warming that is concentrated in the Northern Hemisphere but may exhibit a different pattern to that of the forcing. In-cloud absorption by BC, semi-direct effects and the efficacy of high latitude BC-in-snow and BC-in-sea-ice forcings need to be properly accounted for in the overall climate forcing estimate of BC. This can be done through the concept of the effective forcing, which scales a radiative or adjusted forcing with its climate efficacy.

[583] 3. Climate models show that effective forcing and adjusted forcing are equal within their respective uncertainties for most effects other than snow and ice forcing. This justifies deriving the radiative effects associated with the semi-direct effect from the efficacy of the radiative forcing by atmospheric BC.

[584] 4. There is a threefold range across model studies in temperature response per radiative forcing but only a twofold range in temperature response per adjusted forcing. Therefore, differences in rapid adjustments included in different models account for a fraction of the range of reported temperature responses.

[585] 5. The all-source BC-in-snow adjusted forcing (0.01 to 0.09 W m^{-2} globally averaged) drives equilibrium climate warming of 0.05 to 0.20K in recent climate model studies. Climate response is greatest during local spring and over middle to high northern latitudes. The efficacy of this adjusted forcing is much greater than 1 primarily because all radiative energy is deposited directly within the cryosphere, causing earlier melt of snowpack and driving strong albedo feedback. The adjusted-forcing efficacy is estimated to be 3 with a range of 2 to 4.

[586] 6. Various studies suggest regional circulation and precipitation changes in response to the BC climate forcing. These changes include a northward shift in the Inter-Tropical Convergence Zone and changes in Asian monsoon systems where concentrations of absorbing aerosols are large.

[587] 7. The suggested impact of BC on glacier melting is potentially important, but no model studies sufficiently resolve the glacier energy budget, aerosol transport, and circulation changes in regions of complex topography to assess the importance of this process.

9.2. Introduction to Climate Forcing, Feedback, and Response

[588] A climate forcing is a mechanism that induces a change in the climate system. Most climate forcings are radiative forcings, whereby the induced climate change originates from a modification in the radiative budget of the Earth. More specifically, a radiative forcing is defined by the IPCC as the change in ToA net radiation caused by a climate agent, after stratospheric adjustment, but with everything else being held fixed [*Forster et al*., 2007]. There also exist some rapid adjustments (e.g., some aspects of land use, microphysical effects on precipitation, or the CO_2 physiological forcing). Such forcings do not have an initial radiative driver, but after a rapid adjustment leads to a radiative energy change in the climate system. We term radiative forcings and rapid adjustments as "adjusted forcings" (Table 2 and section 2.3).

[589] The climate system responds to a radiative imbalance through a complex set of mechanisms (called feedbacks), eventually returning to a near equilibrium state [*Boer and Yu*, 2003; *Soden and Held*, 2006]. Climate models show that the equilibrium global temperature change in response to a climate agent is generally linear in radiative forcing, and the proportionality coefficient between these two quantities, denoted λ, is called the climate sensitivity (unit K $(W\ m^{-2})^{-1}$). Climate models further show that although the climate sensitivity is model dependent, it is relatively independent of the climate agent under consideration (within $\pm$20 to 30%, except for snow albedo forcings discussed below). One can define the climate efficacy of a climate agent as the ratio of the climate sensitivity for this climate agent to that for the forcing by CO_2 [*Hansen et al*., 2005]. Efficacies can be defined for either radiative forcing or adjusted forcing (Table 2).

[590] Some studies have shown that climate responses can be categorized into fast feedbacks, also known as rapid adjustments, which respond to forcings on a short timescale (typically days), and slow feedbacks, which are associated

with the global surface temperature response and respond on longer timescales [*Gregory et al.*, 2004; *Andrews and Forster*, 2008]. Different climate agents can induce very different rapid adjustments, whereas slow feedbacks appear to be less dependent on the climate agent. BC affects climate in a number of ways, but those discussed in sections 6 to 8 may all be considered either radiative forcings or rapid adjustments. The direct effect is a radiative forcing. The microphysical effects on clouds are partly radiative forcings and partly rapid adjustments. The cloud semi-direct effect cannot easily be dissociated from the direct effect that causes it and should be seen as a rapid adjustment to the direct radiative forcing rather than a separate forcing, although it can be quantified as a change in radiative flux (i.e., a climate forcing). However, in this assessment, the semi-direct effect is included in a single liquid-cloud effect (which also includes BC microphysical effects on clouds) because modeling procedures make the two difficult to separate (section 7). This calculation also uses the climate efficacy of the direct-effect radiative forcing to determine the semi-direct effect, assuming the efficacy of the adjusted forcing would be one. The snow albedo effect is a combination of radiative forcing and adjustments, some rapid and some less rapid, which tend to amplify this initial forcing (Figure 29). The rapid adjustments can be combined with the radiative forcing to produce an adjusted forcing. This amplified forcing produces further changes in snow cover that drive a snow albedo feedback; this amplifies the temperature response, leading to a high efficacy even when an adjusted forcing is used in determining efficacy.

[591] The response of climate to a relatively uniform radiative forcing such as that of long-lived GHGs, although still uncertain, has been studied in many models, and aspects of its response pattern are consistent among climate models. The response to more heterogeneous radiative forcings is less well understood, and there has been little work in the literature to compare different climate models. Generally there is no direct relationship between the patterns of climate response and the patterns of radiative forcing, except on large scales [*Forster et al.*, 2000]. *Shindell et al.* [2010] performed a multi-model analysis to quantify these scales, using the results of four GCMs. They found that inhomogeneous aerosol forcing caused an impact locally in those GCMs, but the impacts were not confined to those areas and extended quite far in the zonal direction—at least 12000 km—while extending only about 3500 km (or 30° longitude) in the meridional (consistent with modeled transport and modeled removal timescales in the atmosphere). This relationship is illustrated in Figure 31, which shows the geographic distributions of BC emissions, burden, direct radiative forcing, and surface-temperature response for a particular model. The climate response to a regional

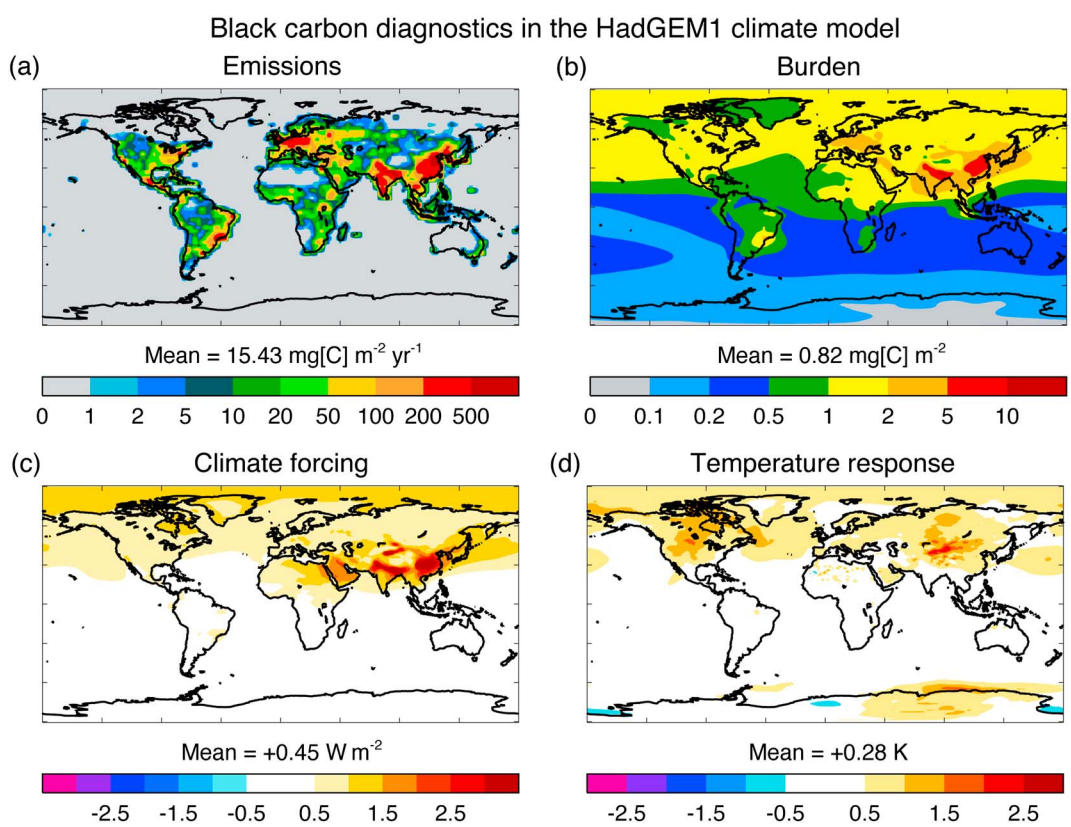

Figure 31. (a) Emissions of BC aerosols (mg BC m^{-2} yr^{-1}), (b) burden of BC aerosols (mg BC m^{-2}), (c) direct radiative forcing due to BC aerosols (W m^{-2}), and (d) equilibrium surface temperature change (K) in response to the BC direct radiative forcing. Adapted from data from the Hadley Centre climate model (HadGEM1) published in *Jones et al.* [2007]. The patterns of burden, radiative forcing, and surface temperature response are considered illustrative because the lifetime of BC is known to be too long in this model.

radiative forcing, such as that by BC, has a regional component and a global component. While the patterns of burden and direct radiative forcing are quite similar, there is no correspondence between the fine-scale patterns of radiative forcing and the surface temperature response. However, both the forcing and the surface temperature response are concentrated in the extratropics of the northern hemisphere.

9.3. Surface Temperature Response to Atmospheric Black Carbon

9.3.1. Global-Mean Temperature Change

[592] Earlier studies on the climate effect of large injections of smoke and dust aerosols (i.e., so-called nuclear winter) are relevant to understanding forcing by BC. *Cess et al*. [1985] showed that for increasing smoke loadings there is a transition from a surface-troposphere heating, induced by the convective coupling of the surface and the troposphere to a surface cooling when this convective coupling breaks down as the vertical structure of the atmosphere is modified. The climate response to BC may differ from a nuclear winter because the aerosol is concentrated in the lower atmosphere, and if the presence of co-emitted species is limited, it may be more absorbing than smoke. *Cook and Highwood* [2004], *Hansen et al*. [2005], and *Ban-Weiss et al*. [2011] added BC to different altitude ranges and showed that radiative forcing was not an effective measure of determining the surface temperature response to BC. The efficacy of the radiative forcing term could even change sign. In contrast, the efficacy of the adjusted forcing that accounted for semi-direct effects was much closer to unity [*Shine et al*., 2003; *Hansen et al*., 2005; *Crook et al*., 2011; *Ban-Weiss et al*., 2011]. The most consistent forcing measure appears to be calculated by allowing tropospheric response but no global mean surface temperature response, either from fixing surface temperature everywhere [*Shine et al*., 2003] or using a regression method [*Ban-Weiss et al*., 2011]. *Hansen et al*. [2005] further showed that for BC in snow the large efficacy of the high-latitude forcing needs to be properly accounted for (see below). The adjusted forcing implicitly accounts for some of the variable efficacy of the direct radiative forcing. The adjusted forcing or the effective forcing (i.e., forcing weighted by efficacy (Table 2)) is a more appropriate measure of BC's ultimate effect on global average temperature.

[593] Table 23 reports BC radiative forcing, adjusted forcing, effective forcing, and surface-temperature response from various climate models. Note that these experiments are generally based on unrealistic BC perturbations and, as such, they are representative of sensitivity rather than the expected magnitude of temperature change or forcing. Therefore, the results in Table 23 should be used qualitatively. Quantitative temperature changes are estimated in section 10, employing our revised forcing estimate. The different models vary in their experimental designs (e.g., BC alone versus BC and co-emitted species, slab ocean model versus fully coupled ocean-atmosphere model), emission rates, and treatment of the effects of BC on climate. Some have a more sophisticated treatment of BC optics, some are better documented in their ability to simulate the present-day climate and the historical period, and some simulate better cloud properties than others. Nevertheless, these results show that effective forcing and adjusted forcings from a single model agree to within their respective uncertainties, justifying our approach for calculating the semi-direct effect. While there is a large range in equilibrium temperature responses across the studies the spread in temperature response per radiative forcing is smaller, covering a threefold range. When the forcings are appropriately scaled to account for rapid adjustments agreement is even better, with only a twofold range in temperature response per adjusted forcing. This finding suggests that differences in rapid adjustments or aerosol processes included in each model are responsible for some of the difference in global average temperature change.

[594] The climate models clearly differ in their cloud responses. For instance, fossil fuel BC causes an increase in high-level clouds in the model of *Jacobson* [2010] due to an enhancement of upper tropospheric water vapor due to surface warming and evaporation and a decrease in low clouds due to enhanced BC warming, including that within cloud drops and interstitially between cloud drops, as discussed in section 7.3.3. These experiments, unlike most other studies, considered OA and other co-emitted species, and included the microphysical effects of BC on liquid and ice clouds.

9.3.2. Regional Surface Temperature Change

[595] As discussed in the introduction, the pattern of surface temperature response can be quite different from the pattern of forcing. The temperature response to BC is a combination of regional response and hemispheric response, with polar and land amplification. There is a reasonable agreement among models that the BC warming is concentrated in the Northern Hemisphere with some polar amplification (Figure 32). However, there is disagreement on the relative warming of the different continents, with some models showing significant warming over North America and Eurasia while others do not. It is unlikely that the differences in experimental setup and range of BC effects included in the four models presented in Figure 32 are sufficient to explain the diversity of results. Some of the model differences could be due to differences in forcing and climate efficacy (or sign of the semi-direct effect). It is difficult, however, to attribute the differences among the models to a particular process or reason without performing a more comprehensive intercomparison. While some models include more BC forcing mechanisms that have been evaluated at different scales (e.g., GATOR), others have been more thoroughly tested regarding their ability to represent the global historical temperature record and climate variability (e.g., NCAR CAM, GISS, and HadGEM2).

[596] There are few systematic studies of the regional impact of BC aerosols from different regions with the exception of the work by *Shindell and Faluvegi* [2009], who looked at the regional impact of atmospheric BC from four latitudinal bands in the GISS climate model. A summary of their results relevant to BC is shown in Figure 33. BC in the 28°N–60°N band is most efficient at inducing warming in the 60°N–90°N band and vice versa. Tropical (28°S to 28°N) BC warms all latitudinal bands, with forcing efficiency increasing in moving from lower to higher latitudes. Finally, it should be noted that atmospheric BC in the 60°N–90°N band cools the surface in that region, possibly because the coupling between the atmosphere and the surface is not strong enough to overwhelm the decrease in solar radiation at the surface induced by BC or because of

Table 23. Summary of Results for Black Carbon in Climate Models[a]

Study	Processes Included	Emissions[b] (Tg BC yr^{-1})	Radiative Forcing ($W m^{-2}$)	Adjusted Forcing ($W m^{-2}$)	Effective Forcing ($W m^{-2}$)	Equilibrium Temperature Response (K)	Notes
Roberts and Jones [2004]	Direct and semi-direct effects	20.24 (×4)	0.78 (×4)		0.48 (×4)	0.44 (×4)	HadSM4. Fossil-fuel BC emissions were quadrupled to increase signal to noise.
Wang [2004]	Direct and semi-direct effects	14	0.35	0.14 ± 0.3		0.07	NCAR CCM3 with slab ocean model from CCM3.6.6. CO_2 climate sensitivity not known.
Hansen et al. [2005]	Direct and semi-direct effects	Not specified	1.03 (×6) BB 0.96 (×2) FF	0.71 ± 0.17 (×6) 0.5 ± 0.1 (×2)	0.76 (×6) 0.59 (×2)	0.27 (×6) 0.35 (×2)	GISS model E. BB = Biomass burning BC only. Experiment E2BCB × 6 (biomass burning BC emissions were multiplied by 6) and E2BCI × 2 (industrial BC emissions were doubled).
Chung and Seinfeld [2005]	Direct and semi-direct effects	7.9	0.33 (Ext) 0.60 (Int)		0.47 (Ext) 0.85 (Int)	0.20 (Ext) 0.37 (Int)	GISS model II-prime with external (Ext) and internal (Int) mixtures
Sokolov [2006]	Direct and semi-direct effects			2.36 (×10)	3.0 (×10)	1.76 (×10)	Earth System Model of Intermediate Complexity. The change in BC has been multiplied by 10.
Jones et al. [2007]	Direct and semi-direct effects. External mixture.	7.9 (year 2000) versus 0.6 (year 1860)	0.45	0.39 ± 0.09	0.28	0.28	Improved version of HadGEM1 coupled to a mixed-layer ocean. Direct and semi-direct effects only. Fossil-fuel BC only.
Jacobson [2010]	Direct (external + internal mixtures), BC inclusion in cloud droplets, snow albedo effect, semi-direct and all cloud effects.	3.18 FS[c] 7.92 FSBSG[c]			0.47[d] 0.78[d]	0.49 0.71	Forcing is an estimate based on an earlier version of the model. CO_2 climate sensitivity $0.6 K (W m^{-2})^{-1}$.

[a]Adjusted forcing includes radiative forcing and rapid adjustments to that forcing quantified as a top-of-atmosphere (ToA) flux change; effective forcing is either radiative or adjusted forcing multiplied by its efficacy (Table 2). Multipliers in brackets refer to the scalings of the BC effect used in integrations to generate a statistically significant response in the climate models.

[b]FF = fossil-fuel BC; FS = fossil-fuel BC + POA; BB = biomass burning BC; FSBSG = fossil-fuel and biofuel BC + POA.

[c]Co-emitted POA is included for FS and all aerosols and gases for FSBSG.

[d]Top-of-atmosphere irradiance changes that include climate response and, thus, are not true effective forcings.

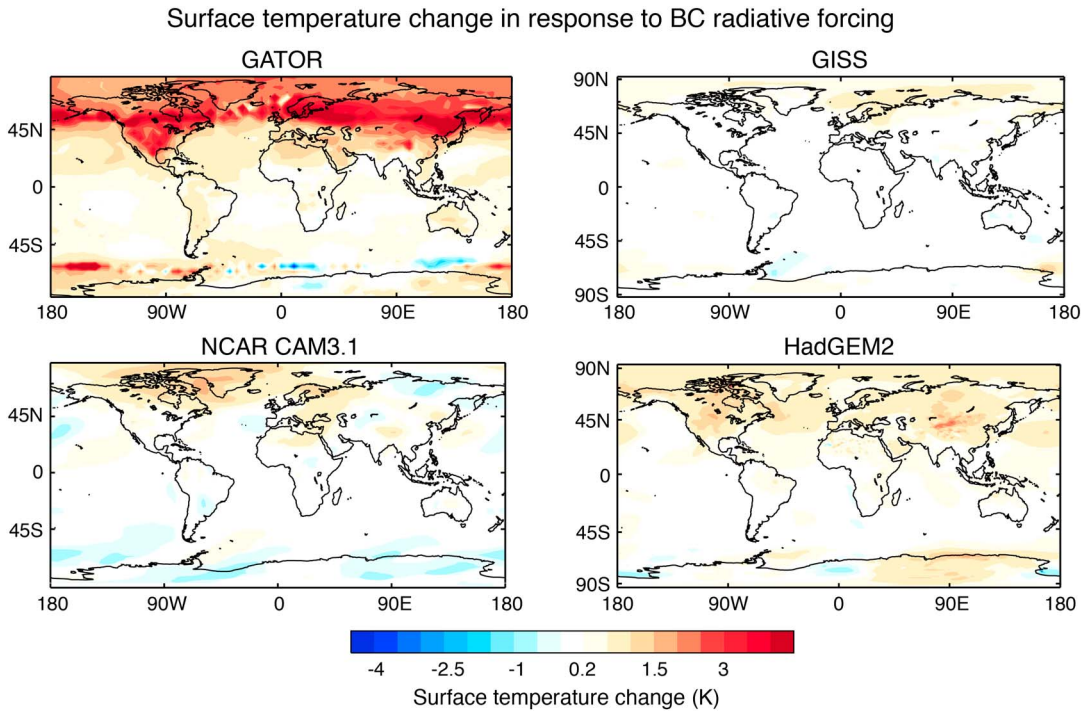

Figure 32. Surface temperature change in response to the BC radiative forcing in different climate models. Note that the experiments differ in their BC emissions, inclusion or not of the snow albedo and indirect effects on clouds, and setup. The panels are labeled with the model name. The details of each model and experimental setups are provided in Table 25.

resulting changes in northward heat transport due to a decreasing latitudinal temperature gradient. These experiments account only for forcing by atmospheric BC; in this same model, when surface forcing from BC deposited to snow and ice is accounted for, the total forcing by BC in the 60°N–90°N latitude band is positive (warming).

[597] It has been further suggested by *Ramanathan and Carmichael* [2008] that absorbing aerosols could have contributed to the observed melting of snowpacks and glaciers in the Himalayan region on the basis that layers of BC aerosol (the so-called atmospheric brown cloud) heat the atmosphere at altitudes up to 3 to 5 km. Evidence for the effectiveness of this mechanism remains elusive. *Menon et al*. [2010] simulate a small decrease in snow and ice cover over the Himalaya associated with the increase in emissions from 1990 to 2000. However, their simulations use observed climatological sea-surface temperatures and neglect any response from the ocean. Moreover, it is unclear to what extent the precipitation changes in their simulations are statistically significant. *Kuhlmann and Quaas* [2010] used lidar measurements from the CALIPSO satellite to assess the importance of aerosols for atmospheric heating rates. They found that (i) in higher layers the shortwave heating was partly balanced by longwave cooling, (ii) the contribution of aerosols to atmospheric heating rate over the Tibetan Plateau was relatively small (typically 0.02K day^{-1}) as compared to neighboring regions (0.2K day^{-1}), and (iii) a large fraction of the aerosol was dust or at least classified as such by CALIPSO. However, *Kuhlmann and Quaas* did not estimate the impact of the aerosol on the surface energy balance. While it is possible that atmospheric BC aerosols have contributed to the melting of snowpack and glacier in the Himalayan region, appropriate testing of the hypothesis would require robust ensembles of high-resolution simulations that can resolve the complex atmospheric flow and surface radiative budget over this region.

9.4. Precipitation Changes Due to Black-Carbon Direct and Semi-Direct Effects

[598] The separation between rapid adjustment and slow feedbacks is particularly useful for examining precipitation responses to forcing. *Andrews et al*. [2010] studied the rapid adjustment associated with a range of climate agents, including BC. They showed that the rapid adjustment in global-mean precipitation correlates negatively with the atmospheric radiative forcing (i.e., the difference between ToA and surface radiative forcing) while the slow response is proportional to the global-mean surface temperature change. Since BC aerosols are responsible for significant atmospheric radiative forcing through absorption of solar radiation, the reduction in precipitation due to the rapid adjustment can dominate over the increase due to the slow feedback. One model showed a global reduction in precipitation of around 0.7% from BC rapid adjustments [*Andrews et al*., 2010]. This result has been confirmed by *Ming et al*. [2010] who found that the decrease in precipitation due to atmospheric heating could dominate over the increase in precipitation due to surface warming for some vertical distributions of the BC aerosol.

[599] Both *Wang* [2007] and *Jones et al*. [2007] found that BC strengthens the Hadley cell in the Northern Hemisphere but weakens it in the Southern hemisphere. This leads to a northward shift in the Inter Tropical Convergence Zone (ITCZ), which appears to be a robust feature of the climate

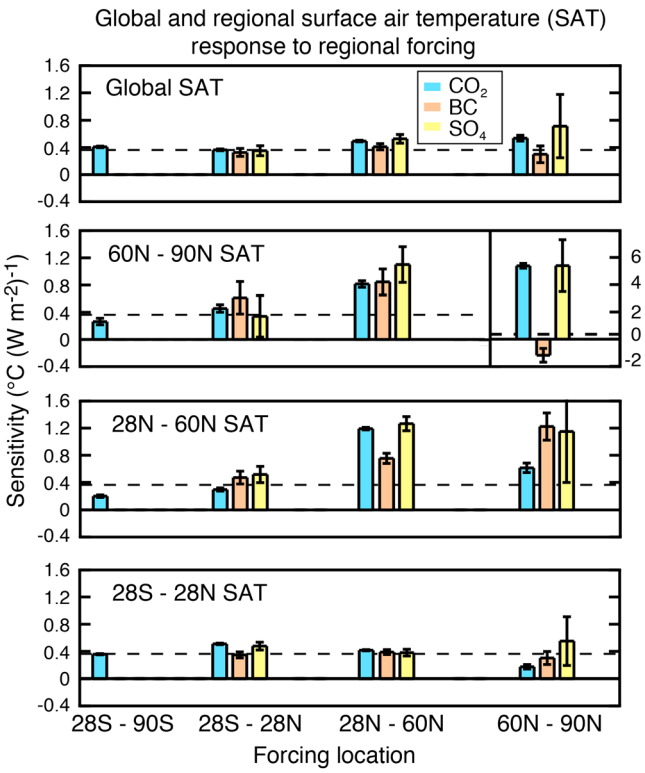

Figure 33. Normalized global and regional surface air temperature (SAT) changes (°C $(\mathrm{W\,m^{-2}})^{-1}$) in response to regional radiative forcings due to CO_2 (blue bars), BC aerosol (no cryosphere) (red bars), and sulfate aerosol (yellow bars). The forcing regions are defined on the horizontal axis as latitudinal bands (Southern Hemisphere middle- and high-latitudes, 28°S–90°S; tropics, 28°S–28°N; Northern Hemisphere mid-latitudes, 28°N–60°N; and Northern Hemisphere high-latitudes, 60°N–90°N). The SAT response regions are labeled in each panel. Adapted from *Shindell and Faluvegi* [2009].

response to BC also supported by earlier experiments [*Roberts and Jones*, 2004; *Chung and Seinfeld*, 2005].

[600] A number of studies have investigated the regional climate responses to BC in particular regions of the world, generally focusing on precipitation changes. Many of these studies examine Asia because of the large concentrations of absorbing aerosols there. Using the GISS model, *Menon et al*. [2002b] simulated a surface warming over most regions in response to absorbing aerosols but a moderate cooling over China. The model also simulates increased precipitation in southern China and over India with a band of decreased precipitation to the south. *Zhang et al*. [2009a] obtained the opposite result using the Community Atmosphere Model (CAM3) when considering carbonaceous aerosol (BC + OC) together. In this case, surface temperature increased in southern China and India and total cloud cover and precipitation decreased. Using the same model, *Liu et al*. [2009b] found that sulfate and BC aerosols have the effect of weakening East Asia monsoons in both the summer and winter seasons.

[601] *Lau et al*. [2006] used the GEOS GCM with fixed sea surface temperature to show that absorption of solar radiation by dust heats the air on the northern and southern slopes of the Tibetan Plateau, which can then rise and create a positive temperature anomaly in the middle to upper troposphere over the Tibetan Plateau. On the southern side, the atmospheric heating is reinforced by anthropogenic emissions of BC over the Indian subcontinent. This can lead to an intensification of the Indian summer monsoon and surface warming over the Tibetan Plateau. While *Lau et al*. found that the effect of BC is important in initiating the monsoon rainfall anomalies over India, it is not enough to produce statistically significant change in the monsoon regime on its own (i.e., without the synergy with dust absorption). Like most of the other earlier studies looking at the regional climate response to BC, this study was performed with an atmosphere-only model, which is a significant limitation because sea surface temperatures are not allowed to respond to the forcing by BC. One could imagine anthropogenic aerosols causing a decrease in sea surface temperature, for example, during the winter monsoon over the Indian Ocean, with consequences for the summer monsoon.

[602] *Wang et al*. [2009a] used the NCAR Community Climate Model version 3 (CAM3) coupled to a slab ocean model to investigate the response of the Indian summer monsoon to scattering and absorbing aerosols. They found that absorbing aerosols cause a northward shift in rainfall (both during the onset of the monsoon and averaged over the monsoon period) that is only weakly offset by the effect of scattering aerosols.

[603] *Meehl et al*. [2008] performed a six-member ensemble of twentieth century simulations with a fully coupled ocean-atmosphere climate model, which confirmed some of the earlier results found with atmospheric models coupled to a slab ocean. In their experiments, BC and OA aerosols increase lower tropospheric heating over south Asia and reduce the amount of solar radiation reaching the surface during the dry season, enhancing precipitation over India in the months of March–April–May. With the onset of the monsoon, the reduced surface temperatures in the Bay of Bengal, Arabian Sea, and over India that extend to the Himalaya act to reduce monsoon rainfall over India itself, with some small increases over the Tibetan Plateau. Precipitation over China generally decreases due to the BC effects. Analysis of single ensemble members from the multiple-forcings experiment suggests that the observed increasing precipitation trends over southern China appear to be associated with natural variability connected to surface temperature changes in the northwest Pacific Ocean. *Rotstayn et al*. [2007] suggest that the effects of Asian aerosols on rainfall could be seen in Australia with an increase in cloudiness and rainfall during the period 1951 to 1996, especially in northwestern Australia. *Bollasina et al*. [2011] and *Shindell et al*. [2012] investigated the impact of aerosol forcing on the South Asian monsoon in the GFDL and GISS GCMs, respectively. *Shindell et al*. found distinct perturbations to the South Asian monsoon as well as to precipitation in the Sahel and southern Europe. *Bollasina et al*. found similar changes and suggested that the changes were part of large-scale circulation changes and had little to do with direct local forcing. *Shindell et al* showed that the precipitation responses were in many places similar to those induced by GHGs but with much greater amplitude per unit forcing.

[604] *Tosca et al*. [2010] also applied the NCAR CAM3 model with a slab ocean model to explore effects of biomass burning emissions over the western equatorial Pacific during intense El Niño episodes, such as the 1997–1998 event. They found that BC and OA emissions from extreme fire years caused sea surface temperature to cool and the atmosphere to warm and that this reduced precipitation by about 10% over greater Indonesia, potentially exacerbating local drought conditions because evapotranspiration reductions were smaller than precipitation changes.

[605] Generally, these studies show that atmospheric heating by BC can have significant effects on precipitation, causing a global reduction via rapid adjustment processes. Model studies have also shown that BC can alter regional precipitation by about 10% and affect circulation patterns such as the monsoon.

9.5. Climate Response to the Snow Albedo Effect

[606] BC deposited to snowpack can significantly reduce snow and ice albedo because of the approximately 5 order-of-magnitude difference in mass absorption cross section between ice and BC, and strong multiple scattering within snow, which enables small mixing ratios of impurities to absorb a disproportionate amount of radiative energy [e.g., *Warren and Wiscombe*, 1980]. BC-induced snow albedo changes exert a small global-mean forcing through radiative forcing and rapid adjustments (i.e., all-source adjusted forcing range of +0.01 to +0.09 W m^{-2} in section 8), but models indicate that snow albedo forcing is unusually effective at warming climate, even when rapid adjustments are accounted for. The high efficacy of the adjusted forcing stems from the following factors:

[607] 1. By definition, all of the forcing energy associated with this mechanism is deposited directly within the cryosphere, a component of the Earth System responsible for strong positive feedback [e.g., *Budyko*, 1969] through the snow (and ice) albedo feedback (*SAF* in Figure 29). Warming of snow and sea ice by deposited BC exacerbates this feedback mechanism in comparison to forcing mechanisms that distribute energy more evenly throughout the planetary envelope, such as GHG forcing.

[608] 2. The mechanism operates mostly at high latitudes, which are uniquely susceptible to surface energy forcings because of stable atmospheric conditions. Smaller lapse rates in high-latitude regions induce shallower mixed layers that permit surface energy forcings to drive larger surface temperature changes. In stratified conditions, the mass of air responding to a surface energy forcing is small, and the energy is not transferred efficiently throughout the system. This condition breaks down with strong warming, however, so that larger forcings have smaller efficacies. It is weaker during summer, when insolation (and therefore radiative forcing via darkening of snow or ice) is greatest [*Forster et al*., 2000].

[609] 3. In some studies, feedbacks driven by changes in snow grain size may also contribute to larger efficacy [*Flanner et al*., 2007] (*GRA* in Figure 29). The reasoning for this result is that BC absorption warms snowpacks so that they age more rapidly, which lowers snow albedo in the near-infrared spectrum. A key uncertainty associated with this process is that snowpack temperature gradient is often a greater controller of snow age than mean temperature [*Flanner and Zender*, 2006], and the influence of absorbing impurities on temperature gradient depends on many factors, including the vertical distribution of impurities and solar absorption, snowpack thermal conductivity, and snowpack-atmosphere coupling.

[610] The relative roles of these three factors are uncertain. *Bellouin and Boucher* [2010] obtained a large climate efficacy in idealized model experiments that do not include the third factor.

[611] Climate response to BC in snow is particularly strong during boreal spring (March–May) over middle to high latitudes [*Flanner et al*., 2009; *Wang et al*., 2011]. Increasing springtime insolation and widespread snow cover in the Northern Hemisphere drive the greatest radiative forcing during this season, and climate response and efficacy are large when the mechanism induces earlier snow melt, as the contrast in albedo between snow-covered and snow-free surfaces is generally much greater than the reduction in albedo caused by BC. A source of enhanced springtime forcing is the retention of impurities at the snow surface during melt (*MBC* in Figure 29; section 8.3.5), but the importance of this effect is largely uncertain and likely varies considerably with location and type of snowpack. *Koch et al*. [2011b] have suggested that even in the absence of the *MBC* feedback (Table 20), 20% of Arctic warming and snow-ice cover loss is a consequence of the BC albedo effect.

[612] Table 24 reports estimates of the BC snow albedo forcing, surface temperature response, and climate efficacy from different model studies. The equilibrium change in global-mean surface temperature ranges from +0.06 to +0.20K for the trustworthiest experiments. The climate response is more localized than that for the BC direct and semi-direct effects with most of the warming over the Arctic region and the Tibetan Plateau and Himalaya. Equilibrium Arctic temperature responses reported from three simulations [*Flanner et al*., 2007; *Koch et al*., 2009a] are 0.50, 0.50, and 1.6K (the latter occurring with strong boreal fire BC emissions in 1998). Climate efficacy for the adjusted forcing is much larger than 1 in all models with most models showing values of 2.0 or more. Based on the spread of adjusted-forcing efficacies given in Table 24, the efficacy of the adjusted forcing by BC in the cryosphere is estimated to be 3, with a range of 2 to 4. These efficacies are used in section 10 to derive effective forcings due to BC in snow and sea ice (Table 2).

[613] Most studies of the climate impact of BC in snow have focused on the global, annual impact or on impacts in the Arctic. However, because most of the energy from this forcing directly impacts snowpack temperatures, local impacts may be large, especially where snowmelt is relied upon as a water source. Recognizing this, *Qian et al*. [2009] applied the Weather Research and Forecasting (WRF) regional model to study the influence of BC deposition on western North America snowpack. They found the largest response during late winter and early spring, with increased net solar radiation caused by reduced snow cover, and subsequent increases in surface air temperature. Climate changes and deposition of BC on snow were both largest over the central Rockies and southern Alberta, where shifts in regional stream flow were also found. An experiment with doubling of regional BC emissions showed a much

Table 24. Summary of Climate Model Studies Focusing on the Snow Albedo Effect[a]

Study	Forcing[b] ($W\,m^{-2}$)	Equilibrium Temperature Response (K)	Climate Sensitivity ($K\,W^{-1}m^2$)	Climate Efficacy (%)	Note
Hansen and Nazarenko [2004]	0.16	0.24	1.5	212	Idealized snow albedo decrease (2.5% in Arctic, 1% in Greenland, and 5% in Northern Hemisphere land snow)
Jacobson [2004a]		0.06[c]			GATOR GCMM range 0.03–0.11K
Hansen et al. [2005]	0.082	0.065		171	GISS model E
Flanner et al. [2007]	0.054[e]	0.15		452[d]	1998 central estimate. NCAR CAM3
Flanner et al. [2007]	0.049[e]	0.10		329[d]	2001 central estimate. NCAR CAM3
Flanner et al. [2007]	0.043[e]				Fossil-fuel and biofuel BC only
Flanner et al. [2007]	0.033[e]				Fossil-fuel BC only
Flanner et al. [2009]	0.057	0.08	1.4	231[f]	Experiment PI4 (pre-industrial climate with fossil and biofuel BC only) NCAR CAM3.1
Koch et al. [2009a]	0.01	0.18			GISS model E. RF is estimated as difference in fluxes from experiments with fixed SST and is not a good approximation.
Bellouin and Boucher [2010]	0.28	0.72	2.6	260	Idealized experiment with HadGEM2-AML. The radiative forcing is for an ad hoc decrease in the land snow albedo of 0.05.
Wang et al. [2011]	0.042[g]	0.071[h]			Idealized snow albedo decrease (2.5% in Arctic, 1% in Greenland, and 5% in Northern Hemisphere land snow)

[a]Specifics of the forcing calculations for all but the *Bellouin and Boucher* [2010] study can be found in Table 19. *Bellouin and Boucher* [2010] were specifically looking at climate response, so this study is excluded from Table 19.
[b]*Bellouin and Boucher* [2010], *Hansen and Nazarenko* [2004], and *Hansen et al.* [2005] forcings are radiative forcings. All other studies included rapid adjustments in the forcings and so are adjusted forcings.
[c]Not equilibrium temperature but 10 year average (including spin up).
[d]Results from *Flanner et al.* [2007] show a large range of climate efficacies which could be due to noise.
[e]ToA forcing is estimated as Fa = 0.91 Fs,snow. CO_2 climate sensitivity is estimated to be 2.47 3.58 = 0.69K W^{-1} m^2.
[f]CO_2 climate sensitivity in *Flanner et al.* [2009] is estimated as 0.89/(5.35ln(380/289)) = 0.89/1.46 = 0.61K W^{-1} m^2.
[g]Surface forcing, Fs.
[h]Temperature response is not equilibrium temperature but a 10 year average, with 1 year spin up. Equilibrium temperature response is not reported so climate sensitivity and climate efficacy are not given.

greater-than-linear climate response in this region. *Qian et al.* [2011] used a global model to look at the influence of BC and dust on the Tibetan Plateau snowpack with a specific focus on the impacts on the Asian hydrological cycle and monsoon climate. In this study, BC and dust in snow were found to produce 5 to 25 W m^{-2} adjusted forcing during spring, reducing spring snowpack over the Tibetan Plateau more than does warming by anthropogenic CO_2 and atmospheric BC. However, *Qian et al.* acknowledge that the global model used grossly overpredicts snow cover in this region (their Figure 2) and, therefore, likely also forcing by BC and dust in snow. These studies highlight the possible strong regional impacts of BC in snow but also emphasize the need for studies that can account for the large variations in terrain, snow cover and BC deposition, especially in mountainous terrain.

Table 25. Description of the Model and Experimental Setup for Figure 32[a]

Model	Experimental Design	BC Sources and State of Mixture	Effects Included	References
GATOR	Present-day emissions versus no emissions; "quasi-equilibrium" climate response using last 10 year average from 15 year experiment; full ocean model	FF + BF (BC + POA + other co-emitted species); evolution from external to internal mixture	Direct; semi-direct; cloud indirect; BC inclusion in water drops and ice crystals; snow albedo effects	*Jacobson* [2010]
GISS	80% of present-day emissions; Equilibrium climate response; full ocean model	80% of FF + BF (only BC); external mixture	Direct; semi-direct; cloud indirect; snow-albedo effects	*Koch and Hansen* [2005]; *Shindell and Faluvegi* [2009].
NCAR CAM3.1	Present-day emissions versus no emissions; equilibrium climate response; slab ocean model	FF + BF (BC + POA); external mixture	Direct; semi-direct; snow albedo effects (and indirect effects)	*Collins et al.* [2006]; *Flanner et al.* [2009]
HadGEM2	Present-day versus pre-industrial emissions; equilibrium climate response; slab ocean model	FF (only BC); external mixture	Direct; semi-direct	*Jones et al.* [2007]

[a]Refer to section 8 for a more detailed description of snow albedo effect.

9.6. Detection and Attribution of Climate Change Due to Black Carbon

[614] As sections 9.3 to 9.5 have outlined, there is evidence of regional climate responses to BC that is manifest in observations. In particular, there is some evidence for a BC effect on (1) regional temperature and precipitation changes [e.g., *Menon et al*., 2010], (2) Arctic temperatures and snow-ice cover [e.g., *Flanner et al*., 2009; *Koch et al*., 2011b], (3) monsoon and other circulation changes [e.g., *Rotstayn et al*., 2007; *Bollasina et al*., 2011; *Shindell et al*., 2012], and (4) Himalayan and North American snow and ice cover [*Qian et al*., 2009; *Qian et al*., 2011]. However, it should be noted that none of these studies formally attribute changes to BC in a statistically rigorous sense.

[615] It is desirable to find a confirmation of the model results on the climate response to BC in the observational climate records. Methods have been developed to detect and attribute climate change to particular climate agents by regressing the spatial and temporal patterns of climate change simulated by the models against the observed patterns. Scaling factors that maximize the fit to the observations provide a measure of whether a particular forcing is detected, by testing the hypothesis that the scaling factors are consistent with a value of zero. When a particular combination of forcings is detected, the scale factors can be used to reconstruct the contribution of each individual forcing to temperature change. Detection and attribution methods have established that the anthropogenic "...greenhouse gas forcing has very likely caused most of the observed global warming over the last 50 years." The cooling due to sulfate aerosols could also be detected [*Hegerl et al*., 2007]. However, it has proven to be more difficult to detect the warming due to BC.

[616] *Jones et al*. [2005] included fossil fuel BC in a detection and attribution analysis with GHG and sulfate aerosols. While the introduction of BC did not affect the attribution of the warming to GHGs, it was not possible to detect the pattern due to BC because it was too similar to the cooling pattern of sulfate aerosols. The influence of carbonaceous aerosols (BC and OA from fossil fuel and biomass burning sources) was detected by *Nagashima et al*. [2006] in the mid part of the twentieth century. However, the relative contribution from BC cannot be deduced from this study.

[617] *Jones et al*. [2011] revisited their earlier work using an ensemble of HadGEM1 model simulations that include different combinations of the GHGs, sulfate aerosols, BC, and natural radiative forcings. They used their detection and attribution method to examine the climate influence of BC from fossil fuel and biofuel combustion sources. The BC forcing included the direct and semi-direct effect but not the snow albedo effect. The climate response to BC was obtained as the difference between a simulation with all forcings and a simulation with all forcings except that from BC. BC was found to have a detectable contribution to the warming over the period 1950–1999 but not over the period 1900–1999 or 1957–2006. The attributed climate change due to BC was 0.41K(century)$^{-1}$ (range 0.20 to 0.60K(century)$^{-1}$) for the period 1950–1999. This corresponds to a warming of about 0.20K (range 0.10 to 0.30K) for the 50 year period. Global warming by industrial-era BC would be about twice as large because 1950 emissions of BC were about half of present-day emissions. Moreover, any committed warming would add only slightly to the equilibrium climate response. Accounting for the snow albedo effect would possibly improve the detection and narrow the uncertainties in the scale factors but would not necessarily result in a larger contribution of BC to the observed warming because the scale factor can compensate for the missing warming in the climate simulations. For the period 1957–2006, the attributed climate change due to BC—not statistically significant—is 0.10K(century)$^{-1}$ (range −0.03 to 0.21K(century)$^{-1}$). Failure to detect the climate response to BC over this period can be due to the discontinuities introduced in the simulations by merging the historical emission inventories until 2000 with the SRES emission projections after 2000.

[618] In conclusion, it can be said that the global warming due to BC can be detected in the observational temperature record but the detection remains very sensitive to the modeling assumptions. The deduced contribution of BC to the observed warming is comparable to that obtained from models alone, but it is not accurate enough to constrain further the various estimates obtained from the models so far. Inclusion of the pattern of warming due to the snow albedo effect and regression of the simulated patterns against both the observed surface and vertical temperature change patterns could contribute to a better detection of the BC signal.

9.7. Conclusions

[619] Figure 34 summarizes our knowledge on the effects of BC on climate. There is agreement among climate models that BC causes a warming that is essentially located in the northern hemisphere. Existing studies have different experimental configurations and consider different processes by which BC affects climate, making comparisons between them difficult. However, there is a smaller range in surface temperature response per unit effective forcing than in effective forcing. Climate models also consistently simulate a northward shift in the Intertropical Convergence Zone in response to BC forcing. Other changes in precipitation are likely, especially the Asian monsoon systems as these regions experience large burdens of BC. However, there is no agreement among models on the patterns of rainfall changes in these regions. High-resolution simulations with coupled ocean-atmosphere models over the Asian region could better address the issue of circulation and precipitation changes due to BC. Darkening of snow and ice surfaces by BC is associated with enhanced melting and an amplification of the surface temperature response in these regions, but the role of BC on glacier melting in the Himalayan and Tibetan Plateau region remains unclear. The climate response to the indirect effect of BC on liquid and ice clouds has not been studied in isolation of the direct and semi-direct effects and remains largely unknown. Detection and attribution studies, which seek the expected patterns of the climate response to the BC forcing in the observational records, have had some limited success, probably because of imperfect modeling assumptions but also because of the disruptive effect of sulfate aerosols.

10. Synthesis of Black-Carbon Climate Effects

10.1. Section Summary

[620] 1. The industrial-era (1750 to 2005) climate forcing of BC is made up of components from its direct radiative forcing, its effect on cloud microphysics, rapid adjustments

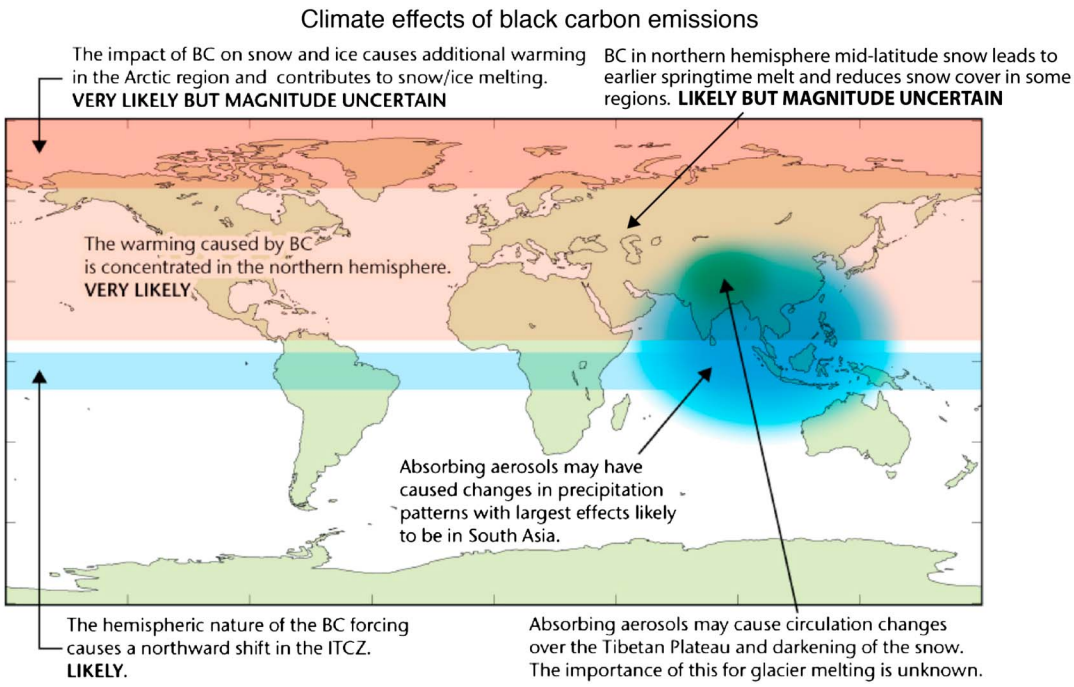

Figure 34. Qualitative summary of our current understanding of the global climate impacts of BC emissions.

to its atmospheric heating, and the effect of BC deposited on snow and sea ice.

[621] 2. Employing radiative forcing alone is inadequate for assessing the climate role of BC in terms of its globally averaged, surface temperature response. In particular, semi-direct effects and the efficacy of high-latitude forcing terms need to be properly accounted for.

[622] 3. The level of scientific understanding of these components is generally assessed as low or very low, making their uncertainty bounds difficult to characterize accurately. It is also difficult to quantify how uncertainties of different terms are correlated, making errors difficult to combine.

[623] 4. With these caveats, the industrial-era total climate forcing of BC is assessed to be +1.1 W m^{-2} with a 90% uncertainty range of +0.17 to 2.1 W m^{-2}, allowing for the correlation of emission uncertainty. This climate forcing has a larger uncertainty range and is likely greater than the radiative forcing from the BC direct effect (+0.71 W m^{-2} with a 90% uncertainty range of +0.08 to +1.27 W m^{-2}). This best estimate of black carbon forcing ranks it as the second most important individual climate-warming agent after carbon dioxide when both direct and indirect effects are included.

[624] 5. In terms of equilibrium global-mean surface temperature change, the total BC climate-forcing estimate for the industrial era would correspond to a warming between 0.1 and 2.0K. Note that not all this warming has been realized in the present day as the climate takes more than a century to reach equilibrium and many co-emitted species have a cooling effect, countering the global-mean warming of BC.

[625] 6. In addition to the direct radiative forcing of BC, adding the positive climate forcings and accounting for the efficacies of BC in snow and BC in sea ice increases the best estimate of forcing. Semi-direct and liquid-cloud effects add negative climate forcing, and cloud absorption and mixed-cloud changes add positive climate forcing. The total of BC cloud effects is estimated to be positive. Including these effects makes the estimate of total BC climate forcing estimate considerably more uncertain than that of direct radiative forcing. In particular, the two positive cloud terms have a very low level of scientific understanding. Without these terms, BC total climate forcing would be +0.65 W m^{-2} with a 90% uncertainty of +0.03 to +1.1 W m^{-2}.

[626] 7. The components of BC climate forcing in addition to the direct radiative forcing are cloud, cloud droplet inclusions, and semi-direct effects (+0.23 W m^{-2} with a 90% uncertainty range of −0.47 to 1.0 W m^{-2}); and BC in snow and BC in ice (+0.13 W m^{-2} with a 90% uncertainty range +0.04 to +0.33 W m^{-2}). See Table 1 for a further breakdown of forcing components.

10.2. Introduction

[627] Earlier sections have discussed emissions of BC, the mechanisms by which BC affects the Earth's radiative balance and BC's various effects on climate. Here we synthesize these discussions to provide best estimates and uncertainty bounds for the role of BC in the current climate using the metric of globally averaged climate forcing. Section 9 pointed out that regional changes and especially changes to the hydrological cycle are how we experience climate change and that such impacts are not represented by global forcing metrics. Nonetheless, in this assessment, we have chosen to use a global forcing metric as it is more comparable across mechanisms and better constrained than other choices.

10.3. Global Climate Forcing Definition

[628] We are ultimately interested in quantifying the impact of BC emissions on the Earth's climate. The definition of radiative forcing employed in IPCC reports [*Forster*

et al., 2007] is the change in net energy (down minus up) at the tropopause since 1750 due to a given mechanism or climate forcing agent, after allowing stratospheric temperatures to adjust to radiative equilibrium. As discussed in section 2.3.2, we retain this definition of forcing relative to a base year but use the term "industrial-era forcing" to indicate that the forcing is based on time rather than wholly attributable to anthropogenic activity. The overall global climate response to BC (encompassing direct, snow, sea-ice, and cloud effects) is also very different from the response to other forcing agents such as the long-lived GHGs (section 9). BC emissions affect clouds, snow, and sea ice (sections 7 and 8). In IPCC reports, some of these effects are classified as part of the cloud albedo effect or represented separately as BC snow albedo forcing, while others are considered part of the climate response. In this assessment, "rapid adjustments" to the forcing are included in the total climate forcing term. Rapid adjustments are where the atmosphere, land, or cryosphere responds to the forcing on a relatively short timeframe compared to that of the global-mean temperature response (Table 2 and section 2.3). In addition for both BC in snow and BC in sea ice, we implicitly include both the rapid adjustment of the snowpack and the climate response to the BC snow and ice albedo changes (i.e., the snow albedo feedback) by accounting for the efficacy of BC snow and ice albedo change in our climate forcing estimate, employing the concept of "effective forcing" discussed next.

[629] The notion of effective forcing means that the radiative forcing is scaled by an efficacy which incorporates the relative strengths of climate feedbacks. This effective forcing is then more representative of the actual radiative impacts of BC [e.g., *Hansen et al*., 2005] (also see Tables 2 and 23). Alternatively, forcings can be calculated from fixed sea-surface temperature experiments or regression techniques [*Hansen et al*., 2005, *Andrews et al*., 2010]. In practice, diverse forcing definitions are used in the different studies we assess and care is required when comparing reported forcings (section 9 and Table 23). For example, the separation of BC forcing into direct, cloud-albedo forcing, and semi-direct forcing is not straightforward (section 7). In this assessment, we have been particularly careful to include all relevant terms when assessing the total climate forcing from BC without double counting (section 2.3.2).

10.4. BC Global Climate Forcing Components and Uncertainties

[630] In this section, we summarize the best estimates of individual climate forcing components for global BC emissions in 2005, compared to 1750. These values are shown in Figure 35 along with 90% uncertainty range estimates. The combined climate forcings represent the known direct and indirect (cloud, snow, and ice) radiative forcings from BC changes plus all known rapid adjustments of clouds and the snowpack (section 8.4). They also capture the high efficacy of high-latitude snow and ice forcings. The sum of these terms represents the total climate forcing of BC. Table 26 summarizes each of the terms evaluated, describes their relation to the forcing definitions described in section 2.3.2, explains how the uncertainty range was determined, and identifies where in this assessment the radiative forcing is estimated in detail. It also presents our general level of scientific understanding, which, following IPCC terminology [*Forster et al*., 2007], is based on an assessment of the nature of assumptions involved, the uncertainties prevailing about the processes that govern the forcing, and the resulting confidence in the numerical value of the estimate. The following sections review these choices.

10.4.1. BC Direct Forcing

[631] The best estimate and range of the direct BC radiative forcing arises from scaled AeroCom model results based on observationally constrained estimates of BC AAOD from AERONET sites (section 6). The finding that large increases in modeled concentrations are warranted in some regions is broadly consistent with comparisons with in situ measurements and space-based observations (sections 5.5.1 and 6.9.3). Emission factors may be the cause of low biomass-burning emissions (section 4.7.2.3). The reason for apparent underestimates in energy-related emissions is unknown, but they occur preferentially in regions with lower emission regulations and sparse combustion source measurements. The uncertainty range comes from a 60 to 70% uncertainty in BC AAOD and a 50% uncertainty in absorption forcing efficiency, due to uncertainties, respectively, in the amount of atmospheric absorption attributed to BC and dust and in the underlying reflectivity of the surface and atmosphere, particularly the presence of clouds below BC (section 6.7). Our assessment of the direct radiative forcing from BC is a +0.71 W m^{-2} best estimate with a 90% uncertainty range of +0.08 W m^{-2} to 1.27 W m^{-2}. Fossil fuel BC emission contributes approximately +0.29 W m^{-2}, biofuel +0.22 W m^{-2}, and open burning +0.20 W m^{-2} (section 11). Figure 35 also presents the preindustrial background plus industrial-era direct forcing from BC. This comprised of emissions from all anthropogenic and natural sources. This all-source climate forcing is evaluated to be +0.88 W m^{-2} with a 90% uncertainty range of +0.17 to +1.48 W m^{-2}.

10.4.2. BC Cloud Indirect Effects

[632] BC effects on clouds, discussed in section 7, are particularly poorly constrained. Many GCM cloud schemes do not reconcile treatments of clouds with small-scale cloud models. The vertical location of BC-containing particles relative to clouds is not well modeled. BC must be collocated with clouds for microphysical effects, and the sign and magnitude of semi-direct effects depend on the BC location relative to the cloud and cloud type. There are general uncertainties regarding the microphysical effects of all aerosols on clouds, and effects of individual species are even more uncertain. Only a few model studies with appropriate diagnostics have focused on the role of BC on these cloud effects. Modeled aerosol microphysics and cloud responses have not yet been closely constrained by observations or comparison with cloud-resolving models. The magnitude of aerosol-induced cloud changes is small compared to the spatial and inter-annual variability in modeled cloud forcing, so quantifying changes due to aerosol forcing is difficult. Our best attempt at assessing likely ranges for these cloud effects is discussed below. These ranges are based on a combination of model results and subjective assessment (Table 26 and section 7). Modeling of aerosol influence on clouds has not elucidated sensitivities to all factors, so it is not possible to develop a true uncertainty as we have for other forcing terms. Instead, the uncertainty is based on model diversity.

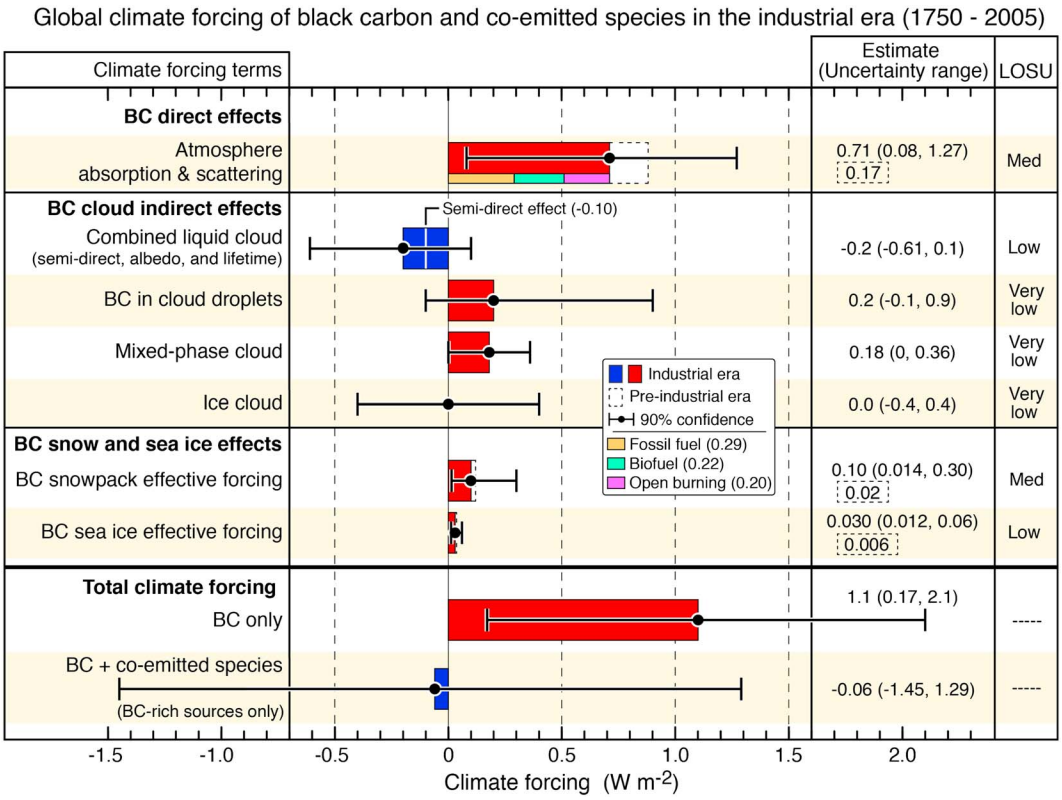

Figure 35. Globally averaged climate forcing in units of $\mathrm{W\,m^{-2}}$ from BC emissions in the year 2005 compared to those in 1750 (the industrial era). The bars and whiskers show the best estimates and uncertainties, respectively, of the different climate forcing terms from BC acting alone. The exception is the bottom bar which shows the net climate forcing from BC and its co-emitted species from BC-rich sources. Whiskers represent the assessed 90% uncertainty range (5% to 95%). The three smaller bars immediately below the direct forcing bar and legend display the separate contributions to industrial-era radiative forcing from fossil fuel, biofuel, and open burning emissions. The white line on the combined liquid-cloud forcing bar indicates the $-0.10 \pm 0.2\,\mathrm{W\,m^{-2}}$ contribution from semi-direct effects. The additional direct forcing of $+0.17\,\mathrm{W\,m^{-2}}$ shown with the dashed line represents the direct radiative forcing from pre-industrial emissions (i.e., prior to 1750). The combined colored and dashed bar represents our estimate of the all-source (i.e., natural plus anthropogenic) direct radiative forcing, namely, a $+0.88\,\mathrm{W\,m^{-2}}$ best estimate with a +0.18 to $+1.47\,\mathrm{W\,m^{-2}}$ uncertainty range (section 6). Likewise, the dashed line on the snow and sea-ice terms corresponds to their additional climate forcing prior to 1750, and the combined bars give their all source forcing (section 8). For snow and ice effects, their adjusted forcing and radiative forcings, respectively, have been scaled by their higher efficacy to give effective forcings as shown. The total climate forcing from all BC effects is shown as $1.1\,\mathrm{W\,m^{-2}}$. The uncertainty for this bar is assessed using a Monte Carlo method that assumes correlated errors in some of the forcing terms (see text for details). The columns on the right give the numeric value for each climate forcing and its uncertainty; they also present a level of scientific understanding (LOSU) for each forcing term. LOSU follows IPCC practice [*Forster et al.*, 2007] and represents our assessment of confidence in our own evaluation of a given climate forcing (see Table 26 and section 10 for further details). See Figure 38 and section 11 for details of the total climate forcing resulting from co-emissions from BC-rich sources shown in the bottom bar.

10.4.2.1. Liquid Cloud and Semi-Direct Effects

[633] The semi-direct effect follows from the in situ heating of the atmosphere from the direct radiative forcing of BC. Heating causes several observed and modeled effects on cloud properties and their distribution, via changes in atmospheric stability and regional circulation. These cloud rapid adjustments can be quantified in $\mathrm{W\ m^{-2}}$. There is good agreement in models that realistic distributions of BC have a semi-direct effect that yields a negative forcing. Our best estimate of the climate forcing from the semi-direct effect ($-0.10 \pm 0.2\ \mathrm{W\ m^{-2}}$) is based on two modeling studies that explicitly calculate the forcing and on five model studies that calculated a reduced radiative-forcing efficacy of BC direct forcing. The reduced efficacy was interpreted as being an adjustment in cloud distributions resulting from BC direct forcing and, therefore, a semi-direct forcing. Semi-direct effects are more properly associated with the "rapid adjustment" component of the direct radiative forcing term. Yet, for consistency with how the cloud indirect effects are estimated in climate models, this forcing is combined with the warm liquid-cloud forcing estimate.

Table 26. Black-Carbon Climate Forcing Terms, Uncertainties, and Level of Scientific Understanding (LOSU)[a]

Climate Forcing Term	Climate Forcing Type	Section	Basis for Best Estimate and Uncertainty Range	Scientific Understanding Basis	LOSU
Direct effect	Radiative forcing from absorption and scattering	6.7	Accounts for uncertainty in optical depth and radiative forcing efficiency. Range comes from model results constrained by ground-based observations.	Well-understood processes and good knowledge of radiative forcing in clear skies. General emission estimates and background clouds are relatively poorly known. Uncertainty remains in reasons for biases in models, compared to observations.	Med
Liquid cloud effect	An adjusted forcing made up from the radiative forcing from microphysical cloud-albedo BC-driven changes, including cloud lifetime and semi-direct (rapid adjustment) effects.	7.4	Range from several model results with different approaches	Microphysical processes well understood. Limited studies have isolated BC effects. Different modeling approaches make separation of semi-direct effects difficult.	Low
Semi-direct effect	Rapid adjustment associated with dynamical cloud changes driven by the BC direct effect	7.3	Range from two model studies and from average efficacy estimates. Implicitly included in liquid cloud forcing estimate.	Basic mechanisms observed and well modeled with good understanding of major processes. More complex fast responses in cloud are poorly constrained.	Low
BC in cloud droplets	Adjusted forcing from changes to cloud droplet absorption characteristics	7.3.3	Based on three studies, exploring different radiative transfer approaches	Uncertainty in the optical properties of mixed particles and the relative size of inclusions; uncertainty in rapid adjustment component.	Very low
Mixed phase cloud effect	Adjusted forcing from cloud albedo and emissivity BC-driven changes.	7.5.2	Range of three model studies	Competing physical mechanisms only partly understood and poorly quantified. Lack of observations.	Very low
Ice cloud effect	Adjusted forcing from cloud albedo and emissivity BC-driven changes.	7.5.3	Two model results highlight different mechanisms to give a wide range of estimated forcing, aviation effects currently excluded.	Plausible physical mechanisms partly understood. Observed aviation BC effects on ice clouds.	Very low
BC-in-snow effect	The effective forcing of BC-driven snow albedo changes, including BC in snow that is in sea ice. Includes rapid adjustments to the snow layer and the snow albedo feedback.	8.6.1	Model results constrained by observations, accounting for uncertainty in emission, BC aging, BC consolidation at the surface with melt, snow cover fraction and mass absorption efficiency.	Derived from a combination of snow reflectivity change and snowpack-surface feedbacks. Failure to adequately account for local dust or soil contributions to snowpack albedo and errors in model snowpack climatology may lead to bias.	Med
BC sea-ice effect	The effective forcing from albedo changes from BC on bare summer sea ice; does not include rapid adjustments to the sea ice or snow on sea ice.	8.6.2	An estimate derived from known physics, observations of BC in Arctic sea ice, and estimates of cloud, snow, ice and melt pond areas.	Poorly quantified snow cover estimates for sea-ice and poor knowledge of stratus cloud distribution. Not yet diagnosed in models.	Low

[a]All forcings are assumed to be over the industrial era (1750–2000). For the direct effect and snow and ice effects, the all-source forcings (i.e., from all anthropogenic and natural forcings) are also included.

[634] Climate forcing due to changes in warm liquid clouds occurs principally from changes in cloud microphysics. Uncertainty results from lack of constraint on particle size, number, and composition. A small amount of BC may reduce CCN by suppressing new particle formation. BC with co-emitted OA make more and better CCN, causing increased cloud albedo and an overall negative radiative forcing. This estimate is based on a limited number of microphysical models that have isolated the effect caused by BC.

[635] BC also causes additional rapid adjustments to cloud, inducing both semi-direct and cloud lifetime changes. These semi-direct and lifetime effects are also included in the estimate of the warm liquid-cloud climate forcing, as the models used to estimate this effect have not separated the microphysical component. The main uncertainty arises from the fact that lifetime effects are inferred from total anthropogenic aerosol studies and the impact of BC aerosol on cloud lifetime has not yet been isolated. The climate forcing for the BC effect on liquid cloud including rapid adjustment and semi-direct effects is assessed to be -0.2 W m^{-2} with a 90% uncertainty range of -0.61 to $+0.10$ W m^{-2}.

10.4.2.2. BC Inclusion in Cloud Drops

[636] BC, when present in cloud drops, changes their absorption characteristics and increases absorption within a cloud. A small number of studies have assessed this radiative forcing and have explored assumptions about the optical properties of mixed particles and their shape. Uncertainties arise due to different optical representations of the BC and droplet combination, which affects in-cloud heating rates, leading to rapid adjustments. This adjustment would be separate from other semi-direct effects. The climate forcing for the effect of BC inclusion in cloud drops, including their rapid adjustment, is assessed to be $+0.2$ W m^{-2} with a 90% uncertainty range of -0.1 W m^{-2} to $+0.9$ W m^{-2}.

10.4.2.3. Mixed-Phase Cloud Effect

[637] Climate forcing through changes in mixed-phase clouds is a mixture of radiative forcing and rapid adjustments. BC acts as an ice nucleus and can thereby produce increased glaciation rates, changes in precipitation, and changes in lifetime (section 7.6.2). The forcing estimate is based on a range of three studies employing anthropogenic BC emissions that has been scaled to total BC emissions in year 2005. Confidence in this forcing value and range is very low as the physical processes are not properly understood. Major uncertainties are that this estimate is based largely on a single model and does not have any observational constraint. The climate forcing for the BC effect on mixed phase cloud is assessed to be $+0.18$ W m^{-2} with a 90% uncertainty range of $+0.0$ to $+0.36$ W m^{-2}.

10.4.2.4. Ice Cloud Effect

[638] BC may affect ice clouds via two mechanisms. First, BC could increase the number of ice particles, which can lead to increased cloud amounts and positive forcing. Second, it can lead to increased numbers of supercooled solution droplets, thereby reducing the atmospheric relative humidity and cloud cover, and resulting in negative forcing. Both these effects are seen in modeling studies. Our estimate of the BC influence on ice cloud is based on two modeling approaches that lead to forcings of different signs for total BC emissions and a third modeling study that found no significant effect (section 7.5.3.4). This climate forcing term is also a mixture of radiative forcing and rapid adjustment. The climate forcing for the BC effect on ice cloud is assessed to be 0.0 W m^{-2} with a 90% uncertainty range of -0.4 to $+0.4$ W m^{-2}.

10.4.3. BC in Snow and Cryosphere Changes

[639] The BC-in-snow forcing estimates arise from changes in snowpack reflectivity and rapid adjustments to that forcing, constituting an adjusted forcing. The best estimate and range is based on a number of model results adjusted based on comparisons to observations of Arctic snow BC concentrations (sections 8.4 and 8.6.1). The lower (upper) bounds on snowpack BC forcing are calculated by adding in quadrature the forcing from low (high) bounds in emissions, rate of snow aging, BC mass absorption efficiency, and snow cover fraction, and using the high (low) bounds in the efficiency of BC scavenging with melt and in the role of dust in reducing snowpack albedo. The range in forcing does not account for uncertainty in the patchiness of snow cover or uncertainties in modeled cloud cover and vegetation cover. It also does not account for possible biases in modeled mid-latitude snow BC concentrations.

[640] The climate forcing for snowpack shown on Figure 35 scales the adjusted forcing by an efficacy of 3 (2 to 4 range) to give an effective forcing that accounts for both rapid adjustments in the snowpack, the strong impact of this forcing on near-surface temperature and the strong snow albedo feedback (section 9). The industrial-era effective forcing for BC in snow is assessed to be $+0.10$ W m^{-2} with a 90% uncertainty range of $+0.014$ to $+0.30$ W m^{-2}. The all-source effective forcing is assessed to be $+0.12$ W m^{-2} with a 90% uncertainty range of $+0.02$ to $+0.36$ W m^{-2}.

10.4.4. BC in Sea Ice

[641] Radiative forcing by BC on summertime sea ice after snow has melted (bare sea ice) is assessed separately and only includes forcing by the direct change in ice albedo with the inclusion of BC; unlike BC in snow, this forcing does not account for rapid adjustments to the snowpack and, thus, is a radiative forcing. Most model studies to date have not included this forcing by BC on bare sea ice, and those that have do not separately diagnose this forcing term. While snow BC forcing is dominant in the spring, bare sea-ice forcing arises due to the enhanced absorption of sunlight in June–July–August–September in the Arctic Ocean. The radiative forcing bounds presented in section 8 are based on estimates of sea-ice coverage, melt-pond area, area of sea ice covered in snow, sea-ice grain size, cloud cover, and average solar irradiance (section 8.6.2). The climate forcing in Figure 35 scales the direct radiative forcing of sea ice by an efficacy of 3 (2 to 4 range). Currently, no modeling study has explicitly calculated this efficacy for BC in sea ice, so we assume the same efficacy as for BC-in-snow effects, as forcing by BC in sea ice directly warms the sea ice and leads to ice melt and, thus, also leads to enhanced albedo feedback. The industrial-era effective forcing for BC in sea ice is assessed to be $+0.030$ W m^{-2} with a 90% uncertainty range of $+0.012$ to $+0.06$ W m^{-2}. The all-source effective forcing is estimated to be $+0.036$ W m^{-2} with a 90% uncertainty range of $+0.016$ to $+0.068$ W m^{-2}.

10.4.5. Net Effect of BC and Co-Emitted Species

[642] It is important to remember that BC is not emitted in isolation. Co-emitted aerosol species such as organic matter, sulfate, and O_3 precursors also affect climate, and many

mitigation actions could affect all of these species. Thus, "climate forcing by BC" is a useful paradigm for exploring physical effects, but it is not a practical one: this forcing could neither be measured individually nor removed from the aerosol mix through mitigation actions.

[643] The lower two bars in Figure 35 demonstrate how the total climate forcing by BC (top bar), compares with the total climate forcing from the mix of BC and its co-emitted species (bottom bar). These combined forcing values require estimates of climate forcing by non-BC species, and section 11 describes how we estimate and combine these values based on previous literature. These additional climate-forcing terms are introduced in Figure 35 to remind the reader of the close coupling between BC and co-emitted species. The remainder of this section continues the discussion of BC alone, and section 11 explores the question of co-emitted species in more depth.

10.5. Uncertainties in BC Global Climate Forcings

[644] Uncertainties in BC global climate forcings arise from many potential sources as discussed below. Except as noted, we have assumed that diversity in model results already reflects these uncertainties.

10.5.1. Atmospheric Burden, Emissions, and Rate of Deposition

[645] Concentrations of BC in the atmosphere and in snow are affected by emissions, lifetime, and removal rates. The range of lifetime estimates is largely due to uncertainties in wet deposition, leading to uncertain concentrations in both the atmosphere and cryosphere. Uncertainties in deposition rates appear to lead to large errors in the atmospheric burden in remote areas (section 5). In the Arctic, variations in wet deposition strongly affect atmospheric BC concentrations [*Garrett et al.*, 2010] and wet deposition rates directly affect surface snow and ice concentrations. Our atmospheric direct forcing estimate is constrained by observations (section 6), although this constraint itself has significant uncertainties. If modeled BC emission rates were larger, they would not have a great effect on forcing estimated here, as models would have a larger burden, and a lower correction to observations would result. A similar argument applies to atmospheric lifetime, although observational constraints are less stringent over oceans. In situ observations of surface snow concentrations have similarly been used to adjust for apparent biases in modeled surface snow concentrations (section 8), though this adjustment does not account for inter-annual variability in snow concentrations.

[646] Large uncertainties in atmospheric burden estimates may result from interpretation of observations. It is difficult to distinguish absorption optical depth attributable to dust from that attributable to BC (sections 5 and 6). Also important for direct radiative forcing and cloud effects is the atmospheric vertical distribution of BC. Vertical distribution varies between models and can lead to factor of 2 differences in direct forcing (section 6). Uncertainties in BC distribution, especially aloft, may cause large changes in cloud effects that are affected by BC concentration (section 7). Although recent observations can help constrain this uncertainty range for the direct forcing, this has not been possible for the cloud effect terms, where this uncertainty is assumed to be captured by the range of model forcing results (section 7).

10.5.2. Selection of Preindustrial Emissions

[647] Industrial-era BC forcing depends on the magnitude and distribution of preindustrial emissions and on atmospheric aerosol transport pathways and deposition rates in the preindustrial climate. Forcing by BC in the cryosphere further depends on the distribution of snow and ice cover in 1750. Shifts in the latitudinal distribution of emissions affect BC atmospheric lifetimes, forcing efficiency, proximity to clouds, and deposition to surface snow and ice. Preindustrial open burning emissions are particularly uncertain, and changes in assumptions about both the magnitude and location of these emissions would alter the estimate of preindustrial forcing. Presently, the largest open-burning emissions are in sub-tropical Africa and South America and are largely anthropogenic (section 4). In contrast, in 1750 there was likely significant open burning from land-clearing activities at northern mid-latitudes. The assumed preindustrial level of aerosol particularly affects non-linear cloud forcing terms.

10.5.3. Scaling to Emission Rate or Atmospheric Burden

[648] We assume in this work that the components of BC forcing generally scale with global emissions or atmospheric burdens. This assumption is reasonably valid for direct forcing. For cloud and cryosphere forcing (sections 7 and 8), this scaling may be valid for small deviations from the modeled state, but it has not been properly evaluated for many of the effects considered here. In particular, this linear scaling may not hold over highly polluted regions or for large estimated changes. For cryosphere BC forcing, changes in the latitudinal distribution of BC emissions between preindustrial and present day makes scaling by emissions to estimate preindustrial forcing particularly uncertain. This is accounted for using modeled estimates of the fraction of total emissions from biomass burning deposited to snow in 1750 versus in present day.

[649] Emissions of co-emitted species and other aerosol, such as dust, also affect direct forcing, cloud forcing, and snow and ice forcing by BC. Uncertainties in the regional pattern of emission are also important for global forcing, as BC emitted in different regions can give different climate forcing per emission due to longer atmospheric lifetime, snow deposition, or above-cloud fraction.

10.5.4. Dependence on Atmospheric and Surface State

[650] Climate forcing estimates depend on the latitudinal distribution of BC, background clouds, surface albedo, the presence of other aerosol, and especially on the relative vertical distributions of clouds and BC. Underlying surface reflectivity, particularly from distributions of snow and ice, are important both for BC-in-snow forcing and accurate determination of the direct effect. For BC in snow, we use uncertainties from one model study to derive the bounds in present-day forcing, which include uncertainty in snow cover. For BC in sea ice, bounds are calculated based on a range in sea-ice cover, snow cover on sea ice, melt ponds on sea ice, and cloud cover. Changes in snow and ice cover from preindustrial to present day are not accounted for in the industrial-era estimates of BC cryosphere forcing (section 8). For the other terms, uncertainty due to atmospheric

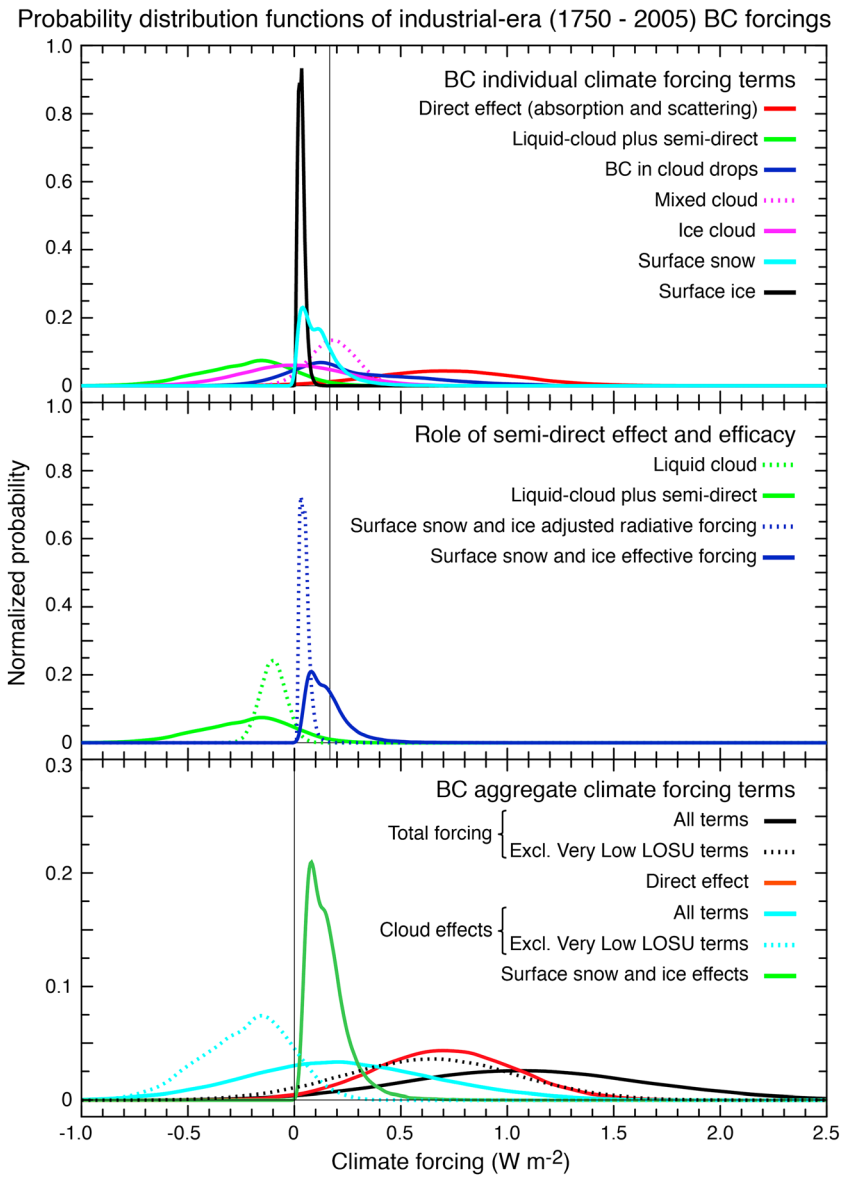

Figure 36. Probability distribution functions (PDFs) of industrial-era (1750–2005) forcings for BC climate forcing terms. Top: Individual PDFs for each climate forcing term. Middle: Before and after PDFs showing the role of the semi-direct effect in modifying the liquid cloud climate forcing term and the role of efficacy in modifying the BC-in-snow and BC-in-ice combined forcing term. Bottom: PDFs of the aggregated climate forcing components and the total climate forcing (see text for details). In the bottom panel, aggregated forcings are presented in two ways: with very low LOSU terms included (solid lines) or excluded (dotted lines). Probabilities are normalized to unity for all terms. Note the different vertical scale in the bottom panel.

state has not been explicitly estimated, but it is assumed to be captured by the range of model results employed.

10.6. Total Forcing Estimates and Comparison With Previous Work

[651] The total climate forcing value and uncertainty in Figure 35 are estimated by combining the estimates and uncertainties of the individual forcing terms. The construction of this error is shown in Figure 36, which shows the error analysis for individual terms (top panel), the role of semi-direct effects and efficacy (middle panel), and the aggregate climate forcing terms (bottom panel). To combine errors, we make a number of assumptions, outlined below.

[652] 1. We assume that the total climate forcing of BC is represented by the sum of individual forcing terms. Efficacies are explicitly included in the individual bars for the BC-on-snow and BC-on-sea-ice terms but not explicitly included for the other terms (center panel of Figure 36). Our summation, therefore, assumes that the efficacy of the combination of the direct radiative forcing terms and the adjusted forcing from the cloud effects and semi-direct effects would be equal to one and, therefore, comparable to the effective snow and sea-ice forcings. This implies that all rapid

adjustment effects are accounted for and the resulting geographical pattern of forcing would not be that different to an equivalent forcing from CO_2 to make a material difference to the efficacy.

[653] 2. To account for covariance between errors in component terms, we assume that emission uncertainties provide the only commonality between the uncertainties of each term. We also assume that emission uncertainty has a negligible effect on the cloud forcing uncertainty, as the large uncertainties are caused by differences in model processes. Emission uncertainty accounts for 50% of the relative uncertainty in direct forcing (section 6) and 32% of the relative uncertainty in snow and sea-ice effective forcing (section 8). This leads to a 0.16 correlation between the direct forcing and the snow and sea-ice terms, and a correlation of 0.1 between the snow and sea-ice terms themselves.

[654] 3. We assume that uncertainties, shown by whiskers on the contributing forcings in Figure 35, represent a 90% (5%–95%) uncertainty range and construct the probability distribution functions (PDFs) in Figure 36 accordingly. The uncertainty of the total climate forcing also assumes that the distribution of probability within a given range is formed from combining either normal or log-normal distributions. Symmetric normal distributions are used for the mixed-phase cloud, ice-cloud, and cloud-droplet inclusion effects. Asymmetric normal distributions are used for the direct effect and the liquid-cloud and semi-direct effects. Asymmetric log-normal distributions are used for the BC-in-snow and the BC-in-sea-ice effects.

[655] Using these assumptions, a Monte Carlo model was run one million times to produce the estimate of climate forcing. The random number sequences generated are used to choose a point to sample in the forcing range, based on a fraction of the area under the probability distribution curve. The forcing value defined by the fractional area is then chosen to represent the forcing for that mechanism during the given iteration. Correlated errors are allowed for by making the appropriate fraction of the random numbers generated match between the direct forcing and the snow and sea-ice terms. To generate correlated errors, a subset of the same random number sequences is used for the correlated forcing terms. For example, 10% of the random number sequence for snow and sea ice identically matches, giving their million-point forcing series a correlation of 0.1. The PDFs for the different climate-forcing terms are shown in Figure 36. Using this methodology, the individual forcing terms are combined to estimate the overall error shown in the total climate-forcing error bar in Figure 35 and the PDF (black line) shown in the bottom panel of Figure 36. The bottom panel also shows subgroups of terms from which the least certain terms are excluded in order to highlight the role of uncertainty in the best estimates. In this assessment, we include all these uncertain terms in our best estimate of the total climate forcing of BC, acknowledging that they add large uncertainty.

[656] Our assessment is that the overall climate forcing for BC is more positive and more uncertain than that from the direct radiative forcing alone (i.e., comparing red and solid black PDFs in the bottom panel of Figure 36). Introducing additional cloud forcing terms increase both the median and spread of climate forcing. Principal results from this uncertainty analysis combined with those in sections 6, 7, and 8 are as follows:

[657] 1. Radiative forcing from the BC direct effect is +0.71 W m^{-2}, with a 90% uncertainty range of +0.08 to +1.27 Wm^{-2}.

[658] 2. The estimate of all-source (i.e., 1750 background plus industrial-era) direct radiative forcing of +0.88 W m^{-2} with a range of +0.17 to +1.48 W m^{-2} is similar to the +0.9 W m^{-2} given by *Ramanathan and Carmichael* [2008].

[659] 3. The globally averaged, industrial-era, total climate forcing from BC is +1.1 W m^{-2} with a 90% uncertainty range of +0.17 to +2.1 W m^{-2}. This distribution gives a 2% chance that the total effect of BC in isolation is actually a cooling effect (negative climate forcing), rather than a warming. It is, therefore, extremely likely (greater than 95% chance) that BC emissions acting alone lead to a present-day overall positive forcing and climate warming. This best estimate of black carbon forcing ranks it as the second most important individual climate-warming agent after carbon dioxide when both direct and indirect effects are included. For comparison, the radiative forcings including indirect effects from emissions of the two most significant long-lived greenhouse gases, carbon dioxide (CO_2) and methane (CH_4), in 2005 were +1.56 and +0.86 W m^{-2}, respectively [*IPCC*, 2007, Table 2.13]. The Monte Carlo procedure produces a central estimate that is slightly different than a simple sum of the forcing terms.

[660] 4. Considering only radiative forcings ignores the changes imposed by rapid adjustments. For BC, all effects need to be considered to get a true representation of the climate forcing. These additional effects are demonstrated in the middle panel of Figure 36, where accounting for many semi-direct effects leads to a more-negative liquid-cloud climate forcing, and accounting for the higher efficacies of BC-in-snow and BC-in-ice forcings leads to a more positive forcing.

[661] 5. While there are large uncertainties in the role of BC effects on clouds, the best estimate of their combined net effect, including the semi-direct effect and cloud droplet inclusions, is +0.23 W m^{-2} with a 90% uncertainty range of −0.47 to +1.0 W m^{-2}. This value is also slightly different than a simple sum of the terms. Therefore, studies that exclude all these cloud effects may have a negative bias in forcing. Many model studies agree that semi-direct and liquid-cloud estimates are negative. However, only a few studies have examined how BC affects cloud absorption and subsequent burnoff, as well as mixed-phase clouds, and these poorly understood effects increase the total positive forcing from +0.65 to +1.1 W m^{-2}. Only one group has estimated the BC forcing effect for ice clouds, indicating that the magnitude could be large but the sign is unknown.

[662] 6. These cloud adjustments also significantly increase the uncertainty in their respective climate forcings and greatly increase the overall large uncertainty in the total climate forcing.

[663] 7. The combined BC on snow and BC on sea-ice effective forcing over the industrial era is estimated to be +0.13 W m^{-2} with a 90% uncertainty range of +0.04 to +0.33 W m^{-2}. The effects of BC on snow and ice is unequivocally a net positive forcing, so any study of BC climate forcing that does not include those effects is biased towards a smaller warming effect.

[664] 8. Uncertainties in cloud forcing are of a different character than uncertainties in direct or snow forcing, and are determined using model diversity rather than the more

rigorous method of identifying governing factors and propagating uncertainties in those factors.

[665] The IPCC Fourth Assessment Report only considered radiative forcing of BC and did not consider its total climate forcing [*Forster et al.*, 2007]. IPCC estimated a 1750-to-2005 fossil fuel BC direct radiative forcing of $+0.2 \pm 0.15$ W m^{-2}, somewhat lower than our direct-forcing estimate of BC from fossil fuel of only +0.29 W m^{-2}. IPCC did not explicitly evaluate the direct forcing of other sources of BC, including biofuel combustion. *Forster et al.* [2007, Table 2.13] lists the direct radiative forcing values for "anthropogenic" BC as obtained from published studies and AeroCom models, which together yield an average of +0.34 W m^{-2} (+0.09 to +0.59 W m^{-2} range). This value is smaller than the best estimate found here of +0.71 W m^{-2} (+0.08 to +1.27 W m^{-2} range). The evolution of forcing estimates between the IPCC tabulation and the present assessment is explained as follows:

[666] 1. Some of the studies in the IPCC tabulation used relatively larger emission estimates. Forcing adjusted to a common bottom-up emission inventory would be lower, as reflected in the reported AeroCom average of +0.27 W m^{-2}.

[667] 2. AAOD and, hence, forcing increase by about 50% when the change in MAC_{BC} due to internal mixing is considered. Applying this correction to the IPCC value would give +0.41 W m^{-2}.

[668] 3. The apparent BC burden in the atmosphere is greater than that in the models. The adjustment required to match industrial-era observations, even after the consideration of increased MAC_{BC}, is an additional factor of 1.9, giving +0.77 W m^{-2}. This value is similar to the +0.84 average in Table 15 but not identical because it is not based on the same models.

[669] 4. The estimated model-average forcing was decreased by 15% to account for the fact that models place BC too high in the atmosphere. This adjustment to the IPCC estimate gives a radiative forcing of +0.65 W m^{-2}.

[670] 5. The remaining difference between the scaled IPCC value of +0.65 W m^{-2} and our direct-forcing estimate of +0.71 comes from the inclusion of model results published since the last IPCC report.

[671] 6. The higher value of forcing presented here is supported by observations of increased MAC_{BC} and underestimated atmospheric absorption. Therefore, our estimate is more robust than the purely model-based estimate in IPCC.

[672] Caution is required when considering total, global-average forcing as the sole metric for expressing the impact of BC emissions on climate change. The climate forcing of BC, and all aerosols, is much more regionally variable than for long-lived GHGs, and this metric does not relate to expected precipitation changes (section 9). These factors may affect the consideration of how BC would be included in climate mitigation strategies (section 13).

[673] The equilibrium surface temperature change associated with the BC climate forcing can be estimated by multiplying the forcing values with estimates of climate sensitivity. *IPCC* [2007] estimated a 5 to 95% likely range for equilibrium warming from a $2\times CO_2$ change of 2.0 to 4.5K. Using a $2\times CO_2$ RF of 3.7 W m^{-2} [*Forster et al.*, 2007] gives a climate sensitivity range between 0.54 and 1.22K W^{-1} m^2. Combining errors of sensitivity in quadrature with the industrial-era total climate-forcing range for BC leads to an equilibrium warming for global mean temperature in the range of 0.1 to 2.0K. This temperature change has not been realized in the present day as the Earth system takes more than a century to reach equilibrium, and many co-emitted species counter the warming of BC. For comparison, the estimated equilibrium warming from the combined effects of all short-lived species from BC-rich sources is between −1.5 and 1.4K.

11. Net Climate Forcing by Black-Carbon-Rich Source Categories

11.1. Section Summary

[674] 1. The net climate forcing of emissions from BC-rich source categories or individual source types depends on the effects of co-emitted species, such as organic carbon, sulfate, and gaseous constituents in addition to all effects of BC.

[675] 2. We use previously developed forcing-per-emission values to provide a comprehensive estimate of forcing from BC-rich source emissions. As for BC, large uncertainties are introduced in estimating cloud effects of co-emitted aerosols and aerosol precursors.

[676] 3. Attribution of direct forcing and cryosphere changes to emitting sources is relatively straightforward. For these effects, net forcing is positive for all BC-rich source categories.

[677] 4. Attribution of forcing by cloud changes and nitrate formation to emitting sources is uncertain because effects on cloud droplets are nonlinear and complex. When this indirect forcing contribution is included, using a simple linear proportionality to emission rate, net climate forcing becomes neutral to negative for all source categories except diesel engines and, with greater uncertainty, some residential solid fuel.

[678] 5. Source categories are often heterogeneous. Individual sources within each category have different profiles of chemical emission components and may have relatively more positive or more negative forcing than the category average might indicate.

[679] 6. Our best estimate of the net climate forcing in the first year after emission from BC-rich sources is −0.06 W m^{-2} with 90% uncertainty bounds of (−1.45, +1.29) W m^{-2}. This net forcing would be +0.22 with a range of (−0.50, +1.08 W m^{-2}) if open burning emissions, which emit high levels of organic matter, were excluded. These values include all effects lasting less than one year, including those from aerosols and short-lived gases.

[680] 7. For most of these source categories, short-lived species have substantial forcing in the first year after emission, and this forcing is significant in comparison with forcing by emissions of all species over longer time scales. When climate forcing by all co-emitted species is integrated over 100 years, the magnitude of integrated forcing by short-lived species from each source category ranges from 5 to 75% of forcing by longer-lived species, including CH_4 and CO_2. The sign of short-lived species can be either positive, enhancing GHG warming, or negative.

[681] 8. Integrating net forcing by aerosols, O_3, CH_4, and CO_2 masks complex spatial patterns in forcing that differ over time. Climate forcing through effects on the CH_4 system tends to offset some of the effects of short-lived species. For diesel engines, longer-term negative forcing via NO_x

offsets short-lived positive forcing; for biofuel sources, longer-term positive forcing via organic gases offsets short-lived negative forcing that is largely attributable to cloud effects.

[682] 9. Reduction of aerosol concentrations by mitigating BC-rich source categories would be accompanied by small to no changes in short-term climate forcing. In contrast, mitigation of other aerosol sources would increase positive short-term climate forcing. All aerosol that is emitted or formed in the lower atmosphere adversely affects public health, so mitigation of most BC-rich source categories offers a method of reducing health impacts with lower risk of adverse effects on climate.

11.2. Introduction

[683] Until this point, we have focused entirely on how BC affects radiative and climate forcing. However, BC is never emitted in isolation. Changes in source magnitudes affect all emitted species, whether those changes are deliberately chosen for mitigation, or occur without intention. Estimates of climate changes caused by BC forcing alone were summarized in the previous section, but those values do not reflect the net climate effect of altering sources whose emissions contain high concentrations of BC (i.e., BC-rich sources).

[684] In this section, we estimate the net climate forcing of emissions from BC-rich sources, considering the major emitted species. Some species that make minor contributions to mass have been ignored. In order to provide the net climate forcing by these sources, estimates of forcing by other species that are co-emitted with BC are also required. As in the presentation for BC, we require consideration of all effects. However, this assessment does not include recommendations for climate forcing by other species and we rely mainly on previous published summaries for these values. Therefore, the resulting quantification should be viewed cautiously. Although accounting for forcing by co-emitted species is fraught with uncertainty, ignoring these effects may convey a mistaken impression about the magnitude or even the sign of net climate forcing by BC-rich sources.

[685] We first discuss the approach to estimating net forcing values for a particular source activity. In section 11.3, we describe methods to estimate forcing-per-emission values for each co-emitted species. Then, in section 11.4, we estimate the net climate effect of the BC-rich source categories summarized in section 4. These categories are aggregates of many individual source types, such as certain types of diesel engines or cooking stoves, whose emission component profile may differ from that of the aggregate category. Estimates of forcing for a few of these individual sources are summarized in section 11.5. In these first sections, we present only forcing by short-lived species (i.e., those with lifetimes less than one year). This near-immediate forcing is attributable primarily to aerosols, their precursors, and emitted O_3 precursors. In section 11.6, this forcing in the very short term is compared with GHG forcing on decadal scales.

11.3. Approach to Estimating Forcing From BC-Rich Source Categories

[686] Determining the net change in climate forcing per change in emission or per change in activity is the goal of this section. This quantitative measure may be thought of as the slope of a curve representing forcing versus activity, at present-day conditions. A fully comprehensive measure would aggregate all effects caused by all emitted pollutants from a particular source. Previous work on this topic has estimated the influence of a particular source either by summarizing direct forcing by all pollutants [*Fuglestvedt et al.*, 2010], or by examining the influence of all pollutants from source sectors with a model that represents multiple climate mechanisms [*Jacobson*, 2004a; *Unger et al.* 2010].

[687] Missing in these progressive studies are systematic methods for incorporating scientific uncertainties, for incorporating findings from other studies that may differ, or for altering findings as knowledge advances. Here, we present the foundations of such a framework. Its essential elements are expert recommendations of the following for each chemical species emitted from a source:

[688] 1. Emission factors for a source activity;

[689] 2. Central values and uncertainties for the radiative forcings, obtained for a defined emission rate;

[690] 3. Central values and uncertainties for rapid adjustments, fast enough to be considered as part of a climate forcing, normalized to a defined emission rate.

[691] We begin with a source activity that emits I pollutants. Each pollutant may have J effects that are best expressed as radiative forcing values, and K effects that are expressed as rapid adjustments. To a first approximation, total climate forcing CF (in W m^{-2}) caused by an emission category (such as diesel), summed across all species emitted, is

$$CF = \sum_{i=1}^{I} EF_i \left(\sum_{j=1}^{J} rforc_{i,j} + \sum_{k=1}^{K} fresp_{i,k} \right) \tag{11.1}$$

where FC is fuel consumption by the activity in kg s^{-1}, and EF_i is the emission factor of pollutant i (kg pollutant (kg fuel)$^{-1}$). The bracket contains forcing terms: $rforc_{i,j}$ is the change in radiative forcing for effect j and species i per emission rate of species i ((W m^{-2}) (kg s^{-1})$^{-1}$), and $fresp_{i,k}$ is the rapid adjustment for effect k and species i given in the same units. Each effect must be carefully distributed among the summations to avoid double counting. Further, this calculation assumes that forcings are additive. Although slight variants of the units given here are used in this section, the principle remains the same.

[692] Ideally the value $rforc_{i,j}$ would be determined as:

$$rforc_{i,j} = \left. \frac{\partial f_j}{\partial e_i} \right|_{PD} \tag{11.2}$$

[693] where f_j is the forcing via mechanism j, e_i is the emission of species i, the notation PD indicates present day, and the partial derivative indicates that no other effects are operating and all other species are held constant. The same is true for the rapid adjustments. In practice, models usually provide total forcing or anthropogenic forcing, not partial derivatives. The assumption of linearity with respect to emission rate is adequate for many of the effects discussed here, but it breaks down for cloud microphysical forcings, as noted in the last section. Incremental changes in emissions are more realistic than removal or addition of entire source categories or pollutant categories. Model studies examining smaller emission changes may clarify whether

Table 27. Basis for Estimates of Climate Forcing by Co-Emitted Species

Climate Forcing Term	Forcing Type	Section Where Discussed	Basis for Best Estimate and uncertainty Range	LOSU[a]
Direct effect	Radiative forcing	11.4.1	Multiple-model ensemble of forcing by sulfate and organic matter; some constraint of overall aerosol effect with observations	High
Liquid cloud effect	Adjusted forcing	11.4.2	Subtract BC liquid-cloud effect from total liquid-cloud effect; partition remainder among atmospheric mass (see text)	Low
Semi direct effect	Rapid adjustment	11.4.3	Possible small absorption by OA ignored; other co-emitted species do not absorb light. No changes in thermal structure induced.	High
Mixed phase cloud effect	Adjusted forcing	11.4.3	Assumed no effect	Very low
Ice cloud effect	Adjusted forcing	11.4.3	Assumed no effect because OA and sulfate are not good ice nuclei	Very low
BC-in-snow effect	Effective forcing[b]	11.4.4	Many have no light absorption; therefore no changes in snow albedo. OA estimated based on measured fraction of absorption due to non-BC constituents.	High (sulfate) Medium (OA)
BC-in-sea-ice effect	Effective forcing	11.4.4	Many have no light absorption; therefore no changes in snow albedo. OA estimated based on measured fraction of absorption due to non-BC constituents.	High (sulfate) Medium (OA)
Gaseous species	Radiative forcing	11.4.5	Forcing per emission from review paper; regional differences not considered	Medium

[a]LOSU = level of scientific understanding.
[b]Effective forcing is the sum of radiative forcing and rapid adjustment.

total forcing divided by emission rate produces reasonable estimates for $rforc_{i,j}$ or $fresp_{,j}$.

[694] Two other challenges in applying equation (11.1) are interactions between species that affect forcing nonlinearly [*Stier et al.*, 2006a], and dependence of forcing on the region of emission [*Berntsen et al.*, 2006; *Naik et al.*, 2007; see section 12]. We acknowledge that further development of equation (11.1) should provide a method to account for these dependences. For the analysis here, we use total forcing divided by emission to approximate $rforc_{i,j}$ and $fresp_{i,j}$ for BC and all co-emitted species.

11.4. Climate Forcing Per Emission for Co-Emitted Aerosols and Precursors

[695] Earlier sections of this assessment examined climate forcing by BC only. As discussed previously, we rely mainly on previous published summaries and analyses for forcing values of co-emitted species and have not evaluated the rigor of these estimates. Table 27 summarizes the basis for our best estimates of forcing per emission for sulfate and organic matter, for all effects that were previously given for BC, and the values used are given in Appendix C (Table C1). The following subsections give more detail about the values chosen.

11.4.1. Direct Effect for Co-Emitted Aerosol and Precursors

[696] Table 28 summarizes global mean estimates of direct radiative forcing and radiative forcing per emission for primary organic aerosol (POA) from a variety of studies. With little absorption, POA leads to a negative radiative forcing. Radiative forcing by total anthropogenic POA varies widely, from -0.06 to -0.49 W m^{-2}, with the smallest estimate coming from the study with one of the largest emissions. Consequently, the relative diversity in the radiative forcing per unit emission is even greater, with values ranging from -0.8 to -7.4 (μW m^{-2})(Gg yr^{-1})$^{-1}$. This diversity is largely due to uncertainty in the radiative forcing per unit mass, which varies from -24 to -198 W m^{-2} g^{-1}. Differences in radiative forcing per unit mass are more likely caused by assumptions about water uptake or optical properties than by differences in its vertical distribution, as most modeling studies do not represent absorption by OA. For radiative forcing by POA from fossil fuel combustion, estimates of radiative forcing vary from -0.01 to -0.09 W m^{-2}, and the forcing per unit emission varies from -0.4 to -19 (μW m^{-2})(Gg yr^{-1})$^{-1}$, which is somewhat larger than that for total POA. A best estimate for POA radiative forcing per mass emitted with 90% uncertainty bounds is -4 ± 3 μW m^{-2} (Gg yr^{-1})$^{-1}$, with greater magnitudes for POA from fossil fuel combustion (-9 ± 9). With our increased estimate of 81000 Gg yr^{-1} (section 11.5), POA radiative forcing is -0.36 W m^{-2}.

[697] Forcing by light-absorbing organic carbon, known as brown carbon, has not been explicitly considered here, although some of the models listed in Table 28 assume a small amount of absorption. *Park et al.* [2010] estimated that positive forcing by brown carbon over East Asia was about 15% as large as that of BC. *Jacobson* [2001b] calculated forcing of all OA with some absorption and found smaller negative forcing of total OA than when no absorption was assumed. *Chung et al.* [2012] assigned about 20% of the carbonaceous aerosol AAOD to brown carbon and estimated

Table 28. Model Results Used to Determine Direct Forcing per Emission for Organic Matter[a]

Model	Reference	Emission (Tg C yr^{-1})		Load (mg m^{-2})	Radiative Forcing (W m^{-2})		NRFmass (W g^{-1})	RF per Emission (W m^{-2})(Tg yr^{-1})$^{-1}$	
		Total POA	FF POA	Total POA	Total POA	FF POA	Total POA	Total POA	FF POA
AeroCom models									
GISS	*Schulz et al.* [2006]	32.5	3.2	1.22	−0.14	−0.03	−115	−0.0043	−0.009
LOA	*Schulz et al.* [2006]	32.5	3.2	1.41	−0.16	−0.04	−113	−0.0049	−0.012
LSCE	*Schulz et al.* [2006]	32.5	3.2	1.50	−0.17	−0.04	−113	−0.0052	−0.012
MPI-HAM	*Schulz et al.* [2006]	32.5	3.2	1.0	−0.10	−0.03	−100	−0.0031	−0.009
SPRINTARS	*Schulz et al.* [2006]	32.5	3.2	1.84	−0.10	−0.01	−54	−0.0031	−0.003
UMI	*Schulz et al.* [2006]	32.5	3.2	1.16	−0.23	−0.06	−198	−0.0071	−0.019
UIO-CTM	*Schulz et al.* [2006]	32.5	3.2	1.12	−0.16	−0.04	−143	−0.0049	−0.012
UIO-GCM	*Schulz et al.* [2006]	32.5	3.2	0.88	−0.06	−0.02	−68	−0.0018	−0.006
Other models									
CAM3	*Bond et al.* [2011]	30	—	—	−0.12	—	—	−0.0040	—
CAM3 ECA	*Kim et al.* [2008]	54.4	—	1.49	−0.19	—	−128	−0.0035	—
GATORG	*Jacobson* [2001b]	73	28	2.55	−0.06	−0.01	−24	−0.0008	−0.0004
LOA	*Reddy et al.*, [2005a, 2005b]	90	7.0	2.33	−0.25	−0.02	−107	−0.0028	−0.003
MOZART	*Ming et al.* [2005]	46	10.1	2.33	−0.34	−0.09	−146	−0.0074	−0.009
SPRINTARS	*Takemura et al.* [2005]	88	14.7	—	−0.49	—	—	−0.0056	—

[a]Global mean emissions of anthropogenic primary organic aerosol (POA) and POA from fossil fuel combustion (FFPOA), mean column burden (load) of POA, mean radiative forcing by total and FFPOA, mean radiative forcing normalized by mean burden (NRFmass), and radiative forcing normalized by emissions. For comparison to emission values in the remainder of the document, 1 Tg = 1000 Gg.

that it had zero forcing rather than negative forcing. A fraction of our BC forcing estimate may in fact be attributable to brown carbon. If brown carbon contributes to atmospheric absorption, its contribution should be removed from the estimate of BC AAOD that is based on observations. The net forcing of brown carbon would be a combination of forcing by absorbing aerosol (presently subsumed in BC) and aerosol that is more highly scattering (presently subsumed in OA), and brown-carbon direct forcing would be about zero. Thus, although we have not explicitly isolated the contribution of brown carbon, the total forcing by BC and OA together would remain about the same.

[698] The most recent IPCC report provides a best estimate of -0.4 ± 0.2 W m^{-2} for direct radiative forcing by anthropogenic sulfate [*Forster et al.*, 2007]. Assuming the AeroCom estimate of 109,000 Gg S yr^{-1} [*Dentener et al.*, 2006], this translates to a range of -3.7 ± 1.8 (μW m^{-2}) (Gg yr^{-1})$^{-1}$ for radiative forcing per mass of S emitted. Emissions used here are 96000 Gg S yr^{-1} from the GAINS database, giving -0.35 W m^{-2} direct forcing.

11.4.2. Liquid Cloud Effect for Co-Emitted Aerosol and Precursors

[699] The effect of co-emitted aerosol on liquid clouds has large uncertainties, both because estimates of the total liquid-cloud radiative forcing of anthropogenic aerosol vary widely, and because studies that isolate the contributions of individual pollutants or sources are scarce. (Exceptions are *Jacobson* [2002] and *Bauer et al.* [2010].) We adopt a preliminary approach to estimating changes in liquid-cloud forcing due to co-emitted species, which we describe first before listing several cautions.

[700] Our preliminary estimate of cloud climate forcing assumes that: (1) the liquid-cloud effect using AeroCom emissions has a central value of -0.9 W m^{-2} for the albedo effect and a range of -1.4 to -0.3 W m^{-2}, as summarized by *Isaksen et al.* [2009]; (2) the lifetime effect is negligible, as inferred from comparisons between GCMs and cloud-resolving models [*Wang et al.*, 2012]; (3) the liquid-cloud change in the studies contributing to the estimate is attributable to submicron species that are considered anthropogenic: BC, organic matter, and sulfate; (4) except for BC, the cloud effect may be apportioned among individual species by mass; and (5) the values of forcing per mass so determined can be used to scale to the new estimates of emission. The latter assumption is approximately justified if particle size is the dominant factor determining the number of CCN, because organic matter and sulfate have similar size distributions. Individual studies to determine liquid-cloud forcing may have used different emission rates; in particular, studies prior to the mid-2000s tended to use much higher OM emissions. However, *Quaas et al.* [2009] gave direct plus indirect forcing values of -1.25 W m^{-2} for 10 models even when they used the lower AeroCom emissions.

[701] Details of the liquid-cloud estimate are given in Appendix C (Tables C2 and C3). Indirect forcing using AeroCom emissions is divided as -0.58 and -0.27 W m^{-2} for sulfate and organic matter, respectively. Sulfate is scaled to the total GAINS emission estimate and organic matter is scaled according to the regional BC scaling in Figure 20. Liquid-cloud indirect effect attributable to 96 Tg yr^{-1} of SO_2 emissions is estimated as -0.51 W m^{-2}, with an uncertainty range of -0.21 to -0.76 W m^{-2}. Liquid-cloud forcing

attributable to 81 Tg yr^{-1} of organic matter is estimated as -0.74 W m^{-2} with an uncertainty range of -1.09 to -0.30 W m^{-2}. The apportionment by mass may overestimate negative forcing by organic matter, as its lower solubility has not been considered in the apportionment. However, a relationship with aerosol optical depth, as suggested by *Quaas et al*. [2009], would yield the same apportionment between sulfate and OA.

[702] Our treatment of liquid-cloud effects deserves several caveats. We caution that the liquid-cloud estimate for SO_2 and POA has not undergone a thorough examination as have the effects of BC. We have chosen to present a more realistic but less rigorous picture for net forcing by sources that are BC-rich, rather than a physically unrealistic depiction that evaluates BC alone. Modeling studies rarely examine the validity of apportioning total liquid-cloud effects among individual species, although *Chuang et al*. [2002] showed that cloud forcing per burden differed by less than 15% for sulfate only, carbonaceous aerosol only, and the combination.

[703] The relationship between cloud forcing, CCN, and emissions is not expected to be linear. Cloud forcing is more sensitive to increased particle concentration in a cleaner atmosphere, as demonstrated for global averages by *Boucher and Pham* [2002]. This is consistent with inferences of low indirect effect over land [*Ruckstuhl et al*., 2010]. Therefore, our linear apportionment could overestimate the impact of the small fraction of total particle mass attributable to BC-rich sources.

[704] Studies disagree on the importance of primary particles, and the relationship between cloud forcing and the emission of primary particles such as BC or POA may not even be monotonic. One study indicates that primary particles play a larger role in cloud formation than other particles [*Adams and Seinfeld*, 2003], while others find that primary emissions suppress nucleation [*Bauer et al*., 2010], and therefore have a much lower influence on CCN than would be expected in the absence of gas-particle interactions [*Merikanto et al*., 2009].

[705] The discussion above indicates that the linear apportionment used here is a zero-order estimate. Yet, present understanding is insufficient to support a different apportionment. Although there is some evidence that forcing-per-emission values may be overestimated, models that account for microphysical interactions [*Bauer et al*., 2010; *Koch et al*., 2011a] have indicated greater forcing-per-emission of POA via liquid-cloud changes than our central value. The uncertainties given here reflect only the uncertainty in the magnitude of the indirect effect, not the uncertainty in apportionment, or regional differences in cloud behavior.

11.4.3. Other Cloud Effects for Co-Emitted Aerosol and Precursors

[706] Other cloud effects (i.e., mixed-phase, ice-cloud, and semi-direct effects) considered for BC are assumed negligible for sulfate and organic matter. These two species may influence water condensation and ice nucleation activity if they are emitted with BC (sections 3.9 and 7.5). This is particularly relevant for cold ice clouds, where BC particles do not become water droplets prior to ice formation. In this case, it is not possible to separate or scale cloud effects from the amount of co-emitted species. Two GCM studies [*Hoose et al*., 2008; *Storelvmo et al*., 2008] suggest that sulfate coating decreases the ability of mineral dust to act as IN. This increases the lifetime of supercooled water clouds, producing negative forcing. These effects have not yet been quantified and are not included here.

[707] In current understanding, aerosols with minimal light absorption have little effect on semi-direct forcing. All such changes are caused by light absorption that heats the atmosphere at various vertical locations (Figure 24). We also do not include the effects of other absorbing material within cloud droplets, although absorbing OA may also contribute to enhanced cloud-droplet absorption [*Jacobson*, 2012]. As an approximation, we have captured the effect of absorbing aerosol by attributing all non-dust AAOD to BC and calculating all effects for that AAOD.

11.4.4. Snow Albedo Forcing for Co-Emitted Aerosol

[708] *Doherty et al*. [2010] found that the light-absorbing aerosol in Arctic snow and sea ice had a strong wavelength dependence, and inferred from this the amount of light absorption due to BC versus other species, specifically brown carbon, mineral dust and soil dust. They reported that 40% of the spectrally weighted light absorption in snow and sea ice is due to these non-BC constituents. Because our estimate of snow albedo forcing was scaled to observations of BC, not of absorbing aerosol, total forcing must be increased to account for additional absorbing material. Only a small fraction of this absorption is due to mineral and soil dust, so we estimate global snow and sea-ice forcing by organic matter from combustion as 20% that of BC. We then scale this value to emissions of organic matter to produce an effective forcing per emission of 0.9 μW m^{-2} (Gg $yr^{-1})^{-1}$ with a range of 0 to 3.0, assuming an efficacy with a central value of 3 and an upper bound of 4. POA from solid-fuel combustion is known to absorb light, while other organic matter is not. Therefore, this forcing was applied only to POA emitted from solid fuel: biofuel, coal, and open biomass burning.

11.4.5. Forcing by Co-Emitted Gaseous Species

[709] Short-lived, co-emitted gaseous species considered here include carbon monoxide (CO), volatile organic compounds (VOCs), and NO_x. These species produce indirect forcing by interacting with tropospheric O_3 and CH_4 and, for NO_x, by producing nitrate. *Fuglestvedt et al*. [2010] summarized studies on radiative forcing by these compounds for the development of metrics. They did not provide recommendations for central values of forcing per emission, but a later study [*Uherek et al*., 2010] used their summary to provide GWP values. We inferred a best estimate of forcing per emission using studies cited by *Fuglestvedt et al*. [2010], as shown in Appendix C (Table C4). For each species, forcing is separated by mechanism, as suggested by *Shindell et al*. [2005]. All species increase O_3, representing a positive forcing that occurs within the first year. NO_x increases nitrate aerosol, giving a negative first-year forcing. These species also alter the lifetime of CH_4, causing forcing that lasts a few decades. CO and VOCs cause a positive forcing, while NO_x causes a negative forcing.

[710] Studies cited in *Fuglestvedt et al*. [2010] gave forcing values for the effects of NO_x emissions on CH_4 and tropospheric O_3 abundances but not for nitrate aerosol resulting from NO_x emission. We estimated a value of forcing per emission by nitrate by assuming that the nitrate forcing summarized by *Forster et al*. [2007] had the same emission base as that for O_3 from NO_x. This method is legitimate for

short-lived species, such as nitrate and O_3 caused by emissions of NO_x or volatile organic compounds. (Present-day forcing values for long-lived species result from all historical emissions that remain in the atmosphere, and cannot be used to estimate forcing per emission.) While *Forster et al.* [2007] attributed all nitrate forcing to NO_x emissions, *Unger et al.* [2010] reported that sectors with substantial ammonia emissions also affect nitrate forcing. The nonlinearity of ammonium, sulfate, nitrate, and NO_x chemistry means that changes in nitrate forcing are difficult to attribute to particular sectors. We assign only 44% of the total nitrate forcing to NO_x emissions, based on the ratio of NO_x-related to total nitrate forcing reported by *Unger et al.* [2010].

11.4.6. Climate Forcing by Secondary Organic Aerosol

[711] Estimating the climate impact of sources using POA alone ignores the complex evolution of organic aerosol throughout the atmosphere. Emitted precursors lead to formation of substantial quantities of SOA [*de Gouw and Jimenez*, 2009]. Oxygenated organic aerosol, thought to be equivalent to SOA, is found wherever measurements are made [*Zhang et al.*, 2007]. SOA yields from diesel engines and wood stoves were estimated to be small in comparison to POA emissions [*Chan et al.*, 2009]. However, observed SOA appears to be much more prevalent than could be explained by models that treat identified SOA precursor molecules [*Robinson et al.*, 2007]. For that reason, mechanisms that account for SOA production have been proposed, using the fraction of emitted vapors with low volatility as inputs [*Donahue et al.*, 2006].

[712] SOA associated with individual sources has not been resolved in climate models. Direct forcing is often provided for POA alone [*Schulz et al.*, 2006], and models of cloud forcing have usually not distinguished POA versus SOA burdens. Simulations by *O'Donnell et al.* [2011] gave a direct effect due to SOA of -0.29 W m^{-2} and an indirect effect of +0.20 W m^{-2}. In this model, which did not include the volatility representation of SOA formation, 90% of the SOA burden came from biogenic sources.

[713] POA : BC ratios may underestimate the total atmospheric OA attributable to each source. Nevertheless, in this analysis, we neglect direct and indirect forcing by SOA. The single estimate of net SOA forcing given above is small, and the chain that relates precursor emissions to concentrations and global forcing is presently limited. We acknowledge, however, that this omission could be a source of bias.

11.4.7. Forcing in Clear and Cloudy Skies

[714] Modeled radiative forcing has been compared with clear-sky and cloudy-sky radiative fluxes observed from space [*Quaas et al.*, 2009; *Lohmann et al.*, 2010]. For that reason, we summarize the clear- and cloudy-sky forcings here. We assume that 30% of BC direct forcing takes place in clear skies [*Zarzycki and Bond*, 2010]. The remainder would be observed in cloudy skies. Clear-sky forcing includes 30% of BC direct forcing (+0.21 W m^{-2}), all OA and sulfate direct forcing, (-0.36 and -0.35 W m^{-2}, respectively), and nitrate direct forcing (-0.16 W m^{-2}) for a total of -0.66 W m^{-2}. Cloudy-sky forcing over liquid clouds includes BC direct forcing in cloudy skies (+0.50 W m^{-2}), BC liquid-cloud forcing including semi-direct effects (-0.20 W m^{-2}), the cloud absorption effect (+0.20 W m^{-2}), and liquid-cloud forcing by OA and sulfate (-0.74 and -0.51 W m^{-2}, respectively) for a total of -0.76 W m^{-2}. It is not clear whether the mixed-phase cloud forcing of +0.18 W m^{-2} would be observed in the analysis of radiances that primarily focus on liquid clouds. *Quaas et al.* [2009] scaled model estimates according to relationships determined from satellite observations to obtain forcing estimates of -0.38 W m^{-2} for clear-sky and -0.70 W m^{-2} for cloudy-sky fluxes. The total forcing estimated here is more negative for clear skies and similar for cloudy skies.

11.5. Net Climate Forcing by BC-Rich Source Categories

[715] Using the values developed in the previous section, total climate forcing by BC-rich source categories can be estimated. Forcing per emission for each effect in W m^{-2} (Gg yr^{-1})$^{-1}$ is multiplied by total emissions, yielding units of W m^{-2}. Forcings by each species emitted within each category are then summed to provide the total industrial-era forcing representing the net forcing from each category. Annual emissions of BC, POA, SO_2, CO, non-methane volatile organic compounds (NMVOCs), and NO_x from each source category were summarized from the GAINS database for the year 2000 for energy-related emissions. Open burning estimates come from the RETRO database. Emissions were adjusted to reflect the observationally based scale factors given in section 6.7, so that energy-related emissions were scaled by factors of 1.1 to 2.5, depending on the category, and open-burning estimates were increased by a factor of about 1.5. Emission rates used are given in Appendix C (Table C5). For energy-related burning, we have assumed that the most uncertain factor is levels of activity with relatively high emission rates, and have adjusted those emissions associated with incomplete combustion (BC, POA, CO, NMVOC) with the scale factors used for BC. For open biomass burning, we assume that the cause of the uncertainty could be the low bias in emission factors of particulate matter (section 4.7.2.3) and adjust BC and OA emissions. Only the effects of POA are included here; some of the gaseous NMVOCs from these sources could form SOA after emission, adding to aerosol-driven forcing mechanisms. This possibility is discussed in section 11.4.6.

[716] Figure 37 shows forcing by short-lived emissions in the BC-rich source categories summarized in Figure 8. These categories comprise 99% of the BC emissions, and the climate forcing includes all aerosol direct, indirect, and snow effects. We also include forcing changes caused by the interaction of CO, VOCs and NO_x with tropospheric O_3. These effects capture most of the forcing that occurs in the first year after emission.

[717] The forcings shown in Figure 37 result from the same treatment as applied in *Forster et al.* [2007]: that is, the values are those that would be observed if year-2000 emission rates continued indefinitely. It differs from IPCC figures because forcing is grouped by source category instead of by species, and because it gives total climate forcing values instead of direct forcing. The species chosen for this figure exert their forcing entirely within the first year after emission. Other emitted species or effects that act over longer time scales are discussed in section 11.7. We have not included effective forcing due to vegetation changes [*Collins et al.*, 2010].

[718] The top bar in Figure 37 shows the forcing components that can be attributed to emissions with high

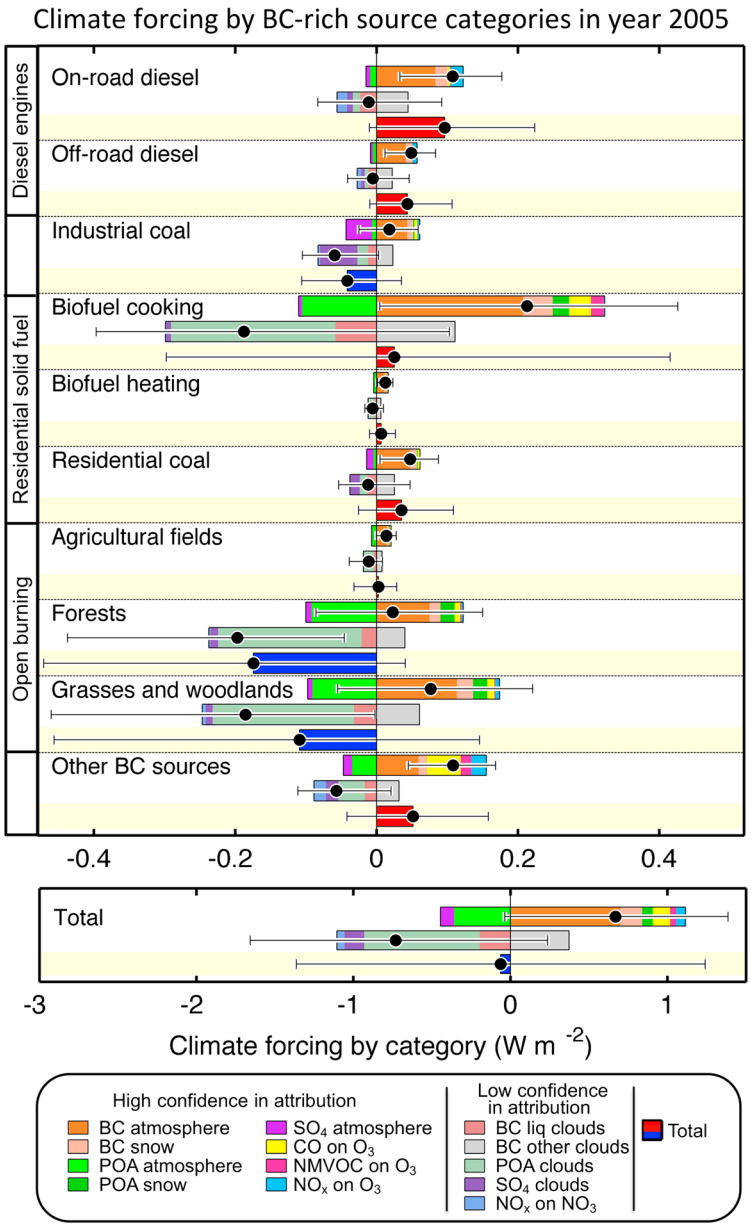

Figure 37. Total climate forcing for BC-rich source categories continuously emitting at year-2000 rates scaled to match observations in 2005. Three sets of climate forcings are shown for each source as bars with a best estimate (black circle) and uncertainty range. The top bar contains the components for which attribution to particular species is straightforward: direct forcing by aerosol and most gases, and cryosphere forcing by aerosol (including climate feedback). The second bar shows the components for which there is less confidence in apportionment to individual species and, therefore, to sources. These components include all cloud indirect effects and forcing by nitrate from NO_x. Effects of BC on liquid clouds include the cloud albedo and semi-direct effects. Other BC-cloud forcings represent the effects of cloud absorption, mixed-phase clouds, and ice clouds. The bottom bar in each group shows estimated net climate forcing by each emission source, combining all forcings and their uncertainties.

confidence: direct forcing by aerosol and gases, effective cryosphere forcing, and cloud response to aerosol absorption. Attribution of liquid-cloud forcing to individual aerosol species or to particular sources is not well developed. We therefore segregate these forcing terms in the second (middle) bar, for which we have less confidence in attribution. The combined liquid-cloud effect, including the albedo and semi-direct effect, is separated from cloud effects that have larger uncertainties and were derived in fewer studies: the cloud absorption effect, the mixed-phase cloud effect, and the ice-cloud effect. Also included in this low-confidence bar is the negative forcing due to nitrate aerosol. The bottom bar shows estimated net forcing by each emission source, or the combination of high-confidence and low-confidence components.

[719] Uncertainties in aerosol forcing only, as discussed throughout this assessment for BC and in earlier sections for other aerosol species, are reflected in Figure 37. Uncertainties in emission factors and gaseous forcing are also

important and are not represented here. A bar centered on the zero line means that forcing has equal probability of being positive or negative; a bar that barely crosses the zero line means that there is a slight uncertainty that the forcing has a different sign than the central estimate. In combining uncertainties, most of the effects are assumed to be independent. However, the best estimates and uncertainties for the effects of individual aerosol species on liquid clouds were derived by a simple subtraction. These cloud uncertainties are assumed to be fully correlated with each other.

[720] As the top bars in Figure 37 demonstrate, the net effect of direct and cryosphere forcing by aerosols and gases is positive with high confidence for many source categories. Inclusion of cloud forcing components (middle bar for each source) makes forcing more negative and increases uncertainty, especially when sources have comparatively large emissions of other aerosols or precursors. Cloud forcing also increases uncertainty in the sign of net forcings (lowest bar for each source). This simple apportionment is subject to several uncertainties, as detailed in section 11.8.

[721] Positive and negative forcing components and sources of uncertainty differ among source categories, as discussed in more detail below. We also compare the values in Figure 37 with the few studies that have examined the total impact of economic sectors. This comparison must be interpreted in light of the fact that BC-rich source categories differ from total sectors.

11.5.1. Diesel Engines

[722] Forcing that can be easily attributed to diesel emissions is positive with high confidence. Both cloud and nitrate forcing reduce the net forcing and increase uncertainty.

[723] BC is a large fraction of aerosol emissions from both on-road and off-road diesel engines. The relative impact of organic matter is low, and negative forcing in the high-confidence category comes primarily from the semi-direct effect. In the low-confidence group, negative cloud forcing, attributable to sulfur, approximately cancels the net positive cloud forcing by BC. This impact is greater in regions where low-sulfur fuel has not been mandated.

[724] In *Unger et al*. [2010], total cloud effects (including semi-direct effects) from all on-road engines are strongly positive and greater than one-half the direct BC forcing. *Bauer et al*. [2010] find that diesel emissions give positive cloud forcing equal to the direct forcing, but this study did not include sulfur emissions. *Jacobson* [2010] found a net decrease in cloud optical depth attributable to total fossil fuel BC, OA, and sulfur, although this study examined the effect of only primary sulfur and aerosol components in order to examine the effect of end-of-pipe particulate controls. The effects of sulfur dioxide co-emitted from diesel engines were not examined.

[725] Negative forcing by nitrate is also substantial in comparison with other forcing mechanisms, in agreement with *Unger et al*. [2010]. Neither *Bauer et al*. [2010] nor *Jacobson* [2010] considered changes in NO_x emissions.

11.5.2. Industrial Coal

[726] Like diesel engines, industrial coal emissions (mostly from small industry) have a relatively large BC component and a small POA component. These emissions also include substantial sulfur, which causes negative forcing for both direct and cloud categories. These strong negative forcings agree with the results of *Unger et al*. [2010].

11.5.3. Residential Solid Fuel

[727] Direct and snow forcings that are easily attributable to residential biofuel (top bar) are also strongly positive. Although POA-to-BC ratios are higher than for diesel engines, negative direct forcing by POA counteracts only about 20% of the BC direct forcing. This negative forcing would be greater if secondary organic aerosol was included here, but it still would not cancel BC forcing. In addition, absorption by OA deposited on snow and changes in tropospheric O_3 due to carbon monoxide and VOC add to positive forcing.

[728] Because these sources also emit POA, however, large negative forcing due to liquid-cloud interactions is predicted and introduces very large uncertainty. With our simple apportionment, these cloud changes are sufficient to make the net forcing near zero. NO_x emissions are low for these sources, so NO_x effects on either O_3 or nitrate forcing play very little role.

[729] A critical question is whether the cloud response due to residential solid fuels offsets the strong positive direct forcing. Models tend to agree that cloud interactions add some negative forcing for these sources, but they disagree on the magnitude. *Unger et al*. [2010] report a positive indirect effect, citing the portion of the semi-direct effect that burns off clouds, but without using aerosol microphysics. *Bauer et al*. [2010] added aerosol microphysics to the same GCM used by *Unger et al*. and found net negative cloud forcing three times greater than the positive direct forcing by BC. *Jacobson* [2010] shows increased cloud optical depth due to biofuel-burning emissions (including gases), but also finds a positive ToA forcing and a warming, suggesting that the cloud changes do not overwhelm the direct forcing. This study also includes ionic components of biofuel-burning emissions that affect water uptake and climate response.

[730] Residential coal emits more BC compared to POA than do residential biofuels. The sulfur-to-BC ratio is much higher than for residential biofuels, and much lower than for industrial coal. This category has net positive direct forcing mainly attributable to BC, and net negative cloud forcing mainly caused by sulfur. The result, with low certainty, is a slight net positive forcing.

11.5.4. Open Biomass Burning

[731] All three categories of open biomass burning emissions contain large POA fractions. As with residential solid fuel, the direct forcing by POA emissions does not fully counteract BC forcing, and forcing via O_3 has a substantial positive contribution. Once again, POA interaction with clouds is responsible for the large negative forcing, and large uncertainties. *Unger et al*. [2010] agree that cloud changes are large and negative. They also simulate a small negative nitrate forcing and a much larger POA direct forcing than calculated here.

11.5.5. Summary of BC-Rich Source Categories

[732] For almost all source categories, net forcing that is easily attributable to individual species (i.e., without clouds and nitrate) is positive with high confidence; that is, the lower limit of uncertainty is well above zero. Categories that emit relatively large quantities of sulfur are exceptions.

[733] The inclusion of forcing via clouds and nitrate makes the estimated impact of each category more negative and

greatly increases the uncertainty. The origins of this negative, uncertain forcing differ among source categories. Sulfate effects on clouds are the primary cause for both residential and industrial coal. For diesel engines, the possible negative forcing comes from nitrate and cloud interactions with sulfate. Interactions between organic matter and clouds are the main source of uncertainty for residential biofuel and open biomass burning.

[734] Confidence in positive net forcing is highest for categories with relatively small quantities of co-emitted aerosols or precursors, such as diesel engines. Except for industrial coal, other energy-related combustion sources have a high probability of producing either positive or negative forcing. These source categories are quite heterogeneous, as discussed further in section 11.6, so that individual emitters may still have net positive forcing.

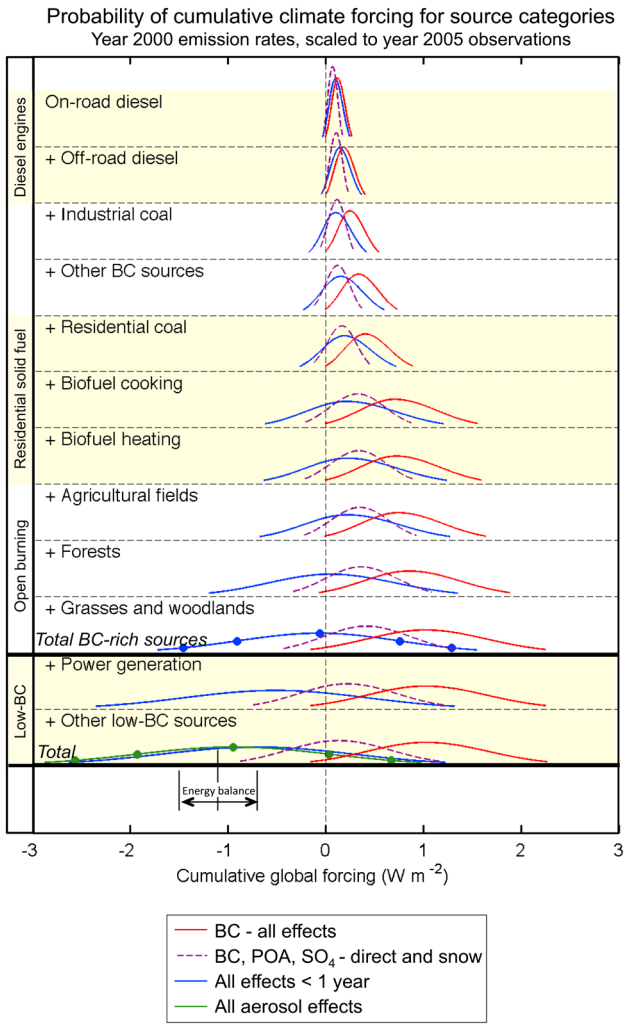

Figure 38. Probability density functions for total climate forcing of short-lived species during the first year after emission by the source categories in Figure 37. Sources emit continuously at year-2000 levels, scaled to match atmospheric concentrations in 2005. Curves labeled "BC-all effects" (red lines) show all effects attributable to BC, including cloud effects. Curves labeled "BC, POA, SO_2" (purple lines) show direct and snow effects for the most commonly considered aerosol species and precursors. Total climate forcing (blue lines) is the sum of first-year forcings by all effects due to BC and co-emitted species, including clouds, gaseous species, and nitrate forcing. Progressing from top to bottom, each curve represents forcing by the sum of the labeled category and all categories above it. The total value and its uncertainty from BC-rich sources and co-emitted species are reproduced as the bottom bar in Figure 35. The lowest set of curves labeled "Other low-BC sources" represents the total effect of aerosol sources. The arrow labeled "energy-balance" represents the central value and one standard deviation of total aerosol forcing from an energy-balance calculation [*Murphy et al.*, 2009]. The curve labeled "All aerosol effects" (green line) excludes gaseous species but includes all other aerosol effects, so is most directly comparable to the energy-balance inference. All curves have identical vertical scales and are normalized to unity. Blue dots on total curves represent central values, 68% confidence intervals (1 σ), and 90% confidence intervals (1.65 σ). Values outside of 95% confidence intervals are not plotted, so the curves do not meet the zero line.

11.5.6. Cumulative Sum of Forcing by BC-Rich Source Categories

[735] Figure 38 demonstrates the fact that BC forcing results from an aggregate of multiple sources by presenting the cumulative sum of source-category forcing from top to bottom. For example, the values listed for "Industrial coal" are the forcing by industrial coal, on-road diesel and off-road diesel. This figure shows probability density functions for total climate forcing by BC alone (red line), for direct forcing by BC and all co-emitted species including organic matter and sulfate (purple line), and by all these species plus the forcing due to cloud changes (blue line). The highest point of each curve is the most likely value. The curve labeled "Other BC sources" is the sum of all categories in Figure 37 and matches the total net forcing in Figure 35. In addition, Figure 38 includes forcing by emissions from two other source groups that emit large quantities of aerosols or precursors, but little BC (less than 1% of the global total).

[736] Figure 38 repeats some messages that appear in Figure 37. The best estimate of BC-only forcing is positive with high confidence, even when cloud forcing is considered. The best estimate of direct and snow forcing by BC and co-emitted species is also positive. However, when cloud forcing is considered, the best estimate of first-year forcing from many categories is only slightly positive because of the counteracting effects of co-emitted species. The figure also emphasizes the important distinctions between source categories. More than half the BC forcing in the aerosol mixture (red line in Figure 38) comes from diesel engines, industrial coal, and residential solid fuels (first six categories). These positive forcings are accompanied by negative direct and cloud forcings that result in climate forcing that is close to neutral (blue line in Figure 38). The remaining BC forcing comes from open burning, and it is accompanied by larger negative forcing. The thick black line separates BC-rich sources from others. The cumulative sum of forcing for the sources above that line is -0.06 W m^{-2} with 90% uncertainty bounds of (-1.45, $+1.29$ W m^{-2}). This total corresponds to the bars in Figure 35, which indicate the net climate effect of BC and co-emitted species. The total of all BC-rich sources excluding open biomass burning (i.e., energy-related sources) is $+0.21$ W m^{-2} (-0.50, $+1.08$ W m^{-2}). This value is similar to the forcing estimate for energy-related emissions of BC and OA by *Kopp and Mauzerall* [2010]. However, this agreement is somewhat coincidental, as our estimate also includes direct and indirect sulfate forcing, semi-direct effects, cloud absorption, and mixed-phase and ice cloud effects. For that reason, our uncertainty is much greater than the *Kopp and Mauzerall* [2010] range of ($+0.02$, $+0.37$ W m^{-2}).

[737] The bottom two source categories in Figure 38 are power generation and a conglomeration of other low-BC sources. These categories emit very low BC amounts but are rich in sulfur and organic matter, and produce most of the net negative aerosol forcing. Including these two categories, forcing by aerosols, short-lived gases, and cloud changes is -0.70 W m^{-2} with 90% uncertainty bounds of (-2.32, $+0.91$ W m^{-2}). Thus, most of the net negative forcing is confined to source categories that are not BC rich. All aerosol that is emitted or formed in the lower atmosphere adversely affects public health, so mitigation of most BC-rich source categories offers a method of reducing health impacts with a lower risk of increasing positive climate forcing.

[738] The green line in the bottom category shows the probability distribution due to aerosol sources alone, excluding short-lived gases. The total is -0.95 W m^{-2} with 90% uncertainty bounds of (-2.57, $+0.67$ W m^{-2}). The central value is slightly less negative than forcing estimated using an energy-balance approach and relying on observations [*Murphy et al.*, 2009]. However, our forcing estimate, which draws on ranges of modeled values, has much greater uncertainty bounds both above and below the central estimate than does the forcing estimate based on observations. It is possible that the broad uncertainty range from indirect effects is overstated.

11.6. Climate Forcing by Selected Sources

[739] Figure 37 presents the magnitude of net forcing by sources in each category, emphasizing the sources with largest activities. These aggregated source categories are not homogeneous, but are made up of individual sources with different chemical emission profiles and rates. In Figure 39, we show forcing by individual sources that are contained within the major emitting categories. To do so, we obtain values for climate forcing per mass of fuel burned by multiplying emission factors (given in Table C6), in mass of pollutant per mass of fuel burned, by the same forcing-per-emission values used for Figure 37 (Tables C1 and C4). Figure 39 shows total climate forcing per source activity, or quantity of fuel burned, emphasizing the difference in emission rates within categories. Sources with higher emission factors for a particular pollutant—usually those with the poorest combustion—have larger climate forcing per fuel burned. These sources are often easier or less expensive to mitigate (section 13). This presentation contrasts with Figure 37, which accentuates categories with large total emissions.

[740] The units of forcing in Figure 39 differ from those in Figure 37 and the standard treatment by IPCC because continuous emissions are not assumed. Instead, the forcing caused by consuming one kg of fuel is integrated over time to give units of (μW m^{-2} yr) (Gg fuel burned)$^{-1}$. This difference is necessary because individual sources are unlikely to continue in perpetuity. However, the species or effects included in this figure have short atmospheric lifetimes, and this forcing occurs entirely during the first year after emission. For this reason, the values in this figure would be the same whether they represented continuous forcing for constant emissions, with units of μW m^{-2} (Gg fuel yr^{-1})$^{-1}$, or integrated forcing from finite consumption, with units of μW m^{-2} yr (Gg fuel)$^{-1}$. Likewise, the values in Figure 37 could represent integrated emissions from the year 2000, with units of W m^{-2} yr.

[741] As in Figure 37, the top bar for each source includes direct forcing by aerosol and gases, cryosphere forcing, and cloud response to aerosol absorption. Other cloud responses and nitrate forcing are given in the middle bar, and the bottom bar shows the total of the two. Uncertainties are calculated in the same manner as for Figure 37 and, again, uncertainties in emission factors are not represented. Similar to the message in Figure 37, the sum of direct, cryosphere and semi-direct forcing by many source types is estimated to be positive. Cloud and nitrate forcing reduce the positive forcing and increase the possibility that the net forcing is negative.

[742] On-road diesel engines are a mix of low-emitting (controlled) engines using low-sulfur fuel and higher-emitting engines implemented in regions with limited regulations. The latter typically use fuel with higher sulfur content. Off-road diesel engines are presently more similar to the high-emitting engines. Modern engines with better combustion emit more NO_x and less PM, as seen in the positive forcing of NO_x on the ozone system. This positive forcing in the first year is counteracted by negative forcing in interactions with methane in later years (section 11.7). In contrast, the positive forcing by less advanced engines is dominated by BC.

[743] As in the category graph in Figure 37, direct and cloud forcing by sulfur are large for both residential and industrial coal sources. Industrial boilers have net negative forcing, but the high BC emission rates more than balance the negative forcing by sulfur for brick kilns and coal cooking stoves. This forcing is highly dependent on coal sulfur content. For example, the brick kiln emissions used in Figure 39 were measured in India, where sulfur content is low. The same source in a region with high-sulfur coal might have a different net forcing. Sources with poor combustion produce more BC compared with sulfur, and are more likely to have positive forcing.

[744] Wood used in many heating stoves (i.e., conventional wood stoves) produces a higher POA : BC ratio than wood for cooking (i.e., mud cooking stoves), while larger heating technologies (i.e., "wood boiler") can have low POA : BC ratios depending on the operation. This difference is apparent in Figure 39, which indicates a lower cloud impact from a conventional wood stove and a near-zero forcing. On the other hand, the best estimate of cooking stove emissions is net positive forcing, although the uncertainty is high. For this specific cooking type of stove, emission factors were taken from in-field measurements. Its net positive forcing contrasts with the net negative value for the entire source category given in Figure 37. This difference results from the choice of emission

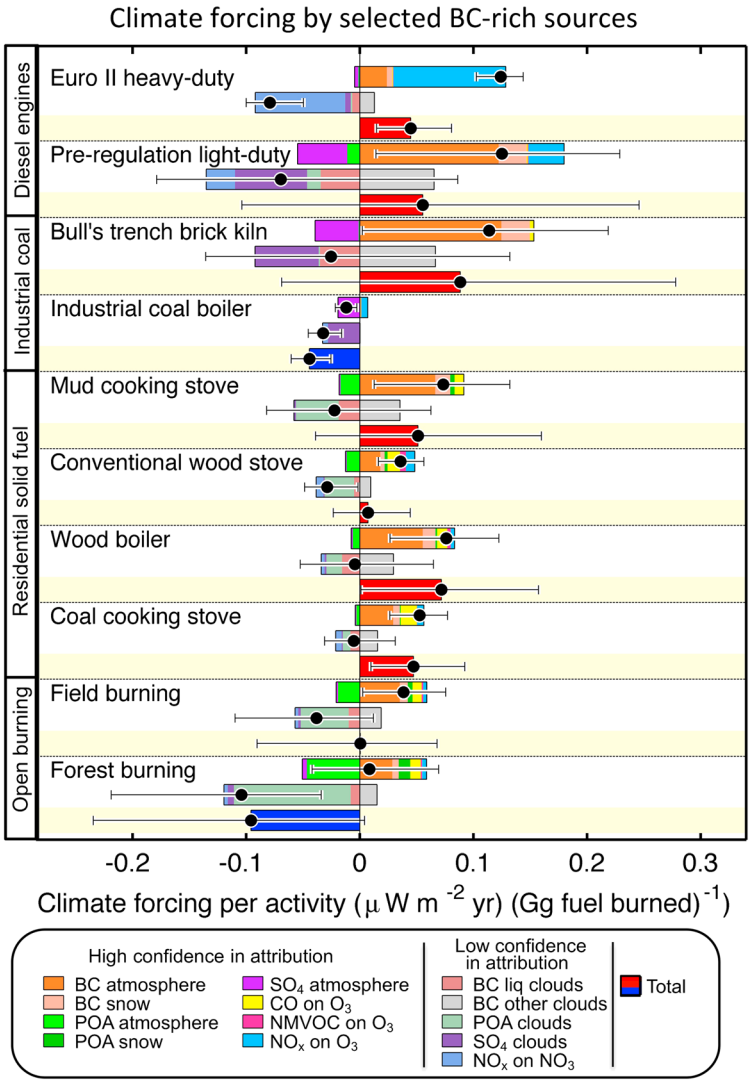

Figure 39. Climate forcing during the first year after emission, for selected individual sources that are subsets of the the categories in Figure 37. As in Figure 37, the three bars for each source correspond to (1) climate-forcing components for which attribution to species and sources can be done with high confidence (direct forcing by gases and aerosols), (2) components for which attribution to individual sources is difficult (cloud changes and nitrate forcing), and (3) total of all components.

factors within the GAINS model (section 4.6.4). Emission factors specific to individual technologies need to be chosen carefully when sources, rather than categories, are scrutinized closely to determine the net effect on forcing.

[745] Profiles of field and forest burning are similar to the category graphs, with important contributions to direct forcing from organic matter and gases, and a net negative forcing due to cloud interactions with POA.

[746] The values in Figure 39 represent the total climate impact of particular sources. They do not reflect the change caused by mitigation actions, which would be the difference between the current climate impact and the impact of the chosen alternative.

11.7. Comparison With Forcing on Longer Time Scales

[747] It is important to consider contributions to climate change beyond the first year after emission. Forcing results both from direct emissions of GHGs (e.g., CO_2 and CH_4) and from short-lived air pollutants interacting with CH_4. While CH_4 is considered a shorter-lived pollutant in some

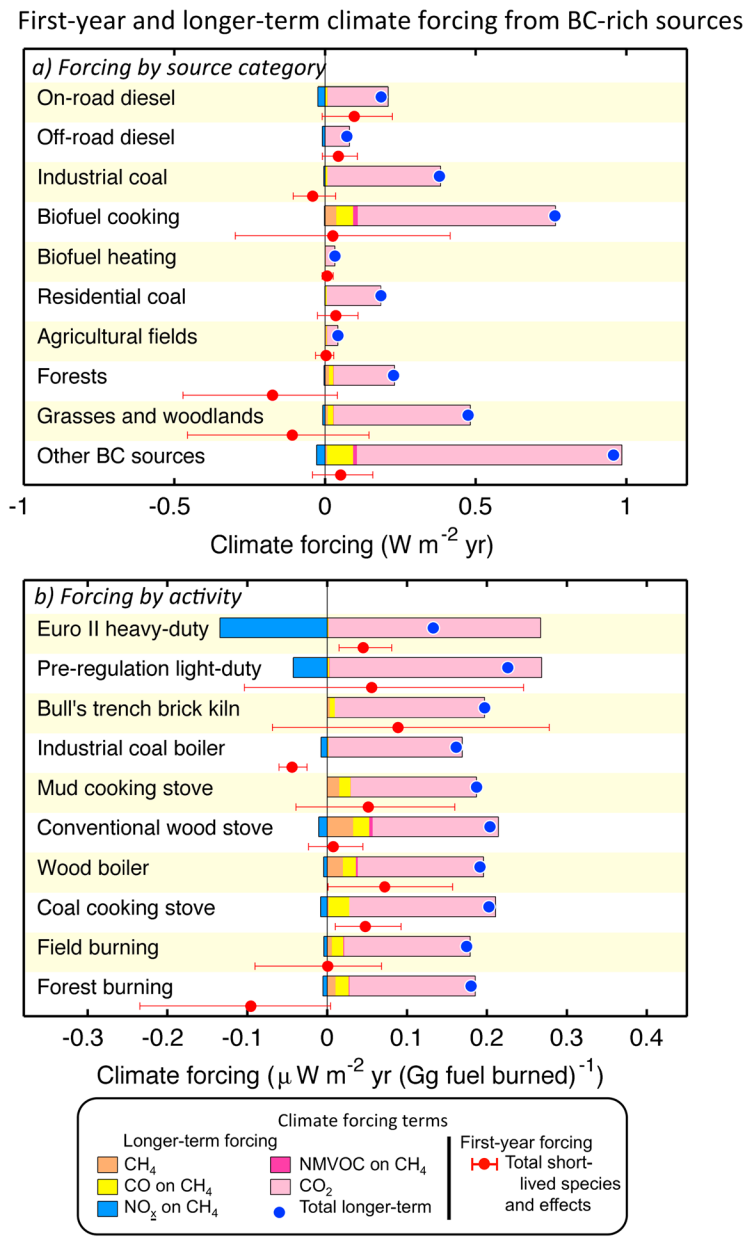

Figure 40. First-year and longer-term climate forcing of BC sources. The forcings are shown by category (top panel) and by source activity (bottom panel) corresponding to the categories in Figures 37 and 39. Totals and individual terms that make up integrated long-term (1–100 year) climate forcings, excluding the first-year forcing, are shown for individual terms and the total forcing with the first-year forcing excluded. The total for the first-year forcing and its uncertainty are also shown in both panels. This figure shows integrated forcing from (a) a single year of emissions (top: 2000 emission rates scaled to match atmospheric observations) or (b) a finite quantity of fuel burned, and does not assume that emissions are sustained.

discussions, its forcing is not contained solely within the first year after emissions as are the forcings of the other constituents discussed earlier in this section. Common practice is to integrate these forcings over 100 years after emission, and these integrated forcings are shown in Figure 40 as bars. Figure 40a shows the longer-lived forcings for year 2000 emissions within each source category in Figure 37, and Figure 40b shows the total forcing per mass of fuel burned for each individual source in Figure 39. For biofuel and open biomass burning, the contribution of CO_2 may not be treated as forcing in traditional GHG accounting, if the biomass consumed is regrown. Only combustion emissions are shown here, so, for example, refrigerants emitted from vehicles are not included.

[748] Figure 40 also shows the estimated forcing from Figures 37 and 39 for comparison (red circles). Because no forcing is exerted by these species or effects after the first year, the 100 year integral is identical to the values already given. The two types of forcing in the figure are distinct: one acts during the first year ("first-year forcing") and one requires longer integration times ("longer-term forcing"). These two groups form a mutually exclusive and collectively exhaustive set of forcing impacts by combustion emissions. Although forcing by CH_4 during the first year after emission is about 10% of its integrated forcing, we classify this as longer-term forcing because of the need for integration.

[749] First-year forcing by BC-rich source categories is substantial but not dominant, with absolute values ranging from 5 to 75% of the integrated long-term forcing. Furthermore, first-year values that appear small in comparison with long-term forcings are usually the small net of two larger values with opposing signs. Thus, emissions from these sources can immediately produce climate forcing that is significant in comparison with the long-term forcing, even if the latter is integrated over 100 years. Regardless of whether any of these sources are chosen for mitigation to reduce climate forcing, changes in these emitters will affect the radiation budget substantially in the near future.

[750] Of particular note are the opposing effects of first-year forcing and longer-term effects on CH_4 for two major source categories. For both on-and off-road diesel engines, the best estimate of first-year forcing is positive, although the uncertainty is high. However, this forcing is countered by the negative forcing after the first year, caused by NO_x emissions that reduce CH_4 concentrations. The opposite effect is seen in another large source, biofuel used for cooking. Its first-year forcing is estimated to be nearly neutral, largely due to the cancelation of cloud and direct forcing. The interaction of short-lived pollutants with the CH_4 budget opposes this negative forcing, and the best estimate of biofuel-burning emissions impact is a slightly positive forcing from aerosol, O_3 and CH_4 interactions. For both of these large BC-rich source categories, the combined forcing by aerosols, O_3 and CH_4 is deceptively small, masking large offsetting terms that may occur during different decades.

11.8. Cautions Regarding Net Forcing Estimates

[751] The values given here represent our best estimate of the global response to worldwide source categories, based on current knowledge. Nevertheless, they should be interpreted in light of the cautions below.

11.8.1. Constraints on Emissions of BC and Co-Emitted Species Are Limited

[752] Total emission estimates are acknowledged to contain uncertainty, and those used for Figures 37 and 38 are determined by scaling modeled atmospheric concentrations to observations. This analysis is hampered because the regions in which the greatest scaling occurs have few observations. We acknowledge that this scaling treatment is subject to many assumptions.

[753] The net forcing and total rely on our assumption that BC and other products of incomplete combustion scale equally. This equal-scaling assumption, especially for OA and BC, affects net forcing in source categories where positive forcing by BC is balanced by negative direct and indirect forcing by OA. The large scaling of OA awaits confirmation beyond the general finding that emissions from biomass burning should increase, and the treatment here has increased OA direct and indirect forcing well above values summarized for the last IPCC report [*Forster et al.*, 2007]. If BC alone should be increased to match atmospheric absorption—perhaps due to poor measurements of BC mass at the point of emission—then all categories in Figure 37 would have greater positive forcing. On the other hand, if larger increases in particulate matter are required to match satellite observations—perhaps due to formation of secondary organic aerosol—then negative forcing in some categories would increase.

11.8.2. Forcing Dependence on Emitting Region Is Not Captured

[754] In developing the figures in this section, we applied globally averaged values of forcing per unit of emission. Some values of forcing per emission depend on the emitting region. The climate forcing per emission of short-lived pollutants depends on the region (and timing) of emission. Thus, the summed climate forcing of all species for a source category emitting in a particular region (or season) may have a different magnitude than the global average, or even a different sign. Atmospheric forcing per emission of BC may vary by about 50% [*Rypdal et al.*, 2009b], and cryosphere forcing is quite dependent on emitting region [*Reddy and Boucher*, 2007; *Shindell et al.*, 2008]. *Bond et al.* [2011] showed that direct radiative forcing by BC and OA is positive in any region when the OA-to-BC ratio was less than 12:1, but when cryosphere forcing was considered for regions near ice, even sources with an OA-to-BC ratio of 30:1 could have positive forcing.

[755] Forcing per emission by gases is also regionally dependent, especially for NO_x, for which values of forcing-per-emission vary by an order of magnitude between the tropics and higher latitudes [*Wild et al.*, 2001].

11.8.3. Regional Impacts Are Not Well Captured by Global Averages

[756] As discussed at the end of section 10, the presentation here measures impact in terms of globally averaged, ToA climate forcing. Globally averaged forcing does not reflect the strong regional impacts of short-lived climate forcers. Forcing that appears small in the global average may be significant over a smaller area and near zero over the rest of the globe. Such regional forcing may induce climate responses different than those of long-lived, well-mixed climate forcers (section 9).

[757] ToA climate forcing does not reflect some societally relevant changes, such as shifts in precipitation. Forcing that

is zero at the top of the atmosphere but alters the distribution of radiation within the atmosphere may still have significant impacts.

11.8.4. Large Uncertainties Remain in Deriving and Apportioning Cloud Impacts

[758] Uncertainty about the sign of forcing is most directly attributable to the uncertainty in cloud forcing by co-emitted species and to lack of knowledge about the magnitude of the total indirect effect itself. This large uncertainty is not unique to BC-rich sources, but reflects the existing state of knowledge regarding clouds. In this analysis, we have included an estimate of cloud impacts because direct forcing alone may give a misleading impression of net impact in terms of both certainty and sign of effect.

[759] Using column burden to assign indirect forcing to OA or sulfate is one plausible method of apportioning the forcing and is consistent with some model studies. This or other methods of apportionment have not been explored by studies combining models and observations. The larger indirect effect predicted by scaling the OA burden has not been evaluated with observations, either.

[760] Reconciling modeled and observed indirect effects is an area of active research. Estimates of warm-cloud forcing have altered over time as models incorporate constraints from satellite measurements [*Lohmann et al.*, 2010]. If the best estimate of warm-cloud microphysical interactions is later revised to be less negative, estimates of net first-year forcing will become more positive for transportation and solid-fuel sources, and less negative for open-burning and sulfur-rich sources.

[761] Negative forcing is ascribed to semi-direct effects of BC, but model responses may depend on BC overlying clouds, an assumption that is questionable in light of observations. If estimates of this effect were weakened (becoming less negative), forcing by all BC sources would also become less negative or more positive.

[762] Enhanced absorption within clouds is highly uncertain. If the forcing attributable to such absorption is as great as that estimated by *Jacobson* [2010], forcing by all BC-rich sources would become strongly positive. Forcing by sources that emit light-absorbing OA or OA precursors, such as biofuel and open biomass burning, would also have greater effects. This potentially large effect is included within our uncertainty bounds, but our central estimate has been more conservative.

[763] The net effect of BC and co-emitted species on mixed-phase and ice clouds depends on the fraction of BC that is ice active. If BC is found to be ice active in the upper troposphere, then the estimate of BC effects on ice clouds may warrant increased positive forcing estimates. On the other hand, if coatings or co-emitted species cause less ice nucleation, then mixed-phase cloud forcings may become more positive.

[764] Forcing by all cloud effects may depend strongly on the region of emission, on co-emissions, or on the environment in which emissions occur, but no study has examined such differences. A more robust treatment would involve examining each individual source with a model that includes all effects described in this assessment, and that also has the ability to examine sensitivity to critical model inputs.

11.8.5. Climate Forcing by Additional Co-Emitted Species May Affect Total Category Forcing

[765] Although forcing by SOA is not included here, it is known to be a large fraction of the atmospheric aerosol. If SOA has a small negative forcing, as some models predict, and if BC-rich sources emit large quantities of SOA precursors, then net forcing estimates will become more negative.

[766] Ionic species such as magnesium and calcium are small fractions of emitted mass and were not included in this analysis. These species are included in biofuel simulations by *Jacobson* [2010], but their effects have not been isolated.

12. Emission Metrics for Black Carbon

12.1. Section Summary

[767] 1. The purpose of an emission metric like the Global Warming potential (GWP) or the Global Temperature Change Potential (GTP) is to put future climate impacts of unit emissions of compounds with different lifetimes and radiative efficiencies on a common scale. Such metrics can be useful not only in legally binding agreements, but also in assessments of net climate impact of different mitigation options affecting emissions of many compounds.

[768] 2. Physically based metrics like the GWP and the GTP for BC emissions can be calculated from estimates of global annual mean climate forcing normalized to BC emissions. For the GTP additional information about the response times of the climate system are needed.

[769] 3. Based on the total climate forcing of BC as given in section 10, the $GWP_{20\text{-yr}}$, $GWP_{100\text{-yr}}$ and $GWP_{500\text{-yr}}$ for BC are 3200, 910 and 280, respectively. The $GTP_{20\text{-yr}}$, $GTP_{50\text{-yr}}$ and $GTP_{100\text{-yr}}$ estimates are 925, 150 and 130, respectively. Uncertainties are (−90, +100%) for the GWPs and (−90, +165%) for the GTPs.

[770] 4. The GWP and GTP metrics vary with the region where BC is emitted by about ±30% based on the results from two studies.

[771] 5. The GWP and GTP metric values (which are all relative to CO_2) increase with decreasing time horizon due to the short lifetime of BC (i.e., removal within a few days to weeks via precipitation and contact with surfaces). The choice of time horizon is a value judgment related to the overall target of the climate policy being considered.

[772] 6. Current climate policies seem to move in the direction of achieving some temperature target. Under such an approach, the time horizon is initially long and the value of a short-lived forcer such as BC is small but grows as the temperature target is approached. A stricter temperature target implies the value of BC grows faster as the temperature target is approached.

[773] 7. BC is not well mixed in the atmosphere because of its short lifetime and has climate forcing mechanisms that differ from most GHGs. Thus, regional changes and impacts on climate variables other than temperature differentiate BC from how most GHGs affect climate. Metrics that attempt to place BC and GHGs on a common global scale are useful in the context of decision making, but because of these differences any such metric should be used with caution.

[774] 8. Co-emission effects, discussed in section 11, are not captured by BC metrics presented here but can be calculated in a similar approach.

12.2. Introduction

[775] The United Nations Framework Convention on Climate Change [UNFCCC, 1992, article 3] carried strong statements about the need for comprehensive (i.e., across all components and sectors) measures that are also cost effective. To achieve this goal, climate policies may target not only CO_2 but also other compounds leading to warming of the system. To facilitate the evaluation of multiple species, a measure that puts climate impacts of emissions of different compounds on a common scale, or a *metric*, is needed [*IPCC*, 1990; *Kandlikar*, 1996; *Fuglestvedt et al.*, 2003; *Forster et al.*, 2007]. In this context, climate impacts are understood as all future impacts imposed from the time of the emission. Since BC has such a short lifetime compared to the long-lived GHGs, the length of time over which future impacts are evaluated (e.g., through the choice of a time horizon in the common metric, the GWP, or through a discount rate) strongly influences the metric value. This is an inevitable challenge in constructing metrics as it fundamentally involves value judgments with respect to how one treats short-term versus long-term climate impacts [e.g., *O'Neill*, 2000; *IPCC*, 2009].

[776] Reductions are often presented in terms of total "CO_2-equivalent" emissions. Based on a metric value M_{BC} for BC and the emissions of EM_{BC} of BC, CO_2-equivalent emissions that can be compared with similarly calculated emissions of other species, are calculated through

$$EM_{CO_2\,eq} = EM_{BC} \cdot M_{BC} \tag{12.1}$$

[777] This CO_2-equivalent value means that emitting EM_{BC} kg of BC would have the same effect (in terms of the impact parameter used in the metric definition) as emitting $EM_{CO2\text{-}eq}$ kg of CO_2 at the same time. In a multi-component climate agreement, such as the Kyoto Protocol, a set of metric values are decided for each component included in the agreement. Note that the Kyoto Protocol does not include BC or other aerosol components. The overall commitments are given in terms of reductions in total CO_2-equivalent emissions, summed up over the all components included in the agreement, and it is then up to each party to the agreement to decide the composition of the total mitigation, depending on the costs of reducing the individual components. An alternative to this "basket" approach would be to agree on commitments for individual components. The role of a metric would then be to provide guidance with respect to how much emissions of one component should be reduced relative to another component, involving the same value judgments discussed above. So-called "multi-basket" approaches have also been proposed [*Fuglestvedt et al.*, 2000; *Rypdal et al.*, 2005; *Jackson*, 2009], where components with similar lifetimes are lumped in separate baskets. Again metrics can be used to help determine the targets for each basket.

[778] The use of metrics is not restricted to legal agreements, but is also very useful for comparing different policies or technological options [e.g., *Jacobson*, 2002] or in assessments of different economic sectors [e.g., *Fuglestvedt et al.*, 2008; *Boucher and Reddy*, 2008; *Berntsen and Fuglestvedt*, 2008].

[779] Metrics have been defined both in terms of physical and economic impacts on climate [*Kandlikar*, 1996; *Fuglestvedt et al.*, 2003, 2010; *Forster et al.*, 2007]. We limit the discussion here to physical metrics, especially those metrics that have already been used in climate change policy. Metrics based on economics are extensions of physical metrics and the extension is of a more generic nature, not particularly related to BC. Metrics based on economics can be designed to allow for cost-benefit optimization by taking damage cost functions into account [*Tol et al.*, 2012]. Different metric concepts can be defined to serve specific policies such as those with a long-term temperature target (e.g., the maximum 2°C as included in the 2009 Copenhagen Accord of the Conference of Parties-15 (COP-15) meeting) [*Manne and Richels*, 2001].

[780] Using equation (12.1) to derive a value of CO_2-equivalent emissions does not ensure that all aspects of climate change are equivalent to those from actual CO_2 emissions, in particular for a very short-lived compound like BC. Equivalence is only obtained with respect to the physical impact chosen in calculating the metric [*O'Neill*, 2000]. Different combinations of compounds with equal total CO_2-equivalent emissions, for example, do not provide equivalence with respect to regional climate impacts or the temporal development of climate change. Although these latter impacts are the key end points of concern, they are farther down the causal chain and, thus, are more difficult to capture with simplified and policy-friendly metrics.

12.3. The GWP and GTP Metrics

[781] Two purely physically based metrics, the GWP and the GTP, have been established in the literature. The absolute GWP (AGWP) can be defined as the integrated climate forcing (F) of a unit-mass pulse emission over a time horizon H. Using climate forcing can take efficacy into account as necessary. The AGWP for a component i with an atmospheric lifetime of τ_i and specific climate forcing of A_i (forcing per unit burden change, W m^{-2} kg^{-1}) can be calculated as:

$$\begin{aligned} AGWP_i(H) &\equiv \int_{t=0}^{H} F(t)dt = \\ &\int_{t=0}^{H} A_i \ \exp(-t/\tau_i) \ dt = \\ &A_i\tau_i(1 - \exp(-H/\tau_i)) \approx A_i\tau_i \end{aligned} \tag{12.2}$$

[782] For all forcing mechanisms involving BC, τ_i is much less than H. The product $A_i\ \tau_i$ (W m^{-2} (kg yr^{-1})$^{-1}$) is the specific normalized climate forcing at steady state for a continuous unit emission. These values can be derived from model simulations that calculate the annual mean climate forcing (F_i) for a given emission, such as the values tabulated in Appendix C.

[783] The generic definition of the absolute GTP (AGTP) can be given as

$$AGTP_i(H) = \int_{0}^{H} F_i(t) \cdot R(H-t)\mathrm{d}t \tag{12.3}$$

where an impulse-response function for the climate system $R(H-t)$ gives the surface temperature response at time H due

to a climate forcing at time t [*Shine et al.*, 2005; *Fuglestvedt et al.*, 2010]. For both the GWP and the GTP the metric values are obtained by dividing the AGWPs and AGTPs by the corresponding AGWP or AGTP values for the reference gas CO_2. The AGWP values for CO_2 for 20, 100 and 500 years time horizon of $2.47 \cdot 10^{-14}$, $8.69 \cdot 10^{-14}$ and $28.6 \cdot 10^{-14}$ W m^{-2} yr (kg CO_2)$^{-1}$ are used to calculate the GWPs [*Forster et al.*, 2007]. *Joos et al.* [2012] show that there is an uncertainty of about ±27% in these values due to various assumptions. The AGTP values for CO_2 used here [*Fuglestvedt et al.*, 2010] are $6.8 \cdot 10^{-16}$, $5.8 \cdot 10^{-16}$ and $5.1 \cdot 10^{-16}$ K (kg CO_2)$^{-1}$ for 20, 50 and 100 year time horizons. The GTP is commonly referred to as an *end-point* metric since equation (12.3) gives the global mean temperature response at time H.

[784] The Kyoto Protocol regulates a basket of six gases, or groups of gases, that are primarily long-lived GHGs. The global warming potential with a 100 year time horizon was chosen as the metric for use in this legal agreement. Metrics are most commonly defined for pulse emissions, since comparisons of future scenarios can readily be carried out by regarding each emission trajectory as a series of pulse emissions [*Berntsen and Fuglestvedt*, 2008]. A special case of a future scenario is constant sustained emissions. *Hansen et al.* [2007] used an alternative GWP defined as change in forcing per change in emission. *Jacobson* [2010] calculated a STRE (Surface Temperature Response per unit Emission) emission index that is defined for sustained emissions, but with a non-standard response function for CO_2.

[785] More recently some alternative physical metrics have been proposed. *Gillett and Matthews* [2010] and *Peters et al.* [2011] introduced the mean GTP and the integrated GTP (iGTP), which are equal concepts, while *Bond et al.* [2011] introduced the *specific forcing pulse*, which is identical to the AGWP without a time horizon and which may be applied to individual regions. The iGTP is a pulse-based emission metric integrating the temperature change from the time of the emission to a given time horizon. There is a close relation between the GWP and the iGTP, with larger differences for short-lived forcers and short time horizons. For BC with a time horizon of 20 years the iGTP is about 40% higher than the GWP [*Peters et al.*, 2011]. Although all of these metrics can be calculated from forcing or effective-forcing values, similar to the GWP and GTP, each is slightly different in the assumption of the response function desired for comparison.

12.4. Calculations of Metric Values for BC

[786] Based on equations (12.2) and (12.3) above, metric values for BC emissions including all relevant processes can be calculated (i.e., the processes summarized in section 10) when the specific normalized climate forcings and the impulse-response function are given. Here we have used the impulse response function from *Boucher and Reddy* [2008]. The detailed method for calculating the AGTPs is given in *Fuglestvedt et al.* [2010] and is not comparable to the equilibrium temperature changes discussed in section 9. Using the estimates for global climate forcing given in section 10 (Figure 35) and the estimated industrial-era emissions of BC of 13,900 Gg yr^{-1} (section 4), the GTP and GWP values for direct BC forcing as well as for the total climate forcing of BC were derived as shown in Figure 41.

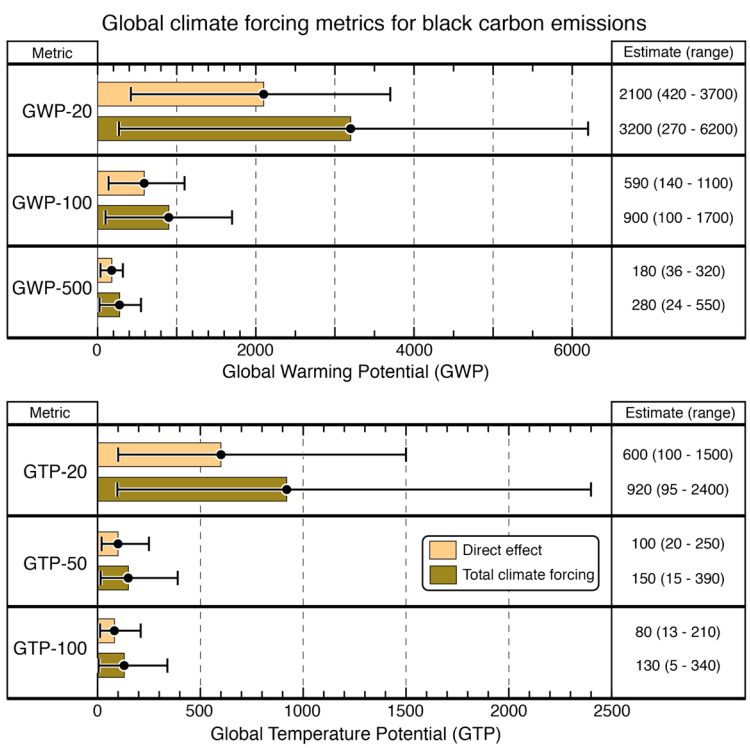

Figure 41. GTP and GWP values for several time horizons for BC climate forcing. Values are shown for the BC direct effect and the total climate forcing. The calculations use the industrial-era climate forcing values displayed in Figure 35 and an annual BC emission of 8700 Gg yr^{-1}. The whiskers represent the uncertainty range as described in the text.

Due to the short lifetime of all BC forcing mechanisms, the annual mean product $A_i\ \tau_i$ can be accurately estimated as the ratio between the annual mean climate forcings (Figure 35) and the annual emissions.

[787] Figure 41 gives global GWP values for the standard 100 year time horizon, as well as values for 20 and 500 years, and GTP values for 20, 50 and 100 years. Since the lifetimes for all forcing mechanisms discussed in section 10 are much shorter than any of the time horizons chosen, each mechanism has the same relative contribution to either GWP or GTP. Although the total forcing assessed in this report is greater than that in previous estimates, the GWP has not increased correspondingly because the estimate of emissions has also increased. It should be noted that the values for GWP_{100} and GTP_{20} are about equal, which is a robust finding in general for short-lived climate forcers [*Fuglestvedt et al.*, 2010]. The GWP and GTP values for the direct effect as given in Figure 41 are about a factor 2 higher than the values given in *Fuglestvedt et al.* [2010]. This is partly because *Fuglestvedt et al.* only considered the direct effects of BC and partly because the estimate for the radiative forcing per unit emission for the direct effects used here (cf. section 6) is higher than the values used by *Fuglestvedt et al.*

12.5. Uncertainties

[788] Relative uncertainties in metric values are assumed to be the same as those given in section 10 for total climate forcing. Normalization of the observationally constrained climate forcing by uncertain annual emissions could in principle change the uncertainty range of the normalized forcing, either increasing or decreasing the uncertainty. Since the forcing estimates are commonly based on combinations of model results and measurements, rigorous propagation of uncertainty is difficult to determine. Although uncertainties in the metric values are of little practical use in formal agreements or trading schemes, where only the central estimates of the metrics are used, they become important when the metric values are used as a first-order assessment of the net effects of different mitigation options. For GTPs, the uncertainties are much larger than for GWPs due to uncertainties in the climate sensitivity and, hence, the temporal response of the climate system. For GTPs in Figure 41, a factor of 2 uncertainty in the impulse response function is included based on the result of *Fuglestvedt et al.* [2010] for GTP_{50} of BC.

[789] Uncertainties in the values of metrics can be classified as structural or scientific. Structural uncertainties refer to the consequences of using different types of metrics for a given application, or to choices about key aspects of a metric such as its time horizon and whether discounting is applied. Scientific uncertainties refer to the range of values that can be calculated for a given metric due to incomplete knowledge of the important aspects of the climate or economic system that relate some anthropogenic emission to climate impacts, damages, or mitigation costs [*IPCC*, 2009]. In previous sections of this paper we present the scientific uncertainties based on the uncertainties for each of the forcing mechanisms for BC as presented in sections 6, 7, and 8, and illustrated in Figure 35. The structural uncertainties, which can be very large, are demonstrated by presenting numerical values for different metrics (GWP and GTP) and for a range of time horizons. The range is between 95 and 2400 for the central estimate for GTP_{20}, and between 120 and 1800 for GWP_{100}. The central value of GWP varies from 280 to 3200 for different time horizons, and that of GTP varies from 120 to 910. Thus, the scientific uncertainties are of the same magnitude as the structural uncertainties.

12.6. Shortcomings of Global Metrics

[790] Some important differences between BC and the long-lived GHGs are not well captured by globally averaged metrics. Because BC absorbs incoming shortwave radiation, BC in the atmosphere causes surface dimming and changes the vertical temperature profile differently than the long-lived GHGs. The various hydrological impacts caused by the dimming from BC are not captured in metrics that are based on global climate forcing or global mean surface temperature change.

[791] Another issue for BC and other short-lived climate forcers is that metric values for global impact (global mean climate forcing for the GWP and global mean temperature for the GTP) depend on the region of the emissions and also on the timing of the emissions due to the short lifetime of BC. Since there have been no studies of the climate forcing due to emissions during different seasons, metric values cannot be differentiated according to when the emission takes place. Two studies have calculated normalized radiative forcings or GWPs for the direct effect and the snow albedo effect for regional emissions [*Rypdal et al.*, 2009b; *Bond et al.*, 2011]. They both find a regional variability of ±30–40% for the direct effect, with the largest forcings typically found for emissions from regions located at low latitudes since there is more solar radiation available. For the snow albedo effect the regional variation is much larger with higher values for high latitude regions where the emitted BC is more likely to be deposited on snow surfaces. The snow albedo effect ranges from practically zero for emissions in the tropics to values that reach 30 to 60 % of the direct effect for emissions in Russia and the former Soviet Union [*Rypdal et al.* [2009b] and *Bond et al.* [2011], respectively], not including an enhanced efficacy factor for the snow albedo effect. Since there is a certain cancelation effect depending on the latitude of the emissions (i.e., high direct forcing occurs with low snow-albedo forcing and vice versa) the total of the two mechanisms shows less regional dependence.

[792] In addition to the potential for different global impacts resulting from BC emitted in different regions, the impact on climate in a given region may depend on where the climate forcing occurs [*Shindell and Faluvegi*, 2009]. So far there has only been one GCM study on this topic, but if it proves to be a robust finding, the location where emission reductions occur to achieve a designed climate benefit will not be completely flexible [*Sarofim et al.*, 2010].

12.7. Choice of Time Horizon

[793] The choice of time horizon for either the GWP or GTP metric is essentially a value judgement, conceptually related to discounting future costs of the impacts of climate change. As discussed by several authors [*Aaheim et al.*, 2006; *Bradford*, 2001; *Johansson et al.*, 2006; *Manne and Richels*, 2001; *Shine et al.*, 2007], for a cost-effective policy that sets a long-term limit on the allowed change in global temperatures [e.g., *COP-15*, 2009], the relative importance of different emissions (i.e., the metric values) will depend

on how far into the future that threshold is likely to be reached. Thus, if the global temperature continues to increase, the metric values of short-lived components will increase as global temperatures get closer to the temperature constraint. If a metric with a dynamic time horizon were incorporated in legally binding agreements or trading schemes, it would be important for the stakeholders to know not only the metric values at the time of the investment in emission reductions, but to have information about the potential change of the metric values over the lifetime of the investment due to shortening of the time horizon as global temperatures get closer to the temperature constraint. Once a threshold is set (e.g., as the 2°C threshold agreed upon in the Copenhagen Accord [*COP-15*, 2009]), it is possible to estimate, with uncertainties, what is the relevant timeframe and how the metric values will evolve over time [e.g., *Manne and Richels*, 2001]. This information can be communicated to decision makers, so that it is taken into account when there are investments in new long-lasting equipment (e.g., power-plants that will be in operation for 40–50 years).

[794] There has been some concern that a policy that increases the focus on short-lived climate forcers like BC would reduce the focus on reduction of CO_2 and other long lived GHGs, with possible severe irreversible long-term climate effects. An assessment by the U.S. National Academy of Sciences went so far as stating that CO_2 emission mitigation and short-term forcing emission mitigation are "...separate control knobs that affect entirely distinct aspects of the Earth's climate, and should not be viewed as substituting for one another" [*NRC*, 2011]. If a metric with a dynamic time-horizon were to be applied to all climate forcers in a cost-effective framework with a long-term temperature constraint (e.g., in accordance with the Copenhagen accords [*COP-15*, 2009]), it can be shown that within this framework short- and long-lived climate forcers can be treated in a common framework and that an increased mitigation of BC does not displace additional CO_2 mitigation [*Berntsen et al.*, 2010]. This is because in a cost-effective framework increased mitigation of BC is only consistent with a higher metric value for BC, which is equivalent to a shorter time horizon. In this framework the only political decision that can shorten the time horizon is to lower the acceptable temperature threshold. The key to this argument is that with a lower threshold the total CO_2-equivalent emissions must be reduced significantly more. Due to the dominant role of CO_2 this means that even if the relative reductions of BC are enhanced, the absolute CO_2 reductions must also be greater if the temperature threshold is decreased [*Berntsen et al.*, 2010].

12.8. Towards Metrics for the Net Effect of Mitigation Options

[795] As shown in section 11 and further discussed in section 13, any mitigation strategy targeting BC reductions will inevitably also change emissions of other species that affect climate. Metrics are suitable tools to make first-order estimates of the net effect of all emission changes [*Berntsen et al.*, 2006; *Boucher and Reddy*, 2008]. Using precalculated metrics for all the relevant species allows for much quicker assessments. Simulating the broader climate effects, including end-point risks and impacts, requires Earth system models which include full coupling between chemistry, radiation, dynamics, clouds, vegetation, etc. However, even if such an Earth system model is applied, the question of how to weigh responses occurring at different times in the future remains.

[796] Section 11 presented the net effect of short-lived emissions from individual source categories. This analysis required estimates of normalized climate forcing for individual species (Appendix C), largely drawing on the comprehensive review of *Fuglestvedt et al.* [2010] but also including the cloud forcing attributable to aerosols and precursors. Although this section presents metric values only for BC, GWPs and GTPs can be derived for the other species by dividing by the appropriate value of AGWP or AGTP for CO_2.

13. Mitigation Considerations for BC-Rich Sources

13.1. Section Summary

[797] 1. Prioritization of BC mitigation options is informed by science questions such as the magnitude of BC emissions by sector and region (section 4), net climate forcing by categories including co-emissions (section 11), impacts on the Arctic (section 8), and direct effects on precipitation (section 9.4). In addition, information on technical and financial feasibility, costs and benefits of mitigation, policy design, and implementation feasibility also inform mitigation options. The major sources of BC are presently in different stages of evolution with regard to technical and programmatic feasibility for near-term mitigation actions.

[798] 2. Regardless of net climate forcing or other climatic effects, all BC mitigation options bring health benefits through reduced particulate matter exposure.

[799] 3. The quality of cost estimates of BC mitigation vary, ranging from robust estimates, for example, for diesel retrofits in industrialized countries to poor estimates for sources such as improved brick kilns in developing countries or open burning.

[800] 4. Diesel engine sources of BC appear to offer the best mitigation potential to reduce near-term climate forcing. In developed countries, retrofitting older diesel vehicles and engines is a key mitigation strategy; in developing countries, transitioning a growing vehicle fleet to a cleaner fleet will be important.

[801] 5. Mitigating emissions from residential solid fuels may yield a reduction in net positive forcing, especially when the longer-term effects on the methane budget are considered. The net effect remains uncertain because of uncertain knowledge regarding the impacts of co-emitted species on clouds. Furthermore, for biofuel use, technology and programs to accomplish mitigation are still emerging.

[802] 6. The net effect of small industrial sources depends on the sulfur content of individual sources, and the feasibility of mitigation is in the emerging phase. Net climate benefits may be possible from individual source types with low sulfur emissions when technology is available.

[803] 7. Estimation, and especially monetization, of the benefits of BC mitigation is a nascent field. CO_2-equivalency metrics serve as a first-order guide to estimating the climate benefits of BC mitigation but do not capture all potential objectives.

[804] 8. Unlike long-lived GHGs, the location, and in some cases timing, of BC emissions may change the climate forcing effect compared to the global average. For example, BC sources that affect the Arctic or other regions with extensive snow and ice cover may offer mitigation potential to reduce climate forcing for those regions. Such regionally specific benefits have not yet been quantified.

[805] 9. Mitigation considerations are ideally informed by how emissions are projected to change over time based on existing policies, so that emphasis is placed on sources whose emissions are expected to grow or remain significant.

13.2. Mitigation Framework for Comprehensive Evaluation

[806] The introduction to this assessment describes a potential role for BC in climate mitigation. Because BC has a short atmospheric lifetime, changes in source activity affect radiative forcing within a few weeks and, therefore, actions that reduce emissions from BC-rich sources could contribute to managing the trajectory of climate forcing. Until this point, this assessment has focused wholly on climate-related physical science. We have treated the suite of climate forcings of BC comprehensively rather than limiting the analysis to direct forcing (section 10), and we have broadened the examination of impacts beyond those of BC alone by including co-emitted species (section 11). In discussing mitigation in this section, we also take a comprehensive view by outlining factors beyond climate science: first, feasibility in technical and policy-related terms; second, health co-benefits from BC mitigation; and third, an economic assessment of whether benefits of mitigation are commensurate with costs. While these factors are important in evaluating mitigation potential, a detailed appraisal of the state of science and policy for mitigating each BC source and in each region is beyond the scope of this assessment. Additional analyses of the potential for BC mitigation can be found in reports such as *UNEP/WMO* [2011a; 2011b], *Arctic Council*, [2011] and *EPA* [2012].

[807] In considering the mitigation of a climate-forcing agent, several principal aspects are involved as illustrated in Figure 42. In the case of BC and co-emitted species, *scientific understanding* addresses what is known about the environmental and health effects of BC emissions and their accumulation in the atmosphere. The net impact of mitigation actions is proportional to the reduction in these effects. For climate, this net impact depends critically on understanding how actions affect both BC and co-emitted species.

[808] Mitigation is generally accomplished with alternatives that provide the same service or function with lower environmental impacts or by reducing the level of service. *Technical feasibility* refers to the availability of these workable alternatives. Even with scientific understanding and technical feasibility in hand, successful mitigation actions further depend on institutional and policy frameworks that can facilitate or enforce widespread implementation of mitigation options. This *programmatic feasibility* refers to the existence of an effective framework, which increases confidence that significant emission reductions could be achieved over a known time frame.

[809] The evolution of each of these principal aspects can be divided into four stages as illustrated in Figure 42. Scientific understanding moves from recognition of an effect (*nascent* stage), to simple estimation that may rely heavily on expert judgment (*emerging* stage). When increased attention to emission sources motivates more sophisticated quantification, advanced models and observations are applied (*solidifying* stage). When multiple estimates are available for the effects, the community can move toward consensus regarding their magnitude and importance (*mature* stage). The goal of this assessment has been moving the understanding of physical science toward the solidifying and mature stages with regard to climate effects.

[810] Evolution or growth of knowledge also occurs with regard to technical feasibility. This evolution often occurs separately from, but parallel to, the development of scientific understanding. It also has a nascent stage, where technical solutions are first envisioned. The emerging stage consists of initial, limited efforts to provide technical solutions and delivery programs. Not until the solidifying stage does the increased attention to environmental or health effects demand effective solutions, so that formal research, development, and evaluation approach completion. Resources are

Aspects and evolutionary phases of mitigation actions

Program Aspect	Program phase			
	I. Nascent	II. Emerging	III. Solidifying	IV. Mature
Scientific Understanding	Recognition	Simple estimation	Detailed quantification	Consensus
Technical Feasibility	Envisioned solution	Successful prototype	Research and development	Production at required scale
Programmatic Feasibility	Experimental interventions	Specialized programs	Pilot programs and scale-up	(Inter)national policies

Figure 42. Conceptual framework for evaluating the feasibility of mitigating environmental impacts. The principal aspects are scientific understanding and technical and programmatic feasibility. Each aspect has evolutionary phases that reach maturity in several steps. Different emission sources are generally at different phases in the evolution of knowledge associated with each mitigation aspect. This assessment has primarily focused on the aspect of scientific understanding.

invariably required to support this leap in capacity. Finally, at the mature stage, the most promising technical mitigation options have been identified that can be carried out at the scales required and with well known costs and benefits. A similar evolution occurs in programmatic feasibility beginning with experimental interventions. Specialized programs then emerge that lead to pilot programs and finally to policies, regulations and institutions that can facilitate, enforce and implement mitigation plans at regional, national or even international scales.

[811] The major sources of BC are presently in different stages with regard to technical and programmatic feasibility. This disparity does not diminish the importance of any source, but it does mean that the near-term feasibility of mobilizing mitigation activities differs among source categories. Section 13.4 gives a brief review of what is known about technical and policy-related feasibility for each of the major BC-rich source categories.

13.3. Costs and Benefits of Mitigation

[812] Mitigation actions generally have both benefits and costs. If the benefits exceed the costs then the action is generally considered desirable. On the other hand, if the costs exceed the benefits, then the action is generally not considered desirable. Formally, a policy is considered optimal if the marginal benefit of the next unit of reductions equals the marginal costs of that unit of reductions, and the current net benefits resulting from that action are greater than zero.

[813] If the benefits of mitigation have been valued in monetary terms, then a cost-benefit approach is possible, but when benefits are difficult or impossible to estimate, the approach of cost effectiveness is often used. Cost effectiveness does not attempt to equate cost and benefits, but rather to identify the least-cost method of reaching a given goal, or most effective use of a given quantity of resources. The goal still requires a metric for comparison; often, this is the total quantity of pollutants reduced or, in more sophisticated analyses, the reduction in physical impacts or damages associated with lower emissions. For example, cost effectiveness can be calculated based on cost per Mg BC reduced, per Mg CO_2 equivalent (section 12), or per degree of global mean temperature reduction. In the case of a cost-benefit analysis, the cost can be compared to the monetized benefits (where feasible for health, climate, or both) of mitigation. Because cost is an important part of such analyses, it is discussed in the next section. Although earlier sections presented emissions in terms of Gg per year, costs are usually tabulated in terms of Mg reductions (1 Gg = 1000 Mg).

[814] The engineering costs of a reduction measure can include capital costs, installation or adoption costs, and fixed or variable operating costs such as changes in fuel demand, future maintenance needs, or labor demands. Estimating the reductions could involve calculating the expected difference in emissions between the baseline and a new projection or using an approximation of calculating the annual reductions multiplied by the expected lifetime of the mitigation project.

13.3.1. Health Benefits

[815] BC is one component of particulate matter that can have adverse effects on human health [*Pope et al*., 2009]. The location of the emission source affects exposure and, hence, the magnitude of health benefit that can come from mitigating that source. To date, public health agencies have not addressed the health effects of BC specifically; rather, the health effects of BC have generally been considered to be associated with the health effects that have been linked to $PM_{2.5}$. As a result, the mitigation literature has traditionally focused on PM rather than explicitly on the BC component. Presently, there is a growing literature on efforts to isolate the specific health effects of BC exposure. As with climate forcing, however, mitigation affects all emissions from a source, so that health effects of BC alone may not be a good estimate of potential benefits from mitigation.

[816] Short-term exposure to $PM_{2.5}$ is likely to be causally associated with mortality from cardiopulmonary diseases, hospitalization and emergency department visits for cardiopulmonary diseases, increased respiratory symptoms, decreased lung function, and physiological changes or biomarkers for cardiac changes [*EPA*, 2009a]. Long-term exposure to $PM_{2.5}$ is likely to be causally associated with mortality from cardiopulmonary diseases and lung cancer, and effects on the respiratory system such as decreased lung function or the development of chronic respiratory disease [*EPA*, 2009a]. Epidemiological evidence explicitly linking BC to such health effects is limited [*Smith et al*., 2009], and simply assigning a fraction of $PM_{2.5}$ health effects to the portion of $PM_{2.5}$ made up by BC is not common, as there are known differential toxicities among PM components, uncertainties about how different mixtures of particulate materials may change toxicity, as well as heterogeneity in the exposure of a population to different PM components. Several studies [*Janssen et al*., 2011; *Ostro et al*., 2010; *Smith et al*., 2010; *Bell et al*., 2009; *Brunekreef et al*., 2009; *Cooke et al*., 2007] describe attempts to differentiate health outcomes among specific components or sources of $PM_{2.5}$.

[817] A study by *Fann et al*. [2009] monetized, on a US dollar per Mg basis (USD Mg^{-1}), the health benefits of reducing carbonaceous particulate material by assuming a differentiated proximity of the receptor populations to sources of carbonaceous PM versus other PM components. *Fann et al*. estimated the health benefits of reducing carbonaceous PM to be on the order of 72 thousand to 2.8 million USD Mg^{-1} in the USA. *UNEP/WMO* [2011a; 2011b] and *Shindell et al*. [2012] assessed the global health benefits of implementing a number of BC measures and found a reduction in annual premature deaths due to outdoor air pollution of 2.3 million (+2.2/−1.6) persons over 30 years of age in 2030. Using a country-specific value of a statistical life, these studies determined a monetized benefit of this mortality reduction of USD 5.1 trillion (+4.7/−3.6). Residential solid-fuel sources of BC also produce high indoor exposures whose effects have been monetized [*Mehta and Shahpar*, 2004].

13.3.2. Valuing Climate Benefits of BC Mitigation

[818] While earlier sections in this assessment discussed climate impact, no value was placed on the reduction of these impacts for use in a cost-benefit assessment. With regard to climate change, the term "benefits" refers to the avoided risks and impacts (Figure 34) associated with less climate change that would be the result of decreased BC emissions. No direct monetization of the benefits of BC reductions for climate change has yet been reported in the literature.

[819] One possible approach to valuation is using metrics (for example, GWP, see section 12) to convert BC emissions into estimates of CO_2-equivalent emissions. BC mitigation estimates in these CO_2-equivalent units would then represent first-order, proxy measures for the climate benefits of BC mitigation actions. Furthermore, the CO_2-equivalent metric also provides a first-order approximation for how the BC mitigation measures compare to other CO_2 and GHG mitigation options. Using the GWP estimates presented in Figure 41, costs of BC mitigation options expressed as USD per tonne of CO_2-equivalent emissions could be compared to consider their competitiveness alongside a range of current monetized per-tonne CO_2 emission estimates. Higher (or lower) CO_2 prices, and a higher (or lower) GWP for BC, would imply more (or fewer) BC mitigation options would be considered to be cost-effective for climate purposes (not accounting for the health benefits described in the previous section).

[820] Monetizing climate benefits of CO_2 reduction is even more uncertain than estimation of health benefits. Impacts of CO_2 emissions are felt globally, over long time periods, are difficult to quantify, and affect a large number of health, economic and environmental systems. Despite these uncertainties, there have been a number of attempts to quantify and monetize these impacts in USD (Mg $CO_2)^{-1}$ (equivalent to USD (tonne $CO_2)^{-1}$) units (referred to as the social cost of CO_2). A meta-analysis of the literature found a median value for the social cost of CO_2 emissions of 47 USD (Mg C)$^{-1}$ under one set of assumptions, with a wide uncertainty range [*Tol*, 2008]. A recent U.S. Department of Energy rule presented a range of values from 17 to 238 USD (Mg C)$^{-1}$ for the year 2010 [*DOE, U. S. Department of Energy*, 2010, Table IV.19]. The few existing policies to date that have resulted in a CO_2 market price can provide another means of gauging acceptable monetization values, as these policies implicitly assigned a value to the reduction of emissions; however, such prices are determined in a manner much different than the analytical approach described above. One example is the European Union Emission Trading Scheme, where European Union Allowance futures prices ranged from about 30 to 90 USD (Mg C)$^{-1}$ during 2011 [see www.theice.com].

[821] It may be feasible to use CO_2-equivalent emissions of BC and the social cost of CO_2 to approximate a monetization of the climate benefits of BC reductions. Along with monetized estimates of the health benefits, this valuation would enable comparison of the net benefits of a BC reduction measure to the net costs of that measure. For example, *UNEP/WMO* [2011b] and *Shindell et al*. [2012] found a net present climate benefit of USD 225 billion (+118/−212) from the reduction of BC and co-emitted species in the year 2030 due to the implementation of several BC measures. However, there are many caveats about using the social cost of CO_2 in such an analysis. Most estimates of the social cost of CO_2 come from evaluating impacts that occur decades in the future. Some estimates of the social cost of carbon even show near-term benefits from slight warming which are outweighed by the larger negative impacts from more extreme warming in the future. In contrast, BC has a very short lifetime. Therefore, both impacts of CO_2 and the resulting valuation should differ from those of BC.

[822] Additionally, several BC impacts are not captured in a globally averaged, climate-forcing based metric. Depending on the location of emission, sources may affect snow- and ice-dominated regions such as the Arctic and the Himalaya. They may also affect climate in ways not represented by global-average climate forcing such as changes in the Asian monsoons (section 9). Some of these issues are outlined in sections 8 and 9, but targeted scientific studies have not yet supported quantification of these additional factors. Therefore, these inquiries are in the emerging phase.

13.4. Technical and Programmatic Feasibility for Individual BC-Rich Source Categories

[823] We briefly review here key mitigation options for each of the major emission source categories, and discuss the mitigation potential for each source with regard to the key factors presented above. The potential for reducing climate forcing presented here is largely based on the global results for emission and forcing categories shown in Figs. 8, 9, 37, and 39. A key caveat is that the analysis in sections 4 and 11 reflect the contribution of all emissions from a given source sector, whereas a mitigation technology may not reduce all of those emissions proportionally. In particular, mitigation that improves combustion without altering activity rates affects only non-CO_2 gases, aerosols, and aerosol precursors.

[824] To date, almost no policies have specifically sought to reduce BC. Most related policies have addressed the more aggregated particulate matter, of which BC is a component, for purposes of improving local air quality and public health. There is therefore a significant amount of literature on the potential and costs of PM emission reductions, but much less literature focused on mitigation options addressing BC specifically.

[825] Many of the mitigation options for PM are identical for BC, but this is not always the case. While a number of studies estimate the costs of mitigating PM, mitigation measures often affect primary PM emissions in a different manner than they affect secondary PM precursor emissions, and sometimes lead to differing reductions of the components of primary PM such as POA and BC. Therefore, mitigation analyses that explicitly determine effects on BC emissions are important. Furthermore, reductions in PM have typically been sought in areas of high concentration, mainly urban areas, and are most easily developed for sources for which end-of-pipe mitigation options are available, such as power plants, vehicles and some industrial processes. Research into mitigation for sources that are more rural in nature is just beginning, especially for those sources that are predominantly located in developing countries, and many of these sources may be important for climate change considerations.

13.4.1. Diesel Engines

[826] Mitigating BC emissions from on-road and off-road diesel sources appears to offer the best potential to reduce net forcing because the net climate forcing is positive and larger than found for other principal source categories. These off-road sources include agricultural, construction and other land-based mobile equipment. From these sources, more than the others in Figure 8, the emission ratio of BC:POA is higher, which reduces the magnitude of negative aerosol forcing terms relative to direct positive forcing. For Euro II

heavy-duty vehicles as shown in Figure 39, NO_x emissions are a substantial contributor to the climate impacts, with offsetting O_3 (warming) and nitrate (cooling) effects in the short term and additional longer-term negative forcing from the NO_x interaction with methane. Therefore, for some diesel sources, the net impact of mitigation options depends on how co-emitted NO_x is affected.

[827] Reductions in mobile-source emissions have been pursued since the 1960s, and technology to reduce emissions from diesel engines is mature. Programs to implement this technology differ by region and type of engine use.

[828] 1. In industrialized countries such as the USA, European Union, and Japan, PM emission standards already effectively control BC emissions from most new diesel vehicles. With the introduction of more stringent PM standards, diesel emissions in these countries are projected to decrease. The rate of reduction largely depends on how quickly older vehicles are retired and replaced with cleaner new vehicles [*EPA*, 2012]. In these countries, continued enforcement and monitoring will be important to deliver the expected emission reductions. Further mitigation of BC from diesel engines is available mainly from retrofits and accelerated vehicle retirement.

[829] 2. In some developing countries, higher-emitting vehicles are still being sold. Accelerating implementation of advanced emission standards in these countries, which requires the use of low-sulfur fuels, would lead to reductions of BC. Monitoring to ensure compliance is also required.

[830] 3. Even in countries with on-road vehicle emission standards, some unregulated or poorly controlled sources remain. For example, regulations may not cover some stationary diesel engines or off-road sources, and better inspection and maintenance programs could address poorly maintained, high-emitting vehicles.

[831] 4. Finally, work still remains to determine the most effective ways to apply existing technology to marine and other off-road engines.

[832] The costs of a diesel particulate-filter retrofit for a heavy duty truck ranging from 5000 to 17,000 USD per vehicle have been reported [*Schrooten et al.*, 2006; *CARB*, 2009], and in some locations (such as the USA, and particularly California) there have been investments of hundreds of millions of dollars in such retrofits. A diesel particulate filter reduces more BC when installed on a large truck than on a small truck if all else is equal, while older vehicles are more polluting per mile but have a shorter remaining lifetime. Therefore, the cost-effectiveness of a diesel retrofit will depend on both the type and age of a vehicle. *Sarofim et al.* [2010] analyzed the potential of diesel retrofits for on-road vehicles to reduce BC emissions in the USA; the study focused on diesel engines that do not meet the more rigorous particulate emission standards that were introduced in the USA in 2007. The study found that costs ranged from 36 thousand USD Mg^{-1} to 318 thousand USD Mg^{-1} BC abated, depending on the age and type of vehicle being retrofitted. The study did not address high emitters or any abatement options besides retrofits. *UNEP* [2011] reported comparable costs for heavy-duty diesel vehicles (i.e., 120 to 200 thousand USD per Mg BC). Installation of filters in new diesel vehicles costs less than retrofitting older vehicles [*EPA*, 2012].

[833] Most developing countries have not yet implemented strict emission standards, and in many cases their fuels are still too sulfur rich to be compatible with diesel particulate filters. Except in the United States, Canada, the European Union, Japan, and some large metropolitan areas in Asia, sulfur fuel levels of 50 ppm or less are not common [*EPA*, 2012, Appendix 4]. Diesel particulate filters can be used with low sulfur fuel (50 ppm) but are more effective when the sulfur content is even lower [*Blumberg et al.*, 2003]. Diesel oxidation catalysts, which can be used to reduce PM emissions even with fuel compositions of several-hundred-ppm sulfur, are ineffective at controlling BC. Some projections [e.g., *Streets*, 2007] reflect the possibility that BC emissions could continue to grow in the transport sector in these regions absent policy interventions, given projected growth in vehicle fleets. *Shindell et al.* [2011] found climate benefits in 2030 as a result of applying European emission standards for diesel vehicles in India and Latin America, with health benefits resulting from the tighter standards in all regions. However, reductions of organic carbon and sulfates make the net climate effect less clear or even lead to warming in some other developing countries such as China.

[834] Non-retrofit reduction options also exist. Reduction of idling through regulation, education, electrification of rest stops, and other means has been explored [e.g., *EPA*, 2009b]. Improved inspection and maintenance, accelerated vehicle retirement, improved efficiency, smart transport algorithms to plan shipping routes, low emission zones, and shifting transport modes to rail and non-motorized transport, can also lead to decreased emissions. These abatement possibilities may generate fuel savings, as well as GHG reductions. Biodiesel use may also lead to lower particulate emissions [*EPA*, 2002].

[835] Diesel retrofits are a good example of how mitigation options do not always reduce all POA species proportionally. Diesel oxidation catalysts reduce OC emissions but offer little BC mitigation benefit [*Shah et al.*, 2007], whereas diesel particulate filters reduce BC with equal or greater effectiveness to other PM components. Diesel particulate filters are also a case where mitigation of some pollutants (BC and POA) may lead to changes in emissions of other pollutants such as an increased NO_2 to NO ratio leading to the potential for higher local O_3 concentrations [*Millstein and Harley*, 2010] or a possible fuel penalty resulting from increased back pressure. As with any end-of-pipe abatement technology, the net climate effect of the installation of a diesel particulate filter will be different from the net effect of the diesel category overall because a filter does not reduce all pollutants equally.

[836] Technical mitigation of diesel engines is in the mature stage for end-of-pipe control, but may have reached only the solidifying stage for retrofit programs. In addition, programs that promote mitigation are in a wide range of phases in less-industrialized countries.

13.4.2. Industry

[837] Figure 37 shows that emissions from industrial sources as a whole are likely to produce net negative direct and indirect climate forcings due to co-emissions, especially sulfur. However, industrial sources are quite heterogeneous, and the aggregated value in Figure 37 masks the fact that individual source profiles have more positive or more negative forcing. For example, emissions from the Bull's trench brick kiln shown in Figure 39, which is an

Indian brick kiln using low-sulfur coal, likely produces positive forcing. Other industrial coal combustion activities discussed in section 4 include small boilers, process heat for brick and lime kilns, and coke production for the steel industry. Knowledge regarding this source category is in an emerging state. Data availability for both activity and emission factors for these sources are poor; estimates of emission magnitudes and composition sometimes have no measurement support.

[838] Extensive work has addressed emission reductions from industrial and manufacturing sources, but these measures may not apply to installations such as brick kilns or coke ovens, which are widespread in developing countries and almost completely absent in developed countries. Likewise, although technical and programmatic feasibility is in advanced stages in industrialized countries, it is still in emerging stages in the developing countries where most BC emissions occur.

[839] Lower-emitting technology and controls exist for both brick kilns [*Heierli and Maithel*, 2008] and coke ovens [*Polenske and McMichael*, 2002; *EPA*, 2008]. These alternatives usually require complete replacement of the installation with more modern technology and thus require large capital outlays (at least 25,000 USD for a more energy efficient technology identified by *Heierli and Maithel* [2008]). To the extent that lower-emitting technologies emit less BC per unit fuel, they would be more beneficial for climate purposes than technologies that strictly improve efficiency (and would therefore reduce BC or sulfur per unit output in equal proportions).

[840] *Rypdal et al*. [2009b] found that industrial source abatement makes up a significant fraction of the least expensive abatement options globally based on extrapolating GAINS model cost curves to the developing world. *Rypdal et al*. did not consider fuel switching as a mitigation option, which is especially important for reductions of residential combustion emissions. *Streets* [2007] found that East Asia was a source of potential industrial reductions of BC emissions, but that existing regulations have already captured a large portion of those reductions in other regions.

[841] In some regions, both coke ovens and brick kilns are being phased out due to developing government action. The fraction of coke produced by traditional or beehive ovens in China has declined after the 1990s [*Huo et al*., 2012], and several South Asian countries have introduced regulations to limit brick kiln operation near urban areas. Improved kilns could also improve efficiency for charcoal production and thereby reduce emissions in Kenya [*Bailis*, 2009]. Potential for addressing these sources could be large. Replacement of a single industrial source would reduce larger quantities of emissions than a replacement of a residential or mobile source and, thus, transaction costs could be lower.

13.4.3. Residential Solid Fuel: Heating

[842] As shown in Figures 8 and 9, wood for heating purposes is a significant source in northern regions such as Europe, North America, and central Asia [see also *Arctic Council*, 2011]. Figure 37 shows little to no potential for reducing global climate forcing from conventional wood stoves by targeting BC emissions because co-emitted species contribute a negative climate forcing, and the net effect of emissions from the residential heating category is uncertain in sign. Like industrial sources, this sector is also heterogeneous. Figure 39 shows that wood boilers specifically offer potential to reduce positive forcing associated with BC emissions. Further, the potential for mitigating climate forcing might be greater in certain regions such as the Arctic. *Quinn et al*. [2011] states that OA co-emitted with BC is unlikely to offset positive climate forcing due to BC when emissions reach the Arctic. Over snow and ice covered surfaces, even OA may exert a positive forcing. Furthermore, as noted in section 7.2, the net aerosol indirect and semi-direct effects in the Arctic may lead to a smaller negative forcing or even positive forcing compared with the global average. *UNEP/WMO* [2011a; 2011b] explored the effect of widespread adoption of pellet stoves and boilers in industrialized countries as well as use of coal briquettes in China, Russia and Eastern Europe, and found that the combination resulted in 0.05°C of avoided warming globally and 0.1°C of avoided warming in the Arctic by 2040.

[843] Wood stoves serving single-family homes can be used as the primary source of heat or as a supplement to conventional heating systems. Stove emissions can be reduced through changes in the stove technology or changes in the nature of the fuel. In the USA, emission limits have been in place for new stoves since 1988. Three major categories of stoves meet modern particulate emission standards: non-catalytic, catalytic, or pellet stoves. Non-catalytic stoves include baffles and secondary combustion chambers for emission reductions whereas catalytic stoves reduce emissions through the use of metals that increase oxidation rates. Catalytic stoves are slightly cleaner and more efficient, but are more expensive and require more maintenance and upkeep. Pellet stoves are designed to burn pellets of sawdust, wood, or other biomass materials. In Europe, several countries (e.g., Nordic countries, Germany, Sweden, and Austria) have introduced voluntary eco-labeling of stoves with standards for efficiency and emissions. Some countries (e.g., Austria, Sweden, Norway, Denmark, Germany) also issued national emission standards for small residential installations; the most comprehensive at this time is a German law from 2010 (*Federal Law Gazette*, 2010). Finally, the European Commission Renewable Directive (2009/28/EC) set combustion efficiency standards while the Ecodesign Directive (2009/125/EC) is being extended to include small residential combustion of solid fuels. These developments mean that the technical feasibility of alternatives is in the mature phase, although programmatic feasibility for widespread implementation may vary considerably by country. While pellet stoves are cleaner than many other options, they may not be cost-effective for users who harvest their own wood for fuel. Prices for these kinds of stoves range from 1000 to 3000 USD; one estimate suggests that the cost-effectiveness of reductions for replacement of a wood stove ranges from 130 USD $(\text{Mg PM})^{-1}$ for a non-catalytic stove to almost 1000 USD $(\text{Mg PM})^{-1}$ for a pellet stove [*Houck and Eagle*, 2006]. Few studies have examined the relative BC to POA ratios for each of these technologies and, therefore, the net climate effect of switching to a less polluting technology may differ from the net climatic impact of the entire category.

[844] Larger boilers for multi-family homes may also be wood-fired, and such installations are found in several European countries. These boilers can range from 150 kW up to 1 MW in size. Little information is available about the

quantities and technologies used in these installations. Cyclones are sometimes used to reduce PM emissions in older installations, but more advanced controls would be required for effective removal of submicron particles, including BC. Newly built installations are often efficient, low-emission pellet, chip, or sawdust boilers.

13.4.4. Residential Solid Fuel: Cooking

[845] Figure 37 shows a slight net positive forcing, with large uncertainty, from biofuel cooking based on emission factors within the GAINS model. Positive forcing by BC is offset by direct and indirect effects of co-emitted organic matter. In contrast, Figure 39 shows a more strongly positive forcing from residential cooking stoves based on in-field measurements, so careful scrutiny of specific technologies is necessary to have confidence in the net effect of mitigation choices. For wood use, changes in the methane budget caused by direct methane and CO emissions add positive forcing in the long term. Therefore, mitigation options that reduce all products of incomplete combustion have the potential to reduce long-term forcing even if first-year forcing is uncertain.

[846] Residential solid fuel is used for cooking primarily in developing countries, and consists of wood, agricultural residues, dung, charcoal, and coal. Improved household energy solutions have been sought for several years. In the early 1980s, forest depletion was the main reason for concern. More recently, in addition to forest depletion, concern is also driven by high PM exposures resulting from indoor solid-fuel use; these exposures lead to severe respiratory ailments and premature deaths numbering in the millions annually [*Smith et al*., 2004]. These activities have largely taken place in the context of development programs without the large-scale investment in environmental measurement or engineering solutions that characterizes the move toward mature technology development.

[847] Stove improvements and fuel switching are the main solutions to reduce environmental and health impacts of household energy use. Early programs that focused on stove efficiency did not always improve air quality [*Smith et al*., 2007], implying that they had little effect on BC. Since that time, stove improvements have included insulating combustion chambers, adding chimneys, and managing air-fuel mixing before and after combustion [*Bryden et al*., 2006]. Chimneys can reduce indoor air pollution and improve combustion by adding draft through the chamber, although some of the reduction in indoor pollution is accomplished by shifting the particulate matter outside [*Johnson et al*., 2006]. Improved stove design has resulted from the advent of emission testing by non-governmental organizations [*MacCarty et al*., 2010], and efforts to promote mass manufacture are also occurring. More advanced combustion technology coupled with a broader understanding of the field has resulted in renewed interest [*World Bank*, 2011]. Nevertheless, understanding of in-use efficiency and emissions as compared with laboratory performance is still limited [*Roden et al*., 2009; *Johnson et al*., 2006; *Johnson et al*., 2008; *Christian et al*., 2010], with in-use emissions typically higher than those measured in laboratory settings. While enhancing efficiency of these stoves decreases total emissions, field measurements indicate that particulate emission per unit fuel is reduced by only up to 50% [*Roden et al*., 2009]. Much of the emission reduction may be POA rather than BC, so that not all mitigation options may reduce total climate forcing.

[848] Air flow management in stoves and cleaner fuels may be required to reduce emissions further. The former can be accomplished either with fans that introduce secondary air or with gasification stoves, which separate fuel devolatilization and combustion. Both fan stoves [*Jetter and Kariher*, 2009] and gasification stoves [*Mukunda et al*., 2010] show very good emission performance in laboratory settings, but they are rare enough in the field that in-use performance is not well characterized. Stoves without chimneys are in the 10–20 USD range, while those with chimneys require more material, individual installation and presently range from 40 to 100 USD. Gasifier stoves are typically 50–100 USD.

[849] Emissions from residential cooking are greatly reduced when the users switch to modern fuels such as liquefied petroleum gas, kerosene, or electricity [*Smith et al*., 2000a; 2000b]. Cleaner fuels can also be provided by processing solid fuels and producing briquettes, pellets, and charcoal made from either wood or agricultural waste. Some programs deliver both stove and fuel [*Zhi et al*., 2009], because performance depends on the combination of the two. However, emissions from fuel production in addition to end-use must be considered in the calculation of climate impact [*Bailis et al*., 2005].

[850] Implementation of cookstove replacement programs is challenging. Cookstove initiatives that do not offer affordable, reliable operation that meets the needs of the main user in real-world settings may not have long-term success [*Hanna et al*., 2012]. Historical programs in China had some success in delivering better wood stoves with chimneys [*Smith et al*., 2007, *Sinton et al*., 2004] but a large, long-standing national program in India may not have affected emissions. These are examples of the importance of addressing implementation feasibility alongside cost and environmental attributes. Most recently, the Global Alliance for Clean Cookstoves was launched as a public-private initiative to address public health and climate change by "…creating a thriving global market for clean and efficient household cooking solutions." Technical and programmatic feasibility for this source category is in the emerging phase.

13.4.5. Open Burning

[851] Figures 37 and 39 show either near-zero or net negative forcing estimates for current baseline emissions from agricultural burning, forest burning and grassland burning. The negative climate forcing from co-emitted POA is substantial for each category, even offsetting the long-term positive forcing caused by effects on the methane budget. These sources, therefore, are not good candidates for BC-focused mitigation actions, if near-term global climate change is the main concern. The exception here, as with residential heating, is if some burning sources affect the Arctic or other snow- and ice-dominated areas or have other significant regional climate impacts (section 8) [*Quinn et al*., 2011].

[852] Work on open burning reduction for BC mitigation is moving from the nascent to the emerging phase of analysis in Figure 42. For open burning sources the preliminary nature of the analysis, resistance to changing management

practices, and difficulties in quantifying reductions may present barriers to implementing mitigation options.

[853] *Sarofim et al*. [2010] analyzed biomass burning abatement potential in the USA by considering mitigation options such as using propane burners on stacked crop residues, backing fires, conservation tillage, soil incorporation, central processing sites, and a number of forestry prescribed-burn mitigation options [derived from *Ottmar et al*., 2001; *EPA*, 1992, 2005; *Massey*, 1997; *WRAP*, 2002; *USDA*, 2005]. Some of the options are estimated to have negative costs: mainly conservation tillage for agriculture [*Massey*, 1997], but also mechanical removal of small trees followed by use of the biomass as feedstock for electricity generation facilities [*USDA*, 2005]. The remaining options for reducing BC emissions for less than 40 thousand USD $(Mg)^{-1}$ all relate to adoption of practices to reduce emissions from prescribed burning of forests or grasslands. While this analysis serves as a representative example of how to develop mitigation cost estimates for open burning, extension of this analysis to regions outside the USA is only appropriate for regions with similar properties in terms of managed forests, grasslands, and agricultural practices.

13.4.6. Other Sources

[854] Marine shipping contributes about 2% of global BC emissions, but may constitute a larger fraction of direct BC emissions in remote regions. In particular, the Arctic is a sensitive region with few other direct sources of BC emissions, where the high surface albedo due to snow and ice cover will reduce the cooling by co-emissions, and where there is potential for increased ship routes in the future as sea ice recedes (though the reduction of sea-ice cover will also lead to a reduced albedo and, therefore, a smaller BC impact over time). If sulfate emissions from ships are controlled for non-climate reasons, the BC-to-sulfate ratio will increase and increase the probability that mitigation would have net climate benefits. For example, new regulations of the United Nations International Maritime Organization will require sulfur content in fuel for marine vessels to be reduced to 0.5% by 2020 [*Winebrake et al*., 2009], and some proposed and existing Emission Control Areas currently have stricter standards than the global standard of 4.5%. However, the fact that most BC emissions from ships occur over low-albedo surfaces in regions where hydrological impacts are less critical means that mitigation of emissions globally is less likely to have climate benefits.

[855] There is interest in better quantifying BC emissions from oil and gas flaring but the work in this area is still preliminary [*Arctic Council*, 2011]. As shown in Table 8, there are a number of other smaller BC sources such as power generation and gasoline engines that have traditionally not been a major target of BC mitigation analysis. However, there have been some exceptions. *Shindell et al*. [2011] show that BC reductions are a key contributor to net cooling resulting from tighter gasoline vehicle standards. There has also been occasional interest in the impacts of BC emissions from aviation despite being less than 1% of global emissions. However, due in part to the altitude of the emissions [*Hendricks et al*., 2005; *Koch and Hansen*, 2005] there is little BC mitigation data available for these sources.

13.5. International Perspective on BC Reductions in Aggregate

[856] In addition to understanding the BC mitigation opportunities and potential for each individual source, as briefly provided above, we present here a more macro perspective for evaluating BC mitigation.

13.5.1. Projected Future Emissions

[857] Mitigation considerations are informed by how emissions are projected to change over time. Future emission drivers include economic development, implementation of air quality policies, technological changes, fuel consumption and quality (including sulfur content), land-use change, and behavioral changes. When using projections to prioritize mitigation, it is important to differentiate between those projections which are solely based on existing policies and drivers, and those that make projections based on a presumption of future regulations due to, for example, an assumption that a richer society will demand cleaner air. For projections based on existing regulations, sectors where emissions are expected to grow over time or remain significant are of more importance than those where emissions are expected to decline—however, for projections which include assumptions about future policies, it is important not to discount mitigation actions that are assumed but not yet implemented. A few studies have looked at future BC projections: *Streets et al*. [2004], *Streets* [2007], *Streets et al*. [2011], *Cofala et al*. [2007], and *Rypdal et al*. [2009b] globally; *Klimont et al*. [2009] in Asia; *Sarofim et al*. [2010] and *EPA* [2012] in the USA, *Rypdal et al*. [2009a] in the USA, European Union, and China; and *Walsh* [2008] for the global transport sector. Using the RAINS (Regional Air Pollution Information and Simulation) model, *Cofala et al*. [2007] estimated a 17% reduction of global anthropogenic BC emissions by 2030 relative to present, mainly due to reductions in the mobile sector (diesel particulate controls) and the domestic sector (less coal use and replacement of traditional stoves). *Streets* [2007] also shows global reductions in BC emissions of 9 to 34% by 2030 relative to present, and highlights some regions and sectors where projected emissions may increase under some scenarios over that time period. The changes depend on assumptions about growth, technology development, and environmental policy creation and enforcement. The growth regions and sectors include residential emissions in Africa, open biomass burning emissions in South America, and transportation emissions in the developing world. Projections by *Streets et al*. [2011] show similar regional differentiation in future trends but with less overall global BC emissions decline by 2030. In these projections, decreases between 2005 and 2030 in Northeast Asia, Southeast Asia, the Pacific, North America and Europe due to further air pollution legislation result in slight net global decreases despite increases in most other regions. It has also been suggested that retreat of Arctic sea ice may increase marine shipping in the Arctic [*Granier et al*., 2006; *Corbett et al*., 2010], which might lead to increased emissions in a region with higher sensitivity to carbonaceous emissions due to snow albedo effects.

[858] Because of the short atmospheric lifetime of BC, the timescale of projections most pertinent to mitigation decisions are those on timescales similar to the lifetime of infrastructure

investments (i.e., two to three decades). Nevertheless, for a long-term perspective, it is also instructive to view how BC and co-emissions of POA are projected within the models that have traditionally been used to produce long-term (i.e., out to year 2100 or even beyond) GHG emission scenarios. Long-term emission scenarios have been developed for the climate projections of the forthcoming IPCC Fifth Assessment Report (www.ipcc.ch), scheduled for publication in 2013. These emission scenarios are referred to as "Representative Concentration Pathways" and based on scenarios from four modeling teams (available at http://www.iiasa.ac.at/web-apps/tnt/RcpDb). These pathways are named according to their 2100 radiative forcing level as reported by the individual modeling teams (the four range from 2.6 to 8.5 W m^{-2}). The radiative forcing estimates are based on the forcing of GHGs and other forcing agents, including BC and OC. The Representative Concentration Pathways do not represent specific futures with respect to climate policy action (or no action). Any differences can be attributed in part to differences between models and scenario assumptions (scientific, economic, and technological). Across the four modeling scenarios, projected patterns of global BC emissions are similar: emissions after 2010 decrease steadily, reaching about half of 2010 emissions by the end of the century (Figure 43) [*RCP Database*, 2009]. Sectorally, there are more differences: global emissions in each major sector increase in at least one model out to 2020, and one model shows an increase in global open burning emissions even out to 2030. Regionally, several scenarios show emission growth in Asia (especially transport) and the Middle East and Africa regions (residential and commercial). Organic carbon emissions show a somewhat less consistent pattern, where, depending on the modeling team or scenario, emissions are projected to remain relatively steady or decline more gradually throughout the century. The economic models that produce these scenarios treat emissions in aggregate and lack engineering details, especially after 2030. Therefore, the projection of declining BC and POA emissions is not based on specific policies or technology shifts, but on the assumption that cleaner fuels are used and emission factors decline as income increases.

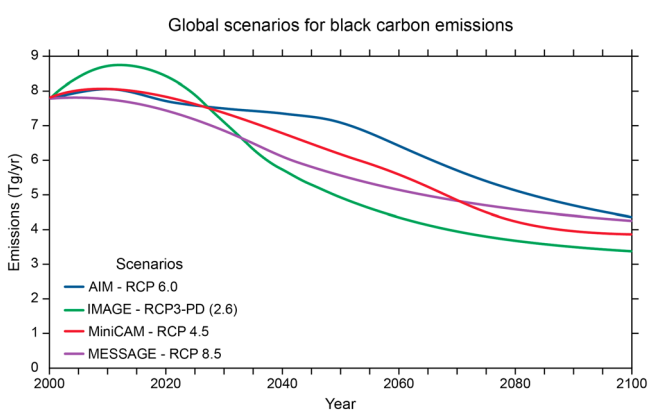

Figure 43. Total global BC emission projections from 2000 to 2100 in the four Representative Concentration Pathway (RCP) scenarios [*Moss et al.*, 2010]. These scenarios are named according to the radiative forcing in 2100 and were developed by four individual modeling groups for use in climate modeling analysis for the IPCC Fifth Assessment Report. Decreasing emissions are a result of expectations of cleaner fuels use and declining emission factors with increasing income.

13.5.2. Comprehensive International Assessments of BC Mitigation Actions

[859] Few studies have examined the potential for BC mitigation across multiple emission sources and across multiple regions within a common economic modeling framework. Simple analyses include those of *Bond and Sun* [2005], *Montgomery et al.* [2009], and *Kandlikar et al.* [2009], who assessed costs and benefits of a few BC mitigation options. Diesel engine retrofits and replacements, cookstove replacements, and super-emitting vehicles are analyzed in all three studies, in addition to gasoline engine and industrial kiln upgrades in a subset of the studies. All three studies identified cookstoves as having the most promising cost-benefit characteristics, whether to achieve climate benefits alone or both climate and health benefits. These studies considered neither the counteracting role of co-emitted aerosols and precursors on indirect effects, nor the additional longer-term positive forcing by co-emitted gases, which could change the results of the analysis.

[860] Analyses by *UNEP/WMO* [2011a; 2011b] and *Rypdal et al.* [2009b] assessed future mitigation strategies to reduce the climate impact of BC and POA from contained combustion. *Rypdal et al.* [2009b] developed cost curves for each of 12 major world regions to describe the technical mitigation potential and costs of reducing BC, as well as co-emitted OC. The cost curves for Europe were generated by the RAINS model, while extrapolations were made for other regions due to lack of detailed region-specific data on technology availability and costs. Because of this extrapolation, the analysis excluded viable alternatives for some sources, especially those for which knowledge is still emerging or is in the early stages of solidifying. For example, small industrial sources and cooking stoves are not widely used in Europe, so replacement technologies were not present in RAINS. Fuel switching was not considered as an option either. These omissions mean that some BC mitigation opportunities are not captured by the analysis. Under these assumptions, in the year 2030, 418 Gg of BC yr^{-1} could be reduced for 4 billion USD annually, 775 Gg for 30 billion USD, and 1200 Gg for 126 billion USD. In comparison, the *Rypdal et al.* study projected that 4400 Gg BC will be emitted in 2030 under current legislation.

[861] While mitigation in the transport sector dominated the suite of feasible reductions in 2030 in the *Rypdal et al.* [2009b] analysis, emission reductions from industrial process activities (such as coke ovens in China and brick kilns in India) are less expensive and, therefore, made up the majority of the first quartile of emissions reductions, as ranked by cost effectiveness.

[862] *UNEP/WMO* [2011a; 2011b] identified several BC mitigation measures that could produce a net global-mean cooling effect. Measures were initially chosen from the GAINS database using one specific value of GWP from the literature. The opportunities identified included tightening of diesel emission standards (i.e., including use of particle filters), brick kiln and coke oven modernization, cookstove improvements, use of efficient pellet stoves for residential heating as well as substitution of coal by coal briquettes, and reduction of agricultural waste burning. Impacts and uncertainties of

the selected measures were then evaluated in more detail. The ultimate analysis of temperature impacts was based on modeling the change in radiative forcing when the mitigation measures were applied in two climate models. The percentage of industrial-era forcing reductions achieved by the measures was scaled by a best estimate and central range of industrial-era forcings. Thus, as in this assessment, modeled BC DRF was increased based on the models' underestimate of BC AAOD relative to observational constraints.

[863] Total BC climate forcing is larger in this assessment (+1.1 W m^{-2}, with uncertainty range of (+0.17 to, +2.1) W m^{-2}) than in the UNEP/WMO Assessment (+0.60, (0.0, +1.0) W m^{-2}) [*UNEP/WMO*, 2011a; 2011b]. Large uncertainties are attributed to indirect effects in both reports. Major differences of our BC forcing compared with the UNEP/WMO assessment are the adjustment to observed absorption, which increases direct forcing; explicit inclusion of the cloud absorption effect; and selection of more negative liquid-cloud effect and more positive mixed-phase cloud effect based on tabulating individual studies.

[864] Additional differences between the two assessments are attributable to the treatment of co-emitted POA, especially its indirect effect. The present assessment attributed indirect forcing to different aerosol species based on total atmospheric mass. Given the lack of constraints from the literature and the lower solubility of OA, the UNEP/WMO Assessment instead attributed indirect effects entirely to sulfate. The total net forcing from co-emitted POA is much smaller in the UNEP/WMO assessment, so that climate benefits of measures tend to be larger than those estimated here. Both assessments stress the uncertainty in attribution of aerosol indirect effects to individual species, and both include large ranges in assessed climate impact.

[865] In the UNEP/WMO Assessment, BC measures were grouped into "technical" and "regulatory" groups. The technical group included primarily diesel measures and the emission reductions produced net cooling, as also suggested here. The regulatory group of measures had impacts whose range encompassed zero, as also found here.

[866] *Shindell et al*. [2012] used the same emission scenarios described above along with detailed climate modeling, and found global mean temperature impacts consistent with the simplified estimates in the UNEP/WMO Assessment. In that model, the combined indirect and semi-direct aerosol forcings resulting from the measures were negative and, hence, augmented rather than offset the reductions in BC DRF. In addition to radiative forcing and global mean climate response, both the UNEP/WMO Assessment and *Shindell et al*. [2012] estimated the impacts of the mitigation measures on health, crop yields, and Arctic temperatures, with large regional precipitation shifts attributed to BC in the climate modeling study.

13.6. Policy Delivery Mechanisms

[867] At the international level, there are forums and agreements where BC mitigation strategies could be addressed. The eight-nation Arctic Council is currently exploring mitigation opportunities for BC, and the Convention on Long-Range Transboundary Air Pollution is exploring the question of how BC could be addressed within its current structure. In 2012, a growing number of nations have announced their support of the voluntary Climate and Clean Air Coalition [http://www.unep.org/ccac] to Reduce Short-Lived Climate Pollutants. Barriers include questions about addressing both long-lived GHGs and short-lived forcers such as BC in a common framework (section 12), and concerns about the consequences of de-emphasizing the importance of long-lived GHGs.

[868] Even if international agreement occurs to move forward with BC reductions, implementation must take place within individual countries. Existing air quality policies may offer the means to deliver near-term mitigation strategies for BC in developed countries and, where such policy frameworks exist, in developing countries where most growth in BC emissions is expected to occur. For example, existing vehicle emission standards for new vehicles, and scrappage and retrofit programs may provide a means of implementing additional BC mitigation in the transportation sector. Other sources may require additional infrastructure for implementation on a large scale, such as reductions of residential cooking emissions in remote areas of developing countries. Some important BC emission sources, such as remote open burning, may lack a policy or program infrastructure supporting reduction. The portfolio of regulations, policies, and programs capable of delivering BC mitigation varies by country, and in some cases could even vary within a country where some air-quality or land-use policies are administered at sub-national levels.

13.7. Synthesis of Considerations for Identifying Important Mitigation Options

[869] Table 29 provides a matrix that presents multiple criteria discussed in this section, and evaluated elsewhere in this assessment, to help identify important mitigation strategies. It summarizes the level of understanding for the following key considerations for identifying promising mitigation opportunities for BC: the magnitude of the emission source (and thus a first-order indication of technical mitigation potential), the potential to reduce net climate forcing, the potential to benefit sensitive regions such as the Arctic, the availability of technologies and management practices, the costs of these strategies, potential health benefits, and implementation feasibility. Not all of the factors for all emission sources can currently be quantified with uniform, or even robust, levels of understanding. The "level of understanding" evaluations in this table are intended to be illustrative and are informed both by quantitative analysis from previous sections of this assessment and by qualitative judgment for some of the non-science factors briefly discussed in this section.

[870] There is considerable variation across BC sources regarding the potential to reduce globally averaged, positive net climate forcing, with many broad emission categories such as residential coal burning, field burning and forest burning offering at best uncertain potential in this regard. If controlling some of these sources preferentially reduces climate forcing in the Arctic or other snow- and ice-dominated regions, or avoids interference with the Asian Monsoon, climate benefits not reflected in Figure 39 may accrue. With regard to technical feasibility, there are known emission mitigation options for most BC sources. However, there is variation in the degree to which these mitigation options are characterized with regard to impacts on BC and co-emissions and costs. Programmatic feasibility also varies. Some emission sources are already associated with a policy

Table 29. Evaluation of Criteria for Mitigation of BC Emission Sources[a]

	Criteria						
Emission Source	Source Magnitude[b]	Global Climate Forcing[c]	Arctic Climate Forcing[d]	Mitigation Technologies or Practices[e]	Mitigation Cost Effectiveness[f]	Health Benefit[g]	Implementation[h]
On-road diesel	H	H	H	H	H	H	H
Off-road diesel	M	H-M	M	H	M	H	H
Industrial coal	M	L	L	M	M-L	H	M
Biofuel cooking	H	H-L	L	M	M	H	L
Biofuel heating	L	M-L	H	M	M	H	M-L
Residential coal	L	H-M	M	M	M	H	M
Agricultural field burning	L	M-L	M	M-L	M	H-M	M-L
Forest burning	H	L	H-M	M-L	H-L	H-L	L
Grass and woodland burning	H	L	L	M-L	H-L	H-L	L

[a]This table presents a qualitative evaluation of several criteria for a range of emission sources that may inform priorities for BC mitigation actions. The first two columns represent criteria for which comprehensive, quantitative analysis is available from previous sections of this assessment. Indicators designate criteria potential as high (H), medium (M), or low (L).

[b]Sources with greater magnitude are considered to have greater technical mitigation potential. See section 4.

[c]Potential to reduce globally averaged climate forcing, based on best estimates from section 11. "High" reflects likely warming effect globally, "Medium" reflects uncertainty regarding global effect, and "Low" reflects likely cooling effect globally.

[d]Potential to reduce Arctic climate forcing, reflecting near-Arctic sources of emissions and albedo effects. See section 8. Other regional effects not captured by global climate forcing, such as changes to Asian Monsoons, could also be considered.

[e]Availability and characterization of mitigation technologies or practices. See section 13.

[f]Magnitude of mitigation costs per unit of BC reduced. See section 13.

[g]Potential to provide health benefits, reflecting likely population exposure. See section 13 for brief discussion.

[h]Potential for near-term implementation at large scales. See section 13 for brief discussion.

infrastructure to deliver mitigation practices at large scale (e.g., diesel sources), whereas other sources (e.g., forest burning) are less amenable to near-term and large-scale policy intervention.

[871] While health effects are not evaluated in this report, there is always the potential to obtain some degree of health benefits by mitigating BC emissions. Emissions that preferentially occur in populated areas have large health impacts, while emissions that occur indoors expose fewer people, but at higher concentrations. The lowest health impacts occur for outdoor emissions that occur at low population density. *UNEP/WMO* [2011a; 2011b] and *Anenberg et al.* [2012] provide detailed evaluations of health impacts from outdoor air.

[872] Diesel sources of BC appear to offer the most promising mitigation opportunities in terms of near-term forcing and maturity of technology and delivery programs. Although some options, such as diesel retrofits, may be costly relative to other BC mitigation options, they may also deliver significant health benefits. Mitigating emissions from residential solid fuels may yield a reduction in net positive forcing. The near-term net effect remains uncertain because of uncertain knowledge regarding the impacts of co-emitted species on clouds, but longer-term forcing by co-emitted species interacting with the methane budget is positive. Furthermore, the evolution of feasibility is still in the emerging phase for these sources. The net effect of small industrial sources depends greatly on the sulfur content of individual sources, and the feasibility of mitigation is in the emerging phase. Individual source types that have low sulfur emissions and for which alternative technology is available could offer net climate benefits.

[873] **Acknowledgments.** This assessment is a contribution of the IGBP-IGAC/WCRP-SPARC Atmospheric Chemistry and Climate Initiative (AC&C). The authors acknowledge financial and technical support from the International Global Atmospheric Chemistry (IGAC) project (http://igac.jisao.washington.edu/index.php), C. Koblinsky of the Climate Program Office of the National Oceanic and Atmospheric Administration (NOAA), H. Maring of the Radiation Sciences Program of the National Aeronautic and Space Administration (NASA), Rose Kendall of CSC, and Beth Tully of Tully Graphics. IGAC funding for this project is via the Joint Institute for the Study of the Atmosphere and Ocean (JISAO) under NOAA Cooperative Agreement NA10OAR4320148, Contribution No. 2035. The authors are grateful to Ray Minjares and the International Council on Clean Transportation (ICCT) and Catherine Witherspoon of the ClimateWorks Foundation for encouragement to undertake this effort. The authors wish to thank the AeroCom modeling community and the AERONET data providers for their great help in providing basic data sets, further analyzed here. Olivier Boucher is thanked for his substantial contribution to section 9 and his careful review and subsequent discussion with the author team on the entire manuscript. We also thank N. Riemer of the University of Illinois for particle-resolved simulation results in Figure 6, N. Mahowald of Cornell University for dust fields in Figure 12, and D. M. Winker of NASA for providing the CALIPSO data in Figure 16. A. Heil is thanked for providing information on biomass fuel loads and M. O. Andreae for providing updates of his biomass burning emission factor compilation. E. Baum, J. Bachmann, R. Minjares, K. Ram, V. Ramanathan, and D. Zaelke are thanked for reading and providing comments that improved the document. T. C. Bond acknowledges support for related work under U.S. EPA RD-83503401, NASA RD-83503401, NSF ATM 08-52775, and DOE DE-SC0006689. Piers Forster acknowledges support from a Royal Society Wolfson Research Merit award. N. Bellouin was supported by the Joint DECC/Defra Met Office Hadley Centre Climate Programme (GA01101). S. Ghan was supported by the U.S. Department of Energy (DOE), Office of Science, Scientific Discovery through Advanced Computing (SciDAC) program, and the DOE Decadal and Regional Climate Prediction using Earth System Models (EaSM) program. The Pacific Northwest National Laboratory is operated for the DOE by Battelle Memorial Institute under contract DE-AC06-76RLO 1830. Y. Kondo was supported by the Ministry of Education, Culture, Sports, Science, and Technology (MEXT), strategic international cooperative program of Japan Science and Technology Agency (JST), and the global environment research fund of the Japanese Ministry of the Environment (A-1101). For P. K. Quinn's work, this is NOAA PMEL contribution no. 3786. M. Schulz received funding support through the EUCAARI project (EU-FP6 Contract 34684). M. Z. Jacobson received funding from the U.S. National Science Foundation. J. W. Kaiser was supported by the European Union Seventh Research Framework Programme (MACC project, contract number 218793). S. G. Warren acknowledges support from U.S. NSF grant ARC-06-12636. H. Zhang was funded by the National Basic Research Program of China (2011CB403405). The views expressed in this paper are those of the authors and do not necessarily reflect the views or policies of the U.S. Environmental Protection Agency.

Appendix A: Author Contributions

[874] The development of this assessment required a large, diverse group of dedicated authors. They synthesized multiple topics in the individual sections and interlinked the topics throughout. Each section required lead-author commitment equivalent to the production of a typical journal paper. The publication of this assessment in a peer-reviewed journal necessitates a first author, thereby precluding the section lead authors from receiving the lead-author credit normally accorded for this level of effort. The author order begins with the first author and three coordinating lead authors (Doherty, Fahey and Forster) followed by the lead authors and contributing authors in alphabetical order. The table below acknowledges the principal contributions of each author in an attempt to further recognize their substantial investment in this assessment.

Table A1. Author Principal Contributions

Section—Topic	Lead Authors	Contributing Authors
2—Introduction	T. C. Bond	
3—Measurements and microphysical properties	P. K. Quinn Y. Kondo	S. Ghan U. Lohmann J. P. Schwarz
4—Emissions	C. Venkataraman M. G. Schultz	T. C. Bond S. K. Guttikunda P. K. Hopke J. W. Kaiser Z. Klimont
5—Constraints on abundance	S. Kinne T. C. Bond	M. Schulz
6—Direct radiative forcing	S. Ghan M. Schulz S. Kinne T. C. Bond H. Zhang	
7—Cloud effects	D. Koch B. Kärcher	T. Storelvmo U. Lohmann
8—Cryosphere changes	S. J. Doherty M. G. Flanner	S. G. Warren
9—Climate response	P. M. Forster	N. Bellouin D. Koch M. G. Flanner S. J. Doherty M. Z. Jacobson D. Shindell C. S. Zender
10—Synthesis	P. M. Forster D. W. Fahey	
11—Net climate forcing	T. C. Bond	
12—Emission metrics	T. Berntsen	
13—Mitigation considerations	B. J. DeAngelo M. C. Sarofim S. Zhang	

Appendix B: Using Sky-Photometer Aerosol Absorption Optical Depth Retrievals to Constrain Black Carbon Models

B1. Background and Methods

[875] Aerosol absorption optical depth (AAOD) associated with BC column amounts is a key factor controlling model estimates of BC DRF. The diversity in modeled BC AAOD is one of the major factors contributing to diversity in estimates of BC DRF. To reduce BC-DRF uncertainty, we use retrievals from a global network of ground-based sun-/sky-radiance observations (AERONET) to adjust the BC AAOD simulated by models. Our AAOD estimates use measurements that cover complete annual cycles for 2000 to 2010 at 171 land sites distributed worldwide, and data from an additional 78 sites with incomplete annual cycles. By applying some assumptions, detailed below, values of BC column absorption (BC AAOD) can be extracted from the AERONET retrievals. These values can be compared to those simulated by models at the same location and time, and regional scale factors for BC AAOD can be determined from the ratio of observationally estimated to simulated BC AAOD. These scale factors are used in this assessment to reduce the bias in models used to determine BC DRF.

[876] Sun and sky radiance observations [*Dubovik and King*, 2000] in the mid-visible range allow inference of the aerosol column absorption in terms of the AAOD (=AOD $\times$ $[1-\omega_0]$) from retrievals of AOD and single-scattering albedo (ω_0) at 550 nm. Regular retrievals for cloud-free conditions with identical instrumentation at many AERONET locations [*Holben et al.*, 1998] provide extensive coverage over continents and islands. A comparison of AAOD retrievals with in situ measurements showed good agreement from 300 to 700 nm and a possible high bias in AERONET AAOD at 880 nm [*Corrigan et al.*, 2008, Figure 16]. However, because retrievals of ω_0 are less certain at low AOD [*Dubovik et al.*, 2000], absorption data for low AOD cases are removed from the official AERONET Version 2.0 product. This filter introduces a positive bias for local statistics of AAOD because only cases with high AOD are counted. To remove this AAOD bias, missing refractive index data in the Version 2.0 data product have been recovered from the lower-quality Version 1.5 data product, so that now low AOD cases are included as well. This procedure adds noise to the retrieved AAOD data set but is expected to reduce the sampling bias (*O. Dubovik*, personal communication, 2008). However, a small positive sampling bias may still exist, because values of ω_0 greater than 1 (negative absorption) are excluded from the data set. The retrieved AAOD is very similar to that from an alternative procedure in which ω_0 is retrieved only from high-AOD observations at each station and applied to all AOD values at that station, thus maximizing the use of Version 2.0 data. The mean AAOD averaged over all samples at all AERONET sites is 0.018 using the Version 1.5 ω_0, which is a factor of 2 smaller than the mean value (0.040) from the version 2.0 retrieval of AAOD.

[877] Refractive indices at 440 nm and 670 nm inferred from the AERONET data are interpolated to 550 nm. Real refractive indices are interpolated linearly and imaginary refractive indices are interpolated in log-log space, which would produce spectral absorption that is well described by the absorption Ångström exponent (equation (3.1)). In the mid-visible solar spectral region, non-BC contributions to absorption are mainly from relatively coarse dust particles. To separate BC AAOD from total AAOD, we assume that BC controls the mid-visible absorption of small (i.e., "fine-mode") aerosol particles and dust controls the absorption of particles larger than 1 μm diameter. This implies that any mid-visible absorption by organic matter, brown carbon or small-sized dust is attributed to BC. This separation by size is possible because the AERONET inversion method provides detailed size-distribution data. We estimate dust AAOD from the super-micron part of the retrieved size distribution and an assumed refractive index of $1.55+0.0015i$ [*Dubovik et al.*, 2002, Table 1]. Finally, BC

AAOD is estimated as the difference between the AERONET total AAOD and the dust AAOD. All calculations are performed at 550 nm.

[878] The AERONET retrieval also provides an estimate of the refractive index, but it applies to the entire aerosol in the column which almost always contains a combination of constituents; thus, the index is not applicable for individual components of the column aerosol such as BC, OA and dust. Thus, we use an assumed value for the dust refractive index rather than a retrieved value from AERONET to calculate the dust contribution to total AAOD. Similarly, assuming the imaginary part of the retrieved refractive index applies to submicron particles yields BC AAOD estimates that are too low if the dust absorption dominates the retrieved refractive index, because the retrieval is strictly valid only for the entire size distribution (section B2).

[879] If AERONET stations provided globally uniform high-resolution coverage for ocean as well as land locations, the AERONET BC-AAOD retrievals could be directly used to constrain model simulations. However, Figure 14 shows that although there are hundreds of AERONET stations distributed across the Earth, coverage is limited to land and is far from homogeneous over land. Additional assumptions are required for locations without AERONET data.

[880] To fill in the gaps between stations we use spatial distributions of BC AAOD from AeroCom simulations [*Kinne et al.*, 2006]. Median values of the set of 15 AeroCom models are used for each month and mapped onto a $1^\circ \times 1^\circ$ latitude-longitude grid. The model ensemble median is, henceforth, referred to as the AeroCom median. The AeroCom BC AAOD is estimated from the BC AOD saved for each model. Based on Mie theory and the assumption of the same BC size distribution (i.e., lognormal with 0.065 μm number mode radius and geometric standard deviation of 1.7) and refractive index (1.7, 0.7*i*) for all models, we use an ω_0 of 0.36 for BC to convert from BC AOD to BC AAOD. To compare AeroCom models that estimate only industrial-era BC AAOD with AERONET observations of total AAOD, we rely on one AeroCom model (LOA) to provide the industrial-era fraction of BC (i.e., (all-source BC AAOD − preindustrial BC AAOD) / (all-source BC AAOD)), thus estimating a preindustrial background AAOD of 0.0004. Using global mean values for both the industrial-era and all-source BC AAOD, this ratio in the LOA model is 0.80, but the ratio among model grid boxes ($1^\circ \times 1^\circ$) varies widely, from near zero in regions with large natural emissions to 97% in regions with large anthropogenic emissions. Modeled global mean values without any scaling are 0.00172 for industrial era BC AAOD and 0.00212 for all-source BC AAOD.

[881] The AeroCom BC-AAOD values do not agree with the AERONET retrievals, so the BC-AAOD distribution from AeroCom is scaled to agree with the AERONET retrievals at the station locations. Errors in emissions or BC scavenging vary spatially, producing different biases, so separate scale factors are calculated for each region (Table B1 and Figure 7). For each region, all AERONET data available for a given month are combined, and from this data set a characteristic regional value is calculated using the average values between the 25% and 75% percentiles. This average is chosen instead of the mean to avoid the impacts of extreme outliers. The same quantity is determined for the AeroCom median field at the locations of AERONET observations. These averages are referred to as the "characteristic values" from AERONET and AeroCom. The ratios of the AERONET to AeroCom characteristic values then define the regional (monthly) scale factors.

[882] Table B1 lists annual mean characteristic values of BC AAOD for each region from the AERONET retrievals and from the AeroCom median model at the same month and locations as the AERONET retrievals. The ratios of the characteristic values (AERONET/AeroCom), also listed in Table B1, define regional scale factors that can be applied to the AeroCom BC AAOD within each region to compensate for regional AeroCom biases. According to Table B1, the ratios are larger than 1 for all regions, but vary widely from region to region (e.g., 1.6 to 6.2 for annual means) and from month to month within a region (e.g., 0.6 to 10.5). The global annual mean of the resulting scaled AeroCom BC AAOD is 0.00605, which is smaller than the average listed in Table B1 for AERONET locations only. The table lists BC AAOD at AERONET sites, where AAOD is higher than the global average, so the global mean after scaling is smaller than the average of the values in the table. This estimate of BC AAOD attributes all fine-mode absorption to BC. When combined with an estimate of fine-mode AOD from MODIS [*Remer et al.*, 2008], this AAOD yields a global, annual average fine-mode single scatter albedo of 0.92.

[883] After scaling to AERONET observations, all-source BC AAOD is 0.00605, and industrial-era BC AAOD is 0.00489, assuming the same scaling applies to preindustrial background BC AAOD because the same biases in BC emission factors, lifetime, and optics apply to preindustrial and present-day simulations. The global average all-source BC AAOD and the industrial-era BC AAOD both increase by a factor of 2.9 because the same scaling is applied to preindustrial conditions. These fractional increases depend on the value of ω_0 assumed in deriving unscaled BC AAOD from the model BC AOD fields, but the scaled BC AAOD value does not. If a more-absorbing aerosol (i.e., lower ω_0) had been chosen, the unscaled model BC AAOD would be greater, the final BC AAOD would be identical, and the percentage increase would be lower. This has no implications for BC DRF, but it does have implications for the emissions inferred after accounting for scaling of BC AAOD.

B2. Uncertainties

[884] Table B2 summarizes estimates of eight sources of uncertainty (95% confidence) in BC AAOD and how each is estimated. We assume that the eight factors contributing to uncertainty are uncorrelated, so that they can be added in quadrature. Two of the uncertainties are asymmetric. The lower and upper uncertainties for all-source BC AAOD are estimated to be −61% and +44%, respectively. For industrial-era BC AAOD, the uncertainties are −71% and +60%, respectively.

[885] 1. *Impact of model spatial pattern*. The regional monthly BC AAOD scale factors are based on existing data pairs (AeroCom/AERONET) for each region and month. The derived scale factor is then applied to all data points of the reference model in that region and month. However, spatial distributions can vary significantly among models, which introduce uncertainty. To quantify this uncertainty, the analysis was performed after replacing the AeroCom median field with fields from three individual models. This

resulted in the following scaled all-source BC AAOD values—AeroCom median model: 0.0060; SPRINTARS: 0.0046; GOCART: 0.0052; and UMI: 0.0064. From the standard deviation of these values, we derive a 25% uncertainty due to the model spatial pattern.

[886] 2. *Characteristic value*. The BC AAOD scale factors for each month and region are based on characteristic values of BC AAOD at the AERONET sites. In this study, the characteristic value is defined by the interquartile average. Other statistical calculations lead to the following all-source BC-AAOD values—average of the 25, 50, and 75 percentile values of the probability distribution: 0.00577; median value: 0.00596; mean: 0.00733; 7 percentiles between 10% and 90% averaged: 0.00635; and interpercentile range of values between 10% and 90% percentiles averaged: 0.00582. From the standard deviation of these estimates, we derive a 18% uncertainty due to the statistical derivation of the BC AAOD characteristic values.

[887] 3. *Limited AERONET sites and sampling*. To quantify the influence of the limited number of AERONET sites used, sub-samples were used to re-estimate the scale factors. Using half of all available AERONET sites in four randomly selected ways produced the following global all-source scaled AeroCom BC-AAOD values: 0.0061, 0.0064, 0.0071, and 0.0057. From this, we derive a 16% uncertainty due to the limited AERONET network coverage.

[888] 4. *Clear-sky bias of AERONET*. A related sampling uncertainty is that AERONET data are acquired only during times of direct sunlight whereas model-simulated BC-AAOD values refer to all times (section 5.4.2.1). This bias is estimated with four AeroCom models (GEOS-Chem, GOCART, OSLO-CTM2, and SPRINTARS) because AERONET retrievals are not possible under cloudy conditions. Simulated BC AAOD on days with AERONET BC-AAOD retrievals were compared to simulated values on all days. Averaging across all models and AERONET sites yields an annual average clear-sky bias of $1\% \pm 5\%$, with the largest bias in SE Asia (15%). An uncertainty of $\pm 5\%$ is therefore applied to our estimate of global, annual average BC AAOD. No correction is made for the 1% annual bias. The effect on radiative forcing could be different than the effect on AAOD depending on the location of BC relative to clouds, but we have not accounted for this uncertainty.

[889] 5. *Transport to unsampled regions*. Scaling burdens over land areas, where AERONET stations are located, should also affect burdens in regions affected by continental outflow. The land-based definition in Figure 7 neglects this influence. To address this deficiency, we extended some regions with large BC outflows partway across the oceans. This procedure increased the global mean BC AAOD by 16%, so we estimate the associated uncertainty to be 16%.

[890] 6. *Dust impact on estimated BC AAOD*. The attribution of AAOD between BC and dust is one of the largest uncertainties. Here we have taken a specific approach to removing dust absorption from the total AAOD, but doing so requires imperfect assumptions. We estimate an asymmetric uncertainty due to the partitioning of AAOD between dust and BC by performing other estimates of BC AAOD from AERONET and propagating these through the model extension. The upper bound of AAOD is obtained by assuming a smaller imaginary refractive index for dust, 0.0006. This yields a BC AAOD of 0.0074, 23% larger than the estimate with imaginary refractive index of 0.0015. For the lower bound, we use the AERONET retrieved refractive index for the total column aerosol, assume that it applies to particles smaller than 1 μm diameter, assume that all absorption by these particles is due to BC, and then integrate absorption over the retrieved sub-1 μm size distribution to estimate BC AAOD. This procedure yields a global mean all-source BC AAOD of 0.0034, 43% smaller than the value estimated from our primary approach. Using the refractive index retrieved for the entire size distribution provides a lower bound for BC AAOD because fine-mode refractive index is generally greater than dust refractive index, as evidenced by the fact that AERONET ω_0 is usually lower than dust ω_0. This method ascribes an AAOD of 0.0052 to non-BC material. For comparison, AeroCom models have a median AOD of 0.023 for dust and compare reasonably well with AERONET observations in dusty regions [*Huneeus et al.*, 2011]. Even with a relatively low ω_0 of 0.95, modeled dust AAOD would be only 0.0011.

[891] 7. *Organic matter impact on BC AAOD*. To extract the AAOD associated with BC, it was assumed that after contributions of larger (dust) aerosol sizes to absorption are removed, the remaining absorption by small particles can be attributed to BC. However, organic aerosol may absorb and is contained in small particles, and it is usually co-emitted with BC. Initial tests with AeroCom median AOD maps for OA and BC and a plausible OA mid-visible imaginary part of the refractive index of 0.005 yielding a co-albedo of 0.027 suggest that 20% of the AAOD of small particles could be attributable to OA. Such an attribution would reduce our estimate of BC AAOD. An asymmetric uncertainty of (0, 20%) is applied to account for this possibility. *Chung et al.* [2012] concluded that absorption by OA is sufficient to offset scattering, so the best estimate of DRF attributable to BC plus absorbing OA would be little affected. Estimates of forcing per emission developed in section 11 may be reasonably accurate, as long as both BC and OA are emitted from the same source.

[892] 8. *Pre-industrial contribution to BC*. Compared with all-source BC, industrial-era BC has an additional uncertainty because the pre-industrial background is unknown. The relative uncertainty in pre-industrial BC emissions may be comparable to the estimated 50% uncertainty in emissions from biomass burning [*Akagi et al.*, 2011; *Vermote et al.*, 2009]. However, the uncertainty in applying the scaling adjustment to pre-industrial AAOD is greater than 50%. We use the previously estimated AAOD of 0.0004 as a low estimate for this preindustrial background and the scaled estimate of 0.0012 as a high estimate. The low pre-industrial value is subtracted from the high value of AAOD for a high estimate, and vice versa.

[893] We acknowledge that there are other sources of uncertainty in using AERONET data that have not been quantified here. These include interpolation of AAOD to 550 nm, removal of climatological NO_2 absorption from the aerosol absorption values, and accounting for dust that absorbs in the fine mode or BC that absorbs in the coarse mode. In addition, the AERONET algorithm is subject to periodic revision and updates that could affect the inferences here.

Table B1. Comparison of BC AAOD From the AeroCom Median Model and AERONET Retrievals in Selected Regions[a]

Region	# Pairs	AeroCom AAOD	AERONET AAOD	Ratio	Min Factor (Month)	Max Factor (Month)
North America	140–220	0.0024	0.0047	1.96	×1.5 (Oct)	×2.3 (Jul)
South America	80–110	0.0049	0.0084	2.49	×1.5 (Jul)	×4.0 (Sep)
Middle East	20–35	0.0042	0.0110	2.63	×1.9 (Feb)	×4.2 (Oct)
Africa	70–110	0.0052	0.0170	3.29	×2.4 (Mar)	×5.0 (Oct)
Europe	90–120	0.0052	0.0083	1.59	×1.1 (May)	×2.3 (Nov)
EECCA	40–60	0.0079	0.0133	1.68	×0.6 (Jun)	×3.2 (Jan)
South Asia	15–20	0.0069	0.0427	6.20	×4.1 (Jun)	×8.1 (Nov)
East Asia	30–60	0.0099	0.0280	2.84	×1.9 (Jul)	×3.4 (Jan)
Southeast Asia	25–30	0.0053	0.0252	4.75	×3.1 (Nov)	×8.2 (Apr)
Japan/Oceania	35–40	0.0015	0.0053	3.57	×1.1 (Jul)	×10.5 (Dec)
Polar land	0–6			1.00		
All oceans	140–210	0.0049	0.0132	2.04	×1.6 (May)	×2.6 (Jan)

[a]Annual averages of monthly interquartile averages of BC AAOD by region. The columns show the (un-adjusted) AeroCom median values at AERONET data locations, the AERONET suggested values, the resulting AERONET to AeroCom annual ratio, and the minimum and maximum regional ratios by month. The reliability of these ratios increases with the number of matching points (column 2), which varies not only by region but also with season.

Table B2. Uncertainties for AeroCom Scaled BC AAOD Based On AERONET Observations[a]

#	Uncertainty Source	Methodology	Uncertainty[b]
1	Impact of model spatial pattern	Comparison of four AeroCom models	±25%
2	Characteristic value	PDF statistics	±18%
3	Limited AERONET sampling	Subsample AERONET sites	±16%
4	Clear-sky bias of AERONET	Use modeling subsamples	±5%
5	Transport into unsampled regions	Extension of large BC source regions	±16%
6	Dust impact on fine-mode AAOD	Estimate using AERONET refractive index for small particles	(−54, +44)%[c] (−44, +23)%[d]
7	Organic matter impact on fine AAOD	Estimated absorption of model organic matter	(−20, 0)%
8	BC AAOD industrial-era component	Assumed uncertainty in background	(0.0004, 0.0012)[c]
	All-source AAOD (#1–7)		(−61, +44)%
	Industrial-era AAOD (#1–8)		(−71, +60)%

[a]Uncertainties added in quadrature.
[b]Values in brackets indicate low and high values of asymmetric uncertainties.
[c]Used for industrial-era AAOD only.
[d]Used for all-source AAOD only

Appendix C: Data Supporting Co-emitted Species Forcings in Section 11

Table C1. Estimates of Forcing Per Emission for Aerosol Species and Precursor SO_2, Grouped by Effect Category[a]

Effect	Central	Low	High
BC atmosphere[b]	51.1	6.5	90.6
BC snow and sea ice	10.3	3.4	24.8
BC liquid clouds[c]	−14.4	−35.8	7.0
BC other clouds[d]	27.3	38.2	59.4
POA atmosphere			
Fossil fuel	−8.6	−17.0	−0.1
Biofuel and open biomass	−4.2	−7.1	−1.2
POA snow[e]	0.9	0.0	3.0
POA clouds	−9.2	−13.5	−3.8
SO_2 atmosphere	−3.7	−5.5	−1.8
SO_2 clouds	−5.3	−7.9	−2.2

[a]Units are $(\mu W\ m^{-2})\ (Gg\ yr^{-1})^{-1}$. Effects correspond to those shown in Figures 37 and 38.
[b]Includes direct forcing.
[c]Includes liquid-cloud albedo and semi-direct effects.
[d]Includes cloud absorption effect and changes in mixed-phase and ice clouds.
[e]Applied to biofuel and open biomass only.

Table C2. Determination of Fraction Used to Apportion Indirect Effect

	Sulfate	Organic Matter
Total industrial-era burden (mg m^{-2})[a]	2.12	1.32
Industrial-era burden, considering associated species (mg m^{-2})[b]	2.83	1.32
Fraction used in apportionment	0.68	0.32

[a]From *Schulz et al*. [2006].
[b]Scaling for sulfate accounts for the mass ratio of $(NH_4)_2SO_4$ to that of $SO_4^{=}$.

Table C3. Estimates of Liquid-Cloud Indirect Effect for Sulfate and Organic Matter[a]

Effect	Central	Low	High	Emission Base (Gg yr^{-1})
Total liquid-cloud effect[b]				
Cloud albedo effect	−0.9	−1.4	−0.3	
BC liquid-cloud effect				
This assessment	−0.10	−0.32	0.12	13,900
Scaled to cloud study emission rate	−0.04	−0.26	0.14	6,100[c]
Sulfate and POA liquid-cloud effect[d]				
Remaining	−0.86	−1.26	−0.35	
Sulfate (68%)	−0.58	−0.86	−0.24	109,000
Organic matter (32%)	−0.27	−0.40	−0.11	30,000
Scaled to final emissions in this study				
Sulfate	−0.51	−0.76	−0.21	96,000
Organic matter	−0.74	−1.09	−0.30	81,000

[a]All values given are forcings in W m^{-2}.
[b]From *Isaksen et al*. [2009]. These values do not include semi-direct effects.
[c]Although some cloud studies could have used a different emission rate, we assumed that the most common rate was the anthropogenic net given in *Dentener et al*. [2006].
[d]Determined for cloud-study emission rates. Fractions for apportionment are from Table C2.

Table C4. Estimates of Forcing Per Emission for Co-Emitted Gaseous Species[a]

Forcing and $GWP_{100\text{-}yr}$	CO	NMVOCs	NO_x (as N)	CH_4
Forcings (μW m^{-2}) (Gg yr^{-1})$^{-1}$				
via short-lived O_3	0.09[b]	0.21[c]	2.8[d]	-
via CH_4	0.15[b]	0.18[c]	−3.8[d]	2.2[b,e]
via nitrate	0	0	−2.0[f]	-
Total	0.24	0.39	−3.2	
$GWP_{100\text{-}yr}$ (dimensionless)	2.8	4.54	−38	

[a]Short-lived O_3 and nitrate forcings are included in first-year forcing shown in Figures 37–39. Longer-lived CH_4 forcing is shown in integrated forcing in Figure 40.
[b]Calculations begin with the $GWP_{100\text{-}yr}$ from *Fuglestvedt et al*. [2010] based on an average of the two models reported in *Berntsen et al*. [2005]. Multiplied by 100-year integral of CO_2 forcing of (0.0086 m W m^{-2}) (Gg yr^{-1})$^{-1}$. Separation of CO into O_3 and CH_4 mechanisms was taken from *Shindell et al*. [2005].
[c]Six VOCs from *Collins et al*. [2002] with weighting recommended by *Fuglestvedt et al*. [2010].
[d]*Wild et al*. [2001] global average.
[e]Although CH_4 does affect short-lived O_3, the resulting forcing is assumed to be included in its total GWP and is subsumed in longer-term forcing. While not precisely accurate for representing first-year forcing, this allocation makes a very small difference.
[f]Calculation begins with total nitrate forcing as given in *Forster et al*. [2007], multiplied by 0.44 to account for the fact that NO_x produces only a fraction of nitrate forcing, with the remainder attributable to ammonia emissions (see text). Forcing-per-emission values are obtained by assuming the same N emission base as the forcing for O_3 attributed to NO_x in *Forster et al*. [2007], so that the ratio between the forcing-per-emission values is the same as the ratio between the forcing values.

Table C5. Emission Rates Used for Figures 37, 39, and 40a[a]

Category	BC	POA	SO_2 (as S)	CO	CH_4	NMVOC	NO_x (as N)	CO_2
On-road	1630	1100	1500	42,000	700	4400	6300	2342
Off-road	810	600	900	7000	0	2800	2400	922
Industry	850	1600	9900	51,000	0	500	1100	4372
Wood/cook	4060	25,300	1200	362,000	17,100	85,200	500	7638
Wood/heat	230	900	100	8000	600	2700	0	344
Coal	930	1100	2500	32,000	200	1300	100	2090
Ag fields	280	1500	100	15,000	1800	2400	0	414
Forests	1470	22,100	2000	96,000	5800	7000	900	2349
Savannas	2230	21,800	1800	121,000	4200	6300	2100	5278
Other rich	1160	4100	3300	557,000	3200	70,500	7500	10,234
Power	20	0	50,100	2000	0	700	6300	7328
Other low	100	300	22,500	51,000	244,500	19,300	3900	5092
Industrial-era total	13,770	80,400	95,900	1,344,000	278,100	203,100	31,100	48,403

[a]All emissions are in $Gg\,yr^{-1}$ except CO_2, which is in Tg. Values are developed beginning with year 2000 emissions given by GAINS (Table 8) and RETRO, scaled to inferred BC emission rates in each region using the scale factors given in section 6 and Appendix B.

Table C6. Emission Factors in ($g\ kg^{-1}$) Used to Develop Figures 39 and 40b

Emission Source	BC	POA	SO_2	CO	CH_4	NMVOC	NO_x	CO_2
Euro II heavy-duty vehicle[a]	0.47	0.1	0.9	7	0.2	1.4	35.3	3087
Pre-regulation truck[a]	2.39	1.3	11.9	11	0.4	3.0	11.2	3087
Bull's Trench brick kiln[b]	2.44	0.1	10.5	41	1.5	0.3	0.0	2182
Industrial coal boiler[c]	0.01	0.0	5.2	5	0.4	0.7	2.1	1947
Mud cooking stove[d]	0.80	5.7	0.3	67	5.6	2.7	1.0	1833
Conventional wood stove[e]	0.36	3.9	0.2	130	15.0	23.6	2.8	1833
Wood boiler[f]	1.09	1.5	0.3	105	9.0	14.0	1.2	1833
Coal cooking stove[g]	0.58	0.8	0.2	166	0.9	0.5	2.2	2130
Field burning[h]	0.69	4.6	0.4	92	2.7	7.0	1.2	1833
Forest burning[h]	0.56	11.2	1.0	107	4.7	5.7	1.4	1833

[a]GAINS implementation of COPERT4 emission factors [*Ntziachristos and Samaras*, 2009].
[b]*Greentech* [2011], except CH_4 and NMVOC values which were not measured. For those gases, one half of *Zhang et al*. [2000] values for coal stoves were used, assumed to scale approximately with CO emissions.
[c]*Wang et al*. [2009b]
[d]*Roden et al*. [2009] in-field data for BC, POA, and CO; *Smith et al*. [2000a, 2000b] for other gases.
[e]*McDonald et al*. [2000], except SO_2, CH_4 and NMVOC from *EPA* [1996].
[f]*Johansson et al*. [2004]; *Rau* [1989].
[g]*Zhang et al*. [2000]; *Zhi et al*. [2008].
[h]*Andreae and Merlet* [2001], except CO_2 from carbon balance.

Table R1. Acronyms and Abbreviations

Acronym	Definition
AAOD	aerosol absorption optical depth
AeroCom	Aerosol Comparison between Observations and Models
AERONET	Aerosol Robotic NETwork
AGTP	absolute global temperature change potential
AGWP	absolute global warming potential
AOD	aerosol optical depth
BB	biomass burning
BC-DRF	black-carbon direct radiative forcing
CALIPSO	Cloud Aerosol Lidar and Infrared Pathfinder Satellite Observations
CAM	Community Atmosphere Model
CAM3	Community Atmosphere Model3
CAM5	Community Atmosphere Model5
CAM-Oslo	Community Atmosphere Model-Oslo
CTM	chemical transport model
DRF	direct radiative forcing

Table R1. (Continued)

Acronym	Definition
ECHAM	European Centre HAmburg Model
EECCA	Eastern Europe, Caucasus and Central Asia
FF	fossil fuel
GAINS	Greenhouse Gas and Air Pollution Interactions and Synergies
GATOR	Gas, Aerosol, TranspOrt, Radiation model
GATOR-GCMOM	Gas, Aerosol, TranspOrt, Radiation - General Circulation, Mesoscale, and Ocean Model
GCM	global climate model
GHG	greenhouse gas
GISS	Goddard Institute for Space Studies
GOCART	Goddard Chemistry Aerosol Radiation and Transport model
GRA	albedo reduction via growth of snow grains with accelerating snow aging
GRB	increase in albedo reduction for a given BC concentration in coarse grained vs. fine-grained snow
GTP	global temperature change potential
GWP	global warming potential
HadGEM	Hadley Centre Global Environmental Model
HIPS	Hybrid Integrating Plate System
IE	indirect effect
IEA	International Energy Agency
IIE	ice cloud indirect effect
IMPACT	Lawrence Livermore National Laboratory (LLNL) Integrated Massively Parallel Atmospheric (IMPACT) Model
IMPROVE	Interagency Monitoring of Protected Visual Environments
IN	ice nuclei
IPCC	Intergovernmental Panel on Climate Change
ISSW	Integrating Sphere Sandwich Spectrophotometer
LES	large-eddy simulation
lidar	light detection and ranging
LOSU	level of scientific understanding
LSCE	Laboratoire des Sciences du Climat et de l'Environnement
MAC	mass absorption cross section
MBC	Increase in surface snow BC concentration via enhanced surface snow melt and retention of BC
MIE	mixed-phase cloud indirect effect
MISR	Multi-angle Imaging Spectroradiometer
MODIS	Moderate Resolution Imaging Spectroradiometer
MPI-HAM	Max Planck Institute-Meterology, Hamburg
MSC	mass scattering cross-section
NASA	National Aeronautics and Space Administration
NCAR	National Center for Atmospheric Research
OMI	Ozone Measurement Instrument
OPAC	Optical Properties of Aerosols and Clouds
PAS	photoacoustic spectrometer
ppm	part per million
PSAP	Particle Soot Absorption Photometer
RAINS	Regional Air Pollution Information and Simulation model
RETRO	Reanalysis of the TROposphere over the last 40 years
RF	radiative forcing
SAF	snow albedo feedback
SBC	change in surface snow BC concentration via change in sublimation
SPEW	Speciated Pollutant Emissions Wizard
SPRINTARS	
SP2	Single Particle Soot Photometer
SST	sea-surface temperature
ToA	top of the atmosphere
TRACE-P	Transport and Chemical Evolution over the Pacific
UIO-CTM	University of Oslo CCM
UMI	University of Michigan
USSR	Union of Soviet Socialist Republics
UTLS	upper-tropsphere-lower-stratosphere
UV	ultraviolet
WIE	warm cloud indirect effect
W	watt
WRF	Weather Research and Forecasting model

Table R2. Chemical Definitions

Chemical	Definition
BC	black carbon
CH_4	methane
CO	carbon monoxide
CO_2	carbon dioxide
EC	elemental carbon
$MgCO_2$	megragram carbon dioxide
NMVOC	non-methane volatile organic compounds
NO	nitric oxide
NO_2	nitrogen dioxide
NO_x	sum of nitric oxide and nitrogen dioxide
OC	organic carbon
OM	organic matter
O_3	ozone
PM	particulate matter
$PM_{2.5}$	particulate matter less than 2.5 micron in diameter
POM	particulate organic matter
rBC	refractory black carbon
S	sulfur
SO_2	sulfur dioxide
VOC	volatile organic compounds

References

Aaheim, H. A., J. S. Fuglestvedt, and O. Godal (2006), Costs savings of a flexible multi-gas climate policy, *Energ. J.*, *S13*, 485–502.

Abbatt, J. P. D., S. Benz, D. J. Cziczo, Z. Kanji, U. Lohmann, and O. Möhler (2006), Solid ammonium sulfate aerosols as ice nuclei: A pathway for cirrus cloud formation, *Science*, *313*(5794), 1770–1773, doi:10.1126/science.1129726.

Abdul-Razzak, H., and S. J. Ghan (2000), A parameterization of aerosol activation: 2. Multiple aerosol types, *J. Geophys. Res.*, *105*(D5), 6837–6844, doi:10.1029/1999JD901161.

Abel, S. J., J. M. Haywood, E. J. Highwood, J. Li, and P. R. Buseck (2003), Evolution of biomass burning aerosol properties from an agricultural fire in southern Africa, *Geophys. Res. Lett.*, *30*(15), doi:10.1029/2003GL017342.

Abu-Allaban, M., A. W. Gertler, and D. H. Lowenthal (2002), A preliminary apportionment of the sources of ambient PM_{10}, $PM_{2.5}$, and VOCs in Cairo, *Atmos. Environ.*., *36*(35), 5549–5557, doi:10.1016/S1352-2310(02)00662-3.

Ackerman, T. P., and O. B. Toon (1981), Absorption of visible radiation in atmosphere containing mixtures of absorbing and nonabsorbing particles, *Appl. Opt.*, *20*(20), 3661–3667, doi:10.1364/AO.20.003661.

Ackerman, A. S., M. P. Kirkpatrick, D. E. Stevens, and O. B. Toon (2004), The impact of humidity above stratiform clouds on indirect aerosol climate forcing, *Nature*, *432*(7020), 1014–1017, doi:10.1038/nature03174.

Ackerman, A. S., O. B. Toon, D. E. Stevens, A. J. Heymsfield, V. Ramanathan, and E. J. Welton (2000), Reduction of tropical cloudiness by soot, *Science*, *288*(5468), 1042–1047, doi:10.1126/science.288.5468.1042.

Adachi, K., S. H. Chung, and P. R. Buseck (2010), Shapes of soot aerosol particles and implications for their effects on climate, *J. Geophys. Res.*, *115*, D15206, doi:10.1029/2009JD012868.

Adams, P. J., and J. H. Seinfeld (2003), Disproportionate impact of particulate emissions on global cloud condensation nuclei concentrations, *Geophys. Res. Lett.*, *30*(5), 1239, doi:10.1029/2002GL016303.

Akagi, S. K., R. J. Yokelson, C. Wiedinmyer, M. J. Alvarado, J. S. Reid, T. Karl, J. D. Crounse, and P. O. Wennberg (2011), Emission factors for open and domestic biomass burning for use in atmospheric models, *Atmos. Chem. Phys.*, *11*, 4039–4072, doi:10.5194/acp-11-4039-2011.

Alfaro, S. C., S. Lafon, J. L. Rajot, P. Formenti, A. Gaudichet, and M. Maille (2004), Iron oxides and light absorption by pure desert dust: An experimental study, *J. Geophys. Res.*, *109*, D08208, doi:10.1029/2003JD004374.

Alfarra, M. R., A. S. H. Prevot, S. Szidat, J. Sandradewi, S. Weimer, V. A. Lanz, D. Schreiber, M. Mohr, and U. Baltensperger (2007), Identification of the mass spectral signature of organic aerosols from wood burning emissions, *Environ. Sci. Technol.*, *41*(16), 5770–5777, doi:10.1021/es062289b.

Allen, R. J., and S. C. Sherwood (2010), Aerosol-cloud semi-direct effect and land-sea temperature contrast in a GCM, *Geophys. Res. Lett.*, *37*, L07702, doi:10.1029/2010GL042759.

Alterskjær, K., J. E. Kristjansson, and C. Hoose (2010), Do anthropogenic aerosols enhance or suppress the surface cloud forcing in the Arctic?, *J. Geophys. Res.*, *115*, D22204, doi:10.1029/2010JD014015.

Amann, M., et al. (2011), Cost-effective control of air quality and greenhouses gases in Europe: Modeling and policy applications, *Environ. Modell. Softw.*, *26*(12), 1489–1501, doi:10.1016/j.envsoft.2011.07.012.

Andreae, M. O., and A. Gelencsér (2006), Black carbon or brown carbon? The nature of light-absorbing carbonaceous aerosols, *Atmos. Chem. Phys.*, *6*, 3131–3148, doi:10.5194/acp-6-3131-2006.

Andreae, M. O., and P. Merlet (2001), Emission of trace gases and aerosols from biomass burning, *Global Biogeochem. Cycles*, *15*(4), 955–966, doi:10.1029/2000GB001382.

Andrews, T., and P. M. Forster (2008), CO_2 forcing induces semi-direct effects with consequences for climate feedback interpretations, *Geophys. Res. Lett.*, *35*(L04), 802, doi:10.1029/2007GL032273.

Andrews, T., P. M. Forster, O. Boucher, N. Bellouin, and A. Jones (2010), Precipitation, radiative forcing and global temperature change, *Geophys. Res. Lett.*, *37*, L14701, 701, doi:10.1029/2010GL043991.

Andrews, E., P. J. Sheridan, and J. A. Ogren (2011), Seasonal differences in the vertical profiles of aerosol optical properties over rural Oklahoma, *Atmos. Chem. Phys.*, *11*, 10661–10676, doi:10.5194/acp-11-10661-2011.

Anenberg, S. C., et al. (2012), Global air quality and health co-benefits of mitigating near-term climate change through methane and black carbon emission controls, *Environ. Health Perspect.*, *120*(6), 831–839.

Ansmann, A., et al. (2008), Influence of Saharan dust on cloud glaciation in southern Morocco during the Saharan Mineral Dust Experiment, *J. Geophys. Res.*, *113*, D04210, doi:10.1029/2007JD008785.

Aoki, T., H. Motoyoshi, Y. Kodama, T. J. Yasunari, S. Konosuke, and H. Kobayashi (2006), Atmospheric aerosol deposition on snow surfaces and its effect on albedo, *Scientific Online Letters on the Atmosphere (SOLA)*, *2*, 13–16, doi:10.2151/sola.2006-004.

Aquila, V., et al. (2011), MADE-in: A new aerosol microphysics submodel for global simulation of insoluble particles and their mixing state, *Geosci. Model Dev.*, *4*, 325–355, doi:10.5194/gmd-4-325-2011.

Arctic Council (2011), An Assessment of Emissions and Mitigation Options for Black Carbon for the Arctic Council, 173 pp., Arctic Council Task Force on Short-Lived Climate Forcers, Arctic Council.

Arellano, A. F., P. S. Kasibhatla, L. Giglio, G. R. van der Werf, and J. T. Randerson (2004), Top-down estimates of global CO sources using MOPITT measurements, *Geophys. Res. Lett.*, *31*(1), L01104, doi:10.1029/2003GL018609.

Arellano, A. F., P. S. Kasibhatla, L. Giglio, G. R. van der Werf, J. T. Randerson, and G. J. Collatz (2006), Time-dependent inversion estimates of global biomass-burning CO emissions using Measurement of Pollution in the Troposphere (MOPITT) measurements, *J. Geophys. Res.*, *111*(D9), 303, doi:10.1029/2005JD006613.

Arnott, W. P., H. Moosmüller, and C. F. Rogers (1997), Photoacoustic spectrometer for measuring light absorption by aerosol: Instrument description, *Atmos. Environ.*, *33*(17), 2845–2852.

Arola, A., G. Schuster, G. Myhre, S. Kazadzis, S. Dey, and S. N. Tripathi (2011), Inferring absorbing organic carbon content from AERONET data, *Atmos. Chem. Phys.*, *11*, 215–225, doi:10.5194/acp-11-215-2011.

Ashbaugh, L. L., W. C. Malm, and W. Z. Sadeh (1985), A residence time probability analysis of sulfur concentrations at Grand-Canyon-National-Park, *Atmos. Environ.*, *19*(8), 1263–1270.

Assamoi, E. M., and C. Liousse (2010), A new inventory for two-wheel vehicle emissions in West Africa for 2002, *Atmos. Environ.*, *44*(32), 3985–3996, doi:10.1016/j.atmosenv.2010.06.048.

Bahadur, R., Y. Feng, L. M. Russell, and V. Ramanathan (2011), Impact of California's air pollution laws on black carbon and their implications for direct radiative forcing, *Atmos. Environ.*, *45*, 1162–1167, doi:10.1016/j.atmosenv.2010.10.054.

Bailis, R. (2009), Modeling climate change mitigation from alternative methods of charcoal production in Kenya, *Biomass Bioenerg.*, *33*(11), 1491–1502, doi:10.1016/j.biombioe.2009.07.001.

Bailis, R., M. Ezzati, and D. M. Kammen (2005), Mortality and greenhouse gas impacts of biomass and petroleum energy futures in Africa, *Science*, *308*(5718), 98–103, doi:10.1126/science.1106881.

Banta, J. R., J. R. McConnell, R. Edwards, and J. P. Engelbrecht (2008), Delineation of carbonate dust, aluminous dust, and sea salt deposition in a Greenland glaciochemical array using positive matrix factorization, *Geochem. Geophys. Geosyst.*, *9*(7), Q07013, doi:10.1029/2007GC001908.

Ban-Weiss, G. A., L. Cao, G. Bala, and K. Caldeira (2011), Dependence of climate forcing and response on the altitude of black carbon aerosols, *Climate Dyn.*, *38*, 897–911, doi:10.1007/s00382-011-1052-y.

Bates, T. S., P. K. Quinn, D. J. Coffman, J. E. Johnson, and A. M. Middlebrook (2005), Dominance of organic aerosols in the marine boundary layer over the Gulf of Maine during NEAQS 2002 and their role in aerosol light scattering, *J. Geophys. Res.*, *110*(D18), 202, doi:10.1029/2005JD005797.

Battye, W., K. Boyer, and T. G. Pace (2002), Methods for improving global inventories of black carbon and organic carbon particulates, Report No. 68-D-98-046, prepared for U.S. Environmental Protection Agency, Research Triangle Park, NC, by EC/R Inc., Chapel Hill, NC.

Bauer, S. E., S. Menon, D. Koch, T. C. Bond, and K. Tsigaridis (2010), A global modeling study on carbonaceous aerosol microphysical characteristics and radiative forcing, *Atmos. Chem. Phys.*, *10*, 4543–4592, doi:10.5194/acpd-10-4543-2010.

Bauer, S. E., D. L. Wright, D. Koch, E. R. Lewis, R. McGraw, L. S. Chang, S. E. Schwartz, and R. Ruedy (2008), MATRIX (Multiconfiguration Aerosol TRacker of mIXing state): An aerosol microphysical module for global atmospheric models, *Atmos. Chem. Phys.*, *8*(20), 6003–6035, doi:10.5194/acp-8-6003-2008.

Baumgardner, D., R. Subramanian, C. Twohy, J. Stith, and G. Kok (2008), Scavenging of black carbon by ice crystals over the northern Pacific, *Geophys. Res. Lett.*, *35*, L22815, doi:10.1029/2008GL035764.

Bell, M. L., K. Ebisu, R. D. Peng, J. M. Samet, and F. Dominici (2009), Hospital admissions and chemical composition of fine particle air pollution, *Am. J. Resp. Crit. Care*, *179*(12), 1115–1120, doi:10.1164/rccm.200808-1240OC.

Bellouin, N., and O. Boucher (2010), Climate response and efficacy of snow forcing in the HadGEM2-AML climate model, *Hadley Centre Technical Note*, No. 82, 8 pp., Met Office, United Kingdom.

Bergstrom, R. W. (1973), Extinction and absorption coefficients of the atmospheric aerosol as a function of particle size, *Contrib. Atmos. Phys.*, *46*, 223–234.

Bergstrom, R. W., P. Pilewskie, P. B. Russell, J. Redemann, T. C. Bond, P. K. Quinn, and B. Sierau (2007), Spectral absorption properties of atmospheric aerosols, *Atmos. Chem. Phys.*, *7*(23), 5937–5943, doi:10.5194/acp-7-5937-2007.

Bergstrom, R. W., P. B. Russell, and P. Hignett (2002), Wavelength dependence of the absorption of black carbon particles: Predictions and results from the TARFOX experiment and implications for the aerosol single scattering albedo, *J. Atmos. Sci.*, *59*(3), 567–577.

Berntsen, T., and J. S. Fuglestvedt (2008), Global temperature responses to current emissions from the transport sectors, *P. Natl. Acad. Sci. USA*, *105 (*49), 19254–19159.

Berntsen, T. K., J. S. Fuglestvedt, M. M. Joshi, K. P. Shine, N. Stuber, M. Ponater, R. Sausen, D. A. Hauglustaine, and L. Li (2005), Response of climate to regional emissions of ozone precursors: Sensitivities and warming potentials, *Tellus B*, *57*(4), 283–304, doi:10.1111/j.1600-0889.2005.00152.x.

Berntsen, T., J. Fuglestvedt, G. Myhre, F. Stordal, and T. F. Berglen (2006), Abatement of greenhouse gases: Does location matter?, *J. Climate*, *74*, 377–411.

Berntsen, T. K., K. Tanaka, and J. S. Fuglestvedt (2010), Does black carbon abatement hamper CO_2 abatement?, *Climatic Change Lett.*, *103*, 627–633, doi:10.1007/s10584-010-9941-3.

Bhave, P. V., G. A. Pouliot, and M. Zheng (2007), Diagnostic model evaluation for carbonaceous $PM_{2.5}$ using organic markers measured in the southeastern US, *Environ. Sci. Technol.*, *41*(5), 1577–1583, doi:10.1021/es061785x.

Birch, M. E., and R. A. Cary (1996), Elemental carbon-based method for monitoring occupational exposures to particulate diesel exhaust, *Aerosol Sci. Technol.*, *25*, 221–241.

Bisiaux, M. M., R. Edwards, J. R. McConnell, M. A. J. Curran, T. D. Van Ommen, A. M. Smith, T. A. Neumann, D. R. Pasteris, J. E. Penner, and K. Taylor (2012), Large scale changes in 20th century black carbon deposition to Antarctica, *Atmos. Chem. Phys.*, *12*, 4107–4115, doi:10.5194/acp-12-4107-2012.

Blumberg, K., M. P. Walsh, and C. Pera (2003), Low-sulfur gasoline and diesel: The key to lower vehicle emissions, Prepared for the International Council on Clean Transportation. (http://www.walshcarlines.com/mpwdocs.html), edited.

Boer, G. J., and B. Yu (2003), Climate sensitivity and response, *Climate Dyn.*, *20*(4), 415–429, doi:10.1007/s00382-002-0283-3.

Bøggild, C. E., R. E. Brandt, K. J. Brown, and S. G. Warren (2010), The ablation zone in northeast Greenland: Ice types, albedos and impurities, *J. Glaciol.*, *56*, 101–113, doi:10.3189/002214310791190776.

Bollasina, M. A., Y. Ming, and V. Ramaswamy (2011), Anthropogenic aerosols and the weakening of the South Asian summer monsoon, *Science*, *334*(6055), 502–505, doi:10.1126/science.1204994.

Bonasoni, P., et al. (2010), Atmospheric brown clouds in the Himalayas: First two years of continuous observations at the Nepal Climate Observatory-Pyramid (5079 m), *Atmos. Chem. Phys.*, *10*(15), 7515–7531, doi:10.5194/acp-10-7515-2010.

Bond, T. C. (2001), Spectral dependence of visible light absorption by carbonaceous particles emitted from coal combustion, *Geophys. Res. Lett.*, *28*(21), 4075–4078.

Bond, T. C., and R. W. Bergstrom (2006), Light absorption by carbonaceous particles: An investigative review, *Aerosol Sci. Technol.*, *40*(1), 27–67.

Bond, T. C., and H. Sun (2005), Can reducing black carbon emissions counteract global warming?, *Environ. Sci. Technol.*, *39*(16), 5921–5926, doi:10.1021/es0480421.

Bond, T. C., T. L. Anderson, and D. Campbell (1999), Calibration and intercomparison of filter-based measurements of visible light absorption by aerosols, *Aerosol Sci. Technol.*, *30*, 582–600.

Bond, T. C., E. Bhardwaj, R. Dong, R. Jogani, S. K. Jung, C. Roden, D. G. Streets, and N. M. Trautmann (2007), Historical emissions of black and organic carbon aerosol from energy-related combustion, 1850–2000, *Global Biogeochem. Cycles*, *21*(2), doi:10.1029/2006GB002840.

Bond, T. C., G. Habib, and R. W. Bergstrom (2006), Limitations in the enhancement of visible light absorption due to mixing state, *J. Geophys. Res.*, *111*(D20), 211, doi:10.1029/2006JD007315.

Bond, T. C., D. G. Streets, K. F. Yarber, S. M. Nelson, J. H. Woo, and Z. Klimont (2004), A technology-based global inventory of black and organic carbon emissions from combustion, *J. Geophys. Res.*, *109*(D14), 203, doi:10.1029/2003JD003697.

Bond, T. C., C. Zarzycki, M. G. Flanner, and D. M. Koch (2011), Quantifying immediate radiative forcing by black carbon and organic matter with the Specific Forcing Pulse, *Atmos. Chem. Phys.*, *11*(4), 1505–1525, doi:10.5194/acp-11-1505-2011.

Bony, S., and J.-L. Dufresne (2005), Marine boundary layer clouds at the heart of tropical cloud feedback uncertainties in climate models, *Geophys. Res. Lett.*, *32*, L20806, doi:10.1029/2005GL023851.

Borghesi, A., and G. Guizzetti (1991), Graphite (C), in Handbook of Optical Constants of Solids, Volume II, edited by E. D. Palik, 449–460 pp., Academic Press, Boston, MA.

Boucher, O., and M. Pham (2002), History of sulfate aerosol radiative forcings, *Geophys. Res. Lett.*, *29*(9), 1308, doi:10.1029/2001GL014048.

Boucher, O., and M. S. Reddy (2008), Climate trade-off between black carbon and carbon dioxide emissions, *Energ. Policy*, *36*, 193–200.

Boucher, O., et al. (1998), Intercomparison of models representing direct shortwave radiative forcing by sulfate aerosols, *J. Geophys. Res.*, *103*(D14), 16979–16998.

Bradford, D. F. (2001), Global change—Time, money and tradeoffs, *Nature*, *410*(6829), 649–650, doi:10.1038/35070707.

Brem, B. T., F. C. M. Gonzalez, S. R. Meyers, T. C. Bond, and M. J. Rood (2012), Laboratory-measured optical properties of inorganic and organic aerosols at relative humidities up to 95%, *Aerosol Sci. Technol.*, *46*(2), 178–190, doi:10.1080/02786826.2011.617794.

Brimblecombe, P. (1977), London air-pollution, 1500–1900, *Atmos. Environ.*, *11*(12), 1157–1162, doi:10.1016/0004-6981(77)90091-9.

Brioude, J., et al. (2009), Effect of biomass burning on marine stratocumulus clouds off the California coast, *Atmos. Chem. Phys.*, *9*(22), 8841–8856, doi:10.5194/acp-9-8841-2009.

Brunekreef, B., R. Beelen, G. Hoek, L. Schouten, S. Bausch-Goldbohm, P. Fischer, B. Armstrong, E. Hughes, M. Jerrett, and P. van den Brandt (2009), Effects of long-term exposure to traffic-related air pollution on respiratory and cardiovascular mortality in the Netherlands: The NLCS-AIR study, *Research Report*, 139, Health Effects Institute, Boston, MA.

Bryden, M., D. Still, P. Scott, G. Hoffa, D. Ogle, R. Bailis, and K. Goyer (2006), Design principles for wood burning cook stoves, EPA-402-K-05-004, Aprovecho Research Center.

Budyko, M. I. (1969), The effect of solar radiation variations on the climate of the Earth, *Tellus*, *21*(5), 611–619.

Bueno, P. A., D. K. Havey, G. W. Mulholland, J. T. Hodges, K. A. Gillis, R. R. Dickerson, and M. R. Zachariah (2011), Photoacoustic measurements of amplification of the absorption cross section for coated soot aerosols, *Aerosol Sci. Technol.*, *45*, 1217–1230, doi:10.1080/02786826.2011.587477.

Cabada, J. C., S. Rees, S. Takahama, A. Khlystov, S. N. Pandis, C. I. Davidson, and A. L. Robinson (2004), Mass size distributions and size resolved chemical composition of fine particulate matter at the Pittsburgh supersite, *Atmos. Environ.*, *38*(20), 3127–3141, doi:10.1016/j.atmosenv.2004.03.004.

Cachier, H., and M. H. Pertuisot (1994), Particulate carbon in Arctic ice, *Analusis*, *22*(7), M34–M37.

Cao, G. L., X. Y. Zhang, and F. C. Zheng (2006), Inventory of black carbon and organic carbon emissions from China, *Atmos. Environ.*, *40*(34), 6516–6527, doi:10.1016/j.atmosenv.2006.05.070.

Cao, J. J., et al. (2005), Characterization and source apportionment of atmospheric organic and elemental carbon during fall and winter of

2003 in Xi'an, China, *Atmos. Chem. Phys.*, *5*, 3127–3137, doi:10.5194/acp-5-3127-2005.

Cao, J. J., et al. (2007), Spatial and seasonal distributions of carbonaceous aerosols over China, *J. Geophys. Res.*, *112*, D22s11, doi:10.1029/2006JD008205.

Cappa, C. D., D. A. Lack, J. B. Burkholder, and A. R. Ravishankara (2008), Bias in filter-based aerosol light absorption measurements due to organic aerosol loading: Evidence from laboratory measurements, *Aerosol Sci. Technol.*, *42*(12), 1022–1032, doi:10.1080/02786820802389285.

Cappa, C. D., et al. (2012), Radiative absorption enhancements due to the mixing state of atmospheric black carbon, *Science*, *337*, 1078–1081, doi:10.1126/science.1223447.

CARB (2009), Technical Support Document: Proposed Regulation for In-Use On-Road Diesel Vehicles, 303, Table XIII-301 pg. 175 pp., California Air Resources Board, Sacramento, CA.

Carmichael, G. R., et al. (2003), Evaluating regional emission estimates using the TRACE-P observations, *J. Geophys. Res.*, *108*(D21), 8810, doi:10.1029/2002JD003116.

Castelvecchi, D. (2009), Subcontinental smut: Is soot the culprit behind melting Himalayan glaciers?, *Sci. Amer., December 15*, http://www.scientificamerican.com/article.cfm?id=subcontinental-smut-himalayas.

Cavalli, F., M. Viana, K. E. Yttri, J. Genberg, and J.-P. Putaud (2010), Toward a standardised thermal-optical protocol for measuring atmospheric organic and elemental carbon: The EUSAAR protocol, *Atmos. Meas. Tech.*, *3*(1), 79–89, doi:10.5194/amt-3-79-2010.

Cesana, G., and H. Chepfer (2012), How well do climate models simulate cloud vertical structure? A comparison between CALIPSO-GOCCP satellite observations and CMIP5 models, *Geophys. Res. Lett.*, *39*, L20803, doi:10.1029/2012GL053153.

Cess, R. D., G. L. Potter, S. J. Ghan, and W. L. Gates (1985), The climatic effects of large injections of atmospheric smoke and dust—A study of climate feedback mechanisms with one-dimensional and 3-dimensional climate models, *J. Geophys. Res.*, *90*(D7), 2937–2950.

Chakrabarty, R. K., H. Moosmüller, L.-W. A. Chen, K. Lewis, W. P. Arnott, C. Mazzoleni, M. K. Dubey, C. E. Wold, W. M. Hao, and S. M. Kreidenweis (2010), Brown carbon in tar balls from smoldering biomass combustion, *Atmos. Chem. Phys.*, *10*(13), 6363–6370, doi:10.5194/acp-10-6363-2010.

Chan, T. W., J. R. Brook, G. J. Smallwood, and G. Lu (2011), Time-resolved measurements of black carbon light absorption enhancement in urban and near-urban locations of southern Ontario, Canada, *Atmos. Chem. Phys.*, *11*(20), 10407–10432, doi:10.5194/acp-11-10407-2011.

Chan, A. W. H., K. E. Kautzman, P. S. Chhabra, J. D. Surratt, M. N. Chan, J. D. Crounse, A. Kurten, P. O. Wennberg, R. C. Flagan, and J. H. Seinfeld (2009), Secondary organic aerosol formation from photooxidation of naphthalene and alkylnaphthalenes: Implications for oxidation of intermediate volatility organic compounds (IVOCs), *Atmos. Chem. Phys.*, *9*, 3049–3060, doi:10.5194/acp-9-3049-2009.

Chan, T. W., et al. (2010), Observations of OM/OC and specific attenuation coefficients (SAC) in ambient fine PM at a rural site in central Ontario, Canada, *Atmos. Chem. Phys.*, *10*(5), 2393–2411, doi:10.5194/acp-10-2393-2010.

Chand, D., R. Wood, T. L. Anderson, S. K. Satheesh, and R. J. Charlson (2009), Satellite-derived direct radiative effect of aerosols dependent on cloud cover, *Nature Geosci.*, *2*(3), 181–184, doi:10.1038/ngeo437.

Charalampopoulos, T. T., H. Chang, and B. Stagg (1989), The effects of temperature and composition on the complex refractive-index of flame soot, *Fuel*, *68*(9), 1173–1179.

Charlson, R. J., and M. J. Pilat (1969), Climate: The influence of aerosols, *J. Appl. Met.*, *8*(5), 1001–1002.

Chen, W. T., R. A. Kahn, D. Nelson, K. Yau, and J. H. Seinfeld (2008), Sensitivity of multiangle imaging to the optical and microphysical properties of biomass burning aerosols, *J. Geophys. Res.*, *113*(D10), 203, doi:10.1029/2007JD009414.

Chen, W. T., Y. H. Lee, P. J. Adams, A. Nenes, and J. H. Seinfeld (2010a), Will black carbon mitigation dampen aerosol indirect forcing?, *Geophys. Res. Lett.*, *37*, L09801, doi:10.1029/2010GL042886.

Chen, T., W. B. Rossow, and Y. C. Zhang (2000), Radiative effects of cloud-type variations, *J. Climate*, *13*, 264–286, doi:10.1175/1520-0442(2000)013<0264:REOCTV>2.0.CO;2.

Chen, L. W. A., J. G. Watson, J. C. Chow, D. W. DuBois, and L. Herschberger (2010b), Chemical mass balance source apportionment for combined $PM_{2.5}$ measurements from U. S. non-urban and urban long-term networks, *Atmos. Environ.*, *44*(38), 4908–4918, doi:10.1016/j.atmosenv.2010.08.030.

Cheng, Y., et al. (2011), Mass absorption efficiency of elemental carbon and water-soluble organic carbon in Beijing, China, *Atmos. Chem. Phys.*, *11*(22), 11497–11510, doi:10.5194/acp-11-11497-2011.

Chevallier, F., M. Fisher, P. Peylin, S. Serrar, P. Bousquet, F. M. Breon, A. Chedin, and P. Ciais (2005), Inferring CO_2 sources and sinks from satellite observations: Method and application to TOVS data, *J. Geophys. Res.*, *110*(D24), 309, doi:10.1029/2005JD006390.

Chevallier, F., A. Fortems, P. Bousquet, I. Pison, S. Szopa, M. Devaux, and D. A. Hauglustaine (2009), African CO emissions between years 2000 and 2006 as estimated from MOPITT observations, *Biogeosciences*, *6*(1), 103–111.

Chin, M., T. Diehl, O. Dubovik, T. F. Eck, B. N. Holben, A. Sinyuk, and D. G. Streets (2009), Light absorption by pollution, dust, and biomass burning aerosols: A global model study and evaluation with AERONET measurements, *Ann. Geophys.*, *27*(9), 3439–3464, doi:10.5194/angeo-27-3439-2009.

Chin, M., P. Ginoux, S. Kinne, O. Torres, B. N. Holben, B. N. Duncan, R. V. Martin, J. A. Logan, A. Higurashi, and T. Nakajima (2002), Tropospheric aerosol optical thickness from the GOCART model and comparisons with satellite and Sun photometer measurements, *J. Atmos. Sci.*, *59*(3), 461–483.

Chow, J. C., and J. G. Watson (2002), Review of $PM_{2.5}$ and PM_{10} apportionment for fossil fuel combustion and other sources by the chemical mass balance receptor model, *Energy Fuel*, *16*(2), 222–260, doi:10.1021/Ef0101715.

Chow, J. C., J. G. Watson, L.-W. A. Chen, W. P. Arnott, and H. Moosmüller (2004), Equivalence of elemental carbon by thermal/optical reflectance and transmittance with different temperature protocols, *Environ. Sci. Technol.*, *38*, 4414–4422.

Chow, J. C., J. G. Watson, D. Crow, D. H. Lowenthal, and T. Merrifield (2001), Comparison of IMPROVE and NIOSH carbon measurements, *Aerosol Sci. Technol.*, *34*(1), 23–34.

Chow, J. C., J. G. Watson, L. C. Pritchett, W. R. Pierson, C. A. Frazier, and R. G. Purcell (1993), The DRI thermal/optical reflectance carbon analysis system: Description, evaluation and applications in U.S. air quality studies, *Atmos. Environ.*, *27A*(8), 1185–1201, doi:10.1016/0960-1686(93)90245-T.

Chowdhury, Z., M. Zheng, J. J. Schauer, R. J. Sheesley, L. G. Salmon, G. R. Cass, and A. G. Russell (2007), Speciation of ambient fine organic carbon particles and source apportionment of $PM_{2.5}$ in Indian cities, *J. Geophys. Res.*, *112*(D15), doi:D15303, 10.1029/2007JD008386.

Christian, T. J., R. J. Yokelson, B. Cardenas, L. T. Molina, G. Engling, and S. C. Hsu (2010), Trace gas and particle emissions from domestic and industrial biofuel use and garbage burning in central Mexico, *Atmos. Chem. Phys.*, *10*(2), 565–584, doi:10.5194/acp-10-565-2010.

Chuang, C. C., J. E. Penner, J. M. Prospero, K. E. Grant, G. H. Rau, and K. Kawamoto (2002), Cloud susceptibility and the first aerosol indirect forcing: Sensitivity to black carbon and aerosol concentrations, *J. Geophys. Res.*, *107*(D21), 4564, doi:10.1029/2000JD000215.

Chung, C. E., and V. Ramanathan (2006), Weakening of North Indian SST gradients and the monsoon rainfall in India and the Sahel, *J. Climate*, *19*(10), 2036–2045.

Chung, S. H., and J. H. Seinfeld (2002), Global distribution and climate forcing of carbonaceous aerosols, *J. Geophys. Res.*, *107*, doi:10.1029/2001JD001397.

Chung, S. H., and J. H. Seinfeld (2005), Climate response of direct radiative forcing of anthropogenic black carbon, *J. Geophys. Res.*, *110*(D11), 102, doi:10.1029/2004JD005441.

Chung, C. E., V. Ramanathan, and D. Decremer (2012), Observationally constrained estimates of carbonaceous aerosol radiative forcing, *Proc. Natl. Acad. Sci. U.S.A.*, *109*(29), doi:10.1073/pnas.1203707109.

Chung, C. E., V. Ramanathan, and J. T. Kiehl (2002), Effects of the South Asian absorbing haze on the northeast monsoon and surface-air heat exchange, *J. Climate*, *15*(17), 2462–2476.

Chung, C. E., V. Ramanathan, D. Kim, and I. A. Podgorny (2005), Global anthropogenic aerosol direct forcing derived from satellite and ground-based observations, *J. Geophys. Res.*, *110*(D24), 207, doi:10.1029/2005JD006356.

Chylek, P., and J. A. Coakley (1974), Aerosols and climate, *Science*, *183*, 75–77.

Chylek, P., and J. Wong (1995), Effect of absorbing aerosol on global radiation budget, *Geophys. Res. Lett.*, *22*(8), 929–931.

Chylek, P., M. K. Dubey, U. Lohmann, V. Ramanathan, Y. J. Kaufman, G. Lesins, J. Hudson, G. Altmann, and S. Olsen (2006), Aerosol indirect effect over the Indian Ocean, *Geophys. Res. Lett.*, *33*, L06806, doi:10.1029/2005GL025397.

Chylek, P., B. Johnson, P. A. Damiano, K. C. Taylor, and P. Clement (1995), Biomass burning record and black carbon in the GISP2 Ice Core, *Geophys. Res. Lett.*, *22*(2), 89–92, doi:10.1029/94GL02841.

Chylek, P., G. B. Lesins, G. Videen, J. G. D. Wong, R. G. Pinnick, D. Ngo, and J. D. Klett (1996), Black carbon and absorption of solar radiation by clouds, *J. Geophys. Res.*, *101*(D18), 23365–23371, doi:10.1029/96JD01901.

Chylek, P., V. Ramaswamy, A. Ashkin, and J. M. Dziedzic (1983a), Simultaneous determination of refractive-index and size of spherical dielectric particles from light-scattering data, *Appl. Opt.*, *22*(15), 2302–2307, doi:10.1364/AO.22.002302.

Chylek, P., V. Ramaswamy, and R. J. Cheng (1984), Effect of graphitic carbon on the albedo of clouds, *J. Atmos. Sci.*, *41*(21), 3076–3084, doi:10.1175/1520-0469(1984)041<3076:EOGCOT>2.0.CO;2.

Chylek, P., V. Ramaswamy, and V. Srivastava (1983b), Albedo of soot-contaminated snow, *J. Geophys. Res.*, *88*(C15), 10837–10843, doi:10.1029/JC088iC15p10837.

Chylek, P., V. Srivastava, L. Cahenzli, R. G. Pinnick, R. L. Dod, T. Novakov, T. L. Cook, and B. D. Hinds (1987), Aerosol and graphitic carbon content of snow, *J. Geophys. Res.*, *92*(D8), 9801–9809, doi:10.1029/JD092iD08p0980.

Clarke, A., and V. Kapustin (2010), Hemispheric aerosol vertical profiles: Anthropogenic impacts on optical depth and cloud nuclei, *Science*, *329*(5998), 1488–1492, doi:10.1126/science.1188838.

Clarke, A. D., and K. J. Noone (1985), Soot in the Arctic snowpack—A cause for perturbations in radiative transfer, *Atmos. Environ.*, *19*(12), 2045–2053, doi:10.1016/0004-6981(85)90113-1.

Clarke, A. D., et al. (2004), Size distributions and mixtures of dust and black carbon aerosol in Asian outflow: Physiochemistry and optical properties, *J. Geophys. Res.*, *109*, D15S09, doi:10.1029/2003JD004378.

Clarke, A., et al. (2007), Biomass burning and pollution aerosol over North America: Organic components and their influence on spectral optical properties and humidification response, *J. Geophys. Res.*, *112*, D12s18, doi:10.1029/2006JD007777.

Cofala, J., M. Amann, Z. Klimont, K. Kupiainen, and L. Hoglund-Isaksson (2007), Scenarios of global anthropogenic emissions of air pollutants and methane until 2030, *Atmos. Environ.*, *41*(38), 8486–8499, doi:10.1016/j.atmosenv.2007.07.010.

Collins, W. J., R. G. Derwent, C. E. Johnson, and D. S. Stevenson (2002), The oxidation of organic compounds in the troposphere and their global warming potentials *Clim. Chang.*, *52*(4), 453–479, doi:10.1023/A:1014221225434.

Collins, W. D., P. J. Rasch, B. A. Boville, J. J. Hack, J. R. McCaa, D. L. Williamson, B. P. Briegleb, C. M. Bitz, S.-J. Lin, and M. Zhang (2006), The formulation and atmospheric simulation of the Community Atmosphere Model Version 3 (CAM3), *J. Climate*, *19*, 2144–2161, doi:10.1175/JCL13760.1.

Collins, W. J., S. Sitch, and O. Boucher (2010), How vegetation impacts affect climate metrics for ozone precursors, *J. Geophys. Res.*, *115*, D23308, doi:10.1029/2010JD014187.

Comiso, J. C., C. L. Parkinson, R. Gersten, and L. Stock (2008), Accelerated decline in the Arctic sea ice cover, *Geophys. Res. Lett.*, *35*(1), 703, doi:10.1029/2007GL031972.

Conant, W. C., A. A. Nenes, and J. H. Seinfeld (2002), Black carbon radiative heating effects on cloud microphysics and implications for the aerosol indirect effect—1. Extended Kohler theory, *J. Geophys. Res.*, *107*, 4604, doi:10.1029/2002jd002094.

Conny, J. M., D. B. Klinedienst, S. A. Wight, and J. L. Paulsen (2003), Optimizing thermal-optical methods for measuring atmospheric elemental (black) carbon: A response surface study, *Aerosol Sci. Technol.*, *37*(9), 703–723, doi:10.1080/02786820300920.

Conway, H., A. Gades, and C. F. Raymond (1996), Albedo of dirty snow during conditions of melt, *Water Resour. Res.*, *32*(6), 1713–1718.

Cook, J., and E. J. Highwood (2004), Climate response to tropospheric absorbing aerosols in an intermediate general-circulation model, *Quart J. Roy. Meteor. Soc.*, *130*(596), 175–191, doi:10.1256/qj.03.64.

Cooke, W. F., and J. J. N. Wilson (1996), A global black carbon aerosol model, *J. Geophys. Res.*, *101*(D14), 19395–19409.

Cooke, W. F., C. Liousse, H. Cachier, and J. Feichter (1999), Construction of a $1° \times 1°$ fossil fuel emission data set for carbonaceous aerosol and implementation and radiative impact in the ECHAM4 model, *J. Geophys. Res.*, *104*(D18), 22137–22162.

Cooke, W. F., V. Ramaswamy, and P. Kasibhatla (2002), A general circulation model study of the global carbonaceous aerosol distribution, *J. Geophys. Res.*, *107*(D16), doi:10.1029/2001JD001274.

Cooke, R. M., A. M. Wilson, J. T. Tuomisto, O. Morales, M. Tainio, and J. S. Evans (2007), A probabilistic characterization of the relationship between fine particulate matter and mortality: Elicitation of European experts, *Environ. Sci. Technol.*, *41*(18), 6598–6605, doi:10.1021/es0714078.

COP-15 (2009), COP-15, Copenhagen Accord, Report of the Conference of the Parties on Its Fifteenth Session, Held in Copenhagen From 7 to 19 December 2009. Addendum. Part Two: Action Taken by the Conference of the Parties at Its Fifteenth Session, United Nations Framework Convention on Climate Change, http://unfccc.int/meetings/copenhagen_dec_2009/items/5262.php2009, 2009.

Corbett, J. J., D. A. Lack, J. J. Winebrake, S. Harder, J. A. Silberman, and M. Gold (2010), Arctic shipping emissions inventories and future scenarios, *Atmos. Chem. Phys.*, *10*, 9689–9704, doi:10.5194/acpd-10-9689-2010.

Corrigan, C. E., G. C. Roberts, M. V. Ramana, D. Kim, and V. Ramanathan (2008), Capturing vertical profiles of aerosols and black carbon over the Indian Ocean using autonomous unmanned aerial vehicles, *Atmos. Chem. Phys.*, *8*(3), 737–747, doi:10.5194/acp-8-737-2008.

Cozic, J., S. Mertes, B. Verheggen, D. J. Cziczo, S. J. Gallavardin, S. Walter, U. Baltensperger, and E. Weingartner (2008), Black carbon enrichment in atmospheric ice particle residuals observed in lower tropospheric mixed phase clouds, *J. Geophys. Res.*, *113*(D15), 209, doi:10.1029/2007JD009266.

Crawford, I., et al. (2011), Studies of propane flame soot acting as heterogeneous ice nuclei in conjunction with single particle soot photometer measurements., *Atmos. Chem. Phys.*, *11*(18), 9549–9561, doi:10.5194/acp-11-9549-2011.

Croft, B., U. Lohmann, R. V. Martin, P. Stier, S. Wurzler, J. Feichter, C. Hoose, U. Heikkila, A. van Donkelaar, and S. Ferrachat (2010), Influences of in-cloud aerosol scavenging parameterizations on aerosol concentrations and wet deposition in ECHAM5-HAM, *Atmos. Chem. Phys.*, *10*(4), 1511–1543, doi:10.5194/acp-10-1511-2010.

Croft, B., U. Lohmann, and K. von Salzen (2005), Black carbon ageing in the Canadian Centre for Climate modeling and analysis atmospheric general circulation model, *Atmos. Chem. Phys.*, *5*, 1931–1949, doi:10.5194/acp-5-1931-2005.

Crook, J. A., P. M. Forster, and N. Stuber (2011), Spatial patterns of modeled climate feedback and contributions to temperature response and polar amplification, *J. Climate*, *24*, 3575–3592, doi:10.1175/2011JCLI3863.1

Cross, E. S., et al. (2010), Soot particle studies—Instrument inter-comparison—Project overview, *Aerosol Sci. Technol.*, *44*(8), 592–611, P

Cziczo, D. J., P. J. DeMott, S. D. Brooks, A. J. Prenni, D. S. Thomson, D. Baumgardner, J. C. Wilson, S. M. Kreidenweis, and D. M. Murphy (2004a), Observations of organic species and atmospheric ice formation, *Geophys. Res. Lett.*, *31*(12), 116, doi:10.1029/2004GL019822.

Cziczo, D. J., D. M. Murphy, P. K. Hudson, and D. S. Thomson (2004b), Single particle measurements of the chemical composition of cirrus ice residue during CRYSTAL-FACE, *J. Geophys. Res.*, *109*(D4), 201, doi:10.1029/2003JD004032.

Cziczo, D. J., et al. (2009), Inadvertent climate modification due to anthropogenic lead, *Nature Geosci.*, *2*(5), 333–336, doi:10.1038/ngeo499.

Darby, D. A., L. H. Burckle, and D. L. Clark (1974), Airborn dust on Arctic pack ice, its composition and fallout rate, *Earth Planet Sci.Lett*, *24*(2), 166–172.

De Angelis, M., J. P. Steffensen, M. Legrand, H. Clausen, and C. Hammer (1997), Primary aerosol (sea salt and soil dust) deposited in Greenland ice during the last climatic cycle: Comparison with east Antarctic records, *J. Geophys. Res.*, *102*(C12), 26681–26698.

de Gouw, J. A., and J. L. Jimenez (2009), Organic aerosols in the Earth's atmosphere, *Environ. Sci. Technol.*, *43*, 7614–7618, doi:10.1021/es9006004.

DeMott, P. J. (1990), An exploratory-study of ice nucleation by soot aerosols, *J. Appl. Meteorol.*, *29*(10), 1072–1079.

DeMott, P. J., Y. Chen, S. M. Kreidenweis, D. C. Rogers, and D. E. Sherman (1999), Ice formation by black carbon particles, *Geophys. Res. Lett.*, *26*, 2429–2432, doi:10.1029/1999GL900580.

DeMott, P. J., D. J. Cziczo, A. J. Prenni, D. M. Murphy, S. M. Kreidenweis, D. S. Thomson, R. Borys, and D. C. Rogers (2003), Measurements of the concentration and composition of nuclei for cirrus formation, *P. Natl. Acad. Sci. USA*, *100*(25), 14655–14660, doi:10.1073/pnas.2532677100.

DeMott, P. J., M. D. Petters, A. J. Prenni, C. M. Carrico, S. M. Kreidenweis, J. L. Collett, and H. Moosmüller (2009a), Ice nucleation behavior of biomass combustion particles at cirrus temperatures, *J. Geophys. Res.*, *114*(D16), 205, doi:10.1029/2009JD012036.

DeMott, P. J., A. J. Prenni, Z. Liu, S. M. Kreidenweis, M. D. Petters, C. H. Twohy, M. S. Richardson, T. Eidhammer, and D. C. Rogers (2010), Predicting global atmospheric ice nuclei distributions and their impact on climate, *P. Natl. Acad. Sci. USA*, *107*, 11217–11222, doi:10.1073/pnas.0910818107.

DeMott, P. J., K. Sassen, M. R. Poellot, D. Baumgardner, D. C. Rogers, S. D. Brooks, A. J. Prenni, and S. M. Kreidenweis (2009b), African dust aerosols as atmospheric ice nuclei, *Geophys. Res. Lett.*, *36*(L07), 808, doi:10.1029/2009GL037639.

Denman, K. L., et al. (2007), Couplings between changes in the climate system and biogeochemistry, in Climate Change 2007: The Physical Science Basis, edited by S. Solomon, D. Qin, M. Manning, Z. Chen, M. Marquis, K. B. Averyt, M. Tigor and H. L. Miller, 129–234 pp., Cambridge University Press, Cambridge, United Kingdom.

Dentener, F., et al. (2006), Emissions of primary aerosol and precursor gases in the years 2000 and 1750: Prescribed data-sets for AeroCom, *Atmos. Chem. Phys.*, *6*, 4321–4344, doi:10.5194/acp-6-4321-2006.

Déry, S. J., and R. D. Brown (2007), Recent northern hemisphere snow cover extent trends and implications for the snow-albedo feedback, *Geophys. Res. Lett.*, *34*(22), L22504, doi:10.1029/2007GL031474.

Deuzé, J. L., et al. (2001), Remote sensing of aerosol over land surfaces from POLDER/ADEOS-1 polarized measurements, *J. Geophys. Res.*, *106*, 4913–4926, doi:10.1029/2000JD900364.

Deville, R. E. L., N. Riemer, and M. West (2011), Weighted Flow Algorithms (WFA) for stochastic particle coagulation, *J. Comput. Phys.*, *230*(23), 8427–8451, doi:10.1016/j.jcp.2011.07.027.

Dickerson, R. R., M. O. Andreae, T. Campos, O. L. Mayol-Bracero, C. Neusuess, and D. G. Streets (2002), Analysis of black carbon and carbon monoxide observed over the Indian Ocean: Implications for emissions and photochemistry, *J. Geophys. Res.*, *107*(D19), 8017, doi:10.1029/2001JD000501.

Diehl, K., and S. K. Mitra (1998), A laboratory study of the effects of a kerosene-burner exhaust on ice nucleation and the evaporation rate of ice crystals, *Atmos. Environ.*, *32*(18), 3145–3151.

Diehl, K., M. Simmel, and S. Wurzler (2006), Numerical sensitivity studies on the impact of aerosol properties and drop freezing modes on the glaciation, microphysics, and dynamics of clouds, *J. Geophys. Res.*, *111*(D07), 202, doi:10.1029/2005JD005884.

Dippel, B., H. Jander, and J. Heintzenberg (1999), NIR FT Raman spectroscopic study of flame soot, *Phys. Chem. Chem. Phys.*, *1*, 4707–4712.

Dobbins, R. A., and C. M. Megaridis (1991), Absorption and scattering of light by polydisperse aggregates, *Appl. Opt.*, *30*(33), 4747–4754.

DOE, U. S. Department of Energy (2010), Final Rule Technical Support Document: Energy Efficiency Program for Commercial and Industrial Equipment: Small Electric Motors, Appendix 15A. Social Cost of Carbon for Regulatory Impact Analysis under Executive Order 12866 13. http://www.epa.gov/oms/climate/regulations/scc-tsd.pdf.

Doherty, S. J., P. K. Quinn, A. Jefferson, C. M. Carrico, T. L. Anderson, and D. Hegg (2005), A comparison and summary of aerosol optical properties as observed in situ from aircraft, ship, and land during ACE-Asia, *J. Geophys. Res.*, *110*(D4), 201, doi:10.1029/2004JD004964.

Doherty, S. J., S. G. Warren, T. C. Grenfell, A. D. Clarke, and R. E. Brandt (2010), Light-absorbing impurities in Arctic snow, *Atmos. Chem. Phys.*, *10*(23), 11647–11680, doi:10.5194/acp-10-11647-2010.

Doherty, S. J., T. C. Grenfell, S. Forsström, D. L. Hegg, S. G. Warren, and R. Brandt (2013), Observed vertical redistribution of black carbon and other light-absorbing particles in melting snow. *J. Geophys. Res.*, *118*, doi:10.1029/2012JD018956.

Donahue, N. M., A. L. Robinson, C. O. Stanier, and S. N. Pandis (2006), Coupled partitioning, dilution, and chemical aging of semivolatile organics, *Environ. Sci. Technol.*, *40*(8), 2635–2643, doi:10.1021/es052297c.

Draine, B. T., and P. J. Flatau (1994), Discrete-dipole approximation for scattering calculations, *J. Opt. Soc. Am. A*, *11*(4), 1491–1499.

Dubovik, O., and M. D. King (2000), A flexible inversion algorithm for retrieval of aerosol optical properties from Sun and sky radiance measurements, *J. Geophys. Res.*, *105*(D16), 20673–20696.

Dubovik, O., B. Holben, T. F. Eck, A. Smirnov, Y. J. Kaufman, M. D. King, D. Tanre, and I. Slutsker (2002), Variability of absorption and optical properties of key aerosol types observed in worldwide locations, *J. Atmos. Sci.*, *59*(3), 590–608.

Dubovik, O., T. Lapyonok, Y. J. Kaufman, M. Chin, P. Ginoux, R. A. Kahn, and A. Sinyuk (2008), Retrieving global aerosol sources from satellites using inverse modeling, *Atmos. Chem. Phys.*, *8*(2), 209–250, doi:10.5194/acp-8-209-2008.

Dubovik, O., A. Smirnov, B. N. Holben, M. D. King, Y. J. Kaufman, T. F. Eck, and I. Slutsker (2000), Accuracy assessment of aerosol optical properties retrieved from Aerosol Robotic Network (AERONET) Sun and sky radiance measurements, *J. Geophys. Res.*, *105*(D8), 9791–9806.

Dusek, U., G. P. Reischl, and R. Hitzenberger (2006a), CCN activation of pure and coated carbon black particles, *Environ. Sci. Technol.*, *40*(4), 1223–1230.

Dusek, U., et al. (2006b), Size matters more than chemistry for cloud-nucleating ability of aerosol particles, *Science*, *312*(5778), 1375–1378.

Dymarska, M., B. J. Murray, L. M. Sun, M. L. Eastwood, D. A. Knopf, and A. K. Bertram (2006), Deposition ice nucleation on soot at temperatures relevant for the lower troposphere, *J. Geophys. Res.*, *111*(D04), 204, doi:10.1029/2005JD006627.

Easter, R. C., S. J. Ghan, Y. Zhang, R. D. Saylor, E. G. Chapman, N. S. Laulainen, H. Abdul-Razzak, L. R. Leung, X. D. Bian, and R. A. Zaveri (2004), MIRAGE: Model description and evaluation of aerosols and trace gases, *J. Geophys. Res.*, *109*(D20), 210, doi:10.1029/2004JD004571.

Eck, T. F., et al. (2003), Variability of biomass burning aerosol optical characteristics in southern Africa during the SAFARI 2000 dry season campaign and a comparison of single scattering albedo estimates from radiometric measurements, *J. Geophys. Res.*, *108*(D13), 8477, doi:10.1029/2002JD002321.

Ekman, A. M. L., A. Engstrom, and C. Wang (2007), The effect of aerosol composition and concentration on the development and anvil properties of a continental deep convective cloud, *Quart J. Roy. Meteor. Soc.*, *133*(627), 1439–1452, doi:10.1002/qj.108.

Eleftheriadis, K., S. Vratolis, and S. Nyeki (2009), Aerosol black carbon in the European Arctic: Measurements at Zeppelin station, Ny-Ålesund, Svalbard from 1998–2007, *Geophys. Res. Lett.*, *36*, L0809, doi:10.1029/2008GL035741.

Elvidge, C. D., K. Baugh, B. Tuttle, D. Ziskin, T. Ghoshet, M. Zhizhin, and D. Pack (2009), Improving satellite data estimation of gas flaring volumes: Year two final report to the GGFR.

Engelbrecht, J. P., L. Swanepoel, J. C. Chow, J. G. Watson, and R. T. Egami (2002), The comparison of source contributions from residential coal and low-smoke fuels, using CMB modeling, *Environ. Sci. Technol.*, *5*(2), 157–167.

EPA (1992), Particulate Matter Best Available Control Measure Technical Guidance Documents for Prescribed Burning and Fugitive Dust, U. S. Environmental Protection Agency, Research Triangle Park, NC.

EPA (1996), Compilation of Air Pollution Emission Factors, Vol. *1, Stationary Point and Area Sources, AP42*, Fifth ed., U.S. Environmental Protection Agency, Washington, DC.

EPA (2002), A Comprehensive Analysis of Biodiesel Impacts on Exhaust Emissions, U. S. Environmental Protection Agency, Draft Technical Report, Ann Arbor, MI.

EPA (2005), AirControlNET Version 4.1 Documentation Report, Prepared by E.H. Pechan & Associates Inc., Springfield, VA.

EPA (2008), Emission Factor Documentation for AP-42: Section 12.2, Coke Production. Finalized by RTI International for U.S. Environmental Protection Agency., Research Triangle Park, NC.

EPA (2009a), Integrated Science Assessment for Particulate Matter, U. S. Environmental Protection Agency, Washington, DC.

EPA (2009b), Available from http://www.epa.gov/ne/eco/diesel/idling.html.

EPA (2012), Report to Congress on Black Carbon, US Environmental Protection Agency, Washington, DC, in preparation.

Essery, R. (1997), Modelling fluxes of momentum, sensible heat and latent heat over heterogeneous snow cover, *Quart J. Roy. Meteor. Soc.*, *123*(543), 1867–1883.

Etyemezian, V., M. Tesfaye, A. Yimer, J. C. Chow, D. Mesfin, T. Nega, G. Nikolich, J. G. Watson, and M. Wondmagegn (2005), Results from a pilot-scale air quality study in Addis Ababa, Ethiopia, *Atmos. Environ.*, *39*(40), 7849–7860, doi:10.1016/j.atmosenv.2005.08.033.

Eyring, V., I. S. A. Isaksen, T. Berntsen, W. J. Collins, J. J. Corbett, O. Endresen, R. G. Grainger, J. Moldanova, H. Schlager, and D. S. Stevenson (2010), Transport impacts on atmosphere and climate: Shipping, *Atmos. Environ. 44*, 4735–4771, doi:10.1016/j.atmosenv.2009.04.059.

Fan, J. W., R. Y. Zhang, W. K. Tao, and K. I. Mohr (2008), Effects of aerosol optical properties on deep convective clouds and radiative forcing, *J. Geophys. Res.*, *113*(D08), 209, doi:10.1029/2007JD009257.

Fann, N., C. Fulcher, and B. Hubbell (2009), The influence of location, source, and emission type in estimates of the human health benefits of reducing a ton of air pollution, *Air Quality, Atmosphere & Health*, *2*(3), doi:10.1007/s11869-009-0044-0.

Federal Law Gazette (2010), First Regulation Implementing the Federal Pollution Control Act, Ordinance on Small and Medium-Sized Combustion Plants—1. BimSchV, 26 January 2010, Federal Law Gazette, Part I, No. 4, Bonn, 2010.

Feingold, G., H. L. Jiang, and J. Y. Harrington (2005), On smoke suppression of clouds in Amazonia, *Geophys. Res. Lett.*, *32*(2), 804, doi:10.1029/2004GL021369.

Ferek, R. J., D. A. Hegg, P. V. Hobbs, P. Durkee, and K. Nielsen (1998), Measurements of ship-induced tracks in clouds off the Washington coast, *J. Geophys. Res.*, *103*(D18), 23199–23206.

Fernandes, S. D., N. M. Trautmann, and D. G. Streets (2007), Global biofuel use, 1850–2000, *Global Biogeochem. Cycles*, *21*(2), doi:10.1029/2006GB002836.

Fetterer, F., and N. Untersteiner (1998), Observations of melt ponds on Arctic sea ice, *J. Geophys. Res.*, *103*(C11), 24821–24835, doi:10.1029/98JC02034.

Fialho, P., M. C. Freitas, F. Barata, B. Vieira, A. D. A. Hansen, and R. E. Honrath (2006), The Aethalometer calibration and determination of iron concentration in dust aerosols, *J. Aerosol. Sci.*, *37*(11), 1497–1506, doi:10.1016/j.jaerosci.2006.03.002.

Flanner, M. G., and C. S. Zender (2006), Linking snowpack microphysics and albedo evolution, *J. Geophys. Res.*, *111*(D12), 208, doi:10.1029/2005JD006834.

Flanner, M. G., K. M. Shell, M. Barlage, D. K. Perovich, and M. A. Tschudi (2011), Radiative forcing and albedo feedback from the Northern Hemisphere cryosphere between 1979 and 2008, *Nature Geosci.*, *4*, 151–155, doi:10.1038/ngeo1062.

Flanner, M. G., C. S. Zender, P. G. Hess, N. M. Mahowald, T. H. Painter, V. Ramanathan, and P. J. Rasch (2009), Springtime warming and reduced snow cover from carbonaceous particles, *Atmos. Chem. Phys.*, *9*(7), 2481–2497, doi:10.5194/acp-9-2481-2009.

Flanner, M. G., C. S. Zender, J. T. Randerson, and P. J. Rasch (2007), Present-day climate forcing and response from black carbon in snow, *J. Geophys. Res.*, *112*(D11), 202, doi:10.1029/2006JD008003.

Fletcher, J. O. (1968), The influence of the Arctic pack ice on climate, *Meteor. Monogr.*, *8*(30), 93–99.

Fornea, A. P., S. D. Brooks, J. B. Dooley, and A. Saha (2009), Heterogeneous freezing of ice on atmospheric aerosols containing ash, soot, and soil, *J. Geophys. Res.*, *114*, D13201, doi:10.1029/2009JD011958.

Forsström, S., J. Ström, C. A. Pedersen, E. Isaksson, and S. Gerland (2009), Elemental carbon distribution in Svalbard snow, *J. Geophys. Res.*, *114*(D19), 112, doi:10.1029/2008JD011480.

Forster, P. M., M. Blackburn, R. Glover, and K. P. Shine (2000), An examination of climate sensitivity for idealised climate change experiments in an intermediate general circulation model, *Climate Dyn.*, *16*(10–11), 833–849.

Forster, P., et al. (2007), Changes in atmospheric constituents and in radiative forcing, in *Climate Change 2007: The Physical Science Basis. Contribution of Working Group I to the Fourth Assessment Report of the Intergovernmental Panel on Climate Change* edited by S. Solomon, D. Qin, M. Manning, Z. Chen, M. Marquis, K. B. Averyt, M. Tignor, and H. L. Miller, Cambridge University Press, New York, NY.

Freitas, S. R., K. M. Longo, M. Diasb, P. L. S. Diasb, R. Chatfield, E. Prins, P. Artaxo, G. A. Grell, and F. S. Recuero (2005), Monitoring the transport of biomass burning emissions in South America, *Environ. Fluid Mech.*, *5*(1-2), 135–167.

Friedlander, S. K. (1973), Chemical element balances and identification of air-pollution sources, *Environ. Sci. Technol.*, *7*(3), 235–240.

Friedman, B., G. Kulkarni, J. Beránek, A. Zelenyuk, J. A. Thornton, and D. J. Cziczo (2011), Ice nucleation and droplet formation by bare and coated soot particles, *J. Geophys. Res.*, *116*, D17203, doi:10.1029/2011JD015999.

Froyd, K. D., D. M. Murphy, T. J. Sanford, D. S. Thomson, J. C. Wilson, L. Pfister, and L. Lait (2009), Aerosol composition of the tropical upper troposphere, *Atmos. Chem. Phys.*, *9*(13), 4363–4385.

Fuglestvedt, J. S., T. K. Berntsen, O. Godal, R. Sausen, K. P. Shine, and T. Skodvin (2003), Metrics of climate change: Assessing radiative forcing and emission indices, *Clim. Chang.*, *58*(3), 267–331.

Fuglestvedt, J. S., T. Berntsen, O. Godal, and T. Skodvin (2000), Climate implications of GWP based reductions in greenhouse gas emissions, *Geophys. Res. Lett.*, *27*, 409–412.

Fuglestvedt, J. S., T. Berntsen, G. Myhre, K. Rypdal, and R. B. Skeie (2008), Climate forcing from the transport sectors, *P. Natl. Acad. Sci. USA*, *105*(2), 454–458.

Fuglestvedt, J. S., K. P. Shine, T. Berntsen, J. Cook, D. S. Lee, A. Stenke, R. B. Skeie, G. J. M. Velders, and I. A. Waitz (2010), Transport impacts on atmosphere and climate: Metrics, *Atmos. Environ.*, *44*(37), 4648–4677, doi:10.1016/j.atmosenv.2009.04.044.

Fuller, K. A. (1995), Scattering and absorption cross sections of compounded spheres. III. Spheres containing arbitrarily located spherical inhomogeneities, *J. Opt. Soc. Am. A*, *12*(5), 893–904, doi:10.1364/JOSA.A.12.000893.

Fuller, K. A., W. C. Malm, and S. M. Kreidenweis (1999), Effects of mixing on extinction by carbonaceous particles, *J. Geophys. Res.*, *104*(D13), 15941–15954, doi:10.1029/1998JD100069.

Fung, K. (1990), Particulate carbon speciation by MnO_2 oxidation, *Aerosol Sci. Technol.*, *12*, 122–127.

Garrett, T. J., and C. Zhao (2006), Increased Arctic cloud longwave emissivity associated with pollution from mid-latitudes, *Nature*, *440*, 787–789, doi:10.1038/nature04636.

Garrett, T. J., C. Zhao, and P. C. Novelli (2010), Assessing the relative contributions of transport efficiency and scavenging to seasonal variability in Arctic aerosol, *Tellus B*, *62*(3), 190–196, doi:10.1111/j.1600-0889.2010.00453.x.

Gayet, J. F., F. Auriol, A. Minikin, J. Strom, M. Seifert, R. Krejci, A. Petzold, G. Febvre, and U. Schumann (2002), Quantitative measurement of the microphysical and optical properties of cirrus clouds with four different in situ probes: Evidence of small ice crystals, *Geophys. Res. Lett.*, *29*(24), 2230, doi:10.1029/2001GL014342.

Gelencsér, A. (2005), Carbonaceous Aerosol, 350 pp, Springer, Dordrecht, The Netherlands.

Gettelman, A., X. Liu, D. Barahona, U. Lohmann, and C. Chen (2012), Climate impacts of ice nucleation, *J. Geophys. Res.*, *117*, D20201, doi:10.1029/2012JD017950.

Ghan, S. J., G. Guzman, and H. Abdul-Razzak (1998), Competition between sea salt and sulfate particles as cloud condensation nuclei, *J. Atmos. Sci.*, *55*(22), 3340–3347, doi:10.1175/1520-0469(19980055<3340:CBSSAS>2.0.CO;2.

Ghan, S. J., X. Liu, R. C. Easter, R. Zaveri, P. J. Rasch, J.-H. Yoon, and B. Eaton (2012), Toward a minimal representation of aerosols in climate models: Comparative decomposition of aerosol direct, semidirect, and indirect radiative forcing, *J. Climate*, *25*(19), 6461–6476, doi:http://dx.doi.org/10.1175/ JCLI-D-11-00650.1.

Giglio, L., T. Loboda, D. P. Roy, B. Quayle, and C. O. Justice (2009), An active-fire based burned area mapping algorithm for the MODIS sensor, *Remote Sens. Environ.*, *113*(2), 408–420, doi:10.1016/j.rse.2008.10.006.

Gildemeister, A. E., P. K. Hopke, and E. Kim (2007), Sources of fine urban particulate matter in Detroit, MI, *Chemosphere*, *69*(7), 1064–1074, doi:10.1016/j.chemosphere.2007.04.027.

Gillett, N. P., and H. D. Matthews (2010), Accounting for carbon cycle feedbacks in a comparison of the global warming effects of greenhouse gases, *Environ. Res. Lett.*, *5*, 034011, doi:10.1088/1748-9326/5/3/034011.

Girard, E., J. P. Blanchet, and Y. Dubois (2005), Effects of Arctic sulphuric acid aerosols on wintertime low-level atmospheric ice crystals, humidity and temperature at Alert, Nunavut, *Atmos. Res.*, *73*(1–2), 131–148, doi:10.1016/j.atmosres.2004.08.002.

Gloersen, P., W. J. Campbell, D. J. Cavalieri, J. C. Comiso, and C. L. Parkinson (1992), Arctic and Antarctic Sea-Ice, 1978–1987: Satellite Passive-Microwave Observations and Analysis *NASA Publication*, SP-511, 290 pp., NASA, Washington, DC.

Goldammer, J. G., and B. Seibert (1990), in Fire in the Tropical Biota. Ecosystem Processes and Global Challenges edited by J. G. Goldammer, 11–31 pp., Springer-Verlag, Berlin-Heidelberg-New York, NY.

Gong, S. L., T. L. Zhao, S. Sharma, D. Toom-Sauntry, D. Lavoue, X. B. Zhang, R. Leaitch, and L. A. Barrie (2010), Identification of trends and inter-annual variability of sulphate and black carbon in the Canadian High Arctic: 1981 to 2007, *J. Geophys. Res.*, *115*, D07305, doi:10.1029/2009JD012943.

Gotschi, T., et al. (2005), Elemental composition and reflectance of ambient fine particles at 21 European locations, *Atmos. Environ.*, *39*(32), 5947–5958, doi:10.1016/j.atmonsenv.2005.06.049.

Graber, E. R., and Y. Rudich (2006), Atmospheric HULIS: How humic-like are they? A comprehensive and critical review, *Atmos. Chem. Phys.*, *6*, 729–753, doi:10.5194/acp-6-729-2006.

Grahame, T. J., and R. B. Schlesinger (2007), Health effects of airborne particulate matter: Do we know enough to consider regulating specific particle types or sources?, *Inhal. Toxicol.*, *19*(6–7), 457–481, doi:10.1080/08958370701382220.

Granier, C., U. Niemeier, J. H. Jungclaus, L. Emmons, P. Hess, J. F. Lamarque, S. Walters, and G. P. Brasseur (2006), Ozone pollution from future ship traffic in the Arctic northern passages, *Geophys. Res. Lett.*, *33*(13), 807, doi:10.1029/2006GL026180.

Graßl, H. (1975), Albedo reduction and radiative heating of clouds by absorbing aerosol particles, *Cont. Atmos. Phys.*, *48*, 199–210.

Greentech (2011), Monitoring of Brick Kilns and Strategies for Cleaner Brick Production in India, Shakti Sustainable Energy, Greentech Knowledge Solutions, New Delhi, India.

Gregory, J. M., W. J. Ingram, M. A. Palmer, G. S. Jones, P. A. Stott, R. B. Thorpe, J. A. Lowe, T. C. Johns, and K. D. Williams (2004), A new method for diagnosing radiative forcing and climate sensitivity, *Geophys. Res. Lett.*, *31*(3), 205, doi:10.1029/2003GL018747.

Grenfell, T. C., S. J. Doherty, A. D. Clarke, and S. G. Warren (2011), Light absorption by particulate impurities in snow and ice determined by spectrophotometric analysis of filters, *Appl. Opt.*, *50*(14), 2037–2048.

Grenfell, T. C., S. P. Neshyba, and S. G. Warren (2005), Representation of a nonspherical ice particle by a collection of independent spheres for scattering and absorption of radiation: 3. Hollow columns and plates, *J. Geophys. Res.*, *110*(D17), 203, doi:10.1029/2005JD005811.

Groblicki, P. J., G. T. Wolff, and R. J. Countess (1981), Visibility-reducing species in the Denver "brown cloud"—I. Relationships between extinction and chemical composition, *Atmos. Environ.*, *15*(12), 2473–2484.

Guazzotti, S. A., et al. (2003), Characterization of carbonaceous aerosols outflow from India and Arabia: Biomass/biofuel burning and fossil fuel combustion, *J. Geophys. Res.*, *108*(D15), 4485, doi:10.1029/2002JD003277.

Guenther, A., T. Karl, P. Harley, C. Wiedinmyer, P. I. Palmer, and C. Geron (2006), Estimates of global terrestrial isoprene emissions using MEGAN (Model of Emissions of Gases and Aerosols from Nature), *Atmos. Chem. Phys.*, *6*, 3181–3210.

Gundel, L. A., R. L. Dod, H. Rosen, and T. Novakov (1984), The relationship between optical attenuation and black carbon concentration for ambient and source particles, *Sci. Total Environ.*, *36*, 197–202.

Gustafsson, O., M. Krusa, Z. Zencak, R. J. Sheesley, L. Granat, E. Engstrom, P. S. Praveen, P. S. P. Rao, C. Leck, and H. Rodhe (2009), Brown clouds over South Asia: Biomass or fossil fuel combustion?, *Science*, *323*(5913), 495–498, doi:10.1126/science.1164857.

Guttikunda, S. K., and P. Jawahar (2012), Application of SIM-air modeling tools to assess air quality in Indian cities, *Atmos. Environ.*, *62*, 551–561, http://dx.doi.org/10.1016/j.atmosenv.2012.08.074.

Haag, W., B. Karcher, J. Strom, A. Minikin, U. Lohmann, J. Ovarlez, and A. Stohl (2003), Freezing thresholds and cirrus cloud formation

mechanisms inferred from in situ measurements of relative humidity, *Atmos. Chem. Phys.*, *3*(5), 1791–1806, doi:10.5194/acp-3-1791-2003.

Hadley, O. L., C. E. Corrigan, T. W. Kirchstetter, S. S. Cliff, and V. Ramanathan (2010), Measured black carbon deposition on the Sierra Nevada snow pack and implication for snow pack retreat, *Atmos. Chem. Phys.*, *10*, 7505–7513, doi:10.5194/acpd-10-7505-2010.

Haeberli, W. (1977), Sahara dust in the Alps—A short review, *Z. Gletscher. Glazialgeol.*, *13*, 206–208.

Hagler, G. S. W., M. H. Bergin, E. A. Smith, and J. E. Dibb (2007a), A summer time series of particulate carbon in the air and snow at Summit, Greenland, *J. Geophys. Res.*, *112*(D21), 309, doi:10.1029/2007JD008993.

Hagler, G. S. W., M. H. Bergin, E. A. Smith, J. E. Dibb, C. Anderson, and E. J. Steig (2007b), Particulate and water-soluble carbon measured in recent snow at Summit, Greenland, *Geophys. Res. Lett.*, *34*(16), L16505, doi:10.1029/2007GL030110.

Hakami, A., D. K. Henze, J. H. Seinfeld, T. Chai, Y. Tang, G. R. Carmichael, and A. Sandu (2005), Adjoint inverse modeling of black carbon during the Asian Pacific Regional Aerosol Characterization Experiment, *J. Geophys. Res.*, *110*(D14), 301, doi:10.11029/12004JD005671.

Hall, A., and X. Qu (2006), Using the current seasonal cycle to constrain snow albedo feedback in future climate change, *Geophys. Res. Lett.*, *33*(3), L03502, doi:10.1029/2005GL025127.

Hallberg, A., J. A. Ogren, K. J. Noone, K. Okada, J. Heintzenberg, and I. B. Svenningson (1994), The influence of aerosol particle composition on cloud droplet formation, *J. Atmos. Chem.*, *19*, 153–171.

Hallett, J., J. G. Hudson, and C. F. Rogers (1989), Characterization of combustion aerosols for haze and cloud formation, *Aerosol Sci. Technol.*, *10*, 70–83.

Hanna, R., E. Duflo, and M. Greenstone (2012), Up in Smoke: The Influence of Household Behavior on the Long-Run Impact of Improved Cooking Stoves, Massachusetts Institute of Technology, Department of Economics Working Paper No. 12-10, Social Science Research Network, http://ssrn.com/abstract=2039004.

Hansen, J., and L. Nazarenko (2004), Soot climate forcing via snow and ice albedos, *P. Natl. Acad. Sci. USA*, *101*(2), 423–428, doi:10.1073/pnas.2237157100.

Hansen, A. D. A., H. Rosen, and T. Novakov (1982), Real-time measurement of the absorption coefficient of aerosol particles, *Appl. Opt.*, *21*(17), 3060–3062.

Hansen, J., M. Sato, P. Kharecha, G. Russell, D. W. Lea, and M. Siddall (2007), Climate change and trace gases, *Philos. Trans. R. Soc. A—Math. Phys. Eng. Sci.*, *365* (1856), 1925–1954, doi:10.1098/rsta.2007.2052.

Hansen, J., M. Sato, and R. Ruedy (1997), Radiative forcing and climate response, *J. Geophys. Res.*, *102*(D6), 6831–6864.

Hansen, J. E., M. Sato, R. Ruedy, A. Lacis, and V. Oinas (2000), Global warming in the twenty-first century: An alternative scenario, *P. Natl. Acad. Sci. USA*, *97*(18), 9875–9880.

Hansen, J., et al. (2005), Efficacy of climate forcings, *J. Geophys. Res.*, *110*(D18), D18104, doi:10.1029/2005JD005776.

Haynes, B. S., and H. G. Wagner (1981), Soot formation, *Prog. Energy Combust. Sci.*, *7*, 229–273.

Haywood, J., and O. Boucher (2000), Estimates of the direct and indirect radiative forcing due to tropospheric aerosols: A review, *Rev. Geophys.*, *38*(4), 513–543.

Haywood, J. M., and V. Ramaswamy (1998), Global sensitivity studies of the direct radiative forcing due to anthropogenic sulfate and black carbon aerosols, *J. Geophys. Res.*, *103*(D6), 6043–6058.

Haywood, J. M., and K. P. Shine (1995), The effect of anthropogenic sulfate and soot aerosol on the clear sky planetary radiation budget, *Geophys. Res. Lett.*, *22*(5), 603–606.

Hazenkamp-von Arx, M. E., et al. (2004), $PM_{2.5}$ and NO_2 assessment in 21 European study centres of ECRHS II: Annual means and seasonal differences, *Atmos. Environ.*, *38*(13), 1943–1953, doi:10.1016/j.atmosenv.2004.01.016.

Heald, C. L., and D. V. Spracklen (2009), Atmospheric budget of primary biological aerosol particles from fungal spores, *Geophys. Res. Lett.*, *36*, L09806, doi:10.1029/2009GL037493.

Heald, C. L., D. J. Jacob, D. B. A. Jones, P. I. Palmer, J. A. Logan, D. G. Streets, G. W. Sachse, J. C. Gille, R. N. Hoffman, and T. Nehrkorn (2004), Comparative inverse analysis of satellite (MOPITT) and aircraft (TRACE-P) observations to estimate Asian sources of carbon monoxide, *J. Geophys. Res.*, *109*(D23), 306, doi:10.1029/2004JD005185.

Hegerl, G. C., F. W. Zwiers, P. Braconnot, N. P. Gillett, Y. Luo, J. A. Marengo Orsini, N. Nicholls, J. E. Penner, and P. A. Stott (2007), Understanding and attributing climate change, in Climate Change 2007: The Physical Science Basis, edited by S. Solomon, D. Qin, M. Manning, Z. Chen, M. Marquis, K. B. Averyt, M. Tigor and H. L. Miller, 129–234 pp., Cambridge University Press, Cambridge, United Kingdom.

Hegg, D. A., S. G. Warren, T. C. Grenfell, S. J. Doherty, and A. D. Clarke (2010), Sources of light-absorbing aerosol in Arctic snow and their seasonal variation, *Atmos. Chem. Phys.*, *10*, 10923–10938, doi:10.5194/acp-10-10923-2010.

Hegg, D. A., S. G. Warren, T. C. Grenfell, S. J. Doherty, T. V. Larson, and A. D. Clarke (2009), Source attribution of black carbon in Arctic snow, *Environ. Sci. Technol.*, *43*(11), 4016–4021.

Heidenreich, R. D., W. M. Hess, and L. L. Ban (1968), A test object and criteria for high resolution electron microscopy, *J. Appl. Crystallogr.*, *1*(1–19).

Heierli, U., and S. Maithel (2008), Brick by brick: The Herculean task of cleaning up the Asian brick industry, in Swiss Agency for Development and Cooperation (SDC), edited by P. Osborn, Natural Resources and Environment Division, Berne, Switzerland.

Heintzenberg, J. (1980), Particle size distribution and optical properties of Arctic haze, *Tellus*, *32*, 251–260.

Heintzenberg, J., and R. J. Charlson (Eds.) (2009), Clouds in the perturbed climate system: Their Relationship to energy balance, atmospheric dynamics, and precipitation, Strüngmann Forum Report, Volume 2, ISBN-10: 0-262-01287-1, The MIT Press, Cambridge, MA.

Heintzenberg, J., K. Okada, and J. Strom (1996), On the composition of non-volatile material in upper tropospheric aerosols and cirrus crystals, *Atmos. Res.*, *41*(1), 81–88.

Heller, W. (1965), Remarks on refractive index mixture rules, *J. Phys. Chem.*, *69*, 1123–1129.

Hendricks, J., B. Kärcher, and U. Lohmann (2011), Effects of ice nuclei on cirrus clouds in a global climate model, *J. Geophys. Res.*, *116*, D18206, doi:10.1029/2010JD015302.

Hendricks, J., B. Karcher, U. Lohmann, and M. Ponater (2005), Do aircraft black carbon emissions affect cirrus clouds on the global scale?, *Geophys. Res. Lett.*, *32*, L12814, doi:10.1029/2005GL022740.

Hess, W. M., and C. R. Herd (1993), Microstructure, morphology, and general physical properties, in Carbon Black, edited by J.-B. Donnet, R. C. Bansal and M.-J. Wang, Marcel Dekker, New York, NY.

Hess, M., P. Koepke, and I. Schult (1998), Optical properties of aerosols and clouds: The software package OPAC, *Bull. Amer. Meteorol. Soc.*, *79*(5), 831–844.

Hicks, S., and E. Isaksson (2006), Assessing source areas of pollutants from studies of fly ash, charcoal, and pollen from Svalbard snow and ice, *J. Geophys. Res.*, *111*(D2), D02113, doi:10.1029/2005JD006167.

Hien, P. D., V. T. Bac, and N. T. H. Thinh (2004), PMF receptor modelling of fine and coarse PM_{10} in air masses governing monsoon conditions in Hanoi, northern Vietnam, *Atmos. Environ.*, *38*(2), 189–201, doi:10.1016/j.atmosenv.2003.09.064.

Higuchi, K., and A. Nagoshi (1977), Effect of particulate matter in surface snow layers on the albedo of perennial snow patches, in Isotopes and Impurities in Snow and Ice, IAHS, Publ. No. 118, 95–97 pp., International Association of Hydrological Sciences, Washington, DC.

Hill, A. A., and S. Dobbie (2008), The impact of aerosols on non-precipitating marine stratocumulus. II: The semi-direct effect, *Quart J. Roy. Meteor. Soc.*, *134*(634), 1155–1165, doi:10.1002/qj.277.

Hirdman, D., J. F. Burkhart, H. Sodemann, S. Eckhardt, A. Jefferson, P. K. Quinn, S. Sharma, J. Ström, and A. Stohl (2010a), Long-term trends of black carbon and sulphate aerosol in the Arctic: Changes in atmospheric transport and source region emissions, *Atmos. Chem. Phys.*, *10*, 9351–9368, doi:10.5194/acp-10-9351-2010.

Hirdman, D., H. Sodemann, J. F. Burkhart, A. Jefferson, T. Mefford, P. K. Quinn, S. Sharma, J. Ström, and A. Stohl (2010b), Source identification of short-lived air pollutants in the Arctic using statistical analysis of measurement data and particle dispersion model output, *Atmos. Chem. Phys.*, *10*, 669–693, doi:10.5194/acp-10-669-2010.

Hitzenberger, R., A. Petzold, H. Bauer, P. Ctyroky, P. Pouresmaeil, L. Laskus, and H. Puxbaum (2006), Intercomparison of thermal and optical measurement methods for elemental carbon and black carbon at an urban location, *Environ. Sci. Technol.*, *40*(20), 6377–6383, doi:10.1021/es051228v.

Holben, B. N., et al. (1998), AERONET—A federated instrument network and data archive for aerosol characterization, *Remote Sens. Environ.*, *66*, 1–16.

Holdsworth, G., K. Higuchi, G. A. Zielinski, P. A. Mayewski, M. Wahlen, B. Deck, P. Chylek, B. Johnson, and P. Damiano (1996), Historical biomass burning: Late 19th century pioneer agriculture revolution in northern hemisphere ice core data and its atmospheric interpretation, *J. Geophys. Res.*, *101*(D18), 23317–23334, doi: 10.1029/96JD01158.

Hoose, C., U. Lohmann, R. Erdin, and I. Tegen (2008), The global influence of dust mineralogical composition on heterogeneous ice nucleation in mixed-phase clouds, *Environ. Res. Lett.*, *3*(2), 5003, doi:10.1088/1748-9326/3/2/025003.

Hopke, P. K. (2010), The application of receptor modeling to air quality data, *Pollution Atmosphérique*, Special Issue, 91–109.

Hopkins, R. J., A. V. Tivanski, B. D. Marten, and M. K. Gilles (2007), Chemical bonding and structure of black carbon reference materials and individual carbonaceous atmospheric aerosols, *J. Aerosol Sci*, *38*(6), 573–591, doi:10.1016/j.jaerosci.2007.03.009.

Horvath, H. (1993), Atmospheric light-absorption - A review, Atmospheric environment part A, *27*(3), 293–317, doi:10.1016/0960-1686(93)90104-7.

Horvath, H. (1997), Systematic deviations of light absorption measurements by filter transmission methods, *J. Aerosol Sci.*, *28*, S55–S56.

Houck, J. E., and B. N. Eagle (2006), Control Analysis and Documentation for Residential Wood Combustion in the MANE-VU Region, OMNI Environmental Services, Alliance for Green Heat, Takoma Park, MD 20912.

Houthuijs, D., et al. (2001), PM_{10} and $PM_{2.5}$ concentrations in Central and Eastern Europe: Results from the Cesar study, *Atmos. Environ.*, *35*(15), 2757–2771.

Hoyle, C. R., B. P. Luo, and T. Peter (2005), The origin of high ice crystal number densities in cirrus clouds, *J. Atmos. Sci.*, *62*(7), 2568–2579.

Hu, Y. T., S. L. Napelenok, M. T. Odman, and A. G. Russell (2009), Sensitivity of inverse estimation of 2004 elemental carbon emissions inventory in the United States to the choice of observational networks, *Geophys. Res. Lett.*, *36*(L15), 806, doi:10.1029/2009GL039655.

Huang, J., Q. Fu, W. Zhang, X. Wang, R. Zhang, H. Ye, and S. G. Warren (2011), Dust and black carbon in seasonal snow across northern China, *Bull. Am. Meteor. Soc.*, *92*, 175–781.

Huang, L., S. L. Gong, C. Q. Jia, and D. Lavoue (2010), Importance of deposition process in simulating the seasonality of the Arctic black carbon aerosol, *J. Geophys. Res.*, *115*, D17207, doi:10.1029/2009JD013478.

Huang, P.-F., B. J. Turpin, M. J. Pipho, D. B. Kittleson, and P. H. McMurry (1994), Effects of water condensation and evaporation on diesel chain-aggregate morphology, *J. Aerosol Sci*, *23*(3), 447–459.

Huebert, B. J., T. S. Bates, P. B. Russell, G. Shi, Y. J. Kim, K. Kawamura, G. Carmichael, and T. Nakajima (2003), An overview of ACE-Asia: Strategies for quantifying the relationships between Asian aerosols and their climatic impacts, *J. Geophys. Res.*, *108*(D23), 8633, doi:10.1029/2003JD003550.

Huneeus, N., F. Chevallier, and O. Boucher (2012), Estimating aerosol emissions by assimilating observed aerosol optical depth in a global aerosol model, *Atmos. Chem. Phys.*, *12*, 4585–4606, doi:10.5194/acpd-12-4585-2012.

Huneeus, N., et al. (2011), Global dust model intercomparison in AeroCom phase I, *Atmos. Chem. Phys.*, *11*(15), 7781–7816, doi:10.5194/acp-11-7781-2011.

Huntzicker, J. J., R. L. Johnson, J. J. Shah, and R. A. Cary (1982), Analysis of organic and elemental carbon in ambient aerosols by a thermal-optical method, in Particulate Carbon: Atmospheric Life Cycle, edited by G. T. Wolff and R. L. Klimisch, 79–88 pp., Plenum Press, New York, NY.

Huo, H., Y. Lei, Q. Zhang, L. Zhao, and K. He (2012), China's coke industry: Recent policies, technology shift, and implication for energy and the environment, *Energ. Policy*, *51*, 397–404 (2012) http://dx.doi.org/10.1016/j.enpol.2012.08.041.

Ichoku, C., and Y. J. Kaufman (2005), A method to derive smoke emission rates from MODIS fire radiative energy measurements, *IEEE Trans. Geosci. Remote Sens.*, *43*(11), 2636–2649.

IPCC (1990), Intergovernmental Panel on Climate Change (IPCC): The Scientific Assessment, UNEP/WMO, Cambridge, United Kingdom.

IPCC (2007), Climate Change 2007: The Physical Science Basis. Contribution of Working Group I to the Fourth Assessment, Report of the Intergovernmental Panel on Climate Change, 996 pp., Cambridge University Press, Cambridge, United Kingdom, and New York, NY, USA.

IPCC (2009), IPCC Expert Meeting on the Science of Alternative Metrics Meeting Report, 82 pp., Grand Hotel, Oslo, Norway.

Isaksen, I. S. A., et al. (2009), Atmospheric composition change: Climate-chemistry interactions, *Atmos. Environ.*, *43*(33), 5138–5192, doi:10.1016/j.atmosenv.2009.08.003.

Iskander, M. F., H. Y. Chen, and J. E. Penner (1991), Resonance optical absorption by fractal agglomerates of smoke aerosols, *Atmos. Environ.*, *25A*(11), 2563–2569.

Ito, A., and J. Penner (2004), Global estimates of biomass burning emissions based on satellite imagery for the year 2000, *J. Geophys. Res.*, *109*(D14), doi:10.1029/2003JD004423, issn: 0148-0227.

Ito, A., and J. Penner (2005), Historical emissions of carbonaceous aerosols from biomass and fossil fuel burning for the period 1870–2000, *Global Biogeochem. Cycles*, *19*(2), doi:10.1029/2004GB002374.

Iversen, T. (1984), On the atmospheric transport of pollution to the Arctic, *Geophys. Res. Lett.*, *11*, 457–460.

Jackson, S. C. (2009), Parallel pursuit of near-term and long-term climate mitigation, *Science*, *326*(5952), 526–527, doi:10.1126/science.1177042.

Jacob, D. J., J. H. Crawford, M. M. Kleb, V. S. Connors, R. J. Bendura, J. L. Raper, G. W. Sachse, J. C. Gille, L. Emmons, and C. L. Heald (2003), Transport and Chemical Evolution over the Pacific (TRACE-P) aircraft mission: Design, execution, and first results, *J. Geophys. Res.*, *108*(D20), 1–19, doi:10.1029/2002JD003276.

Jacob, D. J., et al. (2010), The Arctic Research of the Composition of the Troposphere from Aircraft and Satellites (ARCTAS) mission: Design, execution, and first results, *Atmos Chem Phys*, *10*(11), 5191–5212, doi:10.5194/acp-10-5191-2010.

Jacobson, M. Z. (2000), A physically-based treatment of elemental carbon optics: Implications for global direct forcing of aerosols, *Geophys. Res. Lett.*, *27*(2), 217–220, doi:10.1029/1999GL010968.

Jacobson, M. Z. (2001a), Strong radiative heating due to the mixing state of black carbon in atmospheric aerosols, *Nature*, *409*, 695–697.

Jacobson, M. Z. (2001b), Global direct radiative forcing due to multicomponent anthropgenic and natural aerosols, *J. Geophys. Res.*, *106*, 1551–1568, doi:10.1029/2000JD900514.

Jacobson, M. Z. (2002), Control of fossil-fuel particulate black carbon and organic matter, possibly the most effective method of slowing global warming, *J. Geophys. Res.*, *107*(D19), 4410, doi:10.1029/2001JD001376.

Jacobson, M. Z. (2004a), Climate response of fossil fuel and biofuel soot, accounting for soot's feedback to snow and sea ice albedo and emissivity, *J. Geophys. Res.*, *109*(D21), D21201, doi:10.1029/2004JD004945.

Jacobson, M. Z. (2004b), The short-term cooling but long-term global warming due to biomass burning, *J. Climate*, *17*(15), 2909–2926.

Jacobson, M. Z. (2006), Effects of externally-through-internally-mixed soot inclusions within clouds and precipitation on global climate, *J. Phys. Chem. A*, *110*(21), 6860–6873, doi:10.1021/jp056391r.

Jacobson, M. Z. (2010), Short-term effects of controlling fossil-fuel soot, biofuel soot and gases, and methane on climate, Arctic ice, and air pollution health, *J. Geophys. Res.*, *115*, D14209, doi:10.1029/2009JD013795.

Jacobson, M. Z. (2012), Investigating cloud absorption effects: Global absorption properties of black carbon, tar balls, and soil dust in clouds and aerosols, *J. Geophys. Res.*, *117*, D06205, doi:10.1029/2011JD017218.

Jacobson, M. Z., J. T. Wilkerson, A. D. Naiman, and S. K. Lele (2011), The effects of aircraft on climate and pollution. Part I: Numerical methods for treating the subgrid evolution of discrete size- and composition-resolved contrails from all commercial flights worldwide, *J. Comput. Phys.*, *230*, 5115–5132, doi:10.1016/j.jcp.2011.03.031.

Janssen, N. A., et al. (2011), Black carbon as an additional indicator of the adverse health effects of airborne particles compared with PM_{10} and $PM_{2.5}$, *Environ. Health Perspect.*, *119*, 1691–1699, doi:10.1289/ehp.1003369.

Janzen, J. (1979), The refractive index of carbon black, *J. Colloid Interf. Sci.*, *69*(3), 436–447.

Janzen, J. (1980), Extinction of light by highly nonspherical strongly absorbing colloidal particles—Spectrophotometric determination of volume distributions for carbon-blacks, *Appl. Opt.*, *19*(17), 2977–2985, doi:10.1364/AO.19.002977.

Jenk, T. M., S. Szidat, M. Schwikowski, H. W. Gäggeler, S. Brütsch, L. Wacker, H. A. Synal, and M. Saurer (2006), Radiocarbon analysis in an Alpine ice core: Record of anthropogenic and biogenic contributions to carbonaceous aerosols in the past (1650–1940), *Atmos. Chem. Phys.*, *6*(12), 5381–5390, doi:10.5194/acp-6-5381-2006.

Jensen, E. J., O. B. Toon, S. A. Vay, J. Ovarlez, R. May, T. P. Bui, C. H. Twohy, B. W. Gandrud, R. F. Pueschel, and U. Schumann (2001), Prevalence of ice-supersaturated regions in the upper troposphere: Implications for optically thin ice cloud formation, *J. Geophys. Res.*, *106*(D15), 17253–17266.

Jetter, J. J., and P. Kariher (2009), Solid-fuel household cook stoves: Characterization of performance and emissions, *Biomass Bioenerg.*, *33*, 294–305, doi:10.1016/j.biombioe.2008.05.014.

Johansson, L. S., B. Leckner, L. Gustavsson, D. Cooper, C. Tullin, and A. Potter (2004), Emission characteristics of modern and old-type residential boilers fired with wood logs and wood pellets, *Atmos. Environ.*, *38*(25), 4183–4195, doi:10.1016/j.atmosenv.2004.04.020.

Johansson, D. J. A., U. M. Persson, and C. Azar (2006), The cost of using global warming potentials: Analysing the trade off between CO_2, CH_4 and N_2O, *Clim. Chang.*, *77*(3–4), 291–309, doi:10.1007/s10584-006-9054-x.

Johnson, M. R., and A. R. Coderre (2011), An analysis of flaring and venting activity in the Alberta upstream oil and gas industry, *J. Air Waste Manage. Assoc.*, *61*(2), 190–200, doi:10.3155/1047-3289.61.2.190.

Johnson, K. S., B. de Foy, B. Zuberi, L. T. Molina, M. J. Molina, Y. Xie, A. Laskin, and V. Shutthanandan (2006), Aerosol composition and source apportionment in the Mexico City metropolitan area with PIXE/PESA/STIM and multivariate analysis, *Atmos. Chem. Phys.*, *6*, 4591–4600, doi:10.5194/acp-6-4591-2006.

Johnson, M. R., R. W. Devillers, and K. A. Thomson (2011a), Quantitative field measurement of soot emission from a large gas flare using Sky-LOSA, *Environ. Sci. Technol.*, *45*(1), 345–350, doi:10.1021/es102230y.

Johnson, M., R. Edwards, C. A. Frenk, and O. Masera (2008), In-field greenhouse gas emissions from cookstoves in rural Mexican households, *Atmos. Environ.*, *42*(6), 1206–1222, doi:10.1016/j.atmosenv.2007.10.034.

Johnson, T. M., S. Guttikunda, G. J. Wells, P. Artaxo, T. C. Bond, A. G. Russell, J. G. Watson, and J. West (2011b), Tools for Improving Air Quality Management: A Review of Top-Down Source Apportionment Techniques and Their Application in Developing Countries, ESMAP Publication Series, The World Bank, Washington, DC, USA.

Johnson, B. T., K. P. Shine, and P. M. Forster (2004), The semi-direct aerosol effect: Impact of absorbing aerosols on marine stratocumulus, *Quart J. Roy. Meteor. Soc.*, *130*(599), 1407–1422, doi:10.1256/qj.03.61.

Jones, G. S., N. Christidis, and P. A. Stott (2011), Detecting the influence of fossil fuel and bio-fuel black carbon aerosols on near surface temperature changes, *Atmos. Chem. Phys.*, *11*, 799–816, doi:10.5194/acpd-11-799-2011.

Jones, A., J. M. Haywood, and O. Boucher (2007), Aerosol forcing, climate response and climate sensitivity in the Hadley Centre climate model, *J. Geophys. Res.*, *112*(D20), 211, doi:10.1029/2007JD008688.

Jones, G. S., A. Jones, D. L. Roberts, P. A. Stott, and K. D. Williams (2005), Sensitivity of global-scale climate change attribution results to inclusion of fossil fuel black carbon aerosol, *Geophys. Res. Lett.*, *32*(14), 701, doi:10.1029/2005GL023370.

Jones, H. G., J. W. Pomeroy, D. A. Walker, and R. W. Hoham (Eds.) (2001), Snow Ecology, 398 pp., Cambridge University Press, New York, NY.

Joos, F., et al. (2012), Carbon dioxide and climate impulse response functions for the computation of greenhouse gas metrics: A multi-model analysis, *Atmos. Chem. Phys. Discuss.*, *12*, 19799–19869, doi:10.5194/acpd-12-19799-2012.

Junker, C., and C. Liousse (2008), A global emission inventory of carbonaceous aerosol from historic records of fossil fuel and biofuel consumption for the period 1860–1997, *Atmos. Chem. Phys.*, *8*, 1195–1207, doi:10.5194/acp-8-1195-2008.

Kahn, B. H., A. Gettelman, E. J. Fetzer, A. Eldering, and C. K. Liang (2009a), Cloudy and clear-sky relative humidity in the upper troposphere observed by the A-train, *J. Geophys. Res.*, *114*, D00h02, doi:10.1029/2009JD011738.

Kahn, R. A., D. L. Nelson, M. J. Garay, R. C. Levy, M. A. Bull, D. J. Diner, J. V. Martonchik, S. R. Paradise, E. G. Hansen, and L. A. Remer (2009b), MISR aerosol product attributes and statistical comparisons with MODIS, *IEEE Trans. Geosci. Remote Sens.*, *47*(12), 4095–4114, doi:10.1109/tgrs.2009.2023115.

Kahn, R. A., B. J. Gaitley, M. J. Garay, D. J. Diner, T. F. Eck, A. Smirnov, and B. N. Holben (2010), Multiangle Imaging SpectroRadiometer global aerosol product assessment by comparison with the Aerosol Robotic Network, *J. Geophys. Res.*, *115*, D23209, doi:10.1029/2010JD014601.

Kahn, R., et al. (2009c), Desert dust aerosol air mass mapping in the western Sahara, using particle properties derived from space-based multi-angle imaging, *Tellus B*, *61*(1), 239–251, doi:10.1111/j.1600-0889.2008.00398.x.

Kahnert, M. (2010), On the discrepancy between modeled and measured mass absorption cross sections of light absorbing carbon aerosols, *Aerosol Sci. Technol.*, *44*(6), 453–460, doi:10.1080/02786821003733834.

Kahnert, M., M. Lazaridis, S. Tsyro, and K. Torseth (2004), Requirements for developing a regional monitoring capacity for aerosols in Europe within EMEP, *J. Environ. Monit.*, *6*(7), 646–655, doi:10.1039/b315136k.

Kaiser, J. W., Suttie, M., Flemming, J., Morcrette, J.-J., Boucher, O., and Schultz, M. G. (2009), Global real-time fire emission estimates based on space-borne fire radiative power observations, *AIP Conf. Proc.*, *1100*, 645–648, doi:10.1063/1.3117069.

Kaiser, J. W., et al. (2012), Biomass burning emissions estimated with a global fire assimilation system based on observed fire radiative power, *Biogeosciences*, *9*, 527–554, doi:10.5194/bg-9-527-2012.

Kandlikar, M. (1996), Indices for comparing greenhouse gas emissions: Integrating science and economics, *Energ. Econ.*, *18*, 265–281.

Kandlikar, M., C. Reynolds, and A. Grieshop (2009), A perspective paper on black carbon mitigation as a response to climate change, *Report prepared for the Copenhagen Consensus on Climate*, Copenhagen Consensus Center, Frederiksberg, Denmark.

Kärcher, B., and U. Burkhardt (2008), A cirrus cloud scheme for general circulation models, *Q. J. R. Meteorol. Soc.*, *134*, 1439–1461, doi:10.1002/qj.301.

Kärcher, B., and P. Spichtinger (2009), Cloud-controlling factors of cirrus, in Clouds in the Perturbed Climate System: Their Relationship to Energy Balance, Atmospheric Dynamics, and Precipitation, edited by J. Heintzenberg and R. J. Charlson, 235–268 pp., MIT Press, Cambridge, MA.

Kärcher, B., and J. Ström (2003), The roles of dynamical variability and aerosols in cirrus cloud formation, *Atmos. Chem. Phys.*, *3*, 823–838, doi:10.5194/acp-3-823-2003.

Kärcher, B., and F. Yu (2009), Role of aircraft soot emissions in contrail formation, *Geophys. Res. Lett.*, *36*, L01804, doi:10.1029/2008GL036649.

Kärcher, B., J. Hendricks, and U. Lohmann (2006), Physically based parameterization of cirrus cloud formation for use in global atmospheric models, *J. Geophys. Res.*, *111*(D1), 205, doi:10.1029/2005JD006219.

Kärcher, B., O. Möhler, P. J. DeMott, S. Pechtl, and F. Yu (2007), Insights into the role of soot aerosols in cirrus cloud formation, *Atmos. Chem. Phys.*, *7*(16), 4203–4227, doi:10.5194/acp-7-4203-2007.

Kärcher, B., T. Peter, U. M. Biermann, and U. Schumann (1996), The initial composition of jet condensation trails, *J. Atmos. Sci.*, *53*(21), 3066–3083.

Kasibhatla, P., A. Arellano, J. A. Logan, P. I. Palmer, and P. Novelli (2002), Top-down estimate of a large source of atmospheric carbon monoxide associated with fuel combustion in Asia, *Geophys. Res. Lett.*, *29*(19), doi:10.1029/2002GL015581.

Kasischke, E. S., and N. H. F. French (1995), Locating and estimating the areal extent of wildfires in Alaskan boreal forests using multiple-season AVHRR NDVI composite data, *Remote Sens. Environ.*, *51*(2), 263–275.

Kaufman, Y. J., et al. (1998), Smoke, clouds, and radiation—Brazil (SCAR-B) experiment, *J. Geophys. Res.*, *103*(D24), 31783–31808.

Keene, W. C., R. M. Lobert, P. J. Crutzen, J. R. Maben, D. H. Scharffe, T. Landmann, C. Hely, and C. Brain (2006), Emissions of major gaseous and particulate species during experimental burns of southern African biomass, *J. Geophys. Res.*, *111*(D4), 301, doi:10.1029/2005JD006319.

Khalizov, A. F., H. X. Xue, L. Wang, J. Zheng, and R. Y. Zhang (2009), Enhanced light absorption and scattering by carbon soot aerosol internally mixed with sulfuric acid, *J. Phys. Chem. A*, *113*, 1066–1074, doi:10.1021/jp807531n.

Kim, E., and P. K. Hopke (2007), Source identifications of airborne fine particles using positive matrix factorization and US environmental protection agency positive matrix factorization, *J. Air Waste Manage. Assoc.*, *57*(7), 811–819, doi:10.3155/1047-3289.57.7.811.

Kim, D., C. Wang, A. M. L. Ekman, M. C. Barth, and P. J. Rasch (2008), Distribution and direct radiative forcing of carbonaceous and sulfate aerosols in an interactive size-resolving aerosol-climate model, *J. Geophys. Res.*, *113*(D16), 309, doi:10.1029/2007JD009756.

Kinne, S., et al. (2006), An AeroCom initial assessment—optical properties in aerosol component modules of global models, *Atmos. Chem. Phys.*, *6*, 1815–1834, doi:10.5194/acp-6-1815-2006.

Kirchstetter, T. W., J. Aguiar, S. Tonse, and T. Novakov (2008), Black carbon concentrations and diesel vehicle emission factors derived from coefficient of haze measurements in California: 1967–2003, *Atmos. Environ.*, *42*, 480–491.

Kirchstetter, T. W., T. Novakov, and P. V. Hobbs (2004), Evidence that the spectral dependence of light absorption by aerosols is affected by organic carbon, *J. Geophys. Res.*, *109*(D21), D21208, doi:10.1029/2004JD004999.

Klimont, Z., et al. (2009), Projections of SO_2, NO_x, and carbonaceous aerosol emissions in Asia, *Tellus B*, *61*(4), 602–617, doi:10.1111/j.1600-0889.2009.00428.X.

Knorr, W., V. Lehsten, and A. Arneth (2012), Determinants and predictability of global wildfire emissions, *Atmos. Chem. Phys.*, *61*(4), 6845–6861.

Knox, A., G. J. Evans, J. R. Brook, X. Yao, C. H. Jeong, K. J. Godri, K. Sabaliauskas, and J. G. Slowik (2009), Mass absorption cross-section of ambient black carbon aerosol in relation to chemical age, *Aerosol Sci. Technol.*, *43*(6), 522–532, doi:10.1080/02786820902777207.

Koch, D. (2001), Transport and direct radiative forcing of carbonaceous and sulfate aerosols in the GISS GCM, *J. Geophys. Res.*, *106*(D17), 20311–20332, doi:10.1029/2001JD900038.

Koch, D., and A. D. Del Genio (2010), Black carbon semi-direct effects on cloud cover: Review and synthesis, *Atmos. Chem. Phys.*, *10*(16), 7685–7696, doi:10.5194/acp-10-7685-2010.

Koch, D., and J. Hansen (2005), Distant origins of Arctic black carbon: A Goddard Institute for Space Studies ModelE experiment, *J. Geophys. Res.*, *110*(D4), 204, doi:10.1029/2004JD005296.

Koch, D., S. Menon, A. Del Genio, R. Ruedy, I. Alienov, and G. A. Schmidt (2009a), Distinguishing aerosol impacts on climate over the past century, *J Climate*, *22*(10), 2659–2677, doi:10.1175/2008jcli2573.1.

Koch, D., T. C. Bond, D. Streets, N. Unger, and G. R. van der Werf (2007), Global impacts of aerosols from particular source regions and sectors, *J. Geophys. Res.*, *112*, D02205, doi:10.1029/2005JD007024.

Koch, D., et al. (2009b), Evaluation of black carbon estimations in global aerosol models, *Atmos. Chem. Phys.*, *9*(22), 9001–9026, doi:10.5194/acp-9-9001-2009.

Koch, D., et al. (2011a), Soot microphysical effects on liquid clouds, a multi-model investigation, *Atmos. Chem. Phys.*, *11*(3), 1051–1064, doi:10.5194/acp-11-1051-2011.

Koch, D., et al. (2011b), Coupled aerosol-chemistry-climate twentieth century transient model investigation: Trends in short-lived species and climate responses, *J. Climate*, *24*, 2693–2714, doi:10.1175/2011JCL13582.1.

Koffi, B., et al. (2012), Application of CALIOP layer product to evaluate the vertical distribution of aerosols estimated by global models: AeroCom phase I results, *J. Geophys. Res.*, *117*, D10201, 2012 doi:10.1029/2011JD016858.

Köhler, K. A., P. J. DeMott, S. M. Kreidenweis, O. B. Popovicheva, M. D. Petters, C. M. Carrico, E. D. Kireeva, T. D. Khokhlova, and N. K. Shonija (2009), Cloud condensation nuclei and ice nucleation activity of hydrophobic and hydrophilic soot particles, *Phys. Chem. Chem. Phys.*, *11*(36), 7906–7920, doi:10.1039/b905334b.

Kondo, Y., N. Oshima, M. Kajino, R. Mikami, N. Moteki, N. Takegawa, R. L. Verma, Y. Kajii, S. Kato, and A. Takami (2011a), Emissions of black carbon in East Asia estimated from observations at a remote site in the East China Sea, *J. Geophys. Res.*, *116*, D16201, doi:10.1029/2011JD015637.

Kondo, Y., L. Sahu, N. Moteki, F. Khan, N. Takegawa, X. Liu, M. Koike, and T. Miyakawa (2011b), Consistency and traceability of black carbon measurements made by laser-induced incandescence, thermal-optical transmittance, and filter-based photo-absorption techniques, *Aerosol Sci. Technol.*, *45*(2), 295–312, doi:10.1080/02786826.2010.533215.

Kondo, Y., et al. (2009), Stabilization of the mass absorption cross section of black carbon for filter-based absorption photometry by the use of a heated inlet, *Aerosol Sci. Technol.*, *43*(8), 741–756, doi:10.1080/02786820902889879.

Kondo, Y., et al. (2011c), Emissions of black carbon, organic, and inorganic aerosols from biomass burning in North America and Asia in 2008, *J. Geophys. Res.*, *116*, D08204, doi:10.1029/2010JD015152.

Koop, T., B. P. Luo, A. Tsias, and T. Peter (2000), Water activity as the determinant for homogeneous ice nucleation in aqueous solutions, *Nature*, *406*(6796), 611–614.

Koopmans, A., and J. Koppejan (1997), Agricultural and forest residues: Generation, utilization and availability, in Regional Consultation on Modern Applications of Biomass Energy, FAO, edited, Paper presented at the Regional Consultation on Modern Applications of Biomass Energy, 6-10 January 1997, Kuala Lumpur, Malaysia (see United Nations Food and Agriculture Organization (FAO), 1998) .

Kopacz, M., D. L. Mauzerall, J. Wang, E. M. Leibensperger, D. K. Henze, and K. Singh (2011), Origin and radiative forcing of black carbon transported to the Himalayas and Tibetan Plateau, *Atmos. Chem. Phys.*, *11*, 2837–2852, doi:10.5194/acp-11-2837-2011.

Kopacz, M., et al. (2010), Global estimates of CO sources with high resolution by adjoint inversion of multiple satellite datasets (MOPITT, AIRS, SCIAMACHY, TES), *Atmos. Chem. Phys.*, *10*(3), 855–876.

Kopp, R. E., and D. L. Mauzerall (2010), Assessing the climatic benefits of black carbon mitigation, *Proc. Natl. Acad. Sci. USA*, *107*, 11703–11708, doi:10.1073/pnas.0909605107.

Koren, I., Y. J. Kaufman, L. A. Remer, and J. V. Martins (2004), Measurement of the effect of Amazon smoke on inhibition of cloud formation, *Science*, *303*(5662), 1342–1345, doi:10.1126/science.1089424.

Koren, I., J. V. Martins, L. A. Remer, and H. Afargan (2008), Smoke invigoration versus inhibition of clouds over the Amazon, *Science*, *321*(5891), 946–949, doi:10.1126/science.1159185.

Kristjansson, J. E. (2002), Studies of the aerosol indirect effect from sulfate and black carbon aerosols, *J. Geophys. Res.*, *107*(D15), 4246, doi:10.1029/2001JD000887.

Kuhlmann, J., and J. Quaas (2010), How can aerosols affect the Asian summer monsoon? Assessment during three consecutive pre-monsoon seasons from CALIPSO satellite data, *Atmos. Chem. Phys.*, *10*(10), 4673–4688, doi:10.5194/acp-10-4673-2010.

Kupiainen, K., and Z. Klimont (2007), Primary emissions of fine carbonaceous particles in Europe, *Atmos. Environ.*, *41*, 2156–2170, doi:10.1016/j.atmosenv.2006.10.066.

Kurokawa, J., K. Yumimoto, I. Uno, and T. Ohara (2009), Adjoint inverse modeling of NO_x emissions over eastern China using satellite observations of NO_2 vertical column densities, *Atmos. Environ.*, *43*(11), 1878–1887, doi:10.1016/j.atmosenv.2008.12.030.

Kuwata, M., Y. Kondo, M. Mochida, N. Takegawa, and K. Kawamura (2007), Dependence of CCN activity of less volatile particles on the amount of coating observed in Tokyo, *J. Geophys. Res.*, *112*, D11207, doi:10.1029/2006JD007758.

Kuwata, M., Y. Kondo, and N. Takegawa (2009), Critical condensed mass for activation of black carbon as cloud condensation nuclei in Tokyo, *J. Geophys. Res.*, *114*, D20202, doi:10.1029/2009JD012086.

Laborde, M., P. Mertes, P. Zieger, J. Dommen, U. Baltensperger, and M. Gysel (2012), Sensitivity of the Single Particle Soot Photometer to different black carbon types, *Atmos. Meas. Tech.*, *5*, 1031–1043, doi:10.5194/amt-5-1031-2012.

Lack, D. A., and C. D. Cappa (2010), Impact of brown and clear carbon on light absorption enhancement, single scatter albedo and absorption wavelength dependence of black carbon, *Atmos. Chem. Phys.*, *10*(9), 4207–4220, doi:10.5194/acp-10-4207-2010.

Lack, D. A., C. D. Cappa, D. S. Covert, T. Baynard, P. Massoli, B. Sierau, T. S. Bates, P. K. Quinn, E. R. Lovejoy, and A. R. Ravishankara (2008), Bias in filter-based aerosol light absorption measurements due to organic aerosol loading: Evidence from ambient measurements, *Aerosol Sci. Technol.*, *42*(12), 1033–1041.

Lack, D. A., C. D. Cappa, E. S. Cross, P. Massoli, A. T. Ahern, P. Davidovits, and T. B. Onasch (2009), Absorption enhancement of coated absorbing aerosols: Validation of the photo-acoustic technique for measuring the enhancement, *Aerosol Sci. Technol.*, *43*(10), 1006–1012, doi:10.1080/02786820903117932.

Lack, D. A., J. M. Langridge, R. Bahreinia, C. D. Cappa, A. M. Middlebrook, and J. P. Schwarz (2012), Brown carbon and internal mixing in biomass burning particles, *P. Natl. Acad. Sci. USA*, doi:10.1073/pnas.1206575109.

Lack, D. A., E. R. Lovejoy, T. Baynard, A. Pettersson, and A. R. Ravishankara (2006), Aerosol absorption measurement using photoacoustic spectroscopy: Sensitivity, calibration, and uncertainty developments, *Aerosol Sci. Technol.*, *40*(9), 697–708, doi:10.1080/02786820600803917.

Lall, A. A., and S. K. Friedlander (2006), On-line measurement of ultrafine aggregate surface area and volume distributions by electrical mobility analysis: I. Theoretical analysis, *J. Aerosol. Sci.*, *37*(3), 260–271, doi:10.1016/j.jaerosci.2005.05.021.

Lamarque, J. F., et al. (2010), Historical (1850–2000) gridded anthropogenic and biomass burning emissions of reactive gases and aerosols: methodology and application, *Atmos. Chem. Phys.*, *10*(15), 7017–7039, doi:10.5194/acp-10-7017-2010.

Lance, S., et al. (2009), Cloud condensation nuclei activity, closure, and droplet growth kinetics of Houston aerosol during the Gulf of Mexico Atmospheric Composition and Climate Study (GoMACCS), *J. Geophys. Res.-Atmos.*, *114*, doi:10.1029/2008JD011699.

Lau, K. M., M. K. Kim, and K. M. Kim (2006), Asian summer monsoon anomalies induced by aerosol direct forcing: The role of the Tibetan Plateau, *Climate Dyn.*, *26*(7–8), 855–864, doi:10.1007/s00382-006-0114-z.

Lau, W. K. M., M. K. Kim, K. M. Kim, and W. S. Lee (2010), Enhanced surface warming and accelerated snow melt in the Himalayas and Tibetan Plateau induced by absorbing aerosols, *Environ. Res. Lett.*, *5*(2), doi:10.1088/1748-9326/5/2/025204.

Lavanchy, V. M. H., H. W. Gäggeler, U. Schotterer, M. Schwikowski, and U. Baltensperger (1999), Historical record of carbonaceous particle concentrations from a European high-alpine glacier (Colle Gnifetti, Switzerland), *J. Geophys. Res.*, *104*(D17), 21227–21236, doi:10.1029/1999JD900408.

Law, K. S., and A. Stohl (2007), Arctic air pollution: Origins and impacts, *Science*, *315*(5818), 1537–1540, doi:10.1126/science.1137695.

Lee, S. H., D. M. Murphy, D. S. Thomson, and A. M. Middlebrook (2002), Chemical components of single particles measured with Particle Analysis by Laser Mass Spectrometry (PALMS) during the Atlanta SuperSite Project: Focus on organic/sulfate, lead, soot, and mineral particles, *J. Geophys. Res.*, *107*(D1–D2), 4003, doi:10.1029/2000JD000011.

Lee, K. B., M. W. Thring, and J. M. Beér (1962), On the rate of combustion of soot in a laminar soot flame, *Combustion and Flame*, *6*, 137–145.

Lee, D. S., et al. (2010), Transport impacts on atmosphere and climate: Aviation, *Atmos. Environ.*, *44*(37), 4678–4734, doi:10.1016/j.atmosenv.2009.06.005.

Lefohn, A. S., J. D. Husar, and R. B. Husar (1999), Estimating historical anthropogenic global sulfur emission patterns for the period 1850–1990, *Atmos. Environ.*, *33*(21), 3435–3444.

Legrand, M., S. Preunkert, M. Schock, M. Cerqueira, A. Kasper-Giebl, J. Afonso, C. Pio, A. Gelencsér, and I. Dombrowski-Etchevers (2007), Major 20th century changes of carbonaceous aerosol components (EC, WinOC, DOC, HULIS, carboxylic acids, and cellulose) derived from Alpine ice cores, *J. Geophys. Res.*, *112*(D23), D23S11, doi:10.1029/2006JD008080.

Lei, Y., Q. Zhang, K. B. He, and D. G. Streets (2011), Primary anthropogenic aerosol emission trends for China, 1990–2005, *Atmos. Chem. Phys.*, *11*, 931–954, doi:10.5194/acp-11-931-2011.

Levy, R. C., L. A. Remer, S. Mattoo, E. F. Vermote, and Y. J. Kaufman (2007), Second-generating operational algorithm: Retrieval of aerosol properties over land from inversion of Moderate Resolution Imaging Spectroradiometer spectral reflectance, *J. Geophys. Res.*, *112*, D13211, doi:10.1029/2006JD007811.

Lewis, K., W. P. Arnott, H. Moosmüller, and C. E. Wold (2008), Strong spectral variation of biomass smoke light absorption and single scattering albedo observed with a novel dual-wavelength photoacoustic instrument, *J. Geophys. Res.*, *113*, D16203, doi:10.1029/2007JD009699.

Lewis, K. A., et al. (2009), Reduction in biomass burning aerosol light absorption upon humidification: roles of inorganically-induced hygroscopicity, particle collapse, and photoacoustic heat and mass transfer, *Atmos. Chem. Phys.*, *9*(22), 8949–8966, doi:10.5194/acp-9-8949-2009.

Li, J., M. Posfai, P. V. Hobbs, and P. R. Buseck (2003), Individual aerosol particles from biomass burning in southern Africa: 2. Compositions and aging of inorganic particles, *J. Geophys. Res.*, *108*(D13), 8484, doi:10.1029/2002JD002310.

Liley, J. B., et al. (2003), Black carbon in aerosol during BIBLE B, *J. Geophys. Res.*, *108*(D3), doi:10.1029/2001JD000845.

Lin, C.-I., M. Baker, and R. J. Charlson (1973), Absorption coefficient of atmospheric aerosol: A method for measurement, *Appl. Opt.*, *12*(6), 1356–1363.

Lindesay, J. A., M. O. Andreae, J. G. Goldammer, G. Harris, H. J. Annegarn, M. Garstang, R. J. Scholes, and B. W. vanWilgen (1996), International geosphere-biosphere programme international global atmospheric chemistry SAFARI-92 field experiment: Background and overview, *J. Geophys. Res.*, *101*(D19), 23521–23530.

Liousse, C., J. E. Penner, C. Chuang, J. J. Walton, H. Eddleman, and H. Cachier (1996), A global three-dimensional model study of carbonaceous aerosols, *J. Geophys. Res.*, *101*(D14), 19411–19432.

Liston, G. E. (1995), Local advection of momentum, heat, and moisture during the melt of patchy snow covers, *J. Appl. Meteorol.*, *34*(7), 1705–1715.

Liston, G. E. (1999), Interrelationships among snow distribution, snowmelt, and snow cover depletion: Implications for atmospheric, hydrologic, and ecologic modeling, *J. Appl. Meteorol.*, *38*(10), 1474–1487.

Liston, G. E. (2004), Representing subgrid snow cover heterogeneities in regional and global models, *J. Climate*, *17*(6), 1381–1397.

Liston, G. E., and M. Sturm (2004), The role of winter sublimation in the Arctic moisture budget, *Nordic Hydrology*, *35*(4–5), 325–334.

Liu, L., and M. I. Mishchenko (2005), Effects of aggregation on scattering and radiative properties of soot aerosols, *J. Geophys. Res.*, *110*, D11211, doi:11210.11029/12004JD005649.

Liu, J., S. Fan, L. W. Horowitz, and H. Levy II (2011), Evaluation of factors controlling long-range transport of black carbon to the Arctic, *J. Geophys. Res.*, *116*, D04307, doi:10.1029/2010JD015145.

Liu, X., J. E. Penner, S. J. Ghan, and M. Wang (2007), Inclusion of ice microphysics in the NCAR Community Atmospheric Model Version 3 (CAM3), *J. Climate*, *20*, 4526–4547, doi:10.1175/JCL14264.1.

Liu, X. H., J. E. Penner, and M. H. Wang (2009a), Influence of anthropogenic sulfate and black carbon on upper tropospheric clouds in the NCAR CAM3 model coupled to the IMPACT global aerosol model, *J. Geophys. Res.*, *114*(D03), 204, doi:10.1029/2008JD010492.

Liu, Y. Q., J. Stanturf, and S. Goodrick (2010), Trends in global wildfire potential in a changing climate, *Forest Ecol. Manag.*, *259*, 685–697, doi:10.1016/j.foreco.2009.09.002.

Liu, Y., J. R. Sun, and B. Yang (2009b), The effects of black carbon and sulphate aerosols in China regions on East Asia monsoons, *Tellus B*, *61*(4), 642–656, doi:10.1111/j.1600-0889.2009.00427.X.

Liu, X., et al. (2012), Toward a minimal representation of aerosols in climate models: Description and evaluation in the Community Atmosphere Model CAM5, *Geosci. Model Dev.*, *5*, 709–739, doi:10.5194/gmd-5-709-2012.

Livingston, J. M., et al. (2000), Shipboard sunphotometer measurements of aerosol optical depth spectra and columnar water vapor during ACE-2, and comparison with selected land, ship, aircraft, and satellite measurements, *Tellus B*, *52*(2), 594–619.

Lobert, J. M., D. H. Scharffe, W.-M. Hao, T. A. Kuhlbusch, R. Seuwen, P. Warneck, and P. J. Crutzen (1991), Experimental evaluation of biomass burning emissions: Nitrogen and carbon containing compounds, in Global Biomass Burning: Atmospheric, cIlmatic, and Biospheric Implications, edited by J. S. Levine, Massachussetts Institute of Technology, The MIT Press, Cambridge, Massachusetts.

Lohmann, U. (2002), A glaciation indirect aerosol effect caused by soot aerosols, *Geophys. Res. Lett.*, *29*(4), 1052, doi:10.1029/2001GL014357.

Lohmann, U., and K. Diehl (2006), Sensitivity studies of the importance of dust ice nuclei for the indirect aerosol effect on stratiform mixed-phase clouds, *J. Atmos. Sci.*, *63*(3), 968–982.

Lohmann, U., and J. Feichter (2001), Can the direct and semi-direct aerosol effect compete with the indirect effect on a global scale?, *Geophys. Res. Lett.*, *28*(1), 159–161, doi:10.1029/2000GL012051.

Lohmann, U., and J. Feichter (2005), Global indirect aerosol effects: A review, *Atmos. Chem. Phys.*, *5*, 715–737, doi:10.5194/acp-5-715-2005.

Lohmann, U., and C. Hoose (2009), Sensitivity studies of different aeroso indirect effects in mixed-phase clouds, *Atmos. Chem. Phys.*, *9*(22), 8917–8934, doi:10.5194/acp-9-8917-2009.

Lohmann, U., L. Rotstayn, T. Storelvmo, A. Jones, S. Menon, J. Quaas, A. M. L. Ekman, D. Koch, and R. Ruedy (2010), Total aerosol effect: Radiative forcing or radiative flux perturbation?, *Atmos. Chem. Phys.*, *10*(7), 3235–3246, doi:10.5194/acp-11-931-2011.

Lohmann, U., P. Stier, C. Hoose, S. Ferrachat, S. Kloster, E. Roeckner, and J. Zhang (2007), Cloud microphysics and aerosol indirect effects in the global climate model ECHAM5-HAM, *Atmos. Chem. Phys.*, *7*(13), 3425–3446, doi:10.5194/acp-7-3425-2007.

Lu, Z., D. G. Streets, Q. Zhang, and S. Wang (2012), A novel back-trajectory analysis of the origin of black carbon transported to the Himalayas and Tibetan Plateau during 1996–2010, *Geophys. Res. Lett.*, *39*, L01809, doi:10.1029/2011GL049903.

Lu, Z., Q. Zhang, and D. G. Streets (2011), Sulfur dioxide and primary carbonaceous aerosol emissions in China and India, 1996–2010, *Atmos. Chem. Phys.*, *11*, 9839–9864, doi:10.5194/acp-11-9839-2011.

Lubin, D., and A. S. Simpson (1994), The longwave emission signature of urban pollution: Radiometric FTIR measurement, *Geophys. Res. Lett.*, *21*(1), 37–40, doi:10.1029/93GL03374.

Lund, M. T., and T. Berntsen (2012), Parameterization of black carbon aging in the OsloCTM2 and implications for regional transport to the Arctic, *Atmos. Chem. Phys.*, *12*, 6999–7014, www.atmos-chem-phys.net/12/6999/2012/, doi:10.5194/acpd-11-6999-2012.

Luo, C., N. Mahowald, and J. del Corral (2003), Sensitivity study of meteorological parameters on mineral aerosol mobilization, transport and distribution, *J. Geophys. Res.*, *108*(D15), 4447, doi:10.1029/2003JD0003483.

MacCarty, N., D. Still, and D. Ogle (2010), Fuel use and emissions performance on fifty cooking stoves in the laboratory and related benchmarks of performance, *Energ. Sust. Dev.*, *14*, 161–171.

Mack, M. C., M. S. Bret-Harte, T. N. Hollingsworth, R. R. Jandt, E. A. G. Schuur, G. R. Shaver, and D. L. Verbyla (2011), Carbon loss from an unprecedented Arctic tundra wildfire, *Nature*, *475*(7357), 489–492, doi:10.1038/nature10283.

Magi, B. I., P. V. Hobbs, B. Schmid, and J. Redemann (2003), Vertical profiles of light scattering, light absorption, and single scattering albedo during the dry, biomass burning season in southern Africa and comparisons of in situ and remote sensing measurements of aerosol optical depths, *J. Geophys. Res.*, *108*(D13), 8504, doi:10.1029/2002JD002361.

Mahowald, N. M., D. R. Muhs, S. Levis, P. J. Rasch, M. Yoshioka, C. S. Zender, and C. Luo (2006), Change in atmospheric mineral aerosols in response to climate: Last glacial period, preindustrial, modern, and doubled carbon dioxide climates, *J. Geophys. Res.*, *111*, D10202, doi:10.1029/2005JD006653.

Mallet, M., J. C. Roger, S. Despiau, O. Dubovik, and J. P. Putaud (2003), Microphysical and optical properties of aerosol particles in urban zone during ESCOMPTE, *Atmos. Res.*, *69*(1–2), 73–97.

Mallet, M., J. C. Roger, S. Despiau, J. P. Putaud, and O. Dubovik (2004), A study of the mixing state of black carbon in urban zone, *J. Geophys. Res.*, *109*, D04202, doi:04210.01029/02003JD003940.

Malm, W. C., J. F. Sisler, D. Huffman, R. A. Eldred, and T. A. Cahill (1994), Spatial and seasonal trends in particle concentration and optical extinction in the United States, *J. Geophys. Res.*, *99*(D1), 1347–1370.

Manne, A. S., and R. G. Richels (2001), An alternative approach to establishing trade-offs among greenhouse gases, *Nature*, *410*(6829), 675–677.

Manoli, E., D. Voutsa, and C. Samara (2002), Chemical characterization and source identification/apportionment of fine and coarse air particles in Thessaloniki, Greece, *Atmos. Environ.*, *36*(6), 949–961.

Marcolli, C., S. Gedamke, T. Peter, and B. Zobrist (2007), Efficiency of immersion mode ice nucleation on surrogates of mineral dust, *Atmos. Chem. Phys.*, *7*(19), 5081–5091, doi:10.5194/acp-7-5081-2007.

Marcq, S., P. Laj, J. C. Roger, P. Villani, K. Sellegri, P. Bonasoni, A. Marinoni, P. Cristofanelli, G. P. Verza, and M. Bergin (2010), Aerosol optical properties and radiative forcing in the high Himalaya based on measurements at the Nepal Climate Observatory-Pyramid site (5079 m a.s.l.), *Atmos. Chem. Phys.*, *10*(13), 5859–5872, doi:10.5194/acp-10-5859-2010.

Marinoni, A., P. Cristofanelli, P. Laj, R. Duchi, F. Calzolari, S. Decesari, K. Sellegri, E. Vuillermoz, G. P. Verza, P. Villani, and P. Bonasoni (2010), Aerosol mass and black carbon concentrations, two year-round observations at NCO-P (5079 m, Southern Himalayas), *Atmos. Chem. Phys.*, *10*, 8551–8562, www.atmos-chem-phys.net/10/8551/2010/, doi:10.5194/acpd-10-8551-2010.

Marley, N. A., J. S. Gaffney, J. C. Baird, C. A. Blazer, P. J. Drayton, and J. E. Frederick (2001), An empirical method for the determination of the complex refractive index of size-fractionated atmospheric aerosols for radiative transfer calculations, *Aerosol Sci. Technol.*, *34*, 535–549.

Marlon, J. R., P. J. Bartlein, C. Carcaillet, D. G. Gavin, S. P. Harrison, P. E. Higuera, F. Joos, M. J. Power, and I. C. Prentice (2008), Climate and human influences on global biomass burning over the past two millennia, *Nature Geosci.*, *1*, 697–702, doi:10.1038/ngeo313.

Martins, J. V., P. Artaxo, C. Liousse, J. S. Reid, P. V. Hobbs, and Y. Kaufman (1998a), Effects of black carbon content, particle size, and mixing on light absorption by aerosol from biomass burning in Brazil, *J. Geophys. Res.*, *103*(D24), 32041–32050.

Martins, J. V., P. V. Hobbs, R. E. Weiss, and P. Artaxo (1998b), Sphericity and morphology of smoke particles from biomass burning in Brazil, *J. Geophys. Res.*, *103*(D24), 32051–32057.

Massey, R. (1997), No-Tillage and Conservation Tillage: Economic Considerations, University of Missouri Extension Publication G355, University of Missouri, Columbia, MO.

Massie, S. T., A. Heymsfield, C. Schmitt, D. Muller, and P. Seifert (2007), Aerosol indirect effects as a function of cloud top pressure, *J. Geophys. Res.*, *112*(D6), 202, doi:10.1029/2006JD007383.

Matzl, M., and M. Schneebeli (2006), Measuring specific surface area of snow by near infrared photography, *J. Glaciol.*, *52*, 558–564.

Maykut, G. A., and N. Untersteiner (1971), Some results from a time-dependent thermodynamic model of sea ice, *J. Geophys. Res.*, *76*(6), 1550–1575, doi:10.1029/JC076i006p01550.

Mayol-Bracero, O. L., R. Gabriel, M. O. Andreae, T. W. Kirchstetter, T. Novakov, J. Ogren, P. Sheridan, and D. G. Streets (2002), Carbonaceous aerosols over the Indian Ocean during the Indian Ocean Experiment (INDOEX): Chemical characterization, optical properties, and probable sources, *J. Geophys. Res.*, *107*(D19), 8030, doi:10.1029/2000JD000039.

McConnell, J. R., and R. Edwards (2008), Coal burning leaves toxic heavy metal legacy in the Arctic, *P. Natl. Acad. Sci. USA*, *105*(34), 12140–12144, doi:10.1073/pnas.0803564105.

McConnell, J. R., R. Edwards, G. L. Kok, M. G. Flanner, C. S. Zender, E. S. Saltzman, J. R. Banta, D. R. Pasteris, M. M. Carter, and J. D. W. Kahl (2007), 20th-century industrial black carbon emissions altered Arctic climate forcing, *Science*, *317*(5843), 1381–1384, doi:10.1126/science.1144856.

McCormick, R. A., and J. H. Ludwig (1967), Climate modification by atmospheric aerosols, *Science*, *156*(3780), 1358–1359, doi:10.1126/science.156.3780.1358.

McDonald, J. D., B. Zielinska, E. M. Fujita, J. C. Sagebiel, J. C. Chow, and J. G. Watson (2000), Fine particle and gaseous emission rates from residential wood combustion, *Environ. Sci. Technol.*, *34*, 2080–2091.

McFarquhar, G. M., and H. L. Wang (2006), Effects of aerosols on trade wind cumuli over the Indian Ocean: Model simulations, *Quart J. Roy. Meteor. Soc.*, *132*(616), 821–843, doi:10.1256/qj.04.179.

McFiggans, G., et al. (2006), The effect of physical and chemical aerosol properties on warm cloud droplet activation, *Atmos. Chem. Phys.*, *6*, 2593–2649, doi:10.5194/acp-6-2593-2006.

McKenzie, D., C. L. Raymond, L.-K. B. Kellogg, R. A. Norheim, A. G. Andreu, A. C. Bayard, K. E. Kopper, and E. Elman (2007), Mapping fuels at multiple scales: landscape application of the Fuel Characteristic Classification System, *Can. J. Forest Res.*, *37*, 2421–2437, doi:10.1139/X07-056.

Medalia, A. I., and F. A. Heckman (1969), Morphology of aggregates—II. Size and shape factors of carbon black aggregates from electron microscopy, *Carbon*, *7*, 569–582.

Medalia, A. I., and L. W. Richards (1972), Tinting strength of carbon black, *J. Colloid Interf. Sci.*, *40*(2), 233–252.

Medina, J., A. Nenes, R. E. P. Sotiropoulou, L. D. Cottrell, L. D. Ziemba, P. J. Beckman, and R. J. Griffin (2007), Cloud condensation nuclei closure during the International Consortium for Atmospheric Research on Transport and Transformation 2004 campaign: Effects of size-resolved composition, *J. Geophys. Res.*, *112*(D10), doi:10.1029/2006JD007588.

Meehl, G. A., J. M. Arblaster, and W. D. Collins (2008), Effects of black carbon aerosols on the Indian monsoon, *J. Climate*, *21*(12), 2869–2882, doi:10.1175/2007jcli1777.1.

Mehta, S., and C. Shahpar (2004), The health benefits of interventions to reduce indoor air pollution from solid fuel use: A cost-effectiveness analysis, *Energy Sustain. Dev.*, *8*(3), doi:10.1016/S0973-0826(08)60466-4.

Menon, S., and A. D. Del Genio (2007), Evaluating the impacts of carbonaceous aerosols on clouds and climate, in Human-Induced Climate Change: An Interdisciplinary Assessment edited by M. E. Schlesinger, H. Kheshgi, J. B. Smith, F. C. D. L. Chesnaye, J. M. Reilly, T. Wilson and C. Kolstad, 34–48 pp., Cambridge University Press, Cambridge UK, Cambridge Books Online, doi:10.1017/CBO9780511619472.005.

Menon, S., A. D. Del Genio, D. Koch, and G. Tselioudis (2002a), GCM Simulations of the aerosol indirect effect: Sensitivity to cloud parameterization and aerosol burden, *J. Atmos. Sci.*, *59*(3), 692–713, doi:10.1175/1520-0469(2002)059<0692:gsotai>2.0.co;2.

Menon, S., J. Hansen, L. Nazarenko, and Y. F. Luo (2002b), Climate effects of black carbon aerosols in China and India, *Science*, *297*(5590), 2250–2253.

Menon, S., D. Koch, G. Beig, S. Sahu, J. Fasullo, and D. Orlikowski (2010), Black carbon aerosols and the third polar ice cap, *Atmos. Chem. Phys.*, *10* (10), 4559–4571, doi:10.5194/acp-10-4559-2010.

Merikanto, J., D. V. Spracklen, G. W. Mann, S. J. Pickering, and K. S. Carslaw (2009), Impact of nucleation on global CCN, *Atmos. Chem. Phys.*, *9*(21), 8601–8616, doi:10.5194/acp-9-8601-2009.

Mikhailov, E. F., S. S. Vlasenko, I. A. Podgorny, V. Ramanathan, and C. E. Corrigan (2006), Optical properties of soot-water drop agglomerates: An experimental study, *J. Geophys. Res.*, *111*, D07209, doi:10.1029/2005JD006389.

Miller, S. M., et al. (2008), Sources of carbon monoxide and formaldehyde in North America determined from high-resolution atmospheric data, *Atmos. Chem. Phys.*, *8*(24), 7673–7696, doi:10.5194/acp-8-7673-2008.

Millstein, D. E., and R. A. Harley (2010), Effects of retrofitting emission control systems on in-use heavy diesel vehicles, *Environ. Sci. Technol.*, *44*(13), 5042–5048, doi:10.1021/es1006669.

Ming, J., H. Cachier, C. Xiao, D. Qin, S. Kang, S. Hou, and J. Xu (2008), Black carbon record based on a shallow Himalayan ice core and its climatic implications, *Atmos. Chem. Phys.*, *8*(5), 1343–1352, doi:10.5194/acp-8-1343-2008.

Ming, Y., V. Ramaswamy, P. A. Ginoux, and L. H. Horowitz (2005), Direct radiative forcing of anthropogenic organic aerosol *J. Geophys. Res.*, *110*, D20208, doi:10.1029/2004JD005573.

Ming, Y., V. Ramaswamy, and G. Persad (2010), Two opposing effects of absorbing aerosols on global-mean precipitation, *Geophys. Res. Lett.*, *37*(L13), 701, doi:10.1029/2010GL042895.

Ming, J., C. Xiao, H. Cachier, D. Qin, X. Qin, Z. Li, and J. Pu (2009), Black Carbon (BC) in the snow of glaciers in west China and its potential effects on albedos, *Atmos. Res.*, *92*(1), 114–123.

Minikin, A., A. Petzold, J. Strom, R. Krejci, M. Seifert, P. van Velthoven, H. Schlager, and U. Schumann (2003), Aircraft observations of the upper tropospheric fine particle aerosol in the Northern and Southern Hemispheres at midlatitudes, *Geophys. Res. Lett.*, *30*(10), 1503, doi:10.1029/2002GL016458.

Minvielle, F., G. Cautenet, M. O. Andreae, F. Lasserre, G. Foret, S. Cautenet, J. F. Leon, O. L. Mayol-Bracero, R. Gabriel, P. Chazette, and R. Roca (2004), Modelling the transport of aerosols during INDOEX 1999 and comparison with experimental data—1: Carbonaceous aerosol distribution, *Atmos. Environ.*, *38*(12), 1811–1822, doi:10.1016/j.atmosenv.2003.07.017.

Mishchenko, M. I., L. Liu, L. D. Travis, and A. A. Lacis (2004), Scattering and radiative properties of semi-external versus external mixtures of different aerosol types, *J. Quant. Spectrosc. Radiat. Transfer*, *88*, 139–147.

Moffet, R. C., and K. A. Prather (2009), In-situ measurements of the mixing state and optical properties of soot with implications for radiative forcing estimates, *P. Natl. Acad. Sci. USA*, *106*(29), 11872–11877.

Möhler, O., C. Linke, H. Saathoff, M. Schnaiter, R. Wagner, A. Mangold, M. Kramer, and U. Schurath (2005a), Ice nucleation on flame soot aerosol of different organic carbon content, *Meteor. Z.*, *14*(4), 477–484, doi:10.1127/0941-2948/2005/0055.

Möhler, S., et al. (2005b), Effect of sulfuric acid coating on heterogeneous ice nucleation by soot aerosol particles, *J. Geophys. Res.*, *110*, D11210, doi:10.1029/2004JD005169.

Molina, M., D. Zaelke, K. M. Sarma, S. O. Andersen, V. Ramanathan, and D. Kaniaru (2009), Reducing abrupt climate change risk using the Montreal Protocol and other regulatory actions to complement cuts in CO_2 emissions, *P. Natl. Acad. Sci. USA*, *106*(49), 20616–20621, doi:10.1073/pnas.0902568106.

Mollicone, D., H. D. Eva, and F. Achard (2006), Human role in Russian wild fires, *Nature*, *440*(7083), 436–437, doi:10.1038/440436a.

Montgomery, W. D., R. E. Baron, and S. D. Tuladhar (2009), An Analysis of Black Carbon Mitigation as a Response to Climate Change, Report Prepared for the Copenhagen Consensus on Climate, Copenhagen Consensus Center, Frederiksberg, Denmark.

Moosmüller, H., W. P. Arnott, C. F. Rogers, J. L. Bowen, J. A. Gillies, W. R. Pierson, J. F. Collins, T. D. Durbin, and J. M. Norbeck (2001), Time-resolved characterization of diesel particulate emissions. 2. Instruments for elemental and organic carbon measurements, *Environ. Sci. Technol.*, *35*(10), 1935–1942.

Moosmüller, H., R. K. Chakrabarty, and W. P. Arnott (2009), Aerosol light absorption and its measurement: A review, *J. Quant. Spectrosc. Radiat. Transfer 110*(11), 844–878 doi:10.1016/j.jqsrt.2009.02.035.

Moosmüller, H., R. K. Chakrabarty, K. M. Ehlers, and W. P. Arnott (2011), Absorption Angström coefficient, brown carbon, and aerosols: Basic concepts, bulk matter, and spherical particles, *Atmos. Chem. Phys.*, *11*(3), 1217–1225, doi:10.5194/acp-11-1217-2011.

Moosmüller, H., J. P. Engelbrecht, M. Skiba, G. Frey, R. K. Chakrabarty, and W. P. Arnott (2012), Single scattering albedo of fine mineral dust aerosols controlled by iron concentration, *J. Geophys. Res.*, *117*, D11210, doi:10.1029/2011JD016909.

Moss, R. H., et al. (2010), The next generation of scenarios for climate change research and assessment, *Nature*, *463*, 747–756, doi:10.1038/nature08823.

Moteki, N., and Y. Kondo (2007), Effects of mixing state on black carbon measurements by laser-induced incandescence, *Aerosol Sci. Technol.*, *41*(4), 398–417, doi:10.1080/02786820701199728.

Moteki, N., and Y. Kondo (2010), Dependence of laser-induced incandescence on physical properties of black carbon aerosols: Measurements and theoretical interpretation, *Aerosol Sci. Technol.*, *44*(8), 663–675, doi:10.1080/02786826.2010.484450.

Moteki, N., Y. Kondo, Y. Miyazaki, N. Takegawa, Y. Komazaki, G. Kurata, T. Shirai, D. R. Blake, T. Miyakawa, and M. Koike (2007), Evolution of mixing state of black carbon particles: Aircraft measurements over the western Pacific in March 2004, *Geophys. Res. Lett.*, *34*, L11803, doi:10.1029/2006GL028943.

Moteki, N., Y. Kondo, and S. Nakamura (2010), Method to measure refractive indices of small nonspherical particles: Application to black carbon particles, *J. Aerosol. Sci.*, *41*(5), 513–521, doi:10.1016/J.JAEROSCI.2010.02.013.

Moulliot, F., and C. B. Field (2005), Fire history and the global carbon budget: A $1^\circ \times 1^\circ$ fire history reconstruction for the 20th century, *Glob. Chang. Biol.*, *11*, 398–420, doi:10.1111/j.1365-2486.2005.00920.X.

Mugica, V., E. Ortiz, L. Molina, A. De Vizcaya-Ruiz, A. Nebot, R. Quintana, J. Aguilar, and E. Alcantara (2009), PM composition and source reconciliation in Mexico City, *Atmos. Environ.*, *43*(32), 5068–5074, doi:10.1016/j.atmosenv.2009.06.051.

Muhlbauer, A., and U. Lohmann (2009), Sensitivity studies of aerosol-cloud interactions in mixed-phase orographic precipitation, *J. Atmos. Sci.*, *66*(9), 2517–2538, doi:10.1175/2009jas3001.1.

Mukunda, H. S., S. Dasappa, P. J. Paul, N. K. S. Rajan, M. Yagnaraman, D. R. Kumar, and M. Deogaonkar (2010), Gasifier stoves—Science, technology and field outreach, *Curr. Sci.*, *98*(5), 627–638.

Mullins, J., and A. Williams (1987), The optical properties of soot: a comparison between experimental and theoretical values, *Fuel*, *66*, 277–280.

Murphy, D. M., and T. Koop (2005), Review of the vapour pressures of ice and supercooled water for atmospheric applications, *Quart J. Roy. Meteor. Soc.*, *131*(608), 1539–1565, doi:10.1256/qj.04.94.

Murphy, D. M., J. C. Chow, E. M. Leibensperger, W. C. Malm, M. Pitchford, B. A. Schichtel, J. G. Watson, and W. H. White (2011), Decreases in elemental carbon and fine particle mass in the United States, *Atmos. Chem. Phys.*, *11*, 4679–4686, doi:10.5194/acp-11-4679-2011.

Murphy, D. M., D. J. Cziczo, P. K. Hudson, and D. S. Thomson (2007), Carbonaceous material in aerosol particles in the lower stratosphere and tropopause region, *J. Geophys. Res.*, *112*(D4), 203, doi:10.1029/2006JD007297.

Murphy, D. M., S. Solomon, R. W. Portmann, K. H. Rosenlof, P. M. Forster, and T. Wong (2009), An observationally based energy balance for the Earth since 1950, *J. Geophys. Res.*, *114*(D17), 107, doi:10.1029/2009JD012105.

Myhre, G., et al. (2009), Modelled radiative forcing of the direct aerosol effect with multi-observation evaluation, *Atmos. Chem. Phys.*, *9*, 1365–1392, doi:10.5194/acp-9-1365-2009.

Naeher, L. P., M. Brauer, M. Lipsett, J. T. Zelikoff, C. D. Simpson, J. Q. Koenig, and K. R. Smith (2007), Woodsmoke health effects: A review, *Inhal. Toxicol.*, *19*(1), 67–106.

Nagashima, T., H. Shiogama, T. Yokohata, T. Takemura, S. A. Crooks, and T. Nozawa (2006), Effect of carbonaceous aerosols on surface temperature in the mid twentieth century, *Geophys. Res. Lett.*, *33*(4), 702, doi:10.1029/2005GL024887.

Naik, V., D. L. Mauzerall, L. W. Horowitz, M. D. Schwarzkopf, V. Ramaswamy, and M. Oppenheimer (2007), On the sensitivity of radiative forcing from biomass burning aerosols and ozone to emission location, *Geophys. Res. Lett.*, *34*(3), L03818, doi:10.1029/2006GL028149.

Nakawo, M., C. F. Raymond, and A. Fountain (Eds.) (2000), Debris-Covered Glaciers, 288 pp, IAHS Publication 264, International Association of Hydrological Sciences Press, Oxfordshire, United Kingdom.

Nelson, J. (1989), Fractality of sooty smoke: Implications for the severity of nuclear winter, *Nature*, *339*, 611–613.

Nenes, A., and J. H. Seinfeld (2003), Parameterization of cloud droplet formation in global climate models, *J. Geophys. Res.*, *108*(D14), doi:10.1029/2002JD002911.

Neususs, C., H. Wex, W. Birmili, A. Wiedensohler, C. Koziar, B. Busch, E. Bruggemann, T. Gnauk, nNames>M. Ebert, and D. S. Covert (2002), Characterization and parameterization of atmospheric particle number-, mass-, and chemical-size distributions in central Europe during LACE 98 and MINT, *J. Geophys. Res.*, *107*(D21), 8127, doi:10.1029/2001JD000514.

Nguyen, H. N., et al. (2008), Chemical composition and morphology of individual aerosol particles from a CARIBIC flight at 10 km altitude between 50 degrees N and 30 degrees S, *J. Geophys. Res.*, *113*(D23), 209, doi:10.1029/2008JD009956.

Novakov, T., and C. E. Corrigan (1995), Thermal characterization of biomass smoke particles, *Microchim. Acta*, *119*, 157–166.

Novakov, T., and J. E. Hansen (2004), Black carbon emissions in the United Kingdom during the past four decades: An empirical analysis, *Atmos. Environ.*, *38*(25), 4155–4163.

Novakov, T., M. O. Andreae, R. Gabriel, T. W. Kirchstetter, O. L. Mayol-Bracero, and V. Ramanathan (2000), Origin of carbonaceous aerosols over the tropical Indian Ocean: Biomass burning or fossil fuels?, *Geophys. Res. Lett.*, *27*(24), 4061–4064.

Novakov, T., V. Ramanathan, J. E. Hansen, T. W. Kirchstetter, M. Sato, J. E. Sinton, and J. A. Satahye (2003), Large historical changes of fossil-fuel black carbon aerosols, *Geophys. Res. Lett.*, *30*(6), 1324, doi:10.1029/2002GL016345.

NRC (2011), National Research Council, Climate Stabilization Targets: Emissions, Concentrations, and Impacts Over Decades to Millennia, The National Academies Press, Washington, DC.

Oanh, N. T. K., et al. (2006), Particulate air pollution in six Asian cities: Spatial and temporal distributions, and associated sources, *Atmos. Environ*, *40*(18), 3367–3380, doi:10.1016/j.atmosenv.2006.01.050.

O'Donnell, D., K. Tsigaridis, and J. Feichter (2011), Estimating the direct and indirect effects of secondary organic aerosols using ECHAM5-HAM, *Atmos. Chem. Phys.*, *11*, 8635–8659, doi:10.519/acp-11-8635-2011.

Ogren, J. A., and R. J. Charlson (1983), Elemental carbon in the atmosphere: Cycle and lifetime, *Tellus*, *35B*, 241–254.

Ohara, T., H. Akimoto, J. Kurokawa, N. Horii, K. Yamaji, X. Yan, and T. Hayasaka (2007), An Asian emission inventory of anthropogenic emission sources for the period 1980–2020, *Atmos. Chem. Phys.*, *7*(16), 4419–4444, doi:10.5194/acp-7-4419-2007.

Omar, A. H., et al. (2009), The CALIPSO automated aerosol classification and lidar ratio selection algorithm, *J. Atmos. Oceanic Technol.*, *26*, 1994–2014, doi:10.1175/2009JTECHA1231.1.

O'Neill, B. C. (2000), The jury is still out on global warming potentials, *Clim. Change*, *44*, 427–443.

Ostro, B., M. Lipsett, P. Reynolds, D. Goldberg, A. Hertz, C. Garcia, K. D. Henderson, and L. Bernstein (2010), Long-term exposure to constituents of fine particulate air pollution and mortality: Results from the California teachers study, *Environ. Health Perspect.*, *118*(3), 363–369, doi:10.1289/ehp.0901181.

Ottmar, R. D., J. L. Peterson, B. Leenhouts, and J. E. Core (2001), Smoke management: techniques to reduce or redistribute emissions, in Smoke Management Guide for Prescribed and Wildland Fire: 2001 Edition, editors C.C. Hardy, R. D. Hardy, R. D. Ottmar, J. L. Peterson, J. E. Core, P. Seamon, National Wildfire Coordination Group, Boise, ID 83705, www.nwcg.gov/pms/pubs/SMG/SMG-72.pdf.

Paatero, P. (1997), Least squares formulation of robust non-negative factor analysis, *Chemometr. Intell. Lab.*, *37*(1), 23–35.

Painter, T. H., A. P. Barrett, C. C. Landry, J. C. Neff, M. P. Cassidy, C. R. Lawrence, K. E. McBride, and G. L. Farmer (2007), Impact of disturbed desert soils on duration of mountain snow cover, *Geophys. Res. Lett.*, *34*(12), 502, doi:10.1029/2007GL030284.

Parashar, D. C., R. Gadi, T. K. Mandal, and A. P. Mitra (2005), Carbonaceous aerosol emissions from India, *Atmos. Environ.*, *39*(40), 7861–7871, doi:10.1016/j.atmosenv.2005.08.034.

Paris, J. D., A. Stohl, P. Nédélec, M. Y. Arshinov, M. V. Panchenko, V. P. Shmargunov, K. S. Law, B. D. Belan, and P. Ciais (2009), Wildfire smoke in the Siberian Arctic in summer: Source characterization and plume evolution from airborne measurements, *Atmos. Chem. Phys.*, *9*(23), 9315–9327, doi:10.5194/acp-9-9315-2009.

Park, S. H., S. L. Gong, V. S. Bouchet, W. Gong, P. A. Makar, M. D. Moran, C. A. Stroud, and J. Zhang (2011), Effects of black carbon aging on air quality predictions and direct radiative forcing estimation, *Tellus B*, *63*, 1026–1039, doi:10.1111/j.1600-0889.2011.00558.X.

Park, R. J., D. J. Jacob, M. Chin, and R. V. Martin (2003), Sources of carbonaceous aerosols over the United States and implications for natural visibility, *J. Geophys. Res.*, *108*(D12), 4355, doi:10.1029/2002JD003190.

Park, R. J., M. J. Kim, J. I. Jeong, D. Youn, and S. Kim (2010), A contribution of brown carbon aerosol to the aerosol light absorption and its radiative forcing in East Asia, *Atmos. Environ.*, *44*(11), 1414–1421, doi:10.1016/j.atmosenv.2010.01.042.

Park, K., D. B. Kittelson, M. R. Zachariah, and P. H. McMurry (2004), Measurement of inherent material density of nanoparticle agglomerates, *J. Nanopart. Res.*, *6*(267–272).

Parrish, D. D., D. T. Allen, T. S. Bates, M. Estes, F. C. Fehsenfeld, G. Feingold, R. Ferrare, R. M. Hardesty, J. F. Meagher, J. W. Nielsen-Gammon, R. B. Pierce, T. B. Ryerson, J. H. Seinfeld, and E. J. Williams (2009), Overview of the second Texas air quality study (TexAQS II) and the gulf of Mexico atmospheric composition and climate study (GoMACCS), *J. Geophys. Res.*, *114*, D00f13, doi:10.1029/2009JD011842.

Patterson, E. M., and C. K. McMahon (1984), Absorption characteristics of forest fire particulate matter, *Atmos. Environ.*, *18*(11), 2541–2551.

Pechony, O., and D. T. Shindell (2010), Driving forces of global wildfires over the past millennium and the forthcoming century, *P. Natl. Acad. Sci. USA*, *107*(45), 19167–19170, doi:10.1073/pnas.1003669107.

Penner, J. E., Y. Chen, M. Wang, and X. Liu (2009), Possible influence of anthropogenic aerosols on cirrus clouds and anthropogenic forcing, *Atmos. Chem. Phys.*, *9*(3), 879–896.

Penner, J. E., C. C. Chuang, and K. Grant (1998), Climate forcing by carbonaceous and sulfate aerosols, *Climate Dyn.*, *14*(12), 839–851.

Penner, J. E., H. Eddleman, and T. Novakov (1993), Towards the development of a global inventory for black carbon emissions, *Atmos. Environ.*, *27A*(8), 1277–1295.

Penner, J. E., S. Y. Zhang, and C. C. Chuang (2003), Soot and smoke aerosol may not warm climate, *J. Geophys. Res.*, *108*(D21), 4657, doi:10.1029/2003JD003409.

Penner, J. E., et al. (2001), Aerosols: Their direct and indirect effects, in IPCC, 2001: Climate Change 2001: The Scientific Basis. Contribution of Working Group I to the Third Assessment Report of the

Intergovernmental Panel on Climate Change, 289–348 pp., Cambridge University Press, Cambridge, United Kingdom and New York, NY, USA.

Perlwitz, J., and R. L. Miller (2010), Cloud cover increase with increasing aerosol absorptivity: A counterexample to the conventional semidirect aerosol effect, *J. Geophys. Res.*, *115*(D08), 203, doi:10.1029/2009JD012637.

Perovich, D. K., T. C. Grenfell, B. Light, and P. V. Hobbs (2002), Seasonal evolution of the albedo of multiyear Arctic sea ice, *J. Geophys. Res.*, *107*(C10), 8044, doi:10.1029/2000JC000438.

Peters, G. P., B. Aamaas, T. Berntsen, and J. S. Fuglestvedt (2011), The integrated global temperature change potential (iGTP) and relationships between emission metrics, *Environ. Res. Lett.*, *6*, 044021, doi:10.1088/1748-9326/6/4/044021.

Petters, M. D., M. T. Parsons, A. J. Prenni, P. J. DeMott, S. M. Kreidenweis, C. M. Carrico, A. P. Sullivan, G. R. McMeeking, E. Levin, C. E. Wold, J. L. Collett, and H. Moosmüller (2009), Ice nuclei emissions from biomass burning, *J. Geophys. Res.*, *114*(D07), 209, doi:10.1029/2008JD011532.

Petzold, A., and R. Niessner (1996), Photoacoustic soot sensor for in-situ black carbon monitoring, *Appl. Phys. B—Lasers Opt.*, *63*(2), 191–197.

Petzold, A., M. Gysel, X. Vancassel, R. Hitzenberger, H. Puxbaum, S. Vrochticky, E. Weingartner, U. Baltensperger, and P. Mirabel (2005a), On the effects of organic matter and sulphur-containing compounds on the CCN activation of combustion particles, *Atmos. Chem. Phys.*, *5*, 3187–3203.

Petzold, A., H. Schloesser, P. J. Sheridan, W. P. Arnott, J. A. Ogren, and A. Virkkula (2005b), Evaluation of multiangle absorption photometry for measuring aerosol light absorption, *Aerosol Sci. Technol.*, *39*, 40–51.

Petzold, A., J. Strom, S. Ohlsson, and F. P. Schroder (1998), Elemental composition and morphology of ice-crystal residual particles in cirrus clouds and contrails, *Atmos. Res.*, *49*(1), 21–34.

Philippin, S., A. Wiedensohler, and F. Stratmann (2004), Measurements of non-volatile fractions of pollution aerosols with an eight-tube volatility tandem differential mobility analyzer (VTDMA-8), *J. Aerosol. Sci.*, *35*(2), 185–203, doi:10.1016/j.jaerosci.2003.07.004.

Phillips, V. T. J., P. J. DeMott, and C. Andronache (2008), An empirical parameterization of heterogeneous ice nucleation for multiple chemical species of aerosol, *J. Atmos. Sci.*, *65*(9), 2757–2783, doi:10.1175/2007jas2546.1.

Polenske, K. R., and F. C. McMichael (2002), A Chinese cokemaking process-flow model for energy and environmental analyses, *Energ. Policy*, *30*(10), 865–883, doi:10.1016/S0301-4215(01)00147-1.

Polissar, A., P. Hopke, and J. Harris (2001), Source regions for atmospheric aerosol measured at Barrow, Alaska, *Environ. Sci. Technol.*, *35*, 4214–4226.

Polyakov, I. V., G. V. Alekseev, R. V. Bekryaev, U. Bhatt, R. L. Colony, M. A. Johnson, V. P. Karklin, A. P. Makshtas, D. Walsh, and A. V. Yulin (2002), Observationally based assessment of polar amplification of global warming, *Geophys. Res. Lett.*, *29*(18), 1878, doi:10.1029/2001GL011111.

Pope, C. A., M. Ezzati, and D. W. Dockery (2009), Fine-particulate air pollution and life expectancy in the united states, *N. Engl. J. Med.*, *360*(4), 376–386.

Popovicheva, O., N. M. Persiantseva, N. K. Shonija, P. Demott, K. Köhler, M. Petters, S. Kreidenweis, V. Tishkova, B. Demirdjian, and J. Suzanne (2008), Water interaction with hydrophobic and hydrophilic soot particles, *Phys. Chem. Chem. Phys.*, *10*, 2332–2344, doi:10.1039/B718944N.

Pósfai, M., J. R. Anderson, P. R. Buseck, and H. Sievering (1999), Soot and sulfate particles in the remote marine troposphere, *J. Geophys. Res.*, *104*(D17), 21685–21693.

Pósfai, M., R. Simonics, J. Li, P. V. Hobbs, and P. R. Buseck (2003), Individual aerosol particles from biomass burning in southern Africa: 1. Compositions and size distributions of carbonaceous particles, *J. Geophys. Res.*, *108*(D13), 8483, doi:10.1029/2002JD002291.

Power, M. J., et al (2008), Changes in fire regimes since the Last Glacial Maximum: An assessment based on a global synthesis and analysis of charcoal data, *Climate Dyn.*, *30*, 887–907, doi:10.1007/s00382-007-0334-X.

Pratt, K. A., P. J. DeMott, J. R. French, Z. Wang, D. L. Westphal, A. J. Heymsfield, C. H. Twohy, A. J. Prenni, and K. A. Prather (2009), In situ detection of biological particles in cloud ice-crystals, *Nature Geosci.*, *2*(6), 397–400, doi:10.1038/ngeo521.

Prenni, A. J., P. J. Demott, D. C. Rogers, S. M. Kreidenweis, G. M. McFarquhar, G. Zhang, and M. R. Poellot (2009), Ice nuclei characteristics from M-PACE and their relation to ice formation in clouds, *Tellus B*, *61*(2), 436–448, doi:10.1111/j.1600-0889.2009.00415.X.

Pruppacher, H. R., and J. D. Klett (1997), Microphysics of Clouds and Precipitation, 954 pp., Kluwer Academic Publishers, Dordrecht, The Netherlands.

Puxbaum, H., A. Caseiro, A. Sanchez-Ochoa, A. Kasper-Giebl, M. Claeys, A. Gelencsér, M. Legrand, S. Preunkert, and C. Pio (2007), Levoglucosan levels at background sites in Europe for assessing the impact of biomass combustion on the European aerosol background, *J. Geophys. Res.*, *112*, D23s05, doi:10.1029/2006JD008114.

Qian, Y., M. G. Flanner, L. R. Leung, and W. Wang (2011), Sensitivity studies of the impacts of Tibetan Plateau snowpack pollution on the Asian hydrologic cycle and monsoon climate, *Atmos. Chem. Phys.*, *11*, 1929–1948, doi:10.5194/acp-11-1929-2011.

Qian, Y., W. I. Gustafson, L. R. Leung, and S. J. Ghan (2009), Effects of soot-induced snow albedo change on snowpack and hydrological cycle in western United States based on Weather Research and Forecasting chemistry and regional climate simulations, *J. Geophys. Res.*, *114*(D03), 108, doi:10.1029/2008JD011039.

Quaas, J., et al. (2009), Aerosol indirect effects—General circulation model intercomparison and evaluation with satellite data, *Atmos. Chem. Phys.*, *9*(22), 8697–8717, doi:10.5194/acp-9-8697-2009.

Querol, X., et al (2008), PM speciation and sources in Mexico during the MILAGRO-2006 Campaign, *Atmos. Chem. Phys.*, *8*(1), 111–128, doi:10.5194/acp-8-111-2008.

Quinn, P. K., and T. S. Bates (2005), Regional aerosol properties: Comparisons of boundary layer measurements from ACE 1, ACE 2, aerosols99, INDOEX, ACE Asia, TARFOX, and NEAQS, *J. Geophys. Res.*, *110*(D14), 202, doi:10.1029/2004JD004755.

Quinn, P. K., and D. J. Coffman (1998), Local closure during the First Aerosol Characterization Experiment (ACE1): Aerosol mass concentration and scattering and backscattering coefficients, *J. Geophys. Res.*, *103*(D13), 16575–16596.

Quinn, P. K., T. S. Bates, E. Baum, N. Doubleday, A. M. Fiore, M. Flanner, A. Fridlind, T. J. Garrett, D. Koch, S. Menon, D. Shindell, A. Stohl, and S. G. Warren (2008), Short-lived pollutants in the Arctic: Their climate impact and possible mitigation strategies, *Atmos. Chem. Phys.*, *8*, 1723–1725.

Quinn, P. K., et al. (2011), The impact of black carbon on Arctic Climate, 128 pp., Arctic Monitoring and Assessment Programme (AMAP), Oslo, Norway.

Raes, F., T. Bates, F. McGovern, and M. Van Liedekerke (2000), The 2nd aerosol characterization experiment (ACE-2): General overview and main results, *Tellus B*, *52*(2), 111–125.

Ramachandran, G., and P. C. Reist (1995), Characterization of morphological changes in agglomerates subject to condensation and evaporation using multiple fractal dimensions, *Aerosol Sci. Technol.*, *23*, 431–442.

Ramana, M. V., and V. Ramanathan (2006), Abrupt transition from natural to anthropogenic aerosol radiative forcing: Observations at the ABC-Maldives Climate Observatory, *J. Geophys. Res.*, *111*(D20), doi:10.1029/2006JD007063.

Ramanathan, V., et al (2007), Atmospheric brown clouds: Hemispherical and regional variations in long-range transport, absorption, and radiative forcing, *J. Geophys. Res.*, *112*, D22S21, doi:10.1029/2006JD008124.

Ramanathan, V., and G. Carmichael (2008), Global and regional climate changes due to black carbon, *Nature Geosci.*, *1*(4), 221–227, doi:10.1038/ngeo156.

Ramanathan, V., and Y. Y. Xu (2010), The Copenhagen Accord for limiting global warming: Criteria, constraints, and available avenues, *P. Natl. Acad. Sci. USA*, *107*(18), 8055–8062, doi:10.1073/pnas.1002293107.

Ramanathan, V., C. Chung, D. Kim, T. Bettge, L. Buja, J. T. Kiehl, W. M. Washington, Q. Fu, D. R. Sikka, and M. Wild (2005), Atmospheric brown clouds: Impacts on South Asian climate and hydrological cycle, *P. Natl. Acad. Sci. USA*, *102*(15), 5326–5333, doi:10.1073/pnas.0500656102.

Ramanathan, V., P. J. Crutzen, J. T. Kiehl, and D. Rosenfeld (2001a), Aerosols, climate, and the hydrological cycle, *Science*, *294*(5549), 2119–2124.

Ramanathan, V., et al (2001b), Indian ocean experiment: An integrated analysis of the climate forcing and effects of the great Indo-Asian haze, *J. Geophys. Res.*, *106*(D22),28371–28398, doi:10.1029/2001JD900133.

Randles, C. A., and V. Ramaswamy (2008), Absorbing aerosols over Asia: A Geophysical Fluid Dynamics Laboratory general circulation model sensitivity study of model response to aerosol optical depth and aerosol absorption, *J. Geophys. Res.*, *113*(D21), 203, doi:10.1029/2008JD010140.

Rasch, P. J., W. D. Collins, and B. E. Eaton (2001), Understanding the Indian Ocean Experiment (INDOEX) aerosol distributions with an aerosol assimilation, *J. Geophys. Res.*, *106*(D7), 7337–7355.

Rasch, P. J., et al. (2000), A comparison of scavenging and deposition processes in global models: Results from the WCRP Cambridge Workshop of 1995, *Tellus*, *52B*, 1025–1056.

Rau, J. A. (1989), Composition and size distribution of residential wood smoke particles, *Aerosol Sci. Technol.*, *10*(1), 181–192, doi:10.1080/02786828908959233.

RCP Database (2009), Representative Concentration Pathways (RCP) Database (Version 2.0), International Institute for Applied Systems Analysis (IIASA), http://www.iiasa.ac.at/web-apps/tnt/RcpDb/dsd?Action=htmlpage&page=about., edited.

Reddy, M. S., and O. Boucher (2007), Climate impact of black carbon emitted from energy consumption in the world's regions, *Geophys. Res. Lett.*, *34*, L11802, doi:10.1029/2006GL028904.

Reddy, M. S., O. Boucher, Y. Balkanski, and M. Schulz (2005a), Aerosol optical depths and direct radiative perturbations by species and source type, *Geophys. Res. Lett.*, *32*(12), 803, doi:10.1029/2004GL021743.

Reddy, M. S., O. Boucher, N. Bellouin, M. Schulz, Y. Balkanski, J. L. Dufresne, and M. Pham (2005b), Estimates of global multicomponent aerosol optical depth and direct radiative perturbation in the Laboratoire de Meteorologie Dynamique general circulation model, *J. Geophys. Res.*, *110*, D10s16, doi:10.1029/2004jd004757.

Reddy, M. S., and C. Venkataraman (2002a), Inventory of aerosol and sulphur dioxide emissions from India: Part I—Fossil fuel combustion, *Atmos. Environ.*, *36*, 677–697.

Reddy, M. S., and C. Venkataraman (2002b), Inventory of aerosol and sulphur dioxide emissions from India, Part II—Biomass combustion, *Atmos. Environ.*, *36*(4), 699–712, doi:10.1016.S1352-2310(01)00464-2.

Redemann, J., et al. (2000), Retrieving the vertical structure of the effective aerosol complex index of refraction from a combination of aerosol in situ and remote sensing measurements during TARFOX, *J. Geophys. Res.*, *105*(D8), 9949–9970.

Reff, A., P. V. Bhave, H. Simon, T. G. Pace, G. A. Pouliot, J. D. Mobley, and M. Houyoux (2009), Emissions inventory of $PM_{2.5}$ trace elements across the United States, *Environ. Sci. Technol.*, *43*(15), 5790–5796, doi:10.1021/es802930X.

Reid, J. S., R. Koppmann, T. F. Eck, and D. P. Eleuterio (2005), A review of biomass burning emissions part II: Intensive physical properties of biomass burning particles, *Atmos. Chem. Phys.*, *5*, 799–825, doi:10.5194/acp-5-799-2005.

Reid, J. S., P. V. Hobbs, C. Liousse, J. v. Martins, R. E. Weiss, and T. F. Eck (1998), Comparisons of techniques for measuring shortwave absorption and black carbon content of aerosols from biomass burning in Brazil, *J. Geophys. Res.*, *103*(D24), 32031–32040.

Reid, J. S., et al. (2009), Global monitoring and forecasting of biomass-burning smoke: Description of and lessons from the fire locating and modeling of burning emissions (FLAMBE) program, *IEEE J. Sel. Top. Appl. Earth Observ. Remote Sens.*, *2*(3), 144–162, doi:10.1109/jstars.2009.2027443.

Remer, L. A., et al (2005), The MODIS aerosol algorithm, products, and validation, *J. Atmos. Sci.*, *62*(4), 947–973.

Remer, L. A., et al. (2008), Global aerosol climatology from the MODIS satellite sensors, *J. Geophys. Res.*, *113*, D14S07, doi:10.1029/2007JD009661.

Richardson, M. S., et al. (2007), Measurements of heterogeneous ice nuclei in the western United States in springtime and their relation to aerosol characteristics, *J. Geophys. Res.*, *112*(D2), 209, doi:10.1029/2006JD007500.

Riddle, S. G., M. A. Robert, C. A. Jakober, M. P. Hannigan, and M. J. Kleeman (2008), Size-resolved source apportionment of airborne particle mass in a roadside environment, *Environ. Sci. Technol.*, *42*(17), 6580–6586.

Riemer, N., M. West, R. A. Zaveri, and R. C. Easter (2009), Simulating the evolution of soot mixing state with a particle-resolved aerosol model, *J. Geophys. Res.*, *114*(D9), 202, doi:10.1029/2008JD011073.

Roberts, D. L., and A. Jones (2004), Climate sensitivity to black carbon aerosol from fossil fuel combustion, *J. Geophys. Res.*, *109*(D16), 202, doi:10.1029/2004JD004676.

Robinson, A. L., N. M. Donahue, M. K. Shrivastava, E. A. Weitkamp, A. M. Sage, A. P. Grieshop, T. E. Lane, J. R. Pierce, and S. N. Pandis (2007), Rethinking organic aerosols: Semivolatile emissions and photochemical aging, *Science*, *315*, 1259–1262, doi:10.1126/science.1133061.

Roden, C. A., T. C. Bond, S. Conway, A. B. S. Pinel, N. MacCarty, and D. Still (2009), Laboratory and field investigations of particulate and carbon monoxide emissions from traditional and improved cookstoves, *Atmos. Environ.*, *43*(6), 1170–1181, doi:10.1016/j.atmosenv.2008.05.041.

Rodhe, H., O. Akesson, and C. Persson (1972), An investigation into regional transport of soot and sulfate aerosols, *Atmos. Environ.*, *6*(9), 675–693, doi:10.1016/0004-6981(72)90025-X.

Roeckner, E., P. Stier, J. Feichter, S. Kloster, M. Esch, and I. Fischer-Bruns (2006), Impact of carbonaceous aerosol emissions on regional climate change, *Climate Dyn.*, *27*(6), 553–571, doi:10.1007/s00382-006-0147-3.

Rogers, D. C., P. J. DeMott, S. M. Kreidenweis, and Y. L. Chen (1998), Measurements of ice nucleating aerosols during SUCCESS, *Geophys. Res. Lett.*, *25*(9), 1383–1386.

Rose, D., et al. (2011), Cloud condensation nuclei in polluted air and biomass burning smoke near the mega-city Guangzhou, China—Part 2: Size-resolved aerosol chemical composition, diurnal cycles, and externally mixed weakly CCN-active soot particles, *Atmos. Chem. Phys.*, *11*(6), 2817–2836, doi:10.5194/acp-11-2817-2011.

Rosen, H., A. D. A. Hansen, L. Gundel, and T. Novakov (1978), Identification of the optically absorbing component in urban aerosols, *Appl. Opt.*, *17*(24), 3859–3861.

Rosen, H., A. D. A. Hansen, L. Gundel, and T. Novakov (1979), Identification of the graphitic carbon component of source and ambient particulates by Raman spectroscopy and an optical attenuation technique, in Carbonaceous Particles in the Atmosphere, 229–232 pp. Lawrence Berkeley Laboratory, Berkeley, CA.

Rosen, H., A. D. A. Hansen, and T. Novakov (1984), Role of graphitic carbon particles in radiative transfer in the Arctic haze, *Sci. Total Environ.*, *36*(JUN), 103–110.

Rotstayn, L. D., M. D. Keywood, B. W. Forgan, A. J. Gabric, I. E. Galbally, J. L. Gras, A. K. Luhar, G. H. McTainsh, R. M. Mitchell, and S. A. Young (2009), Possible impacts of anthropogenic and natural aerosols on Australian climate: A review, *Int. J. Climatol.*, *29*, 461–479, doi:10.1002/joc.1729.

Rotstayn, L. D., et al. (2007), Have Australian rainfall and cloudiness increased due to the remote effects of Asian anthropogenic aerosols?, *J. Geophys. Res.*, *112*(D9), 202, doi:10.1029/2006JD007712.

Roy, D. P., P. E. Lewis, and C. O. Justice (2002), Burned area mapping using multi-temporal moderate spatial resolution data—A bi-directional reflectance model-based expectation approach, *Remote Sens. Environ.*, *83*(1–2), 263–286.

Ruckstuhl, C., J. R. Norris, and R. Philipona (2010), Is there evidence for an aerosol indirect effect during the recent aerosol optical depth decline in Europe?, *J. Geophys. Res.*, *115*, D04204, doi:10.1029/2009JD012867.

Russell, L. (2003), Aerosol organic-mass-to-organic-carbon ratios, *Environ. Sci. Technol.*, *37*, 2982–2987.

Russell, P. B., R. W. Bergstrom, Y. Shinozuka, A. D. Clarke, P. F. DeCarlo, J. L. Jimenez, J. M. Livingston, J. Redemann, O. Dubovik, and A. Strawa (2010), Absorption Angstrom Exponent in AERONET and related data as an indicator of aerosol composition, *Atmos. Chem. Phys.*, *10*(3), 1155–1169, doi:10.5194/acp-10-1155-2010.

Russell, P. B., P. V. Hobbs, and L. L. Stowe (1999), Aerosol properties and radiative effects in the United States East Coast haze plume: An overview of the Tropospheric Aerosol Radiative Forcing Observational Experiment (TARFOX), *J. Geophys. Res.*, *104*(D2), 2213–2222.

Rypdal, K., N. Rive, T. Berntsen, H. Fagerli, Z. Klimont, T. K. Mideksa, and J. S. Fuglestvedt (2009a), Climate and air quality-driven scenarios of ozone and aerosol precursor abatement, *Environ. Sci. Policy*, *12*(7), 855–869, doi:10.1016/j.envsci.2009.08.002.

Rypdal, K., N. Rive, T. K. Berntsen, Z. Klimont, T. K. Mideksa, G. Myhre, and R. B. Skeie (2009b), Costs and global impacts of black carbon abatement strategies, *Tellus B*, *61*(4), 625–641, doi:10.1111/j.1600-0889.2009.00430.X.

Rypdal, K., F. Stordal, J. S. Fuglestvedt, and T. Berntsen (2005), Introducing top-down methods in assessing compliance with the Kyoto Protocol, *Climate Policy*, *5*(4), 393–405.

Sahu, S. K., G. Beig, and C. Sharma (2008), Decadal growth of black carbon emissions in India, *Geophys. Res. Lett.*, *35*(2), doi:10.1029/2007GL032333.

Sakurai, H., K. Park, P. H. McMurry, D. D. Zarling, D. B. Kittelson, and P. J. Ziemann (2003), Size-dependent mixing characteristics of volatile and nonvolatile components in diesel exhaust aerosols, *Environ. Sci. Technol.*, *37*, 5487–5495.

Salam, A., H. Bauer, K. Kassin, S. M. Ullah, and H. Puxbaum (2003), Aerosol chemical characteristics of a mega-city in Southeast Asia (Dhaka-Bangladesh), *Atmos. Environ.*, *37*(18), 2517–2528, doi:10.1016/s1352-2310(03)00135-3.

Samset, B. H., and G. Myhre (2011), Vertical dependence of black carbon, sulphate and biomass burning aerosol radiative forcing, *Geophys. Res. Lett.*, *38*, L24802, doi:10.1029/2011GL049697.

Sandu, I., J. L. Brenguier, O. Geoffroy, O. Thouron, and V. Masson (2008), Aerosol impacts on the diurnal cycle of marine stratocumulus, *J. Atmos. Sci.*, *65*(8), 2705–2718, doi:10.1175/2008jas2451.1.

Sarofim, M., B. DeAngelo, R. Beach, K. Weitz, M. Bahner, and A. Zapata (2010), Marginal abatement curves for U.S. black carbon emissions, *J. Integr. Environ. Sci.*, *7*(S1), 279–288, doi:10.1080/19438151003774455.

Satheesh, S. K., and V. Ramanathan (2000), Large differences in tropical aerosol forcing at the top of the atmosphere and Earth's surface, *Nature*, *405*, 60–63, doi:10.1038/35011039.

Sato, M., J. Hansen, D. Koch, A. Lacis, R. Ruedy, O. Dubovik, B. Holben, M. Chin, and T. Novakov (2003), Global atmospheric black carbon inferred from AERONET, *P. Natl. Acad. Sci. USA*, *100*(11), 6319–6324, doi:10.1073/pnas.0731897100.

Schauer, J. J., W. F. Rogge, L. M. Hildemann, M. A. Mazurek, and G. R. Cass (1996), Source apportionment of airborne particulate matter using organic compounds as tracers, *Atmos. Environ.*, *30*(22), 3837–3855.

Schmid, H., et al. (2001), Results of the "carbon conference" international aerosol carbon round robin test stage I, *Atmos. Environ.*, *35*, 2111–2121.

Schmid, B., et al. (2003), Coordinated airborne, spaceborne, and ground-based measurements of massive thick aerosol layers during the dry season in southern Africa, *J. Geophys. Res.*, *108*(D13), 8496, doi:10.1029/2002JD002297.

Schnaiter, M., H. Horvath, O. Möhler, K.-H. Naumann, H. Saathoff, and O. Schock (2003), UV-VIS-NIR spectral optical properties of soot and soot-containing aerosols, *J. Aerosol Sci.*, *34*, 1421–1444, doi:10.1016/S0021-8502(03)00361-6.

Schnaiter, M., C. Linke, O. Möhler, K.-H. Naumann, H. Saathoff, R. Wagner, U. Schurath, and B. Wehner (2005), Absorption amplification of black carbon internally mixed with secondary organic aerosol, *J. Geophys. Res.*, *110*(D19), 204, doi:10.1029/2005JD006046.

Schröder, F. P., B. Karcher, A. Petzold, R. Baumann, R. Busen, C. Hoell, and U. Schumann (1998), Ultrafine aerosol particles in aircraft plumes: In situ observations, *Geophys. Res. Lett.*, *25*(15), 2789–2792.

Schrooten, L., I. De Vlieger, F. Lefebre, and R. Torfs (2006), Costs and benefits of an enhanced reduction policy of particulate matter exhaust emissions from road traffic in Flanders, *Atmos. Environ.*, *40*(5), 904–912, doi:10.1016/j.atmosenv.2005.10.013.

Schultz, M. G., and M. Wooster (2008), Evaluation of a fire radiative power product derived from METEOSAT 8/9 and identification of operational user needs, FREEVAL final report, Band/Volume 23, Darmstadt, Germany.

Schultz, M. G., A. Heil, J. J. Hoelzemann, A. Spessa, K. Thonicke, J. G. Goldammer, A. C. Held, J. M. C. Pereira, and M. van het Bolscher (2008), Global wildland fire emissions from 1960 to 2000, *Global Biogeochem. Cycles*, *22*(2), doi:10.1029/2007GB003031.

Schulz, M., et al. (2006), Radiative forcing by aerosols as derived from the AeroCom present-day and pre-industrial simulations, *Atmos. Chem. Phys.*, *6*, 5225–5246, doi:10.5194/acp-6-5225-2006.

Schuster, G. L., O. Dubovik, B. N. Holben, and E. E. Clothiaux (2005), Inferring black carbon content and specific absorption from Aerosol Robotic Network (AERONET) aerosol retrievals, *J. Geophys. Res.*, *110*, D10S17, doi:10.1029/2004JD004548.

Schwarz, J. P., J. R. Spackman, R. S. Gao, L. A. Watts, P. Stier, M. Schulz, S. M. Davis, S. C. Wofsy, and D. W. Fahey (2010), Global-scale black carbon profiles observed in the remote atmosphere and compared to models, *Geophys. Res. Lett.*, *37*(L18), 812, doi:10.1029/2010GL044372.

Schwarz, J. P., et al. (2006), Single-particle measurements of midlatitude black carbon and light-scattering aerosols from the boundary layer to the lower stratosphere, *J. Geophys. Res.*, *111*(D16), 207, doi:10.1029/2006JD007076.

Schwarz, J. P., et al. (2008a), Coatings and their enhancement of black carbon light absorption in the tropical atmosphere, *J. Geophys. Res.*, *113*(D3), 203, doi:10.1029/2007JD009042.

Schwarz, J. P., et al. (2008b), Measurement of the mixing state, mass, and optical size of individual black carbon particles in urban and biomass burning emissions, *Geophys. Res. Lett.*, *35*(13), 810, doi:10.1029/2008GL033968.

Sedlacek, A. J., E. R. Lewis, L. Kleinman, J. Xu, and Q. Zhang (2012), Determination of and evidence for non-core-shell structure of particles containing black carbon using the Single-Particle Soot Photometer (SP2), *Geophys. Res. Lett.*, *39*, doi:10.1029/2012GL050905.

Seifert, P., A. Ansmann, D. Mueller, U. Wandinger, D. Althausen, A. J. Heymsfield, S. T. Massie, and C. Schmitt (2007), Cirrus optical properties observed with lidar, radiosonde, and satellite over the tropical Indian Ocean during the aerosol-polluted northeast and clean maritime southwest monsoon, *J. Geophys. Res.*, *112*(D17), 205, doi:10.1029/2006JD008352.

Shah, S. D., D. R. Cocker, K. C. Johnson, J. M. Lee, B. L.n Soriano, and J. W. Miller (2007), Reduction of particulate matter emissions from diesel backup generators equipped with four different exhaust aftertreatment devices, *Environ. Sci. Technol.*, *41*(14), 5070–5076, doi:10.1021/es0614161.

Shah, S. D., D. R. Cocker, J. W. Miller, and J. M. Norbeck (2004), Emission rates of particulate matter and elemental and organic carbon from in-use diesel engines, *Environ. Sci. Technol.*, *38*, 2544–2550.

Sharma, S., E. Andrews, L. A. Barrie, J. A. Ogren, and D. Lavoué (2006), Variations and sources of the equivalent black carbon in the high Arctic revealed by long-term observations at Alert and Barrow: 1989–2003, *J. Geophys. Res.*, *111*, D14208, doi:10.1029/2005JD006581.

Sharma, S., J. R. Brook, H. Cachier, J. Chow, A. Gaudenzi, and G. Lu (2002), Light absorption and thermal measurements of black carbon in different regions of Canada, *J. Geophys. Res.*, *107*(D24), 4771, doi:10.1029/2002JD002496.

Shaw, R. A., A. J. Durant, and Y. Mi (2005), Heterogeneous surface crystallization observed in undercooled water, *J. Phys. Chem. B*, *109*(20), 9865–9868, doi:10.1021/jp0506336.

Shea, R. W., B. W. Shea, J. B. Kauffman, D. E. Ward, C. I. Haskins, and M. C. Scholes (1996), Fuel biomass and combustion factors associated with fires in savanna ecosystems of South Africa and Zambia, *J. Geophys. Res.*, *101*(D19), 23551–23568, doi:10.1029/95JD02047.

Sheesley, R. J., J. J. Schauer, and M. L. Orf (2010), Assessing the impact of industrial source emissions on atmospheric carbonaceous aerosol concentrations using routine monitoring networks, *J. Air Waste Manage. Assoc.*, *60*(2), 149–155, doi:10.3155/1047-3289.60.2.149.

Shindell, D., and G. Faluvegi (2009), Climate response to regional radiative forcing during the twentieth century, *Nature Geosci.*, *2*(4), 294–300, doi:10.1038/ngeo473.

Shindell, D. T., G. Faluvegi, N. Bell, and G. A. Schmidt (2005), An emissions-based view of climate forcing by methane and tropospheric ozone, *Geophys. Res. Lett.*, *32*, L04803.

Shindell, D., G. Faluvegi, M. Walsh, S. C. Anenberg, R. V. Dingenen, N. Z. Muller, J. Austin, D. Koch, and G. Milly (2011), Climate, health, agricultural and economic impacts of tighter vehicle-emission standards, *Nature Climate Change*, *1*, 59–66, doi:10.1038/nclimate1066.

Shindell, D., M. Schulz, Y. Ming, T. Takemura, G. Faluvegi, and V. Ramaswamy (2010), Spatial scales of climate response to inhomogeneous radiative forcing, *J. Geophys. Res.*, *115*, D19110, doi:10.1029/2010jd014108.

Shindell, D. T., et al. (2008), A multi-model assessment of pollution transport to the Arctic, *Atmos. Chem. Phys.*, *8*(17), 5353–5372, doi:10.5194/acp-8-5353-2008.

Shindell, D., et al. (2012), Simultaneously mitigating near-term climate change and improving human health and food security, *Science*, *335*(6065), 183–189, doi:10.1126/science.1210026.

Shine, K. P., T. K. Berntsen, J. S. Fuglestvedt, R. B. Skeie, and N. Stuber (2007), Comparing the climate effect of emissions of short- and long-lived climate agents, *Philos. Trans. R. Soc. A—Math. Phys. Eng. Sci.*, *365*(1856), 1903–1914, doi:10.1098/rsta.2007.2050.

Shine, K. P., J. Cook, E. J. Highwood, and M. M. Joshi (2003), An alternative to radiative forcing for estimating the relative importance of climate change mechanisms, *Geophys. Res. Lett.*, *30*(20), 2047, doi:10.1029/2003GL018141.

Shine, K. P., J. S. Fuglestvedt, K. Hailemariam, and N. Stuber (2005), Alternatives to the global warming potential for comparing climate impacts of emissions of greenhouse gases, *Clim. Chang.*, *68*, 281–302.

Shiraiwa, M., Y. Kondo, T. Iwamoto, and K. Kita (2010), Amplification of light absorption of black carbon by organic coating, *Aerosol Sci. Technol.*, *44*(1), 46–54, doi:10.1080/02786820903357686.

Shiraiwa, M., Y. Kondo, N. Moteki, N. Takegawa, Y. Miyazaki, and D. R. Blake (2007), Evolution of mixing state of black carbon in polluted air from Tokyo, *Geophys. Res. Lett.*, *34*, L16803, doi:10.1029/2007GL029819.

Shiraiwa, M., Y. Kondo, N. Moteki, N. Takegawa, L. K. Sahu, A. Takami, S. Hatakeyama, S. Yonemura, and D. R. Blake (2008), Radiative impact of mixing state of black carbon aerosol in Asian outflow, *J. Geophys. Res.*, *113*, D24210, doi:10.1029/2008JD010546.

Simon, M., S. Plummer, F. Fierens, J. J. Hoelzemann, and O. Arino (2004), Burnt area detection at global scale using ATSR-2: The GLOBSCAR products and their qualification, *J. Geophys. Res.*, *109*(D14), doi:10.1029/2003JD003622.

Sinton, J. E., K. R. Smith, J. W. Peabody, L. Yaping, Z. Xiliang, R. Edwards, and G. Quan (2004), An assessment of programs to promote improved household stoves in China, *Energy Sustain. Dev.*, *8*(3), 33–52.

Skeie, R. B., T. Berntsen, G. Myhre, C. A. Pedersen, J. Ström, S. Gerland, and J. A. Ogren (2011), Black carbon in the atmosphere and snow, from pre-industrial times until present, *Atmos. Chem. Phys.*, *11*, 6809–6836, doi:10.5194/acp-11-6809-2011.

Slowik, J. G., K. Stainken, P. Davidovits, L. R. Williams, J. T. Jayne, C. E. Kolb, D. R. Worsnop, Y. Rudich, P. F. DeCarlo, and J. L. Jimenez (2004), Particle morphology and density characterization by combined mobility and aerodynamic diameter measurements. Part 2: Application to combustion-generated soot aerosols as a function of fuel equivalence ratio, *Aerosol Sci. Technol.*, *38*, 1206–1222.

Slowik, J. G., et al. (2007), An inter-comparison of instruments measuring black carbon content of soot particles, *Aerosol Sci. Technol.*, *41*(3), 295–314, doi:10.1080/02786820701197078.

Smith, K. R., R. Uma, V. V. N. Kishore, K. Lata, V. Joshi, J. Zhang, R. A. Rasmussen, and K. A. Khalil (2000a), Greenhouse gases from small-scale combustion devices in developing countries: Household stoves in India, EPA-600/R-00-052, Environmental Protection Agency, Research Triangle Park, NC.

Smith, K. R., R. Uma, V. V. N. Kishore, J. Zhang, V. Joshi, and M. A. K. Khalil (2000b), Greenhouse implications of household stoves: An analysis for India, *Ann. Rev. Energy Environ.*, *25*, 741–763.

Smith, K. R., K. Dutta, C. Chengappa, P. P. S. Gusain, O. Masera, V. Berrueta, R. Edwards, R. Bailis, and K. N. Shields (2007), Monitoring and evaluation of improved biomass cookstove programs for indoor air quality and stove performance: Conclusions from the Household Energy and Health Project, *Energy Sustain. Dev.*, *11*(2), 5–18.

Smith, K. R., J. P. McCracken, L. Thompson, R. Edwards, K. N. Shields, E. Canuz, and N. Bruce (2010), Personal child and mother carbon monoxide exposures and kitchen levels: Methods and results from a randomized trial of woodfired chimney cookstoves in Guatemala (RESPIRE), *J. Expo. Sci. Env. Epid.*, *20*(5), 406–416, doi:10.1038/jes.2010.30.

Smith, K. R., S. Mehta, and M. Maeusezahl-Feuz (2004), Indoor Smoke From Household Solid Fuels, 1435–1493 pp., World Health Organization, Geneva, Switzerland.

Smith, K. R., et al. (2009), Health and climate change 5 public health benefits of strategies to reduce greenhouse-gas emissions: Health implications of short-lived greenhouse pollutants, *Lancet*, *374*(9707), 2091–2103, doi:10.1016/s0140-6736(09)61716-5.

Soden, B. J., and I. M. Held (2006), An assessment of climate feedbacks in coupled ocean-atmosphere models, *J. Climate*, *19*(23), 3354–3360, doi:10.1175/JCLI3799.1.

Sofiev, M., R. Vankevich, M. Lotjonen, M. Prank, V. Petukhov, T. Ermakova, J. Koskinen, and J. Kukkonen (2009), An operational system for the assimilation of the satellite information on wild-land fires for the needs of air quality modelling and forecasting, *Atmos. Chem. Phys.*, *9*(18), 6833–6847, doi:10.5194/acp-9-6833-2009.

Soja, A. J., W. R. Cofer, H. H. Shugart, A. I. Sukhinin, P. W. Stackhouse, D. J. McRae, and S. G. Conard (2004), Estimating fire emissions and disparities in boreal Siberia (1998–2002), *J. Geophys. Res.*, *109*, D14s06, doi:10.1029/2004JD004570.

Sokolik, I. N., and O. B. Toon (1996), Direct radiative forcing by anthropogenic airborne mineral aerosols, *Nature*, *381*, 681–683.

Sokolov, A. P. (2006), Does model sensitivity to changes in CO_2 provide a measure of sensitivity to other forcings?, *J. Climate*, *19*, 3294–3306, doi:10.1175/JCL13791.1.

Solmon, F., F. Giorgi, and C. Liousse (2006), Aerosol modelling for regional climate studies: Application to anthropogenic particles and evaluation over a European/African domain, *Tellus B*, *58*(1), 51–72, doi:10.1111/j.1600-0889.2005.00155.X.

Solomon, P. A., et al. (2003), Overview of the 1999 Atlanta supersite project, *J. Geophys. Res.*, *108*(D7), 8413, doi:10.1029/2001JD001458.

Song, Y., Y. H. Zhang, S. D. Xie, L. M. Zeng, M. Zheng, L. G. Salmon, M. Shao, and S. Slanina (2006), Source apportionment of $PM_{2.5}$ in Beijing by positive matrix factorization, *Atmos. Environ.*, *40*(8), 1526–1537, doi:10.1016/j.atmosenv.2005.10.039.

Sorensen, C. M. (2001), Light scattering by fractal aggregates: a review, *Aerosol Sci. Technol.*, *35*, 648–687.

Spracklen, D. V., K. S. Carslaw, U. Poschl, A. Rap, and P. M. Forster (2011), Global cloud condensation nuclei influenced by carbonaceous combustion aerosol, *Atmos. Chem. Phys.*, *11*(17), 9067–9087, doi:10.5194/acp-11-9067-2011.

Stamnes, K., S. C. Tsay, W. Wiscombe, and K. Jayaweera (1988), Numerically stable algorithm for discrete-ordinate-method radiative-transfer in multiple-scattering and emitting layered media, *Appl. Opt.*, *27*, 2502–2509.

Stavrakou, T., and J. F. Müller (2006), Grid-based versus big region approach for inverting CO emissions using Measurement of Pollution in the Troposphere (MOPITT) data, *J. Geophys. Res.*, *111*(D15), 304, doi:10.1029/2005JD006896.

Stevens, B., and G. Feingold (2009), Untangling aerosol effects on clouds and precipitation in a buffered system, *Nature*, *461*(7264), 607–613, doi:10.1038/nature08281.

Stier, P., J. Feichter, S. Kloster, E. Vignati, and J. Wilson (2006a), Emission-induced nonlinearities in the global aerosol system: Results from the ECHAM4-HAM aerosol-climate model, *J. Climate*, *19*, 3845–3862.

Stier, P., J. H. Seinfeld, S. Kinne, and O. Boucher (2007), Aerosol absorption and radiative forcing, *Atmos. Chem. Phys.*, *7*, 5237–5261.

Stier, P., J. H. Seinfeld, S. Kinne, J. Feichter, and O. Boucher (2006b), Impact of nonabsorbing anthropogenic aerosols on clear-sky atmospheric absorption, *J. Geophys. Res.*, *111*(D18), D18201, doi:10.1029/2006JD007147.

Stith, J. L., C .H. Twohy, P. J. DeMott, D. Baumgardner, T. Campos, R. Gao, and J. Anderson (2011), Observations of ice nuclei and heterogeneous freezing in a Western Pacific extratropical storm, *Atmos. Chem. Phys.*, *11*(13), 6229–6243, doi:10.5194/acp-11-6229-2011.

Stith, J. L., et al. (2009), An overview of aircraft observations from the Pacific Dust Experiment campaign, *J. Geophys. Res.*, *114*(D05), 207, doi:10.1029/2008JD010924.

Stocks, B. J., et al. (2002), Large forest fires in Canada, 1959–1997, *J. Geophys. Res.*, *108*(D1), doi:10.1029/2001JD000484.

Stohl, A. (2006), Characteristics of atmospheric transport into the Arctic troposphere, *J. Geophys. Res.*, *111*(D11), D11306, doi:10.1029/2005JD006888.

Stohl, A., et al. (2007), Arctic smoke and ash: Record high air pollution levels in the European Arctic due to agricultural fires in Eastern Europe in spring 2006, *Atmos. Chem. Phys.*, *7*(2), 511–534, doi:10.5194/acp-7-511-2007.

Stone, E. A., G. C. Lough, J. J. Schauer, P. S. Praveen, C. E. Corrigan, and V. Ramanathan (2007), Understanding the origin of black carbon in the atmospheric brown cloud over the Indian Ocean, *J. Geophys. Res.*, *112*(D22), D22s23, doi:10.1029/2006JD008118.

Storelvmo, T. (2012), Uncertainties in aerosol direct and indirect effects attributed to uncertainties in convective transport parameterizations, *Atmos. Res.*, *118*, 357–369, doi:10.1016/j.atmosres.2012.06.022.

Storelvmo, T., C. Hoose, and P. Eriksson (2011), Global modeling of mixed-phase clouds: The albedo and lifetime effects of aerosols, *J. Geophys. Res.*, *116*, D05207, doi:10.1029/2010JD014724.

Storelvmo, T., J. E. Kristjansson, and U. Lohmann (2008), Aerosol influence on mixed-phase clouds in CAM-Oslo, *J. Atmos. Sci.*, *65*(10), 3214–3230, doi:10.1175/2008jas2430.1.

Streets, D. G. (2007), Dissecting future aerosol emissions: Warming tendencies and mitigation opportunities, *Clim. Chang.*, *81*(3–4), 313–330, doi:10.1007/s10584-006-9112-8.

Streets, D. G., and K. Aunan (2005), The importance of China's household sector for the black carbon emissions, *Geophys. Res. Lett.*, *32*, 1–4.

Streets, D., H. Akimoto, P. Artaxo, Z. Klimont, K. Kupiainen, G. Janssens-Maenhout, and H. Vallack (2011), Black carbon and tropospheric ozone precursors: Driver, emissions and trends, in Integrated Assessment of Black Carbon and Tropospheric Ozone, edited, 282 p., United Nations Environment Programme, Nairobi, Kenya, and World Meteorological Organization, Geneva, Switzerland.

Streets, D. G., T. C. Bond, T. Lee, and C. Jang (2004), On the future of carbonaceous aerosol emissions, *J. Geophys. Res.*, *109*(D24), doi:10.1029/2004JD004902.

Streets, D. G., F. Yan, M. Chin, T. Diehl, N. Mahowald, M. Schultz, M. Wild, Y. Wu, and C. Yu (2009), Anthropogenic and natural contributions to regional trends in aerosol optical depth, 1980–2006, *J. Geophys. Res.*, *114*, doi:10.1029/2008JD011624.

Streets, D. G., K. F. Yarber, J. H. Woo, and G. R. Carmichael (2003a), Biomass burning in Asia: Annual and seasonal estimates and atmospheric emissions, *Global Biogeochem. Cycles*, *17*(4), 1099, doi:10.1029/2003gb002040.

Streets, D. G., Q. Zhang, L. Wang, K. He, J. Hao, Y. Wu, Y. Tang, and G. R. Carmichael (2006), Revisiting China's CO emissions after the Transport and Chemical Evolution over the Pacific (TRACE-P) mission: Synthesis of inventories, atmospheric modeling, and observations, *J. Geophys. Res.*, *111*(D14), 306, doi:10.1029/2006JD007118.

Streets, D. G., et al. (2003b), An inventory of gaseous and primary aerosol emissions in Asia in the year 2000, *J. Geophys. Res.*, *108*(D21), 8809, doi:10.1029/2002JD003093.

Ström, J., and S. Ohlsson (1998), In situ measurements of enhanced crystal number densities in cirrus clouds caused by aircraft exhaust, *J. Geophys. Res.*, *103*(D10), 11355–11361.

Subramanian, R., T. C. Bond, W. Thiansathit, N. T. K. Oanh, K. G. Duleep, I. Paw-armart, and E. Winijkul (2009), Source characterization to support quantification of co-benefits: A piggyback study in Bangkok, Thailand, *Environ. Sci. Technol.*, *43*, 4213–4218.

Subramanian, R., A. Y. Khlystov, and A. L. Robinson (2006), Effect of peak inert-mode temperature on elemental carbon measured using thermal-optical analysis, *Aerosol Sci. Technol.*, *40*(10), 763–780, doi:10.1080/02786820600714403.

Sun, H., L. Biedermann, and T. C. Bond (2007), Color of brown carbon: A model for ultraviolet and visible light absorption by organic carbon aerosol, *Geophys. Res. Lett.*, *34*(17), L17813, doi:10.1029/2007GL029797.

Szidat, S., T. M. Jenk, H. A. Synal, M. Kalberer, L. Wacker, I. Hajdas, A. Kasper-Giebl, and U. Baltensperger (2006), Contributions of fossil fuel, biomass-burning, and biogenic emissions to carbonaceous aerosols in Zurich as traced by C-14, *J. Geophys. Res.*, *111*, D07206, doi:10.1029/2005JD006590.

Takemura, T., T. Nozawa, S. Emori, T. Y. Nakajima, and T. Nakajima (2005), Simulation of climate response to aerosol direct and indirect effects with aerosol transport-radiation model, *J. Geophys. Res.*, *110*(D2), 202, doi:10.1029/2004JD005029.

Tan, Q., W. L. Chameides, D. Streets, T. Wang, J. Xu, M. Bergin, and J. Woo (2004), An evaluation of TRACE-P emission inventories from China using a regional model and chemical measurements, *J. Geophys. Res.*, *109*, D22305, doi:10.1029/2004JD005071.

Targino, A. C., et al. (2009), Influence of particle chemical composition on the phase of cold clouds at a high-alpine site in Switzerland, *J. Geophys. Res.*, *114*(D18), 206, doi:10.1029/2008JD011365.

Tegen, I., P. Hollrig, M. Chin, I. Fung, D. Jacob, and J. Penner (1997), Contribution of different aerosol species to the global aerosol extinction optical thickness: Estimates from model results, *J. Geophys. Res.*, *102* (D20), 23895–23915, doi:10.1029/97JD01864.

Ten Hoeve, J. E., L. A. Remer, and M. Z. Jacobson (2011), Microphysical and radiative effects of aerosols on warm clouds during the Amazon biomass burning season as observed by MODIS: Impacts of water vapor and land cover, *Atmos. Chem. Phys.*, *11*, 3021–3036, doi:10.5194/acp-11-3021-2011.

Textor, C., et al. (2006), Analysis and quantification of the diversities of aerosol life cycles within AeroCom, *Atmos. Chem. Phys.*, *6*, 1777–1813, doi:10.5194/acp-6-1777-2006.

Textor, C., et al. (2007), The effect of harmonized emissions on aerosol properties in global models—An AeroCom experiment, *Atmos. Chem. Phys.*, *7*(17), 4489–4501, doi:10.5194/acp-7-4489-2007.

Thevenon, F., F. S. Anselmetti, S. M. Bernasconi, and M. Schwikowski (2009), Mineral dust and elemental black carbon records from an Alpine ice core (Colle Gnifetti glacier) over the last millennium, *J. Geophys. Res.*, *114*(D17), 102, doi:10.1029/2008JD011490.

Thompson, L. G., S. Hastenrath, and B. Morales-Arnao (1979), Climatic ice core records from the tropical Quelccaya ice cap, *Science*, *203*(4386), 1240–1243.

Tol, R. S. J. (2008), The social cost of carbon: Trends, outliers and catastrophes, *Economics: The Open-Access, Open-Assessment E-Journal*, *2*, 2008–25.

Tol, R. S. J., T. K. Berntsen, B. C. O'Neill, J. S. Fuglestvedt, and K. P. Shine (2012), A unifying framework for metrics for aggregating the climate effect of different emissions, *Environ. Res. Lett.*, *7*, 044006, doi:10.1088/1748-9326/7/4/044006.

Toon, O. B., C. P. McKay, T. P. Ackerman, and K. Santhanam (1989), Rapid calculation of radiative heating rates and photodissociation rates in Inhomogeneous multiple scattering atmospheres, *J. Geophys. Res.*, *94*(D13), 16287–16301, doi:10.1029/JD094iD13p16287.

Torres, O., P. K. Bhartia, J. R. Herman, and Z. Ahmad (1998), Derivation of aerosol properties from satellite measurements of backscattered ultraviolet radiation: Theoretical basis, *J. Geophys. Res.*, *103*, 17099–17110, doi:10.1029/98JD00900.

Torres, O., P. K. Bhartia, J. R. Herman, A. Sinyuk, P. Ginoux, and B. Holben (2002), A long-term record of aerosol optical depth from TOMS observations and comparison to AERONET measurements, *J. Atmos. Sci.*, *59*(3), 398–413.

Tosca, M. G., J. T. Randerson, C. S. Zender, M. G. Flanner, and P. J. Rasch (2010), Do biomass burning aerosols intensify drought in equatorial Asia during El Nino?, *Atmos. Chem. Phys.*, *10*(8), 3515–3528, doi:10.5194/acp-10-3515-2010.

Tsyro, S., D. Simpson, L. Tarrason, Z. Klimont, K. Kupiainen, C. Pio, and K. E. Yttri (2007), Modeling of elemental carbon over Europe, *J. Geophys. Res.*, *112*, D23s19, doi:10.1029/2006JD008164.

Turco, R. P., O. B. Toon, T. P. Ackerman, J. B. Pollack, and C. Sagan (1983), Nuclear winter: Global consequences of multiple nuclear explosions, *Science*, *222*(4630), 1283–1292.

Turetsky, M. R., E. S. Kane, J. W. Harden, R. D. Ottmar, K. L. Manies, E. Hoy, and E. S. Kasischke (2010), Recent acceleration of biomass burning and carbon losses in Alaskan forests and peatlands, *Nature Geosci.*, *4*, 27–31, doi:10.1038/ngeo1027.

Turpin, B. J., R. A. Cary, and J. J. Huntzicker (1990), An in situ, time-resolved analyzer for aerosol organic and elemental carbon, *Aerosol Sci. Technol.*, *12*, 161–171.

Twohy, C. H., and B. W. Gandrud (1998), Electron microscope analysis of residual particles from aircraft contrails, *Geophys. Res. Lett.*, *25*(9), 1359–1362.

Twohy, C. H., and M. R. Poellot (2005), Chemical characteristics of ice residual nuclei in anvil cirrus clouds: Evidence for homogeneous and heterogeneous ice formation, *Atmos. Chem. Phys.*, *5*, 2289–2297.

Twohy, C. H., P. J. DeMott, D. A. Pratt, R. Subramanian, G. L. Kok, S. M. Murphy, T. Lersch, A. J. Heymsfield, Z. E. Wang, K. A. Prather, and J. H. Seinfeld (2010), Relationships of biomass-burning aerosols to ice in orographic wave clouds, *J. Atmos. Sci.*, *67*(8), 2437–2450, doi:10.1175/2010JAS3310.1.

Twomey, S. A. (1959), The nuclei of natural cloud formation. Part II: The supersaturation in natural clouds and the variation of cloud droplet concentrations, *Geofis. Pura. Appl*, *43*, 227–242.

Twomey, S. A. (1991), Aerosols, clouds and radiation, *Atmos. Environ.*, *25A*(11), 2435–2442.

Uekoetter, F. (2005), The strange career of the Ringelmann smoke chart, *Environ. Monit. Assess.*, *106*(1–3), 11–26, doi:10.1007/s10661-005-0756-z.

Uherek, E., et al. (2010), Transport impacts on atmosphere and climate: Land transport, *Atmos. Environ.*, *44*(37), 4772–4816, doi:10.1016/j.atmosenv.2010.01.002.

UNECE (1999), Protocol to the 1979 Convention on Long-Range Transboundary Air Pollution to Abate Acidification, Eutrophication and Ground-Level Ozone. Adopted in Gothenburg, Sweden, on 30 November, 1999. http://www.unece.org/env/lrtap/multi_h1.html.

UNECE (2011), Options for Revising the 1999 Gothenburg Protocol to Abate Acidification, Eutrophication and Ground-level Ozone. ECE/EB.AIR/2011/8 Revised at the 29th Session of the Executive Body of the LRTAP Convention; http://www.unece.org/fileadmin/DAM/env/documents/2011/eb/ebbureau/ece.eb.air.2011.8.-REVISED_1612am_AK.doc.

UNEP (2011), Near-Term Climate Protection and Clean Air Benefits: Actions for Controlling Short-Lived Climate Forcers, 78 pp., United Nations Environment Programme, Nairobi, Kenya.

UNEP/WMO (2011a), Integrated Assessment of Black Carbon and Tropospheric Ozone: Summary for Decision Makers, 38 pp., United Nations Environment Programme, Nairobi, Kenya, and World Meteorological Organization, Geneva, Switzerland.

UNEP/WMO (2011b), Integrated Assessment of Black Carbon and Tropospheric Ozone, 282 pp., United Nations Environment Programme, Nairobi, Kenya, and World Meteorological Organization, Geneva, Switzerland.

UNFCCC (1992), United Nations Framework Convention on Climate Change, 24 pp., United Nations.

Unger, N., T. C. Bond, J. S. Wang, D. M. Koch, S. Menon, D. T. Shindell, and S. Bauer (2010), Attribution of climate forcing to economic sectors, *P. Natl. Acad. Sci. USA*, *107*(8), 3382–3387, doi:10.1073/pnas.0906548107.

USDA (2005), A strategic assessment of forest biomass and fuel reduction treatments in Western states, *Gen. Tech. Rep.*, RMRS-GTR-149, U.S. Department of Agriculture, Forest Service, Rocky Mountain Research Station.

van Aardenne, J. A., F. J. Dentener, J. G. J. Olivier, C. G. M. Klein Goldewijk, and J. Lelieveld (2001), A $1^\circ \times 1^\circ$ resolution data set of historical anthropogenic trace gas emissions for the period 1890–1990. *Global Biogeochem Cycles*, *15*(4), 909–928, doi:10.1029/2000gb001265.

Van Dingenen, R., et al. (2004), A European aerosol phenomenology—1: Physical characteristics of particulate matter at kerbside, urban, rural and background sites in Europe, *Atmos. Environ.*, *38*(16), 2561–2577, doi:10.1016/j.atmosenv.2004.01.040.

Van-Hulle, P., M. Talbaut, M. Weill, and A. Coppalle (2002), Inversion method and experiment to determine the soot refractive index: Application to turbulent diffusion flames, *Meas. Sci. Technol.*, *13*(3), 375–382.

Venkataraman, C., G. Habib, A. Eiguren-Fernandez, A. H. Miguel, and S. K. Friedlander (2005), Residential biofuels in south Asia: Carbonaceous aerosol emissions and climate impacts, *Science*, *307*, 1454–1456.

Venkataraman, C., G. Habib, D. Kadamba, M. Shrivastava, J. F. Leon, B. Crouzille, O. Boucher, and D. G. Streets (2006), Emissions from open biomass burning in India: Integrating the inventory approach with high-resolution Moderate Resolution Imaging Spectroradiometer (MODIS) active-fire and land cover data, *Global Biogeochem. Cycles*, *20*, Gb2013, doi:10.1029/2005gb002547.

Vermote, E., E. Ellicott, O. Dubovik, T. Lapyonok, M. Chin, L. Giglio, and G. J. Roberts (2009), An approach to estimate global biomass burning emissions of organic and black carbon from MODIS fire radiative power, *J. Geophys. Res.*, *114*, D18205, doi:10.1029/2008JD011188.

Viana, M., et al. (2008), Source apportionment of particulate matter in Europe: A review of methods and results, *J. Aerosol. Sci.*, *39*(10), 827–849, doi:10.1016/j.jaerosci.2008.05.007.

Vignati, E., M. Karl, M. Krol, J. Wilson, P. Stier, and F. Cavalli (2010), Sources of uncertainties in modelling black carbon at the global scale, *Atmos. Chem. Phys.*, *10*(6), 2595–2611, doi:10.5194/acp-10-2595-2010.

Virkkula, A., N. C. Ahlquist, D. S. Covert, W. P. Arnott, P. J. Sheridan, P. K. Quinn, and D. J. Coffman (2005), Modification, calibration and a field test of an instrument for measuring light absorption by particles, *Aerosol Sci. Technol.*, *39*, 68–83.

Vogelmann, A. M., A. Robock, and R. G. Ellingson (1988), Effects of dirty snow in nuclear winter simulations, *J. Geophys. Res.*, *93*(D5), 5319–5332.

Wagner, R., T. Ajtai, K. Kandler, K. Lieke, C. Linke, T. Muller, M. Schnaiter, and M. Vragel (2012), Complex refractive indices of Saharan dust samples at visible and near UV wavelengths: A laboratory study, *Atmos. Chem. Phys.*, *12*(5), 2491–2512, doi:10.5194/acp-12-2491-2012.

Walsh, M. P. (2008), Ancillary benefits for climate change mitigation and air pollution control in the world's motor vehicle fleets, *Annu. Rev. Public Health*, *29*, 1–9, doi:10.1146/annurev.publhealth.29.091307.183257.

Wang, C. (2004), A modeling study on the climate impacts of black carbon aerosols, *J. Geophys. Res.*, *109*(D3), 106, doi:10.1029/2003JD004084.

Wang, C. (2007), Impact of direct radiative forcing of black carbon aerosols on tropical convective precipitation, *Geophys. Res. Lett.*, *34*(5), 709, doi:10.1029/2006GL028416.

Wang, C., D. Kim, A. M. L. Ekman, M. C. Barth, and P. J. Rasch (2009a), Impact of anthropogenic aerosols on Indian summer monsoon, *Geophys. Res. Lett.*, *36*(L21), 704, doi:10.1029/2009GL040114.

Wang, Z. L., H. Zhang, and X. S. Shen (2011), Radiative forcing and climate response due to black carbon in snow and ice, *Adv. Atmos. Sci.*, *28*(6), 1336–1344, doi:10.1007/s00376-011-0117-5.

Wang, S., X. Zhao, X. Li, W. Wei, and J. Hao (2009b), Emission characteristics of fine particles from grate firing boilers (in Chinese), *Environ. Sci.*, *30*(4), 963–968.

Wang, S. X., M. Zhao, J. Xing, Y. Wu, Y. Zhou, Y. Lei, K. B. He, L. X. Fu, and J. M. Hao (2010), Quantifying the air pollutants emission reduction during the 2008 Olympic games in Beijing, *Environ. Sci. Technol.*, *44*(7), 2490–2496, doi:10.1021/es9028167.

Wang, M., et al. (2012), Constraining cloud lifetime effects of aerosols using A-Train satellite observations, *Geophys. Res. Lett.*, *39*, L15709, doi:10.1029/2012GL052204.

Ward, D. E., R. A. Susott, J. B. Kauffman, R. E. Babbitt, D. L. Cummings, B. Dias, B. N. Holben, Y. J. Kaufman, R. A. Rasmussen, and A. W. Setzer (1992), Smoke and fire characteristics for cerrado and deforestation burns in Brazil—BASE-B experiment, *J. Geophys. Res.*, *97* (D13), 14601–14619.

Warneke, C., et al. (2009), Biomass burning in Siberia and Kazakhstan as an important source for haze over the Alaskan Arctic in April 2008, *Geophys. Res. Lett.*, *36*(2), L02813, doi:10.1029/2008GL036194.

Warren, S. G. (1982), Optical-properties of snow, *Rev. Geophys.*, *20*(1), 67–89.

Warren, S. G., and A. D. Clarke (1990), Soot in the atmosphere and snow surface of Antarctica, *J. Geophys. Res.*, *95*(D2), 1811–1816.

Warren, S. G., and W. J. Wiscombe (1980), A model for the spectral albedo of snow. II: Snow containing atmospheric aerosols, *J. Atmos. Sci.*, *37*(12), 2734–2745.

Warren, S. G., and W. J. Wiscombe (1985), Dirty snow after nuclear-war, *Nature*, *313*(6002), 467–470.

Warren, S. G., I. G. Rigor, N. Untersteiner, V. F. Radionov, N. N. Bryazgin, Y. I. Aleksandrov, and R. Colony (1999), Snow depth on Arctic sea ice, *J. Climate*, *12*(6), 1814–1829.

Watson, J. G., L. W. A. Chen, J. C. Chow, P. Doraiswamy, and D. H. Lowenthal (2008), Source apportionment: Findings from the US Supersites program, *J. Air Waste Manage. Assoc.*, *58*(2), 265–288, doi:10.3155/1047-3289.58.2.265.

Watson, J. G., J. C. Chow, J. L. Bowen, D. H. Lowenthal, S. Hering, P. Ouchida, and W. Oslund (2000), Air quality measurements from the Fresno Supersite, *J. Air Waste Manage. Assoc.*, *50*(8), 1321–1334.

Watson, J. G., J. C. Chow, and L.-W. A. Chen (2005), Summary of organic and elemental carbon/black carbon analysis methods and intercomparisons, *Aerosol Air Qual. Res.*, *5*(1), 65–102.

Watson, J. G., J. C. Chow, D. H. Lowenthal, L. C. Pritchett, C. A. Frazier, G. R. Neuroth, and R. Robbins (1994), Differences in the carbon composition of source profiles for diesel-powered and gasoline-powered vehicles, *Atmos. Environ.*, *28*(15), 2493–2505.

Watson, J. G., J. C. Chow, D. H. Lowenthal, N. F. Robinson, C. F. Cahill, and D. L. Blumenthal (2002), Simulating changes in source profiles from coal-fired power stations: Use in chemical mass balance of $PM_{2.5}$ in the *Mount Zirkel Wilderness, Energy & Fuels*, *16*(2), 311–324, doi:10.1021/Ef010202w.

Watson, J. G., J. A. Cooper, and J. J. Huntzicker (1984), The effective variance weighting for least-squares calculations applied to the mass balance receptor model, *Atmos. Environ.*, *18*(7), 1347–1355.

Weingartner, E., H. Burtscher, and U. Baltensperger (1997), Hygroscopic properties of carbon and diesel soot particles, *Atmos. Environ.*, *31*(15), 2311–2327.

Weingartner, E., H. Saathof, M. Schnaiter, N. Streit, B. Bitnar, and U. Baltensperger (2003), Absorption of light by soot particles: Determination of the absorption coefficient by means of aethalometers, *J. Aerosol. Sci.*, *34*, 1445–1463.

van der Werf, G. R., J. T. Randerson, L. Giglio, G. J. Collatz, P. S. Kasibhatla, and A. F. Arellano Jr (2006), Interannual variability in global biomass burning emissions from 1997 to 2004, *Atmos. Chem. Phys.*, *6*(11), 3423–3441, doi:10.5194/acp-6-3423-2006.

van der Werf, G. R., J. T. Randerson, L. Giglio, G. J. Collatz, M. Mu, P. S. Kasibhatla, D. C. Morton, R. S. DeFries, Y. Jin, and T. T. van Leeuwen (2010), Global fire emissions and the contribution of deforestation, savanna, forest, agricultural, and peat fires (1997–2009), *Atmos. Chem. Phys.*, *10*, 11707–11735.

Wex, H., G. McFiggans, S. Henning, and F. Stratmann (2010), Influence of the external mixing state of atmospheric aerosol on derived CCN number concentrations, *Geophys. Res. Lett.*, *37*, L10805, doi:10.1029/2010gl043337.

Whitby, E. R., and P. H. McMurry (1997), Modal aerosol dynamics modeling, *Aerosol Sci. Technol.*, *27*(6), 673–688.

Wiacek, A., and T. Peter (2009), On the availability of uncoated mineral dust ice nuclei in cold cloud regions, *Geophys. Res. Lett.*, *36*(L17), 801, doi:10.1029/2009GL039429.

Wilcox, E. M. (2012), Direct and semi-direct radiative forcing of smoke aerosols over clouds, *Atmos. Chem. Phys.*, *12*, (1), 139–149, doi:10.5194/acp-12-139-2012.

Wild, O., M. J. Prather, and H. Akimoto (2001), Indirect long-term global radiative cooling from NO_x emissions, *Geophys. Res. Lett.*, *28* (9), 1719–1722, doi:10.1029/2000GL012573.

Williams, J., M. deReus, R. Krejci, H. Fischer, and J. Ström (2002), Application of the variability-size relationship to atmospheric aerosol studies: Estimating aerosol lifetimes and ages, *Atmos. Chem. Phys.*, *2*, 133–145, doi:10.5194/acp-2-133-2002.

Winebrake, J. J., J. J. Corbett, E. H. Green, A. Lauer, and V. Eyring (2009), Mitigating the health impacts of pollution from oceangoing shipping: An assessment of low-sulfur fuel mandates, *Environ. Sci. Technol.*, *43*(13), 4776–4782, doi:10.1021/es803224q.

Winker, D. M., et al. (2010), The CALIPSO Mission. A Global 3D view of aerosols and clouds, *Bull. Amer. Meteorol. Soc.*, *91*(9), 1211–1229, doi:10.1175/2010bams3009.1.

Wiscombe, W. J., and S. G. Warren (1980), A model for the spectral albedo of snow. I: Pure snow, *J. Atmos. Sci.*, *37*, 2712–2733.

Wofsy, S. C., et. al (2011), HIAPER Pole-to-Pole Observations (HIPPO): Fine-grained, global-scale measurements of climatically important atmospheric gases and aerosols, *Philos. Trans. R. Soc. A-Math. Phys. Eng. Sci.*, *369*(1943), 2073–2086, doi:10.1098/rsta.2010.0313.

Wonaschütz, A., R. Hitzenberger, H. Bauer, P. Pouresmaeil, B. Klatzer, A. Caseiro, and H. Puxbaum (2009), Application of the intergrating sphere method to separate the contributions of brown and black carbon in atmospheric aerosols, *Environ. Sci. Technol.*, *43*(4), 1141–1146, doi:10.1021/es8008503.

Wooster, M. J., G. Roberts, G. L. W. Perry, and Y. J. Kaufman (2005), Retrieval of biomass combustion rates and totals from fire radiative power observations: FRP derivation and calibration relationships between biomass consumption and fire radiative energy release, *J. Geophys. Res.*, *110*(D24), 311, doi:10.1029/2005JD006318.

World Bank (2011), Household Cookstoves, Environment, Health and Climate Change: A New look at an Old Problem, The International Bank for Reconstruction and Development/The World Bank, Washington, DC.

WRAP (2002), Non-Burning Management Alternatives on Agricultural Lands in the Western United States, Volume II: Non-Burning Management Alternatives and Implementation Plan Strategies, Western Air Regional Partnership, Prepared by Eastern Research Group, Inc. (ERG), Sacramento, CA.

Xu, B., M. Wang, D. Joswiak, J. Cao, T. Yao, G. Wu, W. Yang, and H. Zhao (2009a), Deposition of anthropogenic aerosols in a southeastern Tibetan glacier, *J. Geophys. Res.*, *114*, D17209, doi:10.1029/2008JD011510.

Xu, B., T. Yao, X. Liu, and N. Wang (2006), Elemental and organic carbon measurements with a two-step heating gas chromatography system in snow samples from the Tibetan Plateau, *Ann. Glaciol.*, *43*, 257–262, doi:10.3189/172756406781812122.

Xu, B., et al. (2009b), Black soot and the survival of Tibetan glaciers, *P. Natl. Acad. Sci. USA*, *106*(52), 22114–22118, doi:10.1073/pnas.0910444106.

Yang, M., S. G. Howell, J. Zhuang, and B. J. Huebert (2009), Attribution of aerosol light absorption to black carbon, brown carbon, and dust in China—Interpretations of atmospheric measurements during EAST-AIRE, *Atmos. Chem. Phys.*, *9*(6), 2035–2050, doi:10.5194/acp-9-2035-2009.

Yasunari, T. J., P. Bonasoni, P. Laj, K. Fujita, E. Vuillermoz, A. Marinoni, P. Cristofanelli, R. Duchi, G. Tartari, and K. M. Lau (2010), Estimated impact of black carbon deposition during pre-monsoon season from Nepal Climate Observatory—Pyramid data and snow albedo changes over Himalayan glaciers, *Atmos. Chem. Phys.*, *10*(14), 6603–6615, doi:10.5194/acp-10-6603-2010.

Yokelson, R. J., R. Susott, D. E. Ward, J. Reardon, and D. W. T. Griffith (1997), Emissions from smoldering combustion of biomass measured by open-path Fourier transform infrared spectroscopy, *J. Geophys. Res.*, *102*(D15), 18865–18877, doi:10.1029/97JD00852.

Yoshimori, M., and A. J. Broccoli (2008), Equilibrium response of an atmosphere-mixed layer ocean model to different radiative forcing agents: Global and zonal mean response, *J. Climate*, *21*(17), 4399–4423, doi:10.1175/2008jcli2172.1.

Yoshioka, M., N. Mahowald, A. Conley, W. Collins, D. Fillmore, C. Zender, and D. Coleman (2007), Impact of desert dust radiative forcing on Sahel precipitation: Relative importance of dust compared to sea surface temperature variations, vegetation changes and greenhouse gas warming, *J. Climate*, *20*, 1445–1467, doi:10.1175/JCL14056.1.

Young, K. C. (1974), A numerical simulation of wintertime, orographic precipitation. Part I: Description of model microphysics and numerical technique, *J. Atmos. Sci.*, *31*, 1735–1748.

Yu, H., M. Chin, D. M. Winker, A. H. Omar, Z. Liu, C. Kittaka, and T. Diehl (2010), Global view of aerosol vertical distributions from CALIPSO lidar measurements and GOCART simulations: Regional and seasonal variations, *J. Geophys. Res.*, doi:10.1029/2009JD013364.

Yumimoto, K., and I. Uno (2006), Adjoint inverse modeling of CO emissions over Eastern Asia using four-dimensional variational data assimilation, *Atmos. Environ.*, *40*(35), 6836–6845, doi:10.1016/j.atmosenv.2006.05.042.

Yun, Y., and J. E. Penner (2012), Global model comparison of heterogeneous ice nucleation parameterizations in mixed phase clouds, *J. Geophys. Res.*, *117*, D07203, doi:10.1029/2011JD016506.

Zarzycki, C. M., and T. C. Bond (2010), How much can the vertical distribution of black carbon affect its global direct radiative forcing?, *Geophys. Res. Lett.*, *37*, L20807, doi:10.1029/2010GL044555.

Zhang, J., and J. S. Reid (2009), An analysis of clear sky and contextual biases using an operational over ocean MODIS aerosol product, *Geophys. Res. Lett.*, *36*, L15824, doi:10.1029/2009GL038723.

Zhang, Y. H., M. Hu, L. J. Zhong, A. Wiedensohler, S. C. Liu, M. O. Andreae, W. Wang, and S. J. Fan (2008a), Regional integrated experiments on air quality over Pearl River Delta 2004 (PRIDE-PRD2004): Overview, *Atmos. Environ.*, *42*(25), 6157–6173, doi:10.1016/j.atmosenv.2008.03.025.

Zhang, S., J. E. Penner, and O. Torres (2005), Inverse modeling of biomass burning emissions using Total Ozone Mapping Spectrometer aerosol index for 1997, *J. Geophys. Res.*, *110*, D21306, doi:10.1029/2004JD005738.

Zhang, Y. X., J. J. Schauer, Y. Zhang, L. Zeng, Y. Wei, Y. Liu, and M. Shao (2008b), Characteristics of particulate carbon emissions from real-world Chinese coal combustion, *Environ. Sci. Technol.*, *42*, 5068–5073.

Zhang, J., K. R. Smith, Y. Ma, S. Ye, F. Jiang, W. Qi, P. Liu, M. A. K. Khalil, R. A. Rasmussen, and S. A. Thorneloe (2000), Greenhouse gases and other airborne pollutants from household stoves in China: A database for emission factors, *Atmos. Environ.*, *34*, 4537–4549.

Zhang, H., Z.-L. Wang, P.-W. Guo, and Z.-Z. Wang (2009a), A modeling study of the effects of direct radiative forcing due to carbonaceous aerosol on the climate in East Asia, *Adv. Atmos. Sci.*, *26*(1), 57–66, doi:10.1007/s00376-009-0057-5.

Zhang, H., Z.-L. Wang, Z.-Z. Wang, Q.-X. Liu, S. Gong, X.-Y. Zhang, Z.-P. Shen, P. Lu, X.-D. Wei, H.-Z. Che, and L. Li (2012), Simulation of direct radiative forcing of aerosols and their effects on East Asian climate using an interactive AGCM-aerosol coupled system, *Clim. Dyn.*, *38*, 1675–1693, doi:10.1007/s00382-011-1131-0.

Zhang, Q., et al. (2007), Ubiquity and dominance of oxygenated species in organic aerosols in anthropogenically-influenced Northern Hemisphere midlatitudes, *Geophys. Res. Lett.*, *34*, L13801, doi:10.1029/2007gl029979.

Zhang, Q., et al. (2009b), Asian emissions in 2006 for the NASA INTEX-B mission, *Atmos. Chem. Phys.*, *9*(14), 5131–5153, doi:10.5194/acp-9-5131-2009.

Zheng, M., G. R. Cass, J. J. Schauer, and E. S. Edgerton (2002), Source apportionment of $PM_{2.5}$ in the southeastern United States using solvent-extractable organic compounds as tracers, *Environ. Sci. Technol.*, *36*(11), 2361–2371, doi:10.1021/es011275x.

Zheng, M., L. G. Salmon, J. J. Schauer, L. M. Zeng, C. S. Kiang, Y. H. Zhang, and G. R. Cass (2005), Seasonal trends in $PM_{2.5}$ source contributions in Beijing, China, *Atmos. Environ.*, *39*(22), 3967–3976, doi:10.1016/j.atmosenv.2005.03.036.

Zhi, G., Y. Chen, Y. Feng, S. Xiong, J. Li, G. Zhang, G. Sheng, and J. Fu (2008), Emission characteristics of carbonaceous particles from various residential coal-stoves in China, *Environ. Sci. Technol.*, *42*(9), 3310–3315, doi:10.1021/es702247q.

Zhi, G. R., C. H. Peng, Y. J. Chen, D. Y. Liu, G. Y. Sheng, and J. M. Fu (2009), Deployment of coal briquettes and improved stoves: Possibly an option for both environment and climate, *Environ. Sci. Technol.*, *43*, 5586–5591, doi:10.1021/es802955d.

Zhou, L., P. K. Hopke, and W. X. Zhao (2009), Source apportionment of airborne particulate matter for the speciation trends network site in Cleveland, OH, *J. Air Waste Manage. Assoc.*, *59*(3), 321–331, doi:10.3155/1047-3289.s9.3.321.

Zobrist, B., et al. (2006), Oxalic acid as a heterogeneous ice nucleus in the upper troposphere and its indirect aerosol effect, *Atmos. Chem. Phys.*, *6*(10), 3115–3129, doi:10.5194/acp-6-3115-2006.